BEILSTEIN JOURNAL OF ORGANIC CHEMISTRY

Tetrathiafulvalene chemistry

Edited by Peter Skabara and Marc Sallé

Imprint

Beilstein Journal of Organic Chemistry
www.bjoc.org
ISSN 1860-5397
Email: journals-support@beilstein-institut.de

The *Beilstein Journal of Organic Chemistry* is published by the Beilstein-Institut zur Förderung der Chemischen Wissenschaften.

Beilstein-Institut zur Förderung der Chemischen Wissenschaften
Trakehner Straße 7–9
60487 Frankfurt am Main
Germany
www.beilstein-institut.de

BEILSTEIN JOURNAL OF ORGANIC CHEMISTRY

Tetrathiafulvalene chemistry

Peter J. Skabara*[1] and Marc Sallé*[2]

Editorial

Open Access

Address:
[1]WestCHEM, Department of Pure and Applied Chemistry, University of Strathclyde, Glasgow G1 1XL, United Kingdom and
[2]MOLTECH-Anjou, Université d'Angers, UMR CNRS 6200, 2 Bd Lavoisier, 49045 Angers Cedex, France

Email:
Peter J. Skabara* - peter.skabara@strath.ac.uk; Marc Sallé* - marc.salle@univ-angers.fr

* Corresponding author

Keywords:
tetrathiafulvalene; TTF

Beilstein J. Org. Chem. **2015,** *11,* 1528–1529.
doi:10.3762/bjoc.11.167

Received: 10 August 2015
Accepted: 17 August 2015
Published: 01 September 2015

This article is part of the Thematic Series "Tetrathiafulvalene chemistry".

Guest Editor: P. J. Skabara

Tetrathiafulvalene (TTF) is a fascinating system: it is quite rare to find a synthetic molecule endowed with such a simple architecture that is capable of concentrating intense interest from various communities of chemists! This modest-sized molecule which consists of only 14 atoms, was synthesized in the early nineteen seventies [1-3] and since then has proved to be exceptionally popular in various fields of chemistry.

This success results from the conjunction of intrinsic structural and electronic properties: i) structurally, this sulfur-rich bicyclic compound is essentially planar (at least in the radical cation state) and therefore presents, as with most of its substituted derivatives, a good propensity to stack in the solid state. This parameter is favorable for efficient charge delocalization in the solid-state and it is this feature that gave birth to the first conducting and superconducting organic salts (organic metals); the topic of organic conductors remains a very active area of research, attested by thousands of papers from chemists and physicists interested in the transport properties of TTF-based materials [4,5]; ii) this non-aromatic 14 π-electron system is readily oxidized through a reversible process to the corresponding aromatic cation radical and dication species, according to two successive one-electron redox processes. This excellent π-donating ability, coupled to the high stability of both oxidized species, has contributed to the establishment of this unit as a key contemporary building block for the construction of redox-active molecular and supramolecular systems, where an electron-donating capacity is needed and/or when a redox-control has to be considered. It is therefore not surprising that a myriad of TTF derivatives has been produced for various applications. From that point of view, the contrast between the simplicity of the C_6S_4 active framework on one hand and the huge variety of topics that are encompassed by those derivatives is totally incredible. This has been possible thanks to the continuous, creative efforts developed by organic chemists to decorate this unit for specific uses; our special issue in the *Beilstein Journal of Organic Chemistry* Thematic Series presents a snap shot of this highly dynamic field.

A wide community of readers, from synthetic chemists to materials science experts, will find exciting reports (letters, full papers and reviews) spanning the most recent trends from internationally leading groups in this field. The selection of works cover a broad variety of fields that will hopefully serve to inspire the reader, implementing further research into TTF derivatives towards new horizons.

As the guest editors of this Thematic Series in the *Beilstein Journal of Organic Chemistry*, we warmly acknowledge all the authors for their outstanding contributions and the staff of the Beilstein-Institut for their excellent and professional support.

Peter Skabara and Marc Sallé

Glasgow, Angers, August 2015

References

1. Wudl, F.; Smith, G. M.; Hufnagel, E. J. *J. Chem. Soc. D* **1970,** 1453–1454. doi:10.1039/C29700001453
2. Hünig, S.; Kiesslich, G.; Sceutzow, D.; Zhrandik, R.; Carsky, P. *Int. J. Sulfur Chem., Part C* **1971,** 109–122.
3. Coffen, D. L.; Chambers, J. Q.; Williams, D. R.; Garrett, P. E.; Canfield, N. D. *J. Am. Chem. Soc.* **1971,** *93,* 2258–2268. doi:10.1021/ja00738a028
4. Batail, P., Ed. Molecular Conductors. *Chem. Rev.* **2004,** *104,* 4887–5782. doi:10.1021/cr040697x
   See for a dedicated issue.
5. Martín, N. *Chem. Commun.* **2013,** *49,* 7025–7027. doi:10.1039/C3CC00240C
   See for a recent view point.

License and Terms

BEILSTEIN JOURNAL OF ORGANIC CHEMISTRY

Bis(vinylenedithio)tetrathiafulvalene analogues of BEDT-TTF

Erdal Ertas*[1,§], İlknur Demirtas[1] and Turan Ozturk[2,3]

Review

Open Access

Address:
[1]TUBITAK Marmara Research Center, FI, P.O.Box 21, 41470 Gebze-Kocaeli, Turkey, [2]Istanbul Technical University, Science Faculty, Chemistry Department, Organic Chemistry, 34469 Maslak, Istanbul, Turkey and [3]TUBITAK UME, Chemistry Group Laboratories, P.O.Box 54, 41470 Gebze-Kocaeli, Turkey

Email:
Erdal Ertas* - erdal.ertas@tubitak.gov.tr

* Corresponding author
§ Tel: +902626773209; Fax: +902626412309

Keywords:
bis(ethylenedithio)tetrathiafulvalene;
bis(vinylenedithio)tetrathiafulvalene; tetrathiafulvalene

Beilstein J. Org. Chem. **2015,** *11,* 403–415.
doi:10.3762/bjoc.11.46

Received: 28 January 2015
Accepted: 09 March 2015
Published: 27 March 2015

This article is part of the Thematic Series "Tetrathiafulvalene chemistry".

Guest Editor: P. J. Skabara

Abstract

This review aims to give an overview of the current status of our research on the synthesis of π-electron donor bis(ethylenedithio)tetrathiafulvalene (BEDT-TTF, ET) analogues prepared from 1,8-diketones via a ring forming reaction. The new synthesized π-electron donors have vinyl moieties producing extended π-electron delocalization over the substituent phenyl rings at the peripheries.

Introduction

Tetrathiafulvalene (TTF, **1**, Figure 1) was first synthesized in 1960s by Klingsberg's method [1]. Shortly after this, it was synthesized by other research groups and used as a donor molecule in 1970 [2]. Although, in 1972, **1** was demonstrated to be an organic material conductor in the form of its chloride salt [3]. The interest in the chemistry of **1** begun with the discovery of the salt of **1** with 7,7,8,8-tetracyanoquinodimethane (**2**, TTF-TCNQ) in 1973 [4]. Since then, studies have been focused on the syntheses of donor TTF analogues and investigations of the physical properties of their charge-transfer (CT) salts with various acceptors for applications such as electrically conductive materials, super conductive materials, magnetic substances, electrochromic materials, electroluminescent materials, etc. [5-16]. TTF-TCNQ, which is metallic under 54 K and known to be the first true one-dimensional synthetic metal, led to the production of superconducting salts based on TTF type donors containing a heteroatom such as sulfur, selenium, oxygen, etc. [17-20]. Among a large number of tetrathiafulvalene analogues, bis(ethyleneditiho)tetrathiafulvalene (BEDT-TTF, **3**), also known as ET, has been the most studied and has had the largest number of radical cation salts of its CT materials investigated at very low temperature [12,21-24].

In order to improve the properties of TTF type materials, various methods have been applied, including extension of π-conjugation through double bonds [25-30] and fused aromatic

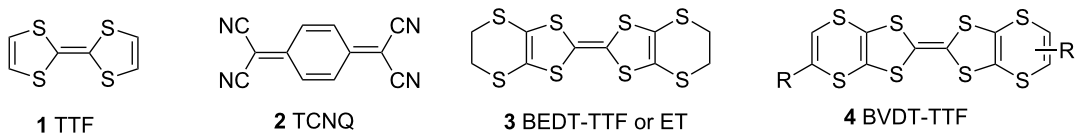

Figure 1: Chemical structure of the TTF analogues and TCNQ.

rings [31-34] and the construction of molecules having acceptor substituents [35-37]. Generally, all these modifications served to produce molecules with better conjugation and improved S···S intermolecular and C–H···anion interactions in determining the solid state properties [35-37]. Bis(vinylenedithio)tetrathiafulvalene (BVDT-TTF) **4** (R = Ph, 4-$CH_3OC_6H_4$, 4-BrC_6H_4, 4-$CH_3C_6H_4$, 4-$O_2NC_6H_4$, 2-thienyl) is a BEDT-TTF analogue possessing π-bonds with aromatic groups on the outer rings (Figure 1) [26,38-41]. Since BEDT-TTF has two ethylene units at the both ends of the molecule, it has a non-planar structure [42]. π-Extended molecules such as **4** with a vinylene group at the end of the BEDT-TTF unit have more planar structures [41,43]. Further, a tetrathiafulvalene with a fused aromatic heterocycle was synthesized as a π-extended donor molecule [28,40]. The most notable superconductivity was observed with the radical cation salts derived from the electron-donor molecule bis(ethylenedithio)tetrathiafulvalene (BEDT-TTF) as a $(BEDT\text{-}TTF)_2Cu[N(CN)_2]Br$ salt at 12.5 K (resistive onset) [24].

The tetrathiafulvalene (TTF) ring system is one of the most intensively studied redox-active organic molecules. It has two easily accessible oxidized states, TTF^+ and TTF^{2+} with potentials of $E_1^{1/2}$ = +0.34 and $E_2^{1/2}$ = +0.78V, respectively, using Ag/AgCl in acetonitrile, (Figure 2) [5,6,44].

TTF analogues have been synthesized by coupling and without coupling methods [45,46]. Depending on the presence of electron-withdrawing groups on the TTF, they exhibit various oxidation potential ranges [15,26]. Recently, TTF and analogues have received widespread attention involving the development of new materials by using various anions to form different charge transfer salts. The physical and electronic properties of their solid states were investigated [13,25,47-49].

We attempt here to provide a summary of the synthesis of differently functionalized and extensively π-electron delocalized conjugated TTF core dithiin- and thiophene-fused donor molecules, obtained from 1,8-diketone ring closure reactions, and coupling reactions, published by our group.

Review

BVDT-TTF analogues from 1,8-diketones

Bis(vinylenedithio)tetrathiafulvalene (BVDT-TTF) **4** (R = Ph, 4-$CH_3OC_6H_4$, 4-BrC_6H_4, 4-$CH_3C_6H_4$, 4-$O_2NC_6H_4$, 2-thienyl) is a fully unsaturated analogue of BEDT-TTF (ET) **3**. It possesses a vinyl moiety at the peripheries in place of the ethylene group of ET. It can also be considered as a tetrathiafulvalene analogue having fused 1,4-dithiin rings as its peripheries. The synthesis was achieved through the reaction of a 1,8-diketone with Lawesson's reagent (LR) [50] or tetraphosphorus decasulfide (P_4S_{10}) [51] Although, in most cases, formation of 1,4-dithiins is the only result, or the major one, a thiophene formation can also take place [46]. So far, eighteen BVDT-TTF analogues have been synthesized (Figure 3).

In 1996, we reported a convenient method of synthesizing fused 1,4-dithiin and thiophene ring systems, possessing functional groups such as Ph 4-$MeOC_6H_4$ and 4-$O_2NC_6H_4$ (Scheme 1) [46]. The synthesis involved treatment of the diketone **6**, produced through the reaction of the readily available dianion **5** [52] with α-haloketones, with Lawesson's reagent **15** to obtain [1,3-dithiolo[4,5-*b*][1,4]dithiin-2-thione **11**, which is an analogue of half ET, as a major product, and the thiophene **13** as a minor product.

After employing different reaction conditions and an in depth study, we suggested that the reaction mechanism involves interaction of **6** with LR **15** (refluxing toluene) initially leading to

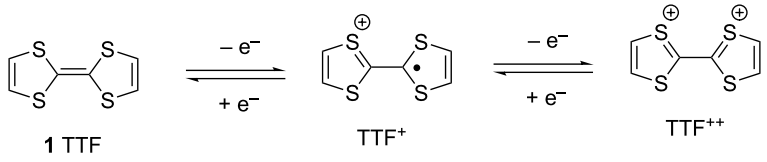

Figure 2: Oxidation states of TTF.

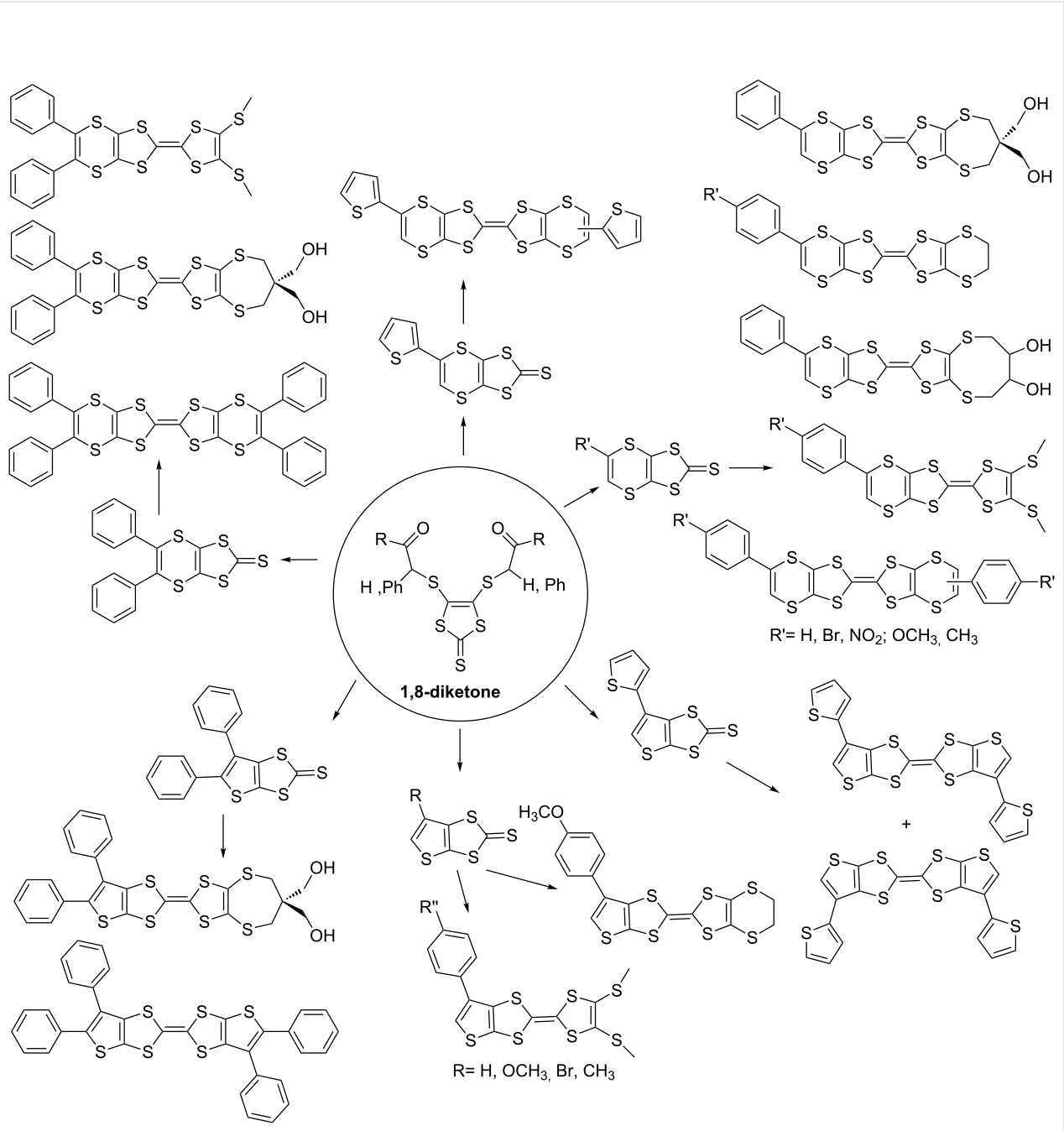

Figure 3: 1,4-Dithiin and thiophene fused TTF analogues from 1,8-diketone.

the formation of enethiols **8**, a tautomer of **7**, then nine-membered ring **9**, rearrangement of which produces **10**. Lastly, the reaction of **10** with fragment **14** of LR would give **11** as a major product (Scheme 1). Rearrangement of the 1,4-dithiin unit of **11** would produce **13** as a minor product through the intermediate **12** by the loss of elemental sulfur. The reaction of a series of 1,8-diketones with LR **15** or P_4S_{10} was further explored in 2003 [53]. With both reactants, 1,4-dithiin **11** was obtained as a major and thiophene **13** as a minor product along with the side products **16**–**19** (Scheme 2).

Depending on the electron-releasing or electron-withdrawing nature of the groups on **6**, the yields for **11** and **13**, with LR varied between 35–52% and from not detected (n.d.) to 18%,

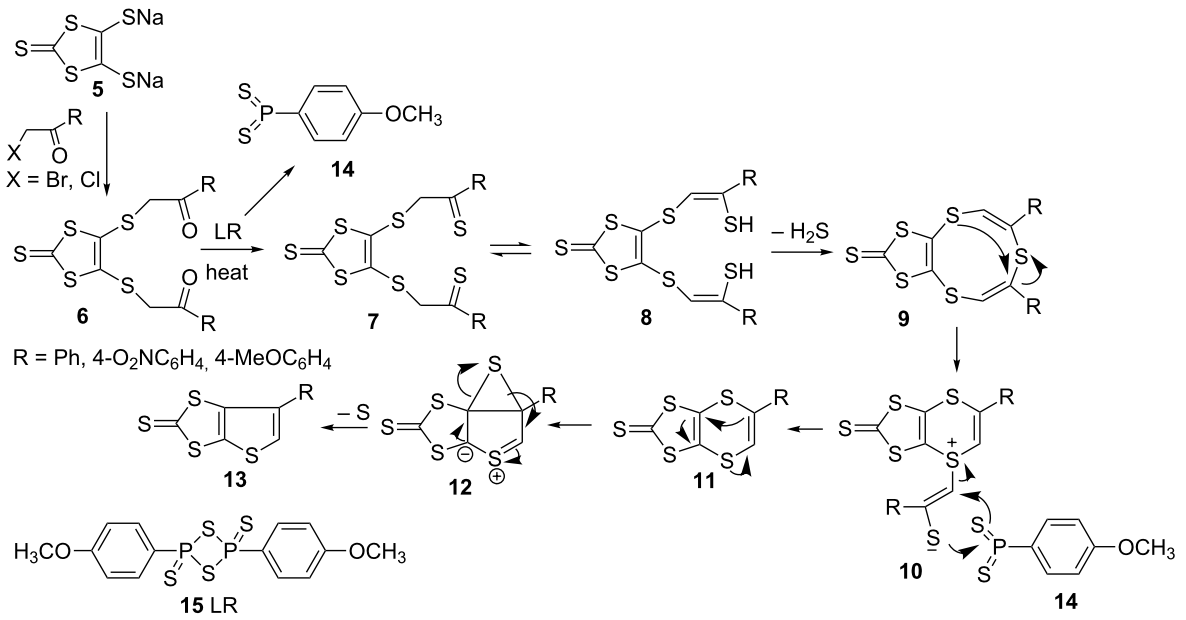

Scheme 1: Reaction mechanism of fused 1,4-dithiin and thiophene ring systems.

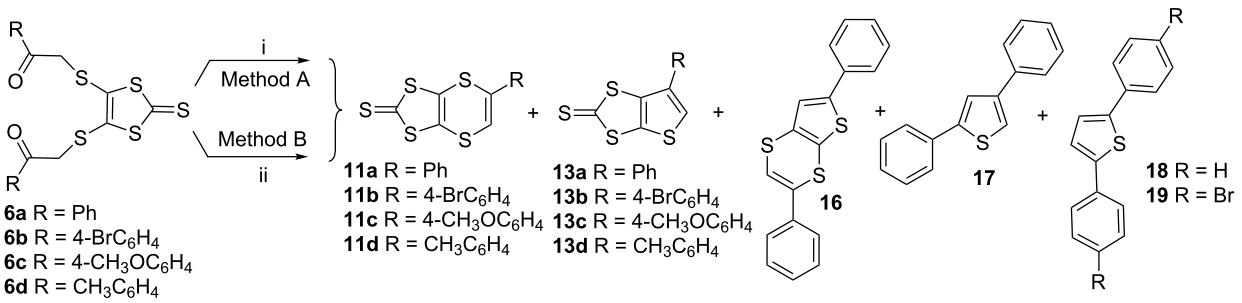

Scheme 2: Reaction conditions (i) LR, toluene, reflux, overnight; (ii) P_4S_{10}, toluene, reflux, 3 h.

respectively, P_4S_{10} gave yields for **11** and **13** from 5 to 49% and n.d. to 27%, respectively. Both of the reagents produced the dithiin as a major product. Compound **13d**, with a thiophene ring, was not obtained with either of the two reagents (Table 1).

A possible reaction mechanism for the formation of **16**–**19** was suggested to involve the intermediate **10** (Scheme 3) [46-53]. A detailed semi-empirical PM3 calculation indicated that the formation of the intermediate **10** is an endothermic process with

Table 1: Ring closure methods and product yields.

Starting material	LR		P_4S_{10}	
	dithiin	thiophene	dithiin	thiophene
6a	**11a** (40%)	**13a** (17%) **16** (15%) **17** (<1%) **18** (9%)	**11a** (49%)	**13a** (n.d.) **17** (8%) **18** (n.d.)
6b	**11b** (35%)	**13b** (18%)	**11b** (40%)	**13b** (2%), **19** (10%)
6c	**11c** (45%)	**13c** (15%)	**11c** (30%)	**13c** (27%)
6d	**11d** (52%)	**13d** (n.d.)	**11d** (5%)	**13d** (n.d.)

n.d.: not detected.

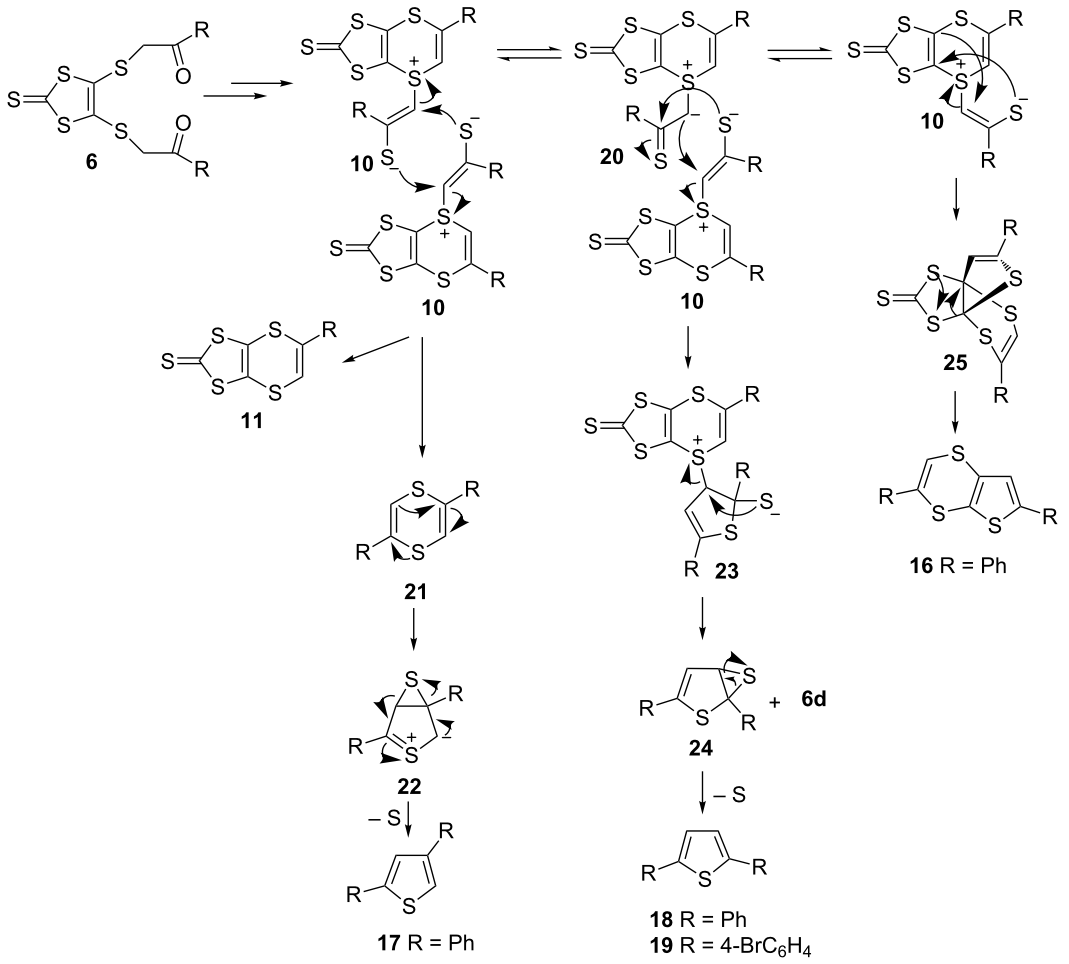

Scheme 3: Proposed mechanism for side products.

ΔH_{rxn}= 29.435 kcal/mol. The reaction of the intermediate **10** with itself could produce the 1,4-dithiin ring **11** and the side product thiophene **17** through the intermediates **21** and **22** by removal of elemental sulfur (Scheme 3). The other side products **18** and **19** were possibly formed from the reaction of **10** with **20**, leading to formation of **23** and **24**, rearrangement of which would then produce **18** and **19**. Moreover, rearrangement of **10** via **25** would result in the formation of **16**. The structures of the side products **16**–**19** can be taken as evidence for the proposed reaction mechanism.

The thione sulfur atoms of **11a**–**d** and **13a**–**c** were converted into their corresponding oxo forms **26a**–**d** and **27a**–**c**, respectively, using mercury acetate (Scheme 4) [46,53,54]. These were then subjected to cross coupling reactions. While the cross couplings of **26a**–**d** with **28** and **31** [53] led to the formation of **29a**–**d** and **32a**–**d**, respectively, along with the self coupling products **4**, **30** and **3**, coupling of **27a**–**c** with **28** gave **33a**–**c** and the self coupling products **34a**–**c** and **30**. The cross coupled product **35** from **27c** and **31** was obtained in a similar manner.

The redox properties of the donor molecules **29a**–**d**, **32a**–**d**, **33a**–**c** and ET **3** were studied by cyclic voltammetry in solution in acetonitrile, containing $NaClO_4$ and dichloromethane, containing tetrabutylammonium tetrafluoroborate ($TBABF_4$) (Table 2 and Table 3). Measurements were performed under a nitrogen atmosphere at room temperature using Pt as working and counter electrodes and Ag/AgCl reference electrode. The oxidation potentials of the coupled products were compared with ET **3**.

The measurements indicated that as the first oxidation potential of ET was higher than the first oxidation potential of **29a**, **29c** and **29d**, the oxidation potential of **29b** was equal to that of

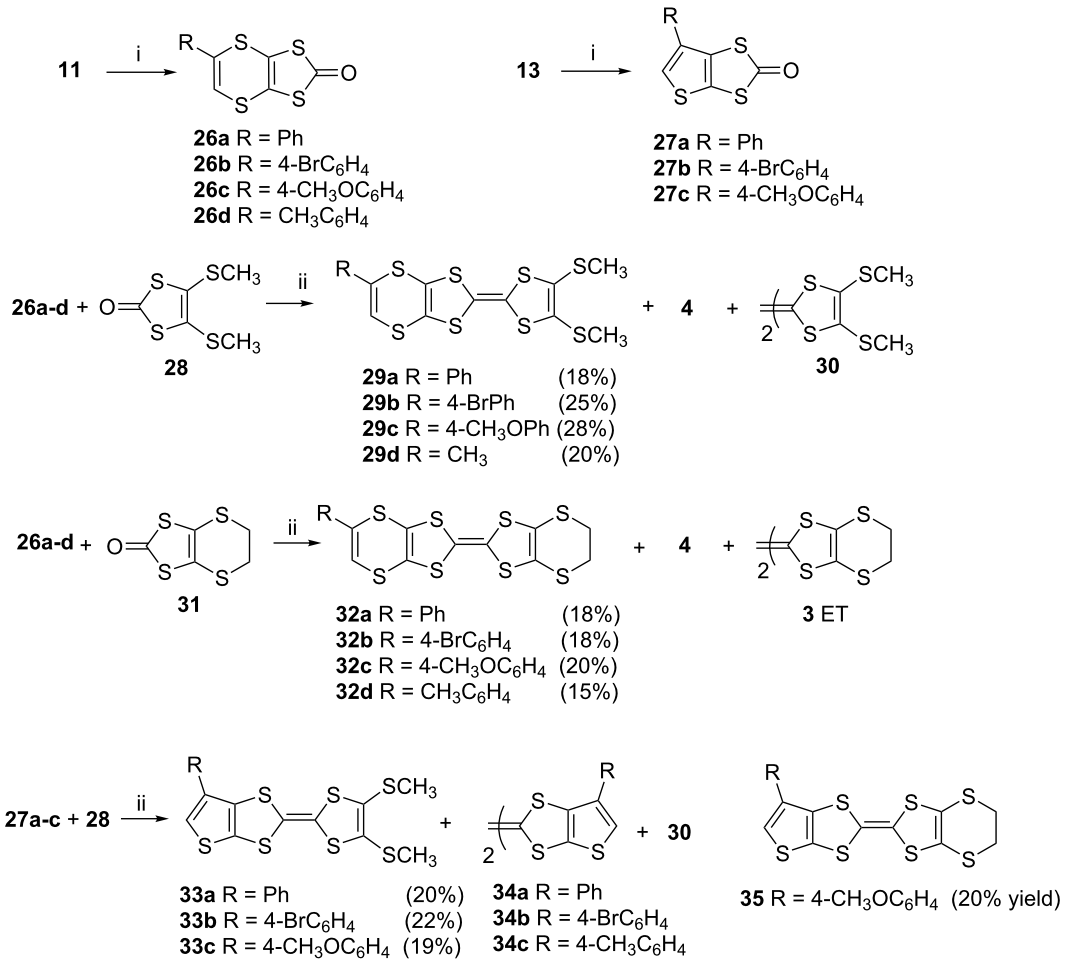

Scheme 4: Reaction conditions (i) $Hg(OAc)_2$, $AcOH/CHCl_3$, rt, 1h; (ii) $(EtO)_3P$, N_2, 3 h, 110 °C.

Table 2: Redox potential of **29** and ET **3**. in 1 mM MeCN solution, $NaClO_4$ (0.1 M) vs Ag/AgCl, 100 mVs^{-1}.

Donor	E^1_{ox} (V)	E^2_{ox} (V)	ΔE_{ox} (V)
29a	0.49	0.63	0.14
29b	0.50	0.63	0.13
29c	0.47	0.72	0.25
29d	0.42	0.66	0.24
3 ET	0.50	0.77	0.27

Table 3: Redox potential of **32a–d** and **33a–c**. and ET **3** in 1 mM CH_2Cl_2 solution, $TBABF_4$ (0.1 M) vs Ag/AgCl, 115 mVs^{-1}.

Donor	E^1_{ox} (V)	E^2_{ox} (V)	ΔE_{ox} (V)
32a	0.66	0.96	0.30
32b	0.60	0.95	0.35
32c	0.68	1.00	0.32
32d	0.64	0.99	0.24
33a	0.59	0.86	0.27
33b	0.51	0.83	0.32
33c	0.62	0.94	0.32
3 ET	0.51	0.85	0.34

ET **3** and the second oxidation potentials of **29a**–**d** were found to be lower than for ET. On the other hand, the first and second oxidation potentials of the donors **33a**–**c** were slightly higher than the oxidation potentials of ET. The oxidation potentials of the donor molecules **32a**–**d** were higher than the ET **3** oxidation potential.

A BEDT-TTF analogue containing phenyl-l,4-dithiin and 2,3-dihydroxybutane-l,4-dithio at the periphery, **43**, was reported as a new highly functionalized donor molecule (Scheme 5) [54].

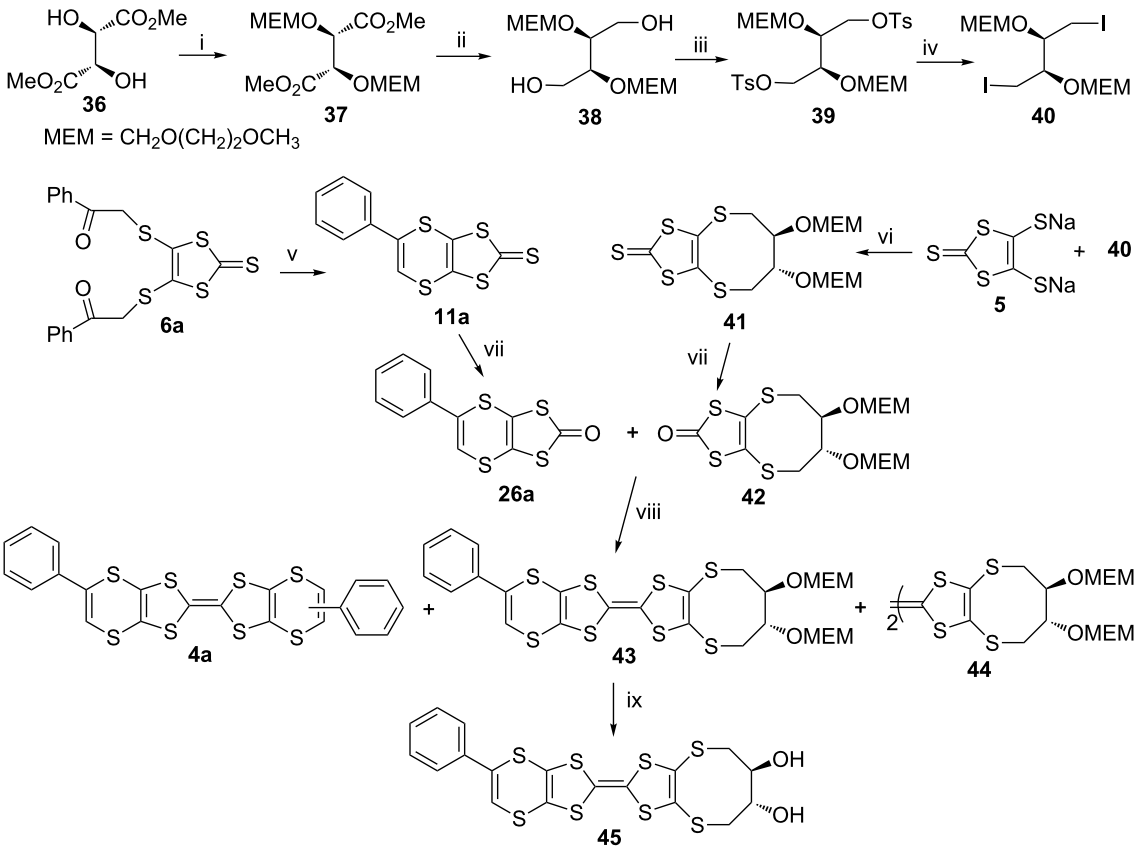

Scheme 5: Reaction conditions (i) iPr_2NEt, MEMCl, THF, rt, 12 h; (ii) $LiAlH_4$, dry ether, rt, 24 h; (iii) tosyl chloride, dry pyridine, 0 °C, 4 h; (iv) KI, dry acetone, N_2, reflux, overnight; (v) dry THF, 75 °C, N_2, 48 h; (vi) P_4S_{10}, toluene, reflux, 3 h; (vii) $Hg(OAc)_2$, AcOH/$CHCl_3$, rt, 2 h; (viii) neat $(EtO)_3P$, N_2, 3 h; (ix) sample in THF at 0 ºC , add 20% HCl, then rt., overnight.

The reaction of diketone **6a**, with LR **15** in refluxing toluene for 3 h gave the dithiin **11a**, which was converted into the oxo form **26a** with mercuric acetate in $CHCl_3$/glacial acetic acid at room temperature in 2 h. Synthesis of **41** was completed in five steps, starting from dimethyl L-tartrate **36**, the hydroxy groups of which were protected by reaction with methoxyethoxymethyl chloride (MEMCl) and then the ester groups of **37** were reduced to alcohols with $LiAlH_4$ to obtain the diol **38**. This was converted into **39** through tosylation of the hydroxy groups with tosyl chloride and then conversion into iodides **40** using potassium iodide. Treatment of **40** with the dianionic salt **5** in dry acetone at room temperature produced **41** [55], which was transformed into the corresponding oxo form **42** by applying the same reaction conditions used to obtain **26a**. Coupling of **26a** with **42** was performed in neat triethyl phosphite at 130 °C for 3 h under a nitrogen atmosphere, which gave a mixture of cross coupled **43** and self coupled products **4a** and **44**. In order to remove the MEM protecting group, **43** was stirred in 20% HCl at room temperature for 2 days, which yielded the ET analogue **45**, having two hydroxy groups.

In 2000, syntheses of 5,6-diphenyl[1,3]dithiolo[4,5-*b*][1,4]dithiin-2-thione **48** and its coupling product **52**, which is a fully unsaturated analogue of BEDT-TTF, were achieved. The 1,8-diketone **47** was easily obtained from the reaction of the dianion **5** (1 equiv) and desyl chloride **46** (2 equiv) in dry ethanol at room temperature for 3 h in 90% yield (Scheme 6) [40].

The ring closure reaction of **47** was performed initially using LR, which produced only the thiophene **50**, similar to the result obtained by another research group [28]. Next, the reaction was conducted with P_4S_{10}, which gave benzylphenyldithiole **49** and the thiophene **50** in 25 and 30% yields. Considering that the reaction could take place through a radical mechanism, it was repeated in the dark using P_4S_{10}. After 3 h of reflux in toluene, the dithiin **48** was successfully obtained in 65% along with a trace of benzylphenyldithiole **49** and the thiophene **50** in 20% yields. The fully unsaturated tetraphenyl analogue **52** of ET was obtained in 90% yield by a coupling reaction of **51**, which was obtained by converting the thione group of **48** to its corres-

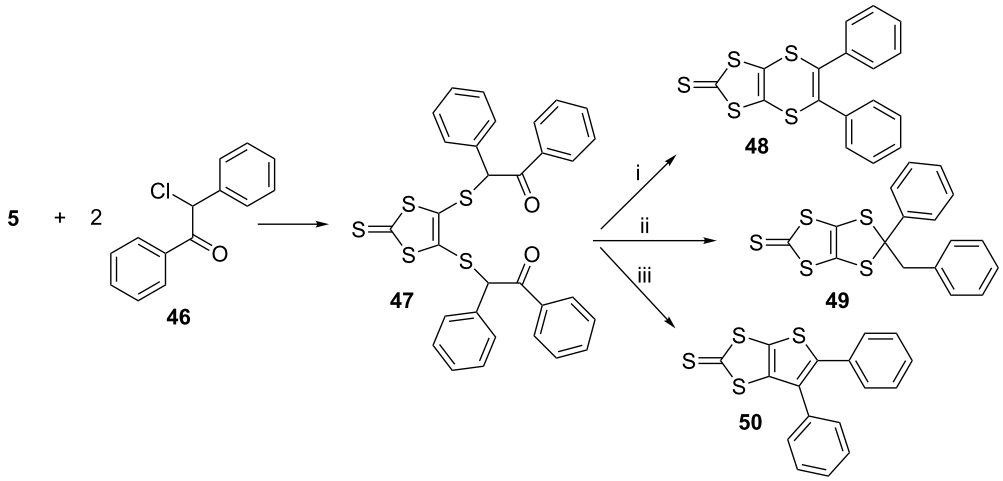

Scheme 6: Reagents and conditions (i) P_4S_{10}, toluene, reflux, dark, 3 h; (ii) P_4S_{10}, toluene, reflux, 3 h; (iii) LR, toluene, reflux, overnight.

ponding oxo form in 85% yield, in hot triethyl phosphite, yielding **52** in 90% yield (Scheme 7).

A charge transfer salt **54** of **52** was prepared with the acceptor 2,3-dichloro-5,6-dicyano-*p*-benzoquinone (DDQ) **53** (1:1) in dichloromethane at room temperature to investigate the optical constant and optical band gap of the complex (Scheme 8) [56]. A solution of the salt was evaporated on a quartz substrate until ≈110 nm thickness of the film was obtained. The film was annealed at 25, 55, 85, 115 and finally at 145 °C for 30 min.

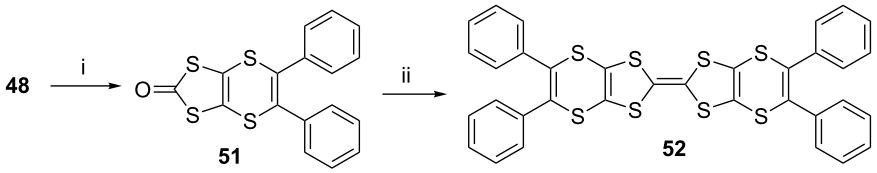

Scheme 7: Reagents and conditions (i) $Hg(OAc)_2$–AcOH, $CHCl_3$, 3 h, rt; (ii) $(EtO)_3P$, 110 °C, N_2, 2 h.

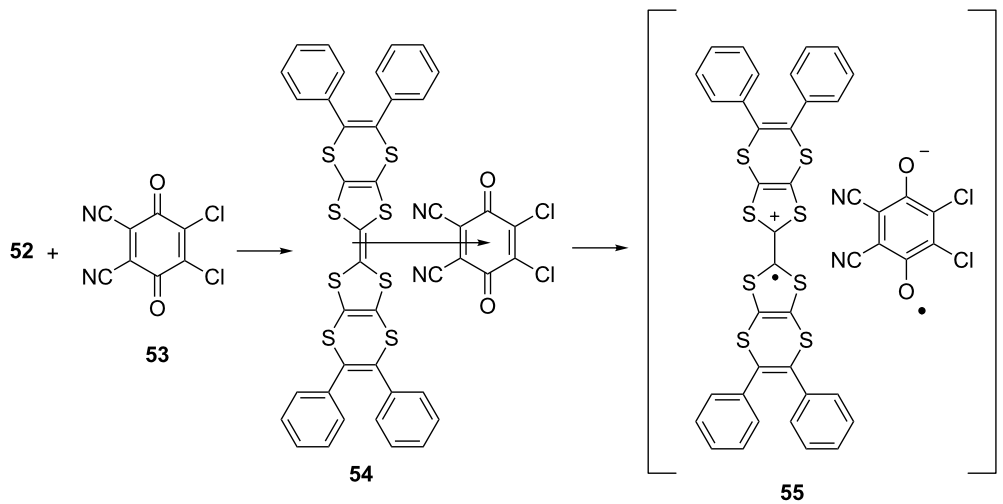

Scheme 8: Charge transfer complex of 5,5',6,6'-tetraphenyl-2,2'-bi([1,3]dithiolo[4,5-*b*][1,4]dithiinylidene) **52** – DDQ **53**.

Electronic transitions of the complex **54**, i.e. n–π* and π–π* transitions, led to the formation of radical ion pairs **55**. The refractive index dispersion and optical constant of the annealed film were examined for each temperature. The absorbance, refractive index, reflectance and transmittance values of the material were found to be between 0.16–0.32, 2.3–2.7, 16–20% and 46–66%, respectively at 400–800 nm wavelength range which clearly indicated that the refractive index, absorbance and reflectance of the complex decreased while transmittance increased with increased annealing temperature.

Our easy synthesis of dithiin-containing compounds led to the production of various BEDT-TTF analogues, comprising monophenyldithiin, diphenyldithiin, diphenylthiophene and diols [40,46,53]. While coupling of **28** with **51** smoothly gave the corresponding ET analogue **56**, its reaction with **57** did not produce any result (Scheme 9) [57]. This could be due to the reaction of the benzylphenyldithiole moiety with triethyl phosphite.

Analogues of ET, having dithiin and thiophene rings along with hydroxy groups were synthesized to provide the possibility of intramolecular hydrogen bonding through the hydroxy groups [57]. The half ET analogue **61** was obtained from the reactions of either the dianion **5** or the zinc-complex **59** with 2-bis(bromomethyl)propane-1,3-diol (**60**, Scheme 10). As the hydroxy groups could lead to side products during the coupling reaction, performed using triethyl phosphite, and the reaction for conversion of the thione group to a keto group with mercury acetate and acetic acid, they were protected by reaction with methoxyethoxymethylchloride ($CH_3OCH_2CH_2OCH_2Cl$, MEMCl) to obtain **62**. The thione group of this compound, was then converted into a keto group to give **63**. Its reaction with **26a–c** in triethyl phosphite led to the formation of cross-coupled product **64a–c**, along with the self coupled one. Following the same procedure, the half ET analogue **65**, possessing a fused diphenylthiophene ring was coupled with **63** to produce **66**, along with self coupled products like **67**. Removal of the MEM groups of both **64** and **66** in dilute HCl/THF mixture resulted in the formation of the target analogues **68a–c** and **69**, having two hydroxy groups. Coupling of the dithiinone **51** with **63** gave **70** and its hydrolysis yielded the ET analogue **71**, possessing diphenyldithiin and two hydroxy groups. Following the same strategy, an ET analogue **72**, having half ET and two hydroxy groups was synthesized to compare the oxidation and reduction potentials of the analogues. The yields of the resultant products are given in Table 4.

Table 4: Yields of the products **64**, **65**, **68–71**.

Product	Yield (%)	Diol	Yield (%)
70	30	**71**	75
65	30	**69**	75
64a	27	**68a**	43
64b	29	**68b**	35
64c	40	**68c**	34

The oxidation and reduction properties of the diphenyl analogues **56**, **69** and **71** and monophenyl analogues **68a–c, 31a** and **29a** were investigated and compared by cyclic voltammetry (CV) (Table 5) with ET **3** and its fully unsaturated tetraphenyl analogue **52**. The CV measurement of the donors was performed in 0.1 M $NaClO_4$/ACN with a scan rate of 100 mVS^{-1} at room temperature, using Pt working and Ag/Ag^+ reference electrodes. The spectroelectrochemical studies were carried out in CH_2Cl_2 containing 0.1 M $TBABF_4$ at room temperature.

The CV studies indicated that while the fully unsaturated **52** and diphenylthiophenedimethylthio **67** had the highest

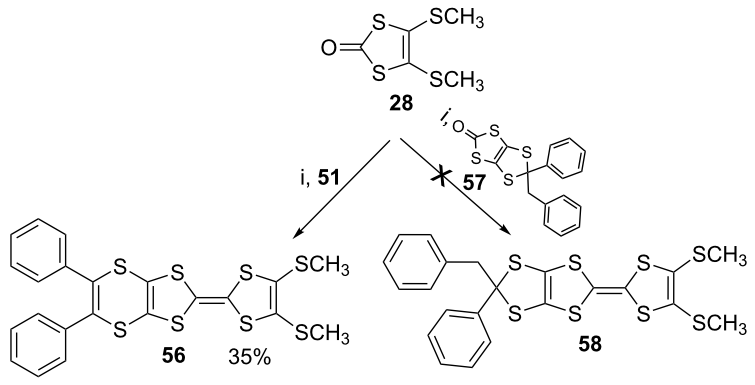

Scheme 9: Reaction conditions (i) $(EtO)_3P$, 110 °C, N_2, 2 h.

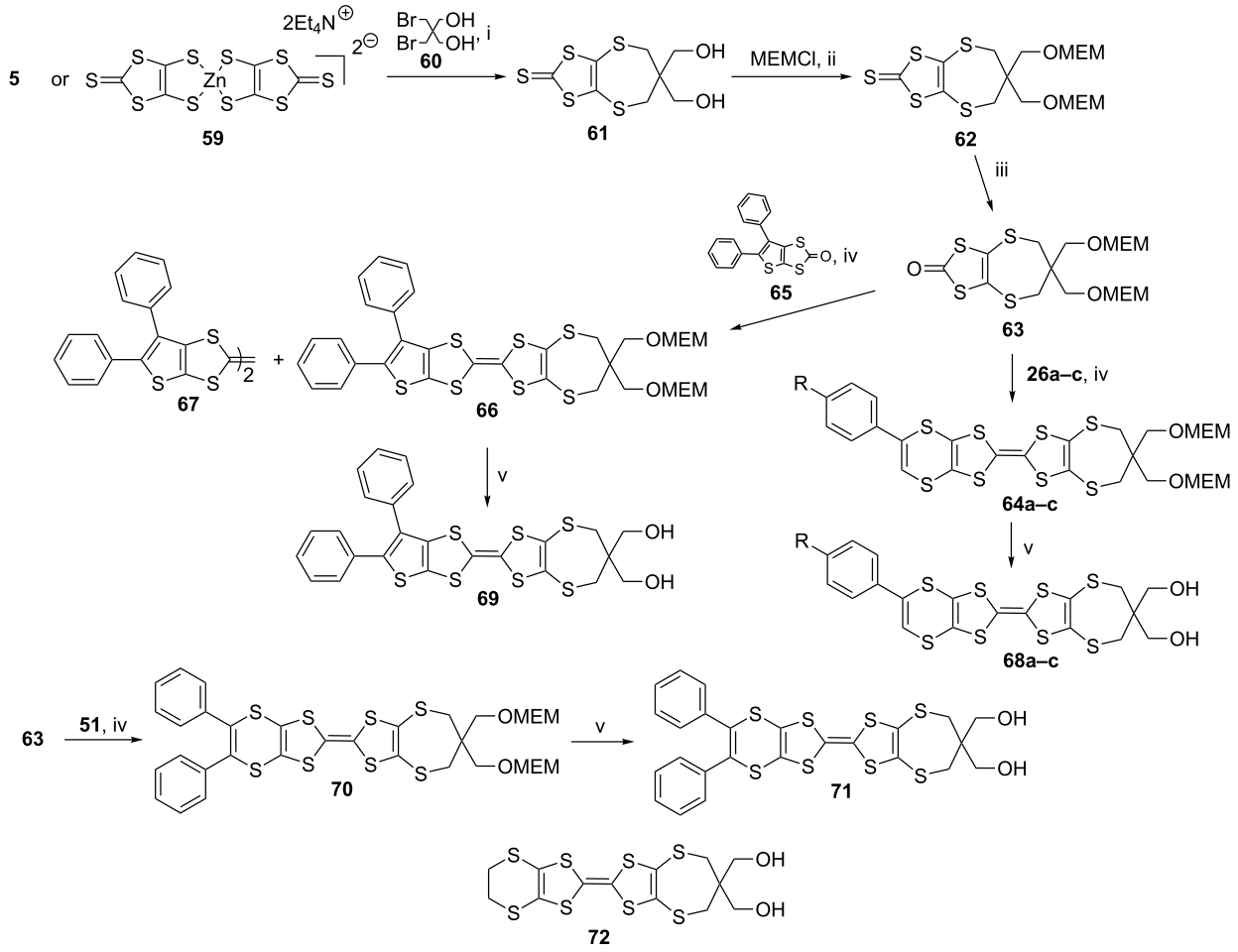

Scheme 10: Reaction conditions (i) EtOH, reflux, overnight; (ii) diisopropylethylamine in CH_2Cl_2, room temperature, overnight; (iii) $(AcO)_2Hg$/AcOH, $CHCl_3$, rt, 3h; iv) $(EtO)_3P$, 110 °C, N_2, 2 h; (v) sample in THF at 0 ºC, add 20% HCl, then rt, overnight.

Table 5: Redox potential of ET **3** and its analogues, ACN solution of 0.1 M $NaClO_4$.

Sample	Oxidation potential (V)		
	E^1_{OX} (V)	E^2_{OX} (V)	ΔE (V)
52	0.72	1.03	0.31
70	0.44	0.70	0.26
66	0.60	0.84	0.24
71	0.41	0.63	0.22
69	0.57	0.80	0.23
56	0.36	0.59	0.23
68a	0.49	0.74	0.25
68b	0.50	0.76	0.26
68c	0.42	0.70	0.28
67	0.72	1.06	0.34
31a	0.49	0.63	0.14
72	0.42	0.70	0.28
29a	0.66	0.96	0.30
3ET	0.46	0.71	0.25

oxidation potentials, diphenyldithiindimethylthio **56** displayed the lowest oxidation potential and combination of dithiin and diol groups led to oxidation potentials comparable with ET **3**.

BEDT-TTF analogues possessing thiophene substituted 1,4-dithiin and thiophene rings were reported in 2013 [58]. Their syntheses began with our standard synthesis of a 1,8-diketone **74** having a thiophene in place of a benzenoid aromatic group (Scheme 11). Reaction of the zinc-complex **59** with four mol equivalents of α-bromoketone **72** gave the diketone **74** in 80% yield, subsequent ring closure of which with P_4S_{10} in acidic and basic conditions produced 1,4-dithiin **75** (75%) and thiophene **76** (57%) rings, respectively. They were then converted into their corresponding oxo forms **77** (65%) and **78** (77%), respectively, with mercury acetate and subjected to the coupling reaction with triethyl phosphite to produce the ET analogues having 1,4-dithiin rings **79** (80%) and thiophene rings **80** and **81** (75%) as inseparable isomers.

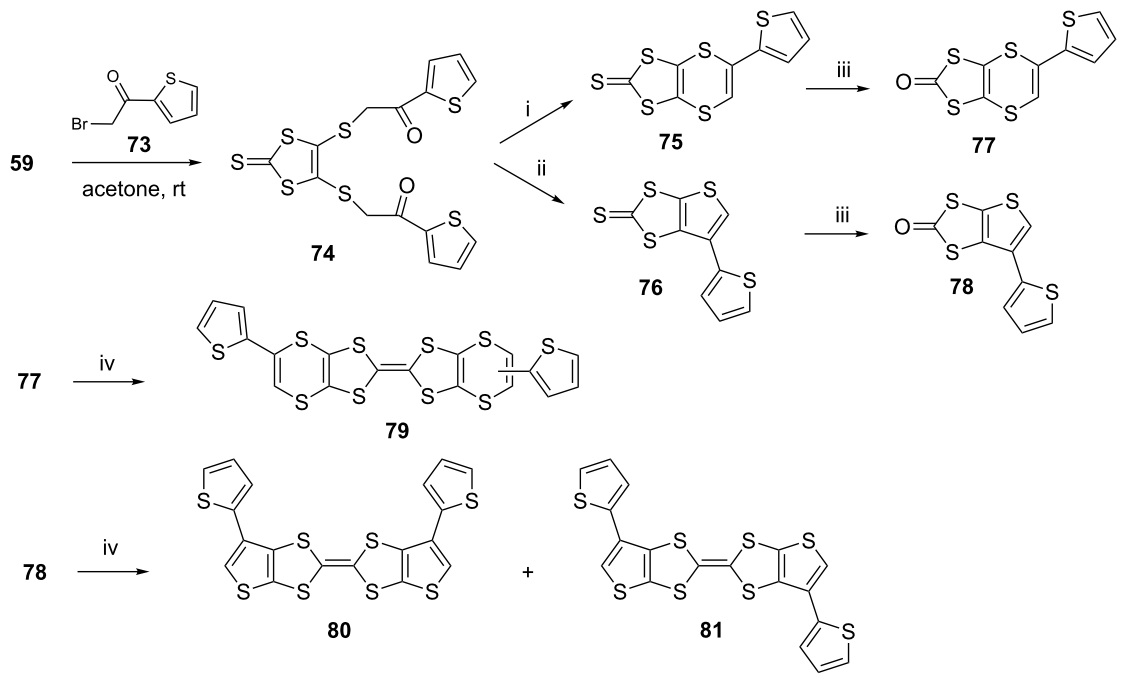

Scheme 11: Reaction and conditions (i) P_4S_{10}, $NaHCO_3$, toluene, reflux, 3 h; (ii) P_4S_{10}, *p*-TSA, toluene, reflux, 3 h; (iii) $(AcO)_2Hg$/AcOH, $CHCl_3$, 3 h, rt; (iv) $(EtO)_3P$, 110 °C, N_2, 2 h.

Unfortunately, all attempts to electropolymerize the analogues failed. Computational studies indicated that the α-carbons of the peripheral thiophenes, where the polymerization was expected to take place, did not exhibit enough spin density.

Conclusion

Bis(ethylenedithio)tetrathiafulvalene (BEDT-TTF, ET) is a unique molecule which has been successfully used as an electronic material that challenges the creativity and inventiveness of chemists in areas such as organic chemistry, materials chemistry, supramolecular chemistry and polymer chemistry. 1,8-Diketones have been demonstrated to be versatile starting materials for the synthesis of various challenging analogues of ET, possessing dithiin and thiophene moieties. This chemistry not only led to the production of the target materials, having interesting electronic properties, but also illustrated challenging synthetic heterocyclic chemistry.

Acknowledgements

We thank Profesor John A. Joule of the University of Manchester for reading the manuscript, and Unsped Global Logistic for financial support.

References

1. Klingsberg, E. *J. Am. Chem. Soc.* **1964,** *86,* 5290–5292. doi:10.1021/ja01077a048
2. Wudl, F.; Smith, G.; Hufnagel, E. *J. Chem. Soc. D* **1970,** 1453–1454. doi:10.1039/C29700001453
3. Wudl, F.; Wobschall, D.; Hufnagel, E. J. *J. Am. Chem. Soc.* **1972,** *94,* 670–672. doi:10.1021/ja00757a079
4. Ferraris, J.; Cowan, D.; Walatka, V. t.; Perlstein, J. *J. Am. Chem. Soc.* **1973,** *95,* 948–949. doi:10.1021/ja00784a066
5. Bryce, M. R. *Chem. Soc. Rev.* **1991,** *20,* 355–390. doi:10.1039/cs9912000355
6. Bryce, M. R. *J. Mater. Chem.* **2000,** *10,* 589–599. doi:10.1039/a908385e
7. Day, P.; Kurmoo, M. *J. Mater. Chem.* **1997,** *7,* 1291–1295. doi:10.1039/a608508c
8. Segura, J. L.; Martin, N. *Angew. Chem., Int. Ed.* **2001,** *40,* 1372–1409. doi:10.1002/1521-3773(20010417)40:8<1372::AID-ANIE1372>3.0.CO;2-I
9. Jerome, D.; Mazaud, A.; Ribault, M.; Bechgaard, K. *J. Phys., Lett.* **1980,** *41,* 95–98. doi:10.1051/jphyslet:0198000410409500
10. Simonsen, K. B.; Svenstrup, N.; Lau, J.; Simonsen, O.; Mørk, P.; Kristensen, G. J.; Becher, J. *Synthesis* **1996,** 407–418. doi:10.1055/s-1996-4216
11. Bryce, M. R. *Adv. Mater.* **1999,** *11,* 11–23. doi:10.1002/(SICI)1521-4095(199901)11:1<11::AID-ADMA11>3.0.CO;2-3
12. Saito, G.; Yoshida, Y. *Bull. Chem. Soc. Jpn.* **2007,** *80,* 1–137. doi:10.1246/bcsj.80.1
13. Caneve, D.; Sallé, M.; Zhang, G.; Zhang, D.; Zhu, D. *Chem. Commun.* **2009,** 2245–2269. doi:10.1039/b818607n
14. Tan, L.; Guo, Y.; Yang, Y.; Zhang, G.; Zhang, D.; Yu, G.; Xu, W.; Liu, Y. *Chem. Sci.* **2012,** *3,* 2530–2541. doi:10.1039/c2sc20303k
15. Akutsu, H.; Yamada, J.-i.; Nakatsuji, S.'i.; Turner, S. S. *Dalton Trans.* **2013,** *42,* 16351–16354. doi:10.1039/c3dt52346b

16. Nielsen, M. B.; Lomholt, C.; Becher, J. *Chem. Soc. Rev.* **2000,** *29,* 153–164. doi:10.1039/a803992e
17. Garín, J.; Orduna, J.; Savirón, M.; Bryce, M. R.; Moore, A. J.; Morisson, V. *Tetrahedron* **1996,** *52,* 11063–11074. doi:10.1016/0040-4020(96)00624-2
18. Imakubo, T.; Okano, Y.; Sawa, H.; Kato, R. *J. Chem. Soc., Chem. Commun.* **1995,** 2493–2494. doi:10.1039/c39950002493
19. Iyoda, M.; Hara, K.; Venkateswara Rao, C. R.; Kuwatani, Y.; Takimiya, K.; Morikami, A.; Aso, Y.; Otsubo, T. *Tetrahedron Lett.* **1999,** *40,* 5729–5730. doi:10.1016/S0040-4039(99)01085-0
20. Suzuki, T.; Yamochi, H.; Srdanov, G.; Hinkelmann, K.; Wudl, F. *J. Am. Chem. Soc.* **1989,** *111,* 3108–3109. doi:10.1021/ja00190a079
21. Kim, Y.-I.; Jeong, C.-K.; Lee, Y.-M.; Choi, S.-N. *Bull. Korean Chem. Soc.* **2002,** *23,* 1754–1758. doi:10.5012/bkcs.2002.23.12.1754
22. Jérome, D. *Science* **1991,** *252,* 1509–1514. doi:10.1126/science.252.5012.1509
23. Williams, J. M.; Schultz, A. J.; Geiser, U.; Carlson, K. D.; Kini, A. M.; Wang, H. H.; Kwok, W.-K.; Whangbo, M.-H.; Schirber, J. E. *Science* **1991,** *252,* 1501–1508. doi:10.1126/science.252.5012.1501
24. Kini, A. M.; Geiser, U.; Wang, H. H.; Carlson, K. D.; Williams, J. M.; Kwok, W.; Vandervoort, K. G.; Thompson, J. E.; Stupka, D. L. *Inorg. Chem.* **1990,** *29,* 2555–2557. doi:10.1021/ic00339a004
25. Abbaz, T.; Bendjeddou, A.; Gouasmia, A.; Villemin, D.; Shirahata, T. *Int. J. Mol. Sci.* **2014,** *15,* 4550–4564. doi:10.3390/ijms15034550
26. Bendikov, M.; Wudl, F.; Perepichka, D. F. *Chem. Rev.* **2004,** *104,* 4891–4945. doi:10.1021/cr030666m
27. Nogami, T.; Inoue, K.; Nakamura, T.; Iwasaka, S.-I.; Nakano, H.; Mikawa, H. *Synth. Met.* **1987,** *19,* 539–544. doi:10.1016/0379-6779(87)90410-3
28. Lee, H.-J.; Kim, Y.-Y.; Noh, D.-Y. *Bull. Korean Chem. Soc.* **1998,** *19,* 1011–1013.
29. Diaz, M. C.; Illescas, B. M.; Martin, N.; Viruela, R.; Viruela, P. M.; Orti, E.; Brede, O.; Zilbermann, I.; Guldi, D. M. *Chem. – Eur. J.* **2004,** *10,* 2067–2077. doi:10.1002/chem.200305555
30. Frère, P.; Skabara, P. J. *Chem. Soc. Rev.* **2005,** *34,* 69–98. doi:10.1039/b316392j
31. Santos, J.; Illescas, B. M.; Martín, N.; Adrio, J.; Carretero, J. C.; Viruela, R.; Ortí, E.; Spänig, F.; Guldi, D. M. *Chem. – Eur. J.* **2011,** *17,* 2957–2964. doi:10.1002/chem.201002674
32. Gao, X.; Wu, W.; Liu, Y.; Qiu, W.; Sun, X.; Yu, G.; Zhu, D. *Chem. Commun.* **2006,** 2750–2752. doi:10.1039/b603632e
33. Yamochi, H.; Saito, G. *Synth. Met.* **1997,** *85,* 1467–1468. doi:10.1016/S0379-6779(96)04437-2
34. Rovira, C.; Veciana, J.; Santalo, N.; Tarres, J.; Cirujeda, J.; Molins, E.; Llorca, J.; Espinosa, E. *J. Org. Chem.* **1994,** *59,* 3307–3313. doi:10.1021/jo00091a017
35. Heuzé, K.; Fourmigué, M.; Batail, P.; Canadell, E.; AubanSenzier, P. *Chem. – Eur. J.* **1999,** *5,* 2971–2976. doi:10.1002/(SICI)1521-3765(19991001)5:10<2971::AID-CHEM2971>3.0.CO;2-S
36. Yamochi, H.; Komatsu, T.; Matsukawa, N.; Saito, G.; Mori, T.; Kusunoki, M.; Sakaguchi, K. *J. Am. Chem. Soc.* **1993,** *115,* 11319–11327. doi:10.1021/ja00077a034
37. Bryce, M. R. *J. Mater. Chem.* **1995,** *5,* 1481–1496. doi:10.1039/jm9950501481
38. Ikegawa, S.; Miyawaki, K.; Nogami, T.; Shirota, Y. *Bull. Chem. Soc. Jpn.* **1993,** *66,* 2770–2772. doi:10.1246/bcsj.66.2770
39. Wallis, J. D.; Griffiths, J.-P. *J. Mater. Chem.* **2005,** *15,* 347–365. doi:10.1039/b412561b
40. Ertas, E.; Ozturk, T. *Chem. Commun.* **2000,** 2039–2040. doi:10.1039/b003714l
41. Nakamura, T.; Iwasaka, S.-i.; Nakano, H.; Inoue, K.; Nogami, T.; Mikawa, H. *Bull. Chem. Soc. Jpn.* **1987,** *60,* 365–368. doi:10.1246/bcsj.60.365
42. Kobayashi, H.; Kobayashi, A.; Sasaki, Y.; Saito, G.; Inokuchi, H. *Bull. Chem. Soc. Jpn.* **1986,** *59,* 301–302. doi:10.1246/bcsj.59.301
43. Jérome, D. *Chem. Rev.* **2004,** *104,* 5565–5592. doi:10.1021/cr030652g
44. Segura, J. L.; Martín, N. *Angew. Chem., Int. Ed.* **2001,** *40,* 1372–1409. doi:10.1002/1521-3773(20010417)40:8<1372::AID-ANIE1372>3.0.CO;2-I
45. Yamada, J.-i.; Amano, Y.; Takasaki, S.; Nakanishi, R.; Matsumoto, K.; Satoki, S.; Anzai, H. *J. Am. Chem. Soc.* **1995,** *117,* 1149–1150. doi:10.1021/ja00108a040
46. Ozturk, T. *Tetrahedron Lett.* **1996,** *37,* 2821–2824. doi:10.1016/0040-4039(96)00396-6
47. Lebedev, V.; Laukhina, E.; Laukhin, V.; Rovira, C.; Veciana, J. *Eur. J. Inorg. Chem.* **2014,** *24,* 3927–3932. doi:10.1002/ejic.201402276
48. Pop, F.; Allain, M.; Auban-Senzier, P.; MartínezLillo, J.; Lloret, F.; Julve, M.; Canadell, E.; Avarvari, N. *Eur. J. Inorg. Chem.* **2014,** *24,* 3855–3862. doi:10.1002/ejic.201400125
49. Zhang, B.; Zhang, Y.; Gao, Z.; Chang, G.; Su, S.; Wang, D.; Guo, Y.; Zhu, D. *Eur. J. Inorg. Chem.* **2014,** *24,* 4028–4032. doi:10.1002/ejic.201402112
50. Ozturk, T.; Ertas, E.; Mert, O. *Chem. Rev.* **2007,** *107,* 5210–5278. doi:10.1021/cr040650b
51. Ozturk, T.; Ertas, E.; Mert, O. *Chem. Rev.* **2010,** *110,* 3419–3478. doi:10.1021/cr900243d
52. Svenstrup, N.; Becher, J. *Synthesis* **1995,** 215–235. doi:10.1055/s-1995-3910
53. Turksoy, F.; Wallis, J. D.; Tunca, U.; Ozturk, T. *Tetrahedron* **2003,** *59,* 8107–8116. doi:10.1016/j.tet.2003.08.042
54. Ozturk, T.; Turksoy, F.; Ertas, E. *Phosphorus, Sulfur Silicon Relat. Elem.* **1999,** *153,* 417–418. doi:10.1080/10426509908546499
55. Horley, G. A.; Ozturk, T.; Turksoy, F.; Wallis, J. D. *J. Chem. Soc., Perkin Trans. 1* **1998,** 3225–3232. doi:10.1039/a804779k
56. Atalay, Y.; Başoğlu, A.; Avcı, D.; Arslan, M.; Ozturk, T.; Ertas, E. *Physica B* **2008,** *403,* 1983–1989. doi:10.1016/j.physb.2007.11.002
57. Ertas, E.; Betul Kaynak, F.; Ozbey, S.; Osken, I.; Ozturk, T. *Tetrahedron* **2008,** *64,* 10581–10589. doi:10.1016/j.tet.2008.08.085
58. Ertas, E.; Bildirir, H.; Sahin, O.; Oksen, I. *Phosphorus, Sulfur Silicon Relat. Elem.* **2013,** *188,* 1835–1844. doi:10.1080/10426507.2013.788005

License and Terms

BEILSTEIN JOURNAL OF ORGANIC CHEMISTRY

TTFs nonsymmetrically fused with alkylthiophenic moieties

Rafaela A. L. Silva, Bruno J. C. Vieira, Marta M. Andrade, Isabel C. Santos, Sandra Rabaça, Dulce Belo* and Manuel Almeida*

Full Research Paper

Open Access

Address:
Centro de Ciências e Tecnologias Nucleares, Campus Tecnológico e Nuclear, Instituto Superior Técnico, Universidade de Lisboa, Estrada Nacional 10, ao km 139,7, 2695-066 Bobadela LRS, Portugal

Email:
Dulce Belo* - dbelo@ctn.ist.utl.pt;
Manuel Almeida* - malmeida@ctn.ist.utl.pt

* Corresponding author

Keywords:
cyclic voltammetry; single-crystal X-ray diffraction; supramolecular chemistry; tetrathiafulvalene (TTF); thiophene

Beilstein J. Org. Chem. **2015,** *11,* 628–637.
doi:10.3762/bjoc.11.71

Received: 27 February 2015
Accepted: 15 April 2015
Published: 05 May 2015

This article is part of the Thematic Series "Tetrathiafulvalene chemistry".

Guest Editor: P. J. Skabara

Abstract

Two new dithiolene ligand precursors, containing fused TTF and alkyl thiophenic moieties 3,3'-{[2-(5-(*tert*-butyl)thieno[2,3-*d*][1,3]dithiol-2-ylidene)-1,3-dithiole-4,5-diyl]bis[sulfanediyl]}dipropanenitrile (α-tbtdt, **1**), and 3,3'-{[2-(5-methylthieno[2,3-*d*][1,3]dithiol-2-ylidene)-1,3-dithiole-4,5-diyl]bis[sulfanediyl]}dipropanenitrile (α-mtdt, **2**), were synthesized and characterized. The electrochemical properties of these electronic donors were studied by cyclic voltammetry (CV) in dichloromethane. Both compounds show two quasi-reversible oxidation processes, versus Ag/AgCl, typical of TTF donors at $E^1_{1/2}$ = 279 V and $E^2_{1/2}$ = 680 V for **1** and $E^1_{1/2}$ = 304 V and $E^2_{1/2}$ = 716 V in the case of **2**. The single-crystal X-ray structure of **1** and of a charge transfer salt of **2**, (α-mtdt)[Au(mnt)$_2$] (**3**), are reported.

Introduction

Since the discovery of the first organic metals and superconductors the field of electronic molecular materials has been largely dominated by derivatives of the organic donor tetrathiafulvalene (TTF) [1]. More than one thousand TTF derivatives have been reported in the last 40 years and many have been at the basis of several conducting, superconducting and other important electronic materials [2-6]. Bisdithiolene–transition metal complexes with square planar structures can be seen as inorganic TTF analogues, in which a transition metal replaces the central double bond. They have similar frontier orbitals to TTF and have been also at the basis of several electronic materials [7]. An additional connection between the TTF derivatives and the bisdithiolene–transition metal complexes was recently provided by complexes with dithiolene ligands incorporating TTF units, which have been at the basis of several highly conducting materials based on a single neutral molecular species [8].

Among the highly extended ligands with TTF moieties, those that also contain thiophenic units have led to a family of complexes with interesting transport and magnetic properties [9,10]. A remarkable example is the neutral complex [Ni(dtdt)$_2$]

(dtdt = 3-{5-[(2-cyanoethyl)thio]-2-(5,6-dihydrothieno[2,3-*d*][1,3]dithiol-2-ylidene-1,3-dithiol-4-yl)thio}propanenitrile), which presents transport properties typical of a metallic system, even when measured in a polycrystalline sample, with an electrical conductivity at room temperature of 200 S/cm. These complexes have been prepared from cyanoethyl-substituted TTF-thiophenedithiolates [9,11]. One of the limitations in the study of these complexes and their possible applications is their low solubility mainly in the neutral state. This limitation can be, in principle, overcome by appropriated functionalization of the ligands as already explored for less extended complexes [12].

Here we report synthesis and characterization of two new sulfur-rich TTF type donors annulated to alkylthiophene rings, 3,3'-{[2-(5-(*tert*-butyl)thieno[2,3-*d*][1,3]dithiol-2-ylidene)-1,3-dithiole-4,5-diyl]bis[sulfanediyl]}dipropanenitrile (α-tbtdt, **1**), and 3,3'-{[2-(5-methylthieno[2,3-*d*][1,3]dithiol-2-ylidene)-1,3-dithiole-4,5-diyl]bis[sulfanediyl]}dipropanenitrile (α-mtdt, **2**) (Scheme 1). These new TTF-type donors can also be converted to transition metal complexes based on extended thiophene/TTF-fused dithiolene ligands. They were obtained by cross-coupling reactions between alkylated thio and oxo compounds. The incorporation of these alkyl groups in the thiophenic ring is expected to increase the solubility of these TTFs and analogous transition metals complexes, enabling their processing from solutions.

Results and Discussion

Synthesis

The TTF donors fused non-symetrically with substituted thiophene moieties **1** and **2** were obtained by the cross coupling, in the presence of trimethyl phosphite, between compounds **I** and **II** and between compounds **III** and **IV**, respectively, following a general procedure for non-symmetrically substituted TTFs [13] as first described by Underhill and co-workers [14] (Scheme 2). 5-(*tert*-Butyl)thieno[2,3-*d*][1,3]dithiol-2-one (**I**)

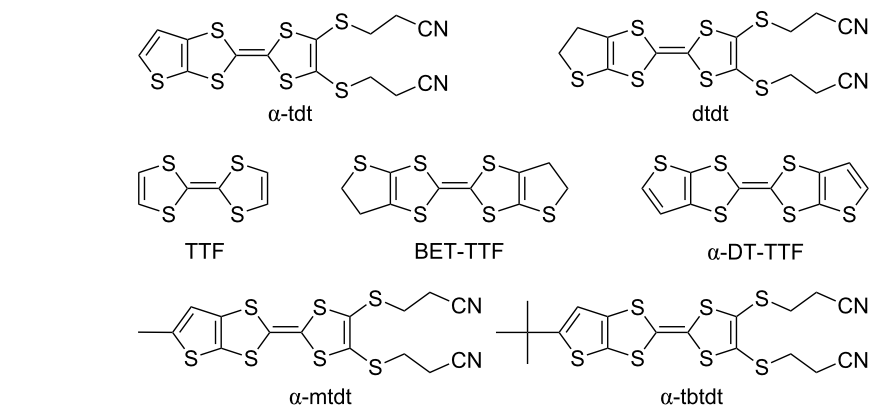

Scheme 1: Molecular diagrams of α-tbtdt (**1**) and α-mtdt (**2**), and related TTF-type donors.

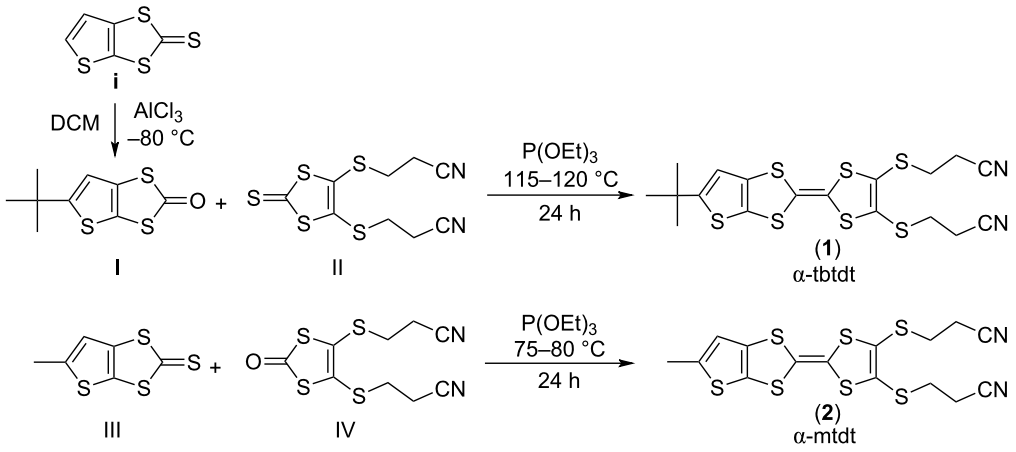

Scheme 2: Synthetic route for compounds **1** and **2**.

was prepared by a low temperature Friedel–Crafts alkylation of 5,6-thieno[2,3-*d*]-1,3-dithiol-2-one (**i**), a new procedure with a better global yield than the one reported previously [15]. 4,5-Bis(2-cyanoethylthio)-1,3-dithiole-2-thione (**II**), was obtained as described before [16] from a bis(tetraethylammonium)bis(2-thioxo-1,3-dithiole-4,5-dithiolate)zincate complex [17], by nucleophilic substitution [14]. Compound **II** was converted in 4,5-bis(2-cyanoethylthio)-1,3-dithiol-2-one (**IV**), using mercuric acetate and acetic acid in chloroform. 5-methylthieno[2,3-*d*][1,3]dithiole-2-thione (**III**) was obtained through a multi-step reaction as previously reported [16].

The preparations of compounds **1** and **2** through the coupling reactions depicted in Scheme 2 also resulted in several byproducts, mainly from homo-coupling reactions. Reaction time, temperature, and amount of solvent were crucial factors for the final yields and for product purity. By optimizing these reaction parameters an acceptable yield of 28% for **1** and a very good yield of 63% for **2** could be obtained after purification through column chromatography, eluting with dichloromethane. The new TTF-type donors are soluble in commonly used organic solvents, such as CH_2Cl_2, $CHCl_3$, acetonitrile and *n*-hexane.

Single crystals suitable for X-ray measurements, could be isolated by slow evaporation of chloroform and *n*-hexane solutions, for **1** and **I**, respectively. Compound **2** crystallizes, from *n*-hexane/CH_2Cl_2 (3:1), in very thin fibres too small for X-ray diffraction. However, thanks to its reasonable solubility in dichloromethane, a charge transfer salt of **2**, (α-mtdt)[Au(mnt)$_2$] (**3**), (mnt = maleonitriledithiolate) could be obtained by electrocrystallization using standard conditions.

Redox properties

The redox properties of the donors **1** and **2** in solution were studied by cyclic voltammetry and the results are collected in Table 1 along with the closely related compounds (DT-TTF = dithiophene-tetrathiafulvalene, BET-TTF = bis(ethylenethio)-tetrathiafulvalene, α-DT-TTF = alpha-dithiophene-tetrathiafulvalene, dtdt = 3-{5-[(2-cyanoethyl)thio]-2-(5,6-dihydrothieno[2,3-*d*][1,3]dithiol-2-ylidene-1,3-dithiol-4-yl)thio}propanenitrile, α-tdt = 3-({5-[(2-cyanoethyl)thio]-2-thieno[2,3-*d*][1,3]dithiol-2-ylidene-1,3-dithiol-4-yl)thio}propanenitrile). Compounds **I** and **II** undergo two separate quasi-reversible one-electron oxidation processes typical of TTF-based donors (Figure 1). Cyclic voltammetry of α-tbtdt in dichloromethane shows a pair of processes at 0.680 V and 0.279 V, vs $Ag/AgNO_3$, which are ascribed to the couples $[\alpha\text{-tbtdt}]^+/[\alpha\text{-tbtdt}]^{2+}$ and $[\alpha\text{-tbtdt}]^0/[\alpha\text{-tbtdt}]^+$, respectively. For α-mtdt, similar quasi-reversible waves are observed at 0.304 V and 0.716 V ascribed to the $[\alpha\text{-mtdt}]^0/[\alpha\text{-mtdt}]^+$ and $[\alpha\text{-mtdt}]^+/[\alpha\text{-mtdt}]^{2+}$ couples, respectively. These electrochemical studies show that α-tbtdt and α-mtdt are easier to oxidise than the related unsubstituted extended TTFs, with higher electron donor ability compared to related TTF-type donors with the exception of BET-TTF.

Table 1: Electrochemical data (oxidation potentials *E* and half wave potentials $E_{1/2}$ for quasi reversible processes), vs $Ag/AgNO_3$ in DCM, of TTF derivatives **1** and **2** as well as of the related donors.

donor	$E_{1,\ D^0/D^+}$ (mV)	$E_{2,\ D^+/D^{2+}}$ (mV)
BET-TTF [18]	215	650
α-DT-TTF [18]	320	730
DT-TTF [18]	542	1015
donor	$E^1_{1/2,\ D^0/D^+}$ (mV)	$E^2_{1/2,\ D^+/D^{2+}}$ (mV)
TTF [19]	370[a]	750[a]
dtdt [11]	639[a]	997[a]
α-tdt [11]	612[a]	906[a]
α-tbtdt (**1**)	279	680
α-mtdt (**2**)	304	716

[a]Data collected in acetonitrile.

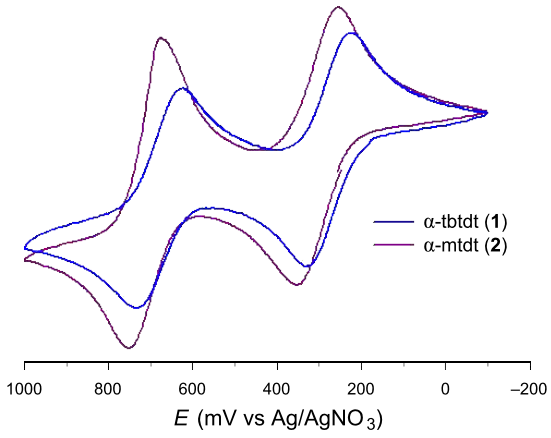

Figure 1: Cyclic voltammogram of α-tbtdt (**1**) and α-mtdt (**2**) (10^{-3} M) in dichloromethane versus $Ag/AgNO_3$, with *n*-Bu_4NPF_6 (10^{-1} M) as supporting electrolyte. Scan rate *v* = 100 mV/s at room temperature.

Crystal structures

Ketone I

Compound **I** crystallises in the orthorhombic system, space group $P2_12_12_1$. The unit cell contains one independent molecule. The terminal sulfur atom presents an orientation disorder as denoted by two nearly identical occupation factors of 49% and 51% for S3 and S3A, respectively (Figure 2). This is most likely the result of orientation disorder of the molecule in the most stable trans configuration, rather than a cis–trans disorder.

The bond lengths are within the expected range for thiophenic dithiol ketones [12,20].

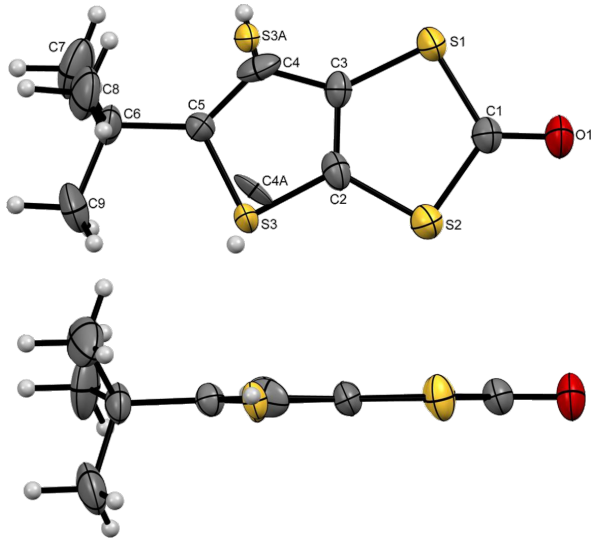

Figure 2: ORTEP view and atomic numbering scheme of **I** with thermal ellipsoids at 50% probability level.

The crystal structure is composed of pairs of side-by-side chains of ketone **1** running parallel to *b*. Within these bi-chains, the molecules are connected by short S···S and S···O interactions with the *tert*-butyl groups pointing outside, in a herringbone fashion (Figure 3b). Molecules in different chains make an angle of circa 39° (Figure 3a). There are no close contacts between bi-chains (Figure 4).

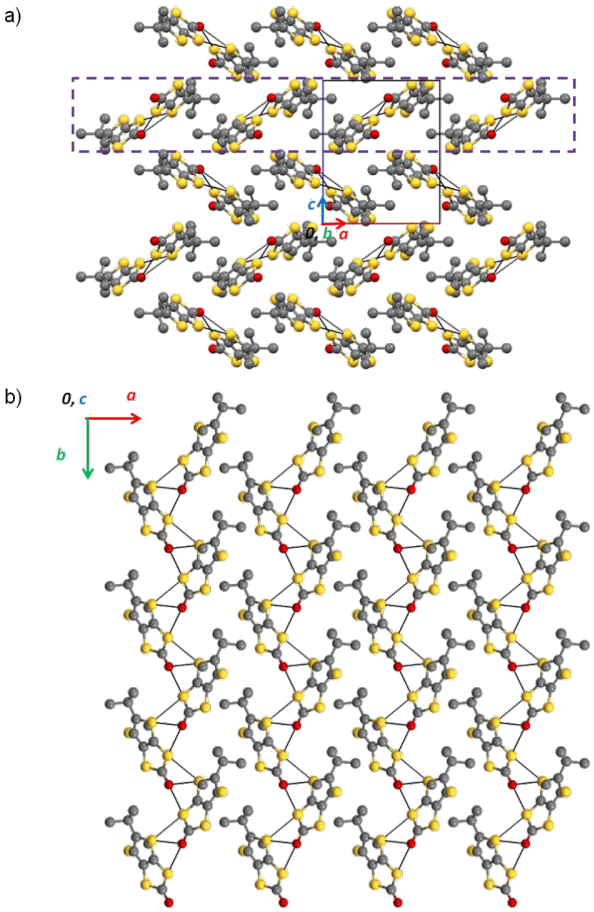

Figure 4: Crystal structure of **I** a) view along the *b* axis, b) Partial view of one layer of bi-chains in the *a*,*b* plane corresponding to the dashed line in a).

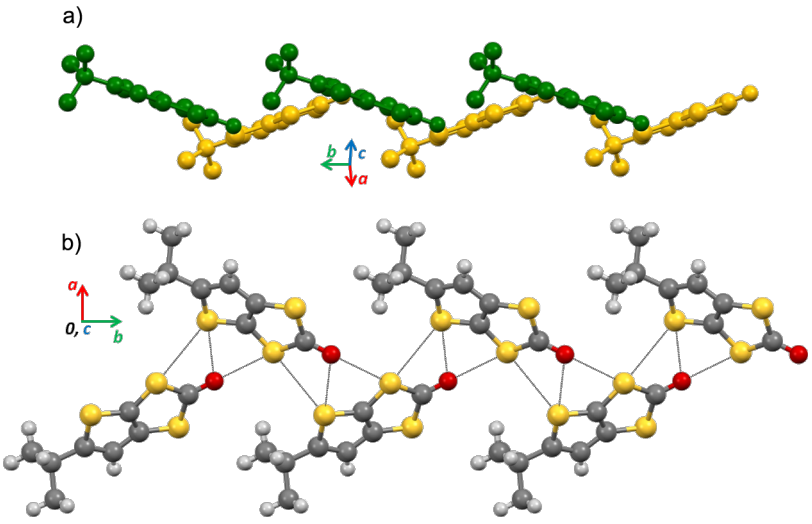

Figure 3: Molecular herringbone bi-chains in the crystal structure of **I**: a) view along the molecular planes and perpendicularly to the chain axis *b*, with molecules in different chains colored differently and b) view along *c*. The short contacts are represented as black dotted lines.

α-tbtdt (**1**)

Compound **1** crystallises in the triclinic system, space group *P*−1. The unit cell contains two independent neutral α-tbtdt molecules that present a slightly boat type distortion of the TTF core. The cyanoethyl groups point in opposite directions of the molecules mean plane (Figure 5). The terminal thiophenic sulfur atoms present, in both molecules, an orientation disorder with occupation factors of 77 and 23% for the pair S8/S8A and 71 and 29% for the pair S1/S1A. The bond lengths of the molecule are within the expected range of values for neutral TTF derivatives [11].

The crystal structure is composed of layers of side-by-side chains of neutral α-tbtdt molecules. Within the chain the molecules are arranged head-to-tail, in a fashion that the cyanoethyl groups point outside the chain and the mean plane of neighbouring molecules is rotated by about 62°. The molecules are connected by several short S···S contacts. Besides these contacts the molecules interact upwards and downwards with other molecules in the same layers, and also with the molecules in the neighbouring layers through short S···S interactions and N···H–C and S···H–C hydrogen bonds (Figure 6).

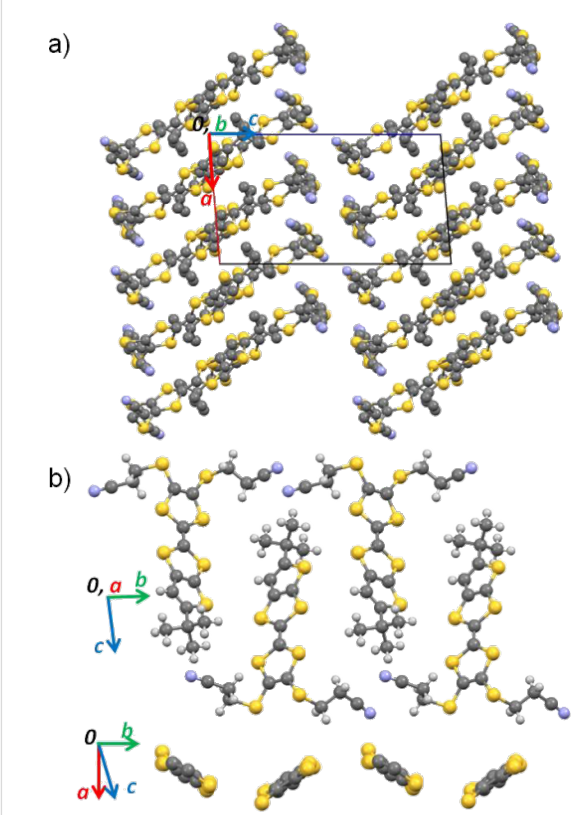

Figure 6: Crystal structure of **1** a) view along the *b* axis; b) Partial view of one chain in the *b*,*c* plane (top) and of the same chain showing the tilt between the molecules along the chain direction (bottom – the cyanoethyl and *tert*-butyl groups were omitted for clarity).

(α-mtdt)[Au(mnt)$_2$] (**3**)

Compound **3** crystallises in the triclinic system, space group *P*−1. The unit cell is composed by one anion $[Au(mnt)_2]^-$ and one fully oxidised donor $[\alpha\text{-mtdt}]^+$. The donor presents orientation disorder as denoted by the sulfur atom position of the

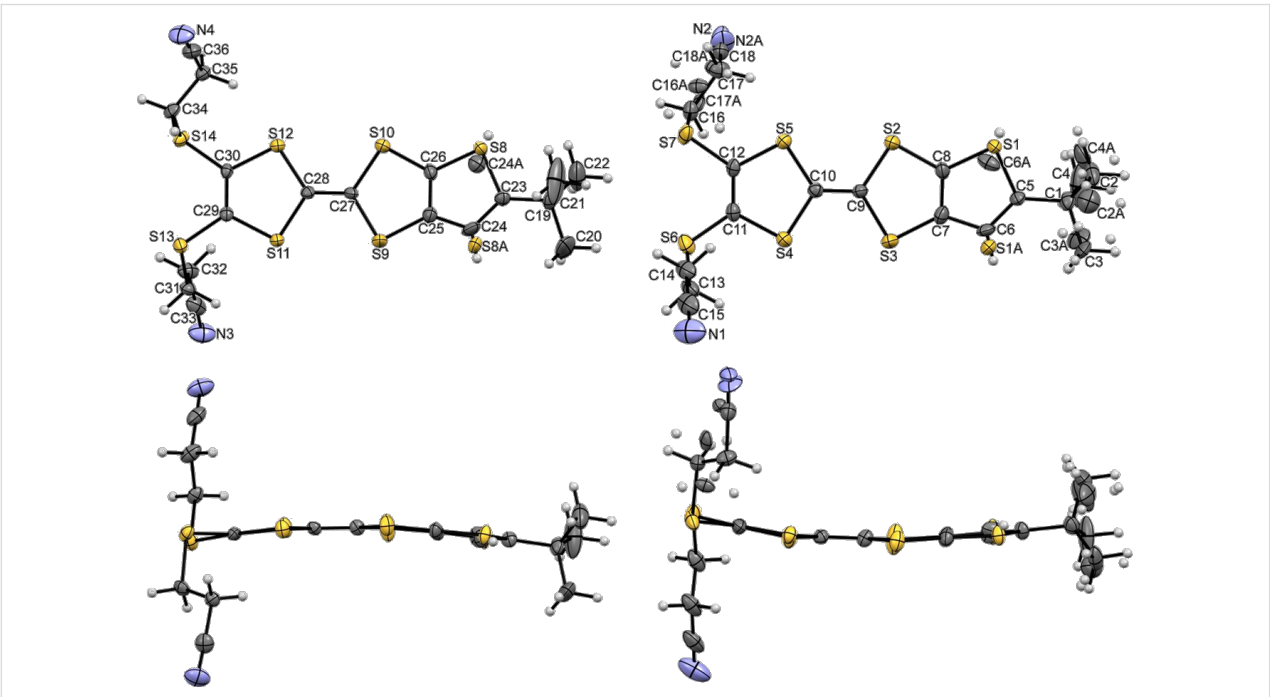

Figure 5: ORTEP views and atomic numbering scheme of α-tbtdt (**1**) with thermal ellipsoids at 50% probability level.

terminal thiophenic ring, with occupation factors of 55% and 45% for S7 and S7A, respectively. The [α-mtdt]$^+$ cation is almost planar, with exception of the –$(CH_2)_2$–CN groups, that point out in the same direction (Figure 7). In both donor and acceptor units, the bond lengths are within the expected range, for monoanionic gold dithiolene complexes [21] and fully oxidised TTF donors [18], namely the Au–S and central C14=C15 double bonds (d_{Au-S} = 2.392(7) Å, $d_{C14=C15}$ = 1.393(4) Å).

The crystal structure of (α-mtdt)[Au(mnt)$_2$] (**3**) is composed of alternated stacks of donor (D)-acceptor (A) molecules, along the *b* axis, with no short contacts between molecules along the stack due to the bulky cyanoethyl and methyl group which prevent a shorter distance between molecular planes. Within the stacks the donor molecules are head-to-head (Figure 8). The interactions between stacks are made in two distinct ways along the molecules long axis: 1) In one side the donor molecules interact, with each other, through the cyanoethyl groups,

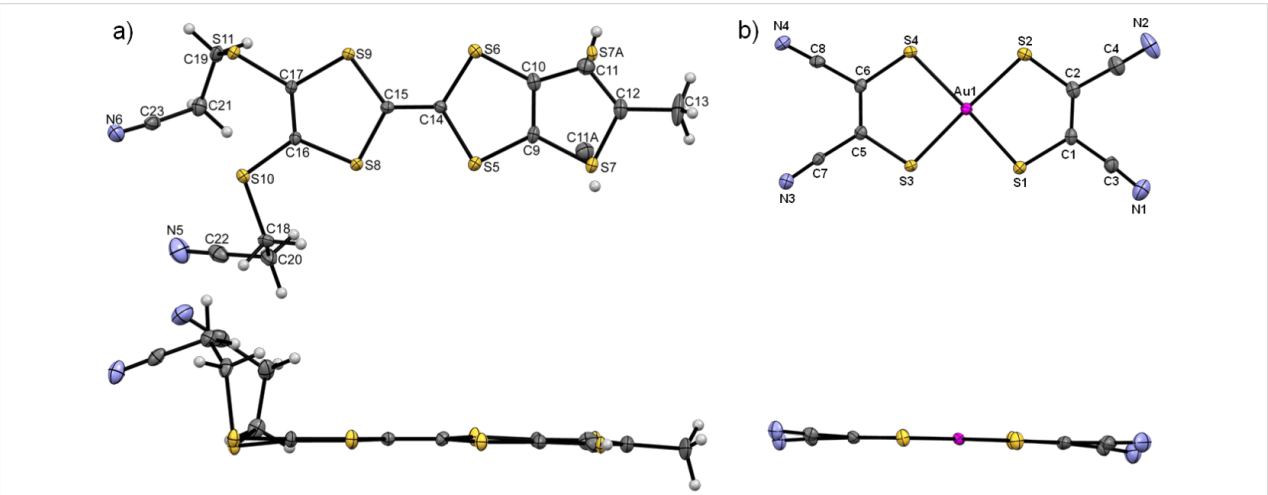

Figure 7: ORTEP views and atomic numbering scheme of a) (α-mtdt)$^+$ and b) [Au(mnt)$_2$]$^-$ in compound **3**, with thermal ellipsoids at 50% probability level.

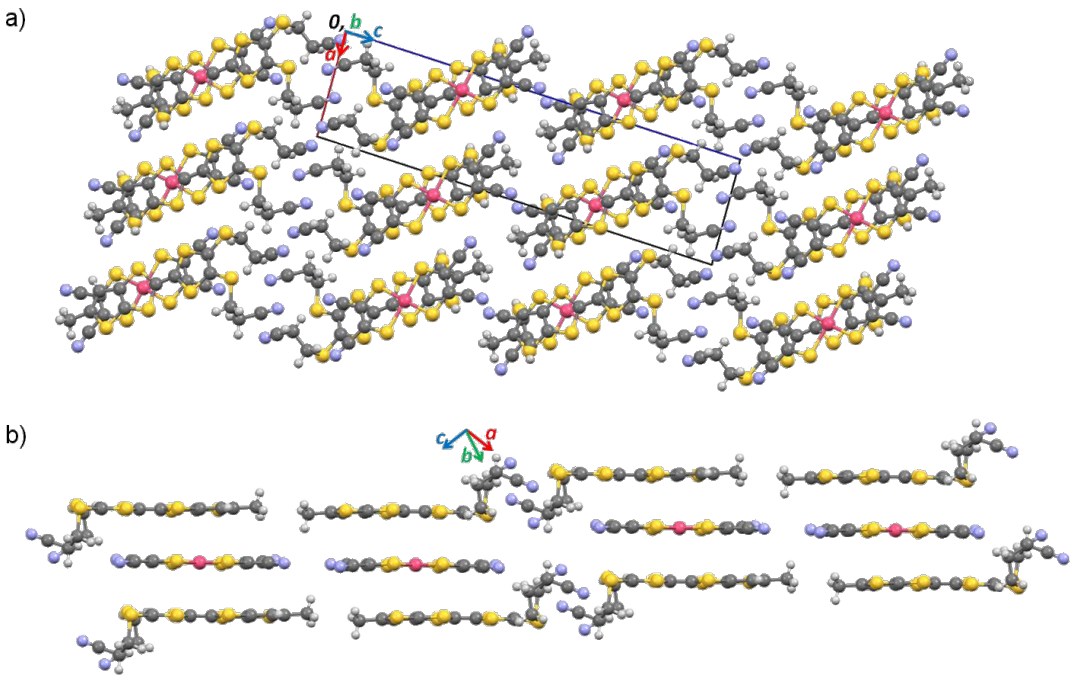

Figure 8: Crystal structure of **3** a) viewed along the *b* axis and b) partial view showing the alternated A–D–A–D stacks and the segregation between the methyl and cyanoethyl groups.

by C–H···N hydrogen bonds and S···N short contacts. There are no interactions between A and D molecules and the stacks are out-of-registry; 2) on the other side the stacking interaction is between the nitrile groups of A and the methyl groups of D, and is mediated by a weak C–H···N hydrogen bond. In this case the stacks are in-registry (Figure 9).

Along the molecules minor axis the stacks are connected by lateral A–D–A–D S···S and N···S short interactions.

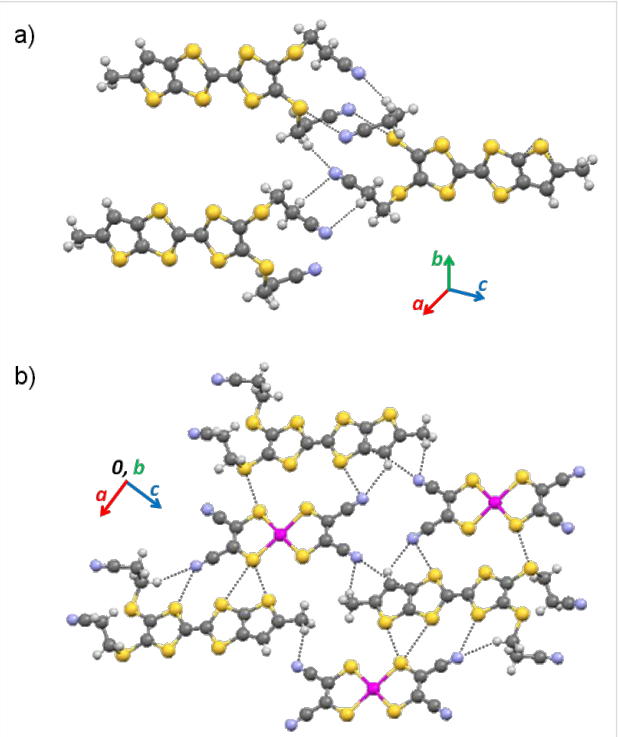

Figure 9: Detail of the crystal structure of **3** showing the short contacts between stacks.

Conclusion

In conclusion two new dithiolene ligand precursors, containing fused TTF and alkyl thiophenic moieties were described. These alkyl substituted compounds present a redox behavior with two processes typical of TTF-type donors with lower oxidation potentials compared with unsubstituted analogues. These molecules can also be used as ligand precursors and are expected to open the way to the preparation of extended dithiolene complexes with increased solubility, which may be processed from solution.

Experimental

Synthesis

All procedures were performed under inert atmosphere, in nitrogen or argon, unless stated otherwise. All solvents were dried according to the standard literature procedures. Compound 5,6-thieno[2,3-*d*]-1,3-dithiol-2-one (**i**) was obtained following the procedure used by Belo and co-workers [21]. Compounds **II** and **IV** were obtained following the literature procedures [16]. 5-Methylthieno[2,3-*d*][1,3]dithiole-2-thione (**III**) was synthesized as previously described [22]. Compounds 3,3'-{[2-(5-(*tert*-butyl)thieno[2,3-*d*][1,3]dithiol-2-ylidene)-1,3-dithiole-4,5-diyl]bis[sulfanediyl]}dipropanenitrile (**1**) and 3,3'-{[2-(5-methylthieno[2,3-*d*][1,3]dithiol-2-ylidene)-1,3-dithiole-4,5-diyl]bis[sulfanediyl]}dipropanenitrile (**2**), were prepared by an analogous procedure to that in [11]. The tetrabuthylammonium salt of $[Au(mnt)_2]^-$ was synthesized and purified as previously described [23]. All other reagents were reagent grade and used as commercially supplied. Column chromatography was carried out using silica gel (0.063 ± 0.2 mm) from SDS. Elemental analyses of the compounds were performed using an EA 110 CE Instruments automatic analyzer. Melting points were studied on a Stuart Scientific SMP2. IR spectra were obtained on a Bruker FTIR Tensor 27 spectrophotometer. ^{1}H NMR and ^{13}C NMR spectra were recorded on a Bruker Avance 300 (300 MHz for ^{1}H) amd a Bruker Avance 400 (100 MHz for ^{13}C) with $CDCl_3$ and CD_2Cl_2 used as solvents and TMS the internal reference. UV–vis spectra were recorded on a UV-1800 Shimadzu spectrophotometer. Mass spectra were obtained in QIT/MS Bruker HCT by collision-induced dissociation (CID).

5-(*tert*-Butyl)thieno[2,3-*d*][1,3]dithiol-2-one (I): 0.536 g of aluminum chloride in 12 mL dichloromethane was cooled to −78 °C in nitrogen atmosphere and a mixture of 0.5 g 5,6-thieno[2,3-*d*][1,3]dithiol-2-one (**i**) and 0.21 mL *t*-BuCl in 6 mL dichloromethane was added dropwise. After stirring for 1 h, the reaction mixture was allowed to warm up to −10 °C and stirred for 3 h, maintaining the temperature between −10 and −5 °C. The product was poured into ice water, neutralized with sodium hydrogen carbonate and extracted with dichloromethane. After drying with magnesium sulfate, the solvent was evaporated. The crude product was purified by column chromatography using *n*-hexane/ethyl acetate (10:1) as eluent and further recrystallized from *n*-hexane to yield 0.616 g (93%) of **I** as white needles. Anal. calcd for $C_9H_{10}OS_3$: C, 46.93; H, 4.38; S, 41.75; found: C, 46.74; H, 4.88; S,42.11; ^{1}H NMR (300 MHz, $CDCl_3$) δ 6.84 (s, 1H), 1.40 (s, 9H); ^{13}C NMR (75 MHz, $CDCl_3$) δ 194.54 (*C*=O), 159.78 (*C*-C(CH_3)$_3$), 126.06 (Ar), 120.02 (Ar), 115.92 (Ar), 35.44 (*C*(CH_3)$_3$), 32.43 (C(*C*H_3)$_3$).

3,3'-{[2-(5-(*tert*-Butyl)thieno[2,3-*d*][1,3]dithiol-2-ylidene)-1,3-dithiole-4,5-diyl]bis[sulfanediyl]}dipropanenitrile, α-tbtdt (1): Compound **I** (300 mg, 1.30 mmol) and compound **II** (395.85 mg, 1.30 mmol) were dissolved in 30 mL of freshly distilled $P(OEt)_3$ in a 50 mL round bottomed flask. The mixture

was heated to 120 °C for 24 h. Upon cooling 100 mL of methanol was added and the mixture was cooled to 20 °C for 24 h. An orange precipitate was recovered by filtration and washed with cold methanol (3 × 20 mL). The solid was furthermore purified by column chromatography using CH_2Cl_2 (R_f = 0.47). Single crystals were obtained by slow evaporation of a chloroform solution of **1**. Yield: 28% (176 mg); Anal. calcd for $C_{18}H_{18}N_2S_7$: C, 44.41; H, 3.72; N, 5.75; S, 46.11; found: C, 44.53; H, 4.00; N, 5.17; S, 46.33; FTIR (KBr): 2960 (m, –CH_2–), 2252 (m, –C≡N), 1634 (m, C=C), 1423 (S, S–CH_2–R) cm^{-1}; ^{1}H NMR (300 MHz, $CDCl_3$) δ 6.61 (s, 1H, –C=CH–C–), 3.10 (t, J = 7.07 Hz, 4H, S–CH_2–CH_2–CN), 2.74 (t, J = 7.06 Hz, 4H, S–CH_2–CH_2–CN), 1.35 (s, 3H, C–$(CH_3)_3$; ^{13}C NMR (100 MHz, CD_2Cl_2) δ 162.47, 131.18, 128.57, 128.44, 123.76, 121.42, 118.00, 115.58 (C6), 108.47, 35.91, 32.27 (C2, C3, C4), 31.83 (C14, C17), 19.26 (C13, C16); UV (CH_2Cl_2) λ_{max}, nm: 334, 305.5; MS *m*/*z* (% relative intensity): 485.9 (M^+, 100); mp 216–217 °C.

3,3'-{[2-(5-Methylthieno[2,3-*d*][1,3]dithiol-2-ylidene)-1,3-dithiole-4,5-diyl]bis[sulfanediyl]}dipropanenitrile, α-mtdt (2): Compound **III** (1.000 g, 4.89 mmol) and compound **IV** (1.468 g, 5.09 mmol) were dissolved in 12 mL of $P(OMe)_3$ in a 50 mL round bottomed flask and stirred for 24 h at 75/80 °C. After cooling to room temperature, 60 mL of methanol was added to the mixture and further cooled down to 15 °C for another 24 h. The orange precipitate was filtered and washed with 3 × 10 mL of methanol and dried under vacuum. This product was purified by column chromatography using CH_2Cl_2 as a solvent (R_f = 0.62). Recrystallization from *n*-hexane/CH_2Cl_2 (3:1) yielded pure **2** (1.38 g, 63%). Anal. calcd for $C_{15}H_{12}N_2S_7$: C, 40.51; H, 2.72; N, 6.30; S, 50.47; found: C, 40.72; H, 2.89; N, 5.97; S, 51.07; FTIR (KBr) 2924 (m, –CH_2–), 2251 (m, –C≡N), 1654 and 1421 (m, C=C), 1425 (S, S–CH_2–R) cm^{-1}; ^{1}H NMR (300 MHz, $CDCl_3$) δ 7.26 (s, 1H, –C=CH–C–), 3.10 (t, J = 7.15 Hz, 4H, S–CH_2–CH_2–CN), 2.74 (t, J = 6.95 Hz, 4H, S–CH_2–CH_2–CN), 1.55 (s, 3H, C–CH_3), ^{13}C NMR (100 MHz CD_2Cl_2) δ 144.49, 131.43, 128.55, 128.44, 123.82, 121.22, 119.00 (C6), 118.00, 108.43, 31.82 (C20, C21), 19.25 (C18, C19), 16.35 (C13); UV (CH_2Cl_2) λ_{max}, nm: 335, 307; MS: *m*/*z* (% relative intensity): 443.9 (M^+, 100); mp 166–167 °C.

(α-mtdt)[Au(mnt)$_2$] (3): Crystals were obtained by electrocrystallisation in a manner analogous to the procedure described in [24]. A dichloromethane solution of **2** and *n*-$Bu_4N[Au(mnt)_2]$, in approximately stoichiometric amounts, was added to the H-shaped cell, with Pt electrodes and in galvanostatic conditions. Dichloromethane was also purified using standard procedures and freshly distilled immediately before its use. The system was sealed under nitrogen and after ca. 3 days, using a current density of 1 μA·cm^{-2}, dark brown plate-shaped crystals were collected in the anode and washed with dichloromethane.

Redox properties

Cyclic voltammetry data were obtained using a BAS C3 Cell Stand. The voltammograms were obtained at room temperature with a scan rate of 100 mV/s, platinum wire working and counter electrodes and a $Ag/AgNO_3$ reference electrode. The measurements were performed on fresh solutions with a concentration of 10^{-3} M, in CH_2Cl_2, that contained *n*-Bu_4NPF_6 (10^{-1} M) as the supporting electrolyte.

Crystal structure determination

X-ray diffraction studies were performed with a Bruker APEX-II CCD detector diffractometer using graphite-monochromated Mo Kα radiation (λ = 0.71073 Å), in the φ and ω scans mode. A semi empirical absorption correction was carried out using SADABS [25]. Data collection, cell refinement and data reduction were done with the SMART and SAINT programs [26]. The structures were solved by direct methods using SIR97 [27] and refined by fullmatrix least-squares methods using the program SHELXL97 [28] using the winGX software package [29]. Non-hydrogen atoms were refined with anisotropic thermal parameters whereas H-atoms were placed in idealised positions and allowed to refine riding on the parent C atom. Molecular graphics were prepared using ORTEP 3 [30].

Crystal data and structure refinement for I: $C_9H_{10}OS_3$, M = 230.35 g·mol^{-1}, crystal size: 0.30 × 0.20 × 0.10 mm, orthorhombic, space group: $P2_12_12_1$, a = 9.4587(5) Å, b = 9.6256(4) Å, c = 11.5993(6) Å, α = β = γ = 90.00°, V = 1056.07(9) $Å^3$, Z = 4, ρ_{calc} = 1.449 g/cm^3, μ = 0.658 mm^{-1}, λ = 0.71073 Å, T = 150(2) K, θ range = 2.75–25.26°, reflections collected: 5280, independent: 1897 (R_{int} = 0.0294), 140 parameters. The structure was solved by direct methods and refined by full-matrix least squares on F^2; final R indices [I > 2sigma(I)]: R_1 = 0.0329, ωR_2 = 0.0767. CCDC 1051179.

Crystal data and structure refinement for compound 1 (α-tbtdt): $C_{18}H_{18}N_2S_7$, M = 486.76 g·mol^{-1}, crystal size: 0.50 × 0.20 × 0.02 mm, triclinic, space group: P−1, a = 9.9526(3) Å, b = 12.2499(3) Å, c = 17.9352(4) Å, α = 81.3810(10)°, β = 85.234(2)°, γ = 89.2040(10)°, V = 2154.46(10) $Å^3$, Z = 4, ρ_{calc} = 1.501g/cm^3, μ = 0.739 mm^{-1}, λ = 0.71073 Å, T = 150(2) K, θ range = 2.93–25.68°, reflections collected: 27683, independent: 8009 (R_{int} =0.0482), 599 parameters. The structure was solved by direct methods and refined by full-matrix least squares on F^2; final R indices [I > 2sigma(I)]: R_1 = 0.0387, ωR_2 = 0.0828. CCDC 1051177.

Crystal data and structure refinement for compound 3 ((α-mtdt)[Au(mnt)$_2$]): $C_{23}H_{12}AuN_6S_{11}$, M = 922.01 g·mol^{-1}, crystal size: 0.40 × 0.10 × 0.04 mm, triclinic, space group: $P\bar{1}$, a = 7.25300(10) Å, b = 8.38770(10) Å, c = 26.2705(4) Å, α = 86.2350(10)°, β = 86.1760(10)°, γ = 71.7200(10)°, V = 1512.47(4) Å^3, Z = 2, ρ_{calc} = 2.025 g/cm^3, μ = 5.652 mm^{-1}, λ = 0.71073 Å, T = 150(2) K, θ range = 2.56–26.37°, reflections collected: 25691, independent: 6102 (R_{int} = 0.0262), 390 parameters. The structure was solved by direct methods and refined by full-matrix least squares on F^2; final R indices [I > 2sigma(I)]: R_1 = 0.0173, ωR_2 = 0.0420. CCDC 1051178.

Supporting Information

Supporting Information File 1

Tables of the selected short contacts and hydrogen bonds in the crystal structure of compounds **I**, **1** and **3**.
[http://www.beilstein-journals.org/bjoc/content/supplementary/1860-5397-11-71-S1.pdf]

Supporting Information File 2

CIF file of compound **I**.
[http://www.beilstein-journals.org/bjoc/content/supplementary/1860-5397-11-71-S2.cif]

Supporting Information File 3

CIF file of compound **1**.
[http://www.beilstein-journals.org/bjoc/content/supplementary/1860-5397-11-71-S3.cif]

Supporting Information File 4

CIF file of compound **3**.
[http://www.beilstein-journals.org/bjoc/content/supplementary/1860-5397-11-71-S4.cif]

Supporting Information File 5

CheckCif for compounds **I**, **1** and **3**.
[http://www.beilstein-journals.org/bjoc/content/supplementary/1860-5397-11-71-S5.pdf]

Acknowledgements

This work was supported by FCT (Portugal) under contract PTDC/QEQ-SUP/1413/2012 and RECI/QEQ-QIN/0189/2012.

References

1. Bendikov, M.; Wudl, F.; Perepichka, D. F. *Chem. Rev.* **2004,** *104,* 4891–4945. doi:10.1021/cr030666m
2. Bryce, M. R.; Nielsen, M. B.; Lomholt, C.; Becher, J. *Chem. Soc. Rev.* **2000,** *29,* 153–164. doi:10.1039/A803992E
3. Bryce, M. R. *J. Mater. Chem.* **2000,** *20,* 589–598. doi:10.1039/a908385e
4. Bryce, M. R. *Chem. Soc. Rev.* **1991,** *20,* 355–390. doi:10.1039/cs9912000355
5. Canevet, D.; Sallé, M.; Zhang, G.; Zhang, D.; Zhu, D. *Chem. Commun.* **2009,** *17,* 2245–2269. doi:10.1039/b818607n
6. Yamada, J.; Sujimoto, T., Eds. *TTF Chemistry, Fundamentals and Apllications of Tetrathiafulvalene;* Kodansha-Springer: Tokyo, Japan, 2004.
7. Roberstson, N.; Cronin, L. *Coord. Chem. Rev.* **2002,** *227,* 93–127. doi:10.1016/S0010-8545(01)00457-X
8. Kobayashi, A.; Fujiwara, E.; Kobayashi, H. *Chem. Rev.* **2004,** *104,* 5243–5264. doi:10.1021/cr030656l
9. Nunes, J. P. N.; Figueira, M. J.; Belo, D.; Santos, I. C.; Ribeiro, B.; Lopes, E. B.; Henriques, R. T.; Gancedo, J. V.; Veciana, J.; Rovira, C.; Almeida, M. *Chem. – Eur. J.* **2007,** *13,* 9841–9849. doi:10.1002/chem.200701050
10. Neves, A. I. S.; Lopes, E. B.; Almeida, M.; Belo, D. *Phys. Status Solidi C* **2012,** *9,* 1137–1139. doi:10.1002/pssc.201100635
11. Belo, D.; Figueira, M. J.; Nunes, J. P. M.; Santos, I. C.; Almeida, M.; Crivillers, N.; Rovira, C. *Inorg. Chim. Acta* **2007,** *360,* 3909–3914. doi:10.1016/j.ica.2007.03.041
12. Neves, A. I. S.; Santos, I. C.; Coutinho, J. T.; Pereira, L. C. J.; Henriques, R. T.; Lopes, E. B.; Alves, H.; Almeida, M.; Belo, D. *Eur. J. Inorg. Chem.* **2014,** 3989–3999. doi:10.1002/ejic.201402048
13. Fabre, J. M. *Chem. Rev.* **2004,** *104,* 5133–5150. doi:10.1021/cr0306440
14. Narvor, N. L.; Robertson, N.; Weyland, T.; Kilburn, J. D.; Underhill, A. E.; Webster, M.; Svenstrup, N.; Becher, J. *Chem. Commun.* **1996,** 1363–1364. doi:10.1039/CC9960001363
15. Nagakubo, J.; Ashizawa, M.; Kawamoto, T.; Tanioka, A.; Mori, T. *Phys. Chem. Chem. Phys.* **2011,** *7,* 14370–14377. doi:10.1039/c1cp21507h
16. Svenstrup, N.; Rasmussen, K. M.; Kruse, T.; Becher, J. *Synthesis* **1994,** 809–812. doi:10.1055/s-1994-25580
17. Wang, C.; Batsanov, A. S.; Bryce, M. R.; Howard, J. A. K. *Synthesis* **1998,** 1615–1618. doi:10.1055/s-1998-2197
18. Silva, R. A. L.; Neves, A. I.; Afonso, M. L.; Santos, I. C.; Lopes, E. B.; Del Pozo, F.; Pfattner, R.; Torrent, M. M.; Rovira, C.; Almeida, M.; Belo, D. *Eur. J. Inorg. Chem.* **2013,** 2440–2446. doi:10.1002/ejic.201201362
19. Lichtenberger, D. L.; Johnston, R. L.; Hinkelmann, K.; Suzuki, T.; Wudl, F. *J. Am. Chem. Soc.* **1990,** *112,* 3302. doi:10.1021/ja00165a007
20. Santos, I. C.; Belo, D.; Mendonça, J.; Figueira, M. J.; Almeida, M.; Rovira, C. *Acta Crystallogr., Sect. E* **2005,** *61,* m2161–m2163. doi:10.1107/S1600536805018234
21. Belo, D.; Alves, H.; Lopes, E. B.; Duarte, M. T.; Gama, V.; Henriques, R. T.; Almeida, M.; Pérez-Benítez, A.; Rovira, C.; Veciana, J. *Chem. – Eur. J.* **2001,** *7,* 511–519. doi:10.1002/1521-3765(20010119)7:2<511::AID-CHEM511>3.0.CO;2-5
22. Kumar, E. V. K. S.; Singh, J. D.; Singh, H. B.; Das, K.; Verghese, B. *Tetrahedron* **1997,** *53,* 11627–11644. doi:10.1016/S0040-4020(97)00732-1
23. Werden, B. G.; Billig, E.; Gray, H. B. *Inorg. Chem.* **1966,** *5,* 78. doi:10.1021/ic50035a019

24. Silva, R. A. L.; Neves, A. I. S.; Lopes, E. B.; Santos, I. C.; Coutinho, J. T.; Pereira, L. C. J.; Rovira, C.; Almeida, M.; Belo, D. *Inorg. Chem.* **2013,** *52,* 5300–5306. doi:10.1021/ic400246y
25. Sheldrick, G. M. *SADABS;* Bruker AXS Inc.: Madison, Wisconsin, USA, 2004.
26. *Bruker. SMART and SAINT;* Bruker AXS Inc.: Madison, Wisconsin, USA, 2004.
27. Altomare, A.; Burla, M. C.; Camalli, M.; Cascarano, G.; Giacovazzo, G.; Guagliardi, A.; Moliterni, A. G. G.; Polidori, G.; Spagna, R. *J. Appl. Crystallogr.* **1999,** *32,* 115. doi:10.1107/S0021889898007717
28. Sheldrick, G. M. SHELXL97, Program for Crystal Structure Refinement, University of Göttingen, Germany, 1997.
29. Farrugia, L. J. *J. Appl. Crystallogr.* **1999,** *32,* 837. doi:10.1107/S0021889899006020
30. Farrugia, L. J. *J. Appl. Crystallogr.* **1997,** *30,* 565. doi:10.1107/S0021889897003117

BEILSTEIN JOURNAL OF ORGANIC CHEMISTRY

Trifluoromethyl-substituted tetrathiafulvalenes

Olivier Jeannin, Frédéric Barrière and Marc Fourmigué*

Full Research Paper

Open Access

Address:
Institut des Sciences Chimiques de Rennes, UMR 6226
CNRS-Université de Rennes I, Campus de Beaulieu, 35042 Rennes, France

Email:
Marc Fourmigué* - marc.fourmigue@univ-rennes1.fr

* Corresponding author

Keywords:
electrochemistry; electron withdrawing group (EWG); fluorine; tetrathiafulvalene (TTF)

Beilstein J. Org. Chem. **2015,** *11,* 647–658.
doi:10.3762/bjoc.11.73

Received: 16 February 2015
Accepted: 15 April 2015
Published: 06 May 2015

This article is part of the Thematic Series "Tetrathiafulvalene chemistry".

Guest Editor: P. J. Skabara

Abstract

A series of tetrathiafulvalenes functionalized with one or two trifluoromethyl electron-withdrawing groups (EWG) is obtained by phosphite coupling involving CF_3-substituted 1,3-dithiole-2-one derivatives. The relative effects of the EWG such as CF_3, CO_2Me and CN on the TTF core were investigated from a combination of structural, electrochemical, spectrochemical and theoretical investigations. Electrochemical data confirm the good correlations between the first oxidation potential of the TTF derivatives and the σ_{meta} Hammet parameter, thus in the order $CO_2Me < CF_3 < CN$, indicating that, in any case, the mesomeric effect of the substituents is limited. Besides, crystal structure determinations show that the deformation of the unsymmetrically substituted dithiole rings, when bearing one, or two different EWG, and attributed to the mesomeric effect of ester or nitrile groups, is not notably modified or counter-balanced by the introduction of a neighboring trifluoromethyl group. DFT calculations confirm these observations and also show that the low energy HOMO–LUMO absorption band found in nitrile or ester-substituted TTFs is not found in TTF-CF_3, where, as in TTF itself, the low energy absorption band is essentially attributable to a HOMO→LUMO + 1 transition. Despite relatively high oxidation potentials, these donor molecules with CF_3 EWG can be involved in charge transfer complexes or cation radical salts, as reported here for the CF_3-subsituted EDT-TTF donor molecule. A neutral charge transfer complex with TCNQ, (EDT-TTF-CF_3)$_2$(TCNQ) was isolated and characterized through alternated stacks of EDT-TTF-CF_3 dimers and TCNQ in the solid state. A radical cation salt of EDT-TTF-CF_3 is also obtained upon electrocrystallisation in the presence of the $FeCl_4^-$ anion. In this salt, formulated as (EDT-TTF-CF_3)($FeCl_4$), the (EDT-TTF-CF_3)$^{+\bullet}$ radical cations are associated two-by-two into centrosymmetric dyads with a strong pairing of the radical species in a singlet state.

Introduction

Following three decades of extensive work toward the elaboration of conducting radical cation salts from tetrathiafulvalene (TTF) derivatives with electron-rich alkyl (tetramethyltetrathiafulvalene: TMTTF, tetramethyltetraselenafulvalene: TMTSF) or thioalkyl (ethylenedithiotetrathiafulvalene: EDT-TTF, bis(ethylenedithio)tetrathiafulvalene: BEDT-TTF) substituents [1], investigations of radical cation salts of tetrathiafulvalenes functionalized by electron-withdrawing groups (EWG) are less

documented, essentially because the presence of such substituents as halogen, acyl, ester, amide or nitrile on the TTF redox core dramatically increases its oxidation potential and destabilizes the radical cation form. This strong anodic shift is particularly noticeable in tetrasubstituted TTFs such as $TTF(CO_2Me)_4$ [2-4], $TTFCl_4$ [5], $TTF(CF_3)_4$ [2], or $TTF(CN)_4$ [3], which oxidize into the radical cation at 0.80, 0.83, 1.05 or 1.12 V vs SCE respectively, to be compared with TTF itself which oxidizes at 0.33 V vs SCE. The associated instability of these radical species in moist air hindered in most cases their isolation in cation radical salts. This is all the more unfortunate since the electronegative atoms (O, N, Hal) within such EWG are expected to be able to engage, in the solid state at the organic–inorganic interface, in a variety of secondary non-bonding interactions such as hydrogen or halogen bonding [6,7], an issue of current strong interest in organic solid state chemistry [8,9]. However, it was also recognized that the introduction of only one or two of such EWG on the TTF core could limit this anodic shift, and accordingly, several tetrathiafulvalenes bearing only one or two ester [10], nitrile [11-14], amide [7,15-17], thioamide [18-20], or halogen [5] substituents were successfully engaged in radical cation salts by electrocrystallization, with intermolecular hydrogen [21-23] of halogen bond interactions [24-27]. Within such TTF derivatives, as reported by Bryce [28], an internal charge transfer (ICT) between the TTF and the EWG moieties increases the hydrophilicity of the TTF head groups and facilitates monolayer formation on the water surface for the preparation of Langmuir–Blodgett films. The structural and electronic properties of a series of ester [15], thioester [29,30], tertiary amide and thioamide [12] TTF derivatives have been then rationalized, based on: (i) the sizeable contribution of the mesomeric form B (Scheme 1) and, (ii) an ICT from the TTF-based HOMO to the EWG-based LUMO, also observed in primary and secondary amides [10]. Another consequence of the contribution of the B form is the shortening of the C–S bond opposite to the EWG, experimentally observed in the structures of such molecules.

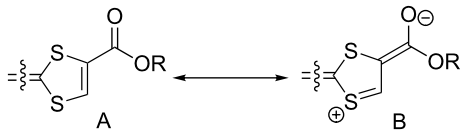

Scheme 1: Mesomeric forms of 1,3-dithiole rings substituted with EWG.

More recently, we have reported another series of TTFs functionalized at various positions with the electron-withdrawing $–CF_3$ (trifluoromethyl) group such as EDT-TTF(CF_3) (**1c**) or EDT-TTF$(CF_3)_2$ (**2cc**) (Scheme 2) [31]. Single-crystal X-ray diffraction measurements revealed the recurrent formation of layered structures with a strong segregation of the fluorinated moieties and formation of fluorine bilayers [32,33], attributed to the amphiphilic character of those TTF derivatives upon CF_3-functionalization. A strong anodic shift of the first oxidation potential was also noted for **1c** and **2cc**, when compared with the unsubstituted EDT-TTF molecule.

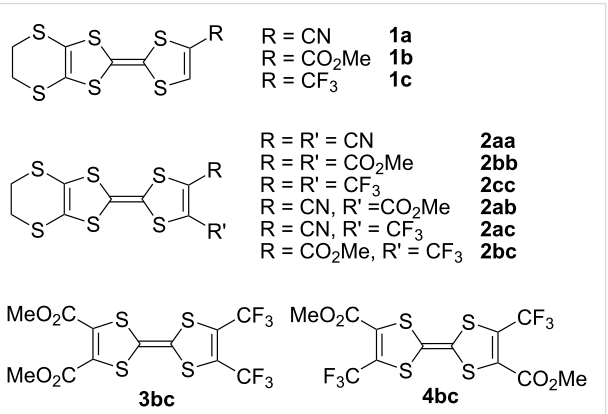

Scheme 2: Investigated TTF derivatives bearing EWG.

This work has been extended here to several novel disubstituted tetrathiafulvalenes bearing one CF_3 group and one ester or nitrile group at the neighboring position as in **2ac** and **2bc** (Scheme 2). These derivatives offer an invaluable opportunity to evaluate the influence of the nature of the EWG on the structural and electronic properties of the TTF redox moiety, taking advantage of the marked differences between the three EWG now available: (i) the strongly electron withdrawing –CN group, (ii) the weaker $–CO_2Me$ group, both with important mesomeric effects, and, (iii) the $–CF_3$ group, expected to exhibit essentially a strong −I inductive effect. Among the nine possible combinations **1** and **2** described above (Scheme 2), the unsymmetrically disubstituted **2ab** and **2ac** have not been reported to date. We describe here the syntheses of **2ac** from **2bc** and the single-crystal X-ray structure determinations of both **2ac** and **2bc** molecules. The preparation of the two positional isomers of bis(trifluoromethyl)-bis(carboxymethyl)tetrathiafulvalene **3bc** and **4bc** is also reported. The evolutions of (i) the geometry of the dithiole ring bearing the EWG, (ii) the electrochemical properties, (iii) the optical absorption (UV–vis) properties will be analyzed within the series, in order to evaluate the role of the CF_3 group as electron-withdrawing substituent on the structural and electronic properties of the tetrathiafulvalene core, by comparison with that of the $–CO_2Me$ or –CN substituents. Furthermore, from the mono-substituted trifluoromethyl derivative **1c**, we were also able to isolate a charge transfer complex with TCNQ and a cation radical salt with $FeCl_4^–$. The structures of both compounds will be de-

scribed, and the geometrical evolutions of the TTF core upon oxidation analyzed by comparison with the structure of neutral **1c**.

Results and Discussion

Syntheses

The reported preparation of **2bc** is based on the coupling reaction of the trithiocarbonate **5** with the dithiocarbonate **6bc**, affording also the symmetrical coupling product **4bc** (Scheme 3) [31]. Further decarboxylation of **2bc** with LiBr/DMF afforded **1c** while reaction with NH_3 in MeOH gives the corresponding primary amide **7** in 63% yield. Its dehydration with $POCl_3$ in sulfolane gives **2ac** in 60% yield.

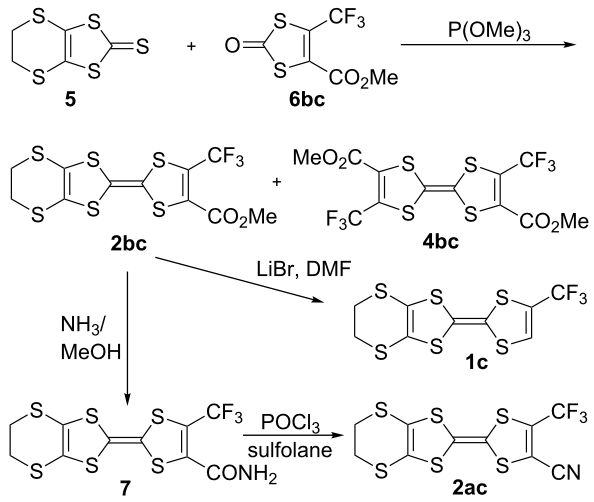

Scheme 3: Synthetic procedures to the CF_3-substituted **4bc**, **1c** and **2ac** molecules.

A similar phosphite-based cross-coupling reaction between the bis(trifluoromethyl)-1,3-dithiole-2-one derivative **9cc** and the diester derivative **10bb** gave the TTF **3bc** in 15% yield (Scheme 4).

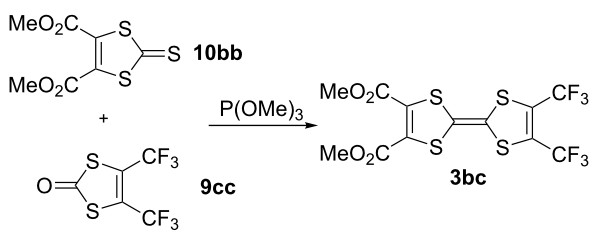

Scheme 4: Synthetic procedure to **3bc**.

With these extensive series at hand, it is now interesting to evaluate the role of the CF_3 group as electron-withdrawing substituent on the structural and electronic properties of the tetrathiafulvalene core and to compare them with those of the $–CO_2Me$ or –CN substituents. This will be done here following two different approaches. First, we report the redox and optical absorption properties of the TTFs in solution, correlated with the electron-withdrawing character of the different substituents. Then, the relative effect of the three EWG on the solid state geometry of the dithiole ring will be described, based on the X-ray crystal structure analyses of four neutral TTF derivatives, i.e., the EDT-TTF derivatives **2ac** and **2bc** and the tetrasubstituted derivatives **3bc** and **4bc**.

Redox properties

Cyclic voltammetry was used to evaluate the evolution of the donor strength with the nature and number of EWG. All derivatives exhibit two reversible oxidation waves. The $E_{1/2}$ values for the EDT-TTF derivatives with one or two EWG are collected in Table 1. Compared with the unsubstituted EDT-TTF parent compound, redox potentials are shifted toward more anodic potentials with the introduction of the EWG with the following order $CO_2Me < CF_3 \leq CN$. Note that this order is also confirmed by the evolution of the redox potentials of the tetrasubstituted TTF derivatives collected in Table 2.

Earlier electrochemical investigations of various tetrathiafulvalene derivatives have shown that the best correlations between the first oxidation potential and the Hammet parameters [39-41] were actually found with the σ_{meta} constant of each substituent on the TTF core [20,42], indicating that, in any case, the mesomeric effect of the substituents was small. A similar satisfactory correlation with all TTF derivatives described here is shown in Figure 1 and demonstrates that the trifluoromethyl

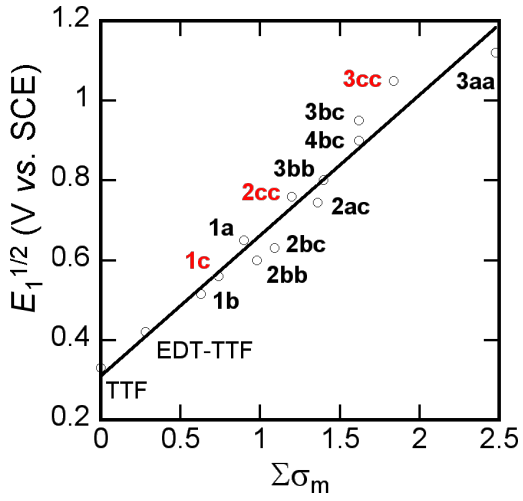

Figure 1: Correlation between the first oxidation potential $E_{1/2}$ and the sum of the Hammet σ_{meta} parameters. TTF that only contain only CF_3 EWG are given in red.

Table 1: Electrochemical and spectroscopic data of the EDT-TTF-RR′ derivatives **1** and **2**. Reported values with other electrochemical references were converted to approximate values vs SCE and are given in italics. Potentials reported vs Fc^+/Fc were converted to SCE by adding 0.39 V. Potentials reported vs Ag/AgCl were converted to SCE by adding −0.045 V. Lowest energy absorption maximum λ_{max} (nm) and molar extinction coefficient ε ($L \cdot mol^{-1} \cdot cm^{-1}$) are determined in CH_2Cl_2 unless otherwise specified).

RR′	solvent	reference electrode	$E_{1/2(ox1)}$ (V)	$E_{1/2(ox2)}$ (V)	references (electrochemistry)	$\Sigma\sigma_{meta}$	λ_{max} (ε)	references (UV–vis)
H, H	CH_3CN	SCE	0.42	0.74	[34,35]	0.28	441 (451) 374 (1266, sh)	this work
H, CO_2Me (**1b**)	CH_3CN	SCE Ag/AgCl	*0.515* 0.56	*0.825* 0.87	[36]	0.63	480 418	[37]
H, CF_3 (**1c**)	CH_2Cl_2	SCE Fc^+/Fc	*0.56* 0.17	*0.99* 0.60	[17]	0.74	374 (2200)	this work
H, CN (**1a**)	PhCN	SCE	0.65	1.0	[9]	0.90	422 (725)	this work
CO_2Me, CO_2Me (**2bb**)	CH_3CN	SCE Ag/AgCl	*0.595* 0.64	*0.905* 0.95	[20]	0.98	443 (1310)	this work
CF_3, CO_2Me (**2bc**)	CH_2Cl_2	SCE Fc^+/Fc	*0.63* 0.24	*0.94* 0.64	[17]	1.09	467 (10800)	this work
CF_3, CF_3 (**2cc**)	CH_2Cl_2	SCE Fc^+/Fc	*0.76* 0.37	*1.15* 0.76	[17]	1.2	422 (990)	this work
CN, CF_3 (**2ac**)	CH_2Cl_2	SCE Fc^+/Fc	*0.745* 0.355	*1.143* 0.753	this work	1.36	464 (760)	this work
CN, CN (**2aa**)			—	—	—	1.52	500 (464)	[11]

Table 2: Electrochemical and spectroscopic data of tetrasubstituted TTF derivatives. $E_{1/2}$ values are reported in V vs SCE reference electrode. Lowest energy absorption maximum λ_{max} (nm) and molar extinction coefficient ε ($L \cdot mol^{-1} \cdot cm^{-1}$) are determined in CH_2Cl_2 unless otherwise specified).

	solvent	$E_{1/2(ox1)}$	$E_{1/2(ox2)}$	references (electrochemistry)	$\Sigma\sigma_{meta}$	λ_{max} (ε)	references (UV–vis)
TTF	CH_3CN	0.33	0.71	[22]	0	446 (263)[a]	[38]
$TTF(CO_2Me)_4$ (**3bb**)	CH_3CN	0.83	1.10	[22]	1.4	445 (1930)	[2,3]
o-$TTF(CO_2Me)_2(CF_3)_2$ (**3bc**)	CH_2Cl_2	0.95	1.28	this work	1.62	437 (2430)	this work
E-$TTF(CO_2Me)_2(CF_3)_2$ (**4bc**)	CH_2Cl_2	0.90	1.23	this work	1.62	467 (2280)	this work
$TFF(CF_3)_4$ (**3cc**)	CH_3CN	1.05	1.28	[2]	1.84	416 (1390)	this work
$TTF(CN)_4$ (**3aa**)	CH_3CN	1.12	1.22	[3]	2.48	502 (2000)	[3]

[a]In CH_3CN.

group anodic shift observed in the order $CO_2Me < CF_3 < CN$ correlate well with the σ_{meta} Hammet constant.

Optical properties

The evolution of the lowest energy absorption bands is also reported for the different TTF derivatives in Table 1 and Table 2. We note that the introduction of the trifluoromethyl group induces a blue shift of these absorptions, by comparison with EWG such as CO_2Me or CN which move the absorption bands toward lower energies This point is actually correlated to the observed color difference, as the trifluoromethyl-substituted TFF derivatives are lightly orange colored, while the ester and cyano TTFs are dark red compounds. In order to rationalize these evolutions, we have performed TD-DFT calculations on the model molecules TTF, TTF-CF_3, TTF-CO_2Me and TTF-CN. The results are shown in Figure 2 and collected in Table 3, where a good correlation is found with the observed absorption bands experimentally observed in the four EDT-TTF derivatives, namely EDT-TTF, EDT-TTF–CF_3 (**1c**), EDT-TTF–CO_2Me (**1b**) and EDT–TTF-CN (**1a**).

Several points need to be emphasized. In pristine TTF as in TTF–CF_3, the strongest, low energy transition is not the HOMO→LUMO transition but the HOMO→LUMO + 1 transition. Indeed, the LUMO in both molecules has a σ character while the LUMO + 1 has a π character. By contrast, the ester and cyano groups (−M EWG) are strongly conjugated with the π system to such a point that the order of the two lowest unoccupied orbitals is inverted. This inversion, with now a LUMO of π character, allows for a direct HOMO→LUMO optical tran-

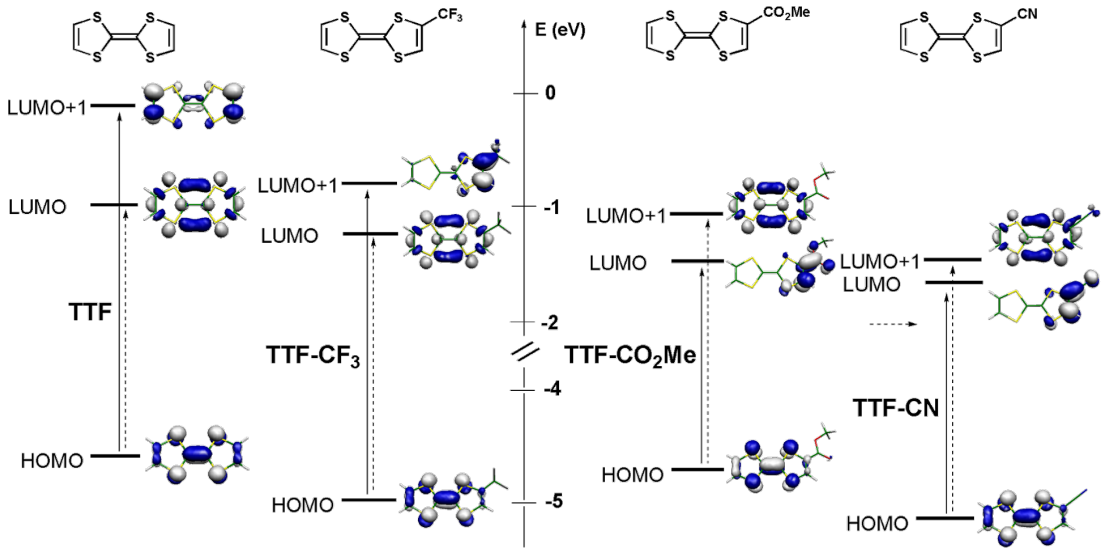

Figure 2: Calculated frontier orbitals of geometry-optimized [B3LYP/6-31G(d)] model compounds TTF, TTF-CF_3, TTF-CO_2Me and TTF-CN, with the lowest energy optical transitions deduced from TD-DFT calculations (see Table 3).

Table 3: Calculated (TD-DFT, B3LYP/6-311G**) optical transitions in the model compounds TTF, TTF–CF_3, TTF–CO_2Me and TTF–CN, and comparison with the experimentally determined values in the analogous EDT-TTF derivatives.

model	transition	oscillator strength *f*	λ_{calc} (nm)	compound	λ_{obs} (nm)
TTF	HOMO→LUMO	0.0000	458.14	EDT-TTF	441 (451)
	HOMO→LUMO + 1[a]	0.0179	361.54		374 (1266, sh)
TTF–CF_3	HOMO→LUMO	0.0009	448.62	**1c**	—
	HOMO→LUMO + 1[a]	0.0203	387.41		374 (2200)
TTF–CO_2Me	HOMO→LUMO	0.0390	471.16	**1b**	480, see [35]
	HOMO→LUMO + 1	0.0001	450.83		418, see [35]
TTF–CN	HOMO→LUMO HOMO→LUMO + 1	0.0018	458.46	**1a**	422 (725)
	HOMO→LUMO HOMO→LUMO + 1	0.0263	452.63		
	HOMO→LUMO + 2[a]	0.0000	333.71		–

[a]The HOMO→LUMO + 4 is also involved in this transition. Cf Supporting Information File 1 for complete TD-DFT calculations.

sition in the two latter compounds. Besides, the −I inductive effect of the trifluoromethyl group stalilizes HOMO, LUMO and LUMO + 1 of TTF. As a consequence, its lower energy absorptions are only slightly shifted by comparison with TTF, as experimentally observed. On the other hand, the strong stabilization of the LUMO in the ester- or cyano-substituted TTFs leads to a large red shift of the low energy absorption of these molecules. Note also that the relative energy of the HOMO of the four different model TTFs is well correlated with the ranking deduced from the electrochemical measurements. The stabilization of the HOMO, associated with the anodic shift of the first oxidation potential is indeed strongest with the cyano group, with the following ordering H < CO_2Me < CF_3 < CN, as discussed above (Table 1 and Table 2).

X-ray crystal structures of the neutral donor molecules

As mentioned in the Introduction, the substitution of one hydrogen atom on the TTF core by one EWG such as ester or cyano group is known to distort the dithiole ring, as illustrated in Scheme 1. In the following, we want to evaluate the extent of this effect in the case of the trifluoromethyl group, and its evolution in competitive situations where two different EWG are on the same dithiole ring. For that purpose, we could obtain

good quality crystals of the trifluoromethyl-substituted EDT-TTF derivatives with either one ester (in **2ac**) or one cyano group (in **2bc**) in ortho position to the CF_3 group. **2ac** crystallizes in the monoclinic system, space group $P2_1$, with one molecule in general position in the unit cell (Figure 3), affected by disorder on the ethylene bridge. On the other hand, **2bc** crystallizes in the triclinic system, space group $P\bar{1}$, with one molecule in general position in the unit cell (Figure 4). The ester group is coplanar with the TTF core and adopts a s-*trans* conformation. In both compounds, the CF_3 group is not disordered as usually observed but adopts a fixed conformation with one fluorine atoms in the TTF mean plane, away from the other substituent. Bond lengths and angles are in the expected range. A dissymmetry of the C–S bonds (*b*, *b*′ in Table 4) in the dithiole ring bearing the different EWG is observed, with in both cases a shortening of the C–S bond close to the CF_3 group. This polarization of the dithiole ring bearing one such EWG has been rationalized by Bryce on the basis of a sizeable contribution of a zwitterionic mesomeric form due to the influence of the EWG of −M character (Scheme 1) [8,17,18]. The fact that in both **2ac** and **2bc** molecules, this shortening affects the C–S bond closest to the CF_3 group demonstrates unambiguously that the mesomeric electron-withdrawing effect of the CN or CO_2Me groups is indeed stronger than that of CF_3.

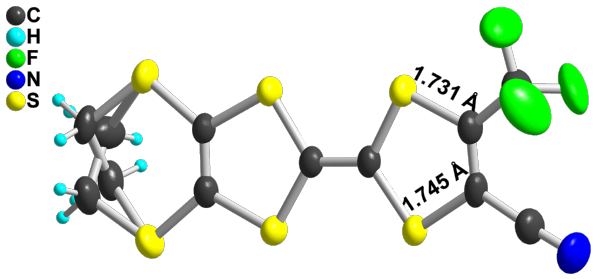

Figure 3: View of the **2ac** molecule. Thermal ellipsoids are shown at the 50% probability level.

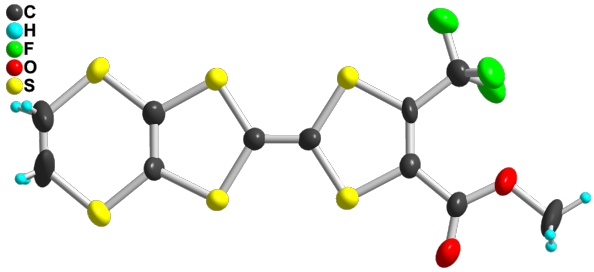

Figure 4: View of the **2bc** molecule. Thermal ellipsoids are shown at the 50% probability level.

A similar effect is also observed on the structure of the symmetrical TTF **4bc**, which was obtained as symmetrical coupling product of **6bc** during the preparation of **2bc** (Scheme 2). **4bc** crystallizes in the orthorhombic system, space group *Pbam*, with two crystallographically independent molecules, each of them located on a mirror plane and on an inversion center (Figure 5). In both molecules, a shorter C−S bond length is observed opposite to the CO_2Me groups (Table 3), demonstrating again here that the (−M) mesomeric effect of the ester group exercises a stronger effect than the (−I) inductive effect of the CF_3 group.

Another interesting insight is provided by the X-ray crystal structure of the other isomer **3bc**, where each dithiole ring is substituted with the same substituents, two CF_3 or two CO_2Me groups (Figure 6). We note first that the C–S bond distances (b) are now equal within the estimated standard deviations. We also observe that the localization of two CF_3 moieties in ortho position to each other leads to a strong positional disorder of the fluorine atoms, at variance with the other structures described

Table 4: Evolution of bonds distances within the dithiole ring in EDT-TTF derivatives substituted with one or two EWG. Definition of the C–S *b* and *b*′ bond distances are given in the scheme below.

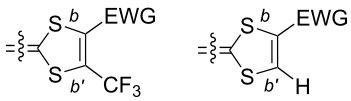

compound	*b*	*b*′	100(*b*′ − *b*)/*b*′	references
CN, CF_3 (**2ac**)	1.745(5)	1.731(9)	−0.8%	this work
CO_2Me, CF_3 (**2bc**)	1.727(23)	1.715(33)	−0.7%	this work
E-TTF$(CF_3)_2(CO_2Me)_2$ (**4bc**)	1.744(4) 1.742(4)	1.734(4) 1.732(4)	–0.6% –0.6%	this work
H, CN (**1a**)	1.760(7)	1.751(6)	−0.5%	[9]
H, CF_3 (**1c**)	1.765(2)	1.737(2)	−1.6%	[17]

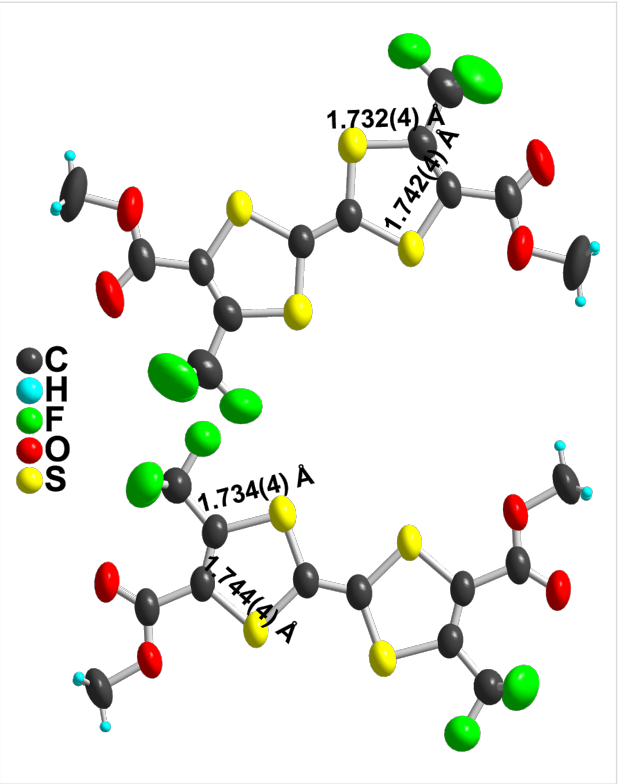

Figure 5: View of the two crystallographically independent **4bc** molecules. Thermal ellipsoids are shown at the 50% probability level.

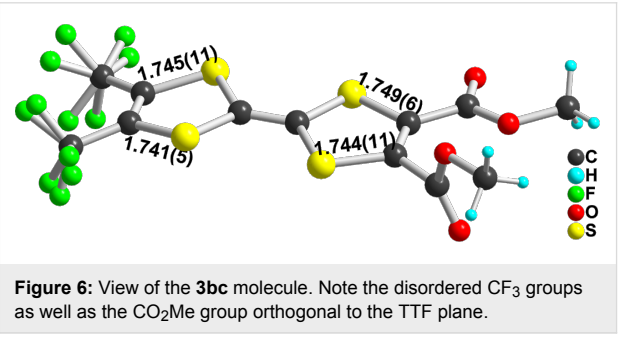

Figure 6: View of the **3bc** molecule. Note the disordered CF_3 groups as well as the CO_2Me group orthogonal to the TTF plane.

above. Furthermore, the two ester groups are not coplanar, one of them lies flat with the TTF core while the other one is almost perpendicular.

Charge-transfer complex and radical cation salt

The relatively low oxidation potential of the mono(trifluoromethyl) derivative **1c** (+0.21 V vs Fc^+/Fc) prompted us to investigate the formation of cation radical salts upon chemical or electrochemical oxidation of **1c**. Indeed, treatment of a solution of **1c** with TCNQ afforded black, crystalline elongated plates which were analyzed to be a 2:1 complex, i.e., (**1c**)$_2$(TCNQ). Electrocrystallization experiments were conducted with **1c** as well as **2cc** with a variety of anions, be they linear such as $AuBr_2^-$, I_3^-, ICl_2^-, tetrahedral (ReO_4^-, $InBr_4^-$) or octahedral (AsF_6^-). In most cases however, the electrochemically generated salts were extremely soluble, a consequence of the presence of the CF_3 groups and there was no crystal growth on the anode. However, with **1c** as electroactive donor molecule and (n-Bu_4N)($FeCl_4$) as electrolyte, layering of the CH_2Cl_2 solutions after electrolysis with pentane afforded crystals of a 1:1 phase formulated as (**1c**)($FeCl_4$).

(**1c**)$_2$(TCNQ) crystallizes in the monoclinic system, space group $P2_1/c$. One TCNQ molecule located on an inversion center and the EDT-TTF-CF_3 molecule in general position in the unit cell generate molecular triads (**1c**)(TCNQ)(**1c**) which stack along the b axis (Figure 7).

The degree of charge-transfer within this system can be anticipated to be close to zero from the comparison of the redox potentials of EDT-TTF-CF_3 ($E_{ox}^{1/2}$ = 0.21 V vs Fc^+/Fc) and TCNQ ($E_{red}^{1/2}$ = −0.23 V vs Fc^+/Fc, 0.17 V vs SCE) [43]. This is also confirmed from the intramolecular bond lengths (Table 5) within the central C_2S_4 core of the donor molecule, close to those observed in neutral EDT-TTF-CF_3 (**2**) itself. The geometry of TCNQ can also give another evaluation of the degree of charge transfer. Based on the large number of reported TCNQ salts, three different correlations between the charge of the molecule and the bond lengths have been reported [44-46]. Applying those three correlations to the TCNQ bond lengths in (**1c**)$_2$(TCNQ), averaged in D_{2h} symmetry, gives calculated charges of −0.08, +0.11 and −0.16, confirming that we are here in presence of a neutral charge-transfer complex rather than a charge-transfer salt.

Note also that this donor–acceptor interaction leads to a strong planarization of the dithiole rings of **1c** in (**1c**)$_2$(TCNQ) with folding angles along the S···S hinge of the two dithiole rings amounting now to 10.13(17)° and 1.90(16)° on the dithioethylene and CF_3 sides, respectively. By comparison, in the neutral donor molecule **1c**, the folding angles amount to 20.59(5) and 19.00(5)° respectively [31]. Such π–π interactions have been shown to derive from quadrupolar interactions between the π systems of both donor and acceptor moieties [47], and their geometrical characteristics to favor the strongest electrostatic interactions between the most electron-rich and electron-poor regions of both partners. In that respect, it appears here that the TCNQ acceptor essentially overlaps with the dithiole ring bearing the dithioethylene substituent, a likely consequence of the electron-withdrawing effect of the CF_3 group on the other dithiole ring (Figure 8).

In the 1:1 salt of EDT-TTF-CF_3 (**1c**) with $FeCl_4^-$, that is (**1c**$^{+\bullet}$)($FeCl_4^-$), oxidation to the radical cation state strongly

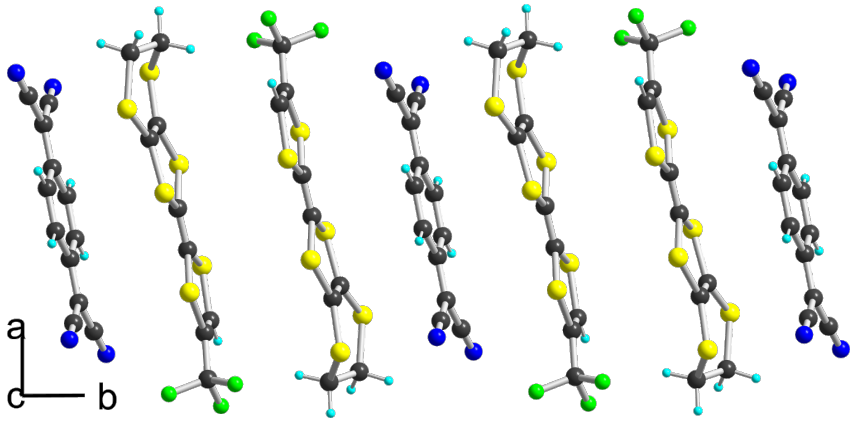

Figure 7: A view of the alternated stacks along the *b* axis in (**1c**)$_2$(TCNQ).

Table 5: Structural characteristics of the C_2S_4 central core in EDT-TTF-CF_3 (**1c**) derivatives. ρ is the charge of **1c** in the different combinations. Bonds *a* (C=C) and *b*, *b*′, *c*, *c*′ ($C_{central}$–S) are identified in the scheme below.

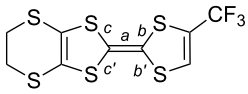

	ρ	*a* (Å)	*b* (Å)	*b*′ (Å)	*c* (Å)	*c*′ (Å)	references
1c	0	1.348(3)	1.755(2)	1.758(2)	1.759(2)	1.759(2)	[17]
(**1c**)$_2$TCNQ	≈0	1.336(4)	1.756(15)	1.763(6)	1.756(6)	1.755(15)	this work
(**1c**)($FeCl_4$)	≈1	1.382(6)	1.727(4)	1.733(4)	1.723(4)	1.708(4)	this work

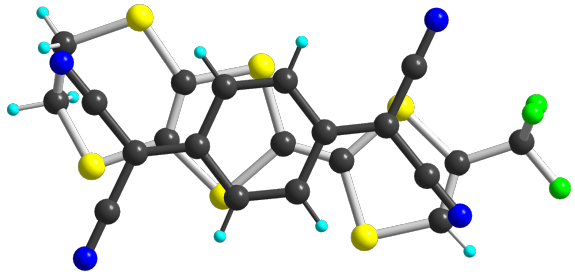

Figure 8: Detail of the overlap between donor and acceptor molecules in (**1c**)$_2$(TCNQ).

affects the central C_2S_4 core of the donor (Table 4) with a lengthening of the C=C central double bond *a*, and an associated shortening of the $C_{central}$–S bonds *b*, *b*′, *c*, *c*′). Note that this effect is stronger on the (*c*, *c*′) $C_{central}$–S bonds of the most electron-rich dithiole ring bearing the dithioethylene substituent.

In the solid state (Figure 9), the molecules are separated from each other by the $FeCl_4^-$ anions in the (*b*,*c*) plane. Along the *a* axis, they interact only laterally with long S···S intermolecular (>3.74 Å) into uniform spin chains. This solid-state arrangement is reminiscent of that observed with the analogous nitrile substituted EDT-TTF, that is EDT-TTF-CN, in the similar 1:1 (EDT-TTF-$CN^{+\bullet}$)($FeBr_4^-$) salt [9], demonstrating that the CF_3 moiety does not play here a crucial role in the solid state organization. Note that both charge transfer complex (**2**)$_2$(TCNQ) and cation radical salt (**2**)($FeCl_4$) are expected to behave as insulators, because of zero charge transfer in the former and full charge-transfer in the latter. We were not able to determine the magnetic response of the $FeCl_4^-$ salt as the crystals are polluted with the starting electrolyte, due to the precipitation technique used to recover these highly soluble salts.

Conclusion

Compared with other EWG such as –CN or –CO_2Me, the CF_3 substituent plays on the TTF electroactive core a peculiar role. From an electrochemical point of view, comparison of the relative role of the CN, CO_2Me and CF_3 EWG shows that, the electron-withdrawing nature of the CF_3 moiety is intermediate between that of the CN and the CO_2Me ones. On the other hand, the structural distortions introduced on the dithiole ring upon substitution with the CN and CO_2Me (−M) EWG are not offset by the competing CF_3 group, confirming its much weaker mesomeric effect on the conjugated dithiole core. Optical prop-

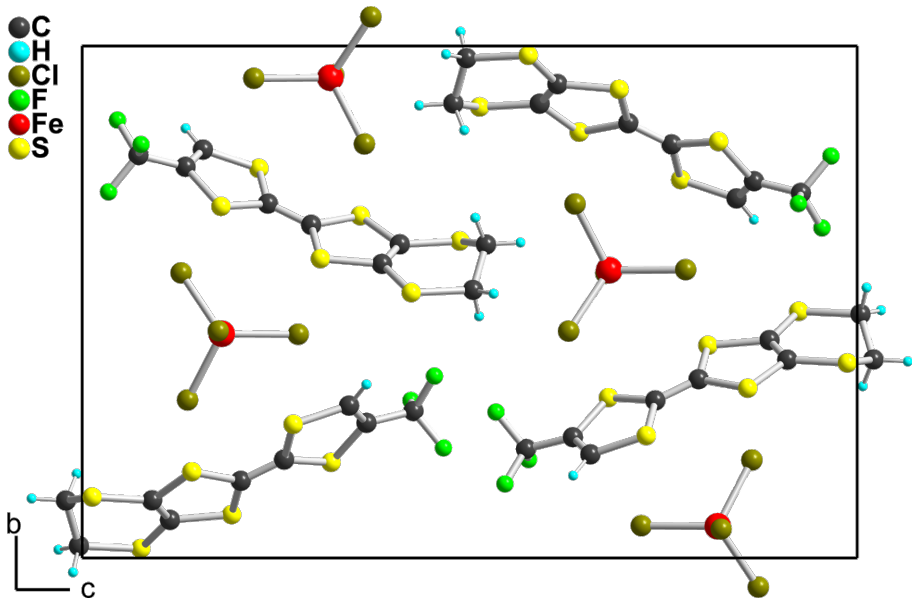

Figure 9: Projection view along the *a* axis of the unit cell of (**1c**$^{+\bullet}$)($FeCl_4^-$).

erties and theoretical calculations have shown that the HOMO–LUMO gap is not much modified in the CF_3-substituted molecules, in sharp contrast with those TTF derivatives with CN or CO_2Me EWG. In the latter indeed, the large stabilization of the LUMO localized on the EWG leads to a strongly decreased HOMO–LUMO gap associated with the well known dark color of these derivatives. Despite relatively high oxidation potentials, these donor molecules with CF_3 EWG can be involved in charge transfer complexes or cation radical salts, as reported here for the CF_3-substituted EDT-TTF donor molecule, in its 2:1 neutral CT complex with TCNQ, (**1c**)$_2$(TCNQ) or its cation radical salt with $FeCl_4^-$. The high solubility brought by the trifluoromethyl substituent strongly limits the isolation of such salts by crystallization.

Experimental

General information

Commercially available reagents were used without further purification. Solvents were distilled under Ar. THF and Et_2O were dried over KOH before distillation from Na/benzophenone. CH_3CN and CH_2Cl_2 were distilled over P_2O_5 and MeOH over Mg/I_2. Column chromatography was performed on silica gel. ^1H, ^{13}C and ^{19}F NMR spectra were obtained on a Bruker Avance DRX500 spectrometer at 500.04 MHz for ^1H, 470.28 MHz for ^{19}F and 125.75 MHz for ^{13}C. Chemical shifts were recorded in parts per million (ppm) downfield from tetramethylsilane (TMS). Coupling constants (*J*) are reported in Hz and refer to apparent peak multiplications. The abbreviations s and q stand for singlet and quartet. Elemental analyses were performed at the Service de Microanalyses, Institut de Chimie des Substances Naturelles (ISCN), Gif/Yvette (France). MALDI-TOF MS spectra were obtained from a Bruker Biflex-IIITM equipped with a 337 nm laser.

Syntheses

Preparation of EDT-TTF($CONH_2$)(CF_3) (7): EDT-TTF(CO_2Me)(CF_3) (**2bc**) [17] (0.2 g, 0.47 mmol) was added to a MeOH solution (20 mL) saturated with gaseous NH_3. The resulting suspension was stirred for 90 min and filtered. The solid was recrystallized from CH_3CN to afford **7** as red–burgundy needles (120 mg, 0.3 mmol). Yield: 63%; mp dec. 150–160 °C; ^1H NMR (d_6-acetone) δ 3.44 (s, 4H), 7.48 ppm (d, 2H); ^{19}F NMR ($CDCl_3$) δ −58.53 (s) ppm. Anal. calcd for $C_{10}H_6F_3NOS_6$: C, 29.62; H, 1.49; N, 3.45; found: C, 29.57; H, 1.34; N, 3.39; MS *m*/*z*: calcd, 404.87, found, 404.90.

Preparation of EDT-TTF(CN)(CF_3) (2ac): A solution of EDT-TTF($CONH_2$)(CF_3) (**7**) (0.3 g, 0.74 mmol) and $POCl_3$ (0.2 mL, 2.15 mmol) in sulfolane (4 mL) is heated under stirring at 110 °C for 5 h. After cooling, the solution is poured in 100 mL of iced water and filtered. The dried precipitate is purified twice by column chromatography on silica gel with dichloromethane elution. Crystals were obtained by diffusion of pentane into a concentrated dichloromethane solution (0.17 g, 0.044 mmol). Yield: 60%; mp 176 °C (CH_2Cl_2/hexane); ^1H NMR ($CDCl_3$) δ 3.32 (s, 4H) ppm; ^{13}C NMR ($CDCl_3$) δ 30.10 (s), 104.58 (s), 107.86 (q, J^3_{CF} = 3.84 Hz), 108.47 (s), 113.97 (s), 114.20 (s), 118.81 (q, J^1_{CF} = 274.47 Hz), 118.30 (s), 138.43 (q, J^2_{CF} = 36.47 Hz) ppm; ^{19}F NMR ($CDCl_3$) δ −59.20 (s) ppm; Anal. calcd for $C_{10}H_4F_3NS_6$: C, 30.99; H, 1.04; N,

3.61; found: C, 30.82; H, 1.01; N, 3.49; MS *m*/*z*: calcd, 386.86, found, 386.69.

Preparation of *o*-TTF(CO_2Me)$_2$(CF_3)$_2$ (3bc): A solution of bis(trifluoromethyl)-1,3-dithiole-2-thione (**9cc**) (2 g, 7 mmol) and bis(carbomethoxy)-1,3-dithiole-2-thione (**10bb**) (6 g, 24 mmol) in $P(OMe)_3$ (15 mL) is heated at 110 °C for 16 h. After evaporation of the solvent under vacuum, the crude residue is purified twice by chromatography on silica gel with pentane/dichloromethane elution (50:50). The red fraction was collected and crystallized from CH_2Cl_2/hexane (0.51 g, 1.1 mmol). Yield: 15%; mp 75°C; ^{1}H NMR ($CDCl_3$) δ 3.86 (s, 6H) ppm; ^{13}C NMR ($CDCl_3$) δ 54.04 (s), 104.74 (s), 114.74 (s), 119.21 (q, J^1_{CF} = 276 Hz) (s), 129.05 (q, J^2_{CF} = 42 Hz), 132.41 (s), 159.83 (s) ppm; ^{19}F NMR ($CDCl_3$) δ −56.25 (s) ppm; Anal. calcd for $C_{12}H_6F_6O_4S_4$: C, 31.58; H, 1.33; found: C, 31.79; H, 1.14; MS *m*/*z*: calcd, 455.91; found, 455.6.

Preparation of (1c)$_2$(TCNQ): EDT-TTF-CH_3 (**1c**) (20 mg, 5.5×10^{-5} mol) and TCNQ (5.6 mg, 2.75×10^{-5} mol) were dissolved in hot CH_3CN (2 mL) and the mixture slowly cooled to room temperature. No crystal formation was observed at this stage. The solution is allowed to stand in a fridge for 15 days to produce thin needles which were filtered and recrystallized by slow evaporation in CH_3CN to give the title compound as elongated black plates (20 mg, 78%); Anal. calcd for $C_{30}H_{14}F_6N_4S_{12}$: C, 38.78; H, 1.52; N, 6.03; found: C, 38.61; H, 1.51; N, 6.08; IR ν_{CN} (KBr): 2222 cm^{-1}.

Preparation of (1c)(FeCl$_4$): The electrocrystallization of **1c** (11 mg) in a CH_2Cl_2 solution (15 mL) of $(Et_4N)(FeCl_4)$ (208 mg) as electrolyte did not afford any crystals. Further layering of the solution recovered from the anodic compartment with pentane afforded dark crystals of a 1:1 phase formulated as (**1c**)$(FeCl_4)$, polluted with the yellow crystals of $(Et_4N)(FeCl_4)$.

Crystallography

Single crystals were mounted on the top of a thin glass fiber. Data were collected either on a Stoe-IPDS at room temperature or on a Nonius KappaCCD diffractometer at 150 K, both equipped with graphite-monochromated Mo Kα radiation

Table 6: Crystallographic data.

compound	**2ac**	**2bc**	**3bc**	**4bc**	(**1c**)$_2$TCNQ	(**1c**)FeCl$_4$
formula	$C_{10}H_4F_3NS_6$	$C_{11}H_7F_3O_3S_6$	$C_{12}H_6F_6O_4S_4$	$C_{12}H_6F_6O_4S_4$	$C_{15}H_7F_3N_2S_6$	$C_9H_5Cl_4F_3FeS_6$
fw	387.50	420.53	456.41	456.41	464.59	560.14
cryst syst	monoclinic	triclinic	monoclinic	orthorhombic	monoclinic	orthorhombic
space group	$P2_1$	$P\bar{1}$	$P2_1/a$	$Pbam$	$P2_1/c$	$P2_12_12_1$
a/Å	5.0849(5)	5.1515(12)	7.4209(8)	28.000(3)	13.2146(15)	5.9348(5)
b/Å	10.9285(12)	11.998(2)	17.0659(17)	8.7129(9)	11.1448(8)	14.4165(15)
c/Å	12.7619(13)	12.974(3)	13.5707(15)	7.2091(7)	13.1662(15)	21.785(2)
α/deg	90	103.96(3)	90	90	90	90
β/deg	97.741(12)	90.02(3)	97.834(13)	90	106.997(13)	90
γ/deg	90	90.45(3)	90	90	90	90
V/Å^3	702.72(13)	778.2(3)	1702.6(3)	1758.8(3)	1854.3(3)	1863.9(3)
Z	2	2	4	4	4	4
d_{calc}/Mg m^{-3}	1.831	1.795	1.781	1.724	1.664	1.996
diffractometer	Stoe-IPDS	Stoe-IPDS	Stoe-IPDS	Stoe-IPDS	Stoe-IPDS	KappaCCD
temp/K	293(2)	293(2)	293(2)	293(2)	293(2)	150(2)
μ/mm^{-1}	0.991	0.910	0.636	0.616	0.768	2.072
θ-range/deg	2.45–25.75	1.75−25.94	1.85–25.85	2.45−25.98	2.44−25.83	2.34−26.02
measured refls	6805	7498	12937	10664	13683	38263
indep. refls	2682	2778	3263	1861	3518	3675
R_{int}	0.0334	0.126	0.0639	0.0815	0.065	0.109
I > 2σ(I) refls	1986	989	2161	833	2190	2932
abs. corr.	multi-scan	none	gaussian	multi-scan	multi-scan	multi-scan
T_{max}, T_{min}	0.786, 0.851	—	0.782, 0.901	0.937, 0.927	0.912, 0.822	0.769,0.733
refined params	199	199	289	151	236	228
R(*F*), *I*>2σ(*I*)	0.0327	0.0442	0.0320	0.0342	0.0339	0.0410
wR(F^2), all	0.0765	0.0909	0.0783	0.0654	0.0814	0.0538
res. Δρ (e Å^{-3})	+0.297, −0.357	+0.29, −0.28	0.211, −0.166	+0.18, −0.16	+0.32, −0.20	+0.41, −0.42

(λ = 0.71073 Å). Structures were solved by direct methods (SHELXS-97) and refined (SHELXL-97) [48] by full-matrix least-squares methods, as implemented in the WinGX software package [49]. Absorption corrections were applied. Hydrogen atoms were introduced at calculated positions (riding model), included in structure factor calculations, and not refined. Crystallographic data are summarized in Table 6.

Computational details

DFT [50,51] calculations were performed with the hybrid Becke-3 parameter exchange functional [52-54] and the Lee–Yang–Parr nonlocal correlation functional [55] (B3LYP) implemented in the Gaussian 03 (revision D.02) program suite [56], using the 6-31G(d) basis set and a quadratically convergent self-consistent field procedure with the default convergence criteria implemented in the program. The X-ray diffraction data of model compounds were used as a starting point for initial geometry optimization calculations. Final geometries are given in Supporting Information File 1. Representation of frontier orbitals included in Figure 2 were generated with Molekel 4.3 [57]. TD-DFT calculations were performed at the B3LYP/6-311G** level of theory, on the previously converged geometries.

Supporting Information

Supporting Information File 1

Optimized geometries of the model molecules TTF, TTF–CN, TTF–CF_3 and TTF–CO_2Me and results of the TD-DFT calculations.
[http://www.beilstein-journals.org/bjoc/content/supplementary/1860-5397-11-73-S1.pdf]

Supporting Information File 2

X-ray data for the reported structures.
[http://www.beilstein-journals.org/bjoc/content/supplementary/1860-5397-11-73-S2.cif]

Acknowledgements

Financial support from Ministry of Higher Education and Research (France) through a Ph.D. grant to O. J. is acknowledged. The authors thank GENCI (France) for allocation of computing time under project c2015085032.

References

1. Batail, P., Ed. Molecular Conductors. *Chem. Rev.* **2004,** *104,* 4887–5781.
2. Hartzler, H. D. *J. Am. Chem. Soc.* **1973,** *95,* 4379–4387. doi:10.1021/ja00794a039
3. Scott, B. A.; Kaufman, F. B.; Engler, E. M. *J. Am. Chem. Soc.* **1976,** *98,* 4342–4344. doi:10.1021/ja00430a070
4. Yoneda, S.; Kawase, T.; Inabe, M.; Yoshida, Z. *J. Org. Chem.* **1978,** *43,* 595–598. doi:10.1021/jo00398a015
5. Jørgensen, M.; Bechgaard, K. *Synthesis* **1989,** 207–208. doi:10.1055/s-1989-27200
6. Imakubo, T.; Sawa, H.; Kato, R. *Synth. Met.* **1995,** *73,* 117–122. doi:10.1016/0379-6779(95)03322-X
7. Fourmigué, M.; Batail, P. *Chem. Rev.* **2004,** *104,* 5379–5418. doi:10.1021/cr030645s
8. Metrangolo, P.; Resnati, G., Eds. *Halogen Bonding: Fundamentals and Applications;* Structure and Bonding, Vol. 126; Springer: Berlin, Germany, 2007. doi:10.1007/978-3-540-74330-9
9. Fourmigué, M. *Curr. Opin. Solid State Mater. Sci.* **2009,** *13,* 36–45. doi:10.1016/j.cossms.2009.05.001
10. Batsanov, A. S.; Bryce, M. R.; Heaton, J. N.; Moore, A. J.; Skabara, P. J.; Howard, J. A. K.; Orti, E.; Viruela, P. M.; Viruela, R. *J. Mater. Chem.* **1995,** *5,* 1689–1696. doi:10.1039/jm9950501689
11. Devic, T.; Bertran, J. N.; Domercq, B.; Canadell, E.; Avarvari, N.; Auban-Senzier, P.; Fourmigué, M. *New J. Chem.* **2001,** *25,* 1418–1424. doi:10.1039/b104640n
12. Cooke, G.; Powell, A. K.; Heath, S. L. *Synthesis* **1995,** 1411–1414. doi:10.1055/s-1995-4124
13. Zhong, Z. J.; You, X.-Z.; Yu, K. *Acta Crystallogr., Sect. C* **1996,** *52,* 449–451. doi:10.1107/S0108270195009942
14. Terkia-Derdra, N.; Andreu, R.; Sallé, M.; Levillain, E.; Orduna, J.; Garin, J.; Orti, E.; Viruela, R.; Pou-Amerigo, R.; Sahraoui, B.; Gorgues, A.; Favard, J.-F.; Riou, A. *Chem. – Eur. J.* **2000,** *6,* 1199–1213. doi:10.1002/(SICI)1521-3765(20000403)6:7<1199::AID-CHEM1199>3.3.CO;2-7
15. Heuzé, K.; Fourmigué, M.; Batail, P. *J. Mater. Chem.* **1999,** *9,* 2373–2379. doi:10.1039/a902852h
16. Baudron, S. A.; Avarvari, N.; Canadell, E.; Auban-Senzier, P.; Batail, P. *Chem. – Eur. J.* **2004,** *10,* 4498–4511. doi:10.1002/chem.200400153
17. Baudron, S. A.; Avarvari, N.; Batail, P.; Coulon, C.; Clérac, R.; Canadell, E.; Auban-Senzier, P. *J. Am. Chem. Soc.* **2003,** *125,* 11583–11590. doi:10.1021/ja0356129
18. Moore, A. J.; Bryce, M. R.; Batsanov, A. S.; Heaton, J. N.; Lehmann, C. W.; Howard, J. A. K.; Robertson, N.; Underhill, A. E.; Perepichka, I. F. *J. Mater. Chem.* **1998,** *8,* 1541–1550. doi:10.1039/a802037j
19. Batsanov, A. S.; Bryce, M. R.; Cooke, G.; Heaton, J. N.; Howard, J. A. K. *J. Chem. Soc., Chem. Commun.* **1993,** 1701–1702. doi:10.1039/c39930001701
20. Batsanov, A. S.; Bryce, M. R.; Cooke, G.; Dhindsa, A. S.; Heaton, J. N.; Howard, J. A. K.; Moore, A. J.; Petty, M. C. *Chem. Mater.* **1994,** *6,* 1419–1425. doi:10.1021/cm00044a046
21. Heuzé, K.; Fourmigué, M.; Batail, P.; Canadell, E.; Auban-Senzier, P. *Chem. – Eur. J.* **1999,** *5,* 2971–2976. doi:10.1002/(SICI)1521-3765(19991001)5:10<2971::AID-CHEM2971>3.0.CO;2-S
22. Heuzé, K.; Mézière, C.; Fourmigué, M.; Batail, P.; Coulon, C.; Canadell, E.; Auban-Senzier, P.; Jérome, D. *Chem. Mater.* **2000,** *12,* 1898–1904. doi:10.1021/cm000143k
23. Heuzé, K.; Fourmigué, M.; Batail, P.; Coulon, C.; Clérac, R.; Canadell, E.; Auban-Senzier, P.; Ravy, S.; Jérome, D. *Adv. Mater.* **2003,** *15,* 1251–1253. doi:10.1002/adma.200305247

24. Devic, T.; Evain, M.; Moëlo, Y.; Canadell, E.; Senzier, P.; Fourmigué, M.; Batail, P. *J. Am. Chem. Soc.* **2003,** *125,* 3295–3301. doi:10.1021/ja0290431
25. Nishijo, J.; Ogura, E.; Yamaura, J.; Miyazaki, A.; Enoki, T.; Takano, T.; Kuwatani, Y.; Iyoda, M. *Solid State Commun.* **2000,** *116,* 661–664. doi:10.1016/S0038-1098(00)00406-3
26. Devic, T.; Domercq, B.; Auban-Senzier, P.; Molinié, P.; Fourmigué, M. *Eur. J. Inorg. Chem.* **2002,** 2844–2849. doi:10.1002/1099-0682(200211)2002:11<2844::AID-EJIC2844>3.0.CO;2-J
27. Domercq, B.; Devic, T.; Fourmigué, M.; Auban-Senzier, P.; Canadell, E. *J. Mater. Chem.* **2001,** *11,* 1570–1575. doi:10.1039/b100103p
28. Bryce, M. R.; Moore, A. J.; Batsanov, A. S.; Howard, J. A. K.; Petty, M. C.; Williams, G.; Rotello, V.; Cuello, A. *J. Mater. Chem.* **1999,** *9,* 2973–2978. doi:10.1039/a905364f
29. Dhindsa, A. S.; Baydal, J. P.; Bryce, M. R.; Petty, M. C.; Moore, A. J.; Lvov, Y. M. *J. Chem. Soc., Chem. Commun.* **1990,** 970–972. doi:10.1039/c39900000970
30. Dsindsa, A. S.; Song, Y. P.; Baydal, J. P.; Bryce, M. R.; L'vov, Y. M.; Petty, M. C.; Yarwood, J. *Chem. Mater.* **1992,** *4,* 724–728. doi:10.1021/cm00021a042
31. Jeannin, O.; Fourmigué, M. *Chem. – Eur. J.* **2006,** *12,* 2994–3005. doi:10.1002/chem.200501078
32. Dautel, O. J.; Fourmigué, M.; Canadell, E. *Chem. – Eur. J.* **2001,** *7,* 2635–2643. doi:10.1002/1521-3765(20010618)7:12<2635::AID-CHEM26350>3.0.CO;2-7
33. Dautel, O. J.; Fourmigué, M. *J. Org. Chem.* **2000,** *65,* 6479–6486. doi:10.1021/jo000518l
34. Garreau, B.; De Montauzon, D.; Cassoux, P.; Legros, J.-P.; Fabre, J.-M.; Saoud, K.; Chakroune, S. *New J. Chem.* **1995,** *19,* 161–171.
35. Fourmigué, M.; Krebs, F. C.; Larsen, J. *Synthesis* **1993,** 509–512. doi:10.1055/s-1993-25894
36. Garín, J.; Orduna, J.; Savirón, M.; Bryce, M. R.; Moore, A. J.; Morisson, V. *Tetrahedron* **1996,** *52,* 11063–11074. doi:10.1016/0040-4020(96)00624-2
37. Papavassiliou, G. C.; Zambounis, J. S.; Mousdis, G. A.; Gionis, V.; Yiannopoulos, S. Y. *Mol. Cryst. Liq. Cryst.* **1988,** *156,* 269–276. doi:10.1080/10441859.1988.11009204
38. Schukat, G.; Richter, A. M.; Fanghänel, E. *Sulfur Rep.* **1987,** *7,* 155–231. doi:10.1080/01961778708082503
39. Values of s_m were taken from O. Exner in *Correlation Analysis in Chemistry*, N. B. Chapman and J. Shorter Eds, Plenum Press, New York, 1978.
40. Carey, F. A.; Sundberg, R. J. *Advanced Organic Chemistry, Part A: Structure and Mechanisms;* Plenum Press: New York, NY, U.S.A., 1984. doi:10.1007/978-1-4757-1143-1
41. The following values were used: MeO_2C: +0.35; F_3C: +0.46; NC: +0.62; $S(CH_2)_2S$: +0.28.
42. Khodorkovsky, V.; Edzina, A.; Neilands, O. *J. Mol. Electron.* **1989,** *5,* 33–36.
43. Wheland, R. C.; Gilson, J. L. *J. Am. Chem. Soc.* **1976,** *98,* 3916–3925. doi:10.1021/ja00429a030
44. Flandrois, S.; Chasseau, D. *Acta Crystallogr., Sect. B* **1977,** *33,* 2744–2750. doi:10.1107/S0567740877009406
45. Kistenmacher, T. J.; Emge, T. J.; Bloch, A. N.; Cowan, D. O. *Acta Crystallogr., Sect. B* **1982,** *38,* 1193–1199. doi:10.1107/S0567740882005275
46. Umland, T. C.; Allie, S.; Kulhman, T.; Coppens, P. *J. Phys. Chem.* **1988,** *92,* 6456–6460. doi:10.1021/j100333a053
47. Hunter, C. A.; Saunders, J. K. M. *J. Am. Chem. Soc.* **1990,** *112,* 5525–5534. doi:10.1021/ja00170a016
48. *SHELX97 - Programs for Crystal Structure Analysis,* Release 97-2; G. M. Sheldrick, 1998.
49. Farrugia, L. J. *J. Appl. Crystallogr.* **1999,** *32,* 837. doi:10.1107/S0021889899006020
50. Hohenberg, P.; Kohn, W. *Phys. Rev. B* **1964,** *136,* 864–871. doi:10.1103/PhysRev.136.B864
51. Parr, R. G.; Yang, W. *Density-Functional Theory of Atoms and Molecules;* Oxford University Press: Oxford, United Kingdom, 1989.
52. Becke, A. D. *Phys. Rev. A* **1988,** *38,* 3098–3100. doi:10.1103/PhysRevA.38.3098
53. Becke, A. D. *J. Chem. Phys.* **1993,** *98,* 1372–1377. doi:10.1063/1.464304
54. Becke, A. D. *J. Chem. Phys.* **1993,** *98,* 5648–5652. doi:10.1063/1.464913
55. Lee, C.; Yang, W.; Parr, R. G. *Phys. Rev. B* **1988,** *37,* 785–789. doi:10.1103/PhysRevB.37.785
56. *Gaussian 03,* Revision D.02; Gaussian, Inc.: Wallingford, CT, 2004.
57. *MOLEKEL,* 4.3; Swiss Center for Scientific Computing: Manno, Switzerland, 2000.

License and Terms

BEILSTEIN JOURNAL OF ORGANIC CHEMISTRY

Copper ion salts of arylthiotetrathiafulvalenes: synthesis, structure diversity and magnetic properties

Longfei Ma, Jibin Sun, Xiaofeng Lu, Shangxi Zhang, Hui Qi, Lei Liu, Yongliang Shao and Xiangfeng Shao*

Full Research Paper

Open Access

Address:
State Key Laboratory of Applied Organic Chemistry, Lanzhou University, Tianshui Southern Road 222, Lanzhou 730000, Gansu Province, China

Email:
Xiangfeng Shao* - shaoxf@lzu.edu.cn

* Corresponding author

Keywords:
antiferromagnetic interaction; arylthio-substituted tetrathiafulvalenes; charge-transfer; crystal structure; magnetic property

Beilstein J. Org. Chem. **2015,** *11,* 850–859.
doi:10.3762/bjoc.11.95

Received: 29 January 2015
Accepted: 15 April 2015
Published: 20 May 2015

This article is part of the Thematic Series "Tetrathiafulvalene chemistry".

Guest Editor: P. J. Skabara

Abstract

The combination of $CuBr_2$ and arylthio-substituted tetrathiafulvalene derivatives (**1**–**7**) results in a series of charge-transfer (CT) complexes. Crystallographic studies indicate that the anions in the complexes, which are derived from $CuBr_2$, show diverse configurations including linear $[Cu(I)Br_2]^-$, tetrahedral $[Cu(II)Br_4]^{2-}$, planar $[Cu(II)_2Br_6]^{2-}$, and coexistence of planar $[Cu(II)Br_4]^{2-}$ and tetrahedral $[Cu(II)Br_3]^-$ ions. On the other hand, the TTFs show either radical cation or dication states that depend on their redox potentials. The central TTF framework on most of TTFs is nearly planar despite the charge on them, whereas the two dithiole rings on molecule **4** in complex **4**·$CuBr_4$ are significantly twisted with a dihedral angle of 38.3°. The magnetic properties of the complexes were elucidated. The temperature-dependent magnetic susceptibility of complex **5**·Cu_2Br_6 shows the singlet–triplet transition with coupling constant $J = -248$ K, and that of **3**·$(CuBr_4)_{0.5}$·$CuBr_3$·THF shows the abrupt change at 270 K caused by the modulation of intermolecular interactions. The thermo variation of magnetic susceptibility for the other complexes follows the Curie–Weiss law, indicating the weak antiferromagnetic interaction at low temperature.

Introduction

Since firstly synthesized in 1970s [1], tetrathiafulvalene (TTF) and its derivatives have been intensively studied to explore functional organic materials [2]. Inspired by the discovery of highly conducting charge-transfer (CT) complex TTF·TCNQ [3] and the first organic superconductor $(TMTSF)_2X$ [4], the chemical modifications on TTF are traditionally aimed at the creation of organic conductors with various electronic ground states [5-10]. It has been well-defined that a subtle modification of TTF would result in a significant effect on the properties of their complexes [5-10]. For example, the complexes of EDO-TTF (4,5-ethylenedioxy-TTF) [11-15] and MeEDO-TTF (4,5-ethylenedioxy-4'-methyl-TTF) [16-19] show the distinct

difference on electrical transport properties. Meanwhile, the modification on TTF, particularly introducing aromatic substituents onto the TTF core, is one of the key strategies to explore functional molecular materials. The resulting TTFs have been employed as electrochemically active units in supramolecular systems and/or molecular devices, which has been summarized in many reviews [20-32]. However, the incorporation of aryl groups onto the TTF core through sulfur bridges, which resulted in arylthio-substituted TTFs (denoted as Ar-S-TTF), has been scarcely reported due to synthetic difficulties [33-36]. Recently, we have disclosed a facile approach toward Ar-S-TTFs [37]. Crystallographic investigations indicate that Ar-S-TTFs show various molecular geometries and packing structures depending on the nature of the peripheral aryls [38,39].

The TTF-based conducting materials are mainly produced as radical cation salts by electrochemical oxidation and CT complexes by chemical oxidation with electron acceptors [5,6]. Most Ar-S-TTFs possess redox potentials higher than that of bis(ethylenedithio)-TTF (BEDT-TTF) [33-39]. Consequently, the complexes of Ar-S-TTFs with electron acceptors such as fullerenes [40,41] and TCNQ [42] show a neutral ground state. However, Ar-S-TTFs can be chemically oxidized by strong electron acceptors such as F_4TCNQ [42] and Keggin-type phosphomolybdic acid [43] to form CT complexes. In comparison with fullerenes and TCNQ, the inorganic salt CuX_2 (X = Cl, Br) is a strong oxidant and has been used to oxidize the TTFs to form organic conductors with diverse electronic ground states [44-54]. Herein, we report the synthesis, structure, and magnetic properties of the complexes of Ar-S-TTFs (**1**–**7**, Scheme 1) with $CuBr_2$. These complexes show diverse structures and properties related to the oxidation state as well as the molecular geometries of TTFs.

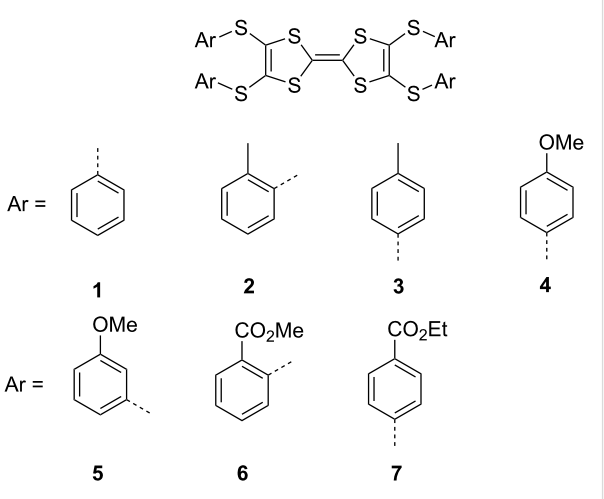

Scheme 1: Chemical structures of arylthio-substituted tetrathiafulvalenes (**1**–**7**).

Results and Discussion

Synthesis

The donor molecules (**1**–**7**, Scheme 1) were synthesized according to our previous report [37,38], and their electrochemical activities as well as the crystal structures have been fully elucidated [38,39]. Since the redox potentials of TTFs are very important in the formation of complexes, particularly on the charge-transfer degree, the first ($E_{1/2}^1$) and the second ($E_{1/2}^2$) redox potentials of **1**–**7** are summarized in Table 1. As reported in the following section, TTFs **1**–**5** have the $E_{1/2}^2 < 0.90$ V and form the dicationic salts by reaction with $CuBr_2$. On the contrary, the $E_{1/2}^2$ values of **6** and **7** are higher than 0.90 V, and these two donor molecules form the radical cation salts by reaction with $CuBr_2$.

Table 1: Electrochemical data of TTFs in this report.[a]

	1	**2**	**3**	**4**	**5**	**6**	**7**
$E_{1/2}^1$ [V]	0.56	0.52	0.51	0.48	0.56	0.62	0.66
$E_{1/2}^2$ [V]	0.89	0.85	0.85	0.83	0.88	0.95	0.96
ΔE [V][b]	0.33	0.33	0.34	0.35	0.32	0.33	0.30

[a]See reference [38], and the redox potentials are recorded vs SCE; [b]$\Delta E = E_{1/2}^2 - E_{1/2}^1$.

The reaction of **1**–**7** with $CuBr_2$ was performed in the mixed solvent of tetrahydrofuran–acetonitrile (THF–CH_3CN; v/v, 1:1) at room temperature. In the low concentration ($<10^{-4}$ mol L^{-1}), a dark green solution was formed, indicating the oxidation of **1**–**7** by $CuBr_2$. When the concentration of the reaction system was increased to higher than 10^{-3} mol L^{-1}, TTFs **1**–**7** afforded the ionic salts showing the same phase as those of the corresponding single crystalline ones. The single crystalline salts were obtained by a conventional two-phase diffusion method. In a typical procedure, the $CuBr_2$ solution in CH_3CN and the solution of TTFs in THF were placed in two different chambers of an H-shape cell, respectively. After several weeks, black single crystalline salts were formed. The compositions of the salts were determined by X-ray single crystal diffraction analyses, as summarized in Table 2.

Crystal structure

The single crystals for all of the present salts were suitable for the X-ray single crystal diffraction analyses. Herein, we report the crystal structures of the typical salts (Figures 1–5), and those of the others are supplied in Supporting Information File 1. As mentioned above, the molecular geometries of Ar-S-TTF are sensitive to the environmental variations, especially the

Table 2: Preparation, composition, yield, and appearance of the salts.[a]

	TTFs		salts[b]	
	amount	composition	amount (yield)	appearance[c]
1	19 mg (0.03 mmol)	**1**·$CuBr_4$	24 mg (80%)	black needle
2	28 mg (0.04 mmol)	**2**·$CuBr_4$	39 mg (91%)	black needle
3	28 mg (0.04 mmol)	**3**·$(CuBr_4)_{0.5}$·$CuBr_3$·THF	46 mg (92%)	black block
4	23 mg (0.03 mmol)	**4**·$CuBr_4$	31 mg (91%)	black needle
5	23 mg (0.03 mmol)	**5**·Cu_2Br_6	33 mg (80%)	black block
6	26 mg (0.03 mmol)	**6**·$CuBr_2$·CH_3CN	26 mg (74%)	black block
7	28 mg (0.03 mmol)	**7**·$CuBr_2$	16 mg (47%)	black cuboid

[a]TTFs were dissolved in 4 mL of THF, and $CuBr_2$ (100 mg, dissolved in 4 mL of CH_3CN) was applied in the synthesis. [b]The compositions were determined by X-ray single crystal diffraction analyses. [c]See the photographs of the crystals in Figure S1 in Supporting Information File 1.

guest components are included in their solid-state matrix. Besides, the bond lengths and the conformation of the central TTF core are sensitive to the charge variation. The charge on TTFs can be estimated according to an empirical formula suggested by Day et al. [55], that is $\delta = (b + c) - (a + d)$. The calculated δ values and the conformation of TTFs **1**–**7** in neutral state and salts are summarized in Table 3. These results indicate that **1**–**5** have the charge of +2, whereas **6** and **7** are radical cations. The central TTF cores on the neutral TTFs show various conformations including chair, planar, and boat conformations. However, the central TTF cores of TTFs in the present salts are planar except that of **4**, where the two dithiole rings are twisted with a dihedral angle of 38.3°. In the following, we will discuss the crystal structures of these salts, including the molecular geometry of TTFs, the structure of anions, and the packing motifs.

1·$CuBr_4$ crystallizes in the orthorhombic *Pbcn* space group with half of molecule **1** and half of $CuBr_4$ crystallographically unique (Figure 1a). The central TTF core on **1** is nearly planar,

Table 3: Selected bond lengths, calculated charge, and conformations of TTFs.

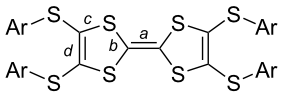

		a [Å]	*b* [Å]	*c* [Å]	*d* [Å]	δ [Å]	charge	conformation
1	neutral[a]	1.325	1.740	1.737	1.325	0.827	0	chair
	complex	1.421	1.689	1.709	1.367	0.608	+2	planar
2	neutral[a]	1.329	1.764	1.750	1.351	0.834	0	planar
	complex	1.422	1.682	1.708	1.364	0.604	+2	planar
3	neutral[a]	1.340	1.757	1.756	1.333	0.840	0	boat
	complex	1.418	1.693	1.704	1.375	0.604	+2	planar
4	neutral[a]	1.342	1.761	1.754	1.339	0.834	0	chair
	complex	1.428	1.685	1.700	1.379	0.578	+2	twist
5	neutral	–	–	–	–	–	–	–
	complex	1.429	1.693	1.710	1.379	0.595	+2	planar
6	neutral[a]	1.336	1.757	1.756	1.345	0.832	0	chair
	complex	1.382	1.716	1.746	1.336	0.744	+1	planar
7	neutral[a]	1.34	1.76	1.76	1.34	0.84	0	planar
	complex	1.39	1.71	1.74	1.35	0.71	+1	planar

[a]See reference [38].

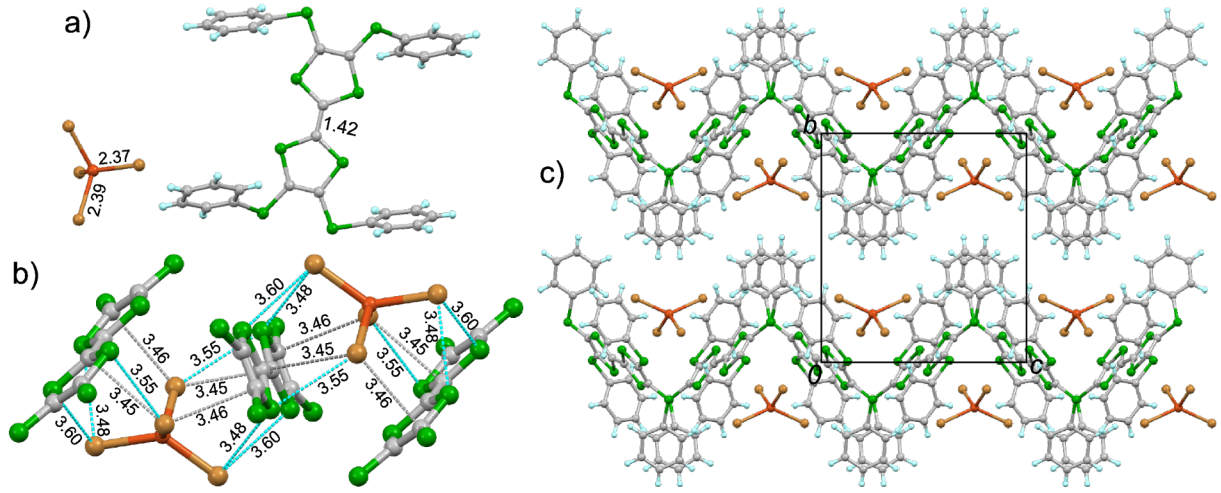

Figure 1: Crystal structure of **1**·$CuBr_4$: a) unit cell contents with the typical bond lengths shown (in Å); b) interactions between the $[Cu(II)Br_4]^{2-}$ ion and the central TTF core of **1**, where the cyan and grey dashed lines represent Br···S and Br···C contacts (Å), respectively; c) packing structure viewed along the *a*-axis.

which is different from the chair conformation in the neutral state. Moreover, the spatial alignment of peripheral phenyls is modulated (see Figure S2 in Supporting Information File 1). The calculated δ value of **1** is 0.608 in the salt, indicating it has the charge of +2 according to the criteria proposed by Day [55]. The inorganic component $CuBr_4$ takes the slightly distorted tetrahedral geometry. The Cu–Br bond lengths are 2.37 and 2.39 Å, which are close to a typical Cu(II)–Br bond length [51-53,56-58]. Thus, the $CuBr_4$ component should have the charge of −2, consistent with the dicationic state of **1**. A $[CuBr_4]^{2-}$ ion is encapsulated by two donor molecules, and there are multiple Br···S (3.48–3.60 Å) and Br···C (3.45–3.46 Å) close contacts [59] between the $[CuBr_4]^{2-}$ ion and the central TTF core of **1** (Figure 1b). Donor molecules form a zig-zag chain alignment along the *c*-axis (Figure 1c), and the $[CuBr_4]^{2-}$ ion locate at the cavity formed by **1**. The spin exchange interaction between Cu(II) on $[CuBr_4]^{2-}$ ions would take place as mediated by the π-orbitals of **1**. The crystal structure of **2**·$CuBr_4$ is reminiscent to that of **1**·$CuBr_4$ as shown in Figure S3 and Figure S4 in Supporting Information File 1.

The crystal structure of **3**·$(CuBr_4)_{0.5}$·$CuBr_3$·THF at room temperature is shown in Figure 2. This salt crystallizes in the triclinic *P*−1 space group, and the asymmetric unit contains one molecule **3**, half of $CuBr_4$, one $CuBr_3$, and one THF. The central TTF core of **3** takes the planar conformation similar to its neutral state, whereas the spatial alignment of the 4-tolyl groups is altered (Figure S6 in Supporting Information File 1). The calculated δ value of **3** in the salt is 0.604, indicating that **3** is oxidized to the dication form. The inorganic component $CuBr_4$ has a planar conformation with a Cu–Br bond length of 2.39 and 2.43 Å (Figure 1a), thus it should be dianionic. On the other hand, the oxygen atom on THF coordinates to the Cu atom on $CuBr_3$ with a Cu–O bond length of 2.08 Å, consequently $CuBr_3$ takes a distorted tetrahedral conformation. The Cu–Br bond length in $CuBr_3$ is 2.33–2.36 Å, indicating that the Cu atom in $CuBr_3$ should be Cu(II). A $[CuBr_4]^{2-}$ ion is sandwiched by two donor molecules through the Br···S (3.65 Å) and Br···C contacts (3.46–3.50 Å), thus, a D–A–D type trimer of [**3**–$CuBr_4$–**3**] is formed as shown in Figure 2b. The neighboring D–A–D trimers shift along the longitudinal axis of **3**, thus form a voidage to accommodate one [$CuBr_3$·THF] as shown in Figure 2c. There are Br···S (3.59–3.62 Å) and Br···C contacts (3.44 Å) between the $[CuBr_3]^-$ ion and molecule **3** in the D–A–D trimer. Consequently, the spin interaction between Cu(II) is expected, which would be mediated through the π-orbitals of **3**. The packing structure of this salt at low temperature (173 K) is very similar to that at room temperature, whereas the intermolecular interactions between the organic and inorganic components are strengthened, particularly for those between [$CuBr_3$·THF] and D–A–D timers (Figure S5 in Supporting Information File 1), which would result in the significant effect on the magnetic property as discussed in the following section.

4·$CuBr_4$ crystallizes in the orthorhombic *Pccn* space group with half of molecule **4** and half of $CuBr_4$ crystallographically independent (Figure 3a). The calculated δ value of **4** in the salt is 0.578, indicating that the charge on **4** should be +2. The two dithiole rings of molecule **4** are significantly twisted with a

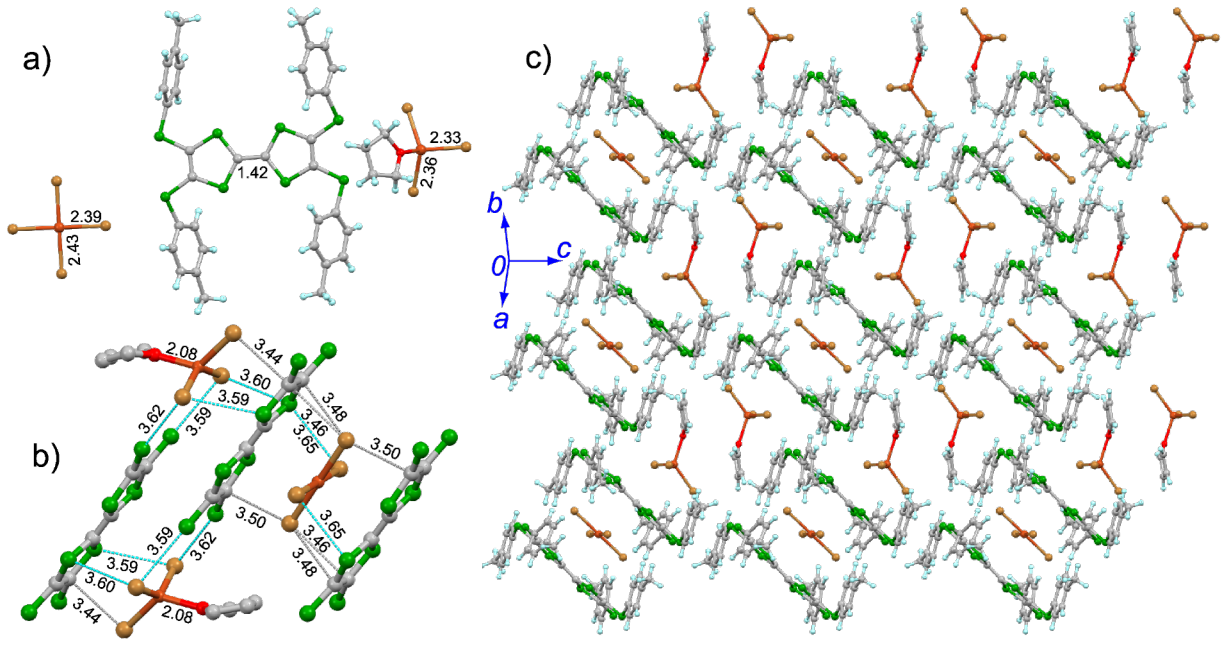

Figure 2: Crystal structure of **3**·$(CuBr_4)_{0.5}$·$CuBr_3$·THF: a) unit cell contents with the typical bond lengths shown (Å), and the structure of planar $[Cu(II)Br_4]^{2-}$ ion is generated by symmetry operation (2-*x*, 2-*y*,1-*z*); b) interaction between the anions and the central TTF core of **3**, where cyan and grey dashed lines represent Br···S and Br···C contacts (Å), respectively; c) packing structure.

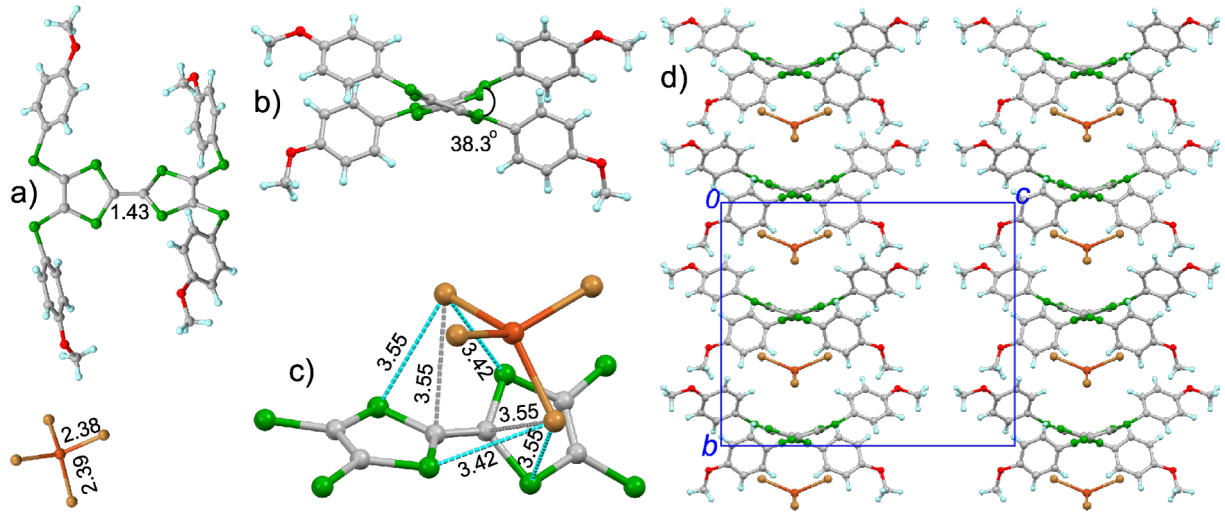

Figure 3: Crystal structure of **4**·$CuBr_4$: a) unit cell contents with the typical bond lengths shown (Å); b) view of molecule **4** along the central C=C bond of the TTF core, and the dihedral angle between two C_3S_2 rings is shown; c) interaction between the $[Cu(II)Br_4]^{2-}$ ion and the central TTF core of **4**, where cyan and grey dashed lines represent Br···S and Br···C contacts (Å), respectively; d) packing structure viewed along the *a*-axis.

dihedral angle of 38.3° as shown in Figure 3b. The $CuBr_4$ component shows the tetrahedral conformation with a Cu–Br bond length of 2.38 and 2.39 Å, thus $CuBr_4$ is a dianion. The $[CuBr_4]^{2-}$ ion locates above the donor molecule, and there are Br···S (3.42–3.55 Å) and Br···C contacts (3.55 Å) between the $[CuBr_4]^{2-}$ ion and **4** as shown in Figure 3c. Molecule **4** and the $[CuBr_4]^{2-}$ ion form the mixed aggregation along the *b*-axis (Figure 3d). Although there is no interaction between the neighbouring donor molecules in the *bc*-plane, the S···S contacts (3.22 Å) are observed between the molecules of **4** along the *a*-axis direction, which would result in the spin exchange interaction between Cu(II).

5·Cu_2Br_6 crystallizes in the triclinic *P*−1 space group with half of molecule **5** and half of Cu_2Br_6 crystallographically independent (Figure 4a). The central TTF core of **5** adopts the planar conformation, and the δ value of **5** in the salt is 0.595, indicating that **5** is oxidized to the dication form. As for the inorganic component Cu_2Br_6, two Cu atoms are connected by two bromine bridges (Br–Cu bond length: 2.47 Å) to form a quasi-planar dianion $[Cu_2Br_6]^{2-}$. Thus, the spin exchange interaction between these two Cu(II) would be significant, as discussed in the following section. Molecule **5** and the $[Cu_2Br_6]^{2-}$ ion form the mixed aggregation along the *b*-axis as shown in Figure 4b. There is no atomic close contact between the organic and inorganic components in a stacking column, whereas one S···S contact (3.57 Å) is observed between the neighbouring molecules of **5** along their longitudinal axis.

6·$CuBr_2$·CH_3CN crystallizes in the triclinic *P*−1 space group, and the asymmetric unit contains half of molecule **6**, half of $CuBr_2$, and half of a CH_3CN solvent molecule (Figure 5a). The central TTF core of **6** has a pseudo-planar conformation, and the calculated δ value of **6** in the salt is 0.744, indicating that **6** is in the radical cation form. The inorganic component $CuBr_2$ is linear, and the Cu–Br bond length is 2.54 Å, which is close to that of a typical Cu(I)–Br bond [51-53,56-58], indicating that $CuBr_2$ has the charge of −1. The organic and inorganic components form the mixed stacks along the *a*-axis as shown in Figure 5b. Moreover, the peripheral aryl groups form the cavity to accommodate a CH_3CN solvent molecule, thus a supramolecular framework is formed in this salt. In the salt of **7** with $CuBr_2$, molecule **7** is also oxidized to the radical cation form and the counter anion is $[CuBr_2]^-$ as shown in Supporting Information File 1 (Figure S11).

Magnetic properties

The temperature-dependent magnetic susceptibilities of the salts were measured on the polycrystalline samples. In the salts of

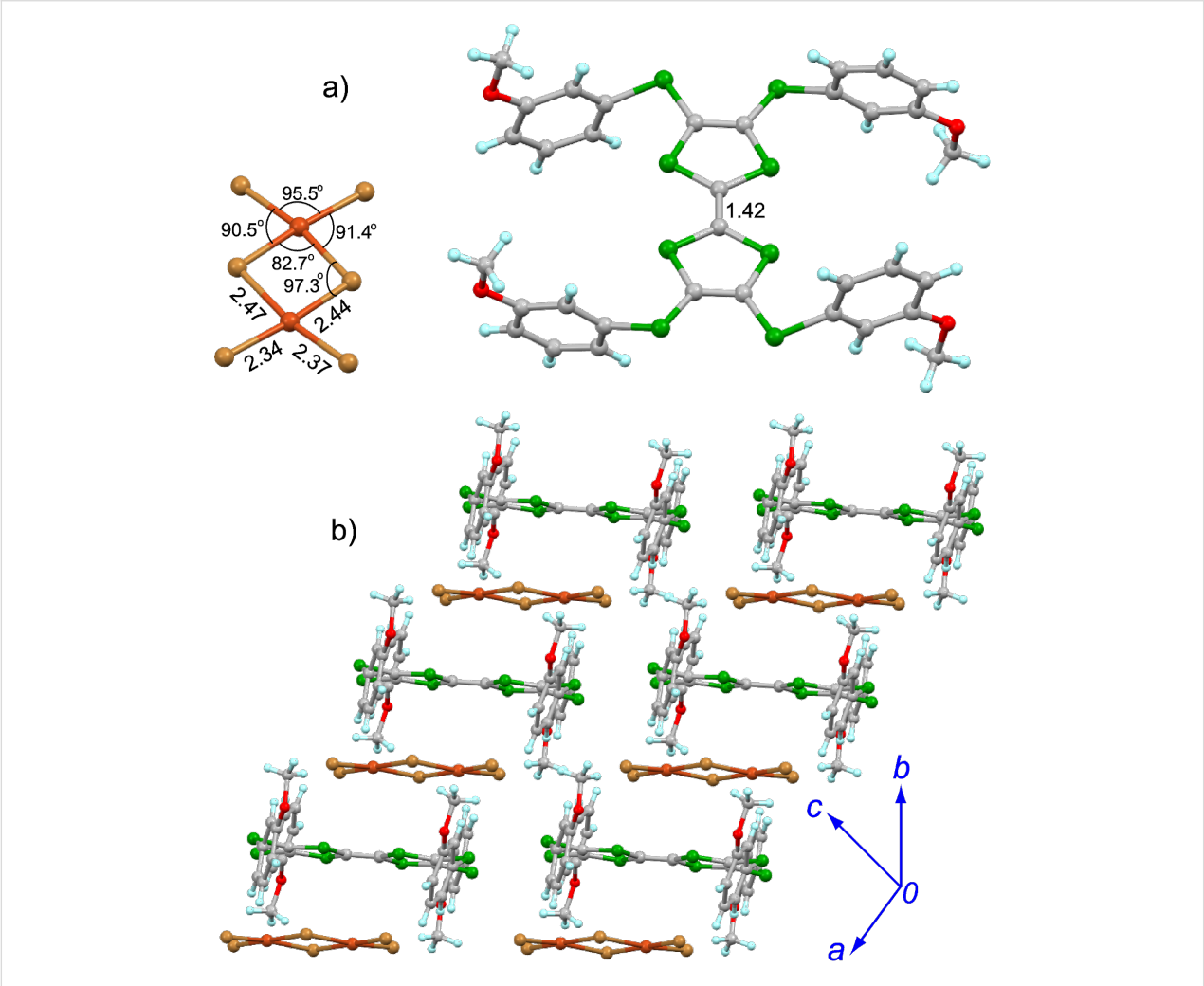

Figure 4: Crystal structure of **5**·Cu_2Br_6: a) unit cell contents with the numeric data indicate the angles and bond lengths (Å); b) packing structure.

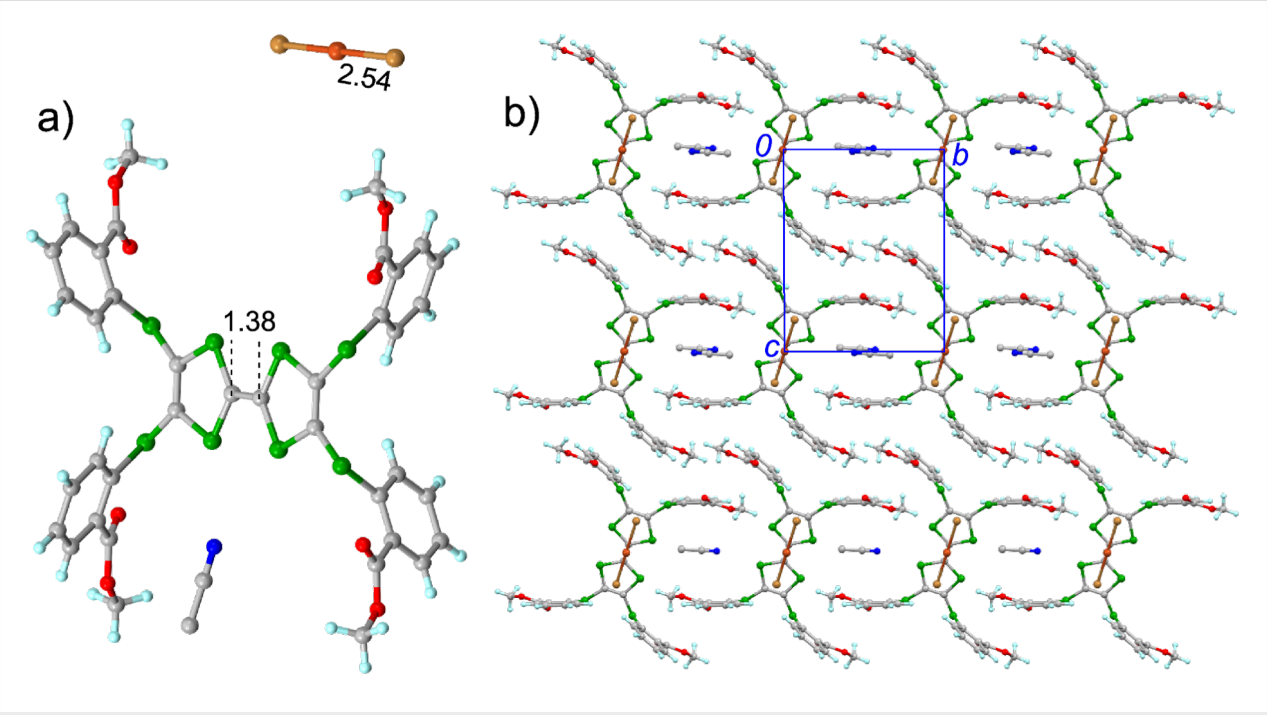

Figure 5: Crystal structure of **6**·$CuBr_2$·CH_3CN: a) unit cell contents with the typical bond lengths shown (Å); b) packing structure viewed along the crystallographic *a*-axis.

1–**5**, the spin susceptibility comes from Cu(II) (S = 1/2), because the TTFs in these salts are oxidized to the dication form and the inorganic components contain Cu(II). On the other hand, spin susceptibility on the salts of **6** and **7** originates from the radical cation, as the inorganic components in these salts contain Cu(I). Figure 6 depicts the temperature-dependent magnetic susceptibilities of the representative salts.

1·$CuBr_4$, **2**·$CuBr_4$, **4**·$CuBr_4$, and **7**·$CuBr_2$ show the similar magnetic properties. The temperature dependence of the magnetic susceptibility follows the Curie–Weiss law, and the spins in these salts show the antiferromagnetic interaction at low temperature. The antiferromagnetic interactions of Cu(II) in **1**·$CuBr_4$, **2**·$CuBr_4$, and **4**·$CuBr_4$ arise from the *d*–π–*d* pathway, as discussed in the crystal structure section. On the other hand, the antiferromagnetic interaction of radical cations in **7**·$CuBr_2$ could be due to the π–π interactions, because the neighbouring donor molecules have a S···S contact (3.30 Å) along the *a*-axis. Figure 6a shows the magnetic susceptibility of **1**·$CuBr_4$ by varying temperature, and the best-fitting parameters for this salt are C = 0.382 emu K mol^{-1} and θ = −5.4 K.

In the case of **3**·$(CuBr_4)_{0.5}$·$CuBr_3$·THF, the temperature dependence of magnetic susceptibility shows the monotonic decrement upon cooling in the temperature range of 300–270 K. Furthermore, an abrupt jump of the magnetic susceptibility is observed at 270 K (see Figure 6b). This abrupt jump could be attributed to the variation of intermolecular interactions as discussed in the crystal structure section. Below 270 K, the temperature dependence of magnetic susceptibility follows the Curie–Weiss law with C = 0.379 emu K mol^{-1} and θ = −4.6 K.

As mentioned in the crystal structure section, two Cu(II) atoms in **5**·Cu_2Br_6 are connected by two bromine bridges, which result in the strong spin interaction between Cu(II) atoms. The temperature-dependent magnetic susceptibility of **5**·Cu_2Br_6 is shown in Figure 6c, which can be well-fitted by the singlet–triplet model [60]. The best-fitting parameters are: J = −243 K which is consistent with the significant magnetic susceptibility dropping at 245 K, f = 0.993, and A = 3.21 × 10^{-4} emu mol^{-1}. The latter two terms reflect the non-zero magnetic susceptibility originated from the crystal defects (the Curie term) and the residue paramagnetic impurities.

$$\chi_{\mathrm{calcd}} = f \cdot \frac{2N_{\mathrm{A}} g^2 \mu_{\mathrm{B}}}{k_{\mathrm{B}} T} \cdot \frac{1}{3 + \exp\left(-\frac{2J}{k_{\mathrm{B}} T}\right)} + (1 - f) \cdot \frac{C}{T} + A$$

Conclusion

We have reported the synthesis, structures, and magnetic properties of the copper ion salts of Ar-S-TTFs **1**–**7**. The present salts show a wide variety of solid state structures and magnetic

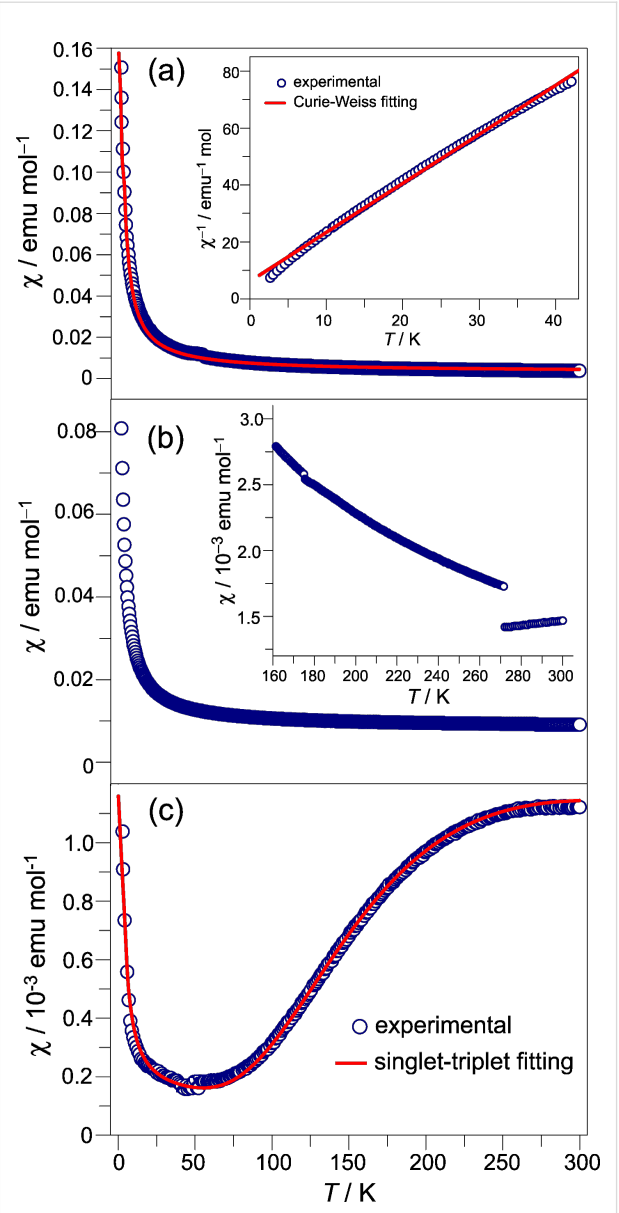

Figure 6: Temperature dependent magnetic susceptibility for the typical salts: a) **1**·$CuBr_4$ with the insert panel depicting the Curie–Weiss fitting (red solid line) in low temperature region; b) **3**·$(CuBr_4)_{0.5}$·$CuBr_3$·THF with the insert panel depicting the magnetic susceptibility at high temperature region; c) **5**·Cu_2Br_6 with the red solid line depicting the singlet-triplet fitting.

properties. The charge on TTFs in the salts depends on their second redox potentials ($E_{1/2}^2$): $E_{1/2}^2 > 0.90$ V, radical cation; $E_{1/2}^2 < 0.90$ V, dication. Except compound **4**, which has the twisted central TTF core in the dicationic salt **4**·$CuBr_4$, the central TTF frameworks of these TTFs are nearly planar despite the charge on them. On the other hand, the anions in the salts show various configurations including the linear $[Cu(I)Br_2]^-$ ion, the tetrahedral $[Cu(II)Br_4]^{2-}$ ion, the planar $[Cu(II)_2Br_6]^{2-}$ ion, the planar $[Cu(II)Br_4]^{2-}$ ion, and the distorted tetrahedral $[Cu(II)Br_3·THF]^-$ ion. As a result of diverse geometries for both donor molecules and counter anions, the present salts show various packing structures, which results in a different spin-exchange interaction pathway as proved by their magnetic properties.

Experimental

Cupric bromide ($CuBr_2$) was purchased from Shanghai Xinbao Fine Chemical Factory (Shanghai, China). Tetrahydrofuran (THF) and acetonitrile (CH_3CN) were distilled over CaH_2 and stored under N_2 atomsphere. Compounds **1**–**7** were synthesized by following our previous reports [37,38].

The electrochemical properties of **1**–**7** were recorded on a RST 5000 electrochemical workstation at a scan rate of 50 mV s^{-1}, with glassy carbon discs as the working electrode, Pt wire as the counter electrode, and a SCE electrode as the reference electrode. The concentration was 5×10^{-4} mol L^{-1} in CH_2Cl_2, and the supporting electrolyte was $(n\text{-Bu})_4N·PF_6$ (0.1 mol L^{-1}). The measurement was performed at 20 °C after bubbling the solution with N_2 gas for 15 min.

The X-ray diffraction measurement was carried out on SuperNova (Agilent) type diffractometer. The crystal structure was solved by a direct method SIR2004 [61] and refined by a full-matrix least-squares method on F^2 by means of SHELXL-97 [62]. The X-ray powder diffraction (XRPD) pattern was recorded on X'Pert PRO (PANalytical). The temperature dependence of the magnetic susceptibility was measured on a SQUID magnetometer of Quantum Design MPMS-XL applying a magnetic field of 1 kOe. The data were corrected for core diamagnetism estimated from the sum of the Pascal constants [63].

Supporting Information

Supporting Information File 1

Selected crystallographic data, crystal structures of **2**·$CuBr_4$ and **7**·$CuBr_2$, and variations of molecular geometries of TTFs at different oxidation states.
[http://www.beilstein-journals.org/bjoc/content/supplementary/1860-5397-11-95-S1.pdf]

Supporting Information File 2

Crystallographic data files of compounds **1**–**7**. These data have been deposited to the Cambridge Crystallographic Data Centre (CCDC) with the registered numbers 1046215–1046222.
[http://www.beilstein-journals.org/bjoc/content/supplementary/1860-5397-11-95-S2.cif]

Acknowledgements

This work was financially supported by National Natural Science Foundation of China (21372111 and 21172104) and Research Fund for the Doctoral Program of Higher Education of China (RFDP 20120211110039). We are grateful to Prof. Bin Chen (Hangzhou Normal University) for the measurement of magnetic susceptibility.

References

1. Wudl, F.; Smith, G. M.; Hufnagel, E. J. *J. Chem. Soc. D* **1970,** 1453–1454. doi:10.1039/C29700001453
2. Yamada, J.; Sugimoto, T., Eds. *TTF Chemistry Fundamentals and Applications of Tetrathiafulvalene;* Kodansha Springer: Berlin, Germany, 2004.
3. Ferraris, J.; Cowan, D. O.; Walatka, V.; Perlstein, J. H. *J. Am. Chem. Soc.* **1973,** *95,* 948–949. doi:10.1021/ja00784a066
4. Jérome, D.; Mazaud, A.; Ribault, M.; Bechgaard, K. *J. Phys., Lett.* **1980,** *41,* 95–98. doi:10.1051/jphyslet:0198000410409500
5. Williams, J. M.; Ferraro, J. R.; Thorn, R. J.; Carlson, K. D.; Geiser, U.; Wang, H. H.; Kini, A. M.; Whangbo, M.-H. *Organic Superconductors (including Fullerenes);* Prentice Hall: Englewood Cliffs, NJ, 1992.
6. Ishiguro, T.; Yamaji, K.; Saito, G. *Organic Superconductors,* 2nd ed.; Springer: Berlin, Germany, 1998.
7. Batail, P., Ed. Molecular Conductors. *Chem. Rev.* **2004,** *104,* 4887–5782.
8. Kagoshima, S.; Kanoda, K.; Mori, T., Eds. Organic Conductors. *J. Phys. Soc. Jpn.* **2006,** *75,* 051001–051802.
9. Lebed, A., Ed. *The Physics of Organic Superconductors and Conductors;* Springer: Berlin, Germany, 2008.
10. Ardavan, A.; Brown, S.; Kagoshima, S.; Kanoda, K.; Kuroki, K.; Mori, H.; Ogata, M.; Uji, S.; Wosnitza, J. *J. Phys. Soc. Jpn.* **2012,** *81,* 011004. doi:10.1143/JPSJ.81.011004
11. Ota, A.; Yamochi, H.; Saito, G. *J. Mater. Chem.* **2002,** *12,* 2600–2602. doi:10.1039/B206293C
12. Ota, A.; Yamochi, H.; Saito, G. *J. Low Temp. Phys.* **2006,** *142,* 425–428. doi:10.1007/BF02679536
13. Chollet, M.; Guerin, L.; Uchida, N.; Fukuya, S.; Shimoda, H.; Ishikawa, T.; Matsuda, K.; Hasegawa, T.; Ota, A.; Yamochi, H.; Saito, G.; Tazaki, R.; Adachi, S.-i.; Koshihara, S.-y. *Science* **2005,** *307,* 86–89. doi:10.1126/science.1105067
14. Onda, K.; Ogihara, S.; Yonemitsu, K.; Maeshima, N.; Ishikawa, T.; Okimoto, Y.; Shao, X.; Nakano, Y.; Yamochi, H.; Saito, G.; Koshihara, S.-y. *Phys. Rev. Lett.* **2008,** *101,* 067403. doi:10.1103/PhysRevLett.101.067403
15. Gao, M.; Lu, C.; Jean-Ruel, H.; Liu, L. C.; Marx, A.; Onda, K.; Koshihara, S.-y.; Nakano, Y.; Shao, X.; Hiramatsu, T.; Saito, G.; Yamochi, H.; Cooney, R. R.; Moriena, G.; Sciaini, G.; Miller, R. J. D. *Nature* **2013,** *496,* 343–346. doi:10.1038/nature12044
16. Shao, X.; Nakano, Y.; Yamochi, H.; Dubrovskiy, A. D.; Otsuka, A.; Murata, T.; Yoshida, Y.; Saito, G.; Koshihara, S.-y. *J. Mater. Chem.* **2008,** *18,* 2131–2140. doi:10.1039/B717621J
17. Shao, X.; Nakano, Y.; Sakata, M.; Yamochi, H.; Yoshida, Y.; Maesato, M.; Uruichi, M.; Yakushi, K.; Murata, T.; Otsuka, A.; Saito, G.; Koshihara, S.-y.; Tanaka, K. *Chem. Mater.* **2008,** *20,* 7551–7562. doi:10.1021/cm802517s
18. Shao, X.; Yoshida, Y.; Nakano, Y.; Yamochi, H.; Sakata, M.; Maesato, M.; Otsuka, A.; Saito, G.; Koshihara, S.-y. *Chem. Mater.* **2009,** *21,* 1085–1095. doi:10.1021/cm803180x
19. Murata, T.; Shao, X.; Nakano, Y.; Yamochi, H.; Uruichi, M.; Yakushi, K.; Saito, G.; Tanaka, K. *Chem. Mater.* **2010,** *22,* 3121–3132. doi:10.1021/cm100051b
20. Bryce, M. R. *Chem. Soc. Rev.* **1991,** *20,* 355–390. doi:10.1039/CS9912000355
21. Adam, M.; Müllen, K. *Adv. Mater.* **1994,** *6,* 439–459. doi:10.1002/adma.19940060603
22. Jørgensen, T.; Hansen, T. K.; Becher, J. *Chem. Soc. Rev.* **1994,** *23,* 41–51. doi:10.1039/CS9942300041
23. Bryce, M. R. *J. Mater. Chem.* **1995,** *5,* 1481–1496. doi:10.1039/JM9950501481
24. Garín, J. *Adv. Heterocycl. Chem.* **1995,** *62,* 249–304. doi:10.1016/S0065-2725(08)60423-7
25. Otsubo, T.; Aso, Y.; Takimiya, K. *Adv. Mater.* **1996,** *8,* 203–211. doi:10.1002/adma.19960080303
26. Coronado, E.; Gómez-García, C. J. *Chem. Rev.* **1998,** *98,* 273–296. doi:10.1021/cr970471c
27. Bryce, M. R. *Adv. Mater.* **1999,** *11,* 11–23. doi:10.1002/(SICI)1521-4095(199901)11:1<11::AID-ADMA11>3.0.CO;2-3
28. Nielsen, M. B.; Lomholt, C.; Becher, J. *Chem. Soc. Rev.* **2000,** *29,* 153–164. doi:10.1039/A803992E
29. Segura, J. L.; Martín, N. *Angew. Chem., Int. Ed.* **2001,** *40,* 1372–1409. doi:10.1002/1521-3773(20010417)40:8<1372::AID-ANIE1372>3.0.CO;2-I
30. Frère, P.; Skabara, P. J. *Chem. Soc. Rev.* **2005,** *34,* 69–98. doi:10.1039/B316392J
31. Canavet, D.; Sallé, M.; Zhang, G.; Zhang, D.; Zhu, D. *Chem. Commun.* **2009,** 2245–2269. doi:10.1039/B818607N
32. Ding, H.; Li, Y.; H, H.; Sun, Y.; Wang, J.; Wang, C.; Wang, C.; Zhang, G.; Wang, B.; Xu, W.; Zhang, D. *Chem. – Eur. J.* **2014,** *20,* 14614. doi:10.1002/chem.201405330
33. Skabara, P. J.; Serebryakov, I. M.; Roberts, D. M.; Perepichka, I. F.; Coles, S. J.; Hursthouse, M. B. *J. Org. Chem.* **1999,** *64,* 6418–6424. doi:10.1021/jo990198+
34. Skabara, P. J.; Roberts, D. M.; Serebryakov, I. M.; Pozo-Gonzalo, C. *Chem. Commun.* **2000,** 1005–1006. doi:10.1039/B001943G
35. Berridge, R.; Serebryakov, I. M.; Skabara, P. J.; Ortí, E.; Viruela, R.; Pou-Amérigo, R.; Coles, S. J.; Hursthouse, M. B. *J. Mater. Chem.* **2004,** *14,* 2822–2830. doi:10.1039/B404545A
36. Kanibolotsky, A. L.; Kanibolotskaya, L.; Gordeyev, S.; Skabara, P. J.; McCulloch, I.; Berridge, R.; Lohr, J. E.; Marchioni, F.; Wudl, F. *Org. Lett.* **2007,** *9,* 1601–1604. doi:10.1021/ol070366h
37. Sun, J.; Lu, X.; Shao, J.; Cui, Z.; Shao, Y.; Jiang, G.; Yu, W.; Shao, X. *RSC Adv.* **2013,** *3,* 10193–10196. doi:10.1039/C3RA41349G
38. Sun, J.; Lu, X.; Shao, J.; Li, X.; Zhang, S.; Wang, B.; Zhao, J.; Shao, Y.; Fang, R.; Wang, Z.; Yu, W.; Shao, X. *Chem. – Eur. J.* **2013,** *19,* 12517–12525. doi:10.1002/chem.201301819
39. Lu, X.; Sun, J.; Liu, Y.; Shao, J.; Ma, L.; Zhang, S.; Zhao, J.; Shao, Y.; Zhang, H.-L.; Wang, Z.; Shao, X. *Chem. – Eur. J.* **2014,** *20,* 9650–9656. doi:10.1002/chem.201402327
40. Sun, J.; Lu, X.; Ishikawa, M.; Nakano, Y.; Zhang, S.; Zhao, J.; Shao, Y.; Wang, Z.; Yamochi, H.; Shao, X. *J. Mater. Chem. C* **2014,** *2,* 8071–8076. doi:10.1039/C4TC01362J
41. Lu, X.; Sun, J.; Zhang, S.; Ma, L.; Qi, H.; Liu, L.; Shao, Y. *Beilstein J. Org. Chem.* submitted.
The combination of Ar-S-TTFs with fullerenes resulted in various type of donor-acceptor type co-crystals.

42. Ma, L.; Lu, X.; Sun, J.; Liu, L.; Qi, H.; Shao, X. to be submitted. The combination of Ar-S-TTFs with TCNQ resulted in the neutral complexes, and that with F_4TCNQ afforded the partially transferred and/or ionic complexes.
43. Zhang, S.; Lu, X.; Sun, J.; Zhao, Y.; Shao, Y.; Shao, X. *CrystEngComm* **2015,** *17*. doi:10.1039/C5CE00510H
The supramolecular assembly of Ar-S-TTF with Keggin-type phosphomolybdic acid resulted in the honey-comb supramolecular frameworks.
44. Siedle, A. R.; Candela, G. A.; Finnegan, T. F.; Van duyne, R. P.; Cape, T.; Kokoszka, G. F.; Woyciejes, P. M.; Hashmall, J. A. *Inorg. Chem.* **1981,** *20,* 2635–2640. doi:10.1021/ic50222a049
45. Inoue, M. B.; Inoue, M.; Fernando, Q.; Nebesny, K. W. *Inorg. Chem.* **1986,** *25,* 3976–3980. doi:10.1021/ic00242a030
46. Day, P.; Kurmoo, M.; Mallah, T.; Marsden, I. R.; Friend, R. H.; Pratt, F. L.; Hayes, W.; Chasseau, D.; Gaultier, J. *J. Am. Chem. Soc.* **1992,** *114,* 10722–10729. doi:10.1021/ja00053a007
47. Marsden, I. R.; Allan, M. L.; Friend, R. H.; Kurmoo, M.; Kanazawa, D.; Day, P.; Bravic, G.; Chasseau, D.; Ducasse, L.; Hayes, W. *Phys. Rev. B* **1994,** *50,* 2118–2127. doi:10.1103/PhysRevB.50.2118
48. Iwamatsu, M.; Kominami, T.; Ueda, K.; Sugimoto, T.; Adachi, T.; Fujita, H.; Yoshino, H.; Mizuno, Y.; Murata, K.; Shiro, M. *Inorg. Chem.* **2000,** *39,* 3810–3815. doi:10.1021/ic0001098
49. Kanehama, R.; Umemiya, M.; Iwahori, F.; Miyasaka, H.; Sugiura, K.-i.; Yamashita, M.; Yokochi, Y.; Ito, H.; Kuroda, S.; Kishida, H.; Okamoto, H. *Inorg. Chem.* **2003,** *42,* 7173–7181. doi:10.1021/ic0344362
50. Matsumoto, T.; Kamada, Y.; Sugimoto, T.; Tada, T.; Noguchi, S.; Nakazumi, H.; Kawakami, T.; Yamaguchi, K.; Shiro, M. *Inorg. Chem.* **2003,** *42,* 8638–8645. doi:10.1021/ic0300971
51. Lu, W.; Zhu, Q.-Y.; Dai, J.; Zhang, Y.; Bian, G.-Q.; Liu, Y.; Zhang, D.-Q. *Cryst. Growth Des.* **2007,** *7,* 652–657. doi:10.1021/cg060490s
52. Ichikawa, S.; Kimura, S.; Takahashi, K.; Mori, H.; Yoshida, G.; Manabe, Y.; Matsuda, M.; Tajima, H.; Yamaura, J. *Inorg. Chem.* **2008,** *47,* 4140–4145. doi:10.1021/ic7019632
53. Wang, Y.; Cui, S.; Li, B.; Zhang, J.; Zhang, Y. *Cryst. Growth Des.* **2009,** *9,* 3855–3858. doi:10.1021/cg900635f
54. Ichikawa, S.; Takahashi, K.; Matsuda, M.; Tajima, H.; Mori, H. *J. Mater. Chem.* **2010,** *20,* 10130–10134. doi:10.1039/C0JM01318H
55. Guionneau, P.; Kepert, C. J.; Bravic, G.; Chasseau, D.; Truter, M. R.; Kurmoo, M.; Day, P. *Synth. Met.* **1997,** *86,* 1973–1974. doi:10.1016/S0379-6779(97)80983-6
56. Pavlyuka, O.; Lis, T.; Mys'kiv, M. G. *Z. Anorg. Allg. Chem.* **2005,** *631,* 1893–1897. doi:10.1002/zaac.200500057
57. Beck, J.; de Oliveira, A. B. *Z. Anorg. Allg. Chem.* **2009,** *635,* 445–449. doi:10.1002/zaac.200801306
58. Kubo, K.; Yamashita, M. *Crystals* **2012,** *2,* 284–293. doi:10.3390/cryst2020284
59. Bondi, A. *J. Phys. Chem.* **1964,** *68,* 441–451. doi:10.1021/j100785a001
60. Kahn, O. *Molecular Magnetism;* Wiley-VCH: Weinheim, Germany, 1993.
61. Burla, M. C.; Caliandro, R.; Camalli, M.; Carrozzini, B.; Cascarano, G. L.; de Caro, L.; Giacovazzo, C.; Polidori, G.; Spagna, R. *J. Appl. Crystallogr.* **2005,** *38,* 381–388. doi:10.1107/S002188980403225X
62. *SHELXL-97, A Program for Crystal Structure Refinement;* University of Göttingen: Göttingen, 1997.
63. Gupta, R. R. Diamagnetism Susceptibility. In *Landolt-Börnstein, New Series II;* Hellwege, K. H.; Hellwege, A. M., Eds.; Springer: Berlin, Germany, 1986; Vol. 16.

License and Terms

BEILSTEIN JOURNAL OF ORGANIC CHEMISTRY

Tuning of tetrathiafulvalene properties: versatile synthesis of *N*-arylated monopyrrolotetrathiafulvalenes via Ullmann-type coupling reactions

Vladimir A. Azov*[1], Diana Janott[1], Dirk Schlüter[1] and Matthias Zeller[2]

Full Research Paper

Open Access

Address:
[1]Department of Chemistry, University of Bremen, Leobener Str. NW 2C, D-28359 Bremen, Germany and [2]One University Plaza, Department of Chemistry, Youngstown State University, Youngstown, OH 44555-3663, USA

Email:
Vladimir A. Azov* - vazov@uni-bremen.de

* Corresponding author

Keywords:
cyclic voltammetry; *N*-arylation; pyrrolotetrathiafulvalene; Ullmann-type coupling; X-ray crystallography

Beilstein J. Org. Chem. **2015,** *11,* 860–868.
doi:10.3762/bjoc.11.96

Received: 17 February 2015
Accepted: 22 April 2015
Published: 21 May 2015

This article is part of the Thematic Series "Tetrathiafulvalene chemistry".

Guest Editor: P. J. Skabara

Abstract

An Ullmann-type coupling reaction was employed for the preparation of several *N*-arylated monopyrrolotetrathiafulvalenes with variable substitution patterns. Spectroscopic and electrochemical properties of the coupling products strongly depend on the electronic nature of the aromatic substituents due to their direct conjugation with the tetrathiafulvalene chromophore. The crystal packing of the arylated monopyrrolotetrathiafulvalenes is primarily defined by networks of C–H···X weak hydrogen bonds and short S···S contacts involving the tetrathiafulvalene moieties.

Introduction

For the last four decades tetrathiafulvalenes [1,2] (Figure 1) **1** have been the subject of extensive studies due to their outstanding electron-donating properties and ability to induce reversible electrochemically-induced switching processes in molecular and supramolecular systems [3,4]. Availability of selective synthetic methods [5,6] gave access to differently substituted tetrathiafulvalene (TTF) moieties which allowed tuning of oxidation potential, donating ability, as well as other physical and chemical properties. The regioselective functionalization of TTF, however, remains problematic due to the presence of four identical attachment sites. Incorporation of the TTF moiety in macrocycles usually leads to poorly separable mixtures of *cis/trans* isomers [7-9]. Even if separation is possible, TTFs are prone to *cis/trans* isomerization, which can be induced by light [10] or traces of acid [11]. These problems are aggravated by the fact that each reversible oxidation–reduction cycle of the TTF moiety always leads to formation of *cis/trans* isomer mixtures.

Bis-pyrrolotetrathiafulvalenes **2** and monopyrrolotetrathiafulvalenes (MPTTFs) **3** represent a significant modification of the TTF backbone featuring a more extended electron-rich

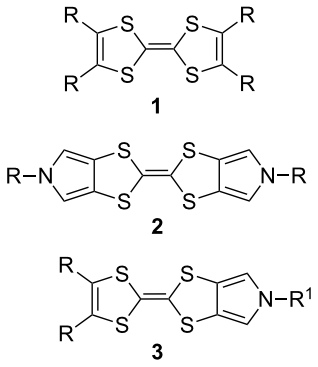

Figure 1: Molecular structures of tetrathiafulvalenes **1**, bis-pyrrolotetrathiafulvalenes **2** and monopyrrolotetrathiafulvalenes **3**.

π-system with only two or three easily accessible attachment points for external substituents, respectively [12,13]. The asymmetric nature of MPTTFs **3** opens the possibility for the introduction of different R- and R^1-groups on the two sides of the TTF moiety. If R^1 = alkyl (or a similar group with an sp^3-hybridized carbon atom), such substituents can be readily attached to the pre-formed MPTTF moiety using a variety of common nucleophilic substitution reactions. In the case of R^1 = aryl, two possible approaches for the preparation of *N*-arylated MPTTF derivatives **4** have been reported (Scheme 1). In the first procedure [14-16], the aryl substituent is incorporated during the initial synthetic steps to form a *N*-aryl-1,3-dithiolo[4,5-*c*]pyrrole-2-thione **5**, which is then coupled to 1,3-dithiole-2-thione **6** in hot triethyl or trimethyl phosphite. Using the second approach [17-19], the aryl group is attached to the MPTTF moiety using a direct copper-mediated Ullmann-type *N*-arylation reaction [20,21]; this method was also used for the preparation of arylated bis-pyrrolotetrathiafulvalenes **2**. Although being reported in the literature, it has so far not found wide spread use and was employed only with a narrow scope of aromatic derivatives with electron-donating substituents and alkylthio-substituted (R = SAlkyl) MPTTFS.

Being interested in the preparation of calix[4]arene receptors with MPTTF moieties directly attached to an aromatic calixarene backbone, we have chosen the copper-catalysed *N*-arylation reaction as a method for coupling of aromatic and MPTTF moieties with each other and successfully employed it for the preparation of two bis-MPTTF-calixarene conjugates, as well as two model low molecular weight aromatic derivatives **4a** and **4c** [22]. To explore the scope of the reaction, we decided to conduct a deeper investigation varying reaction conditions and testing different substituents on the aromatic as well as the MPTTF components of the reaction. It led to the preparation of a family of MPTTF aromatic derivatives, whose properties and crystal structures are discussed below.

Results and Discussion

Synthesis

Our initial synthetic efforts were focused on optimizing reaction conditions using the PrS-MPTTF derivative **7a** [23] and bromoanisole **8a** as starting materials (Scheme 2), as well as comparing two possible copper(I) ligands (Figure 2): *trans*-diaminocyclohexane (DACH) **9a**, which was employed before in *N*-arylations with pyrrolo-TTFs [17-19], and its Schiff base derivative **9b**, which was reported to be one of the most effective ligands in similar *N*-arylation reactions with other substrates [20,21].

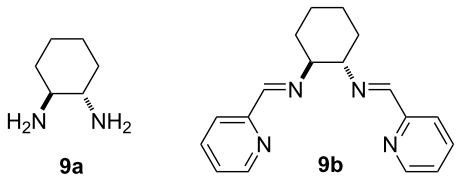

Figure 2: Copper(I) ligands **9a** and **9b**.

Initial experiments gave evidence of much lower efficiency of ligand **9b** in comparison to **9a** in terms of conversion and presence of undesired side-products. Reaction utilizing *trans*-

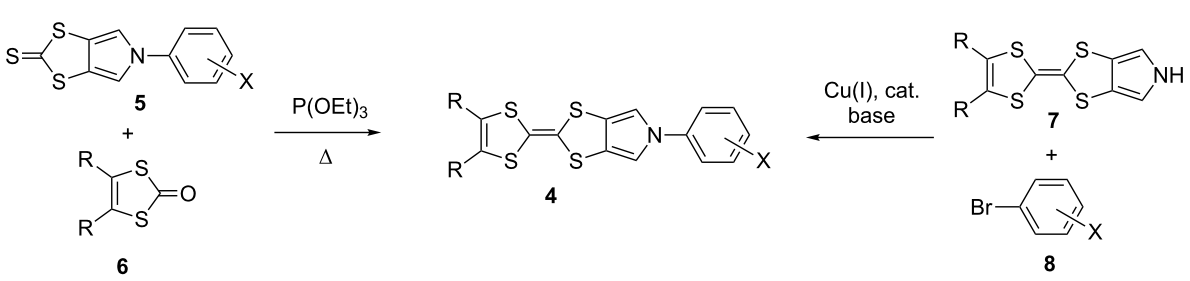

Scheme 1: The two synthetic approaches used for the preparation of arylated monopyrrolotetrathiafulvalenes **1**.

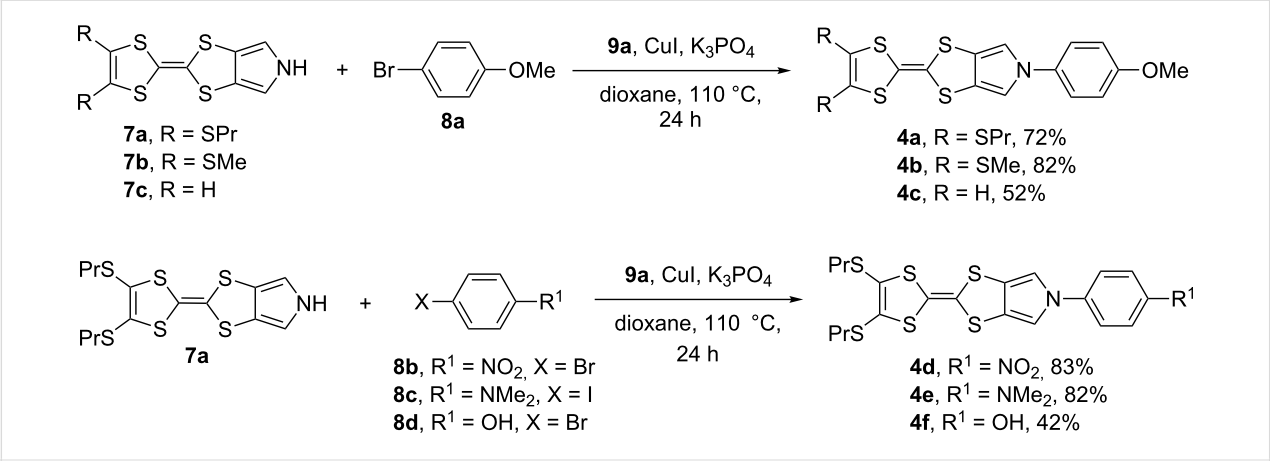

Scheme 2: Synthesis of arylated monopyrrolotetrathiafulvalenes **4a–f**.

diaminocyclohexane **9a**also allowed for fast optimization and reproducibility, which prompted us to focus our attention on the CuI/**9a** catalysis system. Although copper(I) is supposed to play a catalytic role [20,21], smaller CuI loadings led to diminished reaction yields, supposedly due to lower solubility/activity of the CuBr formed in the coupling reaction. Taking into account the affordability of CuI, its excess cannot be considered a disadvantage of the method. Additionally, use of the inexpensive Cu(I) catalyst allows to avoid Buchwald–Hartwig amination [24,25], which employs more expensive Pd-based catalysts for a similar type of C–N coupling reactions.

In a typical procedure, 1 equiv of MPTTF **7a**, **7b** [12], or **7c** [26], 1.5–1.6 equiv of a brominated aromatic derivative, 0.5 equiv of CuI/**9a** and 3–4 equiv of K_3PO_4 were heated at 110–115 °C overnight in absolute dioxane in a Schlenk tube. The reaction yields amounted to 70–80% for stable MPTTF derivatives **4a,b,d,e**, but were lower for **4c** due to sensitivity of the starting material **7b**, as well as for **4f** due to its tendency towards oxidation.

Thus, the *N*-arylation reaction can be readily employed with electron-rich as well as electron-deficient aromatic derivatives, as well as with thioalkyl-substituted and non-substituted MPTTFs. The successful reaction with bromophenol **8d** to form the adduct **4f** also confirmed the possibility of the reaction with hydroxy-substituted aryl derivatives, paving the way for application of this method with non-protected calix[4]arene derivatives [27].

Compounds **4a–c,e,f** (Figure 3) display UV–vis spectra typical for TTF derivatives with absorption maxima at λ_{max} of ca. 310–330 nm as well as a long tail with very low absorption spanning to ca. 500 nm and rendering the yellow colour to the compounds. Thioalkyl TTF derivatives **4a,b,e,f** also show a sloping shoulder at ca. 390 nm, which is missing in the non-substituted **4c**. In contrast, the spectrum of nitro-derivative **4d** displays an additional strong absorption band centred at ca. 425 nm, arising most likely due to charge transfer from the electron-rich MPTTF moiety to the electron-deficient aromatic substituent. This absorption manifests itself in the dark red colour of **4d**, both in solid state as well as in solution.

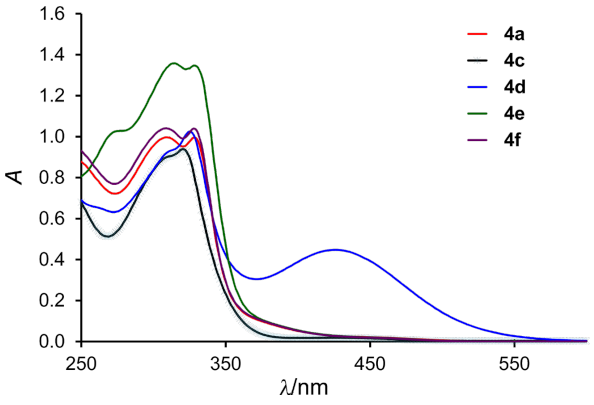

Figure 3: UV–vis spectra of compounds **4a,c–f** (CH_2Cl_2, $c = 4 \times 10^{-5}$ M).

MPTTF derivatives are readily soluble in non-polar organic solvents, such as CH_2Cl_2, toluene or acetone (with the exception of poorly soluble **4c**), giving solutions that are stable at room temperature in air.

Electrochemistry

Solution oxidation potentials of aromatic MPTTF conjugates were determined using cyclic voltammetry (CV) in CH_2Cl_2/Bu_4NClO_4 solution and are summarized in Table 1. The CVs of all compounds displayed two reversible oxidation waves on the cathodic scan (Figure 4) characteristic to TTFs [1], the first one

Table 1: Electrochemical data.[a]

Compound	$E_{1/2}^{ox1}$ (V)	$E_{1/2}^{ox2}$ (V)	$E_{1/2}^{ox3}$ (V)
4a [22]	0.47	0.84	–
4b	0.48	0.83	–
4c [22]	0.40	0.84	–
4d	0.55	0.92	–
4e	0.46	0.84	1.06
4f	0.47	0.86	1.76 (irrev.)

[a]Data were obtained using a one-compartment cell in CH_2Cl_2/0.1 M Bu_4NClO_4, Pt as the working and counter electrodes and a non-aqueous Ag/Ag^+ reference electrode; scan rate 100 mV/s. Values given at room temperature vs SCE; the Fc/Fc^+ couple (0.480 V vs SCE) was used as an internal reference [30].

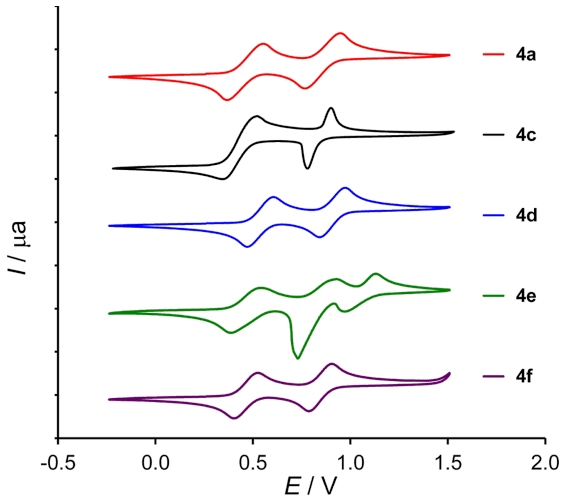

Figure 4: Cyclic voltammograms of compounds **4a,c** [22] and **4d–f** (plotted vs SCE; CH_2Cl_2/0.1 M Bu_4NClO_4).

leading to the radical cation and the second to the dication. Non-substituted derivative **4c** shows a lower first oxidation potential than its alkylS-substituted counterpart **4a,b**, as expected due to the electron-withdrawing effect of the two thioalkyl groups [28,29]. The strong electron-withdrawing effect of the 4-nitrophenyl group in **4d** manifests itself in an increased oxidation potential with a shift of ca. 0.08 V for both oxidation waves. Aromatic electron-donating groups as in **4e** and **4f** do barely influence the potential of the two oxidation waves. Instead, they induce an additional oxidation wave at higher potentials of 1.06 V and 1.77 V, in **4e** and **4f** (see Figure S7, Supporting Information File 1), respectively. For the phenol derivative **4f**, this oxidation is irreversible.

Crystal structures

Compounds **4a,b,d,e** afforded high quality crystals that could be analysed using X-ray crystallography, allowing to unambiguously confirm the identity of the compounds and analyse their structural properties and arrangement in the solid state. Bond lengths and angles in all structures may be considered normal. With the exception of alkylS-substituents, the molecular frameworks of **4a,b,d,e** display relatively low deviations from planarity. Angles between the least-square planes, defined by the heavy atoms of the aromatic ring and neighbouring pyrrole ring do not exceed 17.3° (in **4e**, see Table 2), ensuring good conjugation between the MPTTF and aromatic moieties. Boat-type deviations of the TTF groups (folding along the S–S vectors in the five-membered rings) are minor for electron-deficient **4d** lying below 5°, whereas they are much larger in electron-rich derivatives, where they reach 20.45° in **4a**, 13.58° in **4b** and 11.23° in **4e**. This observation corresponds well with previously reported data: the electron-deficient *N*-Ts derivative has an almost planar arrangement of the TTF moiety, whereas *N*-alkyl derivatives show significant deviation from planarity [12].

Table 2: Angles (°) between the planes of the aromatic ring and neighbouring pyrrole ring in **4a,b,d,e**.

Compound	Molecule1	Molecule 2
4a	3.41	3.42
4b	3.69	12.20
4d	1.36	10.68
4e	13.72	17.28

Interestingly, the crystal structures of all four compounds feature similar packing arrangements with two crystallographically distinct molecules ($Z' = 2$) with quasi-parallel tilted edge-to face arrangements. In the crystal packing, molecules are interconnected by multiple non-classical weak intermolecular hydrogen bonds [31] and C–H···π and S···S interactions, the latter being common in the crystals of sulfur-rich compounds such as TTFs [32]. Most of the close contacts involve the central parts of neighbouring molecules, thus connecting them with each other and leading to formation of supramolecular layers. Parallel layers are only loosely bound to each other [33]. This layered arrangement manifests itself in the crystal morphology: all Ar-MPTTF derivatives crystallize in the form of thin platelets, with the plane of the parallel molecular layers coinciding with the direction normal to the largest crystal face of the platelets. This observation can be rationalized by assuming fast crystal growth within each supramolecular layer, assisted by the presence of directed weak hydrogen bonds as well as C–H···π and S···S interactions. Addition of new parallel layers, connected to the previous layers via dispersive interactions of the van der Waals type, can be assumed to be a much

slower process, leading to plate like crystals that mimic the layered makeup at the molecular level. Crystals of **4d**, for example, form plates with an aspect ratio of 10 and above. Such layered arrangements make these derivatives possible candidates for organic electronics [34] and may serve as a motivation for evaluation of their electronic properties in the solid state.

Figures 5–8 display some aspects of molecular packing of MPTTF derivatives **4a,b,d,e**.

Conclusion

In summary, several arylated monopyrrolotetrathiafulvalene derivatives have been conveniently prepared using a copper-

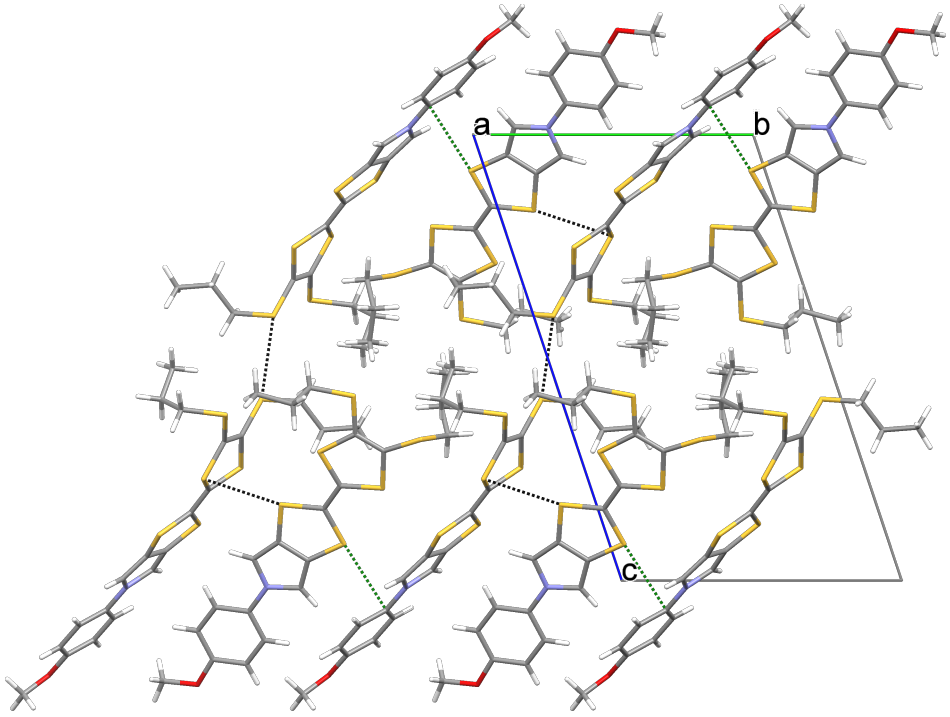

Figure 5: Crystal packing of **4a** viewed along the *a* axis and showing one layer of molecules. Short S···S contacts are shown as black and S···C contacts as green dashed lines. Only the major orientation of the disordered propyl chain is shown.

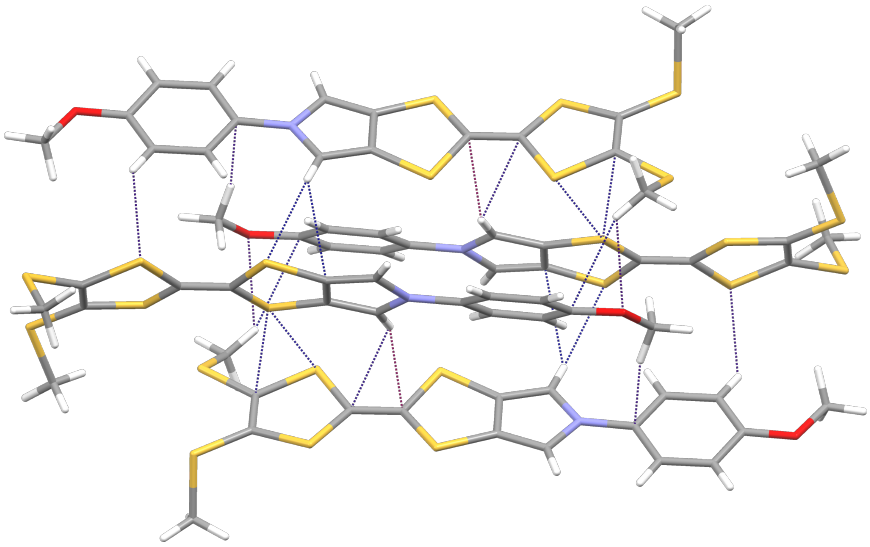

Figure 6: Crystal packing of **4b** showing a group of four molecules interconnected by multiple weak hydrogen bonds, C–H···π, and S···S close contacts.

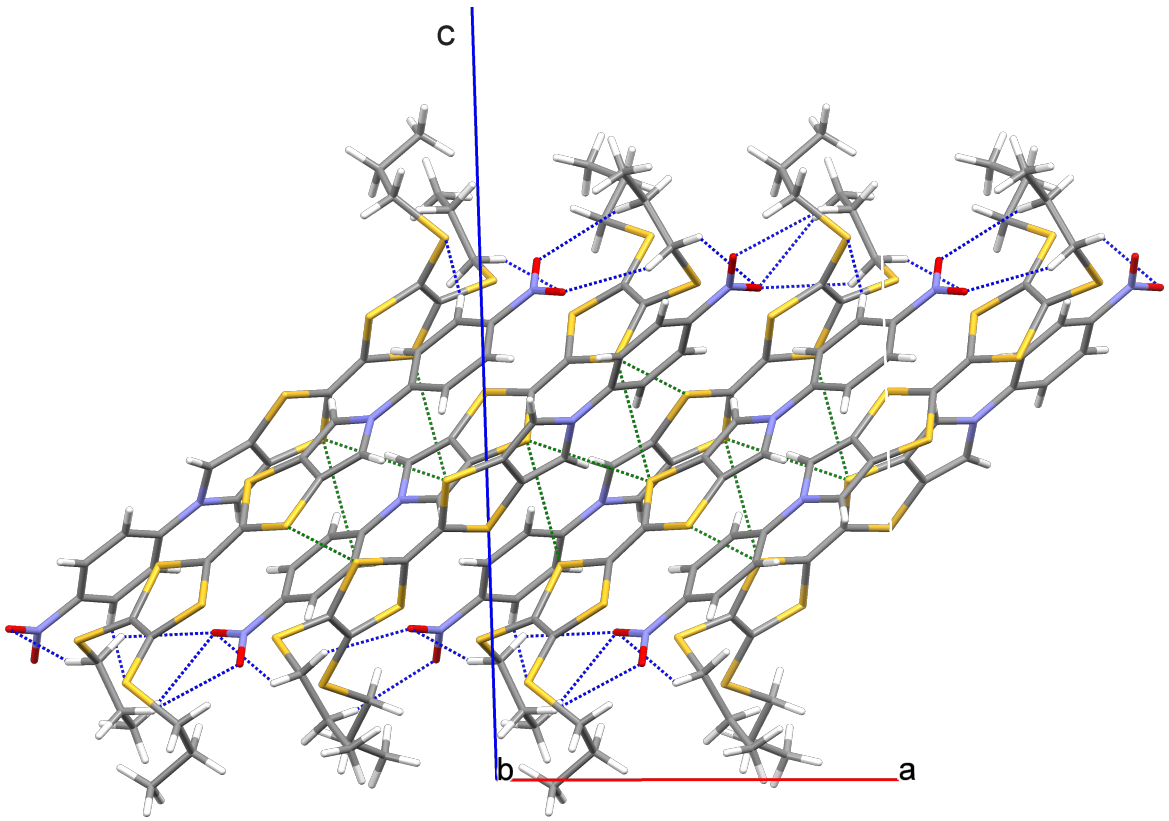

Figure 7: Crystal packing of **4d** viewed along the *b* axis. Molecules of **4d** form layers parallel to the (001) plane being interconnected with each other by means of short S···S contacts (green) and C–H···O_2N weak hydrogen bonds (blue).

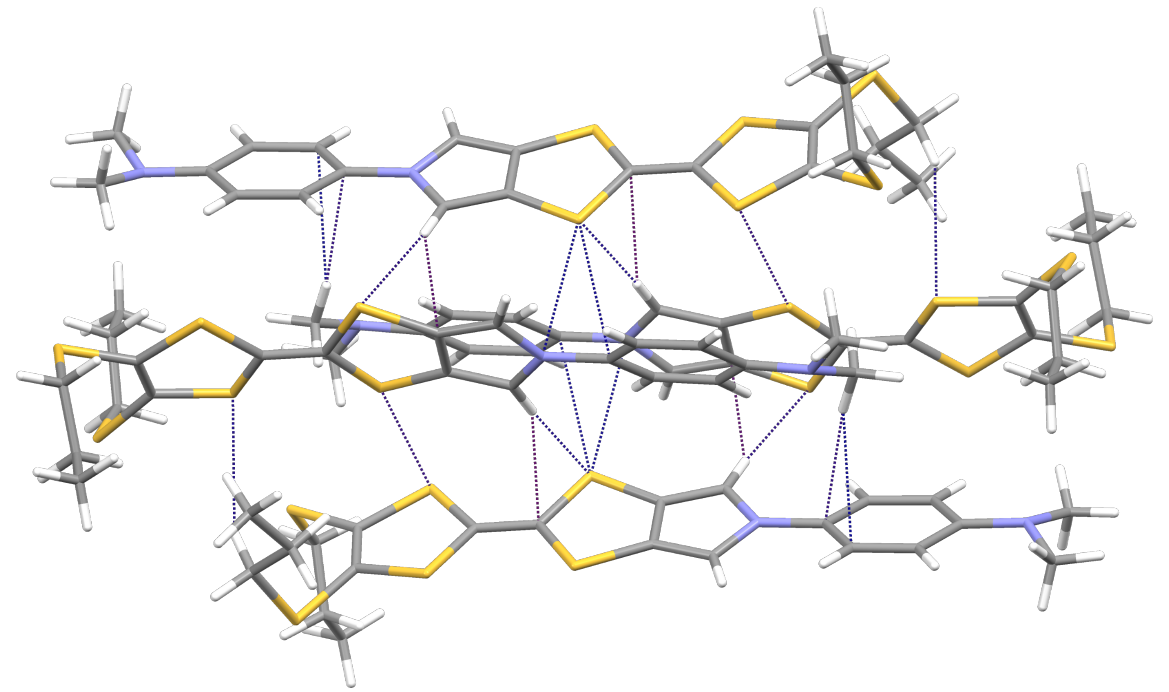

Figure 8: Crystal packing of **4e** showing a group of four molecules interconnected by multiple weak hydrogen bonds, C–H···π, and S···S close contacts.

mediated Ullmann-type *N*-arylation reaction. The reaction was shown to tolerate substituents of different nature on the aromatic group, as well as can be employed with substituted and non-substituted MPTTFs, opening the way for its application for the synthesis of more complex molecular systems, such as conjugates with non-protected calixarenes. New aromatic-MPTTF conjugates were characterized using different analytical methods and X-ray crystallography.

Experimental

Copper-catalyzed *N*-arylation reaction of monopyrrolotetrathiafulvalenes, general procedure. The reaction was performed in a similar manner as described before [22]. A heavy walled Schlenk tube with a wide bore Teflon screw stopcock was charged with MPTTF derivatives **7a**, **7b** or **7c**, CuI, K_3PO_4, (±)-*trans*-1,2-diaminocyclohexane and an aromatic bromide, then absolute dioxane was added via syringe. The reaction mixture was degassed by three freeze-pump-thaw cycles, the vessel was filled with nitrogen, tightly sealed and stirred at 110–115 °C. The reaction was complete in 18–24 h (TLC control). The solvent was removed under reduced pressure directly from the Schlenk tube, the residue was dissolved in CH_2Cl_2, filtered through a plug of celite, and evaporated to dryness. The crude products were triturated with *n*-hexane to remove the unreacted aromatic starting material and then purified by flash chromatography on silica gel to afford pure *N*-arylated MPTTFs.

Preparation and characterization of 2-[4,5-bis(propylthio)-1,3-dithiol-2-ylidene]-5-(4-methoxyphenyl)-5*H*-1,3-dithiolo[4,5-*c*]pyrrole (**4a**) and 2-[1,3-dithiol-2-ylidene]-5-(4-methoxyphenyl)-5*H*-1,3-dithiolo[4,5-*c*]pyrrole (**4c**) was described before [22], also including the X-ray data of **4a** (see Supporting Information File 1 and Supporting Information File 2). For **4a**, corrected oxidation potentials are reported in Table 1.

2-[4,5-Bis(methylthio)-1,3-dithiol-2-ylidene]-5-(4-methoxyphenyl)-5*H*-1,3-dithiolo[4,5-*c*]pyrrole (4b). Prepared from **7b** (0.040 g, 0.119 mmol), CuI (0.023 g, 0.119 mmol), K_3PO_4 (0.020 g, 0.954 mmol), *trans*-diaminocyclohexane (22 µL, 0.179 mmol) and 4-bromoanisole (**8a**, 0.033 g, 0.179 mmol) in 3 mL of dry dioxane. The product was purified by flash chromatography (CH_2Cl_2/cyclohexane, 1:2) to afford bright yellow crystals. X-ray quality crystals were grown by slow evaporation of $CDCl_3$ solution. Yield: 43.2 mg (0.098 mmol, 82%). Mp 198–200 °C; R_f = 0.32 (CH_2Cl_2/cyclohexane, 1:2); ^{1}H NMR (360 MHz, $CDCl_3$) δ 7.25–7.20 (m, 2H), 6.95–6.91 (m, 2H), 6.79 (s, 2H), 3.83 (s, 3H), 2.43 (s, 6H); ^{13}C NMR (90 MHz, $CDCl_3$) δ 158.0, 134.0, 127.1, 121.9, 121.2, 120.2, 114.7, 111.4, 111.1, 55.6, 19.2; UV–vis (CH_2Cl_2) λ_{max} (ε): 309 nm (25600 L·mol^{-1}·cm^{-1}), 329 (24500); MS (EI) *m*/*z* (%): 441 (100) $[M]^{+\bullet}$, 426 (10) $[M - Me]^+$; HRMS (EI) *m*/*z*: $[M]^{+\bullet}$ calcd for $C_{17}H_{15}NOS_6^{+\bullet}$, 440.94780; found, 440.94675; CV (vs SCE, CH_2Cl_2): $E_{1/2}^{ox1}$ = 0.48 V, $E_{1/2}^{ox2}$ = 0.83 V.

2-[4,5-Bis(propylthio)-1,3-dithiol-2-ylidene]-5-(4-nitrophenyl)-5*H*-1,3-dithiolo[4,5-*c*]pyrrole (4d). Prepared from **7a** (0.055 g, 0.140 mmol), CuI (0.014 g, 0.070 mmol), K_3PO_4 (0.089 g, 0.42 mmol), *trans*-diaminocyclohexane (7.5 µL, 0.062 mmol) and 4-bromonitrobenzene (**8b**, 0.045 g, 0.224 mmol) in 2 mL of dry dioxane. The product was purified by flash chromatography (CH_2Cl_2) to afford deep red crystals. X-ray quality crystals were grown by slow evaporation of $CDCl_3$/heptane solution. Yield: 59.7 mg (0.116 mmol, 83%). Mp 240–244 °C; R_f = 0.72 (CH_2Cl_2); ^{1}H NMR (360 MHz, $CDCl_3$) δ 8.33–8.29 (m, 2H), 7.44–7.40 (m, 2H), 6.99 (s, 2H), 2.81 (t, ^3J = 7.2 Hz, 4H), 1.68 (sext, ^3J = 7.2 Hz, 4H), 1.02 (t, ^3J = 7.2 Hz, 6H); ^{13}C NMR (90 MHz, $CDCl_3$) δ 144.7, 144.2, 127.5, 125.8, 125.3, 118.6, 117.3, 113.7, 110.1, 38.2, 23.1, 13.2; UV–vis (CH_2Cl_2) λ_{max} (ε): 325 nm (25600 L·mol^{-1}·cm^{-1}), 426 (11200); MS (EI) *m*/*z* (%): 512 (100) $[M]^{+\bullet}$, 469 (5) $[M - Pr]^{+\cdot}$, 436 (20) $[M - HSPr]^{+\bullet}$; HRMS (EI) *m*/*z*: $[M]^{+\bullet}$ calcd for $C_{20}H_{20}N_2O_2S_6^{+\bullet}$, 511.98435; found, 511.98296; CV (vs SCE, CH_2Cl_2): $E_{1/2}^{ox1}$ = 0.55 V, $E_{1/2}^{ox2}$ = 0.92 V.

2-[4,5-Bis(propylthio)-1,3-dithiol-2-ylidene]-5-(4-dimethylaminophenyl)-5*H*-1,3-dithiolo[4,5-*c*]pyrrole (4e). Prepared from **7a** (0.050 g, 0.128 mmol), CuI (0.012 g, 0.063 mmol), K_3PO_4 (0.082 g, 0.386 mmol), *trans*-diaminocyclohexane (7.5 µL, 0.062 mmol) and 4-iodo-*N,N*-dimethylaniline (**8c**, 0.050 g, 0.202 mmol) in 2 mL of dry dioxane. The product was purified by flash chromatography (CH_2Cl_2/cyclohexane, 1:1) to afford light orange crystals. X-ray quality crystals were grown by slow evaporation of $CDCl_3$/heptane solution. Yield: 53.8 mg (0.105 mmol, 82%); Mp 196–199 °C; R_f = 0.5 (CH_2Cl_2/cyclohexane, 1:1); ^{1}H NMR (360 MHz, CD_2Cl_2) δ 7.22–7.17 (m, 2H), 6.81 (s, 2H), 6.76–6.71 (m, 2H), 2.96 (s, 6H), 2.81 (t, ^3J = 7.2 Hz, 4H), 1.66 (sext, ^3J = 7.2 Hz, 4H), 1.01 (t, ^3J = 7.2 Hz, 6H); ^{13}C NMR (90 MHz, CD_2Cl_2) δ 149.6, 130.7, 127.9, 122.0, 120.6, 119.8, 113.1, 111.9, 111.1, 40.8, 38.5, 23.5, 13.2; UV–vis (CH_2Cl_2) λ_{max} (ε): 314 nm (34000 L·mol^{-1}·cm^{-1}), 330 (33600); MS (EI) *m*/*z* (%): 510 (100) $[M]^{+\bullet}$, 434 (20) $[M - HSPr]^{+\bullet}$; HRMS (EI) *m*/*z*: $[M]^{+\bullet}$ calcd. for $C_{22}H_{26}N_2S_6^{+\bullet}$, 510.04147; found, 510.04104; CV (vs SCE, CH_2Cl_2): $E_{1/2}^{ox1}$ = 0.46 V, $E_{1/2}^{ox2}$ = 0.84 V, $E_{1/2}^{ox3}$ = 1.06 V.

2-[4,5-Bis(propylthio)-1,3-dithiol-2-ylidene]-5-(4-hydroxyphenyl)-5*H*-1,3-dithiolo[4,5-*c*]pyrrole (4f). Prepared from **7a**

(0.049 g, 0.125 mmol), CuI (0.012 g, 0.063 mmol), K_3PO_4 (0.082 g, 0.386 mmol), *trans*-diaminocyclohexane (7.5 µL, 0.062 mmol) and 4-bromophenol (**8d**, 0.035 g, 0.202 mmol) in 2 mL of dry dioxane. The product was purified by flash chromatography (CH_2Cl_2) to afford yellow crystals. Yield: 5 mg (0.052 mmol, 42%); Mp 123–125 °C; R_f = 0.27 (CH_2Cl_2); ^{1}H NMR (200 MHz, $CDCl_3$) δ 7.21–7.14 (m, 2H), 6.91–6.83 (m, 2H), 6.77 (s, 2H), 4.91 (s, 1H), 2.81 (t, ^3J = 7.2 Hz, 4H), 1.66 (sext, ^3J = 7.2 Hz, 4H), 1.01 (t, ^3J = 7.2 Hz, 6H); ^{13}C NMR (50 MHz, $CDCl_3$) δ 153.9, 134.1, 129.7, 127.5, 122.2, 121.4, 119.2, 116.2, 111.4, 38.2, 23.1, 13.2; UV–vis (CH_2Cl_2) λ_{max} (ε): 309 nm (26000 L·mol^{-1}·cm^{-1}), 326 (25900); MS (EI) *m*/*z* (%): 483 (100) $[M]^{+\bullet}$, 440 (5) $[M - Pr]^{+}$, 407 (25) $[M - HSPr]^{+\bullet}$; HRMS (EI) *m*/*z*: $[M]^{+\bullet}$ calcd. for $C_{20}H_{20}N_2O_2S_6^{+\bullet}$, 482.99419; found, 482.99474; CV (vs SCE, CH_2Cl_2): $E_{1/2}^{ox1}$ = 0.47 V, $E_{1/2}^{ox2}$ = 0.86 V, $E_{1/2}^{ox3}$ = 1.77 V.

Supporting Information

Supporting Information File 1

Experimental details, details on electrochemical characterization, ^{1}H and ^{13}C NMR spectra of compounds **4b,d–f**, UV–vis spectrum and CV of **4b**, as well as full crystal structure descriptions.
[http://www.beilstein-journals.org/bjoc/content/supplementary/1860-5397-11-96-S1.pdf]

Supporting Information File 2

Zip archive containing X-ray crystallographic data for **4a** (CCDC 987551), **4b** (CCDC 1049639), **4d** (CCDC 1049638) and **4e** (CCDC 1049637).
[http://www.beilstein-journals.org/bjoc/content/supplementary/1860-5397-11-96-S2.zip]

Acknowledgements

We are grateful to Dr. T. Dülcks, Ms. D. Kemken (MS) and Ms. Ziyan Wang (NMR) for their help with the characterization of new compounds, and Dr. Arunpatcha Nimthong-Roldán for collection of X-ray data and structure refinement for compound **4b**. The X-ray diffractometers were funded by NSF Grants 0087210 and 1337296, Ohio Board of Regents Grant CAP-491, and by Youngstown State University.

References

1. Segura, J. L.; Martín, N. *Angew. Chem., Int. Ed.* **2001,** *40,* 1372–1409. doi:10.1002/1521-3773(20010417)40:8<1372::AID-ANIE1372>3.0.CO;2-I
2. Yamada, J.; Sugimoto, T. *TTF Chemistry. Fundamentals and Applications of Tetrathiafulvalene;* Springer: Heidelberg, Germany, 2004.
3. Becher, J.; Jeppesen, J. O.; Nielsen, K. *Synth. Met.* **2003,** *133–134,* 309–315. doi:10.1016/S0379-6779(02)00379-X
4. Canevet, D.; Sallé, M.; Zhang, G.; Zhang, D.; Zhu, D. *Chem. Commun.* **2009,** 2245–2269. doi:10.1039/b818607n
5. Fabre, J. M. *Chem. Rev.* **2004,** *104,* 5133–5150. doi:10.1021/cr0306440
6. Gorgues, A.; Hudhomme, P.; Sallé, M. *Chem. Rev.* **2004,** *104,* 5151–5184. doi:10.1021/cr0306485
7. Li, Z.-T.; Stein, P. C.; Becher, J.; Jensen, D.; Mørk, P.; Svenstrup, N. *Chem. – Eur. J.* **1996,** *2,* 624–633. doi:10.1002/chem.19960020605
8. Le Derf, F.; Mazari, M.; Mercier, N.; Levillain, E.; Trippé, G.; Riou, A.; Richomme, P.; Becher, J.; Garín, J.; Orduna, J.; Gallego-Planas, N.; Gorgues, A.; Sallé, M. *Chem. – Eur. J.* **2001,** *7,* 447–455. doi:10.1002/1521-3765(20010119)7:2<447::AID-CHEM447>3.0.CO;2-A
9. Azov, V. A.; Cordes, J.; Schlüter, D.; Dülcks, T.; Böckmann, M.; Doltsinis, N. L. *J. Org. Chem.* **2014,** *79,* 11714–11721. doi:10.1021/jo502469z
10. Ballardini, R.; Balzani, V.; Becher, J.; Di Fabio, A.; Gandolfi, M. T.; Mattersteig, G.; Nielsen, M. B.; Raymo, F. M.; Rowan, S. J.; Stoddart, J. F.; White, A. J. P.; Williams, D. J. *J. Org. Chem.* **2000,** *65,* 4120–4126. doi:10.1021/jo0001941
11. Souizi, A.; Robert, A.; Batail, P.; Ouahab, L. *J. Org. Chem.* **1987,** *52,* 1610–1611. doi:10.1021/jo00384a044
12. Jeppesen, J. O.; Takimiya, K.; Jensen, F.; Brimert, T.; Nielsen, K.; Thorup, N.; Becher, J. *J. Org. Chem.* **2000,** *65,* 5794–5805. doi:10.1021/jo000742a
13. Jeppesen, J. O.; Becher, J. *Eur. J. Org. Chem.* **2003,** 3245–3266. doi:10.1002/ejoc.200300078
14. Yin, B.; Yang, Y.; Cong, Z.; Imafuku, K. *Heterocycles* **2004,** *63,* 1577–1584. doi:10.3987/COM-04-10083
15. Balandier, J.-Y.; Chas, M.; Dron, P. I.; Goeb, S.; Canevet, D.; Belyasmine, A.; Allain, M.; Sallé, M. *J. Org. Chem.* **2010,** *75,* 1589–1599. doi:10.1021/jo902529e
16. Nygaard, S.; Leung, K. C.-F.; Aprahamian, I.; Ikeda, T.; Saha, S.; Laursen, B. W.; Kim, S.-Y.; Hansen, S. W.; Stein, P. C.; Flood, A. H.; Stoddart, J. F.; Jeppesen, J. O. *J. Am. Chem. Soc.* **2007,** *129,* 960–970. doi:10.1021/ja0663529
17. Li, H.; Lambert, C. *Chem. – Eur. J.* **2006,** *12,* 1144–1155. doi:10.1002/chem.200500928
18. Li, J.; Zhang, G.; Zhang, D.; Zheng, R.; Shi, Q.; Zhu, D. *J. Org. Chem.* **2010,** *75,* 5330–5333. doi:10.1021/jo1007306
19. Solano, M. V.; DellaPia, E. A.; Jevric, M.; Schubert, C.; Wang, X.; van der Pol, C.; Kadziola, A.; Nørgaard, K.; Guldi, D. M.; Nielsen, M. B.; Jeppesen, J. O. *Chem. – Eur. J.* **2014,** *20,* 9918–9929. doi:10.1002/chem.201402623
20. Monnier, F.; Taillefer, M. *Angew. Chem., Int. Ed.* **2009,** *48,* 6954–6971. doi:10.1002/anie.200804497
21. Sambiagio, C.; Marsden, S. P.; Blacker, A. J.; McGowan, P. C. *Chem. Soc. Rev.* **2014,** *43,* 3525–3550. doi:10.1039/c3cs60289c
22. Düker, M. H.; Schäfer, H.; Zeller, M.; Azov, V. A. *J. Org. Chem.* **2013,** *78,* 4905–4912. doi:10.1021/jo400502t
23. Hansen, J. A.; Becher, J.; Jeppesen, J. O.; Levillain, E.; Nielsen, M. B.; Petersen, B. M.; Petersen, J. C.; Şahin, Y. *J. Mater. Chem.* **2004,** *14,* 179–184. doi:10.1039/b310733g
24. Wolfe, J. P.; Wagaw, S.; Marcoux, J.-F.; Buchwald, S. L. *Acc. Chem. Res.* **1998,** *31,* 805–818. doi:10.1021/ar9600650
25. Hartwig, J. F. *Angew. Chem., Int. Ed.* **1998,** *37,* 2046–2067. doi:10.1002/(SICI)1521-3773(19980817)37:15<2046::AID-ANIE2046>3.0.CO;2-L

26. Nygaard, S.; Hansen, C. N.; Jeppesen, J. O. *J. Org. Chem.* **2007,** *72,* 1617–1626. doi:10.1021/jo061962c
27. D. Schlüter, K. R. Korsching, V. A. Azov, manuscript in preparation for *Eur. J. Org. Chem.*
28. Lichtenberger, D. L.; Johnston, R. L.; Hinkelmann, K.; Suzuki, T.; Wudl, F. *J. Am. Chem. Soc.* **1990,** *112,* 3302–3307. doi:10.1021/ja00165a007
29. Nielsen, M. B.; Jeppesen, J. O.; Lau, J.; Lomholt, C.; Damgaard, D.; Jacobsen, J. P.; Becher, J.; Stoddart, J. F. *J. Org. Chem.* **2001,** *66,* 3559–3563. doi:10.1021/jo010173m
30. Connely, N. G.; Geiger, W. E. *Chem. Rev.* **1996,** *96,* 877–910. doi:10.1021/cr940053x
31. Steiner, T. *Angew. Chem., Int. Ed.* **2002,** *41,* 48–76. doi:10.1002/1521-3773(20020104)41:1<48::AID-ANIE48>3.0.CO;2-U
32. Bryce, M. R.; Devonport, W.; Goldenberg, L. M.; Wang, C. *Chem. Commun.* **1998,** 945–951. doi:10.1039/a800536b
33. See Supporting Information for full details related to crystal structure refinement, ORTEP plots, and tables of close contacts.
34. Bendikov, M.; Wudl, F.; Perepichka, D. F. *Chem. Rev.* **2004,** *104,* 4891–4945. doi:10.1021/cr030666m

License and Terms

BEILSTEIN JOURNAL OF ORGANIC CHEMISTRY

Interactions between tetrathiafulvalene units in dimeric structures – the influence of cyclic cores

Huixin Jiang[1], Virginia Mazzanti[1,2], Christian R. Parker[1], Søren Lindbæk Broman[1], Jens Heide Wallberg[1], Karol Lušpai[3], Adam Brincko[3], Henrik G. Kjaergaard[1], Anders Kadziola[1], Peter Rapta[*3], Ole Hammerich[*1] and Mogens Brøndsted Nielsen[*1]

Full Research Paper

Open Access

Address:
[1]Department of Chemistry, University of Copenhagen, Universitetsparken 5, DK-2100 Copenhagen Ø, Denmark, [2]Sino-Danish Centre for Education and Research (SDC), Niels Jensens Vej 2, DK-8000 Aarhus C, Denmark, and [3]Institute of Physical Chemistry and Chemical Physics, Faculty of Chemical and Food Technology, Slovak University of Technology, Radlinskeho 9, 81237 Bratislava, Slovak Republic

Email:
Peter Rapta* - peter.rapta@stuba.sk;
Ole Hammerich* - o.hammerich@chem.ku.dk;
Mogens Brøndsted Nielsen* - mbn@kiku.dk

* Corresponding author

Keywords:
alkynes; mixed valence; radiaannulene; tetraethynylethene; tetrathiafulvalene

Beilstein J. Org. Chem. **2015,** *11,* 930–948.
doi:10.3762/bjoc.11.104

Received: 27 February 2015
Accepted: 24 April 2015
Published: 02 June 2015

This article is part of the Thematic Series "Tetrathiafulvalene chemistry".

Guest Editor: P. J. Skabara

Abstract

A selection of cyclic and acyclic acetylenic scaffolds bearing two tetrathiafulvalene (TTF) units was prepared by different metal-catalyzed coupling reactions. The bridge separating the two TTF units was systematically changed from linearly conjugated ethyne, butadiyne and tetraethynylethene (*trans*-substituted) units to a cross-conjugated tetraethynylethene unit, placed in either acyclic or cyclic arrangements. The cyclic structures correspond to so-called radiaannulenes having both endo- and exocyclic double bonds. Interactions between two redox-active TTF units in these molecules were investigated by cyclic voltammetry, UV–vis–NIR and EPR absorption spectroscopical methods of the electrochemically generated oxidized species. The electron-accepting properties of the acetylenic cores were also investigated electrochemically.

Introduction

Linking together two redox-active tetrathiafulvalene (TTF) units by a π-conjugated bridge has found immense interest in materials science, in particular in the quest for organic conductors [1-3]. Thus, the materials properties rely on the degree of intra- and intermolecular electronic interactions between neutral and oxidized TTFs. TTF-dimers can potentially exist in five

redox states, 0, +1, +2, +3, and +4, depending on the degree of interactions between the two units. These five redox states have for example been observed in compounds with two TTF units fused to a central benzene or pyrazine ring [4]. If the two TTFs are oxidized at the same potentials in an electrochemical experiment, they behave instead as electrochemically independent redox centres with only weak Coulombic interactions between the cations. Interactions can also be tracked spectroscopically, and while two TTFs might be oxidized at the same or close potentials, the bridge may still convey communication between the units. Works by Otsubo, Iyoda and co-workers [5-7] have shown that two TTFs linked by ethynediyl and buta-1,3-diyndiyl behaved as electrochemically independent redox centres. However, the electronic spectra of the chemically generated radical cations (TTF-bridge-TTF$^{\bullet+}$) were reported to show clear intramolecular intervalence charge-transfer (IVCT) absorption bands with broad maxima around 1300–1400 nm [6].

We have previously found that when separating two TTFs by a cross-conjugated tetraethynylethene (TEE) spacer as in compound **1a** (Figure 1), then the two TTFs behave as independent redox centres that are oxidized at the same potentials in cyclic voltammetry (two two-electron oxidations) [8-10]. However, by bridging the two TTFs with an additional TEE in a cyclic structure, as in the radiaannulene **2a**, communication between the two TTFs is observed in the cyclic voltammetry experiment, and the first two-electron event showed the waves diverging from each other (two stepwise oxidations) [10]. In addition, the intermediate radical cation showed an IVCT absorption at low energy (2257 nm). We became interested in

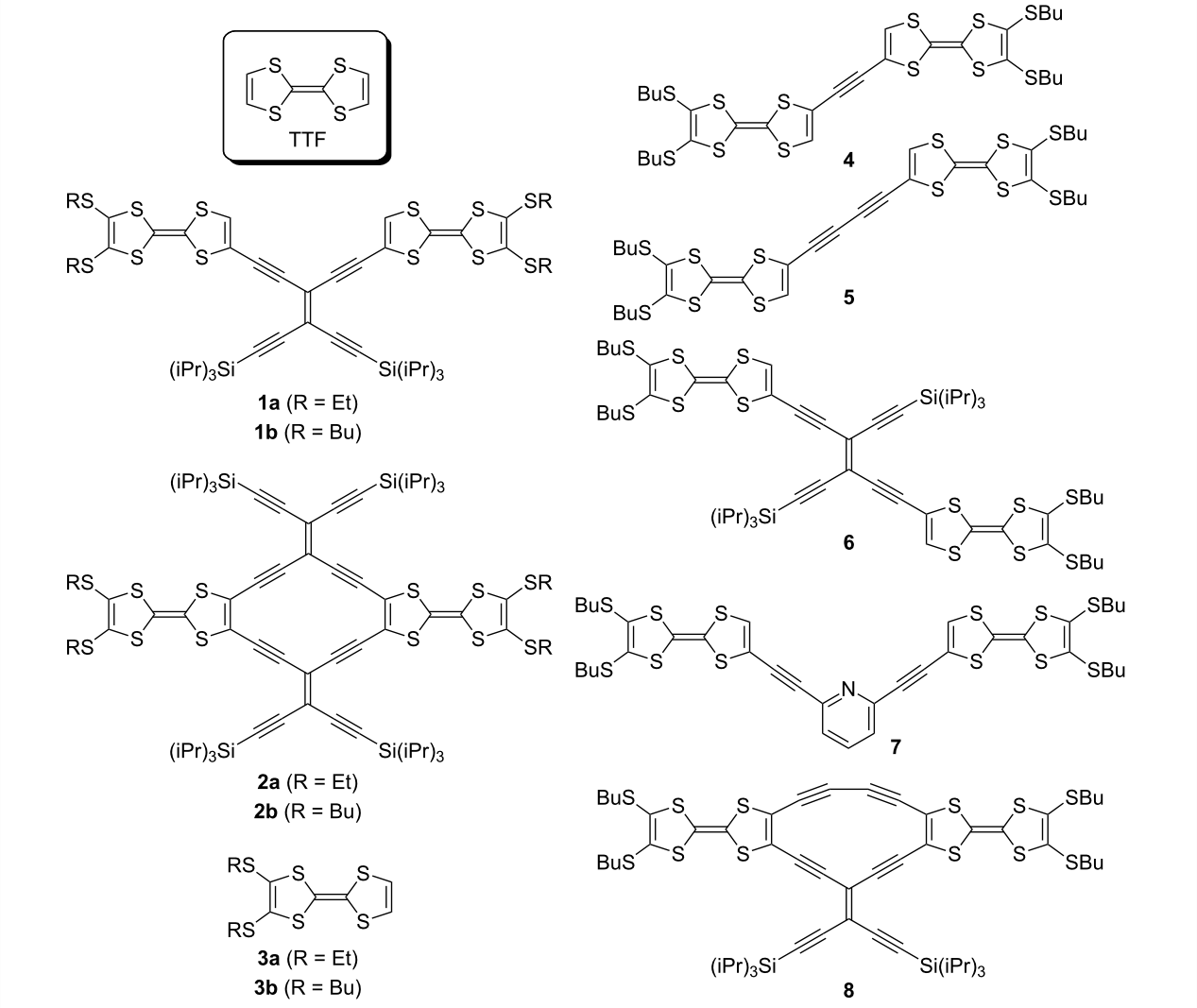

Figure 1: TTF dimers with linearly or cross-conjugated bridging units, acyclic or cyclic bridging units.

elucidating the dependence on acyclic versus cyclic bridging units in more detail by cyclic voltammetry and EPR/UV–vis–NIR spectroelectrochemistry. With regard to conformational flexibility and the lack of it, it deserves mentioning that Low and co-workers [11,12] have shown how rotamers can indeed influence the electronic coupling in bis-ruthenium complexes separated by oligoynediyl spacers. In addition, an increased interaction between redox centres upon linking them together in cyclic structures was previously observed in ferrocene-dimers [13].

Here we present the synthesis and properties of a selection of TTF-dimers as shown in Figure 1. The known TTF **3b** [14] with butylthio substituents, ascertaining good solubility, was used as building block for these dimers. Although ethynediyl- and buta-1,3-diynediyl-bridged dimers were previously studied [1,5-7], we included **4** and **5** in the series in order to be able to compare properties measured under identical conditions. The two TEE-bridged dimers **1b** [15] and **6** have the TTFs arranged in either cross-conjugated or linearly conjugated arrangements. The pyridine-2,6-diyl-bridge present in compound **7** also connects two TTFs in a cross-conjugated pathway. The synthesis of radiaannulene **2b** was very recently described [15], and the properties of **2a** and **2b** are included here for comparison to those of the new unsymmetrical radiaannulene **8** that has a cross-conjugated TEE-diyl and a linearly conjugated buta-1,3-diynediyl bridge between the two TTFs.

Results and Discussion

Synthesis

The synthesis of **4** and **5** was accomplished according to Scheme 1 starting from the known TTF-iodide **9**, readily prepared from compound **3b** [16]. A Sonogashira coupling with trimethylsilylacetylene gave **10** that after desilylation was either subjected to a Sonogashira coupling with **9** to give **4** or to an oxidative Hay coupling to give **5** – using recently developed conditions where 4 Å molecular sieves were added to the reaction mixture to remove water [17].

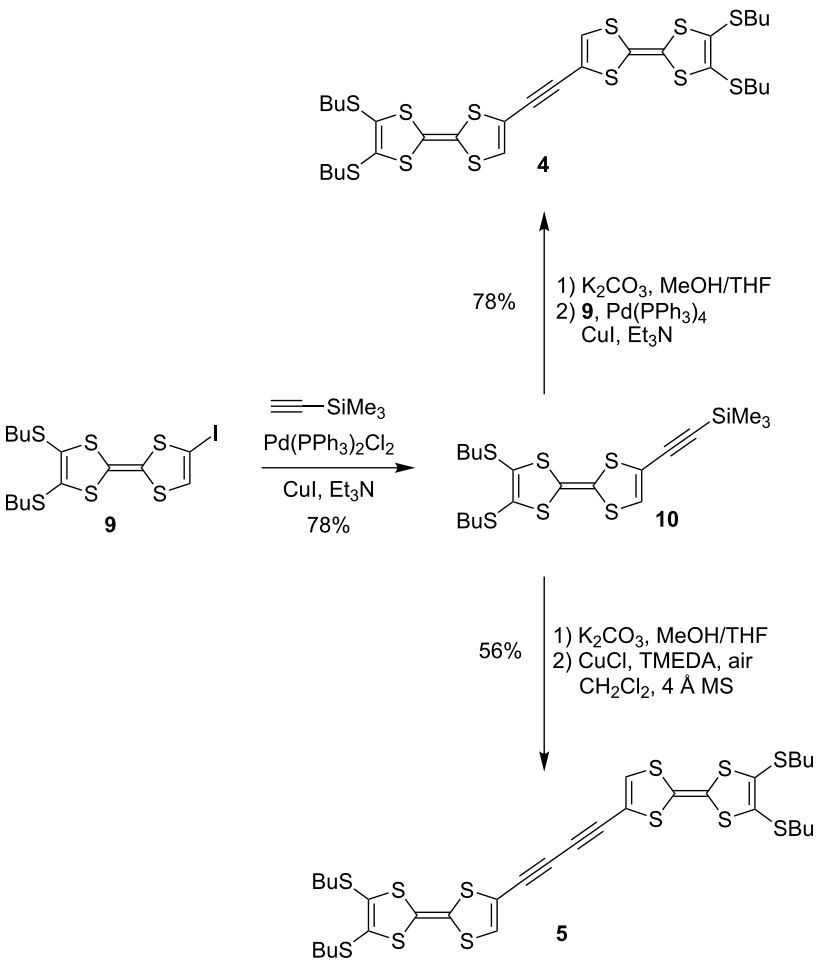

Scheme 1: Synthesis of TTF dimers with alkyne bridges. TMEDA = *N*,*N*,*N*',*N*'-tetramethylethylenediamine. MS = molecular sieves.

Compounds **6** and **7** were prepared by treating **9** with either the *trans*-TEE **11** [18] or 2,6-diethynylpyridine **12** in Sonogashira coupling reactions (Scheme 2). The unsymmetrical radiaannulene **8** was prepared according to Scheme 3. The TEE-TTF derivative **13** [15] was reacted in a Sonogashira coupling with an excess of trimethylsilylacetylene to furnish the product **14**. Removal of the silyl groups and subjecting the intermediate to oxidative Hay conditions in the presence of 4 Å molecular sieves then gave the macrocyclic product **8** in good yield. The structure of **8** was confirmed by X-ray crystallographic analysis (Figure 2). The bond angles in the cyclic core are listed in Figure 3. The butadiyne-diyl unit is bent from linearity – with a C_{TTF}–C≡C angle of 166° and a C≡C–C angle of 170°. The cyclic core is almost planar, while the two TTF units are slightly bent.

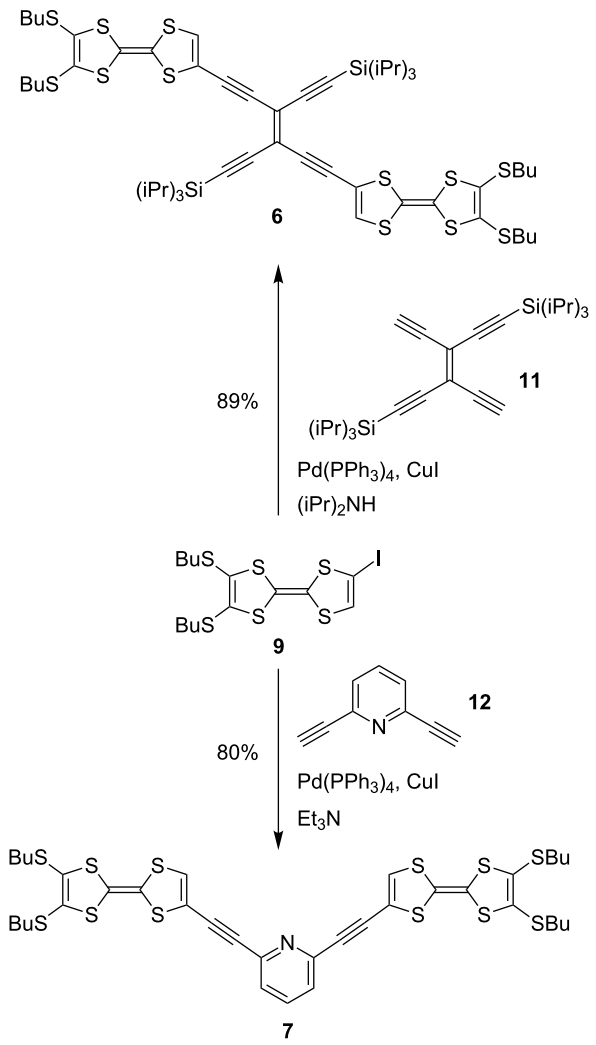

Scheme 2: Synthesis of TTF dimers with TEE and diethynylpyridine bridges.

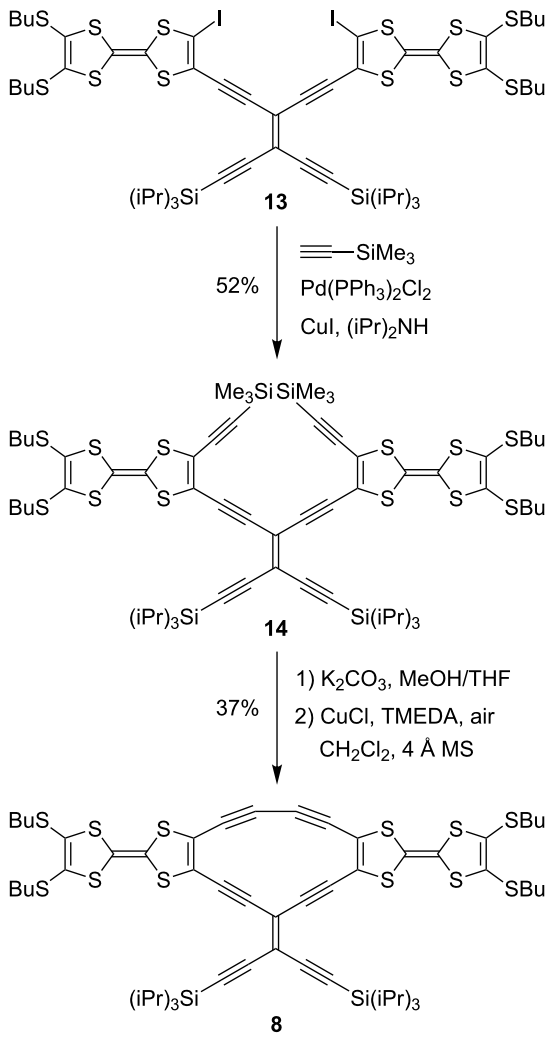

Scheme 3: Synthesis of TTF dimer with radiaannulene core.

Compounds **1b**, **6**, and **8** containing TEE bridging units exhibit longest-wavelength absorption maxima at λ_{max} 529 nm (ε 5800 $M^{-1}cm^{-1}$), 554 nm (ε 12000 $M^{-1}cm^{-1}$), and 651 nm (ε 3900 $M^{-1}cm^{-1}$), respectively, in CH_2Cl_2 (for spectral data of all compounds, see Supporting Information File 1). For radiaannulene **2a** we previously found a longest-wavelength absorption of 644 nm (ε 11000 $M^{-1}cm^{-1}$) [10]. We assign these low-energy bands to charge-transfer absorptions, which are usually observed in π-conjugated systems containing TTF donors and large acetylenic scaffolds that behave as electron acceptors [8-10]. The significant redshifts of the charge-transfer absorptions experienced for **8** and **2a** relative to the absorptions of **1b** and **6** signal the stronger acceptor strength of radiaannulene cores (lower-lying LUMOs) relative to an acyclic TEE unit. This effect was also confirmed by electrochemistry (vide infra). Interestingly, compound **7** containing a diethynylpyridine acceptor unit exhibits the most redshifted absorption of all the

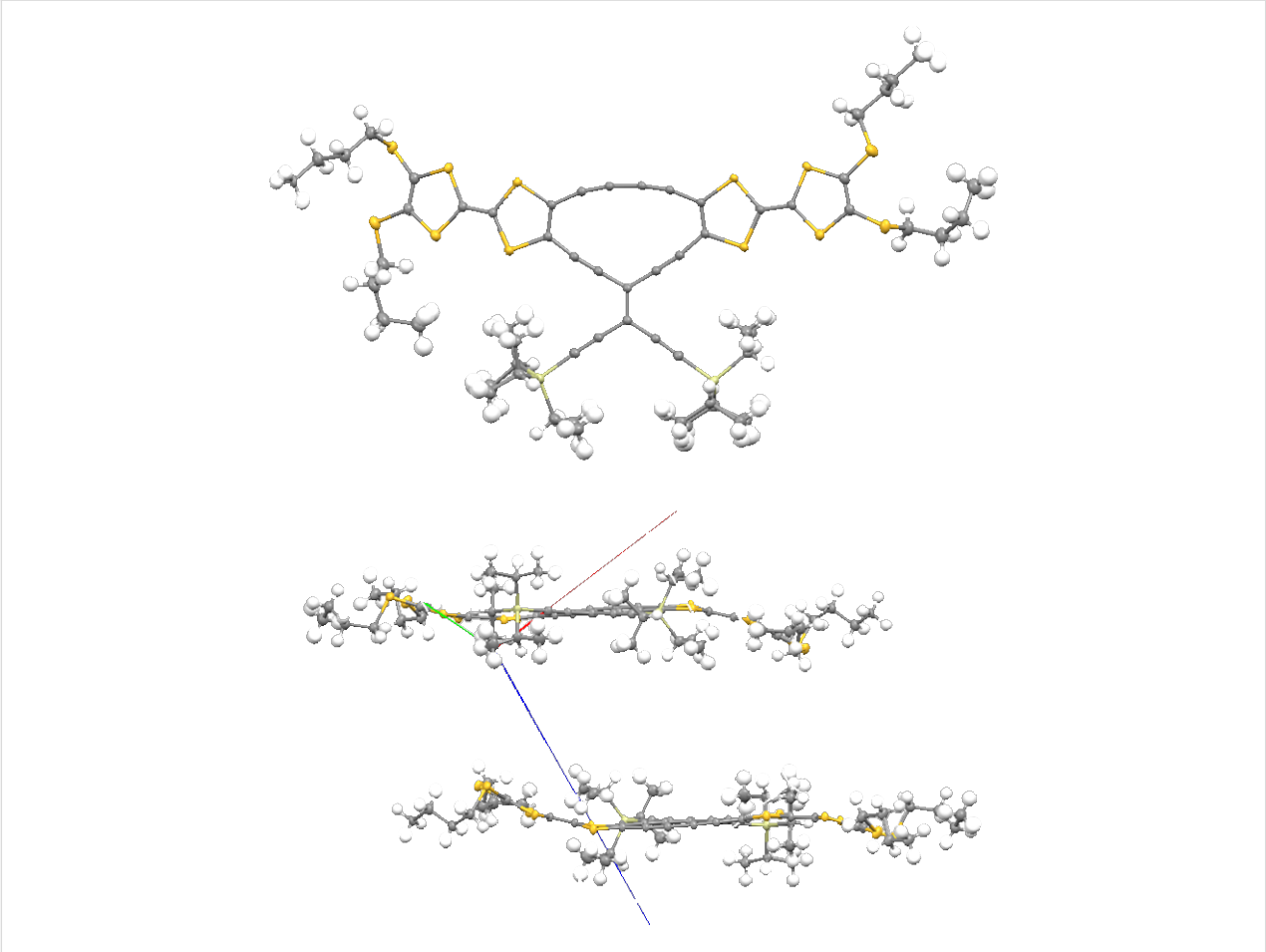

Figure 2: Molecular structure of **8** (top) and packing diagram (bottom). Crystals were grown from CH_2Cl_2/MeOH. CCDC 1050621 contains the supplementary crystallographic data.

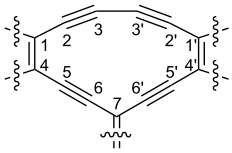

Bond angle (°)	
C1-C2-C3 / C1'-C2'-C3'	166.5 / 166.4
C2-C3-C3' / C2'-C3'-C3	169.6 / 170.0
C4-C1-C2 / C4'-C1'-C2'	120.9 / 120.3
C1-C4-C5 / C1'-C4'-C5'	121.6 / 122.6
C4-C5-C6 / C4'-C5'-C6'	173.0 / 173.1
C5-C6-C7 / C5'-C6'-C7'	178.6 / 177.3
C6-C7-C6'	118.1

Figure 3: Bond angles for the cyclic core of **8** (X-ray crystal structure data).

compounds at λ_{max} 779 nm (ε 210 $M^{-1}cm^{-1}$), but of significantly lower intensity than the charge-transfer absorptions of the TEE compounds.

Electrochemistry

The redox properties of the TTF-bridge-TTF molecules were investigated by cyclic voltammetry and differential pulse voltammetry in CH_2Cl_2 (0.1 M Bu_4NPF_6). For clarity we have broken the discussion of the electrochemistry into two sections, the first being the oxidation of the TTFs and their electronic interactions in comparison to related examples in the literature. The other section deals with the reduction of the molecules.

Oxidation: Cyclic voltammograms of compounds **1a**, **2a**, **3b**, and **4–8** measured at a glassy carbon electrode are shown in Figure 4 [19] and redox potentials are listed in Table 1 together with the shortest TTF (C=C)–TTF (C=C) distance in each structure (obtained from the crystal structures or from DFT calculations). In addition to half-wave potentials obtained from cyclic voltammetry, the table includes peak potentials from differential pulse voltammetry (see Supporting Information File 1, Figure S3). The half-wave redox potentials have been additionally determined for samples **1b** and **2b** (Table 1 and Supporting Information File 1, Figure S4) using cyclic voltam-

metry (with a platinum-wire working electrode in the presence of internal ferrocene potential marker). They are very close to **1a** and **2a**, respectively, as expected. Using **3b** as a reference compound, it is seen that all the other compounds are slightly more difficult to oxidize owing to the presence of the electron-withdrawing alkyne system. The acyclic compounds **1a** and **5**–**7** all undergo two reversible two-electron oxidations; that is, the two TTFs are oxidized at the same potentials when separated by butadiyne, *gem*- or *trans*-TEE, or bis-ethynylpyridine linkers. When two TTFs are closer together via an ethyne spacer (**4**), the two waves are rather broad. In fact, a shoulder can be seen for each wave, which indicates weak interactions between the two units, not only for generating two TTF radical cation units, but also for the final generation of two TTF dication units. This splitting is seen more clearly in the differential pulse voltammograms (Supporting Information File 1, Figure S3). We note that for the SEt derivative of compound **4**, measured under different conditions by Iyoda and co-workers (in PhCN, Bu_4NClO_4), only two two-electron oxidations were reported [6]. For the radiaannulene **2a** removal of two electrons was previously [10] found to occur stepwise with a separation between the first and second oxidations of 90 mV. Thus, despite the long *gem*-TEE bridging units, there is a weak interaction between the TTFs that are separated by a shortest distance of 6.64 Å according to the X-ray crystal structure [10]. For the other radiaannulene, **8**, the first oxidation of each TTF unit was also split into two waves, again indicating interaction between them. In this molecule, the two TTF units are separated by a distance of 6.31 Å.

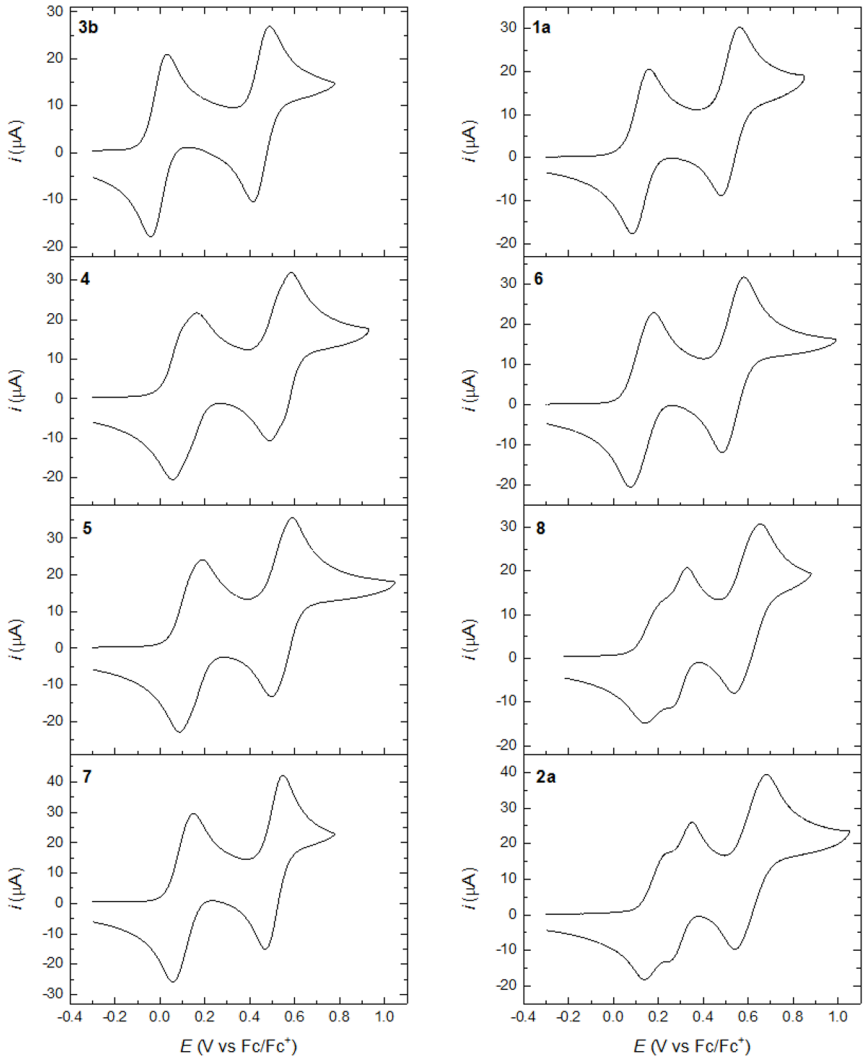

Figure 4: Cyclic voltammograms obtained for the oxidation of compounds **1a** ([10]), **2a** ([10]), and **3b**–**8** (this work, ca. 1 mM) in CH_2Cl_2 (0.1 M Bu_4NPF_6) at a glassy carbon electrode with a scan rate of 0.1 V s^{-1}.

Table 1: Electrochemical data for the oxidation of compounds **1**–**8**.[a]

	Cyclic Voltammetry (CV)			Differential Pulse Voltammetry (DPV)			Shortest TTF–TTF distance / Å
	E_{ox}^1 / V	E_{ox}^2 / V	E_{ox}^3 / V	E_p^1 / V	E_p^2 / V	E_p^3 / V	
1a[b]	+0.12 (2e)	+0.52 (2e)		+0.11 (2e)	+0.51 (2e)		6.88[c]
1b[d]	+0.10 (2e)	+0.50 (2e)					
2a[b]	+0.20 (1e)	+0.29 (1e)	+0.61 (2e)	+0.18 (1e)	+0.29 (1e)	+0.61 (2e)	6.64[e]
2b[d]	+0.18 (1e)	+0.25 (1e)	+0.57 (2e)				
3a[b]	−0.01 (1e)	+0.44 (1e)					n/a
3b	+0.03 (1e)	+0.48 (1e)		−0.01 (1e)	+0.44 (1e)		n/a
4	+0.11[f] (2e)	+0.54[f] (2e)		+0.08 / +0.12[f]	+0.54[f]/+0.56		4.04[c]
5	+0.14 (2e)	+0.54 (2e)		+0.13 (2e)	+0.55 (2e)		6.63[c]
6	+0.13 (2e)	+0.53 (2e)		+0.13 (2e)	+0.50 (2e)		8.92[c]
7	+0.15 (2e)	+0.55 (2e)		+0.10 (2e)	+0.51 (2e)		9.27[c]
8	+0.19[g] (1e)	+0.27[g] (1e)	+0.57 (2e)	+0.21 (1e)	+0.26 (1e)	+0.58 (2e)	6.31[e]

[a]Recorded at a glassy carbon working electrode (if not otherwise stated) in CH_2Cl_2 (0.1 M Bu_4NPF_6), potentials are given vs Fc/Fc^+. CV scan rate: 0.1 V s^{-1}. DPV step potential: 0.0045 V. DPV modulation amplitude: 0.025 V. [b]Data from [10]. [c]Distance(s) obtained by DFT calculations at B3LYP/cc-pVDZ level of theory. [d]Recorded at platinum-wire working electrode. [e]Distance obtained from X-ray crystal structure. [f]Broad signal. [g]Shoulder.

Several bis-TTF molecules and their electrochemical properties have previously been reviewed [1-3]. Here we make a brief discussion of some selected structures of relevance to those studied in this work, as shown in Figure 5. For the directly linked compound **15** [20] and the aryl/heteroaryl mono-bridged compounds **16**, **17** [20] and **18**, **19** [21], only two two-electron oxidations were observed (in PhCN, Bu_4NClO_4). However, incorporation of a Ru centre between two TTF acetylides, complex **20** [22], has been shown to result in a splitting of both the first and second two-electron oxidations of the TTF units (by 110 mV for both). A fifth one-electron event associated to the Ru metal centre was also observed. The two TTFs are 9.37 Å apart, hence further than in the related alkyne compounds **4** and **5**. The strong communication between TTF units in **20** is mediated by the Ru centre, and the bulky ligands possibly also lock the molecule into a conformation where the two TTF units are in co-planarity [22]. The communication dramatically increases when the two TTFs are fused together as in compound **21** [23] or to either a pyrazine or benzene ring [4]. Thus, compounds **21**–**23** all show four distinguishable one-electron oxidation events; in our series, this was only to some extent seen for the C_2-bridged compound **4** as the cyclic radiaannulene cores present in **2a** and **8** only promoted splitting of the first oxidation wave.

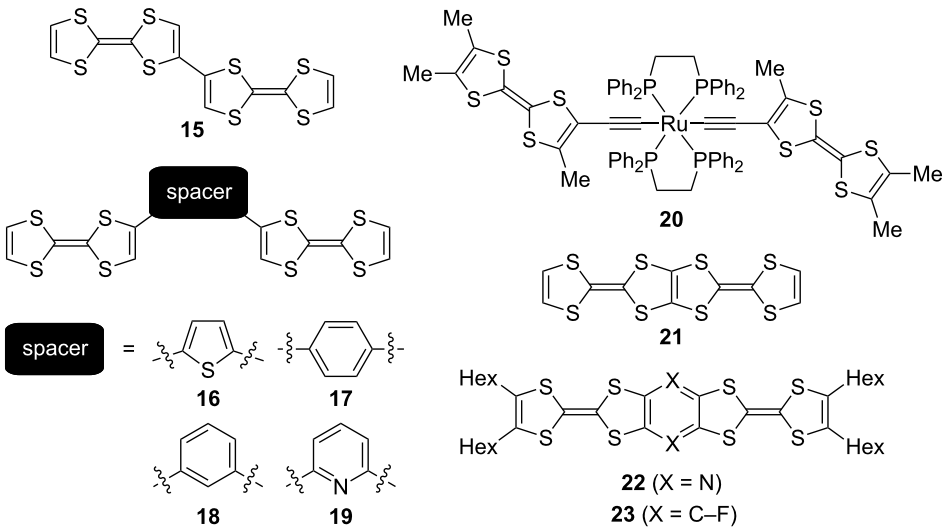

Figure 5: Selected bis-TTFs from literature [20-23].

When taking all the results together, there seem to be some important trends. Placing two TTF units close together by a single bridge does not by itself seem to increase significantly the electronic communication when stepwise oxidations are used as a measure hereof. Instead, fusing directly together the two TTF units, connecting them to a benzene or pyrazine ring, or even to a larger radiaannulene ring, renders them independent redox centres, in all cases when it comes to the first one-electron oxidation of each TTF. Co-planarity of the TTF units seems to play a key role in these structures. This can also be enforced by sterical means and may explain the behaviour of **20**; thus, here the bulky 1,2-bis(diphenylphosphino)ethane (dppe) ligands and the Me group on the TFF might restrict the rotation around the triple bond and sterically keep the two TTFs in the same plane as revealed by the X-ray crystal structure [22]. In compound **18**, the two TTFs are only separated by a *meta*-phenylene bridge, but according to X-ray crystallography they are not co-planar, and no electronic interactions were observed [21]; the cross-conjugated nature of the bridge needs of course to be taken into account here as well. For the derivative of **4** with SEt end-groups instead of SBu groups, we calculate a barrier for rotating the two TTF units around the ethyne bridge of 2.5 kJ mol^{-1} (see Supporting Information File 1). The electronic interactions between two TTFs being spanned by alkynyl or poly-alkynyl bridges are quite poor in comparison to other redox groups. Ferrocene units are only marginally better than TTFs, but the interaction can here also be increased by "doubly-bridging" them [13]. Those redox groups that have shown the best interaction along the all-carbon bridges are the organometallic metal centres $Re(NO)(PPh_3)Cp^*$ [24], Ru(dppe)Cp* [25], and Fe(dppe)Cp* [26] (Cp* = 1,2,3,4,5-pentamethylcyclopentadienyl), showing good communication still well past five carbon–carbon triple bonds between the metal centres.

Reduction: As expected, compound **3b** was found to be non-reducible within the potential window defined by the solvent-supporting electrolyte system (CH_2Cl_2, Bu_4NPF_6). The reduction of the remaining seven compounds falls into three groups; the potentials have been summarized in Supporting Information File 1, Table S2. Compounds **4**, **5**, and **7**, without TEE cores, were found difficult to reduce with poorly defined reduction peaks being observed in the region −2.3 to −2.5 V (Supporting Information File 1, Figure S6). Current corresponding to the oxidation of the initially formed radical anions was not observed during the reverse scan for any of these three compounds. Minor oxidation peaks around −0.75 V may be attributed to the oxidation of intermediate anions presumably formed by further reduction of radical species resulting from protonation by residual water of the radical anions or by protonation of dianions [27]. The corresponding differential pulse voltammograms are shown in Supporting Information File 1, Figure S6. Figure 6 shows the cyclic voltammograms of the four compounds **1a**, **6**, **8** and **2a**, for which reverse current corres-

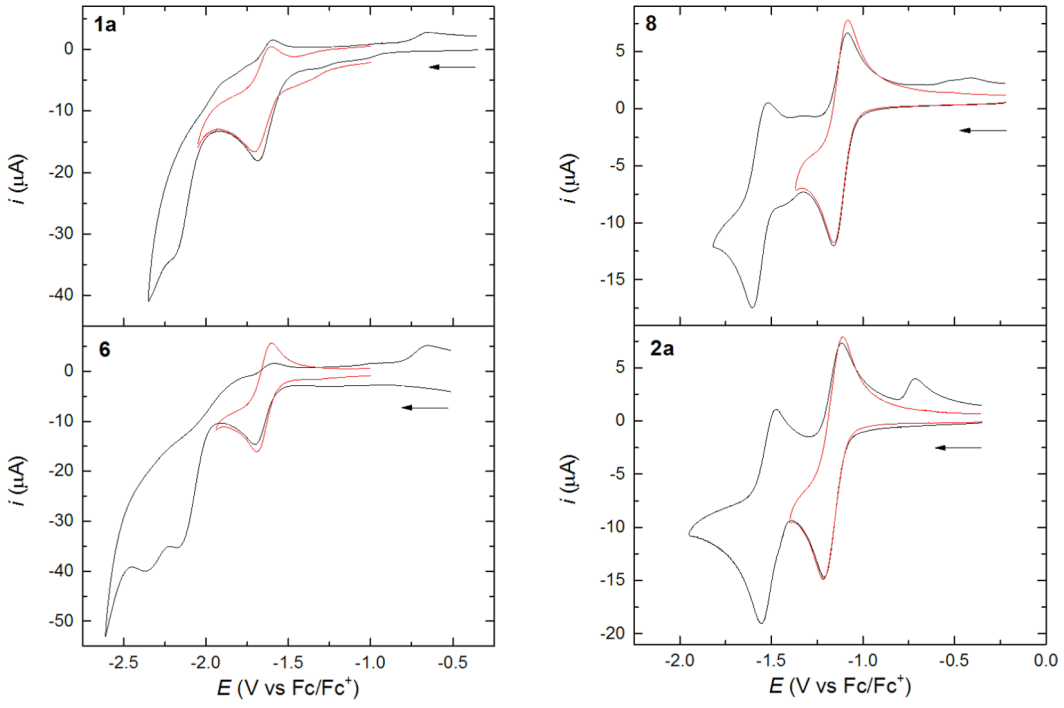

Figure 6: Cyclic voltammograms obtained for the reduction of compounds **1a**, **2a**, **6**, and **8** in CH_2Cl_2 (0.1 M Bu_4NPF_6) at a glassy carbon electrode with a scan rate of 0.1 V s^{-1}. The reduction to the radical anion state only is shown in red color.

ponding to the oxidation of the primarily formed radical anions is clearly seen (DPVs are found in Supporting Information File 1, Figure S5). The further reduction to reactive dianions is seen for **1a** and **6** and, as before, small oxidation peaks, presumably of the same origin as those observed for **4**, **5**, and **7** are seen around −0.75 V during the reverse scan. Most striking is the behaviour of **8** and **2a** for which reversible reduction, not only to the radical anions, but also to the dianions, is clearly seen although even in these two cases the dianions are sufficiently basic to produce minor amounts of the monoprotonation products, the oxidation of which are seen during the reverse scan. We have previously shown that the radiaannulene **2a** is reduced in two sequential one-electron steps at potentials significantly less negative, −1.16 V and −1.52 V vs Fc/Fc^+, than that required to reduce the acyclic TEE compound **1a** (−1.70 V vs Fc/Fc^+) [10]. We explained this readiness of **2a** to accommodate electrons by a gain of aromaticity; a resonance form with a 14 π_z core can be drawn for the dianion and a diatropic ring-current was supported by NICS calculations. The new radiaannulene **8** underwent reversible reductions at −1.12 V and −1.51 V. The readiness of the first reduction may again be explained by the generation of a 14 π_z aromatic core of the radical anion as shown in Figure 7. Thus, again the first reduction occurred at much less negative potential than that of its acyclic components, **1a** and **5** (−1.65 V and −2.35 V vs Fc/Fc^+).

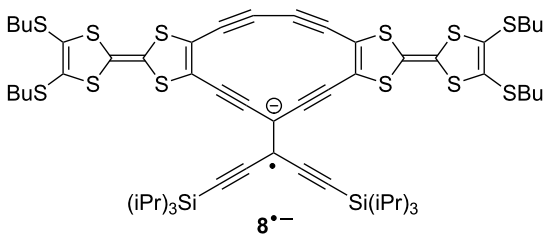

Figure 7: One possible resonance form of the radical anion of **8** with a 14 π_z aromatic core.

UV–vis–NIR and EPR spectra of oxidized species

The EPR and optical (UV–vis–NIR) properties of the oxidized species were studied by in situ spectroelectrochemistry in CH_2Cl_2 (Bu_4NPF_6) at a platinum mesh electrode. Even at low scan rate of 2 mV s^{-1} used for these studies, the reversibility remains unchanged confirming the high stability of the formed radical cation and dication states within each TTF redox site (in further text defined as "polaron" and "bipolaron" states, respectively; see Scheme 4). The small peak separation, ΔE, between the neighbouring voltammetric peaks for the first and the second electron transfer as well as for the third and the fourth electron transfer indicates a weak (but still certain) interaction between the two TTF units in the investigated TTF dimers.

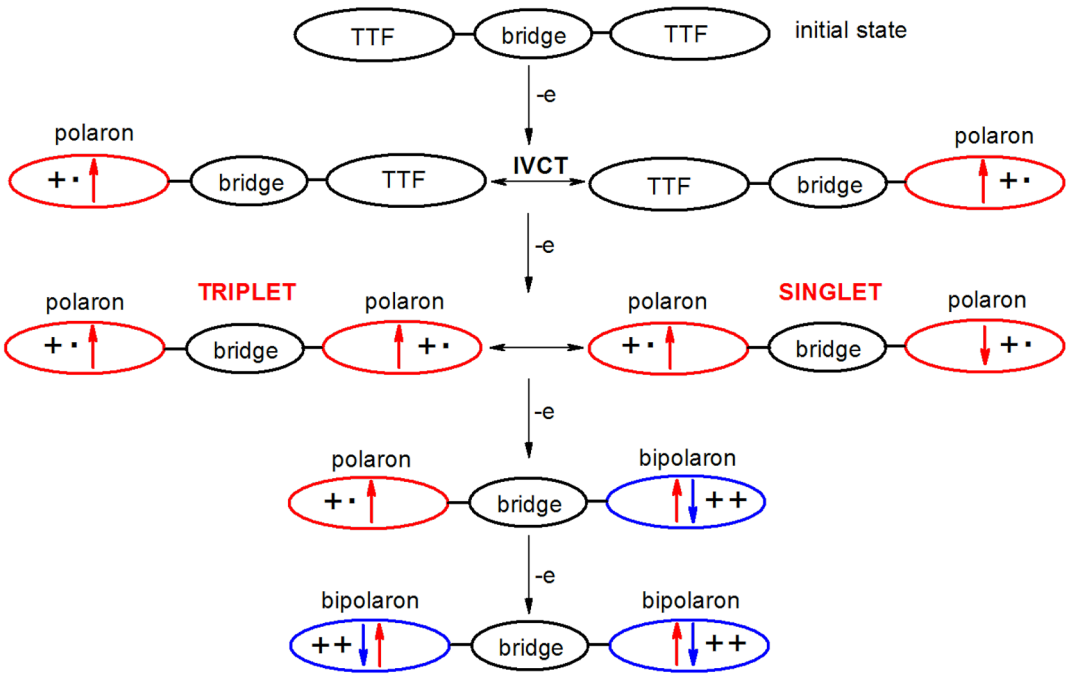

Scheme 4: Spin–spin interactions resulting from oxidation of TTFdimers.

During the in situ oxidation of **1b**, **2b**, **4**, **5**, **6**, and **8** at the first voltammetric double peak, two dominating optical transitions arise, the first one in the region 700–950 nm and the second one in the region 450–550 nm, both characteristic of TTF cation radical (polaron) species [28,29], as illustrated for compound **2b** in Figure 8 and for compound **4** in Figure 9. Simultaneously, singlet EPR spectra with *g*-values around 2.007 were observed (see insets of Figures 8b and 9b) confirming delocalized spin

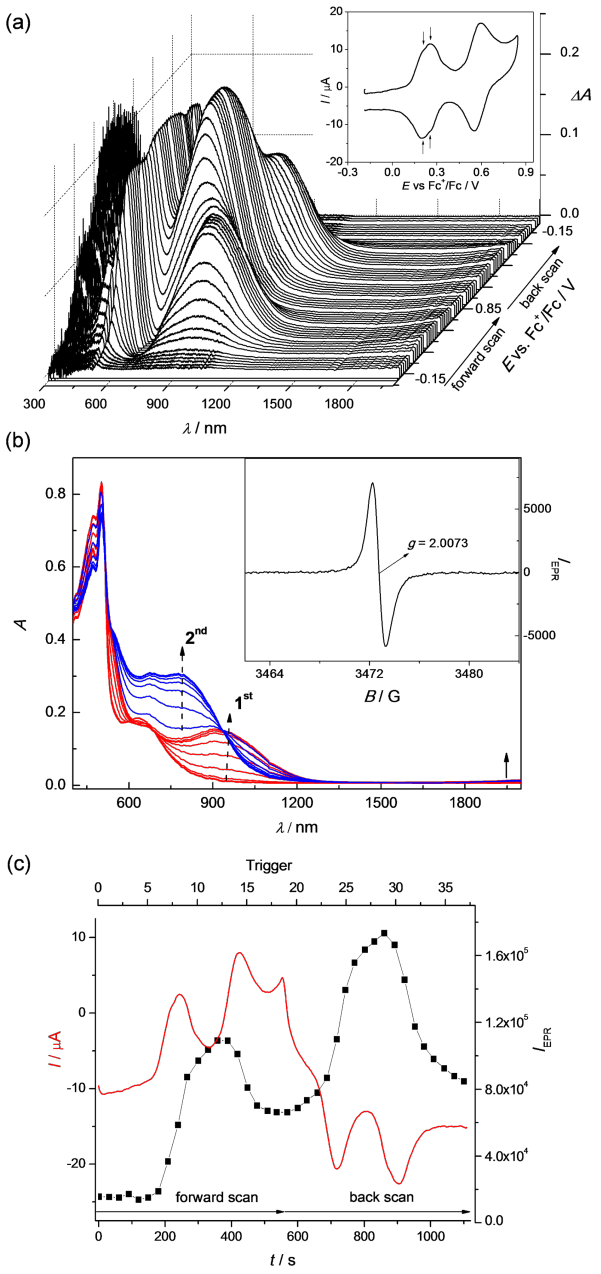

Figure 8: In situ EPR−UV–vis–NIR cyclic voltammetry of **2b** (1 mM) (a) potential dependence of difference vis–NIR spectra with the corresponding cyclic voltammogram (in CH_2Cl_2/0.1 M Bu_4PF_6, scan rate v = 2 mV s^{-1}; the arrows indicate separation between the first and second oxidations); (b) evolution of vis–NIR spectra in forward scan in 2D projection in the region of the first (red lines) and the second (blue lines) voltammetric double peak (inset: representative EPR spectrum of radical species monitored upon oxidation); (c) time dependence of the current (red line) and double-integrated EPR intensity (black solid squares).

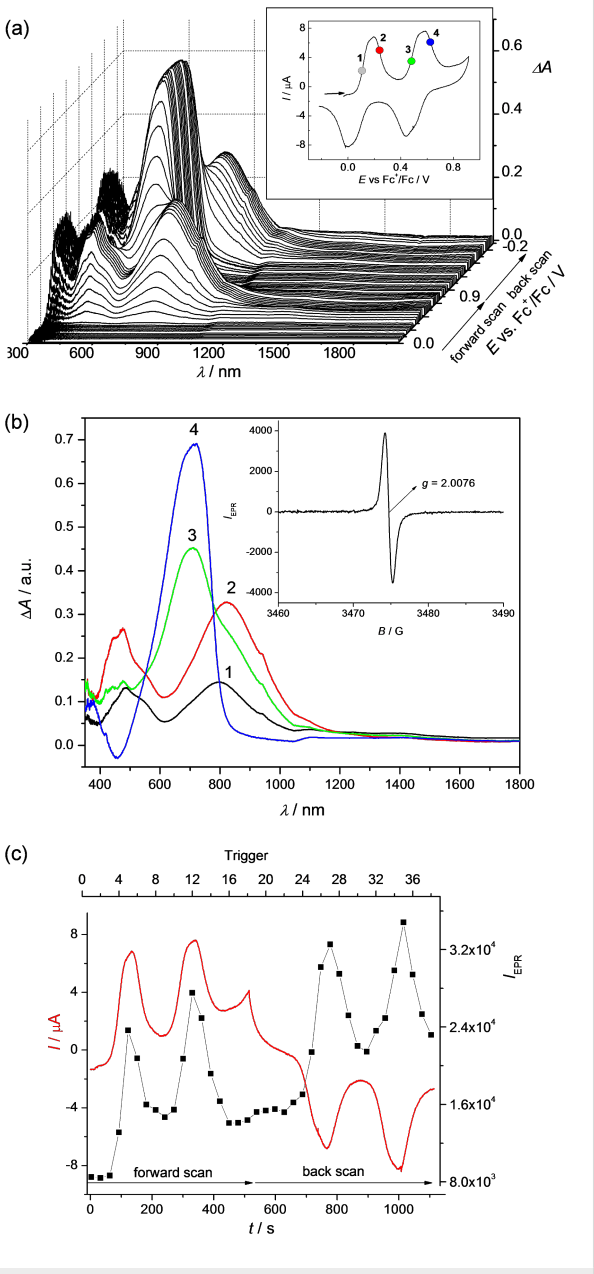

Figure 9: In situ EPR−UV–vis–NIR cyclic voltammetry of **4** (0.4 mM): (a) potential dependence of difference vis–NIR spectra with corresponding cyclic voltammogram (in CH_2Cl_2/0.1 M Bu_4PF_6, scan rate v = 2 mV s^{-1}); (b) selected vis–NIR spectra observed at the foot of the first anodic double peak (1), behind the first voltammetric double peak (2), at the foot of the second anodic double peak (3) and behind the second voltammetric double peak (4); see coloured marked circles in the corresponding voltammogram (inset: representative EPR spectrum of radical species monitored upon oxidation); (c) time dependence of the current (red line) and the double-integrated EPR intensity (black solid squares).

predominantly within the TTF moieties. These data confirm that in the region of the first voltammetric double peak, the only polaronic states are formed in the TTF-dimer. At the second voltammetric double peak, a new dominating absorption band in the region 600–900 arises for all investigated dimers, which corresponds to the formation of doubly charged (bipolaronic) TTF moieties.

Interestingly, it seems that by increasing the interaction between the polaronic species in the dimer we can observe a slight shift of the optical transition characteristic of TTF radical cation going from the first to the second electron transfer as shown in Figure 10. The strongest shifts were observed for dimers **4** and **5** while no shift was found for dimer **1b**. These correspond to Davydov redshifts of head-to-tail $TTF^{\bullet+}$–$TTF^{\bullet+}$, signalling

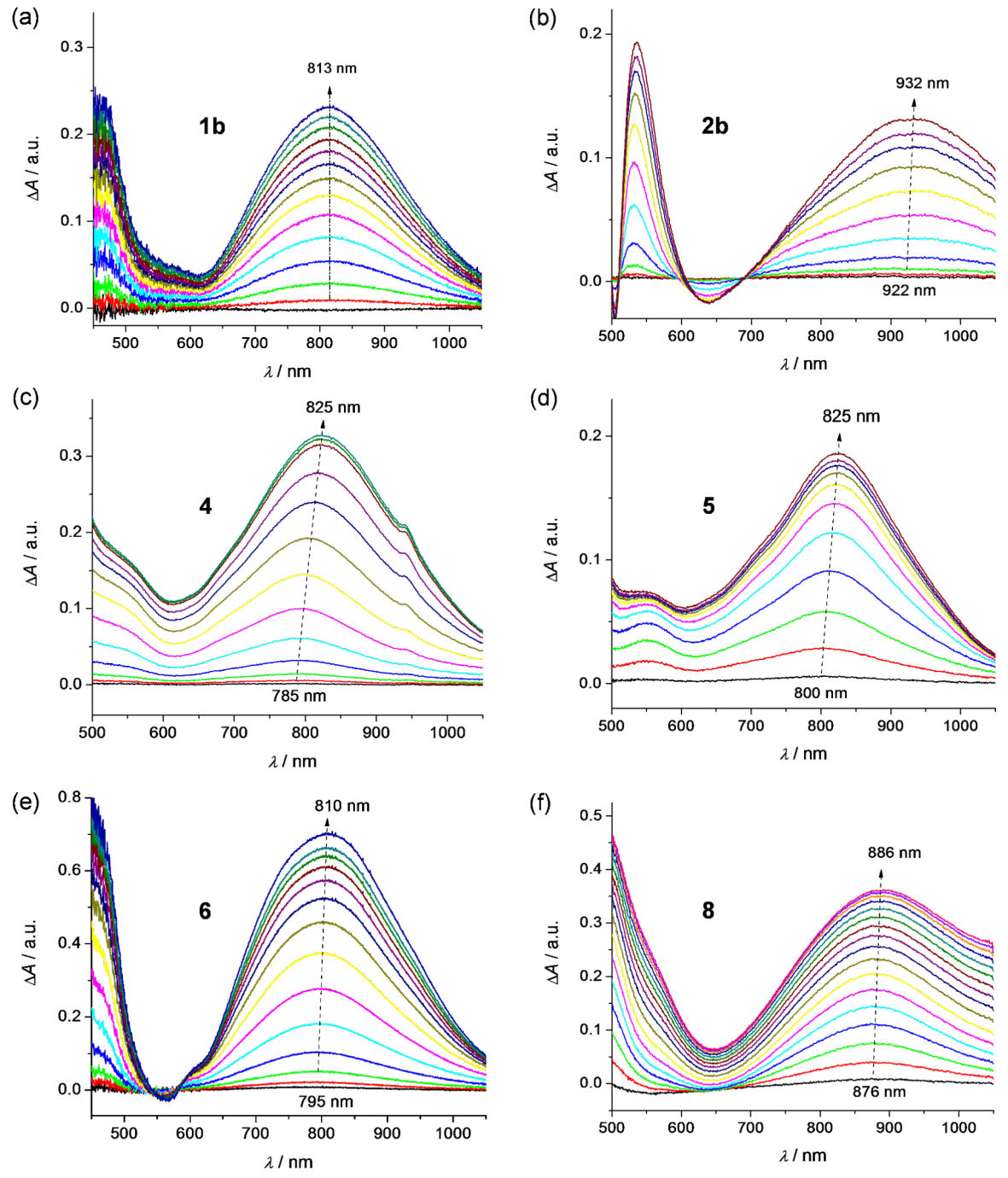

Figure 10: Vis–NIR spectral changes observed during anodic oxidation of each TTF unit to cation radical within the first voltammetric double peak: TTF–TTF → $TTF^{\bullet+}$–TTF → $TTF^{\bullet+}$–$TTF^{\bullet+}$.

intramolecular interactions rather than face-to-face intermolecular interactions [2,30]. Additionally, although all investigated TTF dimers show quite analogous electrochemical and UV–vis–NIR spectroelectrochemical response, the EPR spectroelectrochemical behaviour differs to a certain extent (compare Figure 8c and 9c). Due to a very weak interaction between both mono-charged TTF units in **2b**, the optical spectra of both mono-charged and doubly-charged TTF dimers are very similar and no remarkable changes both in the optical and the EPR spectra were observed in the region of the first cyclovoltammetric double peak. The EPR intensity reaches its maximum behind the first voltammetric double peak (Figure 8c). The maximum of the low energy band of the polaronic TTF species in **2b** is only slightly shifted from 922 nm to 932 nm (small Davydov redshift) upon oxidation in the region of the first voltammetric double peak (Figure 10b). Going to the region of the second voltammetric double peak, the EPR intensity starts to decrease with the minimum behind the second voltammetric double peak, proving the EPR silent character of the TTF dimer tetracation with the optical band at λ_{max} = 810 nm (Figure 8b). Analogous EPR-spectroelectrochemical behavior was observed for compounds **1b**, **6**, and **8** (see Supporting Information File 1, Figures S7–S9). It should be noted that almost the same EPR spectroelectrochemical response was found for concentrated as well as for much diluted solutions (see Supporting Information File 1, Figure S10 for illustration, conc. of **8** at 1 mM vs 0.05 mM).

In EPR–UV–vis–NIR cyclovoltammetric experiments of compounds **4** and **5**, the potential dependencies of the EPR signal are different in comparison to compounds **1b, 2b**, **6**, and **8**. The EPR intensity reaches two maxima in both the forward and back scans. The minimum of EPR intensity was monitored at the second electron transfer as well as at the fourth electron transfer as illustrated for compound **4** in Figure 9c. The increase of the absorbance at dominating band around 790 nm found at the foot of the first anodic double peak for compound **4** corresponds to the increase of the EPR intensity. Simultaneously, a new optical band at 485 nm appears with an additional low-intense NIR band at ca. 1400 nm (see Figure 9b), confirming the primarily formed monocharged dimer $\mathbf{4}^{\bullet+}$, which exhibits an IVCT band as also observed by chemical [6] or electrochemical oxidation (vide infra; also $\mathbf{2b}^{\bullet+}$ exhibited an IVCT band, with maximum >2000 nm, as previously reported for the related species $\mathbf{2a}^{\bullet+}$ [10]). By increasing the electrode potential to the value of the second electron transfer (still in the region of the first anodic double peak), a quite strong shift of the low energy transition from 785 nm to 825 nm (Figure 10c) was observed with simultaneous decrease of the corresponding EPR intensity. Changing the concentration from 0.4 mM to 0.05 mM for sample **4**, the same EPR spectroelectrochemical response was found (see Supporting Information File 1, Figure S11 for illustration). The analogous behaviour was found for compound **5** with the wavelength shift of the low optical band from 800 nm to 825 nm (see Figure 10d and Supporting Information File 1, Figure S12). The EPR silent character of TTF dimer dications found for samples **4** and **5** indicates a substantial interaction of the formed polaronic states leading to the EPR silent species. Interestingly, at the foot of the second anodic double peak, actually corresponding to the third electron transfer, an increase of EPR intensity was monitored confirming that trication of the TTF dimer is paramagnetic. It should be noted that at this anodic potential both optical transitions from polaronic and bipolaronic species are present (see green line 3 in Figure 9b). This confirms that one TTF unit is in its polaronic form while the second one is bipolaron (see Scheme 4). At the potentials behind the second voltammetric double peak, where the absorbance at 715 nm shows a maximum (see blue line 4 in Figure 9b), the EPR intensity has a minimum confirming the EPR silent character of bipolaronic TTF species and that TTF dimer tetracation is EPR silent as expected.

The complex spectroelectrochemical responses may be explained by two possible mechanisms. *The first one* concerns an intramolecular interaction of two polaronic TTF units leading to the EPR silent polaron pair in the singlet state. *The second possibility* could be the formation of intermolecular π-dimers [28,31] represented by the EPR silent tetracationic structures formed from the two doubly charged TTF dimers. After the third electron transfer to each TTF dimer these structures are no more stable and the EPR active TTF dimer trications are formed, which are further immediately charged to the EPR silent TTF dimer tetracations.

As already extensively discussed in [32] concerning the redox properties of self-assembled polyelectrolyte multilayers, consisting of well-defined water-soluble electronically conducting poly-3-(30-thienyloxy)propyltriethylammonium, the spinless doubly charged species can be explained by the interchain or intrachain coupling of two polarons, leading to the formation of dimeric structures between the neighboring chains or to the formation of two polaronic structures in a singlet ground state within the chain [33]. The structures corresponding to polarons and polaron pairs exhibited similar optical spectra and only a small shift in wavelengths was found [32]. It should be noted that the formation of interchain π-dimers is strongly suppressed in dilute solutions. As already mentioned above, we observed the same potential dependence of the EPR signal for compounds **4** and **5** both in the concentrated and in the diluted solutions. This suggests that the doubly charged structures **4** and **5** are in the form of a spinless dication, represented by the two interacting intrachain polarons. Obviously, the optical spectra of

interchain π-dimers of short oligomers are characterized by two optical transitions, which exhibit a rather large blue shift with respect to the two bands of the corresponding radical cations which was not observed for TTF-dimers **4** and **5**.

Going to the region of the second voltammetric double peak, when both TTF segments are already monocharged, the bipolaronic EPR silent TTF structures start to be formed and a new optical band appears in the spectral region between the two polaronic bands (see blue line 4 in Figure 9b and Scheme 4).

For compound **8**, in addition to the small shift of the TTF cation optical band from 876 nm to 886 nm (Figure 10f), we observed also a small shift of *g*-value going to the second electron transfer (see Supporting Information File 1, Figure S9d). This indicates the non-negligible interaction between the polaronic states within the doubly charged TTF dimer **8** but this interaction does not lead to the spinless species as found for **4** and **5**. Both polaronic structures behave as nearly independent and their weak interaction probably leads to the shift in the *g*-value.

NIR absorptions of monocations. Finally, we wanted to examine, in more detail, the broad bands in the NIR region of the spectra of the mixed-valence radical cations. For this objective, compounds **1b**, **4**, **5**, and **8** dissolved in CH_2Cl_2 + 0.1 M Bu_4NPF_6 were studied using another spectroelectrochemical set-up, an optically transparent thin-layer electrochemical Ottle cell equipped with a Pt mini grid working electrode and CaF_2 windows. Figure 11 shows the spectral evolution upon electrolysis of **1b**, **4**, **5**, and **8**. Not surprisingly, compound **1b**, which showed no sign of electronic interactions between the TTF units in the CV (two two-electron oxidations), exhibited no CT absorption band during the oxidation from neutral to dication. Instead, compound **8**, and, in part, compound **4** showed

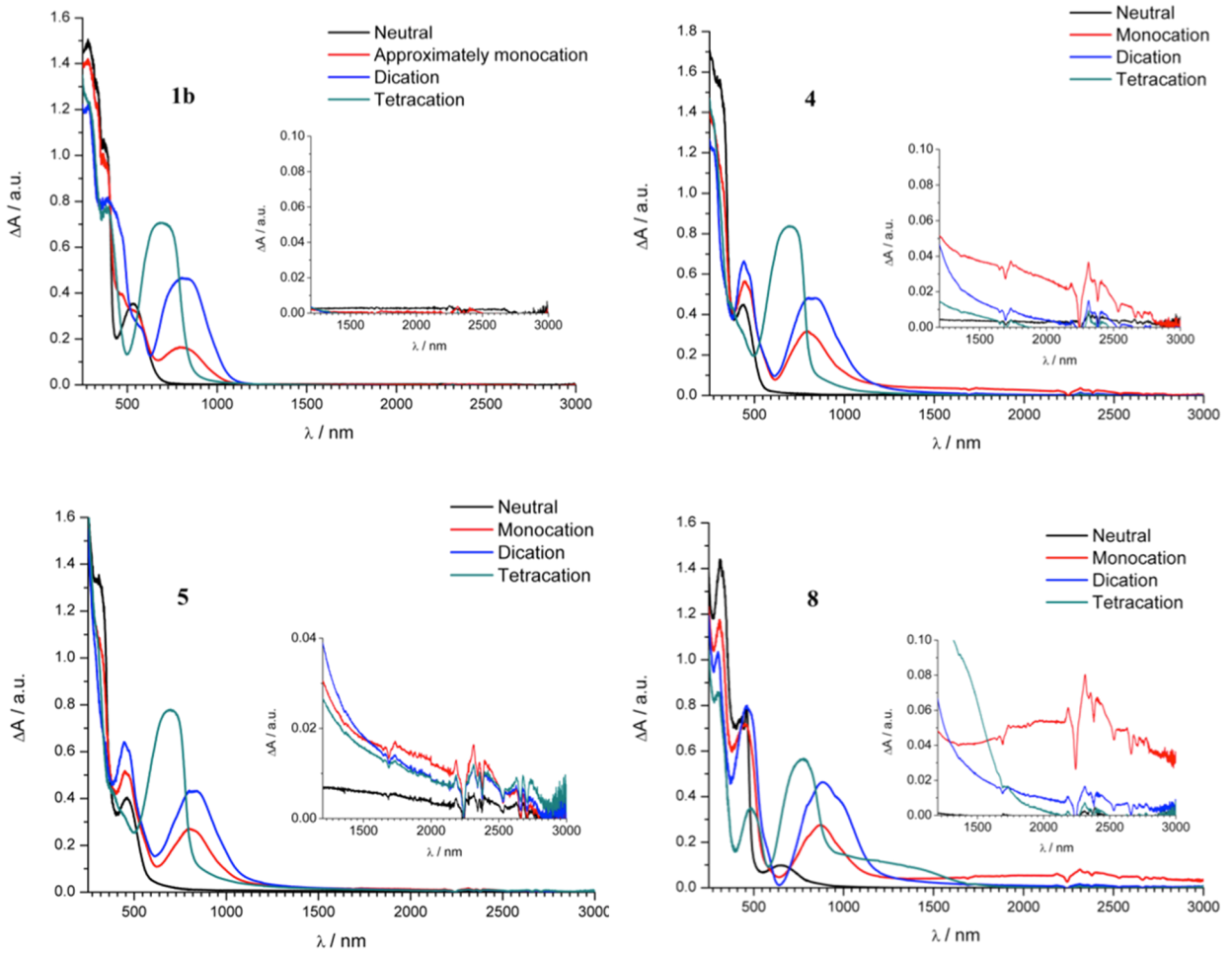

Figure 11: UV–vis–NIR absorptions of **1b** (2.4 mM), **4** (3.5 mM), **5** (2.9 mM), and **8** (1.9 mM) in CH_2Cl_2 + 0.1 M Bu_4NPF_6 at different oxidation states (obtained by electrolysis of the neutral species in an Ottle cell, ultimately generating the tetracation). The insets show expansions of the NIR region. For **1b**, the assignment "approximately monocation" refers to the stage during the electrolysis where this cation is judged to be the major species present.

interactions during the first oxidation of each TTF in the cyclic and differential pulse voltammetry experiments. In accordance hereto, both $\mathbf{4}^{\bullet+}$ and $\mathbf{8}^{\bullet+}$ exhibited broad absorption bands extending to 3000 nm (and apparently beyond for $\mathbf{8}^{\bullet+}$, but, in general, baseline fluctuations add some uncertainty to the intensities of the NIR absorptions and where they exactly end in our spectra). The maximum is around 2300 nm for $\mathbf{8}^{\bullet+}$ (the noise present is due to strong interference from vibrational transitions in the CH_2Cl_2 solvent), while it is somewhat blueshifted for $\mathbf{4}^{\bullet+}$ and seems to agree with the value 1400 nm estimated from the parallel measurement described above (Figure 9b). The NIR absorption of $\mathbf{4}^{\bullet+}$ is in agreement with the broad absorption at 1300 nm reported by Iyoda and co-workers [6] for a derivative of **4** with SEt substituents (measured at one order of magnitude lower concentration, $<10^{-4}$ M, in $MeCN/CH_2Cl_2$ 1:4 using $Fe(ClO_4)_3$ as oxidizing agent). It is difficult to say if the long and weak absorption tail extending to almost 3000 nm observed in our experiment could be an IVCT absorption of the intermolecular mixed valence species, if present. The NIR absorptions of $\mathbf{4}^{\bullet+}$ and $\mathbf{8}^{\bullet+}$ disappeared upon further oxidation to the dications, corroborating the CT character. The position of the more well-defined NIR absorption band of $\mathbf{8}^{\bullet+}$ is close to that of $\mathbf{2a}^{\bullet+}$ at 2257 nm [10]; $\mathbf{2b}^{\bullet+}$ also experiences this absorption according to the EPR-spectroelectrochemistry described above (see Figure 8), but in that experiment, the NIR detection only goes to 2000 nm and therefore does not provide the full NIR absorption band. The neutral spectrum of **8** was not fully regenerated after one cycle (neutral – monocation – dication – tetracation – neutral), presumably due to some degradation (see Supporting Information File 1) although an air-tight Ottle cell was used, filled with solution kept under inert atmosphere. When a TEE is separating the two TTFs in an acyclic structure ($\mathbf{1b}^{\bullet+}$), they are too remote to interact. However, when cyclized into TEE-based radiaannulene structures, $\mathbf{2a}^{\bullet+}$, $\mathbf{2b}^{\bullet+}$, and $\mathbf{8}^{\bullet+}$, interactions appear despite the similar distance between the TTF units as in **1b**. The triisopropylsilyl groups in **2a** and **2b** prevent the formation of face-to-face complexes in which the TTF units interact pairwise (calculations indicate that the TTF units cannot come closer together than approximately 13 Å, see Supporting Information File 1) and the NIR absorptions of the radiaannulene cations are therefore most likely of intramolecular origin. No interaction between the two TTF units was observed in the CV of **5**. There seems, however, to be a very weak CT band around 1700 nm for $\mathbf{5}^{\bullet+}$ with a tail until ca. 3000 nm (but this weak absorption does not disappear fully upon further oxidation). In comparison, Iyoda and co-workers [6] reported a broad absorption at 1200 nm for the monocation of the SEt derivative obtained by chemical oxidation. We also subjected selected compounds to chemical oxidations using tris(4-bromophenyl)aminium hexachloridoantimonate ("magic blue") as oxidant (spectra not shown), but weak NIR absorption bands were here not only present for the monocations of **4**, **5**, and **8**, but also for the higher oxidation states, and it is likely that some decompositions have occurred.

UV–vis–NIR and EPR spectra of reduced species

In cyclic voltammetric studies discussed above, a nearly reversible first cathodic reduction was observed for radiaannulenes **2b** and **8**. At the low scan rates (2 mV s^{-1}) used in spectroelectrochemistry, the cyclic voltammetric peaks become nearly irreversible indicating much lower stability of the formed radical anions in comparison to the corresponding radical cations. Nevertheless, a hint of counter peak in the back anodic scan at low scan rates for both compounds indicates that the primarily formed radical anions could be observed in the EPR spectroelectrochemical experiment. Figure 12 shows the vis–NIR/EPR spectrolectrochemical response found for sample **2b** in CH_2Cl_2 (Bu_4NPF_6) at a platinum mesh electrode. A new dominating absorption band with maximum at 842 nm having a rich vibronic pattern was observed during the in situ reduction in the region of the first cathodic voltammetric peak (a similar absorption at λ_{max} 845 nm was previously found for $\mathbf{2a}^{\bullet-}$ [10]) with the coincident monitoring of narrow single line EPR spectrum with *g*-value of 2.0024 (see Figure 12b). The intensity of the new optical band correlates well with the EPR intensity of the simultaneously-taken narrow EPR spectra (compare Figure 12a and 12c). However, in addition to the narrow EPR singlet line, an additional EPR signal was found (see EPR spectrum marked with asterisks in inset of Figure 12b), the intensity of which increased after prolonged reduction, indicating the formation of a new paramagnetic product by follow-up reactions. Consequently the first EPR signal can be tentatively ascribed to the radical anion $\mathbf{2b}^{\bullet-}$ while the second EPR signal is an unidentified product formed by conversion of this radical anion. Very similar EPR spectra were observed upon cathodic reduction of radiaannulene **8** as shown in Supporting Information File 1, Figure S13. A new optical band at λ_{max} = 653 nm accompanied with a narrow EPR signal at g = 2.0024 were monitored in the region of the first reduction peak. The observed *g*-values close to the free electron value for both anions $\mathbf{2b}^{\bullet-}$ and $\mathbf{8}^{\bullet-}$ are characteristic of delocalized spin and correspond to spin delocalization within the π_z aromatic core.

Conclusion

In conclusion, the interactions between TTF units in dimeric structures depend strongly on the spacer unit in a rather complex manner. The interactions do not only rely on the length of the separation between the units, but also on the rigidity/planarity of the dimer, which can be enforced by cyclic cores. First of all, cyclic radiaannulene cores as spacers promote stepwise oxidation of each TTF unit to its radical cation, via an

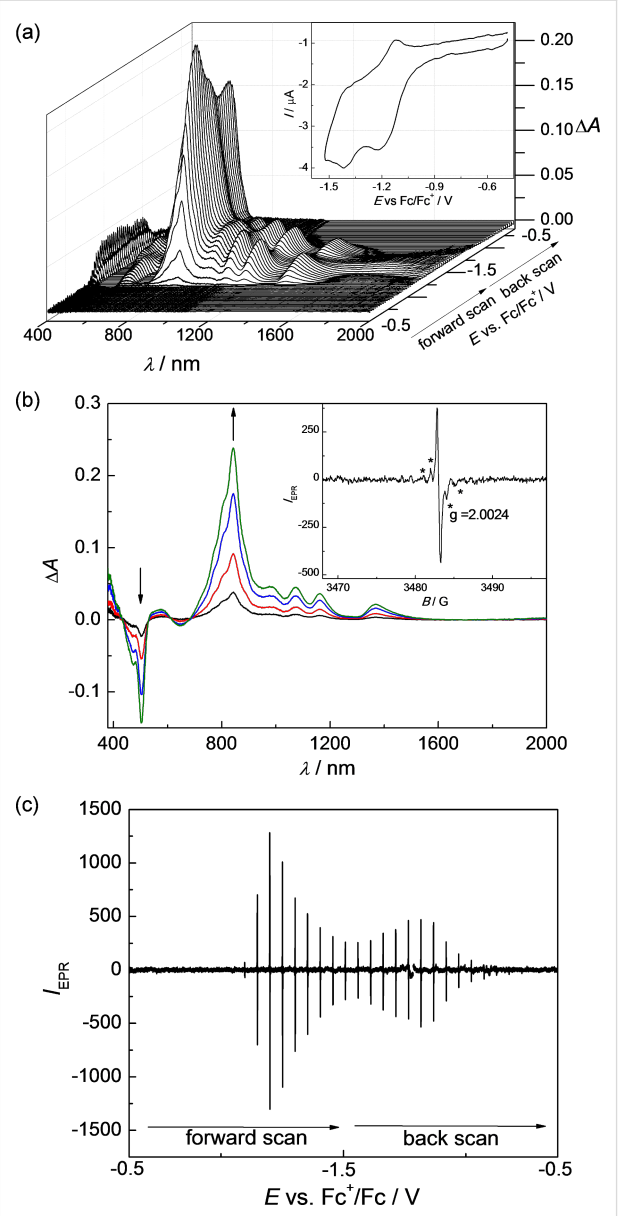

Figure 12: In situ EPR−UV–vis–NIR cyclic voltammetry of **2b** (1 mM) in the cathodic region: (a) potential dependence of vis–NIR spectra with corresponding cyclic voltammogram (in CH_2Cl_2 / 0.1 M Bu_4PF_6, scan rate v = 2 mV s^{-1}); (b) representative difference vis–NIR spectra observed at the first reduction peak (inset: characteristic EPR spectrum of radical species monitored upon reduction); (c) potential dependence of EPR signal monitored during in situ cyclic voltammetric experiment.

intermediate cationic species that exhibits an IVCT band. The generated dication is paramagnetic, signalling two unpaired TTF cation radicals. In contrast, TTF units separated by TEE-bridges in acyclic arrangements, either linearly conjugated or cross-conjugated, behaved as independent redox centres and the intermediate singly-charged *gem*-TEE species did not exhibit IVCT bands. With simple ethynediyl or butadiynediyl spacers in acyclic structures, each TTF unit was also oxidized almost at the same potential, but with some broadening of the first wave for the former compound and its monocation experienced a clear IVCT band, while this band was somewhat weaker for the monocation of the second one. An EPR silent species was generated for the dication of both of these compounds, which signals intramolecular interaction of the two polaronic TTF units as we exclude π-dimerization since the EPR inactivity did not depend on the concentration of the species. A non-negligible interaction between the polaronic states was observed for the dication of the radiaannulene with butadiynediyl and TEE-diyl-bridging units, but in this case, it did not lead to a spinless species. The CT absorptions observed for the radical cations with a short bridge between the two TTF units or a cyclic bridging unit are in general very weak, and it is difficult to make unambiguous assignments of these to intra- and/or intermolecular mixed valence transitions. It is noteworthy, however, that the dications ($TTF^{\bullet+}$–$TTF^{\bullet+}$) experienced Davydov redshifts rather than blueshifts, which signal intramolecular head-to-tail interactions rather than face-to-face π-dimer interactions when both TTF units exist as radical cations (in agreement with the paramagnetic properties). In addition, the triisopropylsilyl groups prevent formation of face-to-face dimers in which all TTFs interact pairwise for those radiaannulenes containing two such bulky groups, pointing to an intramolecular origin of the NIR absorptions.

Finally, the different radiaannulene cores also present redox-active units, undergoing reversible and ready reductions, which we ascribe to some gain in aromaticity upon reduction. On account of these electron-accepting properties, the neutral TTF-radiaannulenes exhibit low-energy CT absorptions.

Experimental

General Methods – Synthesis. Chemicals were purchased from Aldrich, Fluka, and GSF Chemicals and used as received. THF was distilled over the Na/benzophenone couple. Solvents were of HPLC grade and used as received. Thin layer chromatography (TLC) was carried out using aluminum sheets precoated with silica gel 60 F_{254} (Merck 5554). Flash column chromatography was carried out using ROCC or Merck silica gel (40–63 μm). ^{1}H NMR and ^{13}C NMR spectra were recorded on a Bruker instrument (500/126 MHz) with non–inverse cryoprobe using the residual solvent as the internal standard (chloroform-d δ_H = 7.26 ppm, δ_C = 77.16 ppm; dichloromethane-d_2 δ_H = 5.32 ppm, δ_C = 54.00 ppm). All coupling constants are expressed in Hertz (Hz). Melting points were measured on a Reichert melting point apparatus equipped with a microscope and are uncorrected. Mass spectrometry (MS) was performed using Matrix Assisted Laser Desorption Ionization (MALDI); TOF = time-of-flight; FT-ICR = Fourier Transform Ion Cyclotron Resonance. IR spectra were measured

using the attenuated total reflectance (ATR) method on diamond. The relative peak intensities in IR spectra are designated as vw = very weak, w = weak, m = medium, s = strong.

General methods – electrochemistry: Cyclic voltammetry and differential pulse voltammetry were carried out in CH_2Cl_2 containing 0.1 M Bu_4NPF_6 as supporting electrolyte using Autolab PGSTAT12 or CH Instruments 400A or 630B potentiostats. The working electrode was a circular glassy carbon disk (d = 3 mm), the counter electrode was a platinum wire and the reference electrode was a silver wire immersed in the solvent-supporting electrolyte mixture and separated from the solution containing the substrate by a ceramic frit. The potential of the reference electrode was determined vs the ferrocene/ferrocenium (Fc/Fc^+) redox system in a separate experiment. Solutions were purged with nitrogen saturated with CH_2Cl_2 for ten minutes before the measurements were made. Substrate concentrations were in all cases close to 1 mM. All measurements were carried out at room temperature (≈23 °C). **EPR/UV–vis–NIR spectroelectrochemistry:** Commercially available dichloromethane (CH_2Cl_2) and ferrocene (Fc) purchased from Sigma-Aldrich were used without further purification. Tetrabutylammonium hexafluorophosphate (Bu_4NPF_6) of puriss. quality (Fluka) was dried under reduced pressure at 70 °C for 24 h and stored in a desiccator. Cyclic voltammograms (CV) were recorded using a one-compartment electrochemical cell with platinum wires as working and counter electrodes and a Ag wire as a pseudo-reference electrode. Electrochemical measurements were performed under inert argon atmosphere on a PAR 273 potentiostat (EG&G, US) at room temperature. In situ ESR/UV–vis–NIR spectroelectrochemical experiments were performed in an optical ESR cavity (ER 4104OR, Bruker Germany) [34]. EPR spectra were recorded by an EMX X-band CW spectrometer (Bruker, Germany). UV–vis–NIR spectra were measured using the Avantes spectrometer AvaSpec-2048x14-USB2 with an CCD detector and AvaSpec-NIR256-2.2 with an InGaAs detector applying the AvaSoft 7.5 software. Both, the ESR spectrometer and the UV–vis–NIR spectrometer are linked to a HEKA potentiostat PG 390 which triggers both spectrometers. Triggering is performed by the software package PotMaster v2x40 (HEKA Electronik, Germany). For standard in situ ESR/vis–NIR spectroelectrochemical experiments an ESR flat cell was used. A laminated platinum mesh as the working electrode, a silver wire as the pseudo-reference electrode, and a platinum wire as the counter electrode were used in spectroelectrochemical experiments. To reach the nearly thin layer conditions, the electrolyte volume was reduced by inert foil sheets inserted into the flat cell. Experiments were also performed at room temperature in CH_2Cl_2 (0.1 M Bu_4NPF_6) using an optically transparent thin-layer electrochemical (OTTLE) cell equipped with a Pt mini grid working electrode (32 wires cm^{-1}) and CaF_2 windows [35]. The cell was positioned in the sample compartment with the photon source passing through the working electrode mini grid. A narrow slit width setting was chosen in the instrument settings to get good resolution. The UV–vis–NIR spectra were obtained using a Varian Cary 5E spectrophotometer in double beam mode. The controlled-potential electrolysis was carried out using a CH Instruments Model CHI630B potentiostat to manually adjust the potential.

4',5'-Bis(butylthio)-4-(trimethylsilyl)tetrathiafulvalene (10). To a degassed solution of **9** (315 mg, 0.62 mmol) in Et_3N (15 mL) were added $PdCl_2(PPh_3)_2$ (87 mg, 0.12 mmol), CuI (12 mg, 0.06 mmol) and trimethylsilylacetylene (0.70 mL, 5.0 mmol). The mixture was stirred at rt for 3 h after which it became orange. Petroleum spirit (10 mL) was added, the mixture was filtered through a short plug of silica (SiO_2, CH_2Cl_2) and the solvent evaporated in vacuo. Column chromatography (SiO_2, EtOAc/petroleum spirit 1:25) followed by size exclusion column chromatography (Biobeads, S-X3, CH_2Cl_2) afforded compound **10** (230 mg, 78%) as an orange oil. ^{1}H NMR (500 MHz, $CDCl_3$) δ 6.51 (s, 1H), 3.24–2.27 (m, 4H), 1.41 (p, J = 7.3 Hz, 4H), 1.32–1.15 (m, 4H), 0.72–0.52 (m, 6H), 0.00 (s, 9H) ppm; ^{13}C NMR (126 MHz, $CDCl_3$) δ 128.21, 127.66, 125.42, 116.12, 112.62, 109.26, 100.27, 94.97, 36.15, 36.14, 31.91, 31.89, 21.78, 13.74, −0.22 ppm (2 signals missing); MS (MALDI–TOF): m/z = 476 [$M^{\bullet+}$]; HRMS (MALDI+, FT-ICR, dithranol): m/z = 476.02777 [$M^{\bullet+}$] (calcd for $C_{19}H_{28}S_6Si^+$: 476.02790).

1,2-Bis(4,5-bis(butylthio)tetrathiafulvalene)ethyne (4). To a solution of K_2CO_3 (121 mg, 0.88 mmol) in MeOH (30 mL) was added a solution of **10** (56 mg, 0.12 mmol) in THF (5 mL). The mixture was stirred at rt for 20 min, until quantitative conversion was detected by TLC (SiO_2, CH_2Cl_2/heptane 1:4). The mixture was diluted with Et_2O (100 mL), washed with water (3 × 100 mL) and brine (3 × 100 mL). The organic phase was dried over $MgSO_4$ and filtered. Et_3N (15 mL) was added and the solution was concentrated in vacuo until only Et_3N was left. The solution of the desilylated compound in Et_3N was degassed and $Pd(PPh_3)_4$ (21 mg, 0.02 mmol) and CuI (7 mg, 0.04 mmol) were added followed by a degassed solution of **9** in Et_3N (10 mL). After stirring at rt for 3 h, the color changed from orange to red; petroleum spirit was added and the mixture was filtered through a short plug of silica (SiO_2 in CH_2Cl_2) and the solvent evaporated in vacuo. Size exclusion column chromatography (Biobeads, S-X3, CH_2Cl_2) gave compound **4** (73 mg, 78%) as a red amorphous solid. ^{1}H NMR (500 MHz, $CDCl_3$) δ 6.57 (s, 2H), 2.83–2.80 (m, 8H), 1.63–1.59 (m, 8H), 1.46–1.41 (m, 8H), 0.93 (t, J = 7.4 Hz, 6H), 0.92 (t, J = 7.4 Hz, 6H) ppm; ^{13}C NMR (126 MHz, $CDCl_3$) δ 128.28, 127.77, 126.50, 114.90,

111.75, 110.43, 84.61, 36.20, 36.19, 31.98, 31.91, 21.95, 13.75 ppm (2 signals missing); MS (MALDI–TOF): *m/z* = 782 [$M^{\bullet+}$]; HRMS (MALDI+, FT-IRC, dithranol): *m/z* = 781.96161 [$M^{\bullet+}$] (calcd. for $C_{30}H_{38}S_{12}^{+}$: 781.96165).

1,4-Bis(4,5-bis(butylthio)tetrathiafulvalene)-1,3-butadiyne (5). To a solution of K_2CO_3 (190 mg, 1.37 mmol) in MeOH (50 mL) was added a solution of **10** (164 mg, 0.34 mmol) in THF (5 mL). The mixture was stirred at rt for 20 min, until quantitative conversion was detected by TLC (SiO_2, CH_2Cl_2/heptane 1:4). The mixture was diluted with CH_2Cl_2 (150 mL) and washed with brine (3 × 100 mL). The organic phase was dried over $MgSO_4$, filtered and concentrated in vacuo until the total volume was ca. 50 mL. To the obtained solution of the desilylated product in CH_2Cl_2 were added CuCl (3 mg, 0.03 mmol), TMEDA (0.1 mL, 0.67 mmol), and 4 Å molecular sieves (0.12 g), instantly turning the mixture to red. The mixture was stirred vigorously for 2 h, after which it was passed through a short plug of neutralized silica (SiO_2, CH_2Cl_2) and concentrated in vacuo. Size exclusion column chromatography (Biobeads, S-X3, CH_2Cl_2) gave compound **5** (77 mg, 56%) as a red amorphous solid. ^{1}H NMR (500 MHz, $CDCl_3$) δ 6.70 (s, 2H), 2.83–2.79 (m, 8H), 1.63–1.57 (m, 8H), 1.47–1.40 (m, 8H), 0.92 (t, *J* = 7.4 Hz, 6H), 0.92 (t, *J* = 7.4 Hz, 6H) ppm; ^{13}C NMR (126 MHz, $CDCl_3$) δ 129.61, 128.34, 127.70, 114.89, 111.27, 111.20, 77.92, 75.31, 36.19, 31.92, 31.89, 21.79, 13.74 ppm (3 signals missing); MS (MALDI–TOF): *m/z* = 806 [$M^{\bullet+}$]; HRMS (MALDI+, FT-IRC, dithranol): *m/z* = 805.96170 [$M^{\bullet+}$] (calcd. for $C_{32}H_{38}S_{12}^{+}$: 805.96165).

***trans*-TEE-TTF (6).** A solution of **11** (37 mg, 0.09 mmol) in $(iPr)_2NH$ (8 mL) was degassed with argon on an ultrasound bath for 30 min. Then $Pd(PPh_3)_4$ (7 mg, 0.01 mmol), CuI (4 mg, 0.02 mmol), followed by **9** (106 mg, 0.21 mmol) in degassed $(iPr)_2NH$ (2 mL) were added, instantly turning the mixture to dark purple. The mixture was protected from light and stirred at rt for 4 h. Heptane (20 mL) was added and the mixture was filtered through a short plug of silica (SiO_2, CH_2Cl_2) and concentrated in vacuo. Column chromatography (SiO_2, heptane) afforded compound **6** (90 mg, 89%) as a dark purple oil. ^{1}H NMR (500 MHz, CD_2Cl_2) δ 6.63 (s, 2H), 2.86–2.79 (m, 8H), 1.75–1.54 (m, 8H), 1.51–1.39 (m, 8H), 1.23–1.12 (m, 42H), 1.03–0.82 (m, 12H); ^{13}C NMR (126 MHz, CD_2Cl_2) δ 128.76, 128.19, 127.75, 117.30, 115.75, 112.42, 110.47, 105.11, 102.61, 92.01, 90.10, 36.59, 32.42, 32.37, 22.20, 22.19, 19.08, 13.92, 11.87 ppm (2 signals missing); HRMS (MALDI+, FT-ICR, dithranol): *m/z* = 1192.24515 [$M^{\bullet+}$] (calcd for $C_{56}H_{80}S_{12}Si_2^{+}$: 1192.24415).

Compound 7. A flask containing $Pd(PPh_3)_4$ (11 mg, 0.01 mmol), 2,6-bis(ethynyl)pyridine (6.3 mg, 0.05 mmol), and CuI (1 mg, 0.01 mmol) was charged with an argon balloon. A solution of **9** (50 mg, 0.01 mmol) in argon-flushed Et_3N (10 mL) was added and the resulting orange reaction mixture was stirred for 6 h. The reaction was quenched by addition of saturated aqueous NH_4Cl (10 mL) followed by water (100 mL), and the mixture was extracted with CH_2Cl_2 (100 mL). The organic extract was washed with saturated aqueous NH_4Cl (3 × 50 mL), dried with Na_2SO_4, filtered and concentrated in vacuo. Purification by flash column chromatography (SiO_2 pretreated with a 2% solution of Et_3N, CH_2Cl_2/petroleum spirit 1:9 to 1:4, loaded using CCl_4), followed by size-exclusion chromatography (Biobeads S-X3, CH_2Cl_2) gave compound **7** (35 mg, 80%) as a red oil which slowly solidified. M.p. 91–93 °C (CH_2Cl_2). ^{1}H NMR (400 MHz, $CDCl_3$) δ 7.65 (t, *J* = 7.8 Hz, 1H), 7.38 (d, *J* = 7.8 Hz, 2H), 6.71 (s, 2H), 2.82 (t, *J* = 7.3 Hz, 4H), 2.81 (t, *J* = 7.3 Hz, 4H), 1.64–1.60 (m, 8H), 1.47–1.41 (m, 8H), 0.93 (t, *J* = 7.3 Hz, 6H), 0.93 (t, *J* = 7.3 Hz, 6H) ppm; ^{13}C NMR (126 MHz, $CDCl_3$) δ 143.01, 136.78, 128.29, 127.80, 127.65, 126.78, 115.05, 111.99, 110.21, 91.89, 80.97, 36.20, 31.94, 31.92, 21.81, 21.80, 13.76, 13.75 ppm (1 signal missing); HRMS (MALDI+, FT-ICR, dithranol) *m/z* = 882.99032 [$M^{\bullet+}$] (calcd. for $C_{37}H_{41}N^{+}$: 882.98820).

Compound 14. A solution of **13** (99 mg, 0.07 mmol) in $(iPr)_2NH$ (10 mL) was degassed on an ultrasound bath for 30 min. Thereafter, $PdCl_2(PPh_3)_2$ (5 mg, 0.01 mmol), CuI (1 mg, 0.01 mmol), and trimethylsilylacetylene (0.15 mL, 1.03 mmol) were subsequently added. After stirring at rt for 1.5 h, the mixture was filtered through a plug of silica (SiO_2, CH_2Cl_2/petroleum spirit 1:1) and concentrated in vacuo to give compound **14** (49 mg, 52%) as a green oil. ^{1}H NMR (500 MHz, $CDCl_3$) δ 2.81 (t, *J* = 7.3 Hz, 4H), 2.81 (t, *J* = 7.3 Hz, 4H), 1.64–1.58 (m, 8H), 1.46–1.41 (m, 8H), 1.12–1.11 (m, 42H), 0.92 (t, *J* = 7.3 Hz, 6H), 0.92 (t, *J* = 7.3 Hz, 6H), 0.22 (s, 18H) ppm; ^{13}C NMR (126 MHz, $CDCl_3$) δ 127.92, 127.87, 122.84, 120.88, 119.92, 115.19, 112.03, 109.43, 107.77, 105.30, 103.51, 95.07, 94.51, 89.23, 36.22, 31.94, 31.92, 21.80, 18.88, 13.75, 11.41, −0.24 ppm (3 signals missing); HRMS (MALDI+, FT-ICR, dithranol): *m/z* = 1384.32641 [$M^{\bullet+}$] (calcd. for $C_{66}H_{96}S_{12}Si_4^{+}$: *m/z* = 1384.32321).

Radiaannulene 8. To a solution of K_2CO_3 (30 mg, 0.22 mmol) in MeOH (20 mL) was added a solution of **14** (74 mg, 0.05 mmol) in THF (5 mL). The mixture was stirred at rt for 20 min, until quantitative conversion was detected by TLC (SiO_2, CH_2Cl_2/heptane 1:4). The mixture was diluted with CH_2Cl_2 (150 mL) and washed with brine (3 × 100 mL). The organic phase was dried over $MgSO_4$, filtered and concentrated in vacuo until the total volume was ca. 50 mL. To the obtained solution of the desilylated product in CH_2Cl_2 were added CuCl (2 mg, 0.02 mmol), TMEDA (0.1 mL, 0.67 mmol), and 4 Å

molecular sieves (0.06 g). The mixture was stirred vigorously for 2 h, after which it was passed through a short plug of silica (SiO_2, CH_2Cl_2) and concentrated in vacuo. Size exclusion column chromatography (Biobeads, S-X3, CH_2Cl_2) gave compound **8** (24 mg, 37%) as a green oil. Crystals suitable for X-ray crystallography were grown from CH_2Cl_2/MeOH. ^{1}H NMR (500 MHz, $CDCl_3$) δ 2.83–2.80 (m, 8H), 1.64–1.60 (m, 8H), 1.46–1.41 (m, 8H), 1.15–1.14 (m, 42H), 0.93 (t, J = 7.4 Hz, 6H), 0.93 (t, J = 7.4 Hz, 6H) ppm; ^{13}C NMR (126 MHz, $CDCl_3$) δ 128.34, 127.75, 127.59, 121.79, 120.68, 114.29, 108.45, 108.28, 103.90, 98.13, 91.56, 87.85, 86.92, 36.32, 36.28, 31.99, 31.91, 21.82, 21.79, 18.93, 13.74, 13.73, 11.48 ppm (1 signal missing); IR (ATR): 2955s, 2927s, 2863s, 2725vw, 2154w (C≡C), 1716vw, 1676vw, 1461m, 1417w, 1380w, 1346w, 1254m, 1224w, 1201w cm^{-1}; HRMS (MALDI+, FT-ICR, dithranol): m/z = 1238.22912 [M$^{\bullet+}$] (calcd. for $C_{60}H_{78}S_{12}Si_2^+$: m/z = 1238.22851).

Supporting Information

Supporting Information File 1

UV–vis absorption spectra, electrochemical data, UV–vis–NIR absorption spectra of oxidized species, EPR spectra, NMR spectra, and computational data.
[http://www.beilstein-journals.org/bjoc/content/supplementary/1860-5397-11-104-S1.pdf]

Supporting Information File 2

CIF-file of X-ray crystal structure **8**.
[http://www.beilstein-journals.org/bjoc/content/supplementary/1860-5397-11-104-S2.cif]

Acknowledgements

The Villum Foundation is acknowledged for financial support. P.R. thanks the Scientific Grant Agency of the Slovak Republic (Project VEGA/1/0307/14) for financial support.

References

1. Adam, M.; Müllen, K. *Adv. Mater.* **1994,** *6,* 439–459. doi:10.1002/adma.19940060603
2. Iyoda, M.; Hasegawa, M.; Miyake, Y. *Chem. Rev.* **2004,** *104,* 5085–5114. doi:10.1021/cr030651o
3. Lorcy, D.; Bellec, N.; Formigué, M.; Avarvari, N. *Coord. Chem. Rev.* **2009,** *253,* 1398–1438. doi:10.1016/j.ccr.2008.09.012
4. Lahlil, K.; Moradpour, A.; Bowlas, C.; Menou, F.; Cassoux, P.; Bonvoisin, J.; Launay, J.-P.; Dive, G.; Dehareng, D. *J. Am. Chem. Soc.* **1995,** *117,* 9995–10002. doi:10.1021/ja00145a009
5. Otsubo, T.; Kochi, Y.; Bitoh, A.; Ogura, F. *Chem. Lett.* **1994,** *23,* 2047–2050. doi:10.1246/cl.1994.2047
6. Iyoda, M.; Hasegawa, M.; Takano, J.-i.; Hara, K.; Kuwatani, Y. *Chem. Lett.* **2002,** *31,* 590–591. doi:10.1246/cl.2002.590
7. Hara, K.; Hasegawa, M.; Kuwatani, Y.; Enozawa, H.; Iyoda, M. *Chem. Commun.* **2004,** 2042–2043. doi:10.1039/b407200f
8. Andersson, A. S.; Kerndrup, L.; Madsen, A. Ø.; Kilså, K.; Nielsen, M. B.; La Porta, P. R.; Biaggio, I. *J. Org. Chem.* **2009,** *74,* 375–382. doi:10.1021/jo802190q
9. Lincke, K.; Christensen, M. A.; Diederich, F.; Nielsen, M. B. *Helv. Chim. Acta* **2011,** *94,* 1743–1753. doi:10.1002/hlca.201100291
10. Lincke, K.; Frellsen, A. F.; Parker, C. R.; Bond, A. D.; Hammerich, O.; Nielsen, M. B. *Angew. Chem., Int. Ed.* **2012,** *51,* 6099–6102. doi:10.1002/anie.201202324
11. Parthey, M.; Gluyas, J. B.; Schauer, P. A.; Yufit, D. S.; Howard, J. A. K.; Kaupp, M.; Low, P. J. *Chem. – Eur. J.* **2013,** *19,* 9780–9784. doi:10.1002/chem.201301747
12. Parthey, M.; Gluyas, J. B. G.; Fox, M. A.; Low, P. J.; Kaupp, M. *Chem. – Eur. J.* **2014,** *20,* 6895–6908. doi:10.1002/chem.201304947
13. Low, P. J.; Roberts, R. L.; Cordiner, R. L.; Hartl, F. *J. Solid State Electrochem.* **2005,** *9,* 717–731. doi:10.1007/s10008-005-0693-3
14. Hasegawa, M.; Kobayashi, Y.; Hara, K.; Enozawa, H.; Iyoda, M. *Heterocycles* **2009,** *77,* 837–842. doi:10.3987/COM-08-S(F)106
15. Mazzanti, V.; Jiang, H.; Gotfredsen, H.; Morsing, T. J.; Parker, C. R.; Nielsen, M. B. *Org. Lett.* **2014,** *16,* 3736–3739. doi:10.1021/ol5015587
16. Hasegawa, M.; Enozawa, H.; Kawabata, Y.; Iyoda, M. *J. Am. Chem. Soc.* **2007,** *129,* 3072–3073. doi:10.1021/ja069025+
17. Vilhelmsen, M. H.; Jensen, J.; Tortzen, C. G.; Nielsen, M. B. *Eur. J. Org. Chem.* **2013,** 701–711. doi:10.1002/ejoc.201201159
18. Anthony, J.; Boudon, C.; Diederich, F.; Gisselbrecht, J.-P.; Gramlich, V.; Gross, M.; Hobi, M.; Seiler, P. *Angew. Chem., Int. Ed.* **1994,** *33,* 763–766. doi:10.1002/anie.199407631
19. Please notice that the current values given for **2a** in Figure 6 of [10] by a mistake are a factor of 1000 too small.
20. Iyoda, M.; Kuwatani, Y.; Ueno, N.; Oda, M. *J. Chem. Soc., Chem. Commun.* **1992,** 158–159. doi:10.1039/c39920000158
21. Iyoda, M.; Fukuda, M.; Yoshida, M.; Sasaki, S. *Chem. Lett.* **1994,** *23,* 2369–2372. doi:10.1246/cl.1994.2369
22. Vacher, A.; Barrière, F.; Roisnel, T.; Piekara-Sady, L.; Lorcy, D. *Organometallics* **2011,** *30,* 3570–3578. doi:10.1021/om200266q
23. Misaki, Y.; Matsui, T.; Kawakami, K.; Nishikawa, H.; Yamabe, T.; Shiro, M. *Chem. Lett.* **1993,** *22,* 1337–1340. doi:10.1246/cl.1993.1337
24. Dembinski, R.; Bartik, T.; Bartik, B.; Jaeger, M.; Gladysz, J. A. *J. Am. Chem. Soc.* **2000,** *122,* 810–822. doi:10.1021/ja992747z
25. Bruce, M. I.; Cole, M. L.; Ellis, B. G.; Gaudio, M.; Nicholson, B. K.; Parker, C. R.; Skelton, B. W.; White, A. H. *Polyhedron* **2015,** *86,* 43–56. doi:10.1016/j.poly.2014.04.052
26. Lapinte, C. *J. Organomet. Chem.* **2008,** *693,* 793–801. doi:10.1016/j.jorganchem.2007.09.030
27. Parker, V. D.; Tilset, M.; Hammerich, O. *J. Am. Chem. Soc.* **1987,** *109,* 7905–7906. doi:10.1021/ja00259a062
28. Khodorkovsky, V.; Shapiro, L.; Krief, P.; Shames, A.; Mabon, G.; Gorgues, A.; Giffard, M. *Chem. Commun.* **2001,** 2736–2737. doi:10.1039/b104934h
29. Kirketerp, M.-B. S.; Leal, L. A. E.; Varsano, D.; Rubio, A.; Jørgensen, T. J. D.; Kilså, K.; Nielsen, M. B.; Nielsen, S. B. *Chem. Commun.* **2011,** *47,* 6900–6902. doi:10.1039/c1cc11936b
30. Hasegawa, M.; Daigoku, K.; Hashimoto, K.; Nishikawa, H.; Iyoda, M. *Bull. Chem. Soc. Jpn.* **2012,** *85,* 51–60. doi:10.1246/bcsj.20110224
31. Rosokha, S. V.; Kochi, J. K. *J. Am. Chem. Soc.* **2007,** *129,* 828–838. doi:10.1021/ja064166x

32. Rapta, P.; Lukkari, J.; Tarábek, J.; Salomäki, M.; Jussila, M.; Yohannes, G.; Riekkola, M.-L.; Kankare, J.; Dunsch, L. *Phys. Chem. Chem. Phys.* **2004,** *6,* 434–441. doi:10.1039/b308891j
33. van Haare, J. A. E. H.; Havinga, E. E.; van Dongen, J. L. J.; Janssen, R. A. J.; Cornil, J.; Brédas, J.-L. *Chem. – Eur. J.* **1998,** *4,* 1509–1522. doi:10.1002/(SICI)1521-3765(19980807)4:8<1509::AID-CHEM1509>3.0.CO;2-#
34. Matis, M.; Rapta, P.; Lukeš, V.; Hartmann, H.; Dunsch, L. *J. Phys. Chem. B* **2010,** *114,* 4451–4460. doi:10.1021/jp912213v
35. Krejčík, M.; Daněk, M.; Hartl, F. *J. Electroanal. Chem.* **1991,** *317,* 179–187. doi:10.1016/0022-0728(91)85012-E

License and Terms

BEILSTEIN JOURNAL OF ORGANIC CHEMISTRY

Synthesis and characterization of the cyanobenzene-ethylenedithio-TTF donor

Sandrina Oliveira, Dulce Belo, Isabel C. Santos, Sandra Rabaça* and Manuel Almeida*

Letter

Open Access

Address:
C²TN, Instituto Superior Técnico, Universidade de Lisboa, Estrada Nacional 10, P-2695-066 Bobadela LRS, Portugal

Email:
Sandra Rabaça* - sandrar@ctn.ist.utl.pt; Manuel Almeida* - malmeida@ctn.ist.utl.pt

* Corresponding author

Keywords:
cross-coupling; cyanobenzene; cyclic voltammetry; dissymmetric tetrathiafulvalene; electro-active donors

Beilstein J. Org. Chem. **2015,** *11,* 951–956.
doi:10.3762/bjoc.11.106

Received: 18 February 2015
Accepted: 11 May 2015
Published: 03 June 2015

This article is part of the Thematic Series "Tetrathiafulvalene chemistry".

Guest Editor: P. J. Skabara

Abstract

A dissymmetric TTF-type electron donor, cyanobenzene-ethylenedithio-tetrathiafulvalene (CNB-EDT-TTF), was obtained in high yield, by a cross-coupling reaction with triethyl phosphite between 2-thioxobenzo[*d*][1,3]dithiole-5-carbonitrile and 5,6-dihydro-[1,3]dithiolo[4,5-*b*][1,4]dithiin-2-one. This new donor was characterized namely by single crystal X-ray diffraction, cyclic voltammetry, NMR, UV-visible and IR spectroscopy.

Introduction

The tetrathiafulvalene molecule (TTF) and its many derivatives, due to its unique π-donor properties, have been at the basis of the large majority of organic metals and superconductors known so far [1,2]. Their success as building blocks for conducting materials is due to unique π-donor properties of TTF with two oxidized states readily accessible and the possibility of large intermolecular interactions in solid state through rather extended π-orbitals of these flat molecules. The exploration of new TTF derivatives in this context has followed two main guidelines. First, the further extension of the conjugated π-system to render more accessible the different oxidation states, and maximize the intermolecular interactions between planar molecules that tend to be organized in the solid state as stacks or layers with their long axis parallel to each other. Second, the incorporation of additional sulfur and other chalcogen atoms in the molecular periphery to promote side intermolecular interactions along the molecular plane allows a possible 2D or 3D character to the electronic interactions.

More recently there has been an increasing interest in TTF derivatives containing N atoms in their periphery which, while retaining the electroactive behaviour of TTF, could also be able to coordinate to transition metals [3-11]. Some TTF derivatives symmetrically substituted with cyano groups have been reported [12], but non-symmetrically substituted have been a lot less explored with the possible exception of some preligands for dithiolene complexes [13].

Aiming at enlarging this type of electron donors we report here a new non-symmetrically substituted TTF donor with one

dithiin ring and one cyanobenzene ring obtained by a cross coupling reaction. These two rings are expected to enhance the degree of π-delocalization over the molecule when compared with simple TTF, while the presence of the nitrogen atom can favour specific intermolecular interaction at the molecular periphery, either coordinating to other metals as found in other TTF type ligands or promoting weak hydrogen bonds.

Results and Discussion

Synthesis and structure of CNB-EDT-TTF

The synthesis of CNB-EDT-TTF **3** was obtained under a general route to prepare non-symmetrically substituted TTF derivatives by cross coupling of two different 1,3-dichalcogenole-2-chalconegones [14,15], involving the coupling between 2-thioxobenzo[*d*][1,3]dithiole-5-carbonitrile (**1**) [16] and 5,6-dihydro[1,3]dithiolo[4,5-*b*][1,4]dithiin-2-one (**2**) in 1:1.1 ratio in pure triethyl phosphite during 4 hours at 130 °C leading to the formation of **3** in relatively high yield (63%) (Scheme 1). This coupling reaction also gives rise to smaller amounts of BEDT-TTF (14% yield) and dicyanodibenzene tetrathiafulvalene (dcdb-TTF) [13] as byproducts resulting from homocoupling reactions. The separation of the products was easily achieved by chromatography. The dcdb-TTF yield was not determined since due to its insolubility it was retained at the top of the chromatography column. The yield of **3** decreased for longer reaction times and this is likely attributed to the higher formation of insoluble dcdb-TTF.

The CNB-EDT-TTF **3** electron donor is thermally stable, not sensitive to oxygen and soluble in common solvents such as CH_2Cl_2, $CHCl_3$ and AcOEt. The molecular structure and purity of the isolated compound after column chromatography were confirmed by ^1H and ^{13}C NMR spectroscopy, UV–vis and IR spectroscopy, mass spectrometry and elemental analysis.

In the IR spectra of **3**, the characteristic C≡N and C=C stretching absorption bands appeared around 2229 cm^{-1} and 1637 and 1446 cm^{-1}, respectively. The ^1H NMR spectra showed signals at 7.48–7.31 and 3.33 ppm, integrating with ratios expected for the seven protons.

Single crystals of **3** suitable for X-ray analysis were grown by slow evaporation from a dichloromethane solution. The X-ray structural refinement confirm the molecular structure of the compound **3** and was found to crystallize in the monoclinic system, space group $P2_1/n$ with one crystallographically independent molecule in a general position (Figure 1). This molecule is almost planar; the dihydrodithiin ring adopts a half-chair

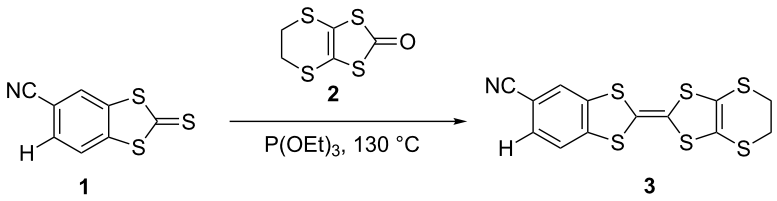

Scheme 1: Synthesis of cyanobenzene-ethylenedithio-tetrathiafulvalene (CNB-EDT-TTF) **3**.

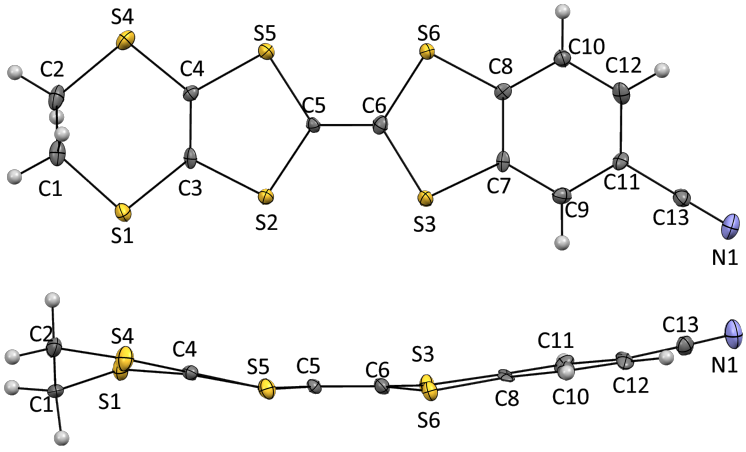

Figure 1: ORTEP diagrams of compound **3** drawn at 30% probability level with the atomic numbering scheme.

conformation with five coplanar atoms. The central C=C bond length (C5–C6 = 1.355(8) Å) is typical of neutral TTF donors [17-20].

The crystal structure is made by piling up molecules head to head forming stacks along the *b* axis (Figure 2) with short S–H contacts (S1–H1B; S4–H2B) in the range 2.751–2.824 Å. Neighbouring stacks are arranged head to tail in the *a,c* plane with several short contacts between molecules in neighbouring stacks S–S, C–N, S–H, N–H (S2–S3; N1–C1; N1–H1A; S2–H9; S5–H10; S6–H10). Short-contact details are given in Table S1 in Supporting Information File 1. Molecules in neighbouring stacks along *a* are tilted by 54.35° (Figure 3).

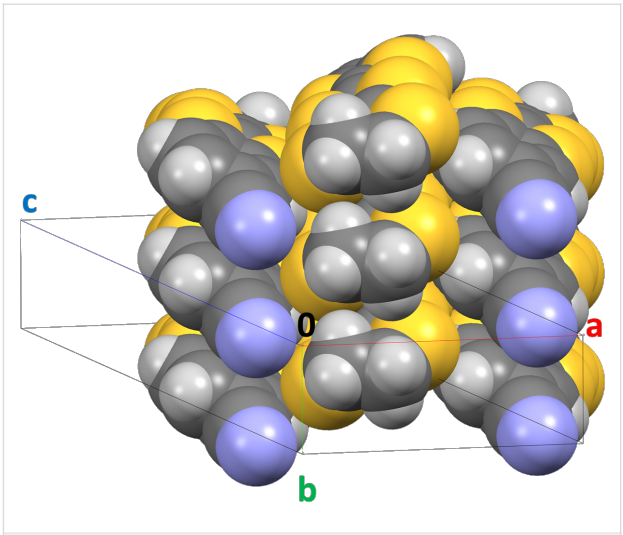

Figure 3: View of three neighbouring molecular stacks in **3**.

Spectroscopic and electrochemical properties

The electronic properties of **3** were investigated by UV–vis absorption spectroscopy in dichloromethane solution. The UV–vis spectra in DCM (Figure S6 in Supporting Information File 1) showed π–π* transitions typical of TTF donors [21], with an intense absorption band centred at approximately at 231 nm and other weaker bands at 269, 305 and 329 nm.

The redox properties of this donor were studied by cyclic voltammetry in dichloromethane using [*n*-Bu_4N][PF_6] as the supporting electrolyte (Figure 4) showing two one-electron quasi-reversible redox waves at 0.405 V and 0.850 V vs $Ag/AgNO_3$ as typical of TTF donors, which are ascribed to the couples $[CNB\text{-}EDT\text{-}TTF]^0/[CNB\text{-}EDT\text{-}TTF]^+$ and $[CNB\text{-}EDT\text{-}TTF]^+/[CNB\text{-}EDT\text{-}TTF]^{2+}$, respectively. Comparing the redox potentials of the new TTF electron donor **3** with the well-known BEDT-TTF donor also measured by us in the same conditions, as shown in Table 1, we can conclude that, as expected, the cyanobenzene group reduces the donor properties, shifting the redox potentials to higher values due to the electron withdrawing effect of the cyano groups possibly with a partial elec-

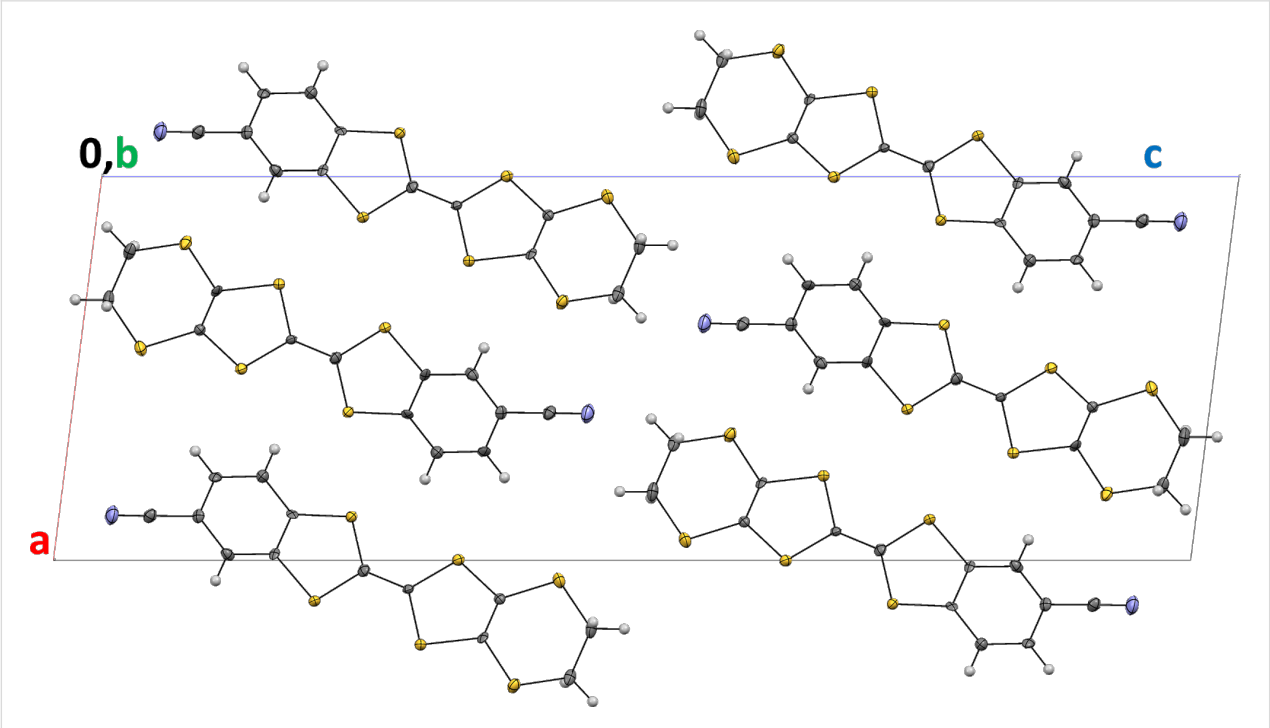

Figure 2: Crystal structure of compound **3** viewed along the *b* axis.

Table 1: Redox potentials for donors in CH_2Cl_2 with [*n*-Bu_4][PF_6] 0.1 M, *E* in V vs Ag/$AgNO_3$ with scan rate = 100 mV s^{-1}.

Donor	Solvent	$E_1^{1/2}$ (V)	$E_2^{1/2}$ (V)
3	DCM	0.405; (0.139[a]; *0.*705[b])	0.850; (0.584[a]; 1.15[b])
BEDT-TTF	DCM	0.234; (−0.320[a]; *0.*534[b])	0.642; (0.376[a]; 0.942[b])
dcdb-TTF [13]	benzonitrile	0.270	0.600
cbdc-TTF [13]	DMF	0.380	0.540

[a]vs Fc/Fc+ and [b]vs SCE.

tron transfer from the donor to the acceptor moiety. This tendency is also in agreement with the redox potentials of other cyanobenzene and pyrazine groups substituted TTFs recently reported by our group [13,22,23].

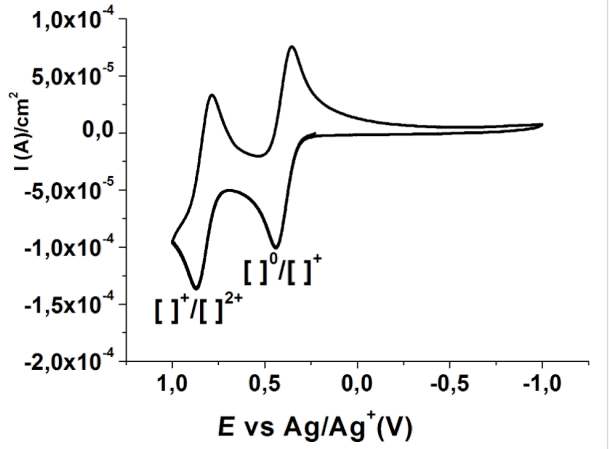

Figure 4: Cyclic voltammogram of **3**.

Conclusion

In conclusion, we have prepared in fair yield a new non-symmetrically substituted cyanobenzene TTF-type electron donor, CNB-EDT-TTF, by a cross coupling reaction followed by chromatographic separation. The crystal structure of this donor is dominated by a large number of S-, C- and N-mediated contacts. CNB-EDT-TTF presents the electroactive behaviour of TTF-type donors although with slightly enhanced oxidation potentials due to the incorporation of the CN group. This new donor is expected to be a valuable building unit to prepare new charge transfer salts where both the dipolar moment and the possibility of metal coordination and other interactions mediated by the cyano group can be further explored to obtain compounds with interesting properties.

Experimental

Materials and methods

Elemental analyses of the compounds were performed using an EA 110 CE Instruments automatic analyzer. Melting points were studied on a Stuart Scientific SMP2. IR spectra were obtained on a Bruker FTIR Tensor 27 spectrophotometer. ^1H and ^{13}C NMR spectra were recorded on Brucker Avance 300 (300 MHz for ^1H) with $CDCl_3$ and $(CD_3)_2SO$ used as solvents respectively and TMS the internal reference. UV–vis spectra were recorded on an UV-1800 Shimadzu spectrophotometer. Cyclic voltammetry data were obtained using a BAS C3 Cell Stand. The voltammograms were obtained at room temperature with a scan rate of 100 mV/s, platinum wire working and counter electrodes and an Ag/$AgNO_3$ reference electrode. The measurements were performed on fresh solutions with a concentration of 10^{-3} M, in CH_2Cl_2, that contained *n*-Bu_4PF_6 (10^{-1} M) as the supporting electrolyte. Mass spectra were obtained with a Bruker HCT electrospray ionization quadrupole ion trap mass spectrometer (ESI-QIT/MS). X-ray diffraction studies were performed with a Bruker APEX-II CCD detector diffractometer using graphite monochromated Mo Kα radiation (λ = 0.71073 Å), in the φ and ω scan modes. A semi empirical absorption correction was carried out using SADABS [24]. Data collection, cell refinement and data reduction were done with the SMART and SAINT programs [25]. The structures were solved by direct methods using SIR97 [26] and refined by full-matrix least-squares methods using the program SHELXL97 [27] using the winGX software package [28]. Non-hydrogen atoms were refined with anisotropic thermal parameters whereas H-atoms were placed in idealised positions and allowed to refine riding on the parent C atom. Molecular graphics were prepared using MERCURY 1.4.2 [29].

General procedure for the synthesis of 3

In freshly destilled triethyl phosphite (10 mL), 2-thioxobenzo[*d*][1,3]dithiole-5-carbonitrile (**1**, 1 mmol, 0.21 g) and 5,6-dihydro[1,3]dithiolo[4,5-*b*][1,4]dithiin-2-one (**2**, 1.1 mmol, 0.23 g) were heated up to 130 °C under N_2 at reflux for 4 h, which led to a formation of an orange precipitate. The precipitate was filtered and washed with cold methanol and dried under vacuum. The product was isolated by silica gel column chromatography with DCM:hexane (3:1) as eluent. Yield 63%; mp 238.6 °C; anal. calcd for $C_{13}H_7NS_6$: C, 42.25; H, 1.91; N, 3.79; S, 52.05; found: C, 41.41; H, 2.45; N, 3.43; S, 49.25; MS *m*/*z* (100%): 369.0 (M^+,100); ^1H NMR ($CDCl_3$, ppm) 7.46 (d,

J = 1 Hz, 1H,), 7.38 (dd, J = 1, 8.1 Hz, 1H,), 7.31 (d, J = 8.1 Hz, 1H), 3.32 (s, 4H); ^{13}C NMR $(CD_3)_2SO$) 142.8, 138.1, 130.9, 126.3, 123.9, 118.7, 113.44, 109.73, 30.11; υ_{max} (KBr)/cm^{-1}: 3062 (m, Ar-H), 2922 (s, CH_2), 2229 (s, C≡N), 1637 and 1446 (m, C=C), and 582 (m, C-S); UV–vis (DCM) λ_{max} = 231 nm.

Crystal structure data: The crystal structure data have been deposited at the Cambridge Crystallographic Data Centre and allocated the deposition number CCDC-1049230 for **3**. These crystallographic data can be obtained free of charge at http://www.ccdc.cam.ac.uk.

Cyanobenzene-ethylenedithio-tetrathiafulvalene **3** crystallized from dichloromethane saturated solution as orange needles, $C_{13}H_7NS_6$ (M_r = 369.59), crystal size 0.35 × 0.22 × 0.18 mm^3, monoclinic, a = 10.8794(6) Å, b = 4.1490(3) Å, c = 31.9854(16) Å, ß = 97.185(4), V = 1432.44 Å^3, Z = 4, ρ_{calcd} = 1.714 g cm^{-3}, space group $P2_1/n$.

Supporting Information

Supporting Information File 1

NMR (^{1}H and ^{13}C), infrared spectra, UV–vis absorption spectra and short contact list of CNB-EDT-TTF.
[http://www.beilstein-journals.org/bjoc/content/supplementary/1860-5397-11-106-S1.pdf]

Acknowledgements

We thank Dr. Joaquim Marçalo for the Mass spectra, ESI-QIT/MS is part of RNEM – Portuguese Mass Spectrometry Network, supported by Fundação para a Ciência e a Tecnologia (FCT). Work partially supported by FCT (Portugal) through contract PTDC/QEQ-SUP/1413/2012, contract RECI/QEQQIN/0189/2012 and contract UID/Multi/04349/2013 project.

References

1. Bendikov, M.; Wudl, F.; Perepichka, D. F. *Chem. Rev.* **2004,** *104,* 4891–4946. doi:10.1021/cr030666m
2. Yamada, J. In *TTF Chemistry Fundamentals and Applications of Tetrathiafulvalene;* Sugimoto, T., Ed.; Kodansha and Springer: Tokyo, 2004.
3. Lorcy, D.; Bellec, N.; Fourmigué, M.; Avarvari, N. *Coord. Chem. Rev.* **2009,** *253,* 1398–1438. doi:10.1016/j.ccr.2008.09.012
4. Pointillart, F.; Golhen, S.; Cador, O.; Ouahab, L. *Dalton Trans.* **2013,** *42,* 1949–1960. doi:10.1039/C2DT32150E
5. Rabaça, S.; Almeida, M. *Coord. Chem. Rev.* **2010,** *254,* 1493–1508. doi:10.1016/j.ccr.2009.12.006
6. Griffiths, J.-P.; Brown, R. J.; Day, P.; Matthews, C. J.; Vital, B.; Wallis, J. D. *Tetrahedron Lett.* **2003,** *44,* 3127–3131. doi:10.1016/S0040-4039(03)00539-2
7. Branzea, D. G.; Fihey, A.; Cauchy, T.; El-Ghayoury, A.; Avarvari, N. *Inorg. Chem.* **2012,** *51,* 8545–8556. doi:10.1021/ic301117h
8. Belhadj, E.; El-Ghayoury, A.; Ripaud, E.; Zorina, L.; Allain, M.; Batail, P.; Mazari, M.; Sallé, M. *New J. Chem.* **2013,** *37,* 1427–1436. doi:10.1039/c3nj00041a
9. Dias, S. I. G.; Neves, A. I. S.; Rabaça, S.; Santos, I. C.; Almeida, M. *Eur. J. Inorg. Chem.* **2008,** 4728–4734. doi:10.1002/ejic.200800660
10. Biet, T.; Cauchy, T.; Avarvari, N. *Chem. – Eur. J.* **2012,** *18,* 16097–16103. doi:10.1002/chem.201201905
11. Biet, T.; Avarvari, N. *CrystEngComm* **2014,** *16,* 6612–6620. doi:10.1039/c4ce00736k
12. Jia, C.; Liu, S.-X.; Ambrus, C.; Labat, G.; Neels, A.; Decurtins, S. *Polyhedron* **2006,** *25,* 1613–1617. doi:10.1016/j.poly.2005.10.037
13. Rabaça, S.; Oliveira, S.; Cerdeira, A. C.; Simão, D.; Santos, I. C.; Almeida, M. *Tetrahedron Lett.* **2014,** *55,* 6992–6997. doi:10.1016/j.tetlet.2014.10.111
14. Fabre, J. M. *Chem. Rev.* **2004,** *104,* 5133–5150. doi:10.1021/cr0306440
15. Fabre, J. M.; Giral, L.; Dupart, E.; Coulon, C.; Manceau, J. P.; Delhaes, P. *J. Chem. Soc., Chem. Commun.* **1983,** 1477–1479. doi:10.1039/c39830001477
16. Cerdeira, A. C.; Afonso, M. L.; Santos, I. C.; Pereira, L. C. J.; Coutinho, J. T.; Rabaça, S.; Simão, D.; Henriques, R. T.; Almeida, M. *Polyhedron* **2012,** *44,* 228–237. doi:10.1016/j.poly.2012.07.010
17. Bouguessa, S.; Gouasmia, A. K.; Golhen, S.; Ouahab, L.; Fabre, J. M. *Tetrahedron Lett.* **2003,** *44,* 9275–9278. doi:10.1016/j.tetlet.2003.10.067
18. Liu, S.-X.; Dolder, S.; Rusanov, E. B.; Stoeckli-Evans, H.; Decurtins, S. *C. R. Chim.* **2003,** *6,* 657–662. doi:10.1016/S1631-0748(03)00118-8
19. Devic, T.; Avarvari, N.; Batail, P. *Chem. – Eur. J.* **2004,** *10,* 3697–3707. doi:10.1002/chem.200305776
20. Belo, D.; Figueira, M. J.; Nunes, J. P. M.; Santos, I. C.; Almeida, M.; Crivillers, N.; Rovira, C. *Inorg. Chim. Acta* **2007,** *360,* 3909–3914. doi:10.1016/j.ica.2007.03.041
21. Camerel, F.; Jeannin, O.; Yzambart, G.; Fabre, B.; Lorcy, D.; Fourmigué, M. *New J. Chem.* **2013,** *37,* 992–1001. doi:10.1039/c3nj41097h
22. Rabaça, S.; Oliveira, S.; Santos, I. C.; Almeida, M. *Tetrahedron Lett.* **2013,** *54,* 6635–6639. doi:10.1016/j.tetlet.2013.09.131
23. Rabaça, S.; Cerdeira, A. C.; Neves, A. I. S.; Dias, S. I. G.; Mézière, C.; Santos, I. C.; Pereira, L. C. J.; Fourmigué, M.; Henriques, R. T.; Almeida, M. *Polyhedron* **2009,** *28,* 1069–1078. doi:10.1016/j.poly.2009.01.015
24. Sheldrick, G. M. SADABS; Bruker AXS: Madison, Wisconsin, USA, 2004.
25. Bruker SMART and SAINT; Bruker AXS: Madison, Wisconsin, USA, 2004.
26. Altomare, A.; Burla, M. C.; Camalli, M.; Cascarano, G. L.; Giacovazzo, C.; Guagliardi, A.; Moliterni, A. G. G.; Polidori, G.; Spagna, R. *J. Appl. Crystallogr.* **1999,** *32,* 115–119. doi:10.1107/S0021889898007717
27. Sheldrick, G. M. SHELXL97, Programs for Crystal Structure Analysis, Release 97-2; Universitat Goettingen, Germany, 2008.
28. Farrugia, L. J. *J. Appl. Crystallogr.* **1999,** *32,* 837–838. doi:10.1107/S0021889899006020
29. Macrae, C. F.; Edgington, P. R.; McCabe, P.; Pidcock, E.; Shields, G. P.; Taylor, R.; Towler, M.; van de Streek, J. *J. Appl. Crystallogr.* **2006,** *39,* 453–457. doi:10.1107/S002188980600731X

License and Terms

The definitive version of this article is the electronic one which can be found at:
doi:10.3762/bjoc.11.106

BEILSTEIN JOURNAL OF ORGANIC CHEMISTRY

Carboxylated dithiafulvenes and tetrathiafulvalene vinylogues: synthesis, electronic properties, and complexation with zinc ions

Yunfei Wang and Yuming Zhao*

Full Research Paper

Open Access

Address:
Department of Chemistry, Memorial University, St. John's, A1B 3X7, NL, Canada

Email:
Yuming Zhao* - yuming@mun.ca

* Corresponding author

Keywords:
complexation; coordination polymers; porosity; redox activity; tetrathiafulvalene

Beilstein J. Org. Chem. **2015,** *11,* 957–965.
doi:10.3762/bjoc.11.107

Received: 26 February 2015
Accepted: 08 May 2015
Published: 03 June 2015

This article is part of the Thematic Series "Tetrathiafulvalene chemistry".

Guest Editor: P. J. Skabara

Abstract

A class of carboxyl and carboxylate ester-substituted dithiafulvene (DTF) derivatives and tetrathiafulvalene vinylogues (TTFVs) has been synthesized and their electronic and electrochemical redox properties were characterized by UV–vis spectroscopic and cyclic voltammetric analyses. The carboxyl-TTFV was applied as a redox-active ligand to complex with Zn(II) ions, forming a stable Zn-TTFV coordination polymer. The structural, electrochemical, and thermal properties of the coordination polymer were investigated by infrared spectroscopy, cyclic voltammetry, powder X-ray diffraction, and differential scanning calorimetric analyses. Furthermore, the microscopic porosity and surface area of the Zn-TTFV coordination polymer were measured by nitrogen gas adsorption analysis, showing a BET surface of 148.2 m^2 g^{-1} and an average pore diameter of 10.2 nm.

Introduction

Tetrathiafulvalene (TTF) has been widely applied as a redox-active building block in organic electronic materials and supramolecular assemblies [1-5], since the first discovery by Wudl and others in the early 1970s that TTF upon interactions with suitable electron acceptors could give rise to charge-transfer complexes exhibiting excellent metallic conductivity [6,7]. The remarkable electron-donating properties of TTF arise from its aromaticity-stabilized cationic states after releasing one and/or two electrons [1-5,8-10]. Tetrathiafulvalene vinylogues (TTFVs) are π-extended analogues of TTF bearing extended vinyl bridges between the two dithiole rings of TTF [9-11]. Similar to their parent TTF, TTFVs are excellent electron donors as well and they can undergo reversible electron transfers under mild redox conditions [11-15]. Of particular interest is the class of aryl-substituted TTFVs which show interesting conformational switching properties governed by redox processes [12,14-16]. For instance, the structure of diphenylated TTFV **1** can be transformed from a pseudo *cis* to a complete *trans* conformation upon oxidation (see Scheme 1). The application of TTFVs in material development began

several decades ago, while the past few years have witnessed surging research activities on integrating TTFVs into a variety of π-conjugated molecular and macromolecular systems [12,17-26]. In many of the studies, the remarkable redox activity and intriguing conformational switching properties of TTFVs were taken advantage of to enhance structural and electronic properties as well as to introduce some "intelligent" functions such as conformational switchability and selectivity in terms of molecular recognition and supramolecular interactions.

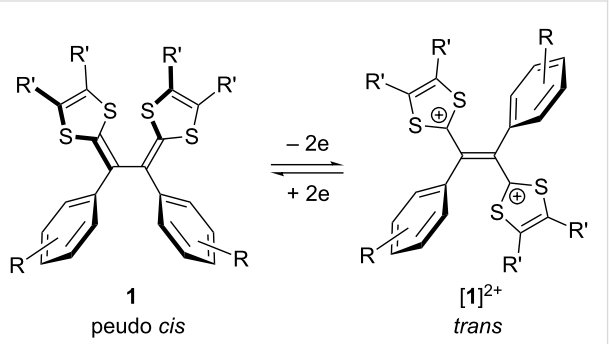

Scheme 1: Redox-induced conformational switching of diphenyl-TTFV **1**.

The synthesis of TTFV structures is usually carried out through a facile iodine-promoted oxidative dimerization reaction of corresponding dithiafulvene (DTF) precursors [27]. This straightforward C–C bond forming reaction has not only allowed TTFV derivatives with different substituents to be readily assembled, but served as an effective methodology to construct the π-conjugated frameworks of some TTFV-based macrocycles and polymers [12,28]. Previously, we have investigated a series of diphenyl-TTFVs with alkynyl groups attached to the phenyl units as synthetic building blocks, through which extension of π-conjugated structures could be conveniently executed via the Pd-catalysed coupling and Cu-catalysed alkyne–azide cycloaddition (i.e., click) reactions [22-26]. In this work, we continued to explore the class of carboxylated diphenyl-TTFVs, in view of the synthetic versatility of the carboxyl group towards various commonly used linkage groups (e.g., amides, esters). The carboxyl group also presents a reliable and useful ligand to coordinate with transition metal ions, which in turn provides easy access to novel organic–inorganic hybrid materials. The most notable example of research in this context is the recent development of metal organic frameworks (MOFs), wherein the design and synthesis of carboxyl functional ligands has played a pivotal role prompting the advancement of this field [29-31]. Very recently, some TTF-based ligands have been employed to achieve organic–inorganic hybrid materials with redox activity [32-35]; however, the use of TTFVs as ligands has not been reported in the literature prior to this work. This article thus describes the first exploration of the synthesis and properties of a carboxylated diphenyl-TTFV **6** (Scheme 2) and its ability to form new redox-active porous materials through the formation of coordination polymer with Zn(II) ions.

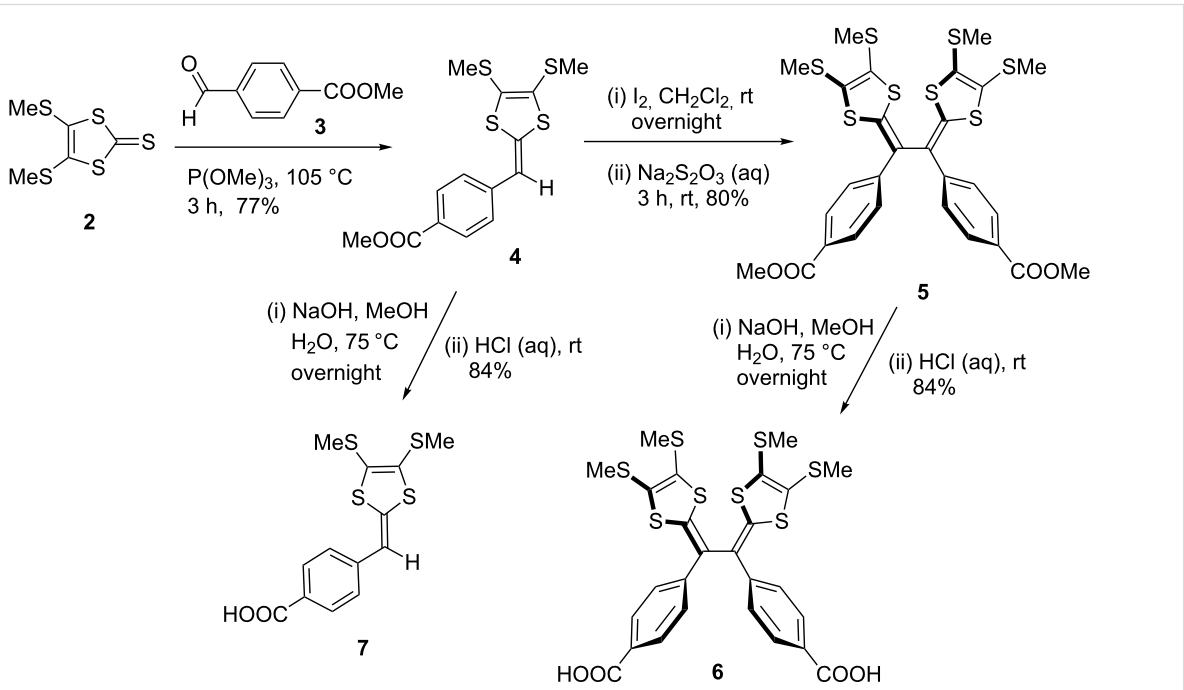

Scheme 2: Synthesis of carboxylated TTFV **6** and DTF **7**.

Results and Discussion

The synthesis of carboxyl-TTFV **6** and its DTF precursor **7** was conducted via a route well established for aryl-substituted TTFV derivatives [22,23]. As shown in Scheme 2, thione **2** was first reacted with benzaldehyde **3** in the presence of trimethylphosphite at 105 °C [36]. This olefination reaction went completion within 3 hours to give DTF **4** in 77% yield after column separation. Compound **4** was then subjected to an oxidative dimerization in CH_2Cl_2 at room temperature using iodine as oxidant. The dimerization gave TTFV **5** as a stable yellow solid in 80% yield. Saponification was then performed on compound **5** in a solution of NaOH in water and methanol to finally afford carboxyl-TTFV **6** in 84% yield. Compound **6** showed relatively poor solubility in non-polar organic solvents, but could be readily dissolved in polar solvents such as MeOH, EtOH, THF, and DMSO. For comparison purposes, carboxyl-DTF **7** was also prepared by hydrolysis of DTF **4** using similar reaction conditions.

With carboxyl-TTFV **6** in hand, the preparation of coordination polymers with Zn(II) ions was undertaken. As outlined in Scheme 3, compound **6** was first mixed with two molar equivalents of $Zn(NO_3)_2{\cdot}6H_2O$ in EtOH, and to this solution triethylamine was allowed to slowly diffuse in [37]. In a period of 4 days, coordination polymer **8** was gradually formed as a yellow coloured crystalline solid, which was insoluble in common solvents. By the same approach, complexes of carboxyl-DTF **7** with Zn(II) ions were also produced as a yellow powder.

The electronic properties of TTFVs **5** and **6** as well as their DTF precursors **4** and **7** were investigated by UV–vis absorption spectroscopy. Figure 1 shows the UV–vis absorption spectra of these compounds, in which the maximum absorption wavelengths (λ_{max}) of all the compounds appear to be nearly identical at ca. 385 nm. There are, however, slight variations in the cut-off energies of long-wavelength absorption bands. The origins of these long-wavelength absorption bands are mainly due to HOMO to LUMO, HOMO to LUMO+1, and HOMO−1 to LUMO+1 transitions according to time-dependent density functional theory (TD-DFT) calculations (see the Supporting Information File 1 for details). The UV–vis data indicates that the degrees of π-delocalization for the TTFVs and DTF compounds are quite similar. This result is congruous with the fact that diphenyl-TTFVs generally prefer a twisted *cisoid* conformation in the ground state [12,15,16], which in theory significantly disrupts the π-delocalization within the molecules. Therefore, even though the molecular sizes of TTFVs **5** and **6** are doubled in comparison with their DTF precursors **4** and **7**, the degrees of π-electron delocalization in these molecules are still retained at a similar level in the ground state.

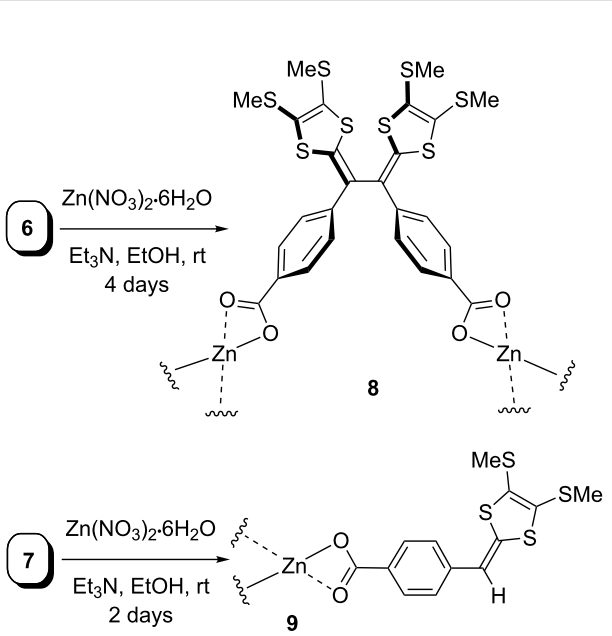

Scheme 3: Complexation of compounds **6** and **7** with Zn(II) ions.

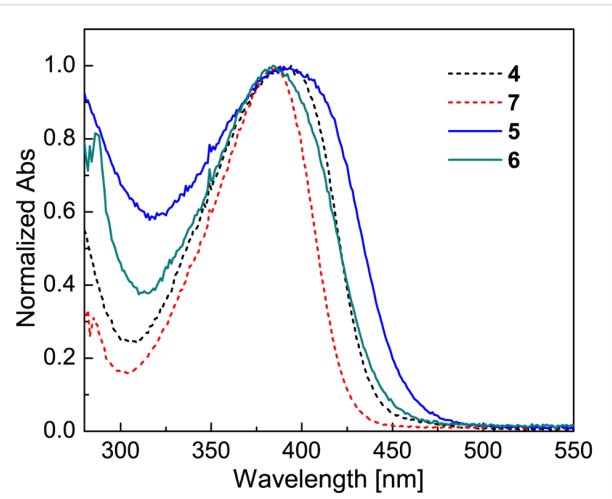

Figure 1: UV–vis spectra of TTFVs **5** and **6** (solid lines) and DTF **4** and **7** (dashed lines). Compounds **4** and **5** were measured in CH_2Cl_2, while compounds **6** and **7** were in THF.

The electrochemical redox properties of compounds **4**–**9** were characterized by cyclic voltammetry, and the detailed cyclic voltammograms are shown in Figure 2. For methyl ester-appended DTF **4** (Figure 2A) an anodic peak was observed at +0.82 V in the first cycle of scan, which is due to the single-electron oxidation of the dithiole moiety into the dithiolium radical cation [15,16]. In the reverse scan, a cathodic peak emerged at +0.54 V which is assigned to the bielectronic reduction of the TTFV product electrochemically generated on the

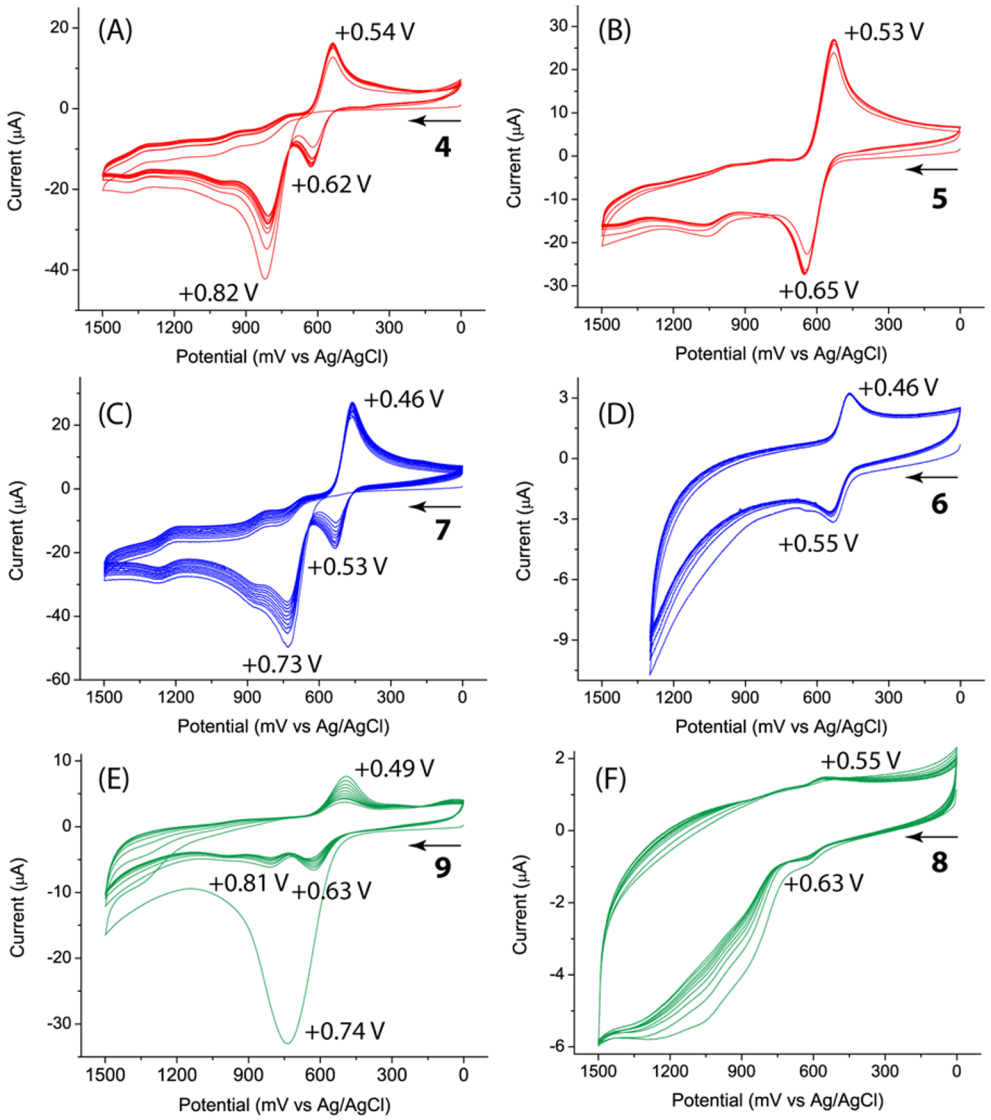

Figure 2: Cyclic voltammograms of compounds **4**–**9**. Experimental conditions: supporting electrolyte: Bu_4NBF_4 (0.1 M), working electrode: glassy carbon, counter electrode: Pt wire, reference electrode: Ag/AgCl (3 M NaCl), scan rate: 200 mV s^{-1}. Compounds **4** (1.5 mM), **5** (0.73 mM), **8**, and **9** were measured in CH_2Cl_2. Compounds **6** (0.76 mM) and **7** (1.5 mM) were measured in CH_3CN.

electrode surface via the DTF dimerization reaction [15,16]. In the following scan cycles, the redox wave pair characteristic of TTFV at E_{pa} = +0.62 V and E_{pc} = +0.54 V was found to gradually increase in intensity as a result of increasing electrochemical dimerization. The same electrochemical patterns can be seen in the cyclic voltammograms of carboxyl-DTF **7** and Zn-DTF complex **9** (Figure 2C and 2E); however, their redox potentials showed a slight degree of variation. Experimentally, the cyclic voltammogram of **9** was determined from its solid thin film compressed on the working electrode surface. It is interesting to note that Zn-DTF complex **9** retained the redox activity and electrochemical reactivity of DTF even in the solid state. The cyclic voltammograms of compounds **5** and **6** both featured a reversible redox wave pair due to the simultaneous bielectronic transfers occurring at the TTFV moieties (Figure 2B and 2D). In the cyclic voltammogram of Zn-TTFV coordination polymer **8** (measured from a solid film prepared in the same way as **9**), the redox wave pair of TTFV is discernible but much weaker than that of Zn-DTF **9** (Figure 2F), suggesting that the electrochemical activity of the coordination polymer is considerably reduced in comparison with the smaller-sized Zn-DTF complex.

The structural properties of Zn-TTFV coordination polymer **8** and Zn-DTF complex **9** were examined by IR spectroscopy (Figure 3). Compared with the IR spectra of carboxyl-TTFV **6**

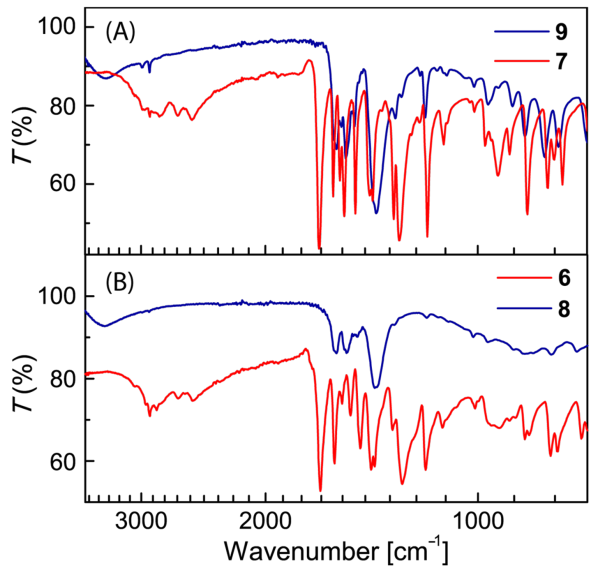

Figure 3: FTIR spectra of compounds **6–9**.

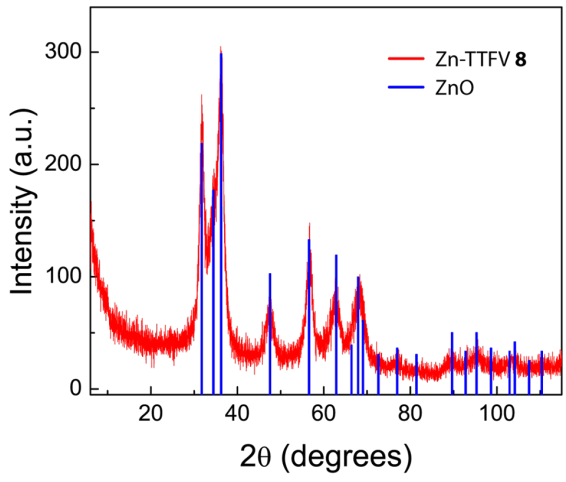

Figure 4: PXRD patterns of the Zn-TTFV coordination polymer **8** (red line) in comparison with the diffraction data of zincite ZnO (blue bars).

and carboxyl-DTF **7**, the vibrational bands of free carboxyl groups were clearly absent in the spectra of **8** and **9**, confirming that the carboxyl groups were completely coordinated with Zn(II) ions. The crystalline properties of coordination polymer **8** were examined by powder X-ray diffraction (PXRD) analysis. The diffraction patterns shown in Figure 4 confirm that coordinate polymer **8** possesses crystallinity in the solid state. Actually, the diffraction patterns were found to bear resemblance to those of zincite ZnO. Such crystalline features hence point to a possibility of the coordination polymer to take some kind of framework-like structures in the solid state with certain microscopic porosity.

To assess the porous properties of Zn-TTFV **8**, nitrogen gas adsorption analysis was conducted at 77 K. The adsorption isotherm shown in Figure 5A indicates a Type-II adsorption behaviour. Application of the Brunauer–Emmett–Teller (BET) model gave a BET surface area of 148.2 m^2 g^{-1} and an adsorption average pore diameter of 10.2 nm. The pore size distribution analysis data revealed that Zn-TTFV coordination polymer **8** carried microporosity primarily in the range of tens of nanometers. Scanning electron microscopic (SEM) imaging was performed on the particles of **8** to show some kind of crystalline-like micromorphology. In line with the gas adsorption results, there were no relatively large pores on the micron scale observable in the particles (see the inset of Figure 5B). On the submicron scale, however, corrugated microporous features could be clearly observed (see Figure 5B). To understand the origin of the micropores, nitrogen gas adsorption experiments were performed on Zn-DTF complex **9**. The experimental

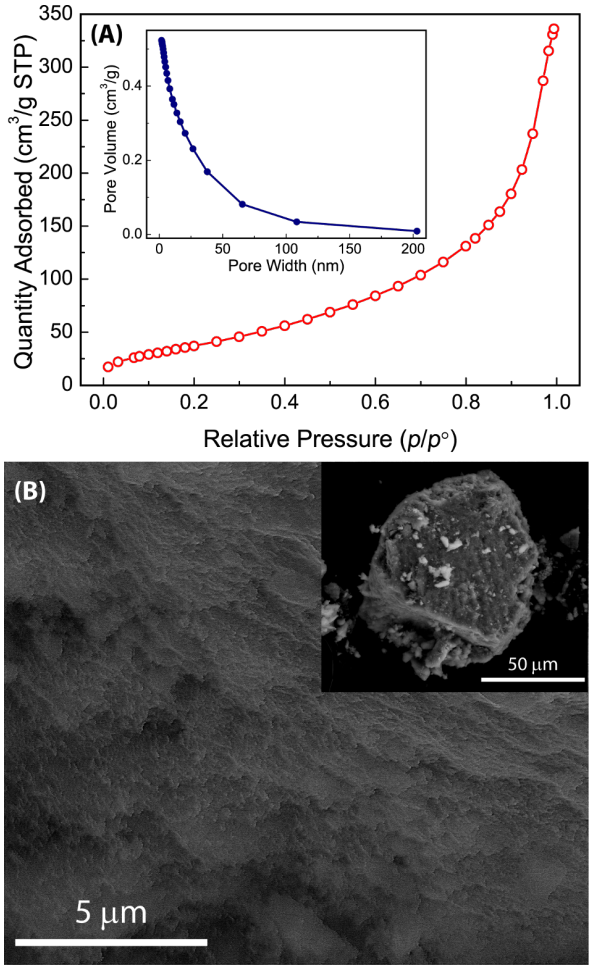

Figure 5: (A) Nitrogen adsorption isotherm of coordination polymer **8** measured at 77 K. Inset: pore size distributions. (B) SEM image of the powder of **8**.

results did not lead to any meaningful measurements of BET surface area and microporosity, indicating a lack of porous structures in the solid of **9**. The major structural difference between Zn-DTF **9** and Zn-TTFV **8** is that **8** assumes crystalline polymeric frameworks as evidenced by PXRD analysis, whereas **9** is in the form of small clusters and amorphous (see Figure S10 in Supporting Information File 1 for the detailed PXRD data of **9**). It is therefore reasonable to propose that the microporosity in **8** is directly related to the coordination polymer structure.

Finally, the thermal stability of coordination polymer **8** and Zn-DTF **9** were evaluated by differential scanning calorimetric (DSC) analysis, and detailed DSC traces are illustrated in Figure 6. The DSC data of Zn-TTFV **8** (Figure 6A) manifested very good thermal stability up to 400 °C, without any significant melting or decomposition except a slight phase transition at 272 °C. Comparatively, the DSC trace of carboxyl-TTFV ligand **6** showed a distinctive melting process at 317 °C, which was immediately followed by a prominent sharp exothermic peak at 326 °C (Figure 6B). The exothermic process is possibly due to a chemical reaction(s); however, the exact reactivity awaits further investigation to clearly elucidate. Zn-DTF **9** gave a moderate endothermic peak at 152 °C and a significant exothermic peak at 358 °C (Figure 6C). For carboxyl-DTF **7**, a notable melting point was observed at 199 °C, and the melting was followed by certain exothermic processes in the range of 200 to 285 °C. The DSC results indicated that the formation of Zn-TTFV coordinate polymer could give rise to considerably improved thermal stability, a property particularly beneficial for practical device and material applications.

Conclusion

In summary, we have synthesized carboxylated diphenyl-TTFV **6** and phenyl-DTF **7** as redox-active ligands to complex with Zn(II) ions. The electronic and electrochemical properties of the TTFV and DTF compounds were found to be in line with other related TTFV and DTF derivatives. Of great interest is that the complexes with Zn(II) ions retain the redox activity and electrochemical reactivity of their TTFV and DTF ligands in the solid state. Another significant added value is the thermal robustness of the Zn-TTFV coordination polymer. Collectively, the good electrochemical and thermal properties point to a promising prospect for them to be further developed into practically useful organic–inorganic hybrid materials through the coordination polymer approach. The Zn-TTFV coordination polymer was also found to be crystalline in nature. At this stage, meaningful single-crystal diffraction data has not yet been successfully determined. Without such data clear understanding of the detailed solid-state structural properties cannot be established.

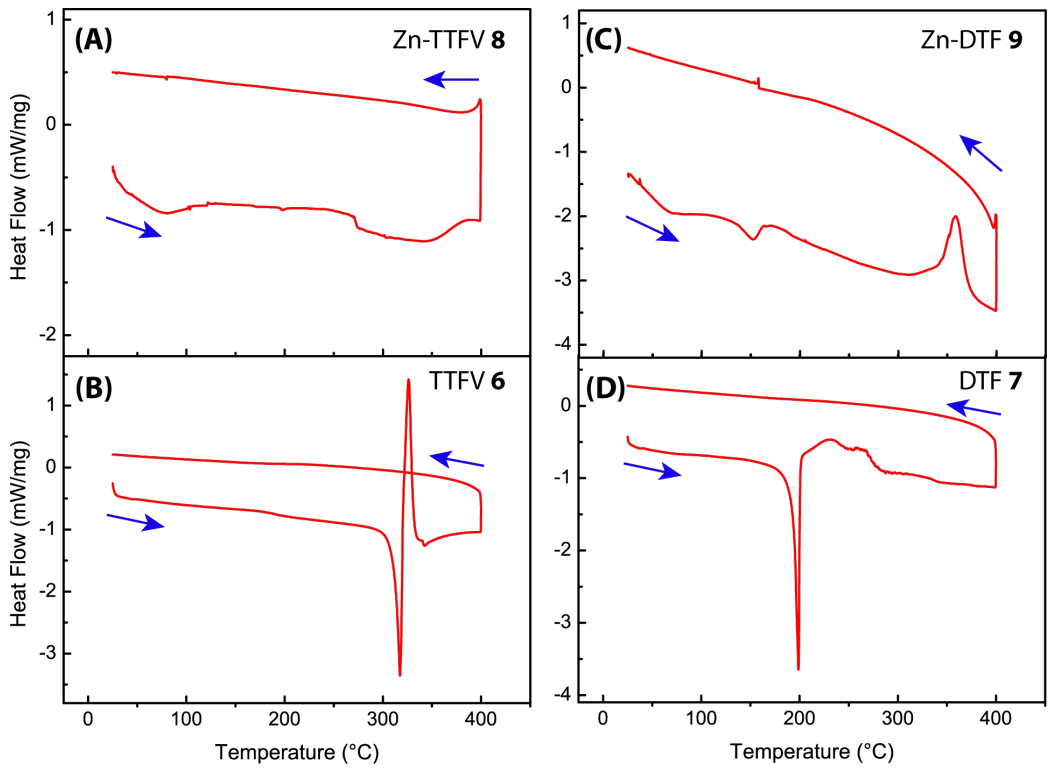

Figure 6: DSC traces of compounds **6**–**9** measured under a nitrogen atmosphere. Scan range: 25–400 °C, scan rate: 10 °C min^{-1}.

Our future work is moving towards tuning the side groups of the TTFV ligand to produce Zn complexes with better crystallinity. Finally, the Zn-TTFV coordination polymer exhibited significant microporosity and surface area. Overall, our current studies have cast a light on the fundamental redox and solid-state properties of the class of TTFV-based organic–inorganic hybrid materials, and the findings disclosed in this article should offer useful guidance to further material design and development.

Experimental

Chemicals were purchased from commercial suppliers and used directly without purification. All reactions were conducted in standard, dry glassware and under an inert atmosphere of nitrogen unless otherwise noted. Evaporation and concentration were carried out with a water-aspirator. Flash column chromatography was performed with silica gel 60 (240-400 mesh). Thin-layer chromatography (TLC) was carried out with silica gel F254 covered on plastic sheets and visualized by UV light. Melting points were measured on a SRS OptiMelt melting point apparatus. ^{1}H and ^{13}C NMR spectra were measured on a Bruker Avance III 300 MHz multinuclear spectrometer. Chemical shifts (δ) are reported in ppm downfield relative to the signal of the internal reference $SiMe_4$. Coupling constants (*J*) are given in Hz. Infrared spectra (IR) were recorded on a Bruker Alfa spectrometer. HRMS analyses were performed on an Agilent 6230 TOF LC/MS instrument using an APPI ionizer. UV–vis absorption spectra were measured on a Cary 6000i spectrophotometer. Cyclic voltammetric analyses were carried out in a standard three-electrode setup controlled by a BASi epsilon workstation. Differential scanning calorimetric (DSC) analyses were performed on a Mettler-Toledo DSC1 calorimeter. Powder X-ray diffraction (PXRD) data was collected on a Rigaku Ultima IV diffractometer equipped with a copper X-ray source with a wavelength of 1.54 nm. Scanning electron microscopy (SEM) was performed on an FEI MLA 650 FEG microscope. BET surface area and pore size analyses were performed on a Micromeritics TriStar II Plus instrument. The degassing was done on a Flow Prep 060 instrument. The calculations were carried out with the MicroActive for TriStar II Plus software (Version 2.02). Thione **2** was prepared according to the procedures we reported previously [22,23].

DTF 4: A mixture of methyl 4-formylbenzoate (**3**, 1.83 g, 11.1 mmol) and thione **2** (3.03 g, 13.4 mmol) in $P(OMe)_3$ (100 mL) was stirred and heated at 105 °C for 3 h. The excess $P(OMe)_3$ was removed by vacuum distillation. The residue was purified by silica column chromatography (EtOAc/hexanes, 1:9) to afford compound DTF **4** (2.93 g, 8.55 mmol, 77%) as a yellow crystalline solid. mp 88.6–90.9 °C; ^{1}H NMR (300 MHz, $CDCl_3$) δ 8.01 (d, *J* = 8.4 Hz, 2H), 7.25 (d, *J* = 8.3 Hz, 2H), 6.51 (s, 1H), 3.91 (s, 3H), 2.44 (d, *J* = 2.8 Hz, 6H) ppm; ^{13}C NMR (75 MHz, $CDCl_3$) δ 166.8, 140.5, 136.2, 129.9, 127.9, 126.7, 126.3, 124.5, 113.3, 52.0, 19.0, 18.9 ppm; FTIR (neat): 2914, 1704, 1599, 1567, 1545, 1492, 1422, 1265, 1175, 1096, 851, 798, 693, 470 cm^{-1}; APPI–HRMS (*m/z*, positive mode): [M^+] calcd for $C_{14}H_{14}O_2S_4$, 341.9877; found, 341.9878.

TTFV 5: A mixture of DTF **4** (0.25 g, 0.73 mmol) and I_2 (0.55 g, 2.2 mmol) in CH_2Cl_2 (100 mL) was stirred at rt overnight. Then a satd $Na_2S_2O_3$ solution (aq, 90 mL) was added. The mixture was stirred for another 3 h at rt. The organic layer was separated, washed with H_2O, dried over $MgSO_4$, and concentrated under vacuum. The residue was purified by silica column chromatography (EtOAc/hexanes, 1:4) to afford compound **5** (0.20 g, 0.29 mmol, 80%) as a yellow solid. mp 183.9–185.4 °C; ^{1}H NMR (300 MHz, $CDCl_3$) δ 7.97 (d, *J* = 8.7 Hz, 4H), 7.46 (d, *J* = 8.7Hz, 4H), 3.89 (s, 6H), 2.44 (s, 6H), 2.38 (s, 6H) ppm; ^{13}C NMR (75 MHz, $CDCl_3$) δ 166.6, 141.1, 140.3, 130.1, 129.1, 127.9, 126.1, 125.5, 122.9, 52.0, 18.9, 18.8 ppm; FTIR (neat): 2942, 2918, 1709, 1600, 1519, 1473, 1430, 1273, 1182, 1107, 766, 713, 465 cm^{-1}; APPI–HRMS (*m/z*, positive mode): [M^+] calcd for $C_{28}H_{26}O_4S_8$, 681.9597; found, 681.9584.

Carboxylated TTFV 6: A mixture of TTFV **5** (50.0 mg, 0.0732 mmol) and NaOH (46.9 mg, 1.17 mmol) in MeOH/H_2O (40 mL, 3:1) was stirred at 75 °C overnight. The solvent MeOH was removed under vacuum, and the residue was diluted to 50 mL with H_2O and acidified to pH 4 with HCl (aq). The precipitate formed was extracted with EtOAc, washed with H_2O, dried over $MgSO_4$, and concentrated under vacuum to afford compound **6** (40.3 mg, 0.0615 mmol, 84%) as a yellow solid. mp 292.9–295.7 °C; ^{1}H NMR (300 MHz, DMSO-d_6) δ 7.94 (d, *J* = 8.5 Hz, 4H), 7.48 (d, *J* = 8.4 Hz, 4H), 2.48 (s, 6H), 2.40 (s, 6H) ppm; ^{13}C NMR (75 MHz, DMSO-d_6) δ 166.7, 140.0, 139.1, 130.0, 128.8, 126.8, 125.9, 125.1, 122.7, 18.2, 18.2 ppm; FTIR (neat): 2916-2536 (br), 1672, 1596, 1515, 1467, 1416, 1280, 1186, 789, 541, 469 cm^{-1}; APPI–HRMS (*m/z*, negative mode) [M^-] calcd for $C_{26}H_{22}O_4S_8$, 653.9284; found, 653.9293.

Carboxylated DTF 7: A mixture of DTF **4** (0.30 g, 0.88 mmol) and NaOH (0.56 g, 14 mmol) in MeOH/H_2O (240 mL, 3:1) was stirred at 75 °C overnight. The solvent MeOH was removed under vacuum, and the residue was diluted to 100 mL with H_2O and acidified to pH 4 with HCl (aq). The precipitate formed was subjected to suction filtration to afford compound **7** (0.24 g, 0.73 mmol, 84%) as a yellow solid. mp 191.0–193.2 °C; ^{1}H NMR (300 MHz, DMSO-d_6) δ 12.86 (s, 1H), 7.94 (d, *J* = 8.4 Hz, 2H), 7.32 (d, *J* = 8.3 Hz, 2H), 6.82

(s, 1H), 2.47 (s, 3H), 2.45 (s, 3H) ppm; ^{13}C NMR (75 MHz, DMSO-d_6) δ 166.9, 139.7, 134.6, 129.7, 127.4, 127.3, 126.3, 122.7, 113.7, 18.3, 18.1 ppm; FTIR (neat): 2914–2540 (br), 1677, 1602, 1567, 1545, 1490, 1408, 1291, 1178, 850, 796, 505, 470 cm^{-1}; APPI−HRMS (*m/z*, negative mode) [M$^-$] calcd for $C_{13}H_{12}O_2S_4$, 327.9720; found, 327.9727.

Zn-TTFV 8: A solution of TTFV **6** (0.12 g, 0.18 mmol) and $Zn(NO_3)_2{\cdot}6H_2O$ (0.11 g, 0.37 mmol) in EtOH (350 mL) was added into a beaker, which was placed in a larger beaker containing Et_3N/EtOH (40 mL, 1:1). The larger beaker was sealed and left standing for 4 days. The precipitate formed within the smaller beaker was collected by centrifugation and rinsed with EtOH to afford Zn-TTFV **8** (50.8 mg) as a yellow solid. FTIR (neat): 3381, 1586, 1535, 1400, 857, 787 cm^{-1}.

Zn-DTF 9: A solution of DTF **7** (20.0 mg, 0.0610 mmol) and $Zn(NO_3)_2{\cdot}6H_2O$ (21.8 mg, 0.0733 mmol) in EtOH (40 mL) was added into a vial, which was placed in a jar containing Et_3N/EtOH (6 mL, 1:2). The jar was sealed and left standing for 2 days. The precipitate formed in the vial was collected by centrifugation and rinsed with EtOH to afford Zn-DTF **9** (15.1 mg) as a yellow solid. FTIR (neat): 3360, 2990, 2916, 1585, 1559, 1538, 1494, 1392, 1187, 803, 768, 472 cm^{-1}.

Supporting Information

Supporting Information File 1

^{1}H and ^{13}C NMR spectra of compounds **4**–**7**, PXRD data of **8** and **9**, thermal gravimetric analysis (TGA) data of **8**, and time-dependent (TD) DFT calculation results for compounds **6** and **7**.
[http://www.beilstein-journals.org/bjoc/content/supplementary/1860-5397-11-107-S1.pdf]

Acknowledgements

We thank the Natural Sciences and Engineering Research Council (NSERC) of Canada, Canada Foundation for Innovation (CFI), and Memorial University for financial support.

References

1. Yamada, J.-i.; Sugimoto, T. *TTF Chemistry: Fundamentals and Applications of Tetrathiafulvalene;* Springer: Berlin, Germany, 2004.
2. Segura, J. L.; Martín, N. *Angew. Chem., Int. Ed.* **2001,** *40,* 1372–1409. doi:10.1002/1521-3773(20010417)40:8<1372::AID-ANIE1372>3.0.CO;2-I
3. Simonsen, K. B.; Becher, J. *Synlett* **1997,** 1211–1220. doi:10.1055/s-1997-1001
4. Nielsen, M. B.; Lomholt, C.; Becher, J. *Chem. Soc. Rev.* **2000,** *29,* 153–164. doi:10.1039/A803992E
5. Canevet, D.; Sallé, M.; Zhang, G.; Zhang, D.; Zhu, D. *Chem. Commun.* **2009,** 2245–2269. doi:10.1039/B818607N
6. Wudl, F.; Wobschall, D.; Hufnagel, E. J. *J. Am. Chem. Soc.* **1972,** *94,* 670–672. doi:10.1021/ja00757a079
7. Ferraris, J.; Cowan, D. O.; Walatka, V.; Perlstein, J. H. *J. Am. Chem. Soc.* **1973,** *95,* 948–949. doi:10.1021/ja00784a066
8. VandeVondele, J.; Lynden-Bell, R.; Meijer, E. J.; Sprik, M. *J. Phys. Chem. B* **2005,** *110,* 3614–3623. doi:10.1021/jp054841+
9. Nielsen, M. B.; Sauer, S. P. A. *Chem. Phys. Lett.* **2008,** *453,* 136–139. doi:10.1016/j.cplett.2008.01.012
10. Bendikov, M.; Wudl, F.; Perepichka, D. F. *Chem. Rev.* **2004,** *104,* 4891–4946. doi:10.1021/cr030666m
11. Frère, P.; Skabara, P. J. *Chem. Soc. Rev.* **2005,** *34,* 69–98. doi:10.1039/B316392J
12. Zhao, Y. M.; Chen, G.; Mulla, K.; Mahmud, I.; Liang, S.; Dongare, P.; Thompson, D. W.; Dawe, L. N.; Bouzan, S. *Pure Appl. Chem.* **2012,** *84,* 1005–1025. doi:10.1351/Pac-Con-11-09-22
13. Roncali, J. *J. Mater. Chem.* **1997,** *7,* 2307–2321. doi:10.1039/A703956E
14. Bryce, M. R.; Coffin, M. A.; Clegg, W. *J. Org. Chem.* **1992,** *57,* 1696–1699. doi:10.1021/jo00032a018
15. Carlier, R.; Hapiot, P.; Lorcy, D.; Robert, A.; Tallec, A. *Electrochim. Acta* **2001,** *46,* 3269–3277. doi:10.1016/S0013-4686(01)00619-3
16. Bellec, N.; Boubekeur, K.; Carlier, R.; Hapiot, P.; Lorcy, D.; Tallec, A. *J. Phys. Chem. A* **2000,** *104,* 9750–9759. doi:10.1021/jp001326x
17. Lorcy, D.; Guerro, M.; Bergamini, J.-F.; Hapiot, P. *J. Phys. Chem. B* **2013,** *117,* 5188–5194. doi:10.1021/jp401537a
18. Gontier, E.; Bellec, N.; Brignou, P.; Gohier, A.; Guerro, M.; Roisnel, T.; Lorcy, D. *Org. Lett.* **2010,** *12,* 2386–2389. doi:10.1021/ol1007422
19. Liang, S.; Zhao, Y.; Adronov, A. *J. Am. Chem. Soc.* **2013,** *136,* 970–977. doi:10.1021/ja409918n
20. Liang, S.; Chen, G.; Zhao, Y. *J. Mater. Chem. C* **2013,** *1,* 5477–5490. doi:10.1039/C3TC30317A
21. Liang, S.; Chen, G.; Peddle, J.; Zhao, Y. *Chem. Commun.* **2012,** *48,* 3100–3102. doi:10.1039/C2CC17935K
22. Chen, G.; Mahmud, I.; Dawe, L. N.; Daniels, L. M.; Zhao, Y. *J. Org. Chem.* **2011,** *76,* 2701–2715. doi:10.1021/jo2000447
23. Chen, G.; Mahmud, I.; Dawe, L. N.; Zhao, Y. *Org. Lett.* **2010,** *12,* 704–707. doi:10.1021/ol9026683
24. Chen, G.; Zhao, Y. *Org. Lett.* **2014,** *16,* 668–671. doi:10.1021/ol403295q
25. Mulla, K.; Shaik, H.; Thompson, D. W.; Zhao, Y. *Org. Lett.* **2013,** *15,* 4532–4535. doi:10.1021/ol402093a
26. Mulla, K.; Dongare, P.; Thompson, D. W.; Zhao, Y. *Org. Biomol. Chem.* **2012,** *10,* 2542–2544. doi:10.1039/C2OB06828A
27. Hapiot, P.; Lorcy, D.; Tallec, A.; Carlier, R.; Robert, A. *J. Phys. Chem.* **1996,** *100,* 14823–14827. doi:10.1021/jp961048v
28. Inagi, S.; Naka, K.; Chujo, Y. *J. Mater. Chem.* **2007,** *17,* 4122–4135. doi:10.1039/B708640G
29. Eddaoudi, M.; Kim, J.; Rosi, N.; Vodak, D.; Wachter, J.; O'Keeffe, M.; Yaghi, O. M. *Science* **2002,** *295,* 469–472. doi:10.1126/science.1067208
30. Cook, T. R.; Zheng, Y.-R.; Stang, P. J. *Chem. Rev.* **2013,** *113,* 734–777. doi:10.1021/cr3002824
31. MacGillivray, L. *Metal-Organic Frameworks: Design and Application;* Wiley & Sons: Hoboken, NJ, USA, 2010.
32. Chen, B.; Lv, Z.-P.; Leong, C. F.; Zhao, Y.; D'Alessandro, D. M.; Zuo, J.-L. *Cryst. Growth Des.* **2015,** *15,* 1861–1870. doi:10.1021/acs.cgd.5b00014

33. Zhu, Q.-Y.; Wang, J.-P.; Qin, Y.-R.; Shi, Z.; Han, Q.-H.; Bian, G.-Q.; Dai, J. *Dalton Trans.* **2011,** *40,* 1977–1983. doi:10.1039/C0DT01152E
34. Ding, Y.; Chen, Q.; Zhong, J.-C.; Munakata, M.; Konaka, H.; Ning, G.-L.; Wang, H.-Z. *Polyhedron* **2008,** *27,* 1393–1400. doi:10.1016/j.poly.2008.01.010
35. Martínez, V.; Gaspar, A. B.; Muñoz, M. C.; Ballesteros, R.; Ortega-Villar, N.; Ugalde-Saldívar, V. M.; Moreno-Esparza, R.; Real, J. A. *Eur. J. Inorg. Chem.* **2009,** 303–310. doi:10.1002/ejic.200800988
36. Christensen, C. A.; Batsanov, A. S.; Bryce, M. R. *J. Org. Chem.* **2007,** *72,* 1301–1308. doi:10.1021/jo062199p
37. Kim, J.; Chen, B.; Reineke, T. M.; Li, H.; Eddaoudi, M.; Moler, D. B.; O'Keeffe, M.; Yaghi, O. M. *J. Am. Chem. Soc.* **2001,** *123,* 8239–8247. doi:10.1021/ja010825o

License and Terms

BEILSTEIN JOURNAL OF ORGANIC CHEMISTRY

Tuning the size of a redox-active tetrathiafulvalene-based self-assembled ring

Sébastien Bivaud, Sébastien Goeb*, Vincent Croué, Magali Allain, Flavia Pop and Marc Sallé*

Letter

Open Access

Address:
Laboratoire MOLTECH-Anjou, Université d'Angers, UMR CNRS 6200, 2 bd Lavoisier, 49045 Angers Cedex, France. Fax: 0033241735439, Tel: 0033241735405

Email:
Sébastien Goeb* - sebastien.goeb@univ-angers.fr; Marc Sallé* - marc.salle@univ-angers.fr

* Corresponding author

Keywords:
coordination; metal-driven; redox; self-assembly; tetrathiafulvalene

Beilstein J. Org. Chem. **2015,** *11,* 966–971.
doi:10.3762/bjoc.11.108

Received: 12 February 2015
Accepted: 07 May 2015
Published: 05 June 2015

This article is part of the Thematic Series "Tetrathiafulvalene chemistry".

Guest Editor: P. J. Skabara

Abstract

The synthesis of a new Pd coordination-driven self-assembled ring M_6L_3 constructed from a concave tetrapyridyl π-extended tetrathiafulvalene ligand (exTTF) is described. The same ligand is also able to self-assemble in a M_4L_2 mode as previously described. Herein, we demonstrate that the bulkiness of the ancillary groups in the Pd complex allows for modulating the size and the shape of the resulting discrete self-assembly, which therefore incorporate two (M_4L_2) or three (M_6L_3) electroactive exTTF sidewalls.

Findings

The coordination-driven approach is a well-established method that has been extensively used to reach more and more sophisticated cage-like discrete molecules [1-19], including redox-active ones [20]. In this context and since this strategy results from one single chemical step (metal to ligand assembly), there is a great interest in controlling the parameters which govern the final size and geometry of the resulting discrete self-assembled structures. Some general trends have first to be considered: i) as awaited from a lower kinetic stability, the ligand exchange process in the case of square-planar Pd(II) complexes is faster than with Pt(II) analogues; ii) the most thermodynamically stable species is formed along the assembly process, but if no evident energetic advantage exists for one structure, a dynamic equilibrium between two or more macrocyclic entities may be observed in solution [21-26]. This is in particular the case with flexible (including long) linear ditopic ligands, which favor the formation of triangle species whereas shorter ones shift the equilibrium towards molecular squares for which the enthalpic gain (less steric constraint) compensates for the entropic penalty. Beside the conformational flexibility of the ligand, parameters such as temperature, concentration and solvent type can influence the equilibrium. Isolation of the species from a given equilibrium has not been often carried out [27,28]. We were able in our case to operate the separation of a mixture of a

triangle and a square [29]. The triangle–square dynamic equilibrium also depends on the nature of the ancillary ligand on the metal corner [21,22,26,30-33]. In particular, steric repulsions due to the ancillary ligand may displace the equilibrium towards the triangular species since the latter offers more space around the metal center. A change in the ancillary group can also lead to a modification of the cavity volume for a given cage [34]. Beyond those results, additional important issues still need to be addressed and concern in particular the possibility to obtain, from one given ligand, one single and stable assembly whose cavity size can be controlled.

We recently depicted the preparation and properties of redox-active rings [29,35] and cages [36-40] integrating the tetrathiafulvalene (TTF) skeleton. In particular, we described self-assembled containers prepared from an electron-rich ligand precursor based on the extended-TTF framework (exTTF) [39].

On this basis, we report herein that the size and the shape of coordination-driven self-assembled redox-active cages, constructed from a exTTF-based tetratopic ligand, can be tuned by modulating the bulkiness of the ancillary group on the metal complex precursor.

The tetrapyridyl-exTTF ligand L1 (Scheme 1, Figure 1a) was synthesized through a palladium catalysed C–H arylation from the naked exTTF [39]. We already reported that the self-assembly process of this tetratopic ligand with *cis*-M(dppf)$(OTf)_2$ (M = Pd or Pt; dppf = 1,1'-bis(diphenylphosphino)ferrocene; OTf = trifluoromethanesulfonate) in nitromethane at 40 °C converged into a single symmetrical M_4L_2 discrete species (Scheme 1, Figure 1b) [39]. It is worth noting that the through space interaction between the phenyl rings of the bulky 1,1'-bis(diphenylphosphino) ferrocene (dppf) coligand and the pyridine moieties force the exTTF unit to increase significantly its curvature in comparison to ligand L1 (56° vs 86° respectively between the 1,3-dithiol-2-ylidene mean planes (Figure 1)). This leads to the formation of the compact M_4L_2 assembly in which the pyridyl units are wedged between the dppf units, producing therefore a robust assembly affording an oblate spheroidal cavity. On this basis and considering the relative flexibility of the large exTTF moiety, we assumed that the bulkiness of the metal complex coligand could be adjusted to tune the macrocycle size and shape.

Complexation of ligand L1 with precursor Pd(en)$(OTf)_2$ (en = 1,2-ethylenediamine) was carried out in DMSO at 40 °C and monitored by ^{1}H NMR. In 30 min, the reaction converged into a unique symmetrical discrete species that could be isolated in more than 90% yield after precipitation in ethyl acetate. In contrast with assembly M_4L_2 for which the presence of through-space interactions (Figure 4a) between the coligand

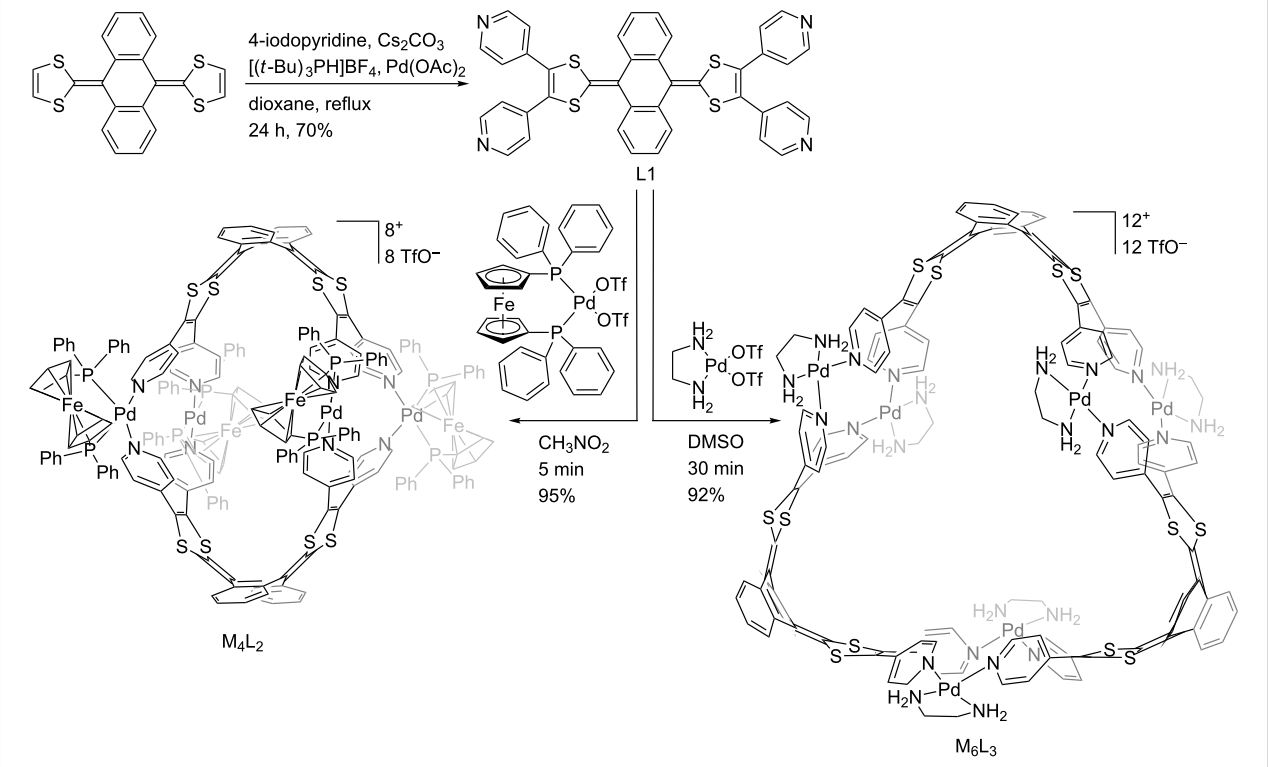

Scheme 1: Synthesis of ligand L1, self-assemblies M_4L_2 and M_6L_3.

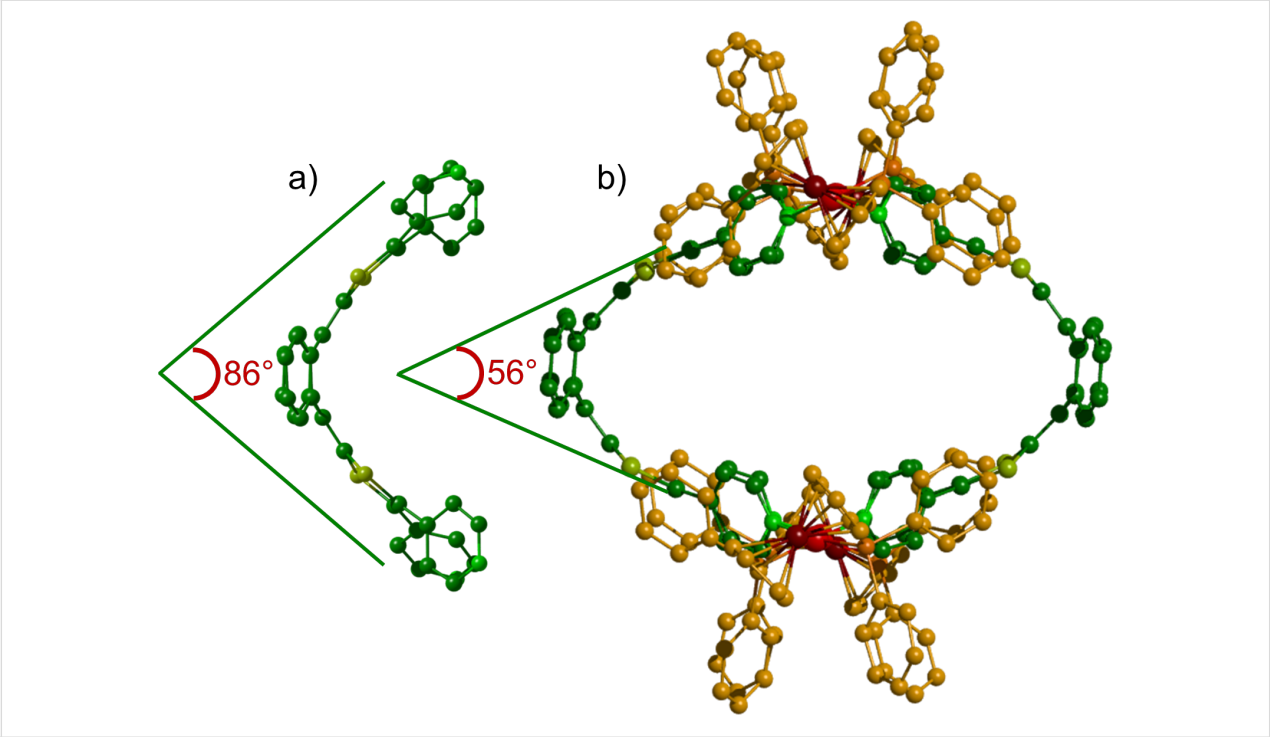

Figure 1: X-ray crystal structures of: (a) ligand L1, (b) self-assembly M_4L_2. For clarity, H atoms and TfO^- counteranions have been omitted.

phenyl units (dppf) and pyridyl groups result in an upfield shift of their signals (Figure 2b) compared to L1, the pyridyl protons are in this case shifted downfield (Figure 2c), as expected from coordination to a metal center. The corresponding DOSY NMR shows only one alignment of signals and confirms the formation of one unique species diffusing in solution with a D value of 6.35×10^{-11} m²·s^{-1} (Figure 2e). An estimated hydrodynamic radius (R_H) of 17.2 Å could be calculated from the Stokes–Einstein equation (T = 298 K) for this new discrete system [41]. This result indicates that the latter is larger than the already described M_4L_2 container (R_H = 10.8 Å (Figure 2d)), and that the corresponding size is compatible with the formation of a M_6L_3 assembly (Scheme 1).

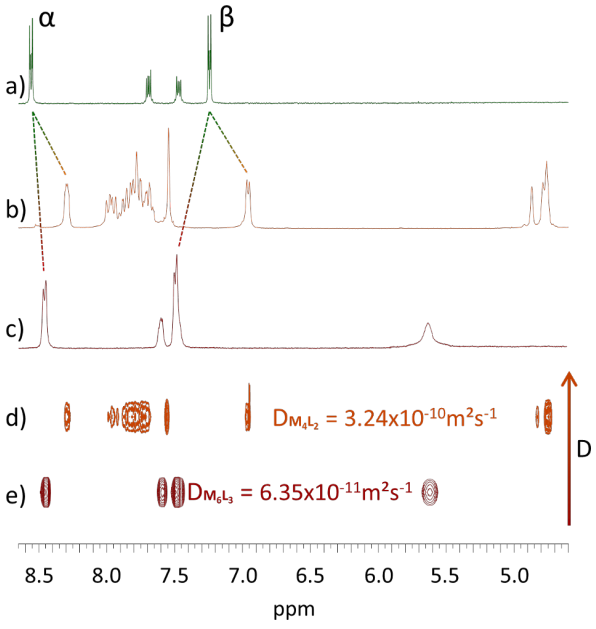

Figure 2: ^{1}H NMR, downfield region (α and β signals correspond respectively to α and β pyridyl protons): (a) L1 (DMSO-d_6), (b) M_4L_2 (CD_3NO_2), (c) M_6L_3 (DMSO-d_6), (d) DOSY NMR of M_4L_2 (CD_3NO_2) and (e) DOSY NMR of M_6L_3 (DMSO-d_6).

ESI–MS mass spectroscopy experiments were carried out in acetone and agree with a M_6L_3 stoichiometry in the gas phase for the new assembly, with multicharged isotopic patterns at m/z = 2278.3, 1468.9, 1064.4, 821.8, corresponding respectively to $[M_6L_3\text{-}10TfO^-]^{2+}$, $[M_6L_3\text{-}9TfO^-]^{3+}$, $[M_6L_3\text{-}8TfO^-]^{4+}$, $[M_6L_3\text{-}7TfO^-]^{5+}$ species and matching perfectly with theoretical ones (Supporting Information File 1, Figure S8).

Single crystals of assembly M_6L_3 were grown by slow diffusion of ethyl acetate in DMSO and allowed for determining unambiguously the solid-state structure by a synchrotron X-ray diffraction study (Figure 3). Whereas the sterically demanding dppf moiety leads to a M_4L_2 structure characterized by i) exTTF moieties which are highly distorted and ii) short interplanar distances between the phenyl units of the ancillary dppf complex and the pyridyl rings (3.5 Å) (Figure 4a), a much less

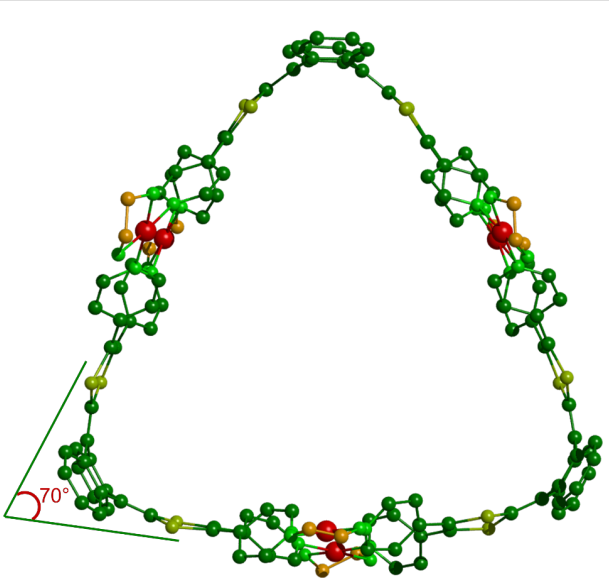

Figure 3: X-ray crystal structure of self-assembly M_6L_3. For clarity, H atoms and TfO^- counteranions have been omitted.

constrained system is observed in the case of the M_6L_3 complex, characterizing a prismatic structure which is not driven by steric effects but which is mainly governed by thermodynamic aspects.

The M_6L_3 assembly forms a trigonal prismatic structure presenting a cavity defined by 17.7 Å high, 19.0 Å edge and 9.5 Å depth. The curvature of the exTTF moiety in the complex (70° between the 1,3-dithiol-2-ylidene mean plans, Figure 3) is intermediate between those observed for the free ligand L1 and the ligand in M_4L_2, which illustrates a lower ring constraint than in M_4L_2. In addition to the expected variation of the *N*(pyridyl)-Pd-*N*(pyridyl) angle within the distorted square planar – i.e. the dppf complex (M_4L_2, 86°) and the en one (M_6L_3, 93°) (Figure 4) –, the change in the ancillary ligand also results in a modification of the rotation angles between the pyridyl units and the 1,3-dithiol-2-ylidene heterocycles. Because of the lower steric demand with the 1,2-ethylenediamine co-ligand, the vicinal pyridyl units are free to rotate around the C-pyridine axis in M_6L_3, resulting in dihedral angles of 40° and 52° in the crystal (Figure 4b). These values are in the same range as those observed in the free ligand L1 (35° and 63°). By comparison, the pyridyl units in complex M_4L_2 are tilted with angles of 52° and −69° in the solid (Figure 4a). Those higher values result from the increased steric demand generated by the dppf coligand.

A cyclic voltammetry study of prism M_6L_3 was carried out in acetonitrile containing 0.1 M NBu_4PF_6 (Figure 5). Compared to ligand L1 which presents the usual electrochemical behavior of

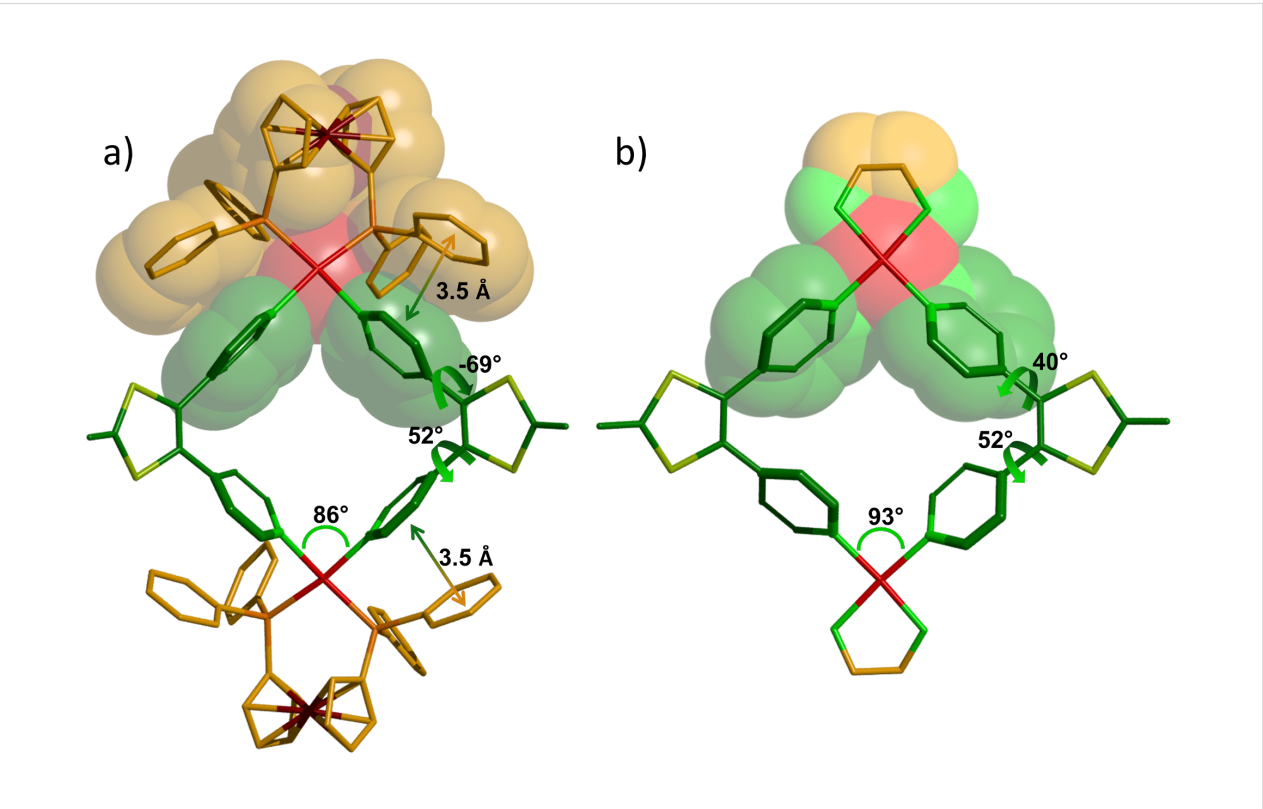

Figure 4: Geometry (from XRD) around two Pd centers in M_4L_2 (a) and M_6L_3 (b). The exTTF moieties have been cut for clarity.

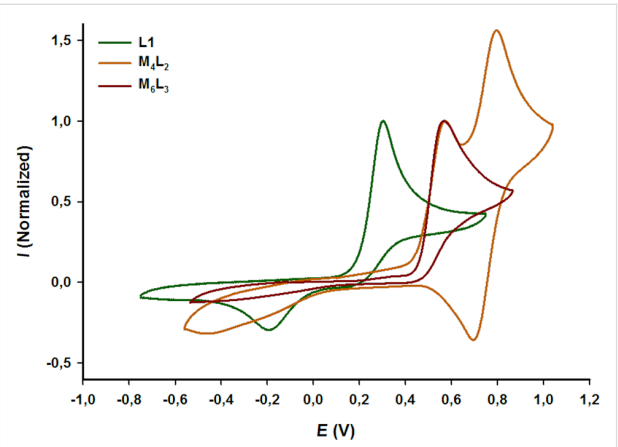

Figure 5: Cyclic voltammogram of L1 ($c = 10^{-3}$ M, CH_3CN/CH_2Cl_2 (v/v 50/50), 0.1 M *n*-Bu_4NPF_6, 100 mV·s^{-1}, Pt), M_4L_2 and M_6L_3 ($c = 10^{-3}$ M, CH_3CN, 0.1 M *n*-Bu_4NPF_6, 100 mV·s^{-1}, Cgr), V vs Fc/Fc^+.

exTTF derivatives, i.e. one poorly electrochemically reversible two-electrons oxidation process, the oxidation of exTTF in self-assembly M_6L_3 is shifted to higher potential (+0.26 V), which is mainly attributed to the coordination to the Pd center. It can be noted that the redox behavior of M_6L_3 is very similar to the one of M_4L_2 [42], with an irreversible oxidation occurring exactly at the same potential (E_{ox} = +0.57 V vs Fc/Fc^+), illustrating the fact that the nature of the ancillary ligand does not impact the electronic properties of exTTF in the corresponding self-assemblies.

In summary, two different coordination-driven discrete self-assemblies varying by the size and the shape can be built from the same tetratopic exTTF-based ligand, simply by changing the ancillary group on the Pd metal center. In particular, whereas a 1,1'-bis(diphenylphosphino)ferrocene co-ligand promotes a clipping of the ligand pyridyl units and leads to a strong curvature of the exTTF moiety integrated in a M_4L_2 coordination cage, the use of a smaller co-ligand leads to the formation of a larger M_6L_3 cavity in which the curvature of the exTTF is closer to ligand L1. The new M_6L_3 system has been fully characterized and exhibits electrochemical properties which are essentially similar to those of M_4L_2, indicating that the strong π-donating ability of the cavity can be maintained while enlarging its size, and illustrating the high potential of the coordination-driven approach in tuning the size and the shape of a target cavity. This approach constitutes a promising strategy to address the design of organic materials (e.g. for organic photovoltaics or molecular electronic devices). Indeed, mastering the geometry of multicomponent redox-active systems offers a unique opportunity to fine-tuning electronic interactions within the material [43], an issue which is of prime importance for optimizing electron transport in organic materials.

Supporting Information

Supporting Information File 1

General methods, synthetic procedures, spectroscopic data.
[http://www.beilstein-journals.org/bjoc/content/supplementary/1860-5397-11-108-S1.pdf]

Supporting Information File 2

X-ray crystallographic data CCDC 1043205.
[http://www.beilstein-journals.org/bjoc/content/supplementary/1860-5397-11-108-S2.cif]

Acknowledgements

The authors gratefully acknowledge the CNRS, the Région des Pays de la Loire and the MENRT for PhD grants (SB and VC), the PIAM (Univ. Angers) and the CRMPO (Univ. Rennes) technical platforms for their assistance in spectroscopic analyses. An access to the synchrotron Soleil – CRISTAL beamline – has been made possible (project 20130173); Drs Pierre Fertey and Sylvain Ravy are warmly acknowledged for their assistance. Finally, the Johnson-Matthey company is acknowledged for the generous providing of palladium salts.

References

1. Amouri, H.; Desmarets, C.; Moussa, J. *Chem. Rev.* **2012,** *112,* 2015–2041. doi:10.1021/cr200345v
2. MacGillivray, L. R. *Angew. Chem., Int. Ed.* **2012,** *51,* 1110–1112. doi:10.1002/anie.201107282
3. Chakrabarty, R.; Mukherjee, P. S.; Stang, P. J. *Chem. Rev.* **2011,** *111,* 6810–6918. doi:10.1021/cr200077m
4. Inokuma, Y.; Kawano, M.; Fujita, M. *Nat. Chem.* **2011,** *3,* 349–358. doi:10.1038/nchem.1031
5. Jin, P.; Dalgarno, S. J.; Atwood, J. L. *Coord. Chem. Rev.* **2010,** *254,* 1760–1768. doi:10.1016/j.ccr.2010.04.009
6. De, S.; Mahata, K.; Schmittel, M. *Chem. Soc. Rev.* **2010,** *39,* 1555–1575. doi:10.1039/b922293f
7. Therrien, B. *Eur. J. Inorg. Chem.* **2009,** 2445–2453. doi:10.1002/ejic.200900180
8. Northrop, B. H.; Zheng, Y.-R.; Chi, K.-W.; Stang, P. J. *Acc. Chem. Res.* **2009,** *42,* 1554–1563. doi:10.1021/ar900077c
9. Stang, P. J. *J. Org. Chem.* **2009,** *74,* 2–20. doi:10.1021/jo801682d
10. Yoshizawa, M.; Klosterman, J. K.; Fujita, M. *Angew. Chem., Int. Ed.* **2009,** *48,* 3418–3438. doi:10.1002/anie.200805340
11. Han, Y.-F.; Jia, W.-G.; Yu, W.-B.; Jin, G.-X. *Chem. Soc. Rev.* **2009,** *38,* 3419–3434. doi:10.1039/b901649j
12. Northrop, B. H.; Chercka, D.; Stang, P. J. *Tetrahedron* **2008,** *64,* 11495–11503. doi:10.1016/j.tet.2008.08.062
13. Northrop, B. H.; Yang, H.-B.; Stang, P. J. *Chem. Commun.* **2008,** 5896–5908. doi:10.1039/b811712h
14. Cooke, M. W.; Chartrand, D.; Hanan, G. S. *Coord. Chem. Rev.* **2008,** *252,* 903–921. doi:10.1016/j.ccr.2008.01.006
15. Dalgarno, S. J.; Power, N. P.; Atwood, J. L. *Coord. Chem. Rev.* **2008,** *252,* 825–841. doi:10.1016/j.ccr.2007.10.010

16. Zangrando, E.; Casanova, M.; Alessio, E. *Chem. Rev.* **2008,** *108,* 4979–5013. doi:10.1021/cr8002449
17. Mukherjee, S.; Mukherjee, P. S. *Chem. Commun.* **2014,** *50,* 2239–2248. doi:10.1039/c3cc49192g
18. Mishra, A.; Kang, S. C.; Chi, K.-W. *Eur. J. Inorg. Chem.* **2013,** 5222–5232. doi:10.1002/ejic.201300729
19. Cook, T. R.; Vajpayee, V.; Lee, M. H.; Stang, P. J.; Chi, K.-W. *Acc. Chem. Res.* **2013,** *46,* 2464–2474. doi:10.1021/ar400010v
20. Croué, V.; Goeb, S.; Sallé, M. *Chem. Commun.* **2015,** *51,* 7275–7289. doi:10.1039/C5CC00597C
21. Uehara, K.; Kasai, K.; Mizuno, N. *Inorg. Chem.* **2010,** *49,* 2008–2015. doi:10.1021/ic100011a
22. Ferrer, M.; Pedrosa, A.; Rodriguez, L.; Rossell, O.; Vilaseca, M. *Inorg. Chem.* **2010,** *49,* 9438–9449. doi:10.1021/ic101150p
23. Ghosh, S.; Mukherjee, P. S. *Inorg. Chem.* **2009,** *48,* 2605–2613. doi:10.1021/ic802254f
24. Sun, Q.-F.; Wong, K. M.-C.; Liu, L.-X.; Huang, H.-P.; Yu, S.-Y.; Yam, V. W.-W.; Li, Y.-Z.; Pan, Y.-J.; Yu, K.-C. *Inorg. Chem.* **2008,** *47,* 2142–2154. doi:10.1021/ic701344p
25. Yamamoto, T.; Arif, A. M.; Stang, P. J. *J. Am. Chem. Soc.* **2003,** *125,* 12309–12317. doi:10.1021/ja0302984
26. Fujita, M.; Sasaki, O.; Mitsuhashi, T.; Fujita, T.; Yazaki, J.; Yamaguchi, K.; Ogura, K. *Chem. Commun.* **1996,** 1535–1536. doi:10.1039/cc9960001535
27. Maeda, H.; Akuta, R.; Bando, Y.; Takaishi, K.; Uchiyama, M.; Muranaka, A.; Tohnai, N.; Seki, S. *Chem. – Eur. J.* **2013,** *19,* 11676–11685. doi:10.1002/chem.201302028
28. Schweiger, M.; Seidel, S. R.; Arif, A. M.; Stang, P. J. *Inorg. Chem.* **2002,** *41,* 2556–2559. doi:10.1021/ic0112692
29. Goeb, S.; Bivaud, S.; Dron, P. I.; Balandier, J.-Y.; Chas, M.; Sallé, M. *Chem. Commun.* **2012,** *48,* 3106–3108. doi:10.1039/c2cc00065b
30. Holló-Sitkei, E.; Tárkányi, G.; Párkányi, L.; Megyes, T.; Besenyei, G. *Eur. J. Inorg. Chem.* **2008,** 1573–1583. doi:10.1002/ejic.200701189
31. Weilandt, T.; Troff, R. W.; Saxell, H.; Rissanen, K.; Schalley, C. A. *Inorg. Chem.* **2008,** *47,* 7588–7598. doi:10.1021/ic800334k
32. Ferrer, M.; Gutiérrez, A.; Mounir, M.; Rossell, O.; Ruiz, E.; Rang, A.; Engeser, M. *Inorg. Chem.* **2007,** *46,* 3395–3406. doi:10.1021/ic062373s
33. Ferrer, M.; Mounir, M.; Rossell, O.; Ruiz, E.; Maestro, M. A. *Inorg. Chem.* **2003,** *42,* 5890–5899. doi:10.1021/ic034489j
34. Fang, Y.; Murase, T.; Sato, S.; Fujita, M. *J. Am. Chem. Soc.* **2013,** *135,* 613–615. doi:10.1021/ja311373f
35. Balandier, J.-Y.; Chas, M.; Goeb, S.; Dron, P. I.; Rondeau, D.; Belyasmine, A.; Gallego, N.; Sallé, M. *New J. Chem.* **2011,** *35,* 165–168. doi:10.1039/C0NJ00545B
36. Goeb, S.; Bivaud, S.; Croué, V.; Vajpayee, V.; Allain, M.; Sallé, M. *Materials* **2014,** *7,* 611–622. doi:10.3390/ma7010611
37. Vajpayee, V.; Bivaud, S.; Goeb, S.; Croué, V.; Allain, M.; Popp, B. V.; Garci, A.; Therrien, B.; Sallé, M. *Organometallics* **2014,** *33,* 1651–1658. doi:10.1021/om401142j
38. Bivaud, S.; Goeb, S.; Balandier, J. Y.; Chas, M.; Allain, M.; Sallé, M. *Eur. J. Inorg. Chem.* **2014,** 2440–2448. doi:10.1002/ejic.201400060
39. Bivaud, S.; Goeb, S.; Croué, V.; Dron, P. I.; Allain, M.; Sallé, M. *J. Am. Chem. Soc.* **2013,** *135,* 10018–10021. doi:10.1021/ja404072w
40. Bivaud, S.; Balandier, J.-Y.; Chas, M.; Allain, M.; Goeb, S.; Sallé, M. *J. Am. Chem. Soc.* **2012,** *134,* 11968–11970. doi:10.1021/ja305451v
41. Cohen, Y.; Avram, L.; Frish, L. *Angew. Chem., Int. Ed.* **2005,** *44,* 520–554. doi:10.1002/anie.200300637
42. M_4L_2 presents an additional reversible redox system located at a higher potential (Eox = +0.80 V vs Fc/Fc+), corresponding to the reversible oxidation of the appended ferrocene Pd co-ligand.
43. Schneebeli, S. T.; Frasconi, M.; Liu, Z.; Wu, Y.; Gardner, D. M.; Strutt, N. L.; Cheng, C.; Carmieli, R.; Wasielewski, M. R.; Stoddart, J. F. *Angew. Chem., Int. Ed.* **2013,** *52,* 13100–13104. doi:10.1002/anie.201307984

License and Terms

BEILSTEIN JOURNAL OF ORGANIC CHEMISTRY

Chiroptical properties of 1,3-diphenylallene-anchored tetrathiafulvalene and its polymer synthesis

Masashi Hasegawa*[1], Junta Endo[1], Seiya Iwata[1], Toshiaki Shimasaki[2] and Yasuhiro Mazaki*[1]

Full Research Paper

Open Access

Address:
[1]Department of Chemistry, School of Science, Kitasato University, 1-15-1 Kitasato, Minami-ku, Sagamihara, Kanagawa 252-0373, Japan and [2]Graduate School of Engineering, Chiba Institute of Technology, 2-17-1 Tsudanuma, Narashino, Chiba 275-0016, Japan

Email:
Masashi Hasegawa* - masasi.h@kitastato-u.ac.jp; Yasuhiro Mazaki* - mazaki@kitasato-u.ac.jp

* Corresponding author

Keywords:
allene; axial chirality; chiroptical properties; redox; tetrathiafulvalene

Beilstein J. Org. Chem. **2015,** *11,* 972–979.
doi:10.3762/bjoc.11.109

Received: 23 February 2015
Accepted: 13 May 2015
Published: 08 June 2015

This article is part of the Thematic Series "Tetrathiafulvalene chemistry".

Guest Editor: P. J. Skabara

Abstract

A novel tetrathiafulvalene dimer, bridged by a chiral 1,3-diphenylallene framework, has been prepared as an optically active compound having strong chiroptical properties. Although a chiral allene bearing strong electron-donating group(s) often undergoes slow photoracemization even in daylight, the present allene is totally configurationally stable under ordinary conditions. Each isomer possesses pronounced chiroptical properties in its ECD spectra reflecting the chiral allene framework. Moreover, the elongation of the chiral main chain was also carried out by direct C–H activation of the TTF unit, and the chiroptical properties of the resulting polymer were also investigated.

Introduction

Recently, there has been a growing interest in chiral π-conjugated systems having strong chiroptical properties because they have great potential for use in optical devices involving polarized light [1-3]. Chiral response, in electronic circular dichroism (ECD) based on an exciton coupling between two adequate π-chromophores, can express a pronounced chiroptical effect over various optical energy regions. Therefore, embedding the chromophores into a chiral rigid framework can be a practical molecular design for ascertaining chiroptical materials [4-7].

A symmetric allene framework is one of the most reliable chiral resources that can preserve a consistent orientation of the chromophores [8,9]. We recently introduced 1,3-bis(tetrathiafulvalenyl)allene derivatives **1**, as a new class of chiral electrochromic (EC) materials consisting of redox-active chromophores and a non-centrochiral framework (Figure 1) [10]. The intensive Cotton effect on the ECD spectra is switchable by tuning the electronic structure of the tetrathiafulvalene (TTF) moieties. However, compound **1** exhibited slow racemization in

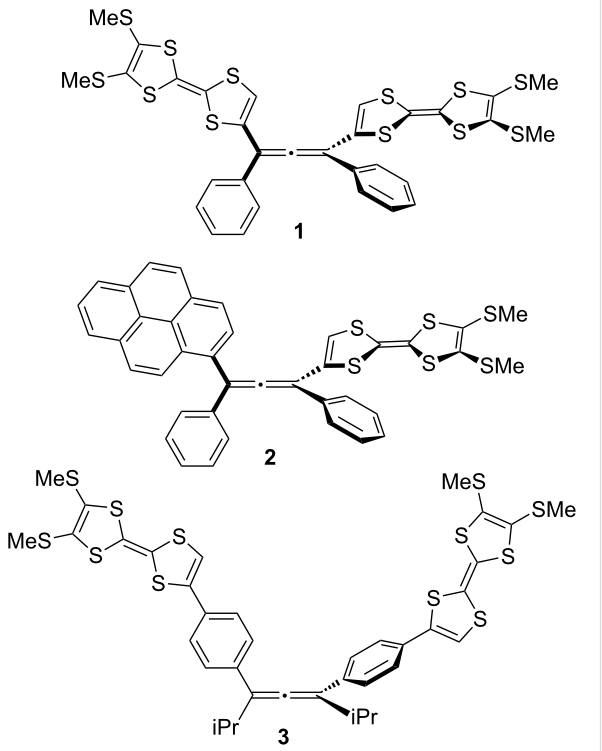

Figure 1: TTF-substituted allenes **1**–**3**.

solution under daylight. The chirality of an allene is configurationally firm in general, because the barrier of the rotation of the allenic double bonds is quite high ($\Delta G^{\ddagger}$ = 180 kJ mol^{-1} for $CH_3CH{=}C{=}CHCH_3$) [11]. In contrast, several allenes directly connected with electron-donating groups occasionally underwent photoracemization [12,13]. Although the mechanism of the photoracemization is not clear, a comparative examination of the racemization rate in **1** and **2**, the latter of which is a dissymmetric allene having a TTF and a pyrenyl group at 1,3-position, suggests that the direct connection of the TTF units may strongly affect the fast racemization [14]. From this point of view, we decided to employ a 1,3-diphenylallene derivative (**3**) as a stable chiral framework. We conceive that the insertion of the phenylene units between the central chiral allene and TTFs would overcome the vulnerability toward the photoracemization under ambient conditions. Previsously, Krause and co-workers reported the first synthesis of a cyclic allenophane involving a racemic 1,3-diphenyl allene unit [15]. In addition, Fallis and co-workers synthesized a cyclic oligoallene based on a chiral 1,3-diphenylallene [16]. More recently, Kijima and co-workers reported the use of a racemic 1,3-diphenylallene framework as a new building block for a π-conjugated polymer [17]. However, there have been few investigations regarding the use of 1,3-diphenylallene as a chiral source and involving the detailed investigations of the chiroptical property. In this paper, we report the synthesis of chiral 1,3-bis(4-(tetrathiafulvalenenyl)phenyl)allene derivative **3** and its chiroptical properties. Furthermore, the first synthesis of a chiral copolymer containing TTFs based on a chiral allenic framework (poly-**3**: PTDPA is also demonstrated.

Results and Discussion

To anchor the TTF groups into the allene framework, we chose a cross-coupling reaction of unknown 1,3-bis(4-iodophenyl)-1,3-diisopropylallene (**9**) with a TTF-zinc intermediate (Scheme 1). Previously, 1,3-bis(2-bromophenyl)allene derivatives were reported by Ready et al. as a precursor of an asymmetric catalyst [18]. To obtain the chiral 1,3-bis(4-bromophenyl)allene (**8**) in a larger scale, we modified the synthesis and the chiral separation process as shown in Scheme 1. Thus, starting with 1-(4-bromophenyl)-2-methylpropanone (**4**), which

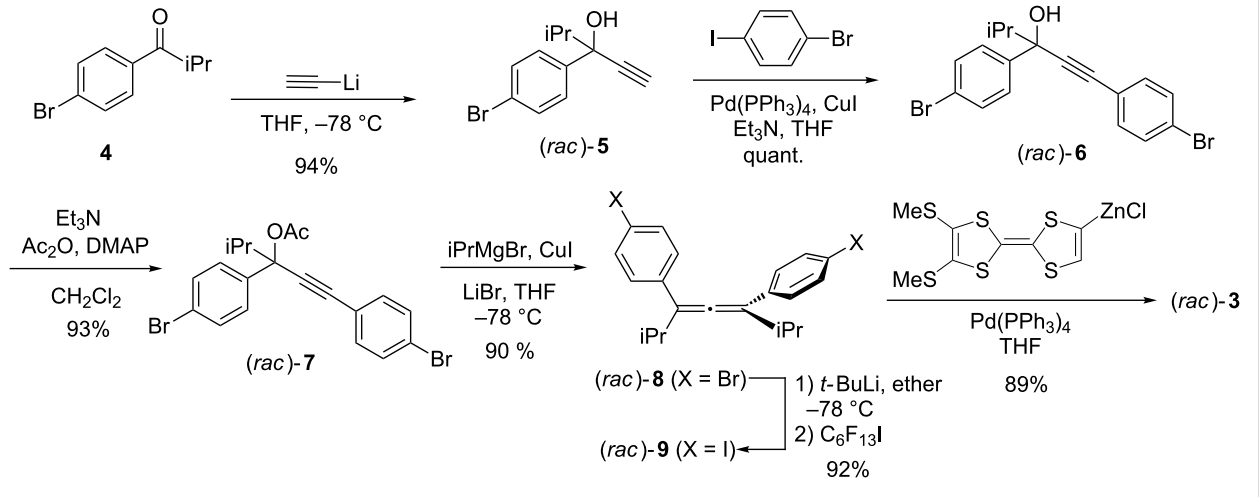

Scheme 1: Synthesis of **3**.

was prepared from bromobenzaldehyde (see Supporting Information File 1), which upon treatment with lithium acetylide at low temperature gave racemic propargyl alcohol **5** in 94% yield. Sonogashira coupling reaction of **5** with 4-bromoiodobenzene gave compound **6** quantitatively. The treatment of **6** with Ac_2O and a catalytic amount of *N*,*N*-dimethyl-4-aminopyridine (DMAP) gave the acetyl ester **7** in 93% yield. The formation of 1,3-bis(4-bromophenyl)-1,3-diisopropylallene (**8**) was achieved by an S_N2'-type reaction of **7** with iPrMgCl–CuI–LiBr at low temperature in 90% yield. This allene was easily transformed into the precursor **9** by halogen exchange with *t*-BuLi followed by the addition of $C_6F_{13}I$ in 92% yield. Subsequently, the reaction of the diiodo precursor **9** with 2 equiv of an organozinc species derived from 4,5-bis(methylthio)TTF [19] in the presence of $Pd(PPh_3)_4$ gave racemic compound **3** in good yield (89%). In the ^{13}C NMR spectrum, the allenic =C= carbon was found to be at 204 ppm, which is a typical value of the linear allene framework. In addition, the FTIR spectrum also exhibited a reasonable vibrational stretching of the C=C=C unit at 1914 cm^{-1}.

Because new symmetrical allenes were subject to optical resolution, the separation of (*rac*)-**3** was carried out by using a recycling HPLC method on a chiral stationary phase (DAICEL Chiralpak IA-3) with hexane/$CHCl_3$/EtOH (v/v = 20:10:0.2) elution. Thus, equimolecular amounts of the optically pure allenes (+)-**3** and (−)-**3**, whose optical rotations ($[\alpha]_D^{25}$) are +726 (*c* 0.853 in CH_2Cl_2) and −721(*c* 0.853 in CH_2Cl_2), respectively, were collected. Similarly, optical resolution of (*rac*)-**9** also provided (+)/(−)-**9** with optical rotations ($[\alpha]_D^{25}$) of +338 (*c* 0.83 in CH_2Cl_2) and −341 (*c* 0.83 in CH_2Cl_2), respectively.

Figure 2 depicted the electronic circular dichroism (ECD) spectra of the enantiomers of (+)/(−)-**3** and (+)/(−)-**9**, and their UV–vis absorption spectra. The ECD spectrum of the (−)-**9** enantiomer exhibited a clear bisignate CD curve with a negative peak at 274 nm and a positive peak at 248 nm. According to the chiral exciton coupling method [20], the spectrum trend of (−)-**9** suggests that the isomer should have the (*R*)-configuration. This assignment was also validated by spectral simulation, obtained from the electronic transition energies and the rotational strengths using TD-DFT calculations [21]. Thus, the intensive Cotton effect is associated with the exciton coupling of the two chromophores of the iodobenzene units. In the ECD spectrum of (+)-**9**, the mirror image of the trend lines of (−)-**9** was found.

The UV–vis absorption spectrum of **3** exhibits absorption maxima at 314 and 405 nm. In the ECD spectra of (+)/(−)-**3**, the Cotton effect was observed over the entire absorption range. A simulated spectrum of **3** with the (*R*)-configuration, calculated

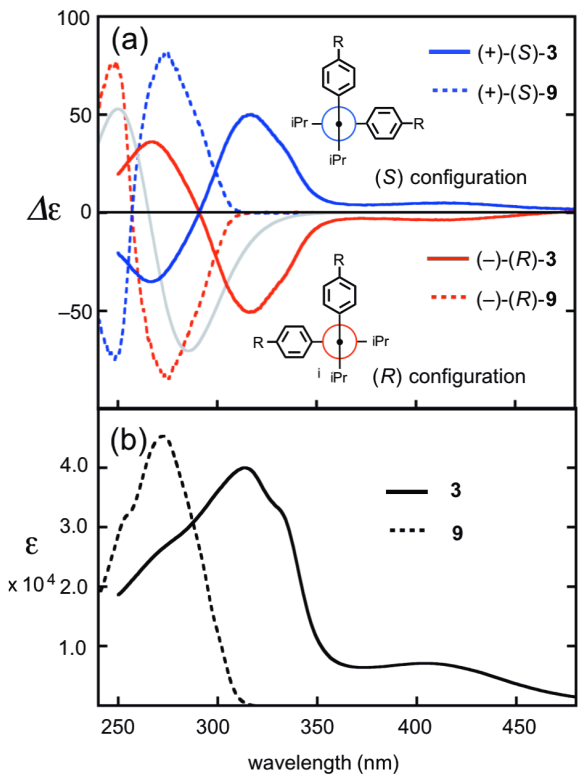

Figure 2: (a) ECD spectra of (*R*)-(−)-**3** (3.5×10^{-5} M), (*S*)-(+)-**3** (3.8×10^{-5} M), (*R*)-(−)-**9** (3.0×10^{-5} M), and (*S*)-(+)-**9** (2.9×10^{-5} M) in CH_2Cl_2 together with the simulated ECD spectra of **3** and **9** in (*R*)-configuration. (b) UV spectra of **3** (3.5×10^{-5} M) and **9** (3.8×10^{-5} M) in CH_2Cl_2.

by TD-DFT (B3LYP/6-31G(d,p)), has moderate resemblance to the spectrum obtained from (−)-**3**. This result is also consistent with the hypothesis from the chiral exciton coupling method. To solidify the absolute configuration, the synthesis of (*R*)-**3** from (*R*)-**9** was carried out separately, and the ECD spectrum of the product from (*R*)-**3** was in complete accord with that of (−)-**9**. Therefore, the absolute configuration of (+)-**3** and (−)-**3** should be (+)-(*S*)-**3** and (−)-(*R*)-**3**, respectively. In the spectra, the intensive Cotton effect was observed at 270 and 316 nm as a bisignate couple, together with broad shoulder tails to ca. 500 nm. The Cotton effect associated with the HOMO–LUMO transition was relatively weak, presumably due to the long-range coupling between two TTF units in the chiral situation. Although allenes **1** and **2**, reported previously, underwent quick photoracemization, the present allenes, **3** and **9**, exhibit photochemical stability without racemization in common organic solvents. It clearly suggests that the insertion of the phenylene units effectively prevents racemization.

To examine the potential of the 1,3-diphenylallene frameworks as a stable chiral resource, a chiral alternate copolymer consisting of TTF and chiral diphenylallene (PTDPA) was

prepared, and its chiroptical properties were investigated. Previously, a racemic conjugated polymer in the literature was prepared by a Suzuki–Miyaura or Yamamoto coupling reaction from (*rac*)-**8** [17]. In contrast, to the best of our knowledge, there is no example of a chiral polymer based on the 1,3-diphenylallene frameworks that can be a unit of copolymer with various types of aryl groups. At this point, we have chosen the direct arylation of TTF in the presence of a palladium catalyst as a key reaction for the chiral polymer synthesis (Scheme 2) [22]. Thus, the chiral allenes, (*R*)-**9** or (*S*)-**9,** react with an active palladium species, prepared in situ from $Pd(OAc)_2$ and $P(t\text{-}Bu)_3{\cdot}HBF_4$ salt in the presence of $CsCO_3$, to give the chiral copolymer of (*R*)-PTDPA and (*S*)-PTDPA, respectively, after purification by column chromatography on polystyrene Biobeads. By using gel permeation chromatography (GPC), the number-average molecular weights (M_n) of the collected PTDPA were in the range of 2800–5600 g mol^{-1} with polydispersity index (PDI) values between 1.01–1.54. These polymers solubilized well in common organic solvents, and they were characterized by their NMR spectra.

Figure 3 depicts normalized UV–vis absorption and ECD spectra of (*R*)-PTDPA and (*S*)-PTDPA, together with (*R*)-**3** and (*S*)-**3**. The polymer exhibited absorption maxima at 310 nm and shoulder absorption at ca. 415 nm, extending up to 600 nm. The shape of the spectrum is quite similar to that of the monomer **3**. The ECD spectra of both enantiomeric polymers exhibited the mirror image. There are two intensive Cotton effects at 318 nm (λ_{first}) and 254 nm (λ_{second}), together with a weak ellipticity in the range of ca. 360–450 nm. The shape of the trend line of PTDPA is similar to that of **3** with the same absolute configuration at the allenic moiety except for the small blue shift of the λ_{second} value of PTDPA (254 nm). Consequently, the chiral situation of the chromophores is preserved in the polymeric structure. However, the Cotton effect associated with the TTF moieties was observed as a relatively weak band, and hence there is not any amplification owing to a higher order structure in the polymer. Moreover, the ECD intensities of both enantiomers did not change under ambient light, at least over several days. Therefore, 1,3-diphenylallene is a reliable chiral source for a chiral polymer having electron-donating units.

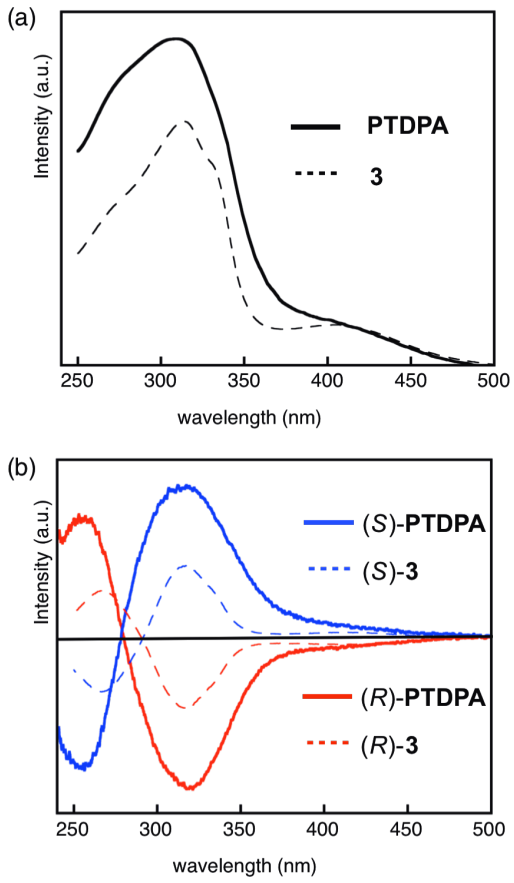

Figure 3: (a) UV–vis absorption spectra of **3** and PTDTA in CH_2Cl_2. (b) Normalized ECD spectra of (*R*)-PTDPA, (*S*)-PTDPA, (*R*)-**3**, and (*S*)-**3** in CH_2Cl_2.

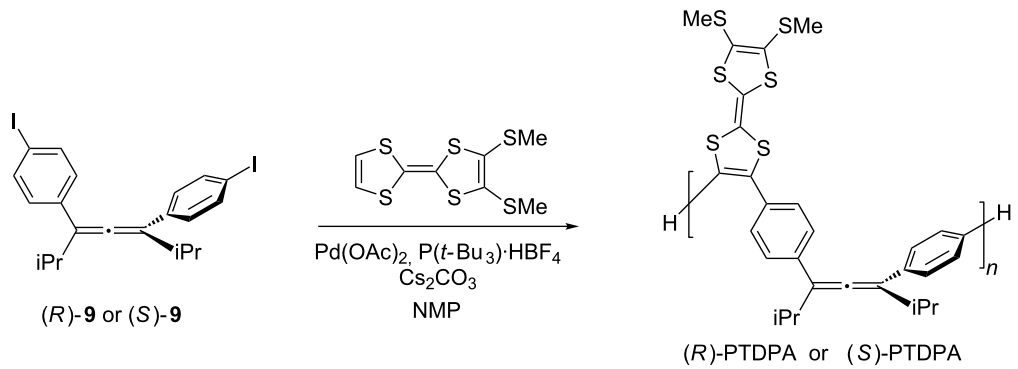

Scheme 2: Synthesis of chiral (*R*)-PTDPA and (*S*)-PTDPA.

The electrochemical properties of **3** and PTDPA were investigated by cyclic voltammetry (CV) analyses (Figure 4 and Table 1). In CVs, there are two sets of reversible redox waves in the conventional potential range. Compound **3** exhibits two two-electron transfer waves at $E^1_{1/2}$ = −0.01 V and $E^2_{1/2}$ = 0.31 V, whereas PTDPA exhibits in a similar manner at $E^1_{1/2}$ = 0.03 V and $E^2_{1/2}$ = 0.30 V. These results suggest that the TTF units in both compounds are oxidized independently to form TTF/TTF$^{\bullet+}$ and, subsequently, TTF$^{\bullet+}$/TTF^{2+}. A small positive shift of $E^1_{1/2}$ in PTDPA is presumably due to the substituent effects of the two phenylene groups in the TTF unit.

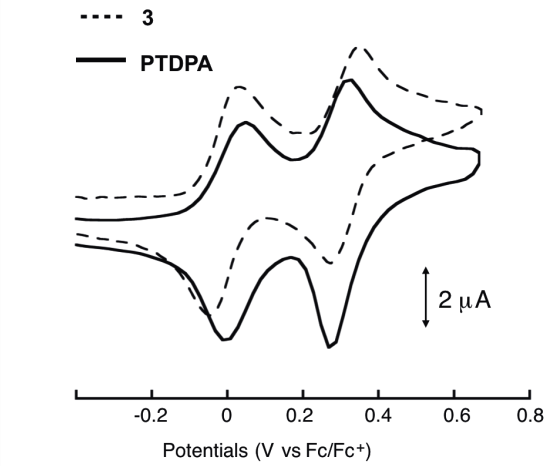

Figure 4: CV of **3** (7.8×10^{-4} M) and PTDPA in PhCN.

Table 1: Redox potentials of **3** and PTDPA.[a]

Compound	$E^1_{1/2}$	$E^2_{1/2}$
3	−0.01	0.31
PTDPA	0.03	0.30

[a]In PhCN containing 0.1 M n-Bu_4ClO_4 at 25 °C. Potentials were measured against an Ag/Ag$^+$ electrode and adjusted to the Fc/Fc$^+$ potential under identical conditions.

To investigate the electronic structures of **3** in various redox states, cationic species of **3**$^{2+}$ and **3**$^{4+}$ were prepared by their reaction with an adequate amount of $Fe(ClO_4)_3$, as the oxidant, in a MeCN/CH_2Cl_2 (v/v = 1:4) solution (Figure 5a). During the sequential addition of between 0 to 2 equivalents of the oxidant, no isosbestic point was seen other than that of **3**/**3**$^{2+}$. Therefore, **3**$^{2+}$ was formed first other than **3**$^{\bullet+}$, suggesting that there is few intramolecular interactions between two TTF units through the central 1,3-diphenylallene moiety. The obtained spectrum of **3**$^{2+}$ is quite similar to those of 4,5-bis(methylthio)tetrathiafulvalenylbenzene radical cation **10**$^{\bullet+}$, which was reported previously [7] (Table 2). In the spectrum of **3**$^{2+}$, the absorption maximum at 810 nm is assigned to an electronic transition to

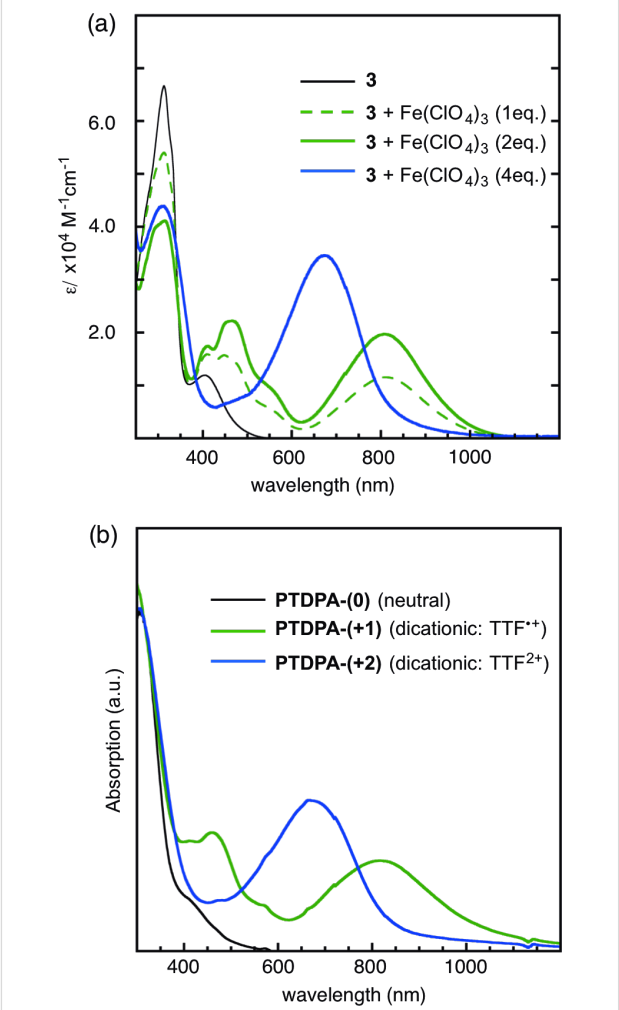

Figure 5: Electronic spectra of (a) **3** and its cationic species, and (b) PTDPA and its cationic states of PTDPA-(+1) and PTDPA-(+2).

the SOMO in the TTF$^{\bullet+}$ moieties. The value was slightly red-shifted compared with that of **10**$^{\bullet+}$ (775 nm). This small bathochromic shift can be ascribed to the conjugation to the central allene moiety. As for the spectrum of **3**$^{4+}$, the absorption maximum at 667 nm, assigned to the HOMO–LUMO transition in the TTF^{2+} moieties, was also red-shifted compared with the corresponding absorption maximum (637 nm) of **10**$^{2+}$.

Similarly, cationic species of PTDPA were also produced by the sequential addition of $Fe(ClO_4)_3$ (Figure 5b). During the oxidation, three phases of PTDPA-(0), PTDPA-(+1), and PTDPA-(+2), corresponding to the oxidation stages involving TTF, TTF$^{\bullet+}$, and TTF^{2+}, respectively, were observed during the oxidation. The spectrum of the intermediate phase of PTDPA-(+1) having absorption maxima at 459 and 816 nm are almost coincident with that of **3**$^{2+}$ (Table 2). With excess addition of the oxidant, the third phase of PTDPA-(+2) appeared, and the spectrum was almost identical to **3**$^{4+}$. The spectral resemblance

Table 2: Absorption maxima of **3**, **10** and PTDPA.[a]

Compound	λ_{max}
3	313 (66600), 405 (11900)
$\mathbf{3}^{2+}$	313 (41100), 412 (17500), 466 (22300), 810 (19700)
$\mathbf{3}^{4+}$	313 (43900), 667 (34600)
10[b]	332 (14800), 393 (3900)
$\mathbf{10}^{\bullet+}$ [b]	256 (18300), 449 (11200), 775 (8100)
$\mathbf{10}^{2+}$ [b]	259 (21500), 646 (17900)
PTDPA-(0)	309, 410
PTDPA-(+1)	459, 816
PTDPA-(+2)	667

[a]Conditions: in CH_2Cl_2-MeCN (v/v = 4:1) solution at 25 °C. The molecular structure of **10** is depicted as follow:

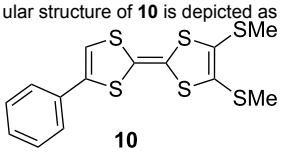

10

[b]Data from [7].

implies that the influence of the central 1,3-diphenylallene on the electronic structure of the TTF units in PTDPA is quite small.

Finally, the ECD spectra of these cation species of **3** and PTDPA were measured (Supporting Information File 1, Figure S15). Contrary to the absorption spectra, there is no distinctive ellipticity based on the cationic species of TTF in any cationic species derived from **3** or PTDPA. Only small changes of λ_{first} and λ_{second} peaks, mainly associated with the 1,3-diphenylallene framework, were observed during the oxidation reactions. In the present chiral system, the chiroptical effects between two TTF units are small due to the long-range exciton coupling, and hence the Cotton effect derived from the electronic transition of the TTF moiety was not clearly seen. However, both chiral compounds of **3** and PTDPA did not undergo the racemization in daylight. Therefore, the chirality was also preserved in the cationic species.

Conclusion

In this paper, we have shown the synthesis and chiroptical properties of a novel chiral TTF dimer linked by a 1,3-diphenylallene framework for the purpose of the development of a stable chiral source without racemization under ambient conditions. The title compound was synthesized from 1,3-bis(4-iodophenyl)-1,3-diisopropylallene (**9**) and organozinc species derived from 4,5-bis(methylthio)TTF. Optical resolution of the enantiomer **3** and its precursor **9** was achieved by a recyclable HPLC on a chiral stationary phase. The ECD spectra were measured, and the obtained spectra allowed for the validation of the absolute configurations based on the TD-DFT method. Although the observed Cotton effect associated with TTF moieties is relatively weak, each chiral allene is stable towards the racemization under ambient light. A chiral copolymer based on TTF and a chiral 1,3-diphenylallene as the main chain scaffold (PTDPA) was also prepared using a direct C–H activation of the TTF framework. The resultant chiral polymers exhibited the characteristic Cotton effect associated with the central chiral 1,3-diphenylallene moieties. The polymer also did not undergo racemization under daylight. Moreover, electrochemical properties were also investigated by the CV method. Cationic species were prepared by the addition of $Fe(ClO_4)_3$ as the oxidant, and their UV and ECD spectra were also recorded. Other molecular designs, including a copolymer based on the 1,3-diphenylallene units, are currently underway to create valuable chiral molecules.

Experimental

4,5-Bis(methylthio)TTF was prepared according to literature procedures [19]. Dehydrated THF and Et_2O were purchased from Wako Pure Chemical Industries, LTd. (Super Dehydrated, Stabilizer Free, H_2O < 10ppm). Anhydrous $ZnCl_2$ (99%) was purchased from Wako Pure Chemical Industries, and dried in vacuo for 4 h with heating over 220 °C. Other commercially available materials were used as received. Column chromatography was carried out using Kanto chemical silica gel 60N, 60–210 μm meshes. ^1H and ^{13}C NMR spectra were recorded on Bruker AVANCE-III-400 (400 MHz for ^1H, 100 MHz for ^{13}C) or on Bruker AVANCE-III-600 (600 MHz for ^1H, 150 MHz for ^{13}C). Spectra are reported (in δ) referenced to internal Me_4Si. Mass spectra were recorded on Thermo Scientific, Exactive Plus Orbitrap Mass Spectrometer with atmospheric pressure chemical ionization (APCI) probe. IR spectra were recorded on JASCO FT/IR-610 spectrometer. Melting points were determined with Yanaco melting point apparatus. Elemental analyses were performed on Perkin Elmer PE 2400-II CHNA/O analyzer. Optical resolution was carried out with recyclable preparative HPLC (JAI Model LC-9204) equipped with Daicel CHIRALPAK-IA3 column (20 Ø × 250 mm). The optical rotations were measured with JASCO P-1300 spectropolarimeter in 1 dm quartz cell at 24 °C. Electronic circular dichroism (ECD) spectra were recorded on JASCO J-725 spectrodichrometer. The spectra were combined after the baseline correction of each measurement. cyclic voltammetry (CV) measurements were performed on Hokuto Denko HZ-5000 electrochemical analyzer. GPC analysis for the polymer products was carried out at 40 °C on a Shodex GPC apparatus equipped with two SB-806M HQ GPC columns (Showa Denko K. K.) and a UV detector. DMF was used as the eluent at a flow rate of 0.5 mL/min. Polystyrene standards with a narrow distribution of molecular weight (M_w: 580–377, 400) were used for molecular weight calibration.

Synthesis of 8: To a solid mixture of dried CuI (5.7 g, 30 mmol) and LiBr (2.6 g, 30 mmol) was added dropwise acetyl ester **7** (6.7 g, 15 mmol) in THF (170 mL) during 15 min at rt, and the mixture was cooled to −78 °C. Then, freshly prepared iPrMgCl (30 mmol) in THF (15 mL) was added dropwise into the mixture at −78 °C. After stirring for 1 h at −78 °C, the mixture was further stirred for 14 h at rt. The resultant mixture was poured into saturated aqueous NH_4Cl solution, and the products were extracted by Et_2O. The organic phase was washed with brine and dried over $MgSO_4$. After evaporation, the crude products were purified on silica gel column chromatography with the elution of hexane. Removal of the solvent afforded **8** as colourless oil (5.8 g, 90%): MS (GC) *m/z* = 432 (50%, M^+: $C_{21}H_{22}{}^{79}Br_2$), 434 (100%, M^+: $C_{21}H_{22}{}^{79}Br^{81}Br$), and 436 (50%, M^+: $C_{21}H_{22}{}^{81}Br_2$); ^{1}H NMR (400 MHz, $CDCl_3$) δ 7.42 (d, *J* = 8.6 Hz, 2H), 7.27 (d, *J* = 8.6 Hz, 2H), 2.91 (septet, *J* = 6.8 Hz), 1.17 (d, *J* = 6.8 Hz, 3H), 1.15 (d, *J* = 6.8 Hz, 3H); ^{13}C NMR (100 MHz, $CDCl_3$) δ 203.0, 135.6, 131.7, 128.0, 120.7, 117.1, 28.8, 22.7, 22.4; IR (neat): 2961, 2926, 2870, 1919, 1489, 1464, 1074, 1009, 825 cm^{-1}; HRMS (APCI-orbitrap) calcd for $C_{21}H_{22}Br_2$ (M^+) 432.0088; found, 432.0089.

Synthesis of 9: To a solution of 1,3-bis(4-bromophenyl)allene derivative **8** (1.0 g, 2.3 mmol) in Et_2O (50 mL) was added dropwise *t*-C_4H_9Li (6.0 mL, 9.8 mmol) at −78 °C under Ar atmosphere. After stirring for 30 min at the same temperature, $C_6F_{13}I$ (1.3 mL, 5.84 mmol) was added dropwise by syringe. The resultant mixture was stirred for 3 h at −78 °C, and then saturated aqueous NH_4Cl solution was poured into the solution at −78 °C. After allowing to warming up to rt, the mixture was extracted by Et_2O. The organic phase was washed with brine and dried over Na_2SO_4. After removal of the solvent, the crude product was purified by column chromatography on silica gel with hexane elution to give colourless oil of **9** (1.0 g, 92%): MS (APCI) *m/z* = 528 (M^+); ^{1}H NMR (400 MHz, $CDCl_3$) δ 7.62 (d, *J* = 8.6 Hz, 2H), 7.14 (d, *J* = 8.6 Hz, 2H), 2.94 (septet, *J* = 6.7 Hz, 1H), 1.17 (d, *J* = 6.8 Hz, 2H), 1.15 (d, *J* = 6.8 Hz, 2H); ^{13}C NMR (100 MHz, $CDCl_3$) δ 202.9, 137.6, 136.0, 128.1, 117.0, 92.2, 28.6, 22.7, 22.4; IR (neat): 2961, 2926, 2869, 1918, 1483, 1463, 1383, 1216 cm^{-1}; HRMS (APCI-orbitrap) calcd for $C_{21}H_{22}I_2$ (M^+) 527.98108; found, 527.98108.

Synthesis of 3: To a solution of 4,5-bis(methylthio)TTF (640 mg, 2.2 mmol) [20] in THF (30 mL) was added dropwise *n*C_4H_9Li (1.3 mL, 2.2 mmol) at –78 °C under Ar atmosphere. After the mixture was stirred for 90 min, a suspension of $ZnCl_2$ (377 mg, 2.8 mmol) in THF (3 mL) was added at −65 °C. The solution was further stirred for 30 min, then 1,3-bis(4-iodophenyl)allene derivative **9** (458 mg, 0.87 mmol) in THF (2.5 mL) and $Pd(PPh_3)_4$ (100 mg, 0.087 mmol) were added into the mixture at –20 °C. The resultant mixture was stirred for 14 h at rt, and then poured into saturated aqueous NH_4Cl solution. The product was extracted by Et_2O, and the organic phase was washed with saturated brine and dried over $MgSO_4$. The crude product was purified by column chromatography on silica gel with CH_2Cl_2/hexane (v/v = 1:4). Recrystallization from CH_2Cl_2/MeOH (v/v = 1:1) solution gave **3** (664 mg, 89%): orange powder; mp: 77.8–79.2 °C; MS (APCI) *m/z* = 865 (M^+ + H); ^{1}H NMR (400 MHz, $CDCl_3$) δ 7.40 (d, *J* = 8.6 Hz, 4H), 7.34 (d, *J* = 8.6 Hz, 4H), 6.48 (s, 2H), 2.97 (sept, *J* = 6.8 Hz, 2H), 2.44 (s, 6H), 2.43 (s, 6H), 1.19 (t, *J* = 6.8 Hz, 12H); ^{13}C NMR (100 MHz, $CDCl_3$) δ 204.2, 136.9, 136.0, 130.8, 127.8, 127.7, 126.7, 126.6, 117.4, 114.8, 112.8, 107.3, 28.7, 22.8, 22.5, 19.4; IR (KBr): 2958, 2918, 2866, 1914, 1568, 1499, 1418, 835, 759 cm^{-1}; anal. calcd for $C_{37}H_{36}S_{12}$: C, 51.35; H, 4.19; found: C, 51.36; H, 4.25.

Synthesis of (*R*)/(*S*)-PTDPA: A mixture of $Pd(OAc)_2$ (8.9 mg, 40 μmol), P(*t*-Bu)$_3$·HBF_4 (35 mg, 120 mmol), Cs_2CO_3 (290 mg, 2.8 mmol) in degassed NMP (1 mL) was stirred for 20 min at 100 °C under Ar atmosphere. Then, (*R*)-**3** (80 mg, 151 μmol) and 4,5-bis(methylthio)TTF (67 mg, 226 μmol) were added to the solution, and the reaction mixture was stirred for 3 days at 100 °C. After cooling to rt, the solvent was removed under reduced pressure, and then the residue and *N*,*N*-diethylphenylazothioformamide (100 mg, 40 μmol), as a metal scavenger, were dispersed in THF (2 mL). The resultant suspension was stirred for 30 min at rt, then further for 1 h at 100 °C. After cooling at rt, the solution was poured into CH_3OH (150 mL). The resulted precipitates were collected by filtration, washing with CH_3OH. The residue on the filter was collected, and then purified by column chromatography on non-polar polystyrene gel (Bio-beads S-X3 Support) with the elution of toluene. The crude product was further purified reprecipitation with toluene-hexane, yielding copolymer of (*R*)-PTDPA as an orange-brown powder (24 mg, 26%). The number-average molecular weight (M_n) was estimated to be 5.6×10^3, and its distribution (M_n/M_w) was estimated to be 1.01: orange-brown powder; ^{1}H NMR (400 MHz, $CDCl_3$) δ 7.13–7.36, 6.46, 2.89, 2.40, 1.14. In similar manner, (*S*)-PTDPA was obtained from the reaction of (*S*)-**3** in 31% yield. Its M_n value was estimated to be 2.8×10^3 and its distribution was estimated to be 1.54.

Supporting Information

Supporting Information File 1

Experimental procedures, characterization data, copies of ^{1}H and ^{13}C NMR charts, recyclable chiral HPLC chart and DFT calculation summary.
[http://www.beilstein-journals.org/bjoc/content/supplementary/1860-5397-11-109-S1.pdf]

Acknowledgements

The authors gratefully acknowledge partial financial aid from Kitasato University Research Grant for young researchers. We also thank to Prof. Dr. Takahiro Tsuchiya for helpful discussion. The calculations were performed at the Research Centre for Computational Science, Okazaki, Japan.

References

1. Mammana, A.; Carroll, G. T.; Feringa, B. L. Circular dichroism of dynamic systems: switching molecular chirality and supramolecular chirality. In *Comprehensive Chiroptical Spectroscopy;* Berova, N.; Polavarapu, P. L.; Nakanishi, K.; Eoody, R. S., Eds.; Wiley: Hoboken, NJ, U.S.A., 2012; Vol. 2, pp 289–316.
2. Feringa, B. L.; van Delden, R. A.; Koumura, N.; Geertsema, E. M. *Chem. Rev.* **2000,** *100,* 1789–1816. doi:10.1021/cr9900228
3. Canary, J. W. *Chem. Soc. Rev.* **2009,** *38,* 747–756. doi:10.1039/b800412a
4. Nishida, J.-i.; Suzuki, T.; Ohkita, M.; Tsuji, T. *Angew. Chem., Int. Ed.* **2001,** *40,* 3251–3254. doi:10.1002/1521-3773(20010903)40:17<3251::AID-ANIE3251>3.0.CO;2-P
5. Deng, J.; Song, N.; Zhou, Q.; Su, Z. *Org. Lett.* **2007,** *9,* 5393–5396. doi:10.1021/ol701822u
6. Pospíšil, L.; Bednárová, L.; Štěpánek, P.; Slavíček, P.; Vávra, J.; Hromadová, M.; Dlouhá, H.; Tarábek, J.; Teplý, F. *J. Am. Chem. Soc.* **2014,** *136,* 10826–10829. doi:10.1021/ja500220j
7. Kobayakawa, K.; Hasegawa, M.; Sasaki, H.; Endo, J.; Matsuzawa, H.; Sako, K.; Yoshida, J.; Mazaki, Y. *Chem. – Asian J.* **2014,** *9,* 2751–2754. doi:10.1002/asia.201402667
8. Diederich, F.; Rivera-Fuentes, P. *Angew. Chem., Int. Ed.* **2012,** *51,* 2818–2828. doi:10.1002/anie.201108001
9. Krause, N.; Hashimi, A. S. K., Eds. *Modern Allene Chemistry;* Wiley-VCH: Weinheim, Germany, 2004.
10. Hasegawa, M.; Sone, Y.; Iwata, S.; Matsuzawa, H.; Mazaki, Y. *Org. Lett.* **2011,** *13,* 4688–4691. doi:10.1021/ol201857f
11. Roth, W. R.; Ruf, G.; Ford, P. W. *Chem. Ber.* **1974,** *107,* 48–52. doi:10.1002/cber.19741070106
12. Alonso-Gómez, J. L.; Rivera-Fuentes, P.; Seiler, P.; Diederich, F. *Chem. – Eur. J.* **2008,** *14,* 10564–10568. doi:10.1002/chem.200801456
13. Odermatt, S.; Alonso-Gómez, L.; Seiler, P.; Cid, M. M.; Diederich, F. *Angew. Chem., Int. Ed.* **2005,** *44,* 5074–5078. doi:10.1002/anie.200501621
14. Hasegawa, M.; Iwata, S.; Sone, Y.; Endo, J.; Matsuzawa, H.; Mazaki, Y. *Molecules* **2014,** *19,* 2829–2841. doi:10.3390/molecules19032829
15. Thorand, S.; Vögtle, F.; Krause, N. *Angew. Chem., Int. Ed.* **1999,** *38,* 3721–3723. doi:10.1002/(SICI)1521-3773(19991216)38:24<3721::AID-ANIE3721>3.0.CO;2-9
16. Clay, M. D.; Fallis, A. G. *Angew. Chem., Int. Ed.* **2005,** *44,* 4039–4042. doi:10.1002/anie.200500484
17. Kijima, M.; Hiroki, K.; Shirakawa, H. *Macromol. Rapid Commun.* **2002,** *23,* 901–904. doi:10.1002/1521-3927(20021001)23:15<901::AID-MARC901>3.0.CO;2-3
18. Pu, X.; Qi, X.; Ready, J. M. *J. Am. Chem. Soc.* **2009,** *131,* 10364–10365. doi:10.1021/ja9041127
19. Hasegawa, M.; Daigoku, K.; Hashimoto, K.; Nishikawa, H.; Iyoda, M. *Bull. Chem. Soc. Jpn.* **2012,** *85,* 51–60. doi:10.1246/bcsj.20110224
20. Berova, N.; Nakanishi, K. Exciton Chirality Method: Principles and Applications. In *Circular dichroism: Principles and Applications;* Nakanishi, K.; Berova, N.; Eoody, R. W., Eds.; Wiley: Hoboken, NJ, U.S.A., 1994; pp 361–398.
21. *Gaussian 09,* Revision D.01; Gaussian, Inc.: Wallingford, CT, U.S.A., 2010.
22. Mitamura, Y.; Yorimitsu, H.; Oshima, K.; Osuka, A. *Chem. Sci.* **2011,** *2,* 2017–2021. doi:10.1039/c1sc00372k

BEILSTEIN JOURNAL OF ORGANIC CHEMISTRY

Glycoluril–tetrathiafulvalene molecular clips: on the influence of electronic and spatial properties for binding neutral accepting guests

Yoann Cotelle, Marie Hardouin-Lerouge, Stéphanie Legoupy, Olivier Alévêque, Eric Levillain* and Piétrick Hudhomme*

Full Research Paper

Open Access

Address:
Université d'Angers, Laboratoire MOLTECH-Anjou, CNRS UMR 6200, 2 Boulevard Lavoisier, F-49045 Angers, France

Email:
Eric Levillain* - eric.levillain@univ-angers.fr;
Piétrick Hudhomme* - pietrick.hudhomme@univ-angers.fr

* Corresponding author

Keywords:
donor–acceptor interactions; glycoluril; molecular clips; supramolecular chemistry; tetrathiafulvalene

Beilstein J. Org. Chem. **2015,** *11,* 1023–1036.
doi:10.3762/bjoc.11.115

Received: 13 March 2015
Accepted: 28 May 2015
Published: 17 June 2015

This article is part of the Thematic Series "Tetrathiafulvalene chemistry".

Guest Editor: P. J. Skabara

Abstract

Glycoluril-based molecular clips incorporating tetrathiafulvalene (TTF) sidewalls have been synthesized through different strategies with the aim of investigating the effect of electrochemical and spatial properties for binding neutral accepting guests. We have in particular focused our study on the spacer extension in order to tune the intramolecular TTF···TTF distance within the clip and, consequently, the redox behavior of the receptor. Carried out at different concentrations in solution, electrochemical and spectroelectrochemical experiments provide evidence of mixed-valence and/or π-dimer intermolecular interactions between TTF units from two closed clips. The stepwise oxidation of each molecular clip involves an electrochemical mechanism with three one-electron processes and two charge-coupled chemical reactions, a scheme which is supported by electrochemical simulations. The fine-tunable π-donating ability of the TTF units and the cavity size allow to control binding interaction towards a strong electron acceptor such as tetrafluorotetracyanoquinodimethane (F_4-TCNQ) or a weaker electron acceptor such as 1,3-dinitrobenzene (*m*-DNB).

Introduction

Thanks to its remarkable redox properties and strong π-donating character demonstrated with the pioneering work of F. Wudl in the early 1970s [1], tetrathiafulvalene (TTF) has become one of the most popular electroactive frameworks used in materials science [2-5]. In addition to the well-known access to molecular conductors [6,7] and TTF-acceptor assemblies [8,9], new concepts have been explored in the field of supramolecular chemistry using the TTF unit as a powerful electroactive

building block [10]. Exploiting its peculiar electronic (two successive reversible oxidation steps giving rise to three stable redox states) characteristics, more and more sophisticated TTF-based supramolecular systems have been designed, being able to operate as machines, chemical sensors, redox-switchable ligands, molecular shuttles, molecular switches and logic gates [11]. Considering that molecular receptors prone to specifically recognize neutral molecules through donor–accceptor interactions are of particular interest [12], the unique π-donating ability and the planar geometry of the TTF building-block are suited to the construction of such receptors. Nevertheless, the incorporation of TTF as a π-donating element in molecular clips or tweezers for recognition of neutral electron acceptor guests is still relatively unexplored [13].

Molecular clips and tweezers can be defined as receptors presenting an open cavity composed of two interaction sites which are separated by a spacer [13-15]. Ideally, these systems are designed with the aim of sandwiching a molecular guest with a high degree of selectivity and control of the interactions between the guest and the sidewalls. While the nature and the flexibility of the spacer between the two sidewalls play a critical role in the recognition process, we were interested in rigidifying the molecular clips in order to favor the "lock and key" model [15]. This rigid structure offers the possibility to orient the interaction sites in a defined manner allowing an increase of the binding strength with the guest. In the last two decades, glycoluril-based molecular clips have shown that they were capable of acting as excellent receptors by exploiting the distance between the two aromatic sidewalls which is usually close to 7 Å. Since then, a large number of host systems based on this principle have been synthesized in order to use them for recognition of aromatic guest molecules through π–π interactions [16,17].

We recently described various glycoluril-based molecular clips **1**–**4** [18,19] (Figure 1) for which the structure varies by: i) the nature of connection between the glycoluril spacer and the TTF sidewalls, ii) the nature of the peripheral substituents on both TTF pincers. In this full research paper we propose to study how these structural parameters influence the electron donating ability of TTF pincers and the size of the cavity and how the control over the inter-TTFs distance within the molecular clip impacts the ability for sandwiching neutral acceptor guests. Those studies are supported by electrochemical analyses (including simulation), time-resolved spectroelectrochemical experiments and UV–visible titrations.

Results and Discussion

Synthesis

We have designed molecular clips **1**–**4** through three different synthetic strategies starting from diphenylglycoluril **5** (Scheme 1). The key building-block **5** is available in multigram scale by reaction of benzil with urea [20]. The first approach leading to molecular clips **1** and **2** is based on a straightforward double nucleophilic substitution leading to a seven-membered ring using 4,5-bis(bromomethyl)-2-thioxo-1,3-dithiole (**6**) [21].

In order to determine the optimized experimental procedure to carry out the urea N-alkylation of compound **5**, we took advantage from literature of previous works realized on glycoluril for such reaction using a 2,3-bis(halogenomethyl)aryl derivative.

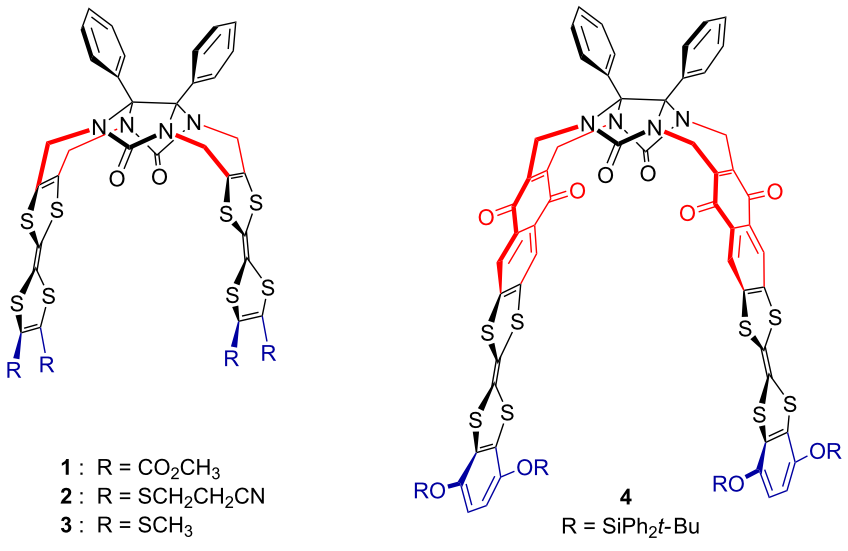

Figure 1: Structures of molecular clips **1–4**.

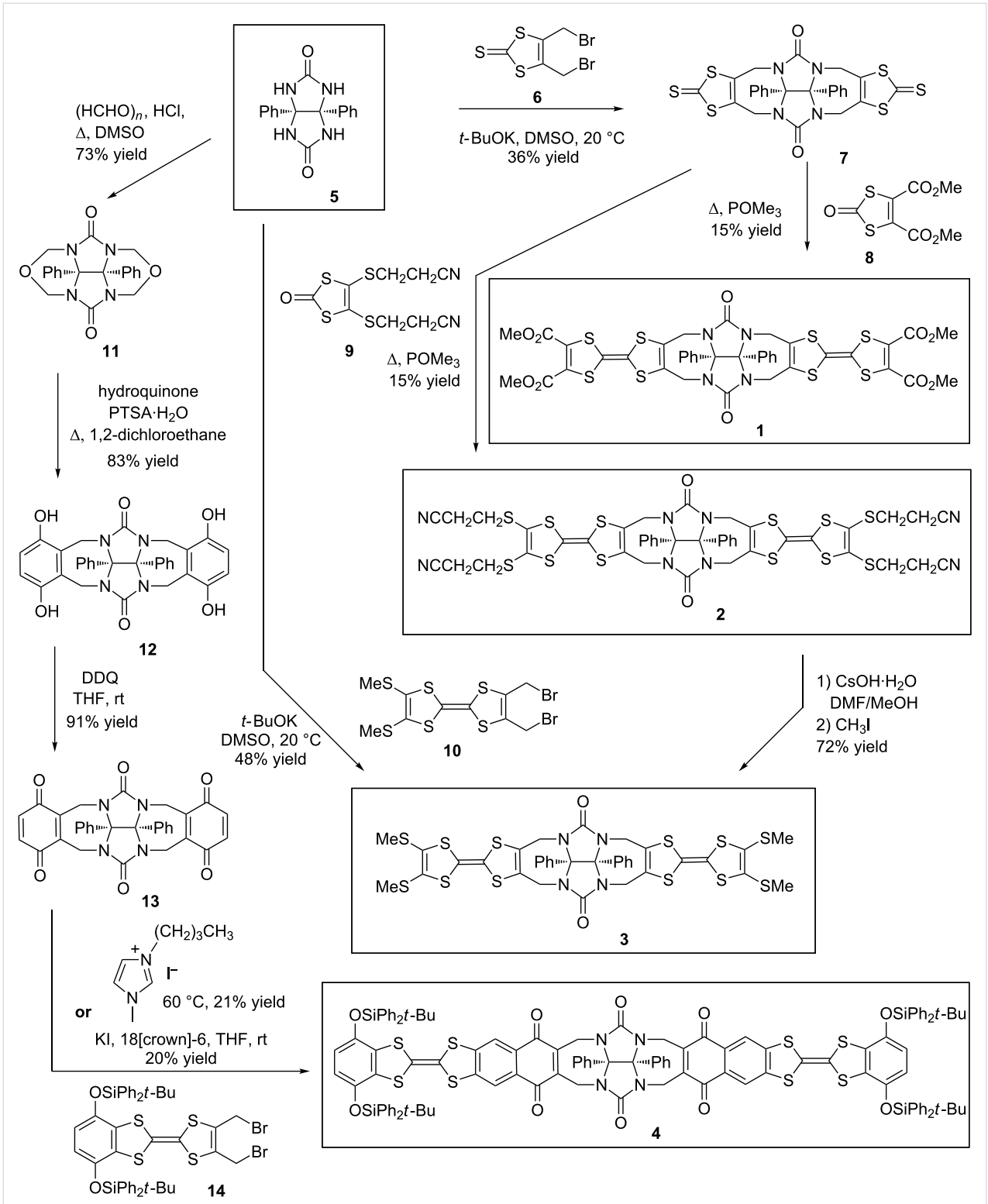

Scheme 1: Different routes developed for the synthesis of molecular clips **1–4**.

Reported procedures were using KOH [22,23], *t*-BuOK [24-26] or NaH [27] as the base with DMSO as an aprotic polar solvent. Different experimental conditions were tested for the reaction between diphenylglycoluril **5** and 4,5-bis(bromomethyl)-2-thioxo-1,3-dithiole (**6**) as the electrophilic reagent (Scheme 2) by varying parameters such as the nature of the base, the reac-

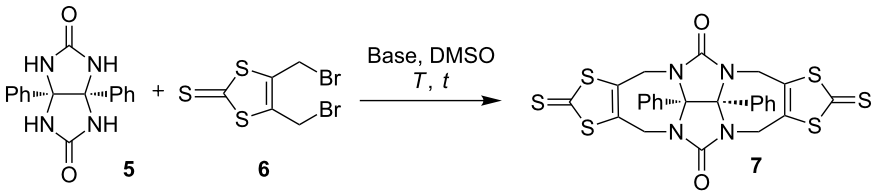

Scheme 2: Reaction between diphenylglycoluril with 4,5-bis(bromomethyl)-2-thioxo-1,3-dithiole.

tion time and the temperature (Table 1). Optimal conditions were using four equivalents of *t*-BuOK in anhydrous DMSO by keeping the temperature at 20 °C with a cryostat apparatus for 3 h. Compound **7** was isolated in 36% yield after purification by silica gel chromatography. We should note that an increase of temperature resulted in the degradation of starting material **6**.

Table 1: Optimized experimental conditions for the synthesis of compound **7**.

Base	Temperature (*T*)	Reaction time (*t*)	Yield [%]
KOH	rt	24 h	6
NaH	rt	24 h	5
KOH	rt	4 h	12
t-BuOK	rt	4 h	19
t-BuOK	Controlled 30 °C	4 h	12
t-BuOK	Controlled 20 °C	3 h	36

This first strategy to reach clips **1** and **2** was considering the trimethylphosphite-mediated cross-coupling reaction involving 2-oxo-1,3-dithiole moiety **8** [28] as an efficient route to prepare dissymmetrical TTF derivatives [29]. The polarity of compounds which were formed was sufficiently different to allow an efficient purification by silica gel chromatography affording molecular clip **1** in 15% yield. This route was successfully applied using compound **9** [30] and clip **2** was also isolated in 15% yield. Target clip **3** was finally obtained in 72% yield by deprotection of precursor **2** using $CsOH{\cdot}H_2O$ in DMF/MeOH mixture [31], followed by the tetraalkylation of tetrathiolate with iodomethane. Considering that this multi-step synthesis was affording molecular clip **3** in an overall 4% yield starting from diphenylglycoluril **5**, we took advantage of the accessibility of 2,3-bis(bromomethyl)TTF **10** [32] bearing methylsulfanyl groups to investigate a more straightforward strategy. Alternatively, the above methodology described for the preparation of compound **7** was efficiently applied to reach molecular clip **2** in 48% yield using similar experimental conditions.

Whereas the synthesis of molecular clips **1**, **2** and **3** uses the nucleophilic substitution onto diphenylglycoluril **5** as a key-step, the introduction of the naphthoquinone spacer in clip **4** required the previous transformation of compound **5** into a glycoluril-based framework possessing quinone moieties for developing a Diels–Alder cycloaddition strategy. Thus compound **12** [33] was prepared in 73% yield by treatment with an excess of hydroquinone in 1,2-dichloroethane using a Friedel–Crafts alkylation as an electrophilic aromatic substitution onto compound **11** [34]. The hydroquinone moieties were subjected to a dehydrogenation reaction using DDQ in THF to reach desired glycolurildiquinone **13** [35] in 91% yield. The Diels–Alder cycloaddition was carried out by treatment of bis-dienophile **13** with TTF derivative **14** [36], able to give rise in situ to the transient diene by reductive elimination using naked iodide [37-39] or the iodo-ionic liquid 1-butyl-3-methylimidazolium iodide [40]. After purification by column chromatography on silica gel, we noted that complete aromatization has occurred concomitantly and molecular clip **4** was isolated in around 20% yield.

Whereas all attempts at growing crystals of molecular clips **1** and **4** of sufficient quality for X-ray analysis have been unsuccessful so far, suitable single crystals were obtained by slow diffusion from a solution of clips **2** and **3** in a CH_2Cl_2/hexane mixture. Considering the central double bond of each TTF moiety, the intramolecular wall-to-wall distance was determined to be equal to 8.25 Å and 7.41 Å for clip **2** and **3**, respectively (Figure 2) [18]. Then the corresponding wall-to-wall distance between the two TTF units was determined by theoretical calculations using the semi-empirical AM1 method in the case of **4** [19]. This distance was estimated to be equal to 9.7 Å indicating that this enlargement around 2 Å was the result mainly of the spatial contribution of the additional naphthoquinone spacer in molecular clip **4**.

Electrochemical properties

The electrochemical behaviour of molecular clips **1**–**4** were determined using cyclic voltammetry experiments (Table 2).

These studies displayed a different electrochemical behavior for clips **1**, **2** and **3** in comparison to clip **4**. In the latter case, the cyclic voltammogram (CV) showed two oxidation waves at

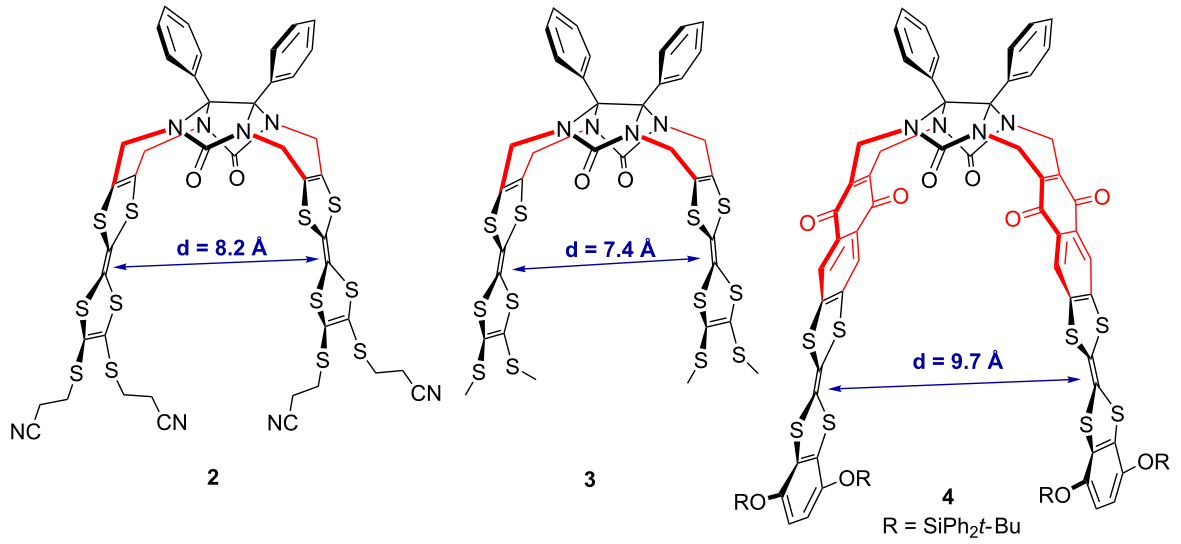

Figure 2: Intramolecular distances between TTF moieties from X-ray analysis for clips **2** and **3** and theoretical calculations for clip **4**.

Table 2: Apparent redox potentials of molecular clips **1, 2, 3** and **4** reported vs Fc^+/Fc in 0.1 M $TBAPF_6/CH_2Cl_2/CH_3CN$ 3:1 on glassy carbon electrode at 100 $mV{\cdot}s^{-1}$. Absolute errors on potentials were found to be around +/−10 mV.

Clip	$E_{app}{}^0{}_{red1}$	$E_{app}{}^0{}_{ox1}$	$E_{app}{}^0{}_{ox1'}$	$E_{app}{}^0{}_{ox2}$
1	–	+0.06	+0.21	+0.51
2	–	+0.03	+0.14	+0.45
3	–	−0.05	+0.06	+0.36
4	−1.05	+0.28		+0.65

$E_{app}{}^0{}_{ox1}$ = +0.28 V and $E_{app}{}^0{}_{ox2}$ = +0.65 V vs Fc^+/Fc corresponding to the successive generation of cation radical then dication species simultaneously on each TTF framework (Figure 3). This unique first two-electron oxidation step indicates that the two TTF units are electrochemically equivalent, thus excluding the presence of intra- or intermolecular electronic interactions between them. It should be noted that the electroactive naphthoquinone acceptor group incorporated in the spacer unit is characterized by a reduction wave ($E_{app}{}^0{}_{red1}$) at −1.05 V vs Fc^+/Fc. On the contrary, the CV of clips **1**–**3** shows a significant splitting of the first oxidation wave ($E_{app}{}^0{}_{ox1}$ and $E_{app}{}^0{}_{ox1'}$), suggesting the presence of intermolecular (between two clips) or intramolecular (within a clip) interactions between two TTF units (i.e., mixed valence and/or π-dimer) [41]. Eventually, the reversible two-electron process (i.e., 1 e^- on each $TTF^{+\cdot}$ unit) for the second oxidation step ($E_{app}{}^0{}_{ox2}$) leading to fully oxidized TTF units is in accordance with independent TTF^{2+} states subject to repulsive electrostatic interactions. Such splitting phenomenon of the first oxidation wave has been previously reported by Azov et al. for TTF-containing molecular tweezers based on a 1,2,4,5-tetramethylbenzene scaffold [42,43].

At this stage, one should keep in mind that the distance between two TTF sidewalls within clips **2** and **3** is quite important (8.2 Å and 7.4 Å, respectively). Such a distance, even though determined in the solid state, does not seem compatible to allow an intramolecular interaction to occur between two TTF units during the first oxidation step. In order to address this issue and to explore possible intermolecular (between two clips) interactions, concentration dependence electrochemical experiments were performed. Cyclic voltammograms were recorded using molecular clip **2** at different concentrations (10^{-3} M, 10^{-4} M and 5×10^{-5} M) (Figure 4).

Importantly, whereas the splitting of the first oxidation wave was perfectly observed at high concentration (10^{-3} M), we noted that the phenomenon was significantly decreased at lower concentration. First, the absence of a splitting or broadening of the first oxidation process at low concentration informed us that the two TTF units are equivalent, thus excluding intramolecular interactions. Secondly, the concentration dependence and the splitting at higher concentrations provided evidence for the existence of intermolecular interactions and the formation of mixed-valence and radical cation dimer states. These results clearly demonstrated the presence of an intermolecular mixed-valence phenomenon.

According to these first results, the following model could be proposed in agreement with the successive oxidation steps in the CV of molecular clips **1**, **2** and **3** (Scheme 3). Because the

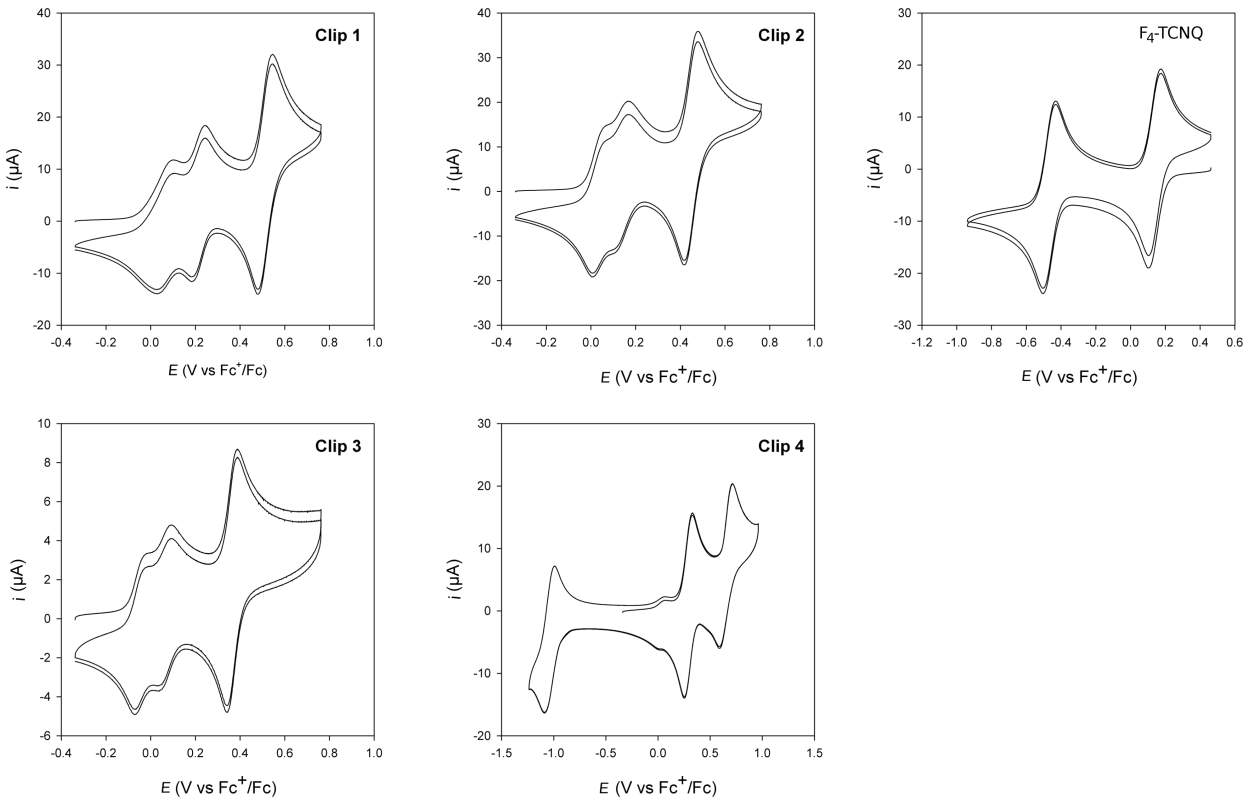

Figure 3: Cyclic voltammograms of molecular clips **1**, **2**, **3**, **4** and F_4-TCNQ at 10^{-3} M in 0.1 M $TBAPF_6/CH_2Cl_2/CH_3CN$ 3:1 on a glassy carbon electrode at 100 mV·s^{-1}.

two TTF units are equivalent, the first oxidation step of the clip involves a one-electron process on each TTF unit, leading to the clip bearing two radical cations. The concentration dependence shown on CVs suggested that this clip with two radical cations stack with and/or without self-assembly affording mixed-valence or π-dimer interactions. At higher potential, the tetra-

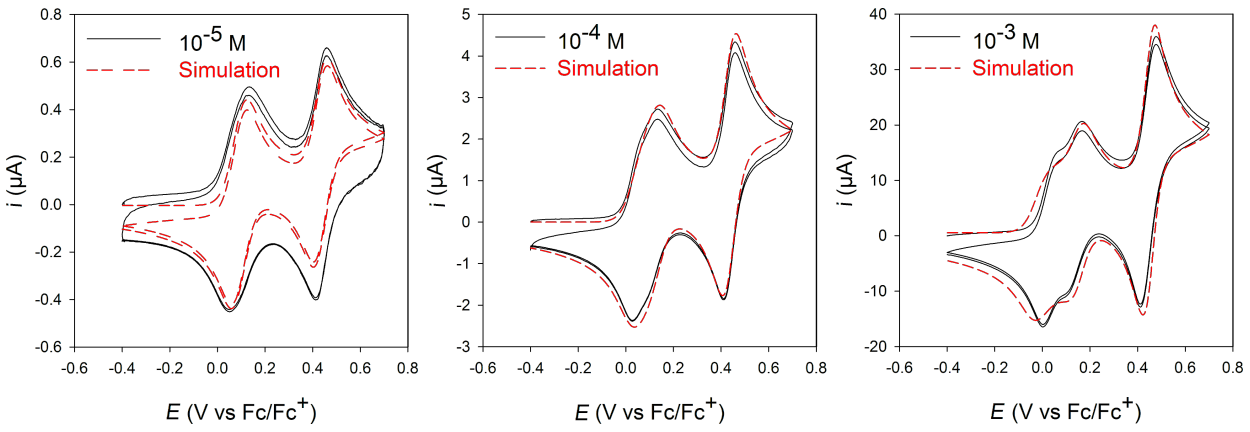

Figure 4: Cyclic voltammograms of molecular clip **2** at different concentrations (left: 10^{-5} M; middle: 10^{-4} M; right: 10^{-3} M) in 0.1 M $TBAPF_6/CH_2Cl_2/CH_3CN$ 3:1 on a glassy carbon electrode at 100 mV·s^{-1}. Red dashed line: electrochemical simulation performed from experiments (E_1 = 0.090 V, E_2 = 0.165 V, E_3 = 0.435 mV, K_{MV} = 11400 M^{-1}, K_{DIM} = 680 M^{-1}, k_f = 1 × 10^9 M^{-1}·s^{-1} for all the forward reactions, α = 0.5 and k_s = 0.01 cm·s^{-1} for all the charge transfers).

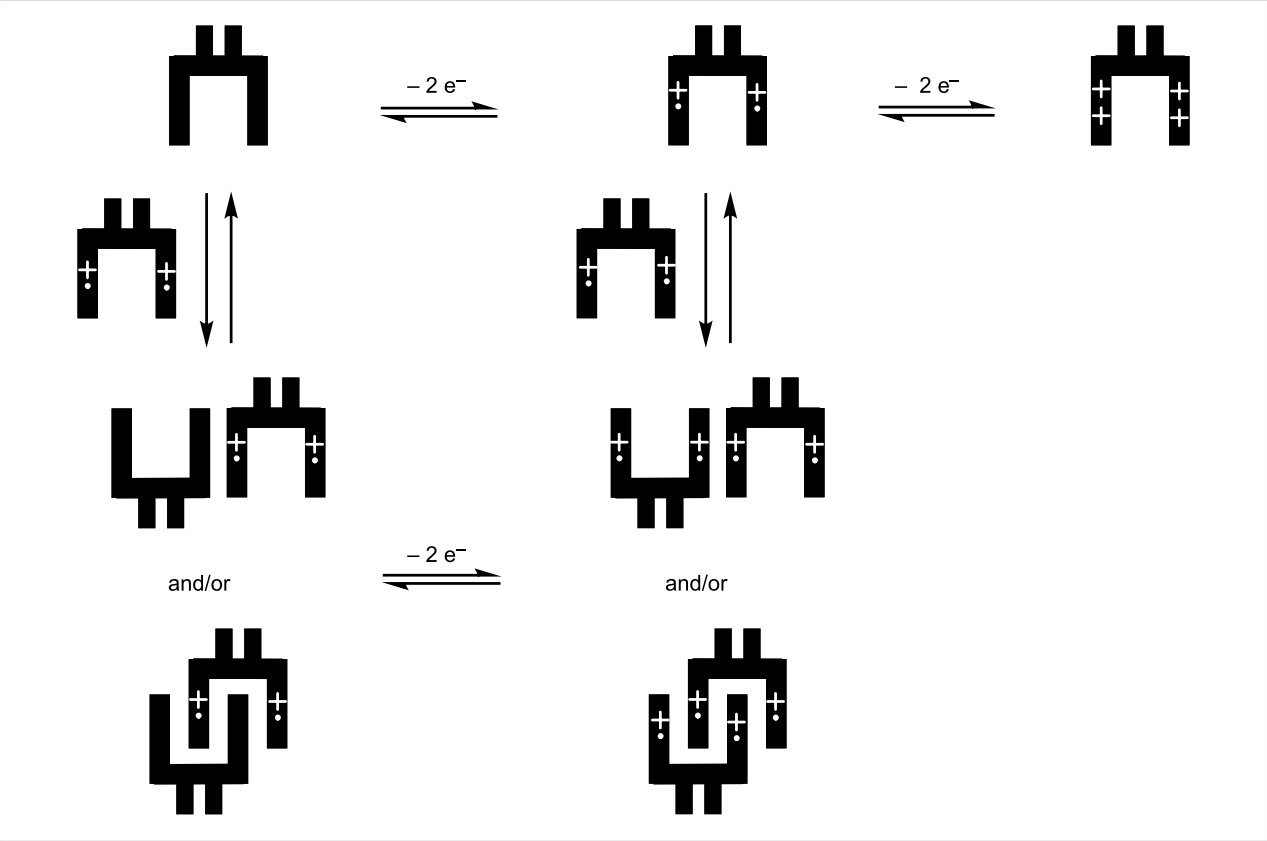

Scheme 3: Graphical representation of the stepwise oxidation of molecular clips **1**, **2** and **3**.

cation is provided by another one-electron process on each TTF unit leading to a clip bearing two dications.

The graphical representation can be simulated by an electrochemical simulation program (DigiElch 7) involving an electrochemical mechanism (Scheme 4) composed by three one-electron processes and two charge-coupled chemical reactions (i.e., formation of mixed-valence and dimerization via a square scheme). Due to the equivalence of the two TTF units, it is important to note that the input value of the concentration of D in Scheme 4 (D represents one TTF unit of the clip) must be twice that of the experimental concentration of a molecular clip. The good agreement between experimental data and modelled CVs over the whole range of concentration supports the graphical representation of the stepwise oxidation of molecular clips **1**, **2** and **3** (Scheme 3).

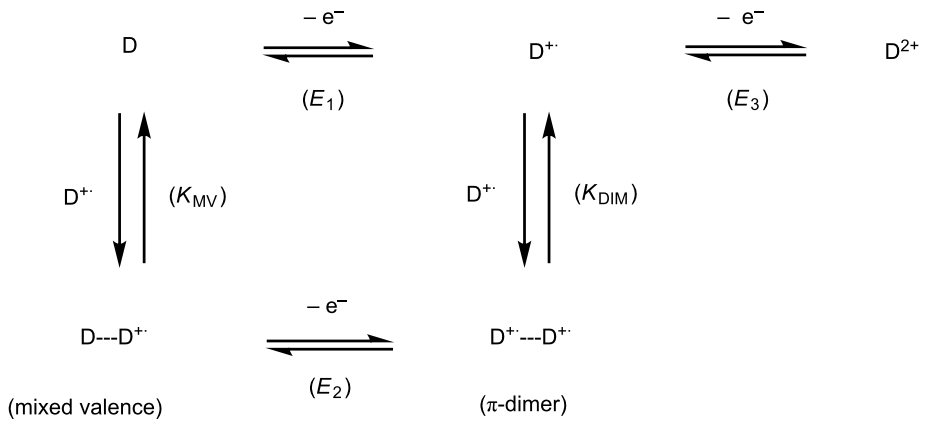

Scheme 4: Electrochemical mechanism used to simulate the CVs of molecular clips **1**, **2** and **3**.

Optical and spectroelectrochemical properties

The optical properties of oxidized states of molecular clip **1** were monitored by UV–vis–NIR spectroscopy, by successive aliquot addition of $NOSbF_6$ (5×10^{-3} M in CH_3CN) used as oxidizing reagent in a solution of clip **1** (10^{-4} M in CH_2Cl_2) in a quartz cell (0.2 cm) (Figure 5). Clip **1** bearing methoxycarbonyl groups at the periphery of the TTF framework was chosen because, to our knowledge, the optical characteristics of such a TTF derivative have not been yet reported. The redox potential (+ 0.87 V vs Fc^+/Fc) of the $NOSbF_6$ reagent is in agreement to allow the oxidation of TTF units. Chemical oxidation led to the rapid disappearance of the band at 320 nm attributed to the neutral TTF derivative and to the concomitant development of new bands characteristic for the cation radical and/or the π-dimer (440, 595 nm), bands which are characteristic for substituted TTF derivatives. After addition of nearly two equivalents of oxidizing reagent, we noted the appearance of the absorption band characteristic of the formation of the TTF dication (340 nm). As soon as we started to add aliquots of $NOSbF_6$ oxidant onto molecular clip **1**, we could observe in the NIR region an absorption band centered at approximately 815 nm and a broad and weak band between 1300–2000 nm.

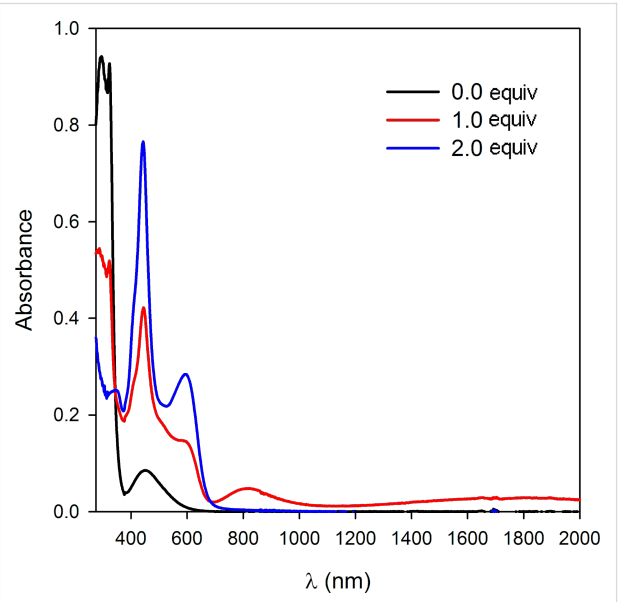

Figure 5: Chemical oxidation of molecular clip **1** (10^{-4} M, CH_2Cl_2) using aliquots of $NOSbF_6$ oxidizing reagent (5×10^{-3} M, CH_3CN).

Known to be a powerful tool for analyzing the formation of π-dimers (DIM) and mixed-valence (MV) systems, time resolved spectroelectrochemical experiments [44-46] were performed on molecular clip **1** in order to probe the first oxidation step at two different concentrations between 350 and 1700 nm in 0.1 M $TBAPF_6/CH_2Cl_2/CH_3CN$ (3:1). At 5×10^{-5} M, only two absorption bands (i.e., 450 and 600 nm) were observed (Figure 6). Confirming a concentration dependence, the absorbance profile at 5×10^{-4} M was different from the one obtained at 5×10^{-5} M. Two additional absorption bands simultaneously emerged at the beginning of the oxidation process and the end of the reduction process: one at 825 nm and a broad band in near infrared range beyond 1300 nm (Figure 6).

In agreement with the simulated concentration–time profiles in thin layer conditions (Figure 6 – bottom), the appearance of the absorption bands centered around 825 and beyond 1300 nm were attributed to the formation of $[(TTF)_2]^+$ mixed-valence dimer [47,48] and the absorption bands centered around 600 nm to the $(TTF^{\cdot+})_2$ π-dimer [49]. The band close to 825 nm could be assigned to cation radicals stack with self-assembly affording mixed-valence. Nevertheless, at this stage, it would be premature to conclude with certainty. The origin of this band is currently under investigation and requires complementary studies to carry out on different substituted molecular clips.

By analogy with unsubstituted TTF derivative, these three bands reasonably support the presence of mixed-valence and cation radical dimers during the oxidation process. Whereas the phenomenon of dimer formation of the TTF cation radical is commonly observed in the solid state, it was also described in solution at low temperature in a concentrated TTF solution [50], or at room temperature in a dilute solution. In the latter case, the characterization of $[(TTF)_2]^{+\cdot}$ mixed-valence dimer and/or $(TTF^{+\cdot})_2$ dimer species concerned systems for which the dimer stabilization is resulting from the close proximity of the two TTF units. That is the case for conjugated bisTTF systems [51], bisTTF-substituted calix[4]arenes [52], or supramolecular architectures such as [3]catenane [53], cucubit[8]uril [54] or self-assembled cages [55] which facilitate the formation of TTF dimers.

Studying the glycoluril-based molecular clip **15** presenting also TTF sidewalls [56,57], Chiu et al. have observed the mixed-valence and radical cation dimer states at high concentration (10^{-3} M) and at room temperature [58]. Indeed, the CV of molecular clip **15** exhibited four consecutive oxidation waves, which were interpreted by a succession of oxidation processes of the TTF sidewalls (Figure 7). These dimer interactions were predicted to exist at room temperature by theoretical investigation realized on this system [59].

By comparison with these results observed for molecular clip **15** [58], it is clear that clips **1–3** exhibit $[(TTF)_2]^{+\cdot}$ mixed-valence dimer and/or $(TTF^{+\cdot})_2$ dimer species but their self-association organization could not be yet demonstrated. The

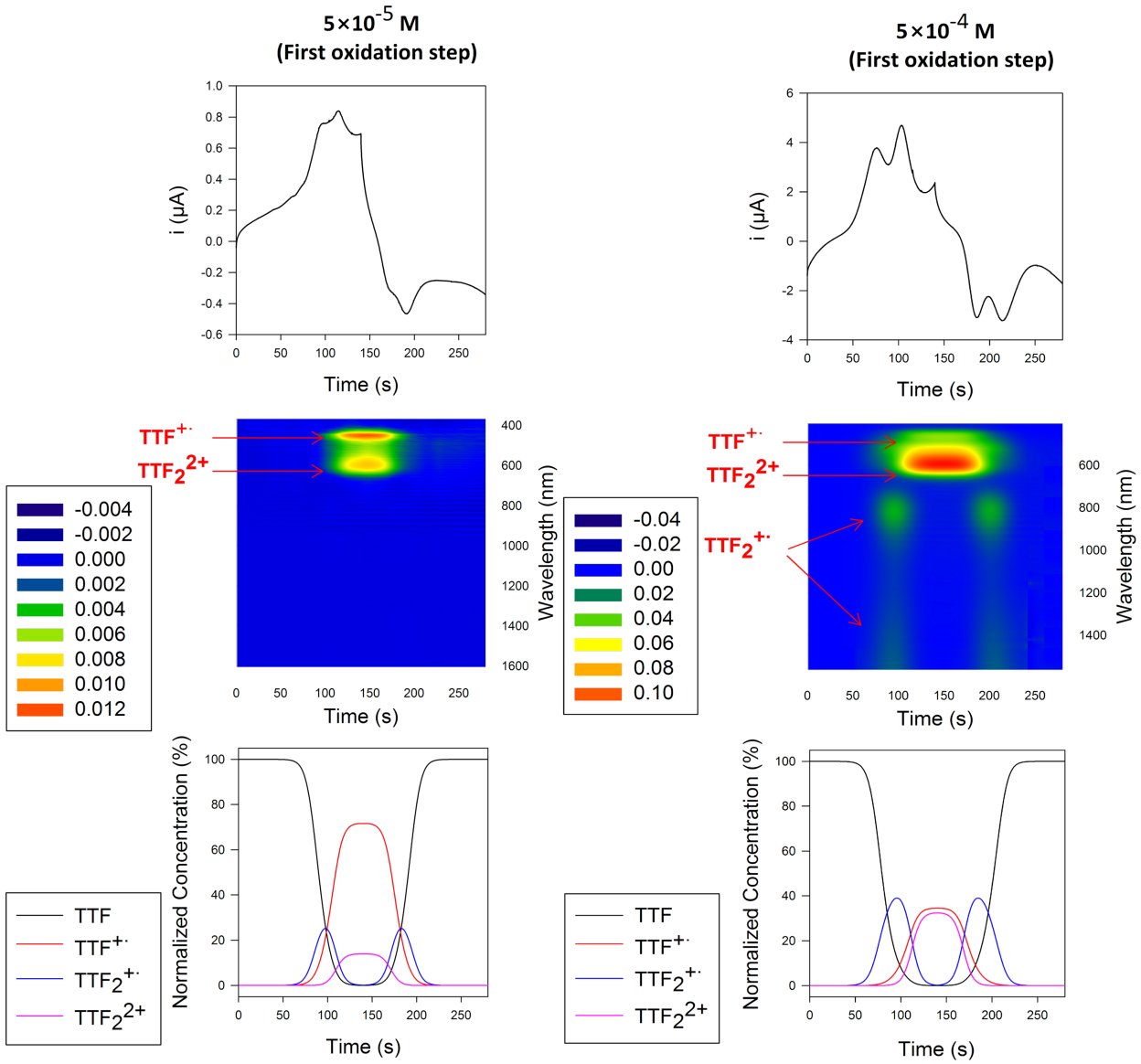

Figure 6: Spectroelectrochemical experiment of molecular clip **1** during the first oxidation step at different concentrations (left: 5 × 10^{-5} M; right : 5 × 10^{-4} M) in 0.1 M $TBAPF_6/CH_2Cl_2/CH_3CN$ (3:1) on glassy carbon on Pt electrode in thin layer conditions (close to 50 µm) electrode at 5 mV·s^{-1} and 293 K. (top) CV in current vs time representation. (middle) 3D representation: *x*-axis = wavelength, *y*-axis = time and *z*-axis = absorbance. (bottom) concentration-time profiles of each simulated species in the thin layer (50 µm) calculated from electrochemical simulations of Figure 4 (E_1 = 0.090 V, E_2 = 0.165 V, E_3 = 0.435 mV, K_{MV} = 11400 M^{-1}, K_{DIM} = 680 M^{-1}, k_f = 1 × 10^9 $M^{-1}·s^{-1}$ for all the forward reactions, α = 0.5 and k_s = 0.01 cm·s^{-1} for all the charge transfers).

presence of more or less sterically bulky groups at the periphery of the TTF moieties does not provide an advantage for the self-assembly of dimers. Moreover, this dimerization phenomenon which is driven by the inclusion of one sidewall into the cavity of the opposing clip is not observed in the solid state for clips **2** and **3** (Figure 8). This typical packing arrangement was previously observed in many cases of glycoluril-based molecular clips containing two aromatic sidewalls [26,60-63]. On the contrary, considering the unit cell for single crystals of clip **2**, X-ray analysis showed that two neighboring molecules of clip **2** appeared in a head-to-tail arrangement and short TTF···TTF intermolecular distances (3.51 Å) were determined between two clips in the solid state.

Binding properties

In order to establish the influence of electronic and spatial properties of the clips towards binding ability of neutral electrodeficient guest molecules, we have chosen compounds **3** and **4** for this study. Molecular clip **3** presents better π-donating ability according to CV study and a smaller interplanar TTF distance

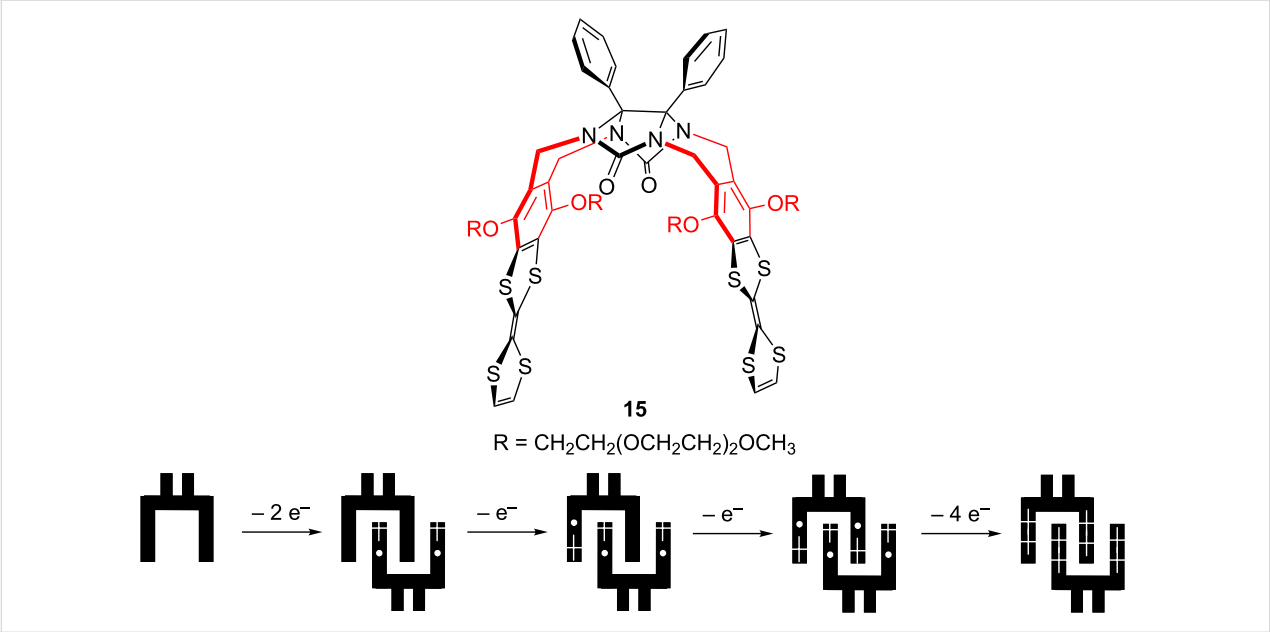

Figure 7: Molecular structure of molecular clip **15** and representation of its stepwise oxidation processes proposed by Chiu et al. [58].

(7.41 Å compared to calculated 9.2 Å for clip **4**). Binding properties were studied using 1,3-dinitrobenzene (*m*-DNB) as a weak and small aromatic electron acceptor molecule. It should be noted that Nolte et al. have successfully observed the complexation of *m*-DNB using a glycoluril-based receptor bearing 2,7-dimethoxynaphthalene walls (K_a = (115 ± 10) M^{-1}) [64]. In the latter case, it was proposed that binding was occurring through an induced-fit mechanism with a recognition process on

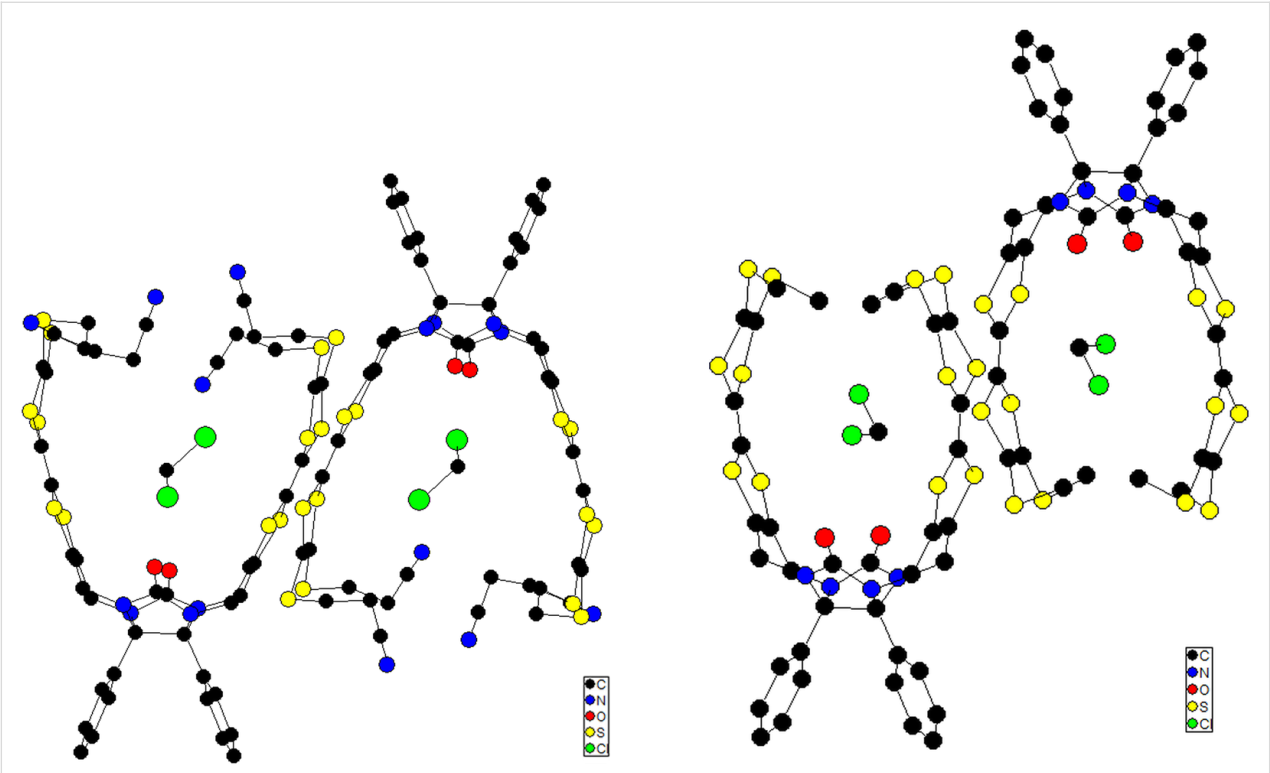

Figure 8: Molecular packing diagram of clips **2** (left) and **3** (right) obtained from X-ray analysis. A molecule of CH_2Cl_2 is included inside the cavity of each clip. Hydrogen atoms are omitted for clarity.

the basis of the size rather than the acceptor strength. We can suppose that the presence of stronger π-donor TTF sidewalls in clip **3** favorize donor–acceptor interactions and consequently the binding properties towards *m*-DNB. We have also checked the influence of the redox properties towards binding ability by studying the strong electrodeficient acceptor F_4-TCNQ.

Interaction with 1,3-dinitrobenzene (*m*-DNB)

The host–guest affinity was detected by UV–visible spectroscopy upon titration of clip **3** (10^{-3} M in *o*-$C_6H_4Cl_2$) with addition of *m*-DNB (10^{-1} M in *o*-$C_6H_4Cl_2$) aliquots. No additional change of the spectra was observed after the addition of one equivalent of *m*-DNB (−1.30 V vs Fc^+/Fc) [65] which is in agreement with the formation of a 1:1 complex. A Job plot carried out in *o*-$C_6H_4Cl_2$ between clip **3** and *m*-DNB shows a maximum at 0.5, confirming the formation of the 1:1 complex (*m*-DNB@clip **3**) (Figure 9 left). The association constant was determined to be $K_a = (7 \pm 3) \times 10^3$ M^{-1} by exploiting the Job plot analysis according to literature [66]. Despite many efforts devoted to the search for a complexation of *m*-DNB using molecular clip **4**, we could not observe any host–guest binding interaction. These results suggest that electronic and spatial properties of the cavity constitute fundamental parameters for binding the *m*-DNB guest. The binding of such a weak electron acceptor was successful for molecular clip **3** presenting the most suitable intramolecular distance between TTF sidewalls and the strongest π-donor ability.

Interaction with tetrafluoroquinodimethane (F_4-TCNQ)

The binding affinity of molecular clip **3** (5×10^{-4} M in CH_2Cl_2) was studied by a UV–visible titration with the electron acceptor F_4-TCNQ (10^{-5} M in CH_2Cl_2). Addition of aliquots of molecular clip **3** onto a F_4-TCNQ solution showed the presence of an isosbestic point at 395 nm with the concomittent formation and increase of bands at 760 and 860 nm which could be attributed to the progressive formation of the F_4-TCNQ radical anion (Figure 10) [67,68]. The increase of the bands around 750 and 850 nm was attributed to the cumulative contribution of the increasing formation of TTF cation radical species and the F_4-TCNQ anion radical.

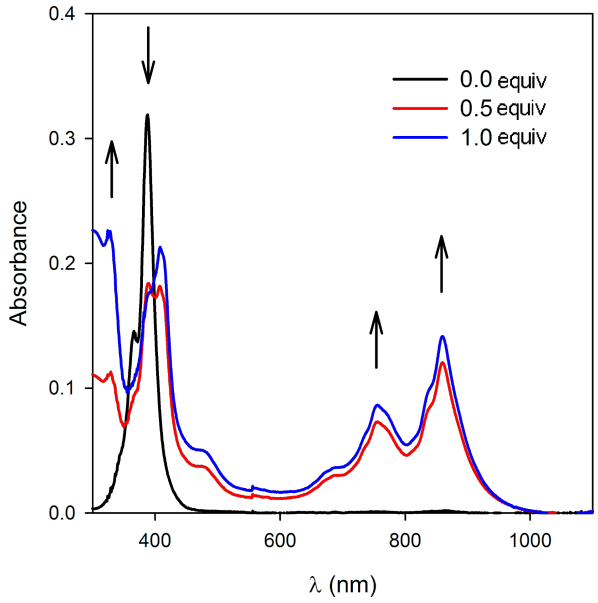

Figure 10: UV–visible absorption spectra of F_4-TCNQ (CH_2Cl_2, 10^{-5} M) upon titration with molecular clip **3** (CH_2Cl_2, 5×10^{-4} M).

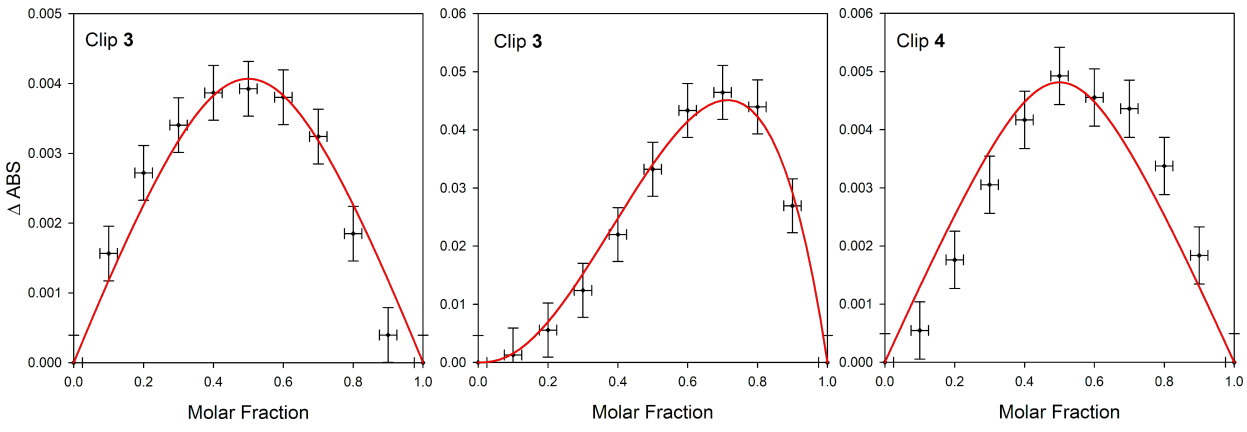

Figure 9: Left: Job plot analysis for DNB vs molecular clip **3** ([**3** + DNB] = 10^{-3} M in *o*-$C_6H_4Cl_2$ at 800 nm) at room temperature. Middle: Job plot for F_4-TCNQ vs molecular clip **3** at room temperature ([**3** + F_4-TCNQ] = 10^{-5} M in CH_2Cl_2 at 860 nm) consistent with a 2:1 binding stoichiometry. Right: Job plot for F_4-TCNQ vs molecular clip **4** at room temperature ([**4** + F_4-TCNQ] = 10^{-5} M in CH_2Cl_2 at 860 nm) in agreement with a 1:1 binding stoichiometry.

A Job plot carried out in CH_2Cl_2 between clip **3** and F_4-TCNQ exhibited a maximum at around 0.7, a finding that corroborates with the formation of a 1:2 complex $(F_4\text{-TCNQ})_2$@clip **3** (Figure 9 middle) with an average binding constant of $K_a = (8 \pm 5) \times 10^8\ M^{-1}$.

Similar studies were carried out using molecular clip **4** and quantitative measurements were performed using UV–visible titration considering the changes in the spectra of F_4-TCNQ at 860 nm upon addition of sensor **4**. The construction of the Job plot is in agreement with the 1:1 binding stoichiometry between clip **4** and F_4-TCNQ with a maximum centered at a molar ratio of 0.5 (Figure 9 right). The high association constant $K_a = (1.3 \pm 0.8) \times 10^6\ M^{-1}$ in CH_2Cl_2 confirms that this rigidified molecular clip **4** is an efficient receptor for F_4-TCNQ guest electron acceptor.

This difference in binding interaction between host molecular clips **3** and **4** towards the F_4-TCNQ guest could be explained by their electrochemical properties. By comparing the first oxidation potential of clips **3** and **4** with the first reduction potential of F_4-TCNQ ($E_{app}{}^0{}_{red1} = +0.14$ V vs Fc^+/Fc – Figure 3), it is clear that F_4-TCNQ guest presents a high reduction potential, sufficient to allow the oxidation of molecular clip **3**. Consequently, the $(F_4\text{-TCNQ})_2$@clip **3** complex should result from a redox interaction between the host and the guest. On the other hand, the oxidation potential of molecular clip **4** is increased due to the introduction of the naphthoquinone spacer. Consequently, the corresponding 1:1 stoichiometry should reasonably correspond to the binding of F_4-TCNQ inside the cavity of clip **4** (Figure 11). This binding of F_4-TCNQ also results from favourable spatial parameters with the increase of the intramolecular distance between the two TTF sidewalls. Thanks to the good π-donor ability of the TTF sidewalls, in combination with a well-suited size of the cavity, it is here demonstrated that molecular clip **4** constitutes one of the rare examples of systems exhibiting good affinity for sandwiching F_4-TCNQ as an electron poor guest.

Conclusion

We have presented original synthetic strategies leading to glycoluril-based molecular clips containing electroactive TTF sidewalls. In particular, the one-step preparation of molecular clip using the N-tetraalkylation of glycoluril constitutes a powerful versatile method allowing an easy access to new architectures for which electrochemical properties can be tuned by simple modification of peripheral substituents on the TTF moiety. Cyclic voltammetry and spectroelectrochemical measurements demonstrated that the mixed-valence state in these fused glycoluril-TTF molecular clips seems to originate from intermolecular TTF interactions, according to measurements at various concentrations and to cyclic voltammogram simulations. Spatial and electrochemical properties were shown to be fundamental parameters towards the binding interaction of a weak (*m*-DNB) or strong (F_4-TCNQ) electrodeficient guest. Consequently, the selectivity for a given target guest could be precisely tuned via the choice of the molecular clip according to its electrochemical and spatial considerations.

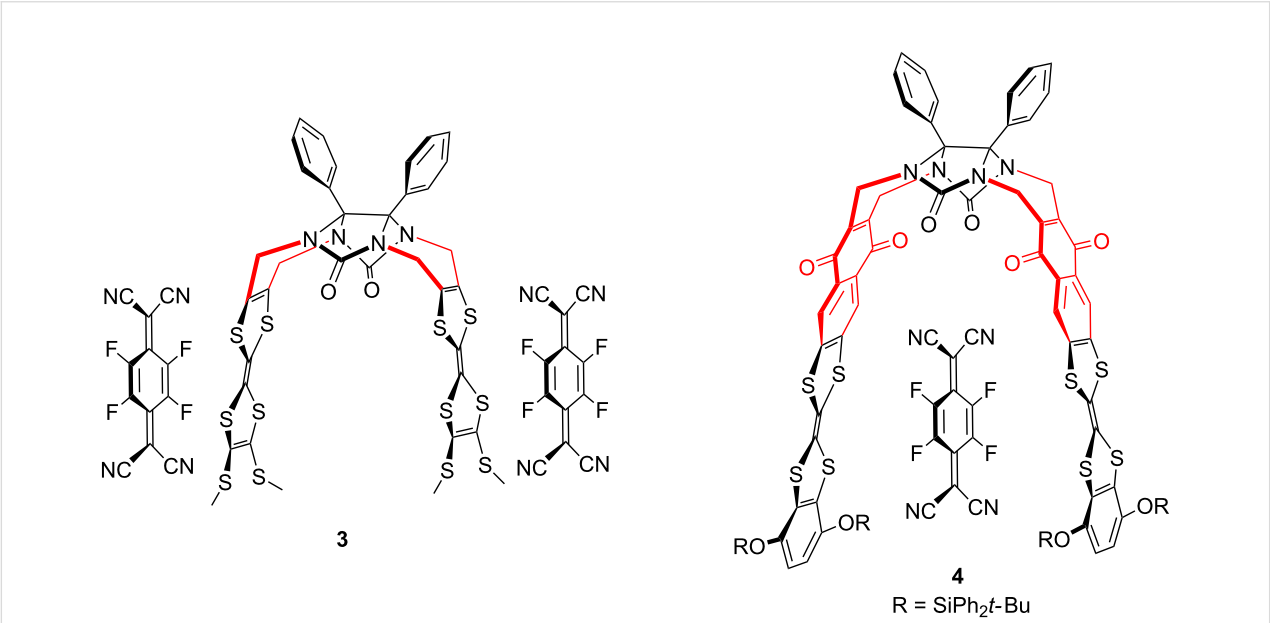

Figure 11: Redox interaction (left) and complexation (right) of F_4-TCNQ with molecular clips **3** and **4**.

Experimental

Synthesis

Molecular clips **1–3** [18] and **4** [19] were synthesized according to our previous reports.

Electrochemical and spectroelectrochemical experiments

Electrochemistry and time-resolved spectroelectrochemistry in solution were performed using the already described home self-made cell [44,45]. Electrochemical measurements were carried out using a platinum wire counter electrode and a silver wire as a quasi-reference electrode with a Biologic SP-150 potentiostat driven by the EC-Lab software including ohmic drop compensation. Experiments were recorded in dry HPLC-grade acetonitrile and dichloromethane with tetrabutylammonium hexafluorophosphate (Bu_4NPF_6, electrochemical grade, Fluka) as supporting electrolyte. All solutions were prepared and transferred into the spectroelectrochemical cell in a glove box containing dry, oxygen-free (<1 ppm) argon, at room temperature.

Spectrophotometric measurements were carried out in direct reflexing mode on the working electrode (i.e., Pt or glassy carbon) with a homemade bench composed of different Princeton Instruments modules (light sources, fibers, monochromators, spectroscopy camera and software). The connection between the light source, the cell and the spectrophotometer is ensured through a "Y-shaped" optical fiber bundle: 18 fibers guide the light to the cell, and 19 fibers collect the reflected light from the cell to visible (320–1080 nm / maximum acquisition frequency 2 MHz) and IR (900–1700 nm / maximum acquisition frequency 8 MHz) CCD detectors. The sensitivity of the spectroscopic measurement (<3 electrons at 100 kHz and <13 electrons at 2 MHz between 320 and 1080 nm; 400 electrons (high gain) and 5000 electrons (low gain) between 900 nm and 1700 nm) allows performing a spectroelectrochemistry experiment under the usual conditions of electrochemistry.

Acknowledgements

This work was supported by the Ministère de la Recherche et de l'Enseignement Supérieur for Ph.D grants to Y. Cotelle and M. Hardouin-Lerouge.

References

1. Wudl, F.; Smith, G. M.; Hufnagel, E. J. *J. Chem. Soc. D* **1970,** 1453–1454. doi:10.1039/C29700001453
2. Bryce, M. R. *J. Mater. Chem.* **2000,** *10,* 589–598. doi:10.1039/A908385E
3. Segura, J. L.; Martín, N. *Angew. Chem., Int. Ed.* **2001,** *40,* 1372–1409. doi:10.1002/1521-3773(20010417)40:8<1372::AID-ANIE1372>3.0.CO;2-I
4. Yamada, J.; Sugimoto, T., Eds. *TTF Chemistry. Fundamentals and applications of tetrathiafulvalene;* Springer Verlag: New York, 2004.
5. Gorgues, A.; Hudhomme, P.; Sallé, M. *Chem. Rev.* **2004,** *104,* 5151–5184. doi:10.1021/cr0306485
6. Batail, P., Ed. Special issue on Molecular Conductors. *Chem. Rev.* **2004,** *104,* 4887–5782.
7. Martín, N. *Chem. Commun.* **2013,** *49,* 7025–7027. doi:10.1039/C3CC00240C
8. Bendikov, M.; Wudl, F.; Perepichka, D. F. *Chem. Rev.* **2004,** *104,* 4891–4946. doi:10.1021/cr030666m
9. Bergkamp, J. J.; Decurtins, S.; Liu, S.-X. *Chem. Soc. Rev.* **2015,** *44,* 863–874. doi:10.1039/C4CS00255E
10. Nielsen, M. O.; Lomholt, C.; Becher, J. *Chem. Soc. Rev.* **2000,** *29,* 153–164. doi:10.1039/A803992E
11. Canevet, D.; Sallé, M.; Zhang, G.; Zhang, D.; Zhu, D. *Chem. Commun.* **2009,** 2245–2269. doi:10.1039/B818607N
12. Steed, J. W.; Atwood, J. L. *Supramolecular Chemistry,* 2nd ed.; John Wiley & Sons Ltd, 2009.
13. Hardouin-Lerouge, M.; Hudhomme, P.; Sallé, M. *Chem. Soc. Rev.* **2011,** *40,* 30–43. doi:10.1039/b915145c
14. Chen, C.-W.; Whitlock, H. W., Jr. *J. Am. Chem. Soc.* **1978,** *100,* 4921–4922. doi:10.1021/ja00483a063
15. Leblond, J.; Petitjean, A. *ChemPhysChem* **2011,** *12,* 1043–1051. doi:10.1002/cphc.201001050
16. Sijbesma, R. P.; Nolte, R. J. M. *Top. Curr. Chem.* **1995,** *175,* 25–56. doi:10.1007/3-540-58800-0_17
17. Rowan, A. E.; Elemans, J. A. A. W.; Nolte, R. J. M. *Acc. Chem. Res.* **1999,** *32,* 995–1006. doi:10.1021/ar9702684
18. Cotelle, Y.; Allain, M.; Legoupy, S.; Hudhomme, P. *Org. Lett.* **2014,** *16,* 2590–2593. doi:10.1021/ol500458e
19. Hardouin-Lerouge, M.; Cotelle, Y.; Legoupy, S.; Hudhomme, P. *New J. Chem.* **2014,** *38,* 5341–5348. doi:10.1039/c4nj00617h
20. Butler, A. R.; Leitch, E. *J. Chem. Soc., Perkin Trans. 2* **1980,** 103–105. doi:10.1039/P29800000103
21. Hudhomme, P.; Le Moustarder, S.; Durand, C.; Gallego-Planas, N.; Mercier, N.; Blanchard, P.; Levillain, E.; Allain, M.; Gorgues, A.; Riou, A. *Chem. – Eur. J.* **2001,** *7,* 5070–5083. doi:10.1002/1521-3765(20011203)7:23<5070::AID-CHEM5070>3.0.CO;2-6
22. Reek, J. N. H.; Kros, A.; Nolte, R. J. M. *Chem. Commun.* **1996,** 245–247. doi:10.1039/CC9960000245
23. Elemans, J. A. A. W.; Rowan, A. E.; Nolte, R. J. M. *J. Am. Chem. Soc.* **2002,** *124,* 1532–1540. doi:10.1021/ja012061i
24. Creaven, B. S.; Gallagher, J. F.; McDonagh, J. P.; McGinley, J.; Murray, B. A.; Whelan, G. S. *Tetrahedron* **2004,** *60,* 137–143. doi:10.1016/j.tet.2003.10.084
25. Wu, A.; Chakraborty, A.; Witt, D.; Lagona, J.; Damkaci, F.; Ofori, M. A.; Chiles, J. K.; Fettinger, J. C.; Isaacs, L. *J. Org. Chem.* **2002,** *67,* 5817–5830. doi:10.1021/jo0258958
26. Wang, Z.-G.; Zhou, B.-H.; Chen, Y.-F.; Yin, G.-D.; Li, Y.-T.; Wu, A.-X.; Isaacs, L. *J. Org. Chem.* **2006,** *71,* 4502–4508. doi:10.1021/jo0603375
27. Bogaschenko, T. Yu.; Lyapunov, A. Yu.; Kikot, L. S.; Mazepa, A. V.; Botoshansky, M. M.; Fonari, M. S.; Kirichenko, T. I. *Tetrahedron* **2012,** *68,* 4757–4764. doi:10.1016/j.tet.2012.04.009
28. Easton, D. B. J.; Leaver, D. *Chem. Commun.* **1965,** 585–586. doi:10.1039/C19650000585
29. Fabre, J.-M. *Chem. Rev.* **2004,** *104,* 5133–5150. doi:10.1021/cr0306440
30. Svenstrup, N.; Rasmussen, K. M.; Hansen, T. K.; Becher, J. *Synthesis* **1994,** 809–812. doi:10.1055/s-1994-25580

31. Simonsen, K. B.; Becher, J. *Synlett* **1997,** 1211–1220. doi:10.1055/s-1997-1001
32. Hudhomme, P.; Liu, S.-G.; Kreher, D.; Cariou, M.; Gorgues, A. *Tetrahedron Lett.* **1999,** *40,* 2927–2930. doi:10.1016/S0040-4039(99)00325-1
33. Smeets, J. W. H.; Sijbesma, R. P.; Van Dalen, L.; Spek, A. L.; Smeets, W. J. J.; Nolte, R. J. M. *J. Org. Chem.* **1989,** *54,* 3710–3717. doi:10.1021/jo00276a037
34. Butler, A. R.; Hussain, I. *J. Chem. Soc., Perkin Trans. 2* **1981,** 310–316. doi:10.1039/P29810000310
35. Sijbesma, R. P.; Kentgens, A. P. M.; Lutz, E. T. G.; van der Maas, J. H.; Nolte, R. J. M. *J. Am. Chem. Soc.* **1993,** *115,* 8999–9005. doi:10.1021/ja00073a015
36. Baffreau, J.; Dumur, F.; Hudhomme, P. *Org. Lett.* **2006,** *8,* 1307–1310. doi:10.1021/ol060011i
37. Gautier, N.; Mercier, N.; Riou, A.; Gorgues, A.; Hudhomme, P. *Tetrahedron Lett.* **1999,** *40,* 5997–6000. doi:10.1016/S0040-4039(99)01162-4
38. Kreher, D.; Liu, S.-G.; Cariou, M.; Hudhomme, P.; Gorgues, A.; Mas, M.; Veciana, J.; Rovira, C. *Tetrahedron Lett.* **2001,** *42,* 3447–3450. doi:10.1016/S0040-4039(01)00494-4
39. Hudhomme, P. *C. R. Chim.* **2006,** *9,* 881–891. doi:10.1016/j.crci.2005.11.008
40. Bénard, C. P.; Geng, Z.; Heuft, M. A.; VanCrey, K.; Fallis, A. G. *J. Org. Chem.* **2007,** *72,* 7229–7236. doi:10.1021/jo0709807
41. Spanggaard, H.; Prehn, J.; Nielsen, M. B.; Levillain, E.; Allain, M.; Becher, J. *J. Am. Chem. Soc.* **2000,** *122,* 9486–9494. doi:10.1021/ja000537c
42. Azov, V. A.; Gómez, R.; Stelten, J. *Tetrahedron* **2008,** *64,* 1909–1917. doi:10.1016/j.tet.2007.11.110
43. Skibiński, M.; Gómez, R.; Lork, E.; Azov, V. A. *Tetrahedron* **2009,** *65,* 10348–10354. doi:10.1016/j.tet.2009.10.052
44. Gaillard, F.; Levillain, E. *J. Electroanal. Chem.* **1995,** *398,* 77–87. doi:10.1016/0022-0728(95)04144-1
45. Dias, M.; Hudhomme, P.; Levillain, E.; Perrin, L.; Sahin, Y.; Sauvage, F.-X.; Wartelle, C. *Electrochem. Commun.* **2004,** *6,* 325–330. doi:10.1016/j.elecom.2004.01.010
46. Alévêque, O.; Levillain, E.; Sanguinet, L. *Electrochem. Commun.* **2015,** *51,* 108–112. doi:10.1016/j.elecom.2014.12.014
47. Torrance, J. B.; Scott, B. A.; Welber, B.; Kaufman, F. B.; Seiden, P. E. *Phys. Rev. B* **1979,** *19,* 730–741. doi:10.1103/PhysRevB.19.730
48. Andreu, R.; Garín, J.; Orduna, J. *Tetrahedron* **2001,** *57,* 7883–7892. doi:10.1016/S0040-4020(01)00766-9
49. Khodorkovsky, V.; Shapiro, L.; Krief, P.; Shames, A.; Mabon, G.; Gorgues, A.; Giffard, M. *Chem. Commun.* **2001,** 2736–2737. doi:10.1039/B104934H
50. Rosokha, S. V.; Kochi, J. K. *J. Am. Chem. Soc.* **2007,** *129,* 828–838. doi:10.1021/ja064166x
51. Gautier, N.; Samuel, R.; Şahin, Y.; Levillain, E.; Leroy-Lhez, S.; Hudhomme, P. *Org. Lett.* **2004,** *6,* 1569–1572. doi:10.1021/ol049620l
52. Lyskawa, J.; Sallé, M.; Balandier, J.-Y.; Le Derf, F.; Levillain, E.; Allain, M.; Viel, P.; Palacin, S. *Chem. Commun.* **2006,** 2233–2235. doi:10.1039/B518275A
53. Coskun, A.; Spruell, J. M.; Barin, G.; Fahrenbach, A. C.; Forgan, R. S.; Colvin, M. T.; Carmieli, R.; Benítez, D.; Tkatchouk, E.; Friedman, D. C.; Sarjeant, A. A.; Wasielewski, M. R.; Goddard, W. A., III; Stoddart, J. F. *J. Am. Chem. Soc.* **2011,** *133,* 4538–4547. doi:10.1021/ja110584c
54. Ziganshina, A. Y.; Ko, Y. H.; Jeon, W. S.; Kim, K. *Chem. Commun.* **2004,** 806–807. doi:10.1039/B316651A
55. Yoshizawa, M.; Kumazawa, K.; Fujita, M. *J. Am. Chem. Soc.* **2005,** *127,* 13456–13457. doi:10.1021/ja053508g
56. Chen, P.-N.; Chiang, P.-T.; Chiu, S.-H. *Chem. Commun.* **2005,** 1285–1287. doi:10.1039/b417823h
57. Chiang, P.-T.; Cheng, P.-N.; Lin, C.-F.; Liu, Y.-H.; Lai, C.-C.; Peng, S.-M.; Chiu, S.-H. *Chem. – Eur. J.* **2006,** *12,* 865–876. doi:10.1002/chem.200500676
58. Chiang, P.-T.; Chen, N.-C.; Lai, C.-C.; Chiu, S.-H. *Chem. – Eur. J.* **2008,** *14,* 6546–6552. doi:10.1002/chem.200800213
59. Fumanal, M.; Capdevila-Cortada, M.; Miller, J. S.; Novoa, J. J. *J. Am. Chem. Soc.* **2013,** *135,* 13814–13826. doi:10.1021/ja405352p
60. Reek, J. N. H.; Elemans, J. A. A. W.; de Gelder, R.; Beurskens, P. T.; Rowan, A. E.; Nolte, R. J. M. *Tetrahedron* **2003,** *59,* 175–185. doi:10.1016/S0040-4020(02)01480-1
61. Chen, Y.; She, N.; Meng, X.; Yin, G.; Wu, A.; Isaacs, L. *Org. Lett.* **2007,** *9,* 1899–1902. doi:10.1021/ol0704340
62. Wu, A.; Chakraborty, A.; Fettinger, J. C.; Flowers, R. A.; Isaacs, L. *Angew. Chem., Int. Ed.* **2002,** *41,* 4028–4031. doi:10.1002/1521-3773(20021104)41:21<4028::AID-ANIE4028>3.0.CO;2-2
63. She, N.; Gao, M.; Cao, L.; Wu, A.; Isaacs, L. *Org. Lett.* **2009,** *11,* 2603–2606. doi:10.1021/ol900858d
64. Sijbesma, R. P.; Wijmenga, S. S.; Nolte, R. J. M. *J. Am. Chem. Soc.* **1992,** *114,* 9807–9813. doi:10.1021/ja00051a013
65. Macías-Ruvalcaba, N. A.; Evans, D. H. *J. Electroanal. Chem.* **2007,** *602,* 77–81. doi:10.1016/j.jelechem.2006.12.001
66. Renny, J. S.; Tomasevich, L. L.; Tallmadge, E. H.; Collum, D. B. *Angew. Chem., Int. Ed.* **2013,** *52,* 11998–12013. doi:10.1002/anie.201304157
67. Jain, A.; Rao, K. V.; Mogera, U.; Sagade, A. A.; George, S. J. *Chem. – Eur. J.* **2011,** *17,* 12355–12361. doi:10.1002/chem.201101813
68. Bivaud, S.; Balandier, J.-Y.; Chas, M.; Allain, M.; Goeb, S.; Sallé, M. *J. Am. Chem. Soc.* **2012,** *134,* 11968–11970. doi:10.1021/ja305451v

License and Terms

BEILSTEIN JOURNAL OF ORGANIC CHEMISTRY

Donor–acceptor type co-crystals of arylthio-substituted tetrathiafulvalenes and fullerenes

Xiaofeng Lu, Jibin Sun, Shangxi Zhang, Longfei Ma, Lei Liu, Hui Qi, Yongliang Shao and Xiangfeng Shao*

Full Research Paper

Open Access

Address:
State Key Laboratory of Applied Organic Chemistry, Lanzhou University, Tianshui Southern Road 222, Lanzhou 730000, Gansu Province, P. R. China

Email:
Xiangfeng Shao* - shaoxf@lzu.edu.cn

* Corresponding author

Keywords:
arylthio-substituted tetrathiafulvalene; co-crystal; donor–acceptor system; fullerene

Beilstein J. Org. Chem. **2015,** *11,* 1043–1051.
doi:10.3762/bjoc.11.117

Received: 08 February 2015
Accepted: 01 June 2015
Published: 19 June 2015

This article is part of the Thematic Series "Tetrathiafulvalene chemistry".

Guest Editor: P. J. Skabara

Abstract

A series of donor–acceptor type co-crystals of fullerene (as the acceptor) and arylthio-substituted tetrathiafulvalene derivatives (Ar-S-TTF, as the donor) were prepared and their structural features were thoroughly investigated. The formation of co-crystals relies on the flexibility of Ar-S-TTF and the size matches between Ar-S-TTF and fullerene. Regarding their compositions, the studied co-crystals can be divided into two types, where types I and II have donor:acceptor ratios of 1:1 and 1:2, respectively. Multiple intermolecular interactions are observed between the donor and acceptor, which act to stabilize the structures of the resulting co-crystals. In the type I co-crystals, the fullerene molecule is surrounded by four Ar-S-TTF molecules, that is, two Ar-S-TTF molecules form a sandwich structure with one fullerene molecule and the other two Ar-S-TTF molecules interact with the fullerene molecule along their lateral axes. In the type II co-crystals, one fullerene molecule has the donor–acceptor mode similar to that in type I, whereas the other fullerene molecule is substantially surrounded by the aryl groups on Ar-S-TTF molecules and the solvent molecules.

Introduction

Tetrathiafulvalene (TTF) [1-3] and its derivatives have attracted significant interest for decades. This is because this unique heterocycle system has provided most of the organic conductors possessing diverse electronic ground states [4-11]. Owing to their good electron donating ability and reversible electrochemical activity, TTF derivatives have recently been employed as building blocks for functional supramolecular systems [12-22]. Among the TTF-based supramolecular systems, those involving fullerene molecules are of growing interest due to their potential application in organic voltaics [20]. The TTF–fullerene dyad is a typical donor–acceptor (D–A) system, where TTFs and fullerenes act as donors and acceptors,

respectively. The TTF–fullerene dyad can be constructed by (1) connection of two components through covalent bonds [23-27] or (2) supramolecular assembly between TTFs (as host) and fullerene (as guest) [28-41].

For the formation of the host–guest type supramolecular system, the shape and size complementarity between TTFs and fullerenes are key factors that give rise to the effective surface contact for the stabilization of the resulting supramolecular structures. Because pristine TTF cannot form good enough surface contact with fullerenes due to the shape and size mismatch [42], chemical modifications of TTF have been carried out. To this regard, introduction of substituents onto the peripheral sites [43-54] and expansion of the π-systems have been reported [55-59]. As reported, the π-extended TTFs (exTTF) can encapsulate fullerenes in solution, and form the inclusion complex with fullerenes as well [28-37]. Very recently, we have disclosed a facile approach toward the arylthio-substituted TTFs (hereafter denoted as Ar-S-TTF) [60-62], which bear four aryl groups on the peripheral positions of the TTF core through the sulfur bridges. The Ar-S-TTF molecules are size and shape matched for fullerenes (C_{60}/C_{70}), and the peripheral aryls show large rotational freedom that could adjust their spatial alignment to adapt to the environmental variations [61].

Regarding the structural feature of Ar-S-TTF, we have performed the complexation of Ar-S-TTFs with C_{60}/C_{70}, and found that Ar-S-TTF could form D–A type inclusion complexes with C_{60}/C_{70} [63]. Crystallographic investigation reveals that the multidimensional interaction networks consisting of a central TTF core, peripheral aryls, and fullerenes are the key factors to stabilize the resulting supramolecular structures. Meanwhile, the solid state absorption study indicates that the inclusion complexes display a photoexcited electronic transition between Ar–S–TTF and C_{60}/C_{70}. To gain further insight into the structural features of Ar-S-TTF upon complexation with C_{60}/C_{70}, we have carried out the preparation a series of [(Ar-S-TTF)–(fullerene)] co-crystals and investigated their solid state structure, as reported herein. In this report we focus on the synthesis, composition (donor:acceptor ratio), and crystal structure of the resulting co-crystals.

Results and Discussion

Synthesis and compositions

On the basis of hundreds of experimental runs, we found that the Ar-S-TTFs possessing the first redox potential ($E_{1/2}{}^1$) smaller than 0.6 V could form the co-crystal-type complexes with fullerene molecules C_{60} and/or C_{70}, whereas those with $E_{1/2}{}^1 > 0.6$ V could not afford the desired complexes. The complexes obtained thus far are intrinsically neutral [63], which means the charge transfer does not take place between Ar-S-TTF and fullerenes in the ground state. In this regard, the $E_{1/2}{}^1$ values of Ar-S-TTFs would not affect the formation of co-crystals. On the other hand, the interaction between the aryls and fullerene molecules is very important to stabilize the structure of the co-crystals as reported in the crystal structures section. For Ar-S-TTFs exhibiting $E_{1/2}{}^1 > 0.6$ V, the aryl groups are more electron deficient than the phenyl [61,62]. The interaction between the electron-deficient aryls and fullerenes is weak; consequently, these TTFs ($E_{1/2}{}^1 > 0.6$ V) could not form the co-crystals with fullerenes.

Among the [(Ar-S-TTF)–(fullerene)] complexes obtained to this point, the complexes of Ar-S-TTFs **1**–**8** (Scheme 1) with C_{60}/C_{70} were cropped in the single crystalline form, and the others were obtained as powdery samples with difficult to determine compositions. The [(Ar-S-TTF)–(fullerene)] co-crystals were prepared by evaporating the mixed solution of Ar-S-TTF and the corresponding fullerenes at room temperature. As a typical example, compound **1** (12.8 mg, 2 mmol) and C_{60} (7.2 mg, 1 mmol) were dissolved in carbon disulfide (CS_2, 7 mL), and the resulting mixed solution was then placed in the dark hood and left standing without disruption. After 2 weeks, the black block-like single crystalline complex was cropped, and the composition of the complex was determined to be **1**·$(C_{60})_2$·$(CS_2)_2$ on the basis of the X-ray single crystal structure analysis. The synthetic conditions, compositions, yields, and morphologies for the 11 complexes are summarized in Table 1.

Concerning the compositions (donor:acceptor ratio), most of the co-crystals could be divided into two types (I and II), except for **2**·$(C_{70})_4$·$(PhCl)_2$. The ratio of donor:acceptor (abbreviated as D:A) for the type I and type II co-crystals are 1:1 and 1:2, respectively. No solvent molecule was involved in most of the type I co-crystals, except for **4**·C_{60}·CS_2, which contains a small, linear solvent, CS_2. On the other hand, all of the type II co-crystals contain solvent molecules in their matrix. Since one Ar-S-TTF is capable of encapsulating a fullerene molecule [63], the larger ratio of fullerenes would result in the formation of additional void space by fullerene molecules, which could potentially accommodate the solvent molecules. In a previous report, we have proposed that C_{70} tends to form co-crystals with a larger acceptor ratio [63]. However, the present results suggest that this prediction would not hold because both C_{60} and C_{70} form the type I and type II co-crystals with Ar-S-TTFs as shown in Table 1. The D:A ratio for the co-crystals results from the cooperative effects of the geometry of Ar-S-TTF (particularly the peripheral aryls), the shape and size of the fullerene molecules, and the solvent molecules. Although we cannot presently provide a clear estimation of the D:A ratio of the

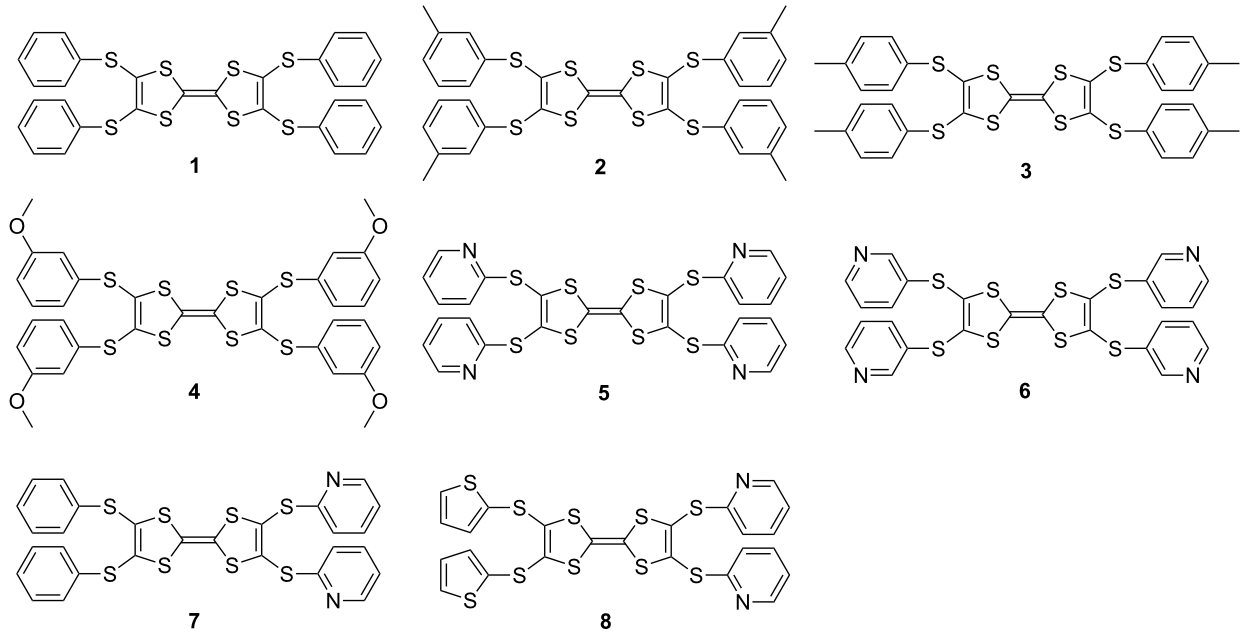

Scheme 1: Chemical structures of Ar-S-TTFs **1**–**8**.

Table 1: Experimental conditions for the preparation of the co-crystals.

	Donor	Acceptor	Solvent[a]	Complex[b]	Appearance
C_{60} complexes	**1**, 12.8 mg	C_{60}, 7.2 mg	CS_2, 7 mL	**1**·$(C_{60})_2$·$(CS_2)_2$, 7.3 mg	Black block
	1, 7 mg	C_{60}, 5.7 mg	PhCl, 6 mL	**1**·$(C_{60})_2$·PhCl, 7.5 mg	Black block
	2, 6.9 mg	C_{60}, 5.5 mg	PhCl, 14 mL	**2**·C_{60}, 8.2 mg	Black plate[c]
	4, 34.1 mg	C_{60}, 14.4 mg	CS_2, 14 mL	**4**·C_{60}·CS_2, 29.2 mg	Black block[c]
	6, 10 mg	C_{60}, 11 mg	PhCl, 9 mL	**6**·$(C_{60})_2$·$(PhCl)_2$, 17.1 mg	Black block
	7, 14.4 mg	C_{60}, 5.5 mg	PhCl, 12 mL	**7**·C_{60}, 8.8 mg	Black plate
	8, 14.6 mg	C_{60}, 5.5 mg	PhCl, 12 mL	**8**·C_{60}, 9.7 mg	Black block
C_{70} complexes	**1**, 9 mg	C_{70}, 5.9 mg	PhCl, 12 mL	**1**·C_{70}, 9.2 mg	Black plate
	2, 6.9 mg	C_{70}, 4.2 mg	PhCl, 10 mL	**2**·$(C_{70})_4$·$(PhCl)_2$, 6.1 mg	Black prism
	3, 13.8 mg	C_{70}, 8.4 mg	PhCl, 10 mL	**3**·$(C_{70})_2$·$(PhCl)_2$, 6 mg	Black prism[c]
	5, 6.5 mg	C_{70}, 4.2 mg	PhCl, 8 mL	**5**·C_{70}, 4.1 mg	Black block

[a]CS_2: carbon disulfide, PhCl: chlorobenzene; [b]the compositions of the co-crystals were determined by X-ray single crystal structure analysis; [c]see reference [63].

co-crystals, this work further demonstrates that Ar-S-TTFs are promising candidates to serve as receptors for fullerenes and have diverse supramolecular structures.

Crystal structures

The single crystalline structure of the complex is suitable for X-ray single crystal diffraction measurements. In most cases, the fullerene molecules and solvent molecules are disordered. The disorder of fullerenes and solvents cannot be suppressed even at low temperature, and can thus be characterized as having statistic rather than rotational disorder. The selected crystallographic data are summarized in Tables S1 and S2 in Supporting Information File 1. In the following sections, the structures of the type I and type II co-crystals will be discussed in sequence.

Type I co-crystals

The type I co-crystals include four C_{60} complexes and two C_{70} complexes, namely, **2**·C_{60}, **4**·C_{60}·CS_2, **7**·C_{60}, **8**·C_{60}, **1**·C_{70}, and **5**·C_{70}. It should be noted that we recently reported the structures of **2**·C_{60} and **4**·C_{60}·CS_2 [63]. As a typical example of the newly obtained co-crystals, the structure of **5**·C_{70} is discussed

here, and those of **7**·C_{60}, **8**·C_{60}, and **1**·C_{70} are provided in the Supporting Information File 1 (Figures S4–S15).

Complex **5**·C_{70} crystallizes in the triclinic space group *P*-1 with one molecule **5** and one C_{70} crystallographically unique (Figure 1a). The central TTF core on molecule **5** has a chair conformation. The molecular geometry of **5** in the co-crystal, both the spatial alignment of pyridyl groups and the conformation of the TTF core, is very close to its neutral crystalline form obtained in CS_2 [61]. The C_{70} molecule is surrounded by four molecules **5** (Figure 1b), and the long axes of C_{70} and TTF5 are almost parallel to each other. A pair of **5** and a C_{70} molecule in a sandwich configuration is stabilized by multiple intermolecular atomic close contacts [64]: C–S of 3.33–3.36 Å and C–C of 3.17–3.40 Å. The other two molecules of **5** have C–S contacts (3.23–3.50 Å) with C_{70} along their lateral axes. Moreover, the C–C contacts (3.18–3.36 Å) are also observed between the peripheral pyridyl groups and C_{70}. Compound **5** and C_{70} form separated layers (Figures S1–S3 in Supporting Information File 1), and the arrangement of C_{70} molecules in the *ac*-plane is shown in Figure 1c. The center-to-center distances between C_{70} molecules along the (*a*−*c*) and (*a*+*c*) directions are 10.2 Å and 10.6 Å, respectively. The former is close to the short axis of C_{70} (10 Å), thus C_{70} molecules form one-dimensional (1D) columnar arrays along this direction. The structural features for both donor–acceptor interaction mode and fullerene arrangement of **7**·C_{60}, **8**·C_{60}, and **1**·C_{70} are very similar to that of **5**·C_{70}.

Type II co-crystals

Among the type II co-crystals, the structure of **3**·$(C_{70})_2$·$(PhCl)_2$ has been reported [63]. Herein, we report the structures of **1**·$(C_{60})_2$·$(CS_2)_2$ and **1**·$(C_{60})_2$·PhCl, and that of **6**·$(C_{60})_2$·$(PhCl)_2$ is provided in the Supporting Information File 1 (Figures S25–S29).

Complex **1**·$(C_{60})_2$·$(CS_2)_2$ crystallizes in the triclinic space group *P*-1. The asymmetric unit contains half a molecule of **1**, two halves of C_{60} (**A** and **B**), and one CS_2 molecule. The central C_6S_4 moieties of both molecules **1** (**A** and **B**) are nearly planar. Molecule **A** is disordered and surrounded by four molecules of **1**. The donor–acceptor interaction mode for molecule **A** is very similar to those in type I co-crystals (Figure 2a): a pair of molecules of **1** forms a sandwich structure with **A** through multiple interactions (C–S, 3.50 Å; C–C, 3.20–3.38 Å), and the other two molecules of **1** interact with **A** along their lateral axes. On the other hand, the C_{60} molecule **B** is ordered and surrounded by four phenyl groups with multiple C–C contacts (3.19–3.38 Å) as shown in Figure 2b. **1** and C_{60} form separated layers (Figures S16–S17 in Supporting Information File 1). The

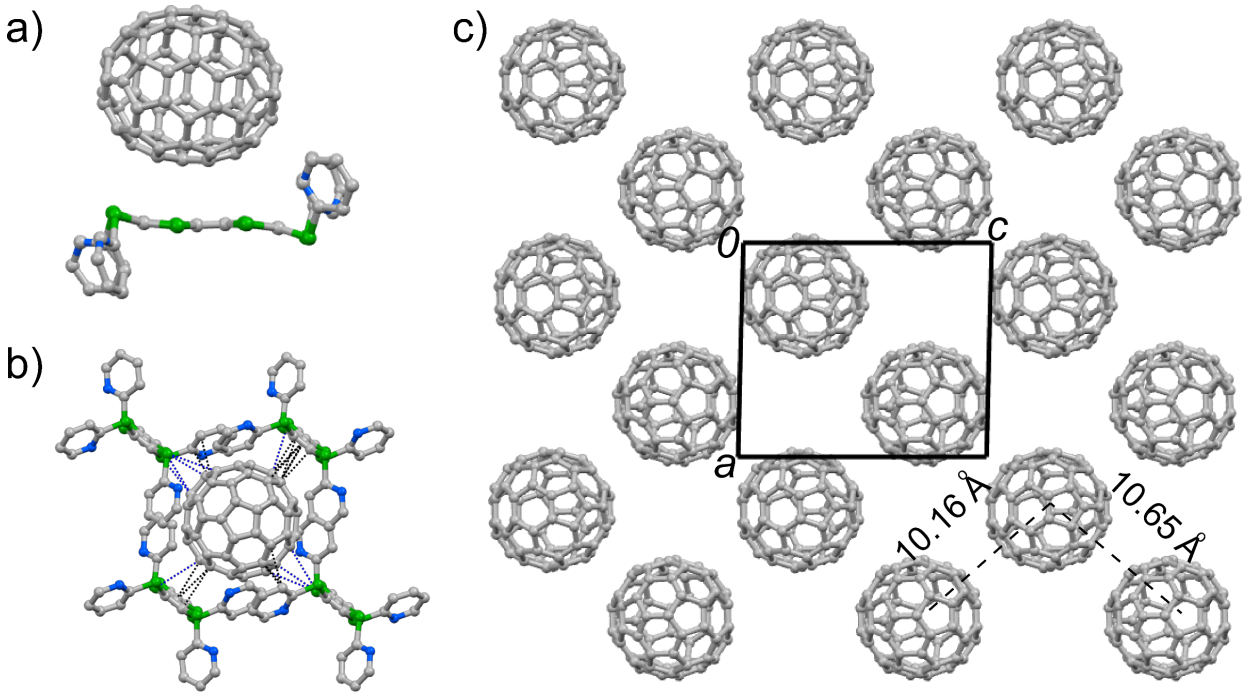

Figure 1: Crystal structure of **5**·C_{70}. a) Unit cell contents viewed along the short axis of **5**; b) Interactions between **5** and C_{70}, where the blue and black dashed lines represent the C–S and C–C contacts, respectively; c) packing motif of C_{70} molecules viewed along the *b*-axis. The grey, blue and green spheres represent carbon, nitrogen and sulfur atoms, respectively, and the hydrogen atoms are omitted for clarity.

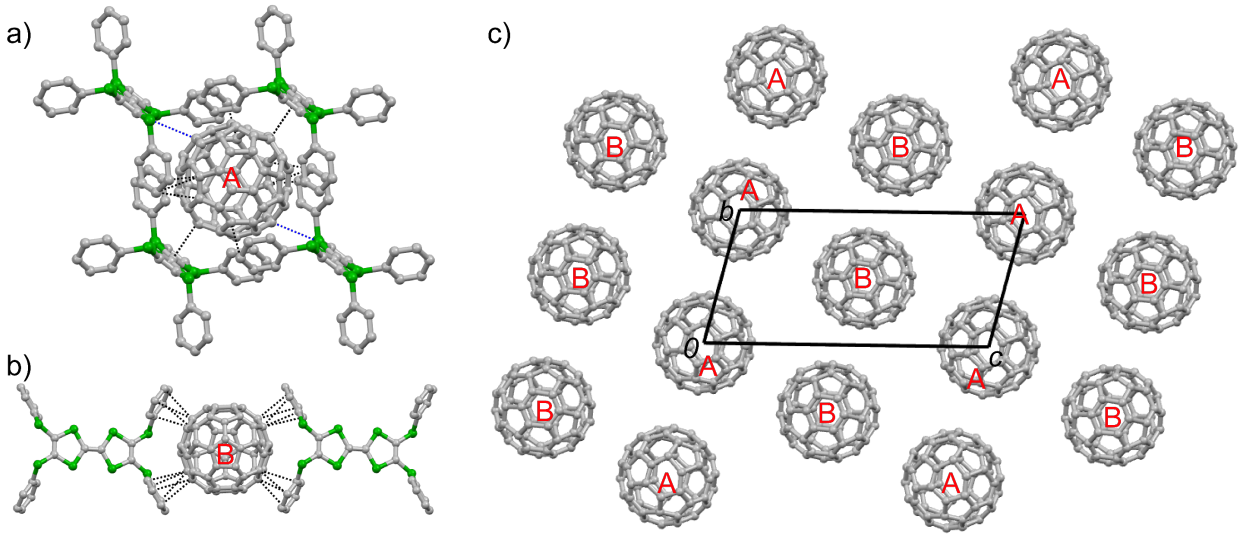

Figure 2: Crystal structure of **1**·$(C_{60})_2$·$(CS_2)_2$. a) Interactions of C_{60} molecule **A** with **1**, where the blue and black dashed lines indicate the C–S and C–C contacts between **1** and C_{60}, respectively. b) Interactions of C_{60} molecule **B** with **1**; c) packing motifs of C_{60}, depiction along the *a*-axis. The hydrogen atoms and solvent molecules are omitted for clarity.

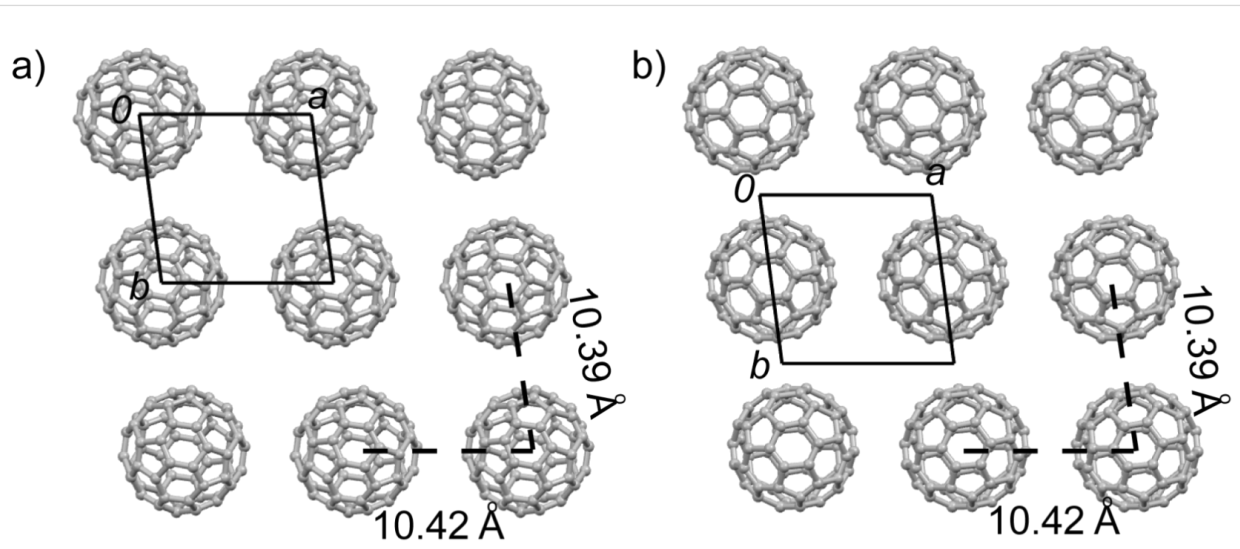

Figure 3: Packing motifs of C_{60} molecules **A** (a) and **B** (b) of **1**·$(C_{60})_2$·$(CS_2)_2$ in the crystallographic *ab*-plane with the center-to-center distance between the neighboring C_{60} molecules shown.

packing structure of C_{60} in the *bc*-plane is shown in Figure 2c. Molecules **A** and **B** form two kinds of two-dimensional (2D) sheets in the *ab*-plane as shown in Figure 3, and two sheets alternate along the *c*-axis. In both 2D sheets, the center-to-center distances between adjacent C_{60} molecules are 10.4 Å along the *a*- and *b*-axes.

Complex **1**·$(C_{60})_2$·PhCl crystallizes in the triclinic space group *P*-1. Unlike **1**·$(C_{60})_2$·$(CS_2)_2$, the asymmetric unit of **1**·$(C_{60})_2$·PhCl contains one molecule of **1**, four halves of C_{60} (**A**, **B**, **C**, and **D**), and one PhCl molecule. The central TTF core of **1** is in a planar conformation. As shown in Figure S18 in Supporting Information File 1, C_{60} molecules **A** and **B** have a donor–acceptor interaction mode similar to those in the type I co-crystals, and several C–C (3.17–3.39 Å) and C–S (3.46–3.49 Å) contacts are observed between the central TTF core of **1** and C_{60} molecules. On the other hand, C_{60} molecules **C** and **D** are surrounded by the phenyl groups of **1** and solvent molecules PhCl (Figure S19 in Supporting Information File 1). The donor and acceptor molecules that form the separated

layers are shown in Figures S20–S24 (Supporting Information File 1). Molecules **A** and **B** form a 2D sheet in the *ab*-plane (Figure S23 in Supporting Information File 1), where **A** and **B** form the different columnar arrays along the *a*-axis. The center-to-center distances between the adjacent C_{60} molecules are around 10.4 Å along the *a*- and *b*-axes. Molecules **C** and **D** also form the 2D sheet in the *ab*-plane (Figure S24 in Supporting Information File 1), and the configuration of the molecular arrays is similar to that in the **AB** sheet. The **AB** and **CD** sheets alternate along the crystallographic *c*-axis.

Co-crystal **2**·$(C_{70})_4$·$(PhCl)_2$

This complex crystallizes in the monoclinic space group *C*2/*n*, and the asymmetric unit contains half of molecule **2**, two C_{70} molecules (**A** and **B**), and two halves of PhCl molecules. The central C_6S_4 moiety of molecule **2** is nearly planar. In types I and II co-crystals, fullerene molecules are encapsulated by Ar-S-TTF molecules. However, in **2**·$(C_{70})_4$·$(PhCl)_2$, molecule **2** penetrates into the void space formed by C_{70} molecules due to the large A:D ratio (4:1). Referring Figure 4, one molecule **2** is surrounded by six C_{70} neighbors. Along the longitudinal and lateral axes of molecule **2**, four **A** molecules are located to show multiple donor–acceptor interactions (Figure 4a): C–C contacts (3.22–3.37 Å) between *p*-tolyl moieties and C_{70} along the longitudinal axis of **2**, and C–S contacts (3.44, 3.47Å) between the central TTF core and C_{70} along the lateral axis of molecule **2**. On the other hand, two **B** molecules are located above and below the mean plane of **2** (Figure 4b), and there are C–S (3.44–3.50 Å) and C–C (3.13, 3.35 Å) contacts between the C_{70} molecules and the central TTF core of **2**. The C_{70} molecules form the 3D network of the present co-crystals. As shown in Figure S30 Supporting Information File 1, one **A** molecule is surrounded by five **B** molecules, and one **B** molecule is surrounded by five **A** molecules. There are multiple C–C close contacts (3.20–3.38 Å) between the neighboring C_{70} molecules along the different directions, which result in the 3D carrier transport pathway [38-41].

Structural comparison

As has previously been reported, the van der Waals length of the C_6S_8 core in the Ar-S-TTF molecule is about 12.8 Å [61,63], which is larger than the van der Waals diameters of C_{60} (10 Å) and C_{70} (11 Å) [65,66]. In this regard, a single Ar-S-TTF molecule is able to encapsulate C_{60}/C_{70}, and the size difference between C_{60} and C_{70} would not be the sole factor determining the composition of the co-crystal. The D:A ratio for the co-crystal is attributed to the cooperation of the geometry of the Ar-S-TTF (particularly the geometry and rotational freedom of the peripheral aryls), the shape and the size of the fullerene molecules, and the solvent molecules. Furthermore, the dynamic effect on the crystal growth is also taken into account.

Additionally, the D:A ratio of the co-crystal plays a significant role on the donor–acceptor interaction mode and the packing motif of the fullerenes. In the type I co-crystals (D:A = 1:1), the donor–acceptor interactions mainly exist between the central TTF core of the Ar-S-TTF and the fullerene molecules. Therefore, Ar-S-TTF serves as the host and the fullerene molecule is the guest. The fullerene molecules form the 1D columnar stacks with a center-to-center distance of around 10.3 Å, which is comparable with that of superconducting C_{60} complexes with alkali metals (e.g.,10.29 Å in $RbCs_2C_{60}$) [67]. When the ratio of fullerene molecules increases (i.e., the type II co-crystals, D:A = 1:2), one fullerene molecule is substantially encapsulated by the central TTF core of Ar-S-TTF, and another

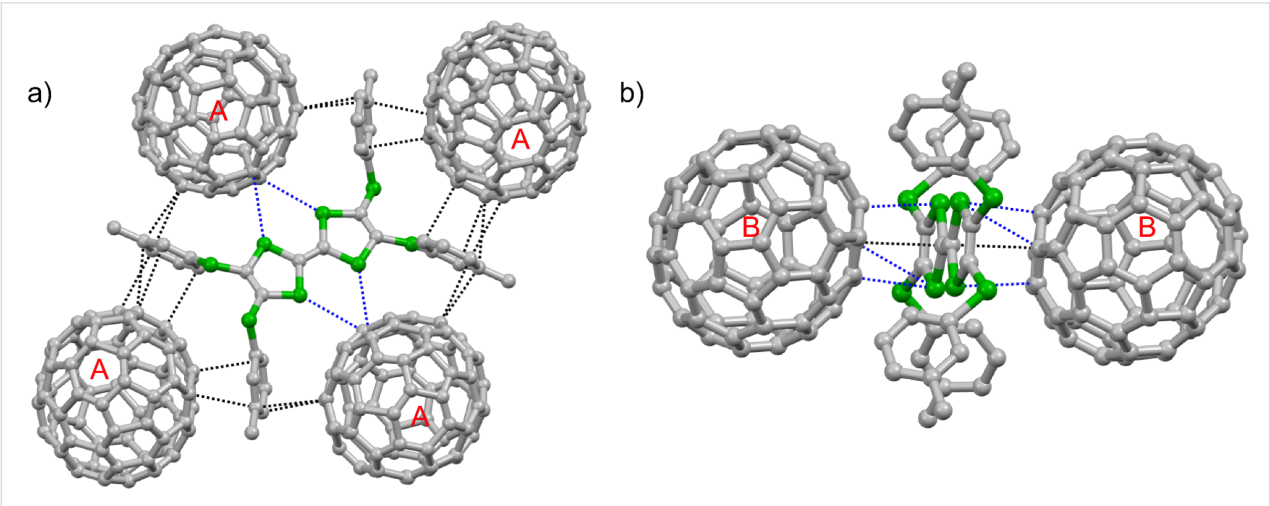

Figure 4: Crystal structure of **2**·$(C_{70})_4$·$(PhCl)_2$. a) Interactions between C_{70} molecule **A** and **2**; b) Interactions between C_{70} molecule **B** and **2**. The blue and black dashed lines indicated the intermolecular C–S and C–C contacts, respectively. The hydrogen atoms are omitted for clarity.

fullerene molecule is surrounded by the aryls on the Ar-S-TTF and solvent molecules. In this case, the Ar-S-TTF molecule still acts as the host for at least one of the fullerene molecules. Moreover, the dimensionality of the packing motifs of fullerene molecules increases, resulting in a 2D network through multiple van der Waals forces. Upon further increase of the ratio of fullerene molecules in the co-crystal (e.g., **2**·$(C_{70})_4$·$(PhCl)_2$), the packing structure becomes dominated by the C_{70} molecule, which forms the 3D network. The Ar-S-TTF and solvent molecules serve as the guests to occupy the void formed by the C_{70} molecules.

The present results demonstrate that Ar-S-TTF molecules have three key features that enable formation of donor–acceptor type co-crystals with fullerenes: (1) size and shape complementarity, (2) flexibility, and (3) the ability to introduce an additional interaction with fullerene by peripheral aryls. While the interactions between the TTF framework and fullerenes have been observed in many TTF–fullerene supramolecular systems [38-41], the rotational freedom of the peripheral aryls on Ar-S-TTF causes the aryls to locate at the appropriate positions to form additional interactions with fullerenes. This therefore enhances the stability of the resulting co-crystals. By complexation with Ar-S-TTF molecules, the 1D columnar array, 2D sheets, and 3D networks of fullerene molecules have been successfully established, resulting in the carrier transport pathway, in principle. However, the ground state of the present co-crystals is intrinsically neutral, as demonstrated by the IR spectra (Figures S34–S40 in Supporting Information File 1). To improve the functionality of the co-crystals, one interesting strategy would be the generation of itinerant carriers in the co-crystals, i.e., charge transfer between the donor and acceptor in the ground state.

Conclusion

In summary, we have prepared eleven donor–acceptor type co-crystals of Ar-S-TTFs with fullerenes (C_{60}/C_{70}), and performed thorough investigations on their solid state structures. These co-crystals mainly belong to two types according to the donor:acceptor ratios (D:A), types I and II having D:A of 1:1 and 1:2, respectively. The composition of the co-crystals is thought to be the cooperative consequence of the molecular geometry of Ar-S-TTF, the shape and size of the fullerene molecule, the solvent adduct, and the crystallization dynamics. The donor–acceptor interaction mode and the packing motif of the fullerenes largely depend on the composition of the co-crystal. The present results suggest that Ar-S-TTF molecules would be promising receptors for fullerenes as they are easily accessible. Meanwhile, Ar-S-TTFs possess the unique structural features to encapsulate fullerenes. That means the size matches with that of fullerenes and the flexibility is helpful to adapt to the shape of the fullerenes, which is supported by the additional stabilization force from the peripheral aryls moieties. Moreover, by varying the peripheral aryls and solvents, the 1D, 2D, and 3D packing motifs of fullerenes can be selectively achieved.

Supporting Information

Supporting Information File 1

Additional experimental data.
[http://www.beilstein-journals.org/bjoc/content/supplementary/1860-5397-11-117-S1.pdf]

Supporting Information File 2

Crystallographic data in CIF format.
[http://www.beilstein-journals.org/bjoc/content/supplementary/1860-5397-11-117-S2.cif]

Acknowledgements

This work was financially supported by National Natural Science Foundation of China (21372111 and 21172104) and Research Fund for the Doctoral Program of Higher Education of China (RFDP 20120211110039).

References

1. Wudl, F.; Smith, G. M.; Hufnagel, E. J. *J. Chem. Soc. D* **1970,** 1453. doi:10.1039/C29700001453
2. Coffen, D. L.; Chambers, J. Q.; Williams, D. R.; Garrett, P. E.; Canfield, N. D. *J. Am. Chem. Soc.* **1971,** *93,* 2258. doi:10.1021/ja00738a028
3. Hünig, S.; Kiesslich, G.; Scheutzow, D.; Zahradnik, R.; Carsky, P. *Int. J. Sulfur Chem., Part C* **1971,** *6,* 109. doi:10.1016/0368-2048(73)80012-X
4. Williams, J. M.; Ferraro, J. R.; Thorn, R. J.; Carlson, K. D.; Geiser, U.; Wang, H. H.; Kini, A. M.; Whangbo, M. H. *Organic Superconductors (including Fullerenes);* Prentice Hall: Englewood Cliffs, NJ, U.S.A., 1992.
5. Ishiguro, T.; Yamaji, K.; Saito, G. *Organic Superconductors,* 2nd ed.; Springer: Berlin, Germany, 1998.
6. Batail, P., Ed. Molecular Conductors. *Chem. Rev.* **2004,** *104,* 4887–5782.
7. Kagoshima, S.; Kanoda, K.; Mori, T., Eds. Organic Conductors. *J. Phys. Soc. Jpn.* **2006,** *75,* 051001–051802.
8. Lebed, A. *The Physics of Organic Superconductors and Conductors;* Springer: Berlin, Germany, 2008.
9. Ardavan, A.; Brown, S.; Kagoshima, S.; Kanoda, K.; Kuroki, K.; Mori, H.; Ogata, M.; Uji, S.; Wosnitza, J. *J. Phys. Soc. Jpn.* **2012,** *81,* 011004.
10. Ferraris, J.; Cowan, D. O.; Walatka, V.; Perlstein, J. H. *J. Am. Chem. Soc.* **1973,** *95,* 948. doi:10.1021/ja00784a066
11. Jérome, D.; Mazaud, A.; Ribault, M.; Bechgaard, K. *J. Phys., Lett.* **1980,** *41,* 95. doi:10.1051/jphyslet:0198000410409500
12. Bryce, M. R. *Chem. Soc. Rev.* **1991,** *20,* 355. doi:10.1039/CS9912000355

13. Adam, M.; Müllen, K. *Adv. Mater.* **1994,** *6,* 439. doi:10.1002/adma.19940060603
14. Jørgensen, T.; Hansen, T. K.; Becher, J. *Chem. Soc. Rev.* **1994,** *23,* 41. doi:10.1039/CS9942300041
15. Garían, J. *Adv. Heterocycl. Chem.* **1995,** *62,* 249. doi:10.1016/S0065-2725(08)60423-7
16. Coronado, E.; Gómez-García, C. J. *Chem. Rev.* **1998,** *98,* 273. doi:10.1021/cr970471c
17. Bryce, M. R. *Adv. Mater.* **1999,** *11,* 11. doi:10.1002/(SICI)1521-4095(199901)11:1<11::AID-ADMA11>3.0.CO;2-3
18. Nielsen, M. B.; Lomholt, C.; Becher, J. *Chem. Soc. Rev.* **2000,** *29,* 153. doi:10.1039/A803992E
19. Segura, J. L.; Martín, N. *Angew. Chem., Int. Ed.* **2001,** *40,* 1372. doi:10.1002/1521-3773(20010417)40:8<1372::AID-ANIE1372>3.0.CO;2-I
20. Bendikov, M.; Wudl, F.; Perepichka, D. F. *Chem. Rev.* **2004,** *104,* 4891. doi:10.1021/cr030666m
21. Frère, P.; Skabara, P. J. *Chem. Soc. Rev.* **2005,** *34,* 69. doi:10.1039/B316392J
22. Canevet, D.; Sallé, M.; Zhang, G.; Zhang, D.; Zhu, D. *Chem. Commun.* **2009,** 2245. doi:10.1039/B818607N
23. Martín, N.; Sánchez, L.; Seoane, C.; Andreu, R.; Garín, J.; Orduna, J. *Tetrahedron Lett.* **1996,** *37,* 5979. doi:10.1016/0040-4039(96)01235-X
24. Martín, N.; Sánchez, L.; Herranz, M. Á.; Guldi, D. M. *J. Phys. Chem. A* **2000,** *104,* 4648. doi:10.1021/jp9941458
25. Giacalone, F.; Segura, J. L.; Martín, N.; Guldi, D. M. *J. Am. Chem. Soc.* **2004,** *126,* 5340. doi:10.1021/ja0318333
26. Fernández, G.; Pérez, E. M.; Sánchez, L.; Martín, N. *Angew. Chem., Int. Ed.* **2008,** *47,* 1094. doi:10.1002/anie.200703049
27. Fernández, G.; Pérez, E. M.; Sánchez, L.; Martín, N. *J. Am. Chem. Soc.* **2008,** *130,* 2410. doi:10.1021/ja710505h
28. Pérez, E. M.; Sánchez, L.; Fernández, G.; Martín, N. *J. Am. Chem. Soc.* **2006,** *128,* 7172. doi:10.1021/ja0621389
29. Pérez, E. M.; Sierra, M.; Sánchez, L.; Torres, M. R.; Viruela, R.; Viruela, P. M.; Ortí, E.; Martín, N. *Angew. Chem., Int. Ed.* **2007,** *46,* 1847. doi:10.1002/anie.200604327
30. Fernández, G.; Sánchez, L.; Pérez, E. M.; Martín, N. *J. Am. Chem. Soc.* **2008,** *130,* 10674. doi:10.1021/ja8018498
31. Isla, H.; Gallego, M.; Pérez, E. M.; Viruela, R.; Ortí, E.; Martín, N. *J. Am. Chem. Soc.* **2010,** *132,* 1772. doi:10.1021/ja910107m
32. Huerta, E.; Isla, H.; Pérez, E. M.; Bo, C.; Martín, N.; de Mendoza, J. *J. Am. Chem. Soc.* **2010,** *132,* 5351. doi:10.1021/ja1006993
33. Grimm, B.; Santos, J.; Illescas, B. M.; Muñoz, A.; Guldi, D. M.; Martín, N. *J. Am. Chem. Soc.* **2010,** *132,* 17387. doi:10.1021/ja108744a
34. Canevet, D.; Gallego, M.; Isla, H.; de Juan, A.; Pérez, E. M.; Martín, N. *J. Am. Chem. Soc.* **2011,** *133,* 3184. doi:10.1021/ja111072j
35. Fukuzumi, S.; Ohkubo, K.; Kawashima, Y.; Kim, D. S.; Park, J. S.; Jana, A.; Lynch, V. M.; Kim, D.; Sessler, J. L. *J. Am. Chem. Soc.* **2011,** *133,* 15938. doi:10.1021/ja207588c
36. Zhou, Z.; Qin, Y.; Xu, W.; Zhu, D. *Chem. Commun.* **2014,** *50,* 4082. doi:10.1039/c4cc00741g
37. Nielsen, K. A.; Cho, W.-S.; Sarova, G. H.; Petersen, B. M.; Bond, A. D.; Becher, J.; Jensen, F.; Guldi, D. M.; Sessler, J. L.; Jeppesen, J. O. *Angew. Chem., Int. Ed.* **2006,** *45,* 6848. doi:10.1002/anie.200602724
38. Izuoka, A.; Tachikawa, T.; Sugawara, T.; Suzuki, Y.; Konno, M.; Saito, Y.; Shinohara, H. *J. Chem. Soc., Chem. Commun.* **1992,** 1472. doi:10.1039/C39920001472
39. Konarev, D. V.; Semkin, V. N.; Graja, A.; Lyubovskaya, R. N. *J. Mol. Struct.* **1998,** *450,* 11. doi:10.1016/S0022-2860(98)00408-6
40. Saito, G.; Sasaki, H.; Aoki, T.; Yoshida, Y.; Otsuka, A.; Yamochi, H.; Drozdova, O. O.; Yakushi, K.; Kitagawa, H.; Mitani, T. *J. Mater. Chem.* **2002,** *12,* 1640. doi:10.1039/B110605H
41. Konarev, D. V.; Khasanov, S. S.; Saito, G.; Otsuka, A.; Lyubovskaya, R. N. *J. Mater. Chem.* **2007,** *17,* 4171. doi:10.1039/B704371F
42. Pérez, E. M.; Marín, N. *Chem. Soc. Rev.* **2008,** *37,* 1512. doi:10.1039/B802589B
43. Yamada, J.; Sugimoto, T., Eds. *TTF Chemistry: Fundamentals and Applications of Tetrathiafulvalenes;* Springer: Berlin, Germany, 2004.
44. Hervé, K.; Liu, S.-X.; Cador, O.; Golhen, S.; Gal, Y. L.; Bousseksou, A.; Stoeckli-Evans, H.; Decurtins, S.; Ouahab, L. *Eur. J. Inorg. Chem.* **2006,** 3498. doi:10.1002/ejic.200600351
45. Jia, C.; Liu, S.-X.; Tanner, C.; Leiggener, C.; Neels, A.; Sanguinet, L.; Levillain, E.; Leutwyler, S.; Hauser, A.; Decurtins, S. *Chem. – Eur. J.* **2007,** *13,* 3804. doi:10.1002/chem.200601561
46. Murata, T.; Morita, Y.; Yakiyama, Y.; Fukui, K.; Yamochi, H.; Saito, G.; Nakasuji, K. *J. Am. Chem. Soc.* **2007,** *129,* 10837. doi:10.1021/ja072607m
47. Zhu, Q.-Y.; Liu, Y.; Lu, W.; Zhang, Y.; Bian, G.-Q.; Niu, G.-Y.; Dai, Y. *Inorg. Chem.* **2007,** *46,* 10065. doi:10.1021/ic700672e
48. Wu, J.-C.; Liu, S.-X.; Keene, T. D.; Neels, A.; Mereacre, V.; Powell, A. K.; Decurtins, S. *Inorg. Chem.* **2008,** *47,* 3452. doi:10.1021/ic800138x
49. Fujiwara, H.; Sugishima, Y.; Tsujimoto, K. *Tetrahedron Lett.* **2008,** *49,* 7200. doi:10.1016/j.tetlet.2008.10.001
50. Zhu, Q.-Y.; Huo, L.-B.; Qin, Y.-R.; Zhang, Y.-P.; Lu, Z.-J.; Wang, J.-P.; Dai, J. *J. Phys. Chem. B* **2010,** *114,* 361. doi:10.1021/jp908399r
51. Jaggi, M.; Blum, C.; Marti, B. S.; Liu, S.-X.; Leutwyler, S.; Decurtins, S. *Org. Lett.* **2010,** *12,* 1344. doi:10.1021/ol1002708
52. Mitamura, Y.; Yorimitsu, H.; Oshima, K.; Osuka, A. *Chem. Sci.* **2011,** *2,* 2017. doi:10.1039/C1SC00372K
53. Lincke, K.; Frellsen, A. F.; Parker, C. R.; Bond, A. D.; Hammerich, O.; Nielsen, M. B. *Angew. Chem., Int. Ed.* **2012,** *51,* 6099. doi:10.1002/anie.201202324
54. Ueno, R.; Fujino, D.; Yorimitsu, H.; Osuka, A. *Chem. – Eur. J.* **2013,** *19,* 7156. doi:10.1002/chem.201300623
55. Yamashita, Y.; Kobayashi, Y.; Miyashi, T. *Angew. Chem., Int. Ed. Engl.* **1989,** *28,* 1052. doi:10.1002/anie.198910521
56. Christensen, C. A.; Batsanov, A. S.; Bryce, M. R. *J. Org. Chem.* **2007,** *72,* 1301. doi:10.1021/jo062199p
57. Kato, T.; Origuchi, C.; Shinoda, M.; Adachi, C. *Jpn. J. Appl. Phys.* **2011,** *50,* 050202. doi:10.1143/JJAP.50.050202
58. Yamashita, M.; Kuzuhara, D.; Aratani, N.; Yamada, H. *Chem. – Eur. J.* **2014,** *20,* 6309. doi:10.1002/chem.201304997
59. Nielsen, K. A.; Cho, W.-S.; Jeppesen, J. O.; Lynch, V. M.; Becher, J.; Sessler, J. L. *J. Am. Chem. Soc.* **2004,** *126,* 16296. doi:10.1021/ja044664a
60. Sun, J.; Lu, X.; Shao, J.; Cui, Z.; Shao, Y.; Jiang, G.; Yu, W.; Shao, X. *RSC Adv.* **2013,** *3,* 10193. doi:10.1039/C3RA41349G
61. Sun, J.; Lu, X.; Shao, J.; Li, X.; Zhang, S.; Wang, B.; Zhao, J.; Shao, Y.; Fang, R.; Wang, Z.; Yu, W.; Shao, X. *Chem. – Eur. J.* **2013,** *19,* 12517. doi:10.1002/chem.201301819
62. Lu, X.; Sun, J.; Liu, Y.; Shao, J.; Ma, L.; Zhang, S.; Zhao, J.; Shao, Y.; Zhang, H.-L.; Wang, Z.; Shao, X. *Chem. – Eur. J.* **2014,** *20,* 9650. doi:10.1002/chem.201402327

63. Sun, J.; Lu, X.; Ishikawa, M.; Nakano, Y.; Zhang, S.; Zhao, J.; Shao, Y.; Wang, Z.; Yamochi, H.; Shao, X. *J. Mater. Chem. C* **2014,** *2,* 8017. doi:10.1039/c4tc01362j
64. Bondi, A. *J. Phys. Chem.* **1964,** *68,* 441. doi:10.1021/j100785a001
65. Krätschmer, W.; Lamb, L. D.; Fostiropoulos, K.; Huffman, D. R. *Nature* **1990,** *347,* 354. doi:10.1038/347354a0
66. Hawkins, J. M.; Lewis, T. A.; Loren, S. D.; Meyer, A.; Heath, J. R.; Saykally, R. J.; Hollander, F. J. *J. Chem. Soc., Chem. Commun.* **1991,** 775. doi:10.1039/C39910000775
67. Tanigaki, K.; Prassides, K. *J. Mater. Chem.* **1995,** *5,* 1515. doi:10.1039/JM9950501515

License and Terms

BEILSTEIN JOURNAL OF ORGANIC CHEMISTRY

A hybrid electron donor comprising cyclopentadithiophene and dithiafulvenyl for dye-sensitized solar cells

Gleb Sorohhov[1], Chenyi Yi[2], Michael Grätzel[2], Silvio Decurtins[1] and Shi-Xia Liu[*1]

Full Research Paper

Open Access

Address:
[1]Departement für Chemie und Biochemie, Universität Bern, Freiestrasse 3, CH-3012 Bern, Switzerland and [2]Laboratory of Photonics and Interfaces, Institute of Chemical Science and Engineering, École Polytechnique Fédérale de Lausanne (EPFL), Station 6, CH-1050 Lausanne, Switzerland

Email:
Shi-Xia Liu[*] - liu@dcb.unibe.ch

* Corresponding author

Keywords:
donor–acceptor systems; dye-sensitized solar cells; electrochemistry; intramolecular charge transfer; Knoevenagel reaction; tetrathiafulvalene

Beilstein J. Org. Chem. **2015,** *11,* 1052–1059.
doi:10.3762/bjoc.11.118

Received: 17 April 2015
Accepted: 05 June 2015
Published: 22 June 2015

This article is part of the Thematic Series "Tetrathiafulvalene chemistry".

Guest Editor: P. J. Skabara

Abstract

Two new photosensitizers featured with a cyanoacrylic acid electron acceptor (A) and a hybrid electron donor (D) of cyclopentadithiophene and dithiafulvenyl, either directly linked or separated by a phenyl ring, were synthesized and characterized. Both of them undergo two reversible oxidations and strongly absorb in the visible spectral region due to a photo-induced intramolecular charge-transfer (ICT) transition. To a great extent, the electronic interaction between the D and A units is affected by the presence of a phenyl spacer. Without a phenyl ring, the D unit appears more difficult to oxidize due to a strong electron-withdrawing effect of the A moiety. In sharp contrast, the insertion of the phenyl ring between the D and A units leads to a broken π-conjugation and therefore, the oxidation potentials remain almost unchanged compared to those of an analogue without the A group, suggesting that the electronic coupling between D and A units is relatively weak. As a consequence, the lowest-energy absorption band shows a slight hypsochromic shift upon the addition of the phenyl spacer, indicative of an increased HOMO–LUMO gap. In turn, the direct linkage of D and A units leads to an effective π-conjugation, thus substantially lowering the HOMO–LUMO gap. Moreover, the application in dye-sensitized solar cells was investigated, showing that the power conversion efficiency increases by the insertion of the phenyl unit.

Introduction

Dye-sensitized solar cells (DSSCs) have been intensively investigated as an alternative to silicon-based solar cells [1-4]. Although devices with the most commonly used dyes based on polypyridyl transition-metal complexes show excellent photovoltaic performances with high power conversion efficiencies of over 11% [4], metal-free organic dyes have significant advantages in several aspects. These comprise for example large molar extinction coefficients, ease of synthesis, fine-

tuning of structural and electronic properties, and low-cost production [1-4]. Particularly, the hitherto best DSSC based on organic sensitizers shows an efficiency of 10.3% [5]. Among the most efficient organic dyes are those featured with an electron-donor (D) and an electron-acceptor (A) unit linked through a π-bridge, leading to a broad and intense optical absorption band in the visible spectral region due to an effective intramolecular charge transfer (ICT) from D to A units. To develop high-efficient DSSCs, a variety of organic donors [2,6-8] have been used in the construction of photosensitizers. Not surprisingly, tetrathiafulvalene (TTF), as a strong π-electron donor, has been incorporated into different D–π–A systems for numerous potential applications [9-14]. However, TTF-sensitized solar cells have rarely been explored [15-17], mainly due to the high-lying HOMO energy levels leading to a thermodynamically unfavorable dye regeneration. To overcome this problem, we recently applied a Schiff-base reaction to obtain a rigid and planar quinoxaline-fused TTF-based dye that shows an intense optical ICT absorption over a wide spectral range and a substantially stabilized HOMO, leading to a power conversion efficiency of ca. 6.5% [17]. This example represents the currently best performance for TTF-sensitized solar cells. An alternative approach is based on dithiafulvene (DTF), which from a structural point of view, can be treated as half of a TTF unit. DTF-based D–π–A sensitizers have been proven quite promising with high power conversion efficiencies of up to 8.3% [18,19].

Taking into account all these considerations, we set ourselves the synthetic task to prepare two new molecular dyes (Figure 1) configured with DTF-substituted 4,4-dihexyl-4*H*-cyclopenta[2,1-*b*:3,4-*b'*]dithiophene (CPDT) as an electron-donor and cyanoacrylic acid as an electron-acceptor moiety. The incorporation of the rigid and coplanar electron-donating moiety CPDT to the DTF core could increase the electron-donating ability of the dyes, beneficial for the electron-injection process. In addition, on the one hand, the presence or absence of a phenyl ring between the D and A units in the organic sensitizers is expected to tailor the frontier orbital energy level, which is an essential aspect for good device performance. On the other hand, the presence of side chains on both DTF and CPDT moieties could prevent dye aggregation and thus retard charge recombination. Herein, we describe the preparation, characterization and the electronic properties of two new organic dyes as well as their application in DSSCs.

Results and Discussion

Synthesis

Under Knoevenagel condensation reaction conditions, the corresponding aldehydes **4** and **7** can readily react with cyanoacetic acid leading to the target sensitizers **1** and **2**, as depicted in Scheme 1. For the synthesis of the aldehyde precursor **4**, the Horner–Wadsworth–Emmons (HWE) reaction [20] of 4,5-bis(hexylthio)-1,3-dithiole-2-thione with the dialdehyde CPDT **3** [21] was successfully applied. The preparation of the latter was accomplished in 57% yield through the reaction of 4,4-dihexyl-4*H*-cyclopenta[2,1-*b*:3,4-*b'*]dithiophene [22] with oxalyl chloride in the presence of DMF. However, the synthesis of the key intermediate **7** involves the protection of one aldehyde group as an acetal using pinacol prior to HWE reaction of **5** with 4,5-bis(hexylthio)-1,3-dithiole-2-thione, followed by deprotection under acidic conditions. Aldehyde **5** was readily obtained by palladium-catalyzed Suzuki–Miyaura coupling reaction between 4,4,5,5-tetramethyl-2-(4-(4,4,5,5-tetramethyl-1,3-dioxolan-2-yl)phenyl)-1,3,2-dioxaborolane and 6-bromo-4,4-dihexyl-4*H*-cyclopenta[2,1-*b*:3,4-*b'*]dithiophene-2-carbaldehyde [23]. All these new precursors and the two target dyes **1** and **2** were purified by chromatography and characterized by NMR and HRMS analyses.

Electronic properties

To estimate the energy values of the frontier orbitals (HOMO and LUMO) of dyes **1** and **2** that are essential for the evaluation of two critical processes in DSSC devices, namely the electron injection from the photo-excited sensitizer to the TiO_2

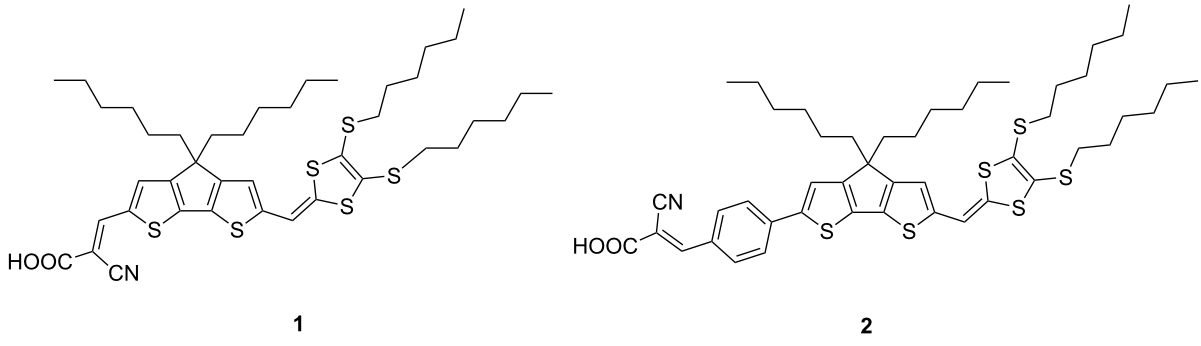

Figure 1: Chemical structures of the target dyes **1** and **2**.

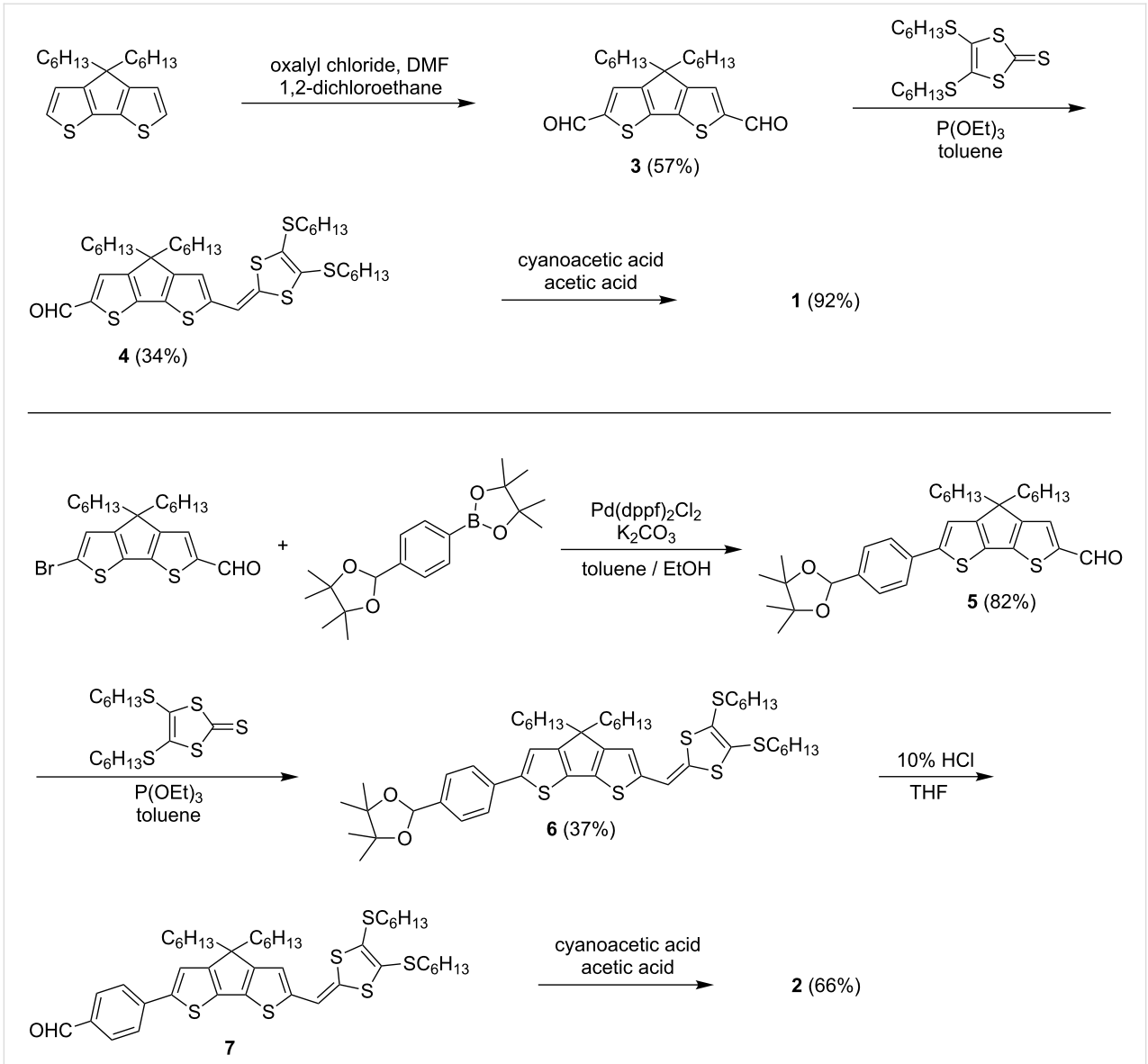

Scheme 1: Synthetic routes to the target dyes **1** (top) and **2** (bottom).

conduction band and the dye regeneration, the corresponding electrochemical and photophysical properties were investigated. As depicted in Figure 2, cyclic voltammograms of dyes **1** and **2** in CH_2Cl_2 show two reversible oxidation waves. To gain additional insight into the redox processes, the cyclic voltammetry of the reference compound **6** was carried out as well. The latter undergoes two reversible oxidations at 0.44 V and 0.75 V vs Fc^+/Fc, hence at values which are lower than the oxidation potentials of the individual components DTF [24] and CPDT [25]. This observation indicates the formation of an extended hybrid donor as the HOMO is delocalized over the DTF and CPDT moieties. Compared to **6**, dye **2** is only marginally more difficult to oxidize as evidenced by slightly more positive values for both oxidation potentials (0.02 V and 0.03 V, respectively, Table 1). This is due to the electron-withdrawing effect of the cyanoacrylic acid. Obviously, the electronic interaction between D and A units is fairly weak because the π-conjugation is partially broken upon the insertion of the phenyl ring which can adopt a non-coplanar conformation. In contrast to **2**, **1** is much more difficult to oxidize as its oxidation potentials (0.63 V and 0.99 V vs Fc^+/Fc) are substantially shifted to positive values by 0.17 V and 0.21 V, respectively, suggesting a stronger electronic interaction between the D and A moieties. Clearly, the insertion of the phenyl ring has a significant effect on the redox potentials. Moreover, the energies of the HOMO levels of dyes **1** and **2** are −5.36 eV and −5.17 eV, respectively (Table 1), and thus they are lower than the energy level of the Co^{3+}/Co^{2+} redox shuttle [26,27]. It can

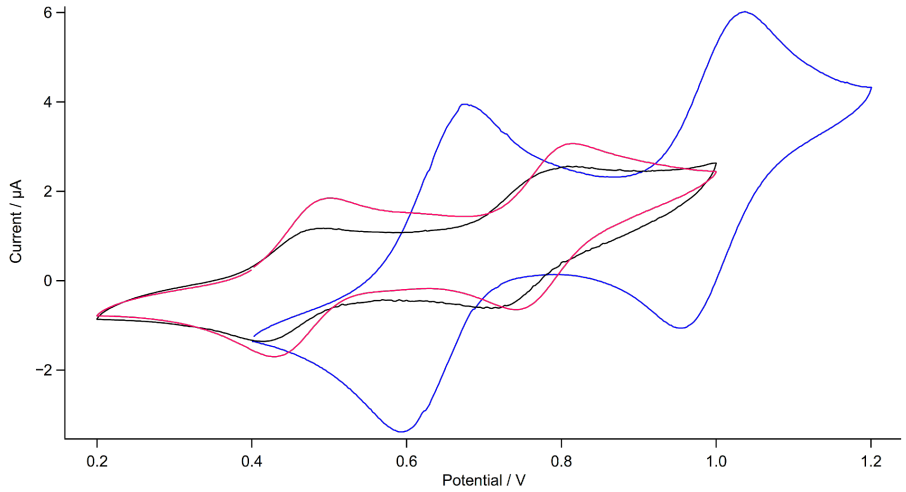

Figure 2: Cyclic voltammograms of **1** (blue line), **2** (red line) and **6** (black line) in CH_2Cl_2 (0.1 M Bu_4NPF_6; Pt working electrode; scan rate 100 mV s^{-1}).

Table 1: Optical and electrochemical data, HOMO and LUMO energy levels of the dyes **1** and **2**.

	λ_{max} (nm)	ε (M^{-1} cm^{-1})	E_g^{opt} (eV)[a]	$E_{1/2}^1$ (V)[b]	$E_{1/2}^2$ (V)[b]	E_{HOMO} (eV)[c]	E_{LUMO} (eV)[d]
1	577	74500	1.82	0.63	0.99	−5.36	−3.54
2	548	56700	1.86	0.46	0.78	−5.17	−3.31

[a]The optical band gap is estimated from the onset of the lowest-energy absorption band. [b]The oxidation potential of Fc^+/Fc against Ag/AgCl was recorded in a CH_2Cl_2/Bu_4NPF_6 (0.1 M) solution to be 0.49 V, therefore the half-wave potentials are converted to Fc^+/Fc by subtracting 0.49 V from the corresponding Ag/AgCl values. [c]The HOMO level is calculated from the onset of the first oxidation potential in cyclic voltammetry, according to the equation $E_{HOMO} = [-e(E_{onset} + 4.8)]$ eV, where 4.8 eV is the energy level of ferrocene below the vacuum level. [d]The LUMO level is estimated according to the equation $E_{LUMO} = [E_g^{opt} + E_{HOMO}]$ eV.

therefore be deduced that the oxidized dyes can efficiently be regenerated.

The UV–vis absorption measurements of sensitizers **1** and **2** were performed in CH_2Cl_2 solutions and the spectra are shown in Figure 3. Both of them reveal quite similar absorption patterns with an intense and broad absorption band in the visible region peaking at 577 nm (17330 cm^{-1}) and 548 nm (18250 cm^{-1}), respectively, with high extinction coefficients on the order of 6×10^4 M^{-1} cm^{-1} (Table 1). The lowest-energy absorption band is attributed to ICT transitions originating from electronic excitations from MOs spread over the hybrid donor to the MO localized on the cyanoacrylic acid. Compared to **2**, sensitizer **1** shows for the lowest-energy absorption band a higher extinction coefficient and a slight red shift by virtue of the more extended π-conjugation. Based on the onset of the lowest-energy absorption band, the HOMO–LUMO gap is estimated to be 1.82 eV for **1** and 1.86 eV for **2**. Therefore, the values of their LUMO energy levels of −3.54 eV and −3.31 eV (Table 1) ensure an efficient electron injection from the photoexcited dyes to TiO_2. As a consequence, the direct linkage of the D and A units leads to an effective π-conjugation and a planar molecular configuration, thus substantially lowering the HOMO–LUMO gap, while the insertion of the phenyl spacer causes a partially interrupted π-conjugation, hence the electronic interactions between the D and A units are weaker. This result is in good agreement with the aforementioned electrochemical data.

Photovoltaic properties

DSSC devices based on sensitizers **1** and **2** were investigated with both I^-/I^{3-} and Co^{2+}/Co^{3+} electrolytes and the detailed photovoltaic parameters, such as short-circuit photocurrent density (J_{sc}), open-circuit voltage (V_{oc}), fill factor (*FF*), and power conversion efficiency (η) are listed in Table 2. As depicted in Figure 4, the presence of the phenyl spacer has a pronounced effect on the DSSC device performances. Although dye **1** has a slightly better light-harvesting ability and the HOMO level of **2** is energetically higher than that of **1**, both the J_{sc} and V_{oc} values increase on going from **1** to **2**, leading to an increase of the η value from 2.18% to 4.12% with cobalt tris(bipyridine)-based redox mediator. With iodide/triiodide

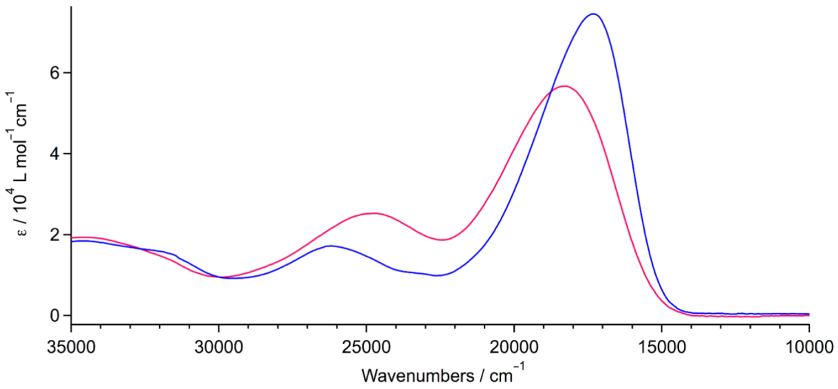

Figure 3: Electronic absorption spectra of **1** (blue line) and **2** (red line) in CH_2Cl_2 solutions.

Table 2: Photovoltaic performances of DSSCs based on dyes **1** and **2**.

	J_{sc} (mA cm^{-2})	V_{oc} (mV)	*FF*	η(%)
1 (Co^{2+}/Co^{3+})	3.97	632	0.78	2.18
2 (Co^{2+}/Co^{3+})	7.27	687	0.77	4.12
1 (I^-/I^{3-})	9.26	485	0.72	3.19
2 (I^-/I^{3-})	12.26	493	0.69	4.13

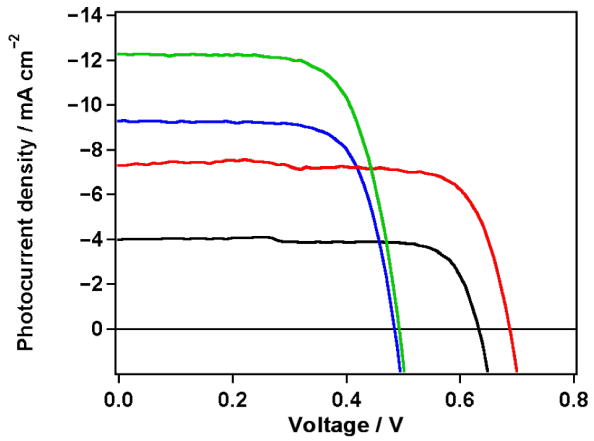

Figure 4: Photovoltaic performance of the two sensitizers. Photocurrent density (*J*) as a function of voltage (V) for **1** (black and blue curves) and **2** (red and green curves) measured under standard air mass 1.5 and simulated sunlight at 1000 W/m^2 intensity.

as redox shuttle, both devices based on dye **1** and dye **2** showed higher photocurrent densities of 9.26 mA cm^{-2} and 12.26 mA cm^{-2}, respectively. However, they showed lower photovoltages of 485 mV and 493 mV. As a result, in the presence of the iodine-based electrolyte, the PCEs for **1** and **2** were 3.19% and 4.13%, respectively. The higher photocurrent of dye **2** is probably due to a lower charge recombination because of the large distortion between the donor and the anchoring acceptor. On the other hand, the planar structure of **1** with full π-conjugation increases the propensity of dye aggregation on the TiO_2 surface, leading to a decrease of the electron-injection yield, too.

Overall, the dyes show a relatively poor DSSC performance compared to the analogous systems reported in the literature so far [18,19], which is mainly due to substantial charge recombination losses during the electron-injection process, very probably caused by self-aggregation on the TiO_2 surface and fast back-electron transfer upon photoexcitation.

Conclusion

In summary, we have synthesized two new organic photosensitizers featured with a DTF–CPDT hybrid as an electron donor and a cyanoacrylic acid either directly linked or linked through a phenyl spacer. Both of them show two reversible oxidations and strongly absorb in the visible spectral region. As evidenced by electrochemical and optical data, the electronic interaction between the D and A units is greatly affected by the presence of a phenyl spacer. For dye **1**, without a phenyl ring, the D unit appears more difficult to oxidize due to a strong the electron-withdrawing effect of the A moiety, and also the lowest-energy absorption band shows a slight bathochromic shift compared to that for dye **2** with a phenyl spacer. As a consequence, the direct linkage of the D and A units leads to an effective π-conjugation,

thus substantially lowering the HOMO–LUMO gap and increasing the light-harvesting ability. The application in dye-sensitized solar cells was further investigated, showing that the power conversion efficiency increases by insertion of a phenyl ring spacer. To further enhance the device performance by retarding charge recombination upon photoexcitation and increasing the charge injection efficiency, appropriate modifications of the structures of sensitizers based on the DTF–CPDT hybrid donor are currently undertaken.

Experimental

General

Air and/or water-sensitive reactions were conducted under nitrogen in dry, freshly distilled solvents. ^{1}H NMR and ^{13}C NMR spectra were recorded on a Bruker Avance 300 spectrometer operating at 300 MHz for ^{1}H and 75.5 MHz for ^{13}C. Chemical shifts are reported in parts per million (ppm) and are referenced to the residual solvent peak (chloroform, ^{1}H = 7.26 ppm, ^{13}C = 77.0 ppm; dichloromethane, ^{1}H = 5.32 ppm, ^{13}C = 54.00). Coupling constants (*J*) are given in Hertz (Hz). Peak multiplicities are described in the following way: s, singlet; d, doublet; t, triplet; m, multiplet. HRMS data were obtained with electrospray ionization (ESI). Cyclic voltammetry was performed in a three-electrode cell equipped with a platinum-disk working electrode, a glassy carbon counter electrode, and Ag/AgCl was used as the reference electrode. The electrochemical experiments were carried out under dry conditions and an oxygen-free atmosphere in dichloromethane with 0.1 M $Bu_4N(PF_6)$ as a supporting electrolyte. The voltammograms were recorded on a PGSTAT 101 potentiostat. Absorption spectra were recorded on a Perkin Elmer Lambda 900 UV/Vis/NIR spectrometer.

Synthesis of 3: In a similar manner as described in [22], oxalyl chloride (0.872 g, 6.86 mmol) was added to a cold solution of 4,4-dihexyl-4*H*-cyclopenta[2,1-*b*:3,4-*b'*]dithiophene (0.301 g, 0.86 mmol) and *N,N*-dimethylformamide (0.502 g, 6.87 mmol) in 1,2-dichloroethane (10 mL) at 0 °C under nitrogen protection. After stirring at constant temperature for 3 h, saturated sodium acetate aqueous solution (20 mL) was added to the reaction mixture. The mixture was further stirred at room temperature for 2 h, then extracted with dichloromethane for three times. The combined organic layer was washed with brine (100 mL), water (100 mL), and dried over anhydrous sodium sulfate. After removing solvent under reduced pressure, the residue was purified by column chromatography on silica gel using hexane/dichloromethane 1:1 (v/v) as eluent to yield **3** as a yellow solid (0.198 g, 57%). ^{1}H NMR (300 MHz, $CDCl_3$) δ 9.91 (s, 2H), 7.62 (s, 2H), 1.95–1.87 (m, 4H), 1.21–1.10 (m, 12H), 0.96–0.78 (m, 10H) ppm; ^{13}C NMR (75 MHz, $CDCl_3$) δ 183.0, 161.5, 146.8, 145.2, 129.6, 37.7, 31.7, 29.8, 29.7, 24.8, 22.7, 14.1 ppm; ESIMS (*m/z*): $[M + H]^+$ calcd for $C_{23}H_{31}O_2S_2$, 403.18; found, 403.18.

Synthesis of 4: A solution of 4,5-bis(hexylthio)-1,3-dithiole-2-thione (0.160 g, 0.5 mmol) in toluene (50 mL) was added dropwise into a hot solution of **3** (0.212, 0.5 mmol) and triethyl phosphite (10 mL) in toluene (50 mL) under nitrogen protection. The resulting mixture was stirred at reflux overnight. After removing the solvent under reduced pressure, the residue was purified by column chromatography on silica gel using dichloromethane/ethyl acetate 9:1 (v/v) as eluent to yield **4** as a red oil (0.122 g, 34%). ^{1}H NMR (300 MHz, $CDCl_3$) δ 9.80 (s, 1H), 7.52 (s, 1H), 6.70 (s, 2H), 2.91–2.81 (m, 4H), 1.90–1.79 (m, 4H), 1.71–1.59 (m, 4H), 1.46–1.08 (m, 28H), 0.90 (t, *J* = 6.0 Hz, 6H), 0.81 (t, *J* = 6.0 Hz, 6H) ppm; ^{13}C NMR (75 MHz, $CDCl_3$) δ 182.4, 163.0, 157.4, 148.3, 146.0, 142.8, 134.4, 132.6, 129.9, 129.0, 126.3, 118.1, 108.4, 54.1, 37.9, 36.5, 36.4, 31.7, 29.8, 29.7, 28.4, 24.6, 22.7, 14.1 ppm; ESIMS (*m/z*): $[M]^+$ calcd for $C_{38}H_{56}OS_6$, 720.27; found, 720.26.

Synthesis of 1: A mixture of **4** (52 mg, 0.07 mmol), 2-cyanoacetic acid (85 mg, 1 mmol) and ammonium acetate (13 mg) in acetic acid (15 mL) was refluxed for 12 h at 120 °C under nitrogen protection. After cooling, the mixture was poured into water. The precipitate was collected by filtration and washed with water. The residue purified by column chromatography on silica gel using dichloromethane/methanol/acetic acid 95:4:0.5 (v/v) as eluent to give **1** as a purple solid (49 mg, 92%). ^{1}H NMR (300 MHz, CD_2Cl_2) δ 8.33 (s, 1H), 7.61 (s, 1H), 6.76 (s, 1H), 6.74 (s, 1H), 2.94–2.81 (m, 4H), 1.97–1.83 (m, 4H), 1.75–1.60 (m, 4H), 1.49–1.39 (m, 4H), 1.38–1.27 (m, 12H), 1.22–1.09 (m, 12H), 0.90 (t, *J* = 6.0 Hz, 6H), 0.81 (t, *J* = 6.0 Hz, 6H) ppm; ^{13}C NMR (75 MHz, CD_2Cl_2) δ 169.5, 165.2, 158.8, 152.2, 148.3, 136.4, 134.8, 134.7, 132.7, 129.5, 127.1, 118.7, 117.7, 108.7, 54.6, 38.4, 36.9, 36.8, 32.2, 31.9, 30.4, 30.3, 30.2, 28.8, 25.1, 23.2, 14.4 ppm; ESIMS (*m/z*): $[M]^+$ calcd for ($C_{41}H_{57}NO_2S_6$), 787.27; found, 787.27.

Synthesis of 5: In a similar manner as described in [23], $Pd(dppf)Cl_2$ (0.101 g, 0.12 mmol), 4,4,5,5-tetramethyl-2-(4-(4,4,5,5-tetramethyl-1,3-dioxolan-2-yl)phenyl)-1,3,2-dioxaborolane (0.451 g, 1.35 mmol), and K_2CO_3 (0.502 g, 3.61 mmol) were added to a solution of 6-bromo-4,4-dihexyl-4*H*-cyclopenta[2,1-*b*:3,4-*b'*]dithiophene-2-carbaldehyde (0.453 g, 0.66 mmol) in toluene/ethanol 1:1 (10 mL) in a microwave vial. The reaction mixture was heated in a microwave reactor at 100 °C for 1 h. After cooling to room temperature, the resulting mixture was poured into water and extracted with dichloromethane. The organic phase was washed with water (3 × 150 mL), dried over anhydrous sodium sulfate and concentrated under reduced pressure. The residue was purified by

column chromatography on on silica gel using hexane/dichloromethane 1:1 (v/v) as eluent to give **5** as a yellow oil (0.312 g, 82%). ^{1}H NMR (300 MHz, $CDCl_3$) δ 9.83 (s, 1H), 7.63 (d, J = 6.0 Hz, 2H), 7.56 (s, 1H), 7.53 (d, J = 6.0 Hz, 2H), 7.22 (s, 1H), 6.00 (s, 1H), 1.96–1.82 (m, 4H), 1.34 (s, 6H), 1.28 (s, 6H), 1.23–1.10 (m, 12H), 1.03–0.92 (m, 4H), 0.81 (t, J = 6.0 Hz, 6H) ppm; ^{13}C NMR (75 MHz, $CDCl_3$) δ 182.6, 163.4, 157.8, 149.2, 148.0, 143.4, 140.0, 135.0, 134.8, 130.0, 127.1, 125.6, 118.0, 99.6, 82.9, 54.3, 37.8, 31.7, 29.8, 24.7, 24.4, 22.7, 22.3, 14.1 ppm; ESIMS (*m/z*): $[M]^+$ calcd for $C_{35}H_{46}O_3S_2$, 578.29; found, 578.29.

Synthesis of 6: A solution of 4,5-bis(hexylthio)-1,3-dithiole-2-thione (0.090 g, 0.2 mmol) in toluene (50 mL) was added dropwise into a hot solution of **5** (0.101 g, 0.2 mmol) and triethyl phosphite (5 mL) in toluene (100 mL) under nitrogen protection. The resulting mixture was stirred at reflux overnight. After removing the solvent under reduced pressure, the residue was purified by column chromatography using hexane/dichloromethane 2:1 (v/v) as eluent on silica gel to give **6** as a yellow oil (0.066 g, 37%). ^{1}H NMR (300 MHz, $CDCl_3$) δ 7.59 (d, J = 8.2 Hz, 2H), 7.49 (d, J = 8.2 Hz, 2H), 7.17 (s, 1H), 6.69 (s, 1H), 6.66 (s, 1H), 5.99 (s, 1H), 2.90–2.80 (m, 4H), 1.87–1.79 (m, 4H), 1.72–1.61 (m, 4H), 1.47–1.39 (m, 4H), 1.37–1.25 (m, 20H), 1.22–1.10 (m, 12H), 1.02–0.93 (m, 4H), 0.90 (t, J = 6.9 Hz, 6H), 0.81 (t, J = 6.8 Hz, 6H) ppm; ^{13}C NMR (75 MHz, $CDCl_3$) δ 158.5, 158.3, 144.0, 141.3, 138.7, 136.5, 136.1, 135.6, 128.3, 127.0, 125.0, 118.5, 117.9, 109.3, 99.8, 82.8, 54.1, 38.1, 36.4, 36.3, 31.8, 31.5, 29.9, 29.8, 28.4, 24.6, 24.4, 22.8, 22.7, 22.3, 14.2 ppm; ESIMS (*m/z*): $[M]^+$ calcd for $C_{50}H_{72}O_2S_6$, 896.39; found, 896.38.

Synthesis of 7: A solution of **6** (0.107 g, 0.119 mmol) in 10% HCl/THF (1:2, 30 mL) was heated at 50 °C for 3 h and then poured into water. The organic layer was extracted with dichloromethane and washed with water (3 × 100 mL), then dried over anhydrous sodium sulfate, and filtered. The solvent was removed under reduced pressure and the crude product (0.84 g, red-orange oil) was used without further purification. ESIMS (*m/z*): $[M]^+$ calcd for $C_{44}H_{60}OS_6$, 796.30; found, 796.29.

Synthesis of 2: Crude **7** (0.84 g), 2-cyanoacetic acid (0.050 g, 0.588 mmol) and ammonium acetate (11 mg) in acetic acid (10 mL) were refluxed for 12 h at 120 °C under nitrogen. After cooling, the mixture was poured into water. The precipitate was collected by filtration and washed with water. The residue was purified by column chromatography on silica gel using dichloromethane/methanol/acetic acid 97:3:0.5 (v/v) as eluent to give **2** as a purple solid (0.69 g, 66%). ^{1}H NMR (300 MHz, DMSO-d_6) δ 8.24 (s, 1H), 8.04 (d, J = 8.5 Hz, 2H), 7.82 (d, J = 8.5 Hz, 2H), 7.75 (s, 1H), 6.99 (s, 1H), 6.92 (s, 1H), 2.94–2.84 (m, 4H), 1.92–1.83 (m, 4H), 1.67–1.56 (m, 4H), 1.46–1.35 (m, 4H), 1.33–1.23 (m, 12H), 1.18–1.05 (m, 12H), 0.91–0.83 (m, 6H), 0.76 (t, J = 7.0 Hz, 6H) ppm; ^{13}C NMR (75 MHz, DMSO-d_6) δ 158.9, 158.8, 141.80, 141.8, 138.7, 137.7, 134.8, 131.4, 129.7, 127.80, 127.6, 124.5, 124.5, 120.4, 118.8, 109.6, 53.4, 36.8, 35.3, 35.1, 30.7, 30.5, 29.1, 29.0, 28.7, 27.2, 23.8, 21.7, 13.5 ppm; ESIMS (*m/z*): $[M]^+$ calcd for ($C_{47}H_{61}NO_2S_6$), 863.30; found, 863.30.

Fabrication of DSSCs

In a similar manner as described in [15], electrodes with a 4 μm or 8 μm transparent layer and a 4 μm scattering layer of TiO_2 were screen-printed on fluorine-doped tin oxide (FTO). After sintering at 500 °C for 0.5 h and cooling to room temperature, the electrodes were treated with 20 mM $TiCl_4$ solution at 70 °C for 0.5 h. The films were sintered at 500 °C for 0.5 h and cooled to 80 °C before dipping into the dye solution (0.1 mM dye with 0.3 mM chenodeoxycholic acid in a mixture of THF/ethanol 1:1) for 12 h. After the sensitization, the electrodes were rinsed with acetonitrile and dried in air. The cells were sealed with a Surlyn film and platinized FTO counter electrode. The composition of the cobalt complex-based electrolyte of this study is 0.2 M $[Co(bpy)_3][B(CN)_4]_2$, 0.05 M $[Co(bpy)_3][B(CN)_4]_3$, 0.1 M lithium bis(trifluoromethanesulfonyl)imide, 0.5 M 4-*tert*-butylpyridine in acetonitrile. The composition of the iodine-based electrolyte is 1-methyl-3-propylimidazolium iodide (PMII; 1 M), iodine (60 mM), 4-*tert*-butylpyridine (0.5 M), and lithium perchlorate (0.1 M) in acetonitrile.

Acknowledgements

Financial support for this research by the Swiss National Science Foundation (Grant No. 200021-147143) is gratefully acknowledged.

References

1. Grätzel, M. *Acc. Chem. Res.* **2009,** *42,* 1788–1798. doi:10.1021/ar900141y
2. Hagfeldt, A.; Boschloo, G.; Sun, L.; Kloo, L.; Pettersson, H. *Chem. Rev.* **2010,** *110,* 6595–6663. doi:10.1021/cr900356p
3. Higashino, T.; Imahori, H. *Dalton Trans.* **2015,** *44,* 448–463. doi:10.1039/C4DT02756F
4. Li, L.-L.; Diau, E. W.-G. *Chem. Soc. Rev.* **2013,** *42,* 291–304. doi:10.1039/C2CS35257E
5. Zeng, W.; Cao, Y.; Bai, Y.; Wang, Y.; Shi, Y.; Zhang, M.; Wang, F.; Pan, C.; Wang, P. *Chem. Mater.* **2010,** *22,* 1915–1925. doi:10.1021/cm9036988
6. Mishra, A.; Fischer, M. K. R.; Bäuerle, P. *Angew. Chem.* **2009,** *121,* 2510–2536. doi:10.1002/ange.200804709
   Angew. Chem. Int. Ed. **2009,** *48,* 2474–2499. doi:10.1002/anie.200804709
7. Bai, Y.; Zhang, J.; Zhou, D.; Wang, Y.; Zhang, M.; Wang, P. *J. Am. Chem. Soc.* **2011,** *133,* 11442–11445. doi:10.1021/ja203708k

8. Basheer, B.; Mathew, D.; George, B. K.; Reghunadhan Nair, C. P. *Sol. Energy* **2014,** *108,* 479–507. doi:10.1016/j.solener.2014.08.002
9. Canevet, D.; Sallé, M.; Zhang, G.; Zhang, D.; Zhu, D. *Chem. Commun.* **2009,** 2245–2269. doi:10.1039/B818607N
10. Bergkamp, J. J.; Decurtins, S.; Liu, S.-X. *Chem. Soc. Rev.* **2015,** *44,* 863–874. doi:10.1039/C4CS00255E
11. Lapadula, G.; Trummer, D.; Conley, M. P.; Steinmann, M.; Ran, Y.-F.; Brasselet, S.; Guyot, Y.; Maury, O.; Decurtins, S.; Liu, S.-X.; Copéret, C. *Chem. Mater.* **2015,** *27,* 2033–2039. doi:10.1021/acs.chemmater.5b00306
12. Jia, H.; Ding, J.; Hauser, A.; Decurtins, S.; Liu, S.-X. *Asian J. Org. Chem.* **2014,** *3,* 198–202. doi:10.1002/ajoc.201300144
13. Wu, J.; Dupont, N.; Liu, S.-X.; Neels, A.; Hauser, A.; Decurtins, S. *Chem. – Asian J.* **2009,** *4,* 392–399. doi:10.1002/asia.200800322
14. Schuler, B.; Liu, S.-X.; Geng, Y.; Decurtins, S.; Meyer, G.; Gross, L. *Nano Lett.* **2014,** *14,* 3342–3346. doi:10.1021/nl500805x
15. Geng, Y.; Pop, F.; Yi, C.; Avarvari, N.; Grätzel, M.; Decurtins, S.; Liu, S.-X. *New J. Chem.* **2014,** *38,* 3269–3274. doi:10.1039/c4nj00428k
16. Wenger, S.; Bouit, P.-A.; Chen, Q.; Teuscher, J.; Di Censo, D.; Humphry-Baker, R.; Moser, J.-E.; Delgado, J. L.; Martín, N.; Zakeeruddin, S. M.; Grätzel, M. *J. Am. Chem. Soc.* **2010,** *132,* 5164–5169. doi:10.1021/ja909291h
17. Amacher, A.; Yi, C.; Yang, J.; Bircher, M. P.; Fu, Y.; Cascella, M.; Grätzel, M.; Decurtins, S.; Liu, S.-X. *Chem. Commun.* **2014,** *50,* 6540–6542. doi:10.1039/C4CC02696A
18. Guo, K.; Yan, K.; Lu, X.; Qiu, Y.; Liu, Z.; Sun, J.; Yan, F.; Guo, W.; Yang, S. *Org. Lett.* **2012,** *14,* 2214–2217. doi:10.1021/ol300477b
19. Wan, Z.; Jia, C.; Duan, Y.; Chen, X.; Lin, Y.; Shi, Y. *Org. Electron.* **2013,** *14,* 2132–2138. doi:10.1016/j.orgel.2013.05.011
20. Imakubo, T.; Iijima, T.; Kobayashi, K.; Kato, R. *Synth. Met.* **2001,** *120,* 899–900. doi:10.1016/S0379-6779(00)00932-2
21. Marco, A. B.; Martinez de Baroja, N.; Franco, S.; Garin, J.; Orduna, J.; Villacampa, B.; Revuelto, A.; Andreu, R. *Chem. – Asian J.* **2015,** *10,* 188–197. doi:10.1002/asia.201402870
22. Li, R.; Liu, J.; Cai, N.; Zhang, M.; Wang, P. *J. Phys. Chem. B* **2010,** *114,* 4461–4464. doi:10.1021/jp101222s
23. Leandri, V.; Ruffo, R.; Trifiletti, V.; Abbotto, A. *Eur. J. Org. Chem.* **2013,** 6793–6801. doi:10.1002/ejoc.201300962
24. Woolridge, K.; Goncalves, L. C.; Bouzan, S.; Chen, G.; Zhao, Y. *Tetrahedron Lett.* **2014,** *55,* 6362–6366. doi:10.1016/j.tetlet.2014.09.110
25. Zimmer, H.; Mark, H. B., Jr.; Wehmeier, M. *Phosphorus, Sulfur Silicon Relat. Elem.* **1997,** *123,* 45–56. doi:10.1080/10426509708044197
26. Tsao, H. N.; Yi, C.; Moehl, T.; Yum, J.-H.; Zakeeruddin, S. M.; Nazeeruddin, M. K.; Grätzel, M. *ChemSusChem* **2011,** *4,* 591–594. doi:10.1002/cssc.201100120
27. Wang, X.; Yang, J.; Yu, H.; Li, F.; Fan, L.; Sun, W.; Liu, Y.; Koh, Z. Y.; Pan, J.; Yim, W.-L.; Yan, L.; Wang, Q. *Chem. Commun.* **2014,** *50,* 3965–3968. doi:10.1039/c4cc00577e

License and Terms

BEILSTEIN JOURNAL OF ORGANIC CHEMISTRY

Single-molecule conductance of a chemically modified, π-extended tetrathiafulvalene and its charge-transfer complex with F_4TCNQ

Raúl García[1], M. Ángeles Herranz[1], Edmund Leary[*2], M. Teresa González[2], Gabino Rubio Bollinger[3], Marius Bürkle[4], Linda A. Zotti[5], Yoshihiro Asai[4], Fabian Pauly[6], Juan Carlos Cuevas[5], Nicolás Agraït[2,3] and Nazario Martín[*1,2]

Full Research Paper

Open Access

Address:
[1]Departamento de Química Orgánica, Facultad de Química, Universidad Complutense, E-28040 Madrid, Spain, [2]Fundación IMDEA Nanoscience, Campus de Cantoblanco, Universidad Autónoma, E-28048 Madrid, Spain, [3]Departamento de Física de la Materia Condensada, and Instituto "Nicolás Cabrera", Universidad Autonoma de Madrid, E-28049 Madrid, Spain, [4]Nanosystem Research Institute, National Institute of Advanced Industrial Science and Technology (AIST), Tsukuba, Ibaraki 305-8568, Japan, [5]Departamento de Física Teórica de la Materia Condensada, Universidad Autónoma de Madrid, Spain and [6]Department of Physics, University of Konstanz, D-78457 Konstanz, Germany

Email:
Edmund Leary[*] - edmund.leary@imdea.org; Nazario Martín[*] - nazmar@quim.ucm.es

* Corresponding author

Keywords:
break junction measurements; charge-transfer complex; DFT-based transport; molecular electronics; tetrathiafulvalene

Beilstein J. Org. Chem. **2015,** *11,* 1068–1078.
doi:10.3762/bjoc.11.120

Received: 11 March 2015
Accepted: 22 May 2015
Published: 24 June 2015

This article is part of the Thematic Series "Tetrathiafulvalene chemistry".

Guest Editor: P. J. Skabara

Abstract

We describe the synthesis and single-molecule electrical transport properties of a molecular wire containing a π-extended tetrathiafulvalene (exTTF) group and its charge-transfer complex with F_4TCNQ. We form single-molecule junctions using the in situ break junction technique using a homebuilt scanning tunneling microscope with a range of conductance between 10 G_0 down to 10^{-7} G_0. Within this range we do not observe a clear conductance signature of the neutral parent molecule, suggesting either that its conductance is too low or that it does not form a stable junction. Conversely, we do find a clear conductance signature in the experiments carried out on the charge-transfer complex. Due to the fact we expected this species to have a higher conductance than the neutral molecule, we believe this supports the idea that the conductance of the neutral molecule is very low, below our measurement sensitivity. This idea is further supported by theoretical calculations. To the best of our knowledge, these are the first reported single-molecule conductance measurements on a molecular charge-transfer species.

Introduction

The development of molecular electronics is a current challenge in nanoscience. The ultimate goal is to fabricate different electronic devices based on a variety of active elements such as wires, transistors, diodes or switches (to name just a few), where each is built from individual, suitably functionalized molecules. Although the controlled handling of molecules to form reliable molecule-based circuits remains a demanding task, modern organic synthesis allows the design and preparation of nearly any challenging molecule [1].

Among the aforementioned electroactive elements, the study of molecular wires has received great attention and, in this regard, a great variety of molecules of different nature involving single, double and triple C–C bonds (conjugated or not) have been extensively studied [2-4]. Furthermore, most of these systems have been covalently connected to a great variety of different anchor groups in order to improve the connection to various metal electrodes. However, despite the huge number of molecular systems that find application as wires, the use of electroactive molecules exhibiting different oxidation states that can modify/control the conductance through the wire have been considerably less studied.

In the realm of organic chemistry there are a great variety of organic compounds able to show different redox states that are very appealing candidates to be used as wires and/or switches in molecular electronics. In this regard, molecules having redox centers such as viologen [5,6], aniline [7,8], thiophene [9], anthraquinone [10] and ferrocene [11] have been previously studied. However, a particularly suitable redox-active molecule for molecular electronics is the well-known electron donor tetrathiafulvalene (TTF) molecule. Pristine TTF, as well as the tetraselenafulvalene analogue (TSF), have been previously reported. In this study, the authors hypothesized that in the Au–TTF–Au junctions, the molecule is connected to the electrodes in a face-to-face overlapping configuration [12]. In contrast, since the first report on a suitably functionalized TTF as a molecular wire using two thioacetate anchoring groups [13], most of the TTF derivatives synthesized for this purpose have been functionalized with sulfur atoms as alligator clips. These belong either to a fused ring on the TTF [14], or to a chain covalently connected to the TTF core bearing a thiol group at the end [15,16]. Furthermore, extended TTF cruciform molecules, formed by two orthogonally placed, π-conjugated moieties bearing the 1,3-dithiole rings at the ends, have also been used for single-molecule measurements [17].

A singular TTF analogue is the so-called π-extended TTF (exTTF, (9,10-bis(1,3-dithiol-2-ylidene)-9,10-dihydroanthracene) which, in contrast to pristine TTF that exhibits two oxidation peaks to form the radical cation and dication species, shows only one oxidation peak involving a two electron process to form the dication state. Furthermore, the geometrical properties of exTTF are quite different from pristine TTF. Thus, whereas TTF is mostly planar in the neutral form, exTTF is a highly distorted, out-of-plane molecule with a butterfly shape in its neutral state. It undergoes a dramatic gain of planarity and aromaticity upon oxidation (Figure 1) [18,19]. This gain of stability upon oxidation has been skillfully used in a variety of D–π–A systems, namely exTTF–π-bridge–C_{60} derivatives, for determining the attenuation factor of the molecular wire (oligomer) acting as the π-bridge [20-22].

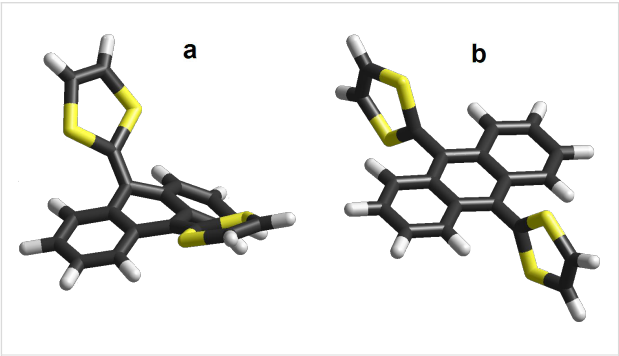

Figure 1: Depictions of 9,10-bis(1,3-dithiol-2-ylidene)-9,10-dihydroanthracene (exTTF) in the (a) neutral form and (b) in the oxidized (2+) state. In the oxidized state the two positive charges reside on the two 1,3-dithiole rings.

In this paper, we describe the synthesis of a new exTTF derivative, suitably functionalized with two (*p*-acetylthio)phenylethynyl substituents at positions 2 and 6 of the anthracene central core. We then describe single-molecule conductance measurements on this new derivative, along with measurements of the charge-transfer complex formed with F_4TCNQ. Finally, we present theoretical calculations to understand its electrical transport properties.

Results and Discussion

Synthesis and characterization of molecular wire 5

The synthesis of the target molecule is shown in Scheme 1 and starts from the previously reported 2,6-diiodo-exTTF **1** [23]. Reaction of **1** under Sonogashira conditions (Pd(II), CuI, DIPEA) with trimethylsilylacetylene affords the symmetrically substituted exTTF **2** in good yield. Further removal of the trimethylsilyl group is easily achieved by treatment with potassium carbonate, yielding the free terminal alkyne **3** in quantitative yield. The introduction of the two anchor groups in **3** is carried out through a second Sonogashira reaction. The coupling of 2,6-diethynyl-exTTF **3** with 1-acetylthio-4-iodoben-

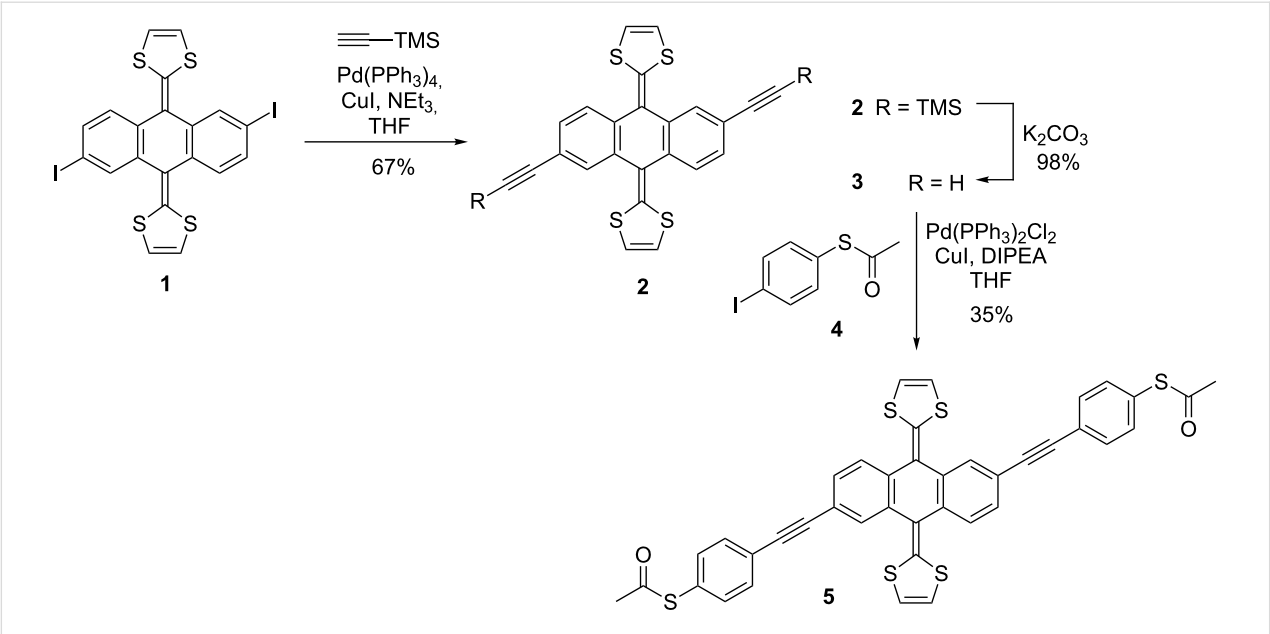

Scheme 1: Synthetic route to the target exTTF-based molecular wire **5**.

zene (**4**), in the presence of Pd(II) and copper iodide and DIPEA in THF, led to the target molecule **5** in moderate yield (35%). Compound **4** was obtained in one step and with high yield from 1,4-diiodobenzene by reaction with *n*-BuLi in ether, followed by reaction with S_8, and eventually, acetyl chloride [24].

All new compounds were fully characterized by spectroscopic and electrochemical means. Interestingly, compounds **2**, **3** and **5** showed similar ^{1}H NMR spectra due to their symmetry resulting in relatively simple spectra, which confirms the proposed structures. In particular, compound **5** exhibits the methyl groups as a singlet at 2.45 ppm, and the protons corresponding to the 1,3-dithiole rings appear as a singlet at 6.37 ppm. In the ^{13}C NMR of the target molecule **5**, the carbonyl groups appear at 192.4 ppm and the carbons of the alkyne moieties at 88.0 and 90.4 ppm, with the terminal methyl groups at 28.7 ppm.

The redox properties of compound **5** (0.2 mM) were determined by cyclic voltammetry at room temperature in THF using $TBAPF_6$ (0.1 M) as a supporting electrolyte under argon atmosphere and at a scan rate of 0.1 Vs^{-1}. The electrochemical cell consisted of a glassy carbon working electrode, $Ag/AgNO_3$ reference electrode and a Pt wire counter electrode. It is worth mentioning that ferrocene was not employed as the inner reference since its oxidation potential overlaps with that of the exTTF unit. Similar to pristine exTTF, the new exTTF derivative **5** exhibited only one quasi-reversible oxidation peak, involving a two-electron process to form the dication state [25,26]. This oxidation peak appears at E_{pa} = 217 mV (ΔE = 285 mV, peak-to-peak separation), which is quite similar to the oxidation peak found for pristine exTTF (E_{pa} = 244 mV, ΔE = 350 mV) (Figure 2).

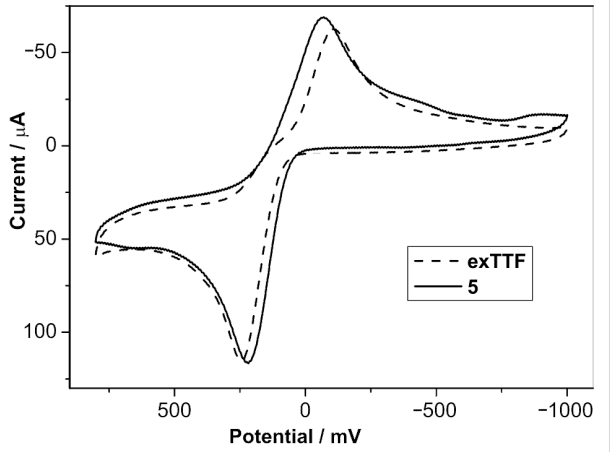

Figure 2: Cyclic voltammograms of compound **5** and pristine exTTF (at concentrations of approximately 0.2 mM) using THF as a solvent and $TBAPF_6$ (0.1 M) as a supporting electrolyte. Scan rate: 0.1 Vs^{-1}.

Break junction measurements

Neutral molecule

We first tried to form neutral-molecule molecular junctions. Simply, compound **5** can be seen as an analogue of an oligo(phenylene ethynylene), specifically an OPE3-dithiol compound (where 3 indicates the total number of phenyl rings), in which the central phenyl ring has been substituted by an exTTF unit. We could, therefore, expect compound **5** to form molecular junctions in a similar way to the OPE3-dithiol, which

readily does so either in solution, or under solvent-free conditions as recently reported [27]. Hence, as a starting point, we followed the same sample preparation conditions as previously with the OPE3-dithiol [27]. We prepared 0.1–1 mM solutions of compound **5** in both 1,2,4-trichlorobenzene (TCB) or mesitylene/tetrahydrofuran (Mes/THF 4:1), and exposed a clean gold substrate to the solution for a period of approximately 30 min. The sample was then dried under a flow of argon and mounted inside the scanning tunneling microscope (STM). All experiments were then performed under solvent-free, ambient conditions. In order to form molecular junctions of compound **5**, we followed the break junction technique [28]. During the experiment, the variation in conductance (G) is recorded while an STM tip is moved vertically (z) in and out of contact with a gold substrate, forming and breaking gold nanocontacts (G vs z trace). When the two gold electrodes (the STM tip and the substrate) are in contact, or in close enough proximity, one or more molecules of the compound adsorbed on the surface can bridge the two electrodes. This binding occurs through one of the terminal groups (thiols in this case) to each of the electrodes, hence forming a molecular junction. In this configuration, when separating the electrodes (larger z values), we observe conductance plateaus while the gold nanocontact or a molecular junction remains intact during the pulling. The plateaus then end abruptly when the junction is broken.

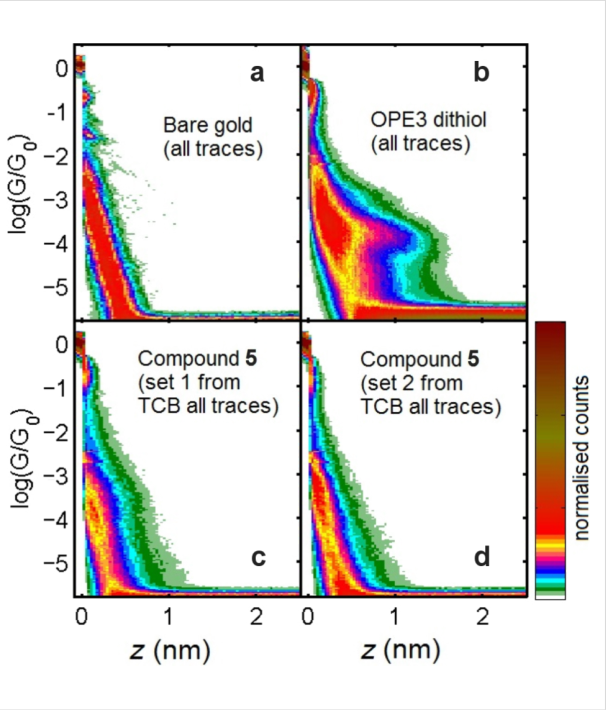

Figure 3: 2D histograms resulting from break junction experiments on an unmodified gold sample (a), OPE3-dithiol drop-cast from TCB (26% of traces displayed plateaus around 10^{-4} G_0) (b), compound **5** drop-cast from TCB (c) and, compound **5** dip-cast from dichloromethane (d). All measurements were performed in dry ambient conditions.

Figure 3c and 3d show the 2D histograms consisting of several thousand individual G vs z traces recorded in a break junction experiment in the presence of compound **5**. These are compared with those recorded on an unmodified gold substrate and in the presence of OPE3-dithiol. These histograms include all the measured traces without filtering out the tunneling-only traces from those with plateaus. One can see that the colored region of the 2D histogram of OPE3-dithiol extends significantly to larger inter-electrode distances than the unmodified gold substrate. Also, it does so within a narrow band of conductance values (roughly between $\log(G/G_0) = -3$ and -4.5). This 2D profile exemplifies the presence of plateaus occurring in a narrow region of conductance. In the 2D histograms of compound **5**, we can also see that the colored region extends to higher electrode interdistance values (z) than for the unmodified gold substrate. However, as opposed to the case of OPE-dithiol, there is no clear protuberance in the histogram that would indicate the concentration of plateaus at a given conductance value.

Therefore, in order to determine whether the signature of compound **5** is simply very weak, we performed a trace separation process to build histograms of only the traces displaying plateaus. Figure 4 shows the results of this separation for the traces considered in Figure 3. In particular, for compound **5**, two separation steps were carried out, resulting in three categories of traces: (1) those with only a smooth exponential decay (Figure 4a and Figure 4d, labeled "No Plat."), (2) those with poorly-defined plateaus (Figure 4b and Figure 4e, labeled "Plat. 1"), and (3) those with well-defined plateaus (Figure 4c and Figure 4f, labeled "Plat. 2"). We considered the conductance range between $\log(G/G_0) = -5.3$ and -0.5 and established that a trace has a plateau whenever a z interval (Δz) longer than 0.15 nm is needed to observe a change of conductance $\Delta\log(G/G_0) = 0.12$ along the trace. Amongst these traces, we separate the well-defined plateaus as those traces for which a Δz larger than 0.2 nm is needed to observe a $\Delta\log(G/G_0) = 0.1$ along the trace. These are empirical criteria which gave us the best separation results. We see that the histograms built from the trace of the third group present protuberances, suggesting that molecular junctions are successfully formed from compound **5**.

From a close inspection of Figure 4c and Figure 4f, we see that the plateau conductance in these experiments varies by more than 2 orders of magnitude (between $\log(G/G_0) = -3$ and -5), significantly greater than OPE3-dithiol, and also that they extend to between 1 and 2 nm. However, it is important to note here that the percentage of traces with well-defined plateaus (given in parentheses in Figure 4) is very low. Even with a total number of 5000 measured traces, the final number of traces

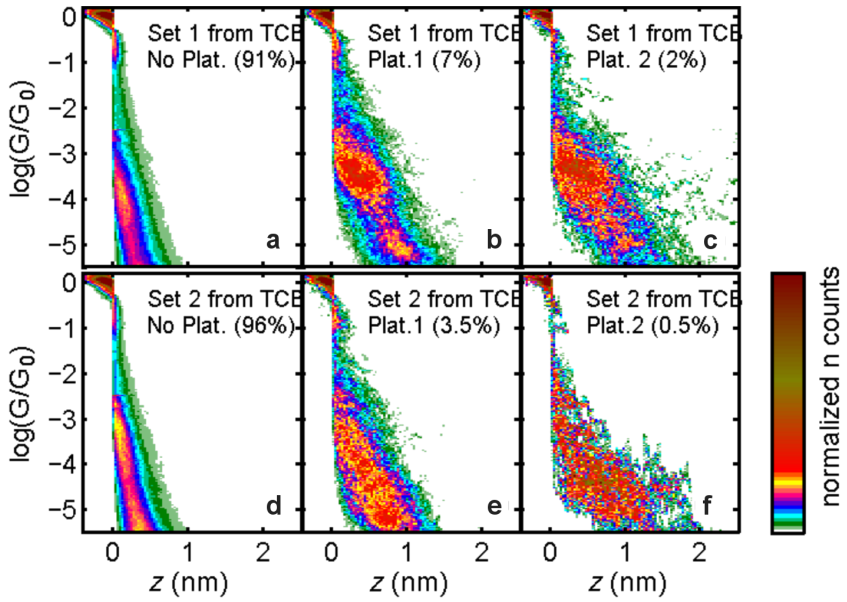

Figure 4: 2D histograms corresponding to compound **5** after exposing a gold substrate to the solution of the compound in TCB. For each measurement, the traces were separated into 3 groups: traces with no plateau (No Plat.), traces with poorly defined plateaus (Plat. 1), and traces with well-defined plateaus (Plat. 2). See text for details on the separation process. The percentage of traces included in each group is indicated in the brackets.

with well-defined plateaus is less than 50 traces. We also note here that these results correspond to the most successful measurement runs, and the percentage of traces with plateaus was even lower in other cases. We stress that under the same experimental conditions, we obtained percentages of around 35% of well-defined plateaus for OPE3-dithiol.

We have recently measured the conductance of a series of molecules based on a similar OPE3 backbone, also terminated with thiols, but with differing numbers of dithiafulvalene (DTF) substituents placed at various positions along the OPE backbone [17]. One of the main structural differences with these molecules compared to compound **5** is that conjugation is maintained along the OPE3 backbone. For this series of compounds, we could observe a clear signature for each, which was similar to the unmodified OPE3. We showed that the presence of the DTF side groups does not influence the low-bias conductance and secondly, and that their presence does not significantly hinder molecular junction formation. Different to the measurements carried out thus far on compound **5**, we carried out these measurements using dichloromethane as the deposition solvent, and since the results were clear, we decided to applied this also to compound **5**. The sample was prepared by exposing the gold to a solution of compound **5** in dichloromethane (DCM) for 1 h, followed by drying the sample with a flow of N_2. The results of these measurements are shown in Figure 5.

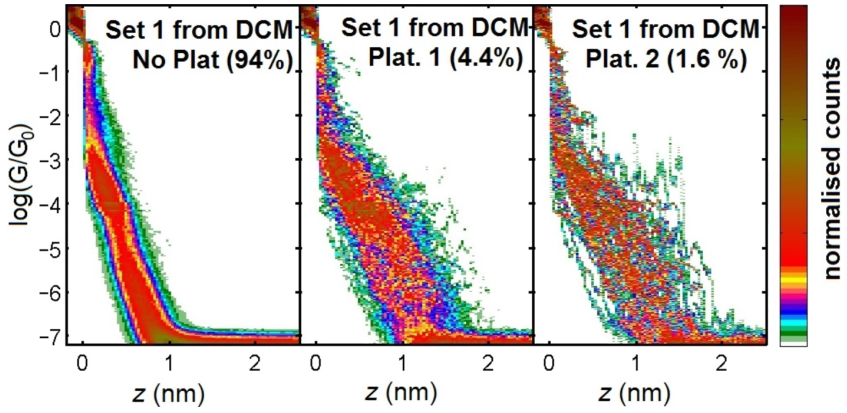

Figure 5: 2D histograms corresponding to compound **5** after exposing a gold substrate to a solution of the compound in DCM. The traces were separated into three groups as described in Figure 4. The total number of traces recorded was 3830.

As with the measurements on compound **5** using the TCB drop-casting method, after dip-casting from DCM, we could observe the presence of G(z) plateaus, in this case down to just above 10^{-7} G_0 facilitated by the use of larger gains. The percentage of traces displaying these plateaus was again low, however, and similar to that found before, with less than 2% fitting the well-defined criteria. From the 2D histograms in Figure 4, we see again that no favored region of conductance develops after separating the junctions displaying plateaus (labeled Plat. 1 and Plat. 2). This, we believe, indicates that whilst the formation of molecular junctions is possible, it is unclear exactly how the molecule binds in these junctions. The low percentage of molecular junction formation can be considered consistent with our observations on the OPE3 series with DTF side groups, in that the presence of sulfur atoms in the center of the molecule slightly reduces the probability of forming junctions. This is likely because the mobility of the molecule over the surface is reduced, which in turn makes it difficult for molecules to diffuse into the freshly created nanogaps.

The lack of a clear molecular signature may ultimately be due to several reasons. Aside from reducing the probability of junction formation, the sulfur atoms in the center of the molecule can also bind to the electrodes during the evolution of the junctions, preventing the wire from becoming fully stretched. This is a distinct possibility for this molecule due to the well-known interaction of the parent extended-TTF and gold [29]. An alternative explanation for the lack of a clear signal for compound **5** is that its end-to-end conductance is too low for it to be observed in our setup. If this is the case, this would mean the conductance is lower than 10^{-7} G_0. This is quite likely due to the cross-conjugated nature of the exTTF unit, and the known effect this has on conductance.

Conductance measurements on the exTTF-F_4TCNQ charge-transfer complex

Despite the lack of a clear signal for the neutral molecule, we decided to proceed by trying to form the charge-transfer (CT) complex of compound **5** with 7,7,8,8-tetracyanoquinodimethane (TCNQ). When combining two equimolar solutions of the two compounds in DCM, we observed no color change, suggesting no complexation. The solvent was then changed to acetonitrile, a more polar solvent better able to stabilize complex formation, but this too did not give the anticipated strong color change. Only when the solution was heated at reflux for 3 h under ambient conditions and a large excess of TCNQ was added (5 equiv), a dark green color developed. UV–vis absorption spectroscopy confirmed the formation of a CT complex (Supporting Information File 1, Figure S1). To ensure the quantitative formation of the CT complex, a more straightforward method compatible with the conductance measurements was considered. Specifically, we switched from TCNQ to the stronger acceptor 2,3,5,6-tetrafluoro-7,7,8,8-tetracyanoquinodimethane (F_4TCNQ). This produced a clear change of color as soon as the first drops of the acceptor were added to the solution of compound **5** in DCM, yielding a green solution. We monitored the formation of the CT complex by recording the UV–vis spectrum of the solution. As successive amounts of the acceptor are added to the solution of the donor, the peak at 448 nm of the neutral donor species decreases and new peaks appear between 600–900 nm that grow with the addition of more acceptor and also methanol (see Supporting Information File 1, Figure S2). Specifically, we observe three peaks at 689 nm, 764 nm and 867 nm, which can be assigned to the radical anion F_4TCNQ species [30]. For the break junction measurements, it was necessary to avoid having an excess of the acceptor because F_4TCNQ forms molecular junctions itself due to its four terminal cyano groups (see Supporting Information File 1, Figure S7). Hence, we formed the charge-transfer (CT) complex by adding approximately 0.5 mL of a 10^{-4} M solution of F_4TCNQ in DCM to a 1 mL 10^{-4} M solution of compound **5**. In this way, we can avoid having significant amounts of free acceptor on the surface. This, however, means we do not exactly know the ratio of donor to acceptor in our case. It is known that the CT complex of the parent exTTF with TCNQ forms in a 1:4 ratio [31]. However, as we have evidence of the formation of a radical anion of F_4TCNQ, we believe a donor to acceptor ratio of 1:2 is more likely, for which there is a precedent in a substituted exTTF complex with TCNQ [32]. We then allowed 24 h for the molecules to adsorb onto the gold in order to obtain as high a density of molecules as possible. This increases the possibility that a significant fraction of the solution is still the free donor species. Although there will still be some of the neutral donor species present on the surface, as we have shown that this molecule does not give a clear signal in break junction experiments, there will be no problem of signal overlap with the CT complex.

In contrast to the neutral form of compound **5**, a significant percentage of conductance plateaus for the CT complex sample were observed. They were found fall into two main groups, labeled as high and low conductance. Figure 6a shows examples of individual G(z) traces displaying conductance plateaus. Firstly, we separate traces showing only tunneling (Figure 6b) from those containing plateaus (Figure 6c) using the following criteria: z interval (Δz) longer than 0.12 nm needed to observe a change of conductance $\Delta\log(G/G_0) = 0.16$. We then further divided the traces into two more groups for those with plateaus above or below $\log(G/G_0) = -3.8$. Dividing the traces using a value slightly above or below this does not change the separation significantly as the difference between the two types of plateaus is clear. By fitting a Gaussian function to the

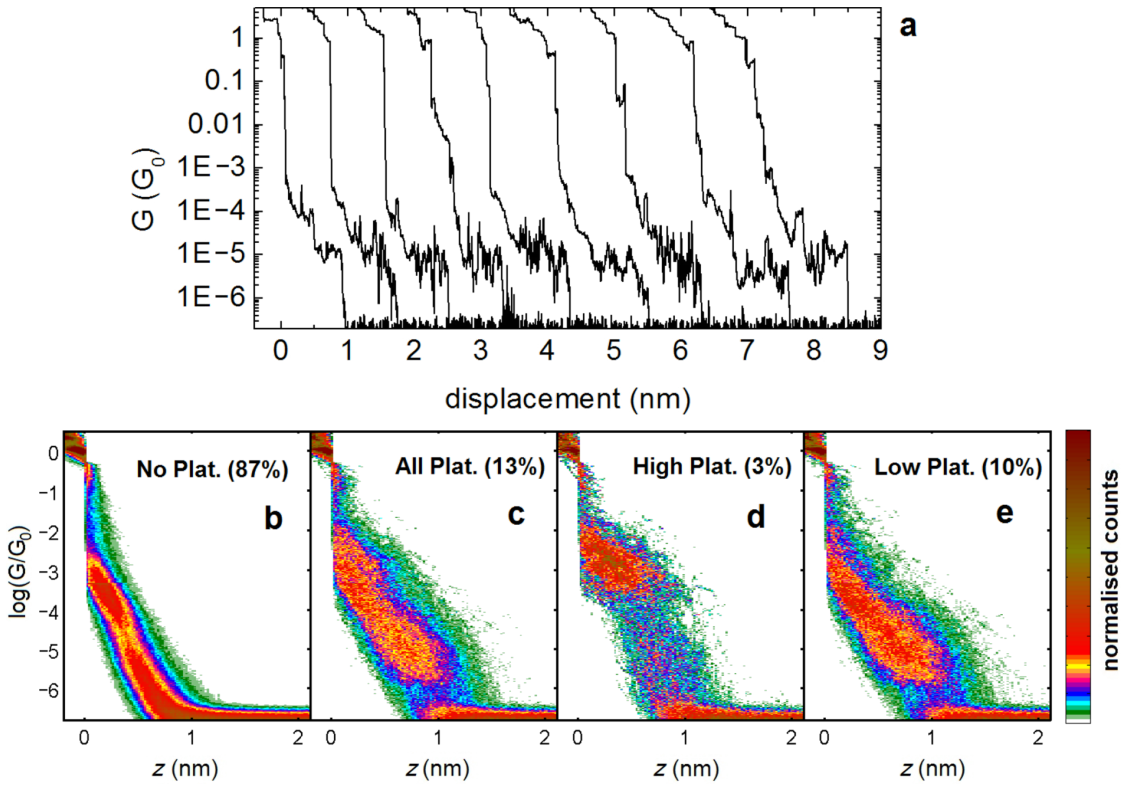

Figure 6: a) Examples of individual G(*z*) traces showing clear conductance plateaus. b–e) 2D histograms corresponding to the CT complex between compound **5** and F_4TCNQ after exposing a gold substrate to the solution of the complex in DCM. The traces are separated into four groups: b) traces without plateaus; c) traces with plateaus between log(G/G_0) = −0.5 and −6.0. From these traces the traces were divided into high and low plateau groups: d) traces with plateaus above log(G/G_0) = −3.8; e) traces with plateaus below log(G/G_0) = −3.8. The total number of traces recorded was 4868.

histograms we find peak positions of log(G/G_0) = −3.0 for the high group, and log(G/G_0) = −4.7 for the low group (see Supporting Information File 1, Figure S6 for the 1D histograms). We also measured the junction break-off distance for the two groups (which we define as the separation required to move from log(G/G_0) = −0.5 to either log(G/G_0) = −4 for the high plateaus, or log(G/G_0) = −6.1 for the low plateaus). We found mean values of 0.65 ± 0.25 nm and 1.14 ± 0.30 nm for the high and low groups, respectively (see Supporting Information File 1, Figure S3 for break-off histograms). We repeated the measurements using a freshly prepared CT complex and gold electrodes, and obtained a very similar result for the low conductance group (see Supporting Information File 1, Figures S4 and S5). In the repeated measurement, however, we did not observe a signal in the high conductance region, above 10^{-3} G_0.

As can be seen from the separation of plateaus into high and low groups, the two types generally occur independently. The origin of the high conductance state is difficult to be totally sure about. The two groups may arise from independent chemical species, in which case it would be natural to label the high group as junctions for which transport takes place through a molecule of F_4TCNQ. The length and conductance are similar to the control test we carried out on only this molecule (see Supporting Information File 1, Figure S7). It may also be possible that the high conductance state arises through contact to the central part of the CT complex and one of the terminal thiol groups. We observed a similar feature for the neutral molecule (see Figure 4b and Figure 4c) although for the neutral molecule, this signal was never very reproducible. The low group, on the other hand, fits well with conductance taking place across the whole molecule (i.e., thiol to thiol). We calculate an S–S distance of 2.4 nm for the CT complex (substituting the dihydroanthracene core of compound **5** for anthracene). We estimate the amount of gold retraction to be 0.5 nm, which then gives a real Au–Au separation of 1.64 ± 0.30 nm for the mean breaking distance of the low group, corresponding well with the length of the molecule. The fact that the molecule does not seem to fully stretch inside the junctions (unlike the OPE3-dithiol) may be due to the bulky nature of the complex, which contains many groups with the potential to interact with gold.

We cannot be totally sure of the species which gives rise to the low conductance state in so much as we do not know its exact

charge and ratio of donor to acceptor molecules. It is conceivable that some charge is transferred to the electrodes upon molecular junction formation, as is common for molecular junctions [33]. However, it is well known that the cationic (1+) state of exTTF is less thermodynamically stable than the dication (2+) [34], resulting in inverted oxidation potentials of the cation and dication. Additionally, it is known that the resonance between the neutral and dication is impossible due to the strong difference in geometries. Thus, it is more than plausible that the molecule retains its cationic state in the junction. We further point out that in several recent studies, a very similar conductance was found for a molecule that is structurally similar and contains only the anthracene central group. In a study by Hong et al., a conductance peak was found at $\log(G/G_0) = -4.5$, which is close to the low conductance group we observe [10]. As it is known that the oxidation of exTTF compounds results in the planarization and aromatization of the central three rings to the anthracene unit, the similarity in conductance is perhaps indicative of these changes. We have also recently shown that adding substituents to the central phenyl rings of OPE wires has no noticeable influence on the molecular conductance (groups were tested ranging from electron-withdrawing fluorine to electron-donating methoxy groups) [35]. It is also rational to suppose that the, albeit charged, dithiole side groups of our CT complex would not strongly modify the conductance of the otherwise neutral anthracene-containing wire. Finally, we point out that recent conductive AFM measurements carried out on self-assembled monolayers of anthracene and anthraquinone OPE derivatives showed a difference of approximately two orders of magnitude between their respective conductance values [36]. This would fit with our hypothesis that the conductance of the neutral exTTF molecule, which has a similar bonding pattern to anthraquinone, is below our experimental resolution, based on the value we measure for the CT complex.

Ab initio calculations

To gain insight into the conduction mechanism of compound **5**, we performed theoretical calculations based on a combination of density functional theory (DFT) and Green's functions techniques within the framework of the Landauer theory for coherent transport. The complete technical details are reported in Supporting Information File 1.

We first optimized the geometry of the molecule in the gas phase. The HOMO was found to be localized on the exTTF unit, which presented the expected butterfly shape, while the LUMO appeared delocalized over the whole molecule (Figure 7).

Subsequently, we constructed two kinds of metal–molecule–metal junctions, where the molecule is bound to a gold

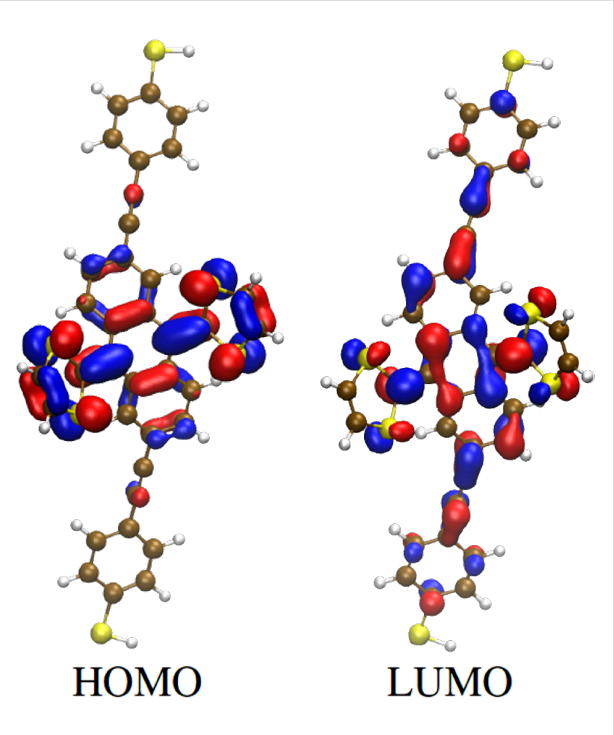

Figure 7: Frontier orbitals of compound **5** in the gas phase.

cluster in a top and hollow position, respectively (Figure 8). We then computed the zero-bias electron transmission following the procedure explained in Supporting Information File 1. The corresponding transmission curves are shown in Figure 9. Notice that the molecular HOMO–LUMO gap was corrected, following the procedure previously reported [37]. The HOMO and all other occupied orbital energies were shifted by $\Sigma_{occ}=-IP-\varepsilon_H+\Delta_{occ}$, while the LUMO and all other unoccupied orbital levels were shifted by $\Sigma_{virt}=-EA-\varepsilon_L+\Delta_{virt}$. Here, Δ_{occ} (Δ_{virt}) is the image charge correction for the occupied (unoccupied) states, ε_H (ε_L) is the Kohn–Sham energy of the gas phase HOMO (LUMO), and IP(EA) is the gas phase ionization potential (electron affinity). All quantities are reported in Table 1 for both binding geometries.

The alignment of the Breit–Wigner resonances related to both the HOMO and LUMO (at approximately −1 and 2.7 eV from the Fermi level, respectively) do not show a strong dependence on the binding geometry (Figure 9). The electron transport is dominated by the HOMO, although interference features (resonance–antiresonance pairs) appear in the energy region close to the Fermi level. This is not surprising, given the spatial extension of the frontier orbitals, in particular of the HOMO, which is localized on the ex-TTF unit only. In fact, Fano resonances are known to arise when a "pendant" orbital, which is weakly coupled to the electrodes, is coupled to an orbital delocalized over the main axis of the molecular wire [38,39].

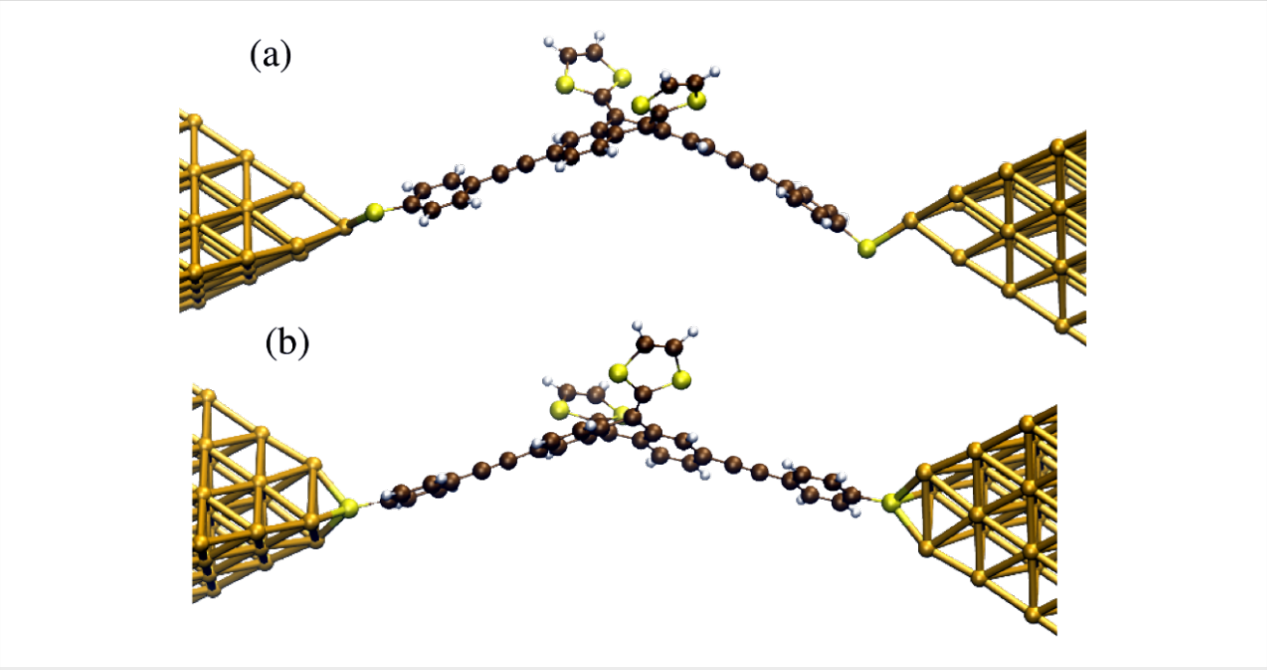

Figure 8: Top a) and hollow b) binding geometries of **5** to a gold cluster in metal–molecule–metal junctions.

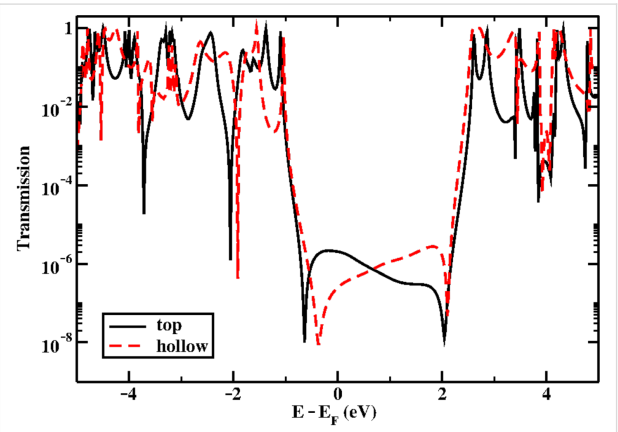

Figure 9: Transmission as a function of energy for the top and hollow binding geometries.

Table 1: Kohn–Sham HOMO and LUMO, ionization potential (IP), electron affinity (EA) and image charge correction for occupied Δ_{occ} and Δ_{virt} unoccupied orbitals. All quantities are in eV.

	HOMO	IP	Δ_{occ}	LUMO	EA	Δ_{virt}
top	−4.27	5.68	−0.35	−2.54	−1.16	−0.38
hollow	−4.27	5.68	−0.32	−2.54	−1.16	−0.33

The computed conductance values, evaluated as the transmission at the Fermi level, are in the range 10^{-6} to 10^{-7} G_0. These low conductance values are at the limit of what we can observe experimentally. This, therefore, would be consistent with the idea that the real conductance of the molecule is too low to be recorded in the experiments. Nevertheless, we cannot absolutely rule out the possibility that the molecule does not form molecular junctions in the experiments.

Conclusion

We have synthesized a molecular wire containing a π-extended tetrathiafulvalene (exTTF) group and studied its single-molecule electrical transport properties along with those of its charge-transfer complex with F_4TCNQ. Within the accessible conductance range (10 to 10^{-7} G_0) we did not observe a clear conductance signature of the neutral parent molecule. This alone could suggest either that its conductance is too low or that it does not form stable junctions. We did, however, find a clear conductance signature in the experiments carried out on the charge-transfer complex. As complexation with the acceptor oxidizes the molecule by removing two electrons from the exTTF group, thus converting it from a buckled and cross-conjugated group into a planar aromatic group, we predict the CT species to have a higher conductance than the neutral molecule. This, we believe, supports the idea that the conductance of the neutral molecule is very low, below our measurement sensitivity. This would make the conductance difference between the neutral and CT species at least two orders of magnitude. This can be considered as favorable for the use of single molecules as chemical sensors, in which analyte molecules may bind to a backbone to alter its conductance. Further combinations of donors and acceptors should be explored in order to evaluate this potential.

Supporting Information

Supporting Information File 1

Detailed experimental procedures for the synthesis and characterization of **5**, break junction experiments and theoretical methods.
[http://www.beilstein-journals.org/bjoc/content/supplementary/1860-5397-11-120-S1.pdf]

Acknowledgements

We thank Dr. Jose Manuel Santos Barahona for help with preparing the CT complex with TCNQ, and recording and interpreting the UV–vis spectra. Financial support by the European Commission (EC) FP7 ITN "MOLESCO" Project No. 606728, the European Research Council (ERC-436 2012 ADG_20120216-Chirallcarbon), the CAM (PHOTOCARBON project S2013/MIT-2841, NANOFRONTMAG-CM project S2013/MIT-2850 and MAD2D project S2013/MIT-3007), FP7-ENERGY-2012-1-2STAGE-number 309223 (PHOCS) and the Spanish MICINN/MINECO through the programs MAT2011-25046, MAT2014-57915-R and PRI-PIBUS-2011-1067 is acknowledged. MB was partly supported by a FY2012 (P12501) Postdoctoral Fellowship for Foreign Researchers from the Japan Society for Promotion of Science (JSPS) and by a JSPS KAKENHI, "Grant-in-Aid for JSPS Fellows", grant no. 24·02501. YA is also thankful to another KAKENHI, "Grant-in-Aid for Scientific Research on Innovation Areas, Molecular Architectonics: Orchestration of Single Molecules for Novel Functions" (#25110009). LAZ was supported by the Spanish MICINN under Grant MAT2011-23627. FP acknowledges support by the Carl-Zeiss foundation and the Collaborative Research Center 767 "Controlled Nanosystems: Interaction and Interfacing to the Macroscale".

References

1. Leary, E.; La Rosa, A.; González, M. T.; Rubio-Bollinger, G.; Agraït, N.; Martín, N. *Chem. Soc. Rev.* **2015,** *44,* 920–942. doi:10.1039/C4CS00264D
2. Guldi, D. M.; Nishihara, H.; Venkataraman, L., Eds. Molecular wires. *Chem. Soc. Rev.* **2015,** *4,* 835–1030. doi:10.1039/C5CS90010G
3. Forrest, S. R.; Thompson, M. E., Eds. Organic Electronics and Optoelectronics. *Chem. Rev.* **2007,** *107,* 923–1386. doi:10.1021/cr0501590
4. Guldi, D. M.; Illescas, B. M.; Atienza, C. M.; Wielopolski, M.; Martín, N. *Chem. Soc. Rev.* **2009,** *38,* 1587–1597. doi:10.1039/b900402p
5. Haiss, W.; van Zalinge, H.; Higgins, S. J.; Bethell, D.; Höbenreich, D.; Schiffrin, D. J.; Nichols, R. J. *J. Am. Chem. Soc.* **2003,** *125,* 15294–15295. doi:10.1021/ja038214e
6. Gittins, D. I.; Bethell, D.; Schiffrin, D. J.; Nichols, R. J. *Nature* **2000,** *408,* 67–69. doi:10.1038/35040518
7. Chen, F.; He, J.; Nuckolls, C.; Roberts, T.; Klare, J. E.; Lindsay, S. *Nano Lett.* **2005,** *5,* 503–506. doi:10.1021/nl0478474
8. Chen, F.; Nuckolls, C.; Lindsay, S. *Chem. Phys.* **2006,** *324,* 236–243. doi:10.1016/j.chemphys.2005.08.052
9. Xu, B. Q.; Li, X. L.; Xiao, X. Y.; Sakaguchi, H.; Tao, N. J. *Nano Lett.* **2005,** *5,* 1491–1495. doi:10.1021/nl050860j
10. Hong, W.; Valkenier, H.; Mészáros, G.; Manrique, D. Z.; Mishchenko, A.; Putz, A.; Moreno García, P.; Lambert, C.; Hummelen, J. C.; Wandlowski, T. *Beilstein J. Nanotechnol.* **2011,** *2,* 699–713. doi:10.3762/bjnano.2.76
11. Xiao, X.; Brune, D.; He, J.; Lindsay, S.; Gorman, C. B.; Tao, N. *Chem. Phys.* **2006,** *326,* 138–143. doi:10.1016/j.chemphys.2006.02.022
12. Taniguchi, M.; Tsutsui, M.; Shoji, K.; Fijiwara, H.; Kawai, T. *J. Am. Chem. Soc.* **2009,** *131,* 14146–14147. doi:10.1021/ja905248e
13. Giacalone, F.; Ángeles Herranz, M.; Grüter, L.; González, M. T.; Calame, M.; Schönenberger, C.; Arroyo, C.; Rubio-Bollinger, G.; Vélez, M.; Agraït, N.; Martín, N. *Chem. Commun.* **2007,** 4854–4856. doi:10.1039/b710739k
14. Li, M.-J.; Long, M.-Q.; Chen, K.-Q.; Xu, H. *Solid State Commun.* **2013,** *157,* 62–67. doi:10.1016/j.ssc.2012.12.001
15. Leary, E.; Higgins, S. J.; van Zalinge, H.; Haiss, W.; Nichols, R. J.; Nygaard, S.; Jeppesen, J. O.; Ulstrup, J. *J. Am. Chem. Soc.* **2008,** *130,* 12204–12205. doi:10.1021/ja8014605
16. Liao, J.; Agustsson, J. S.; Wu, S.; Schönenberger, C.; Calame, M.; Leroux, Y.; Mayor, M.; Jeannin, O.; Ran, Y.-F.; Liu, S.-X.; Decurtins, S. *Nano Lett.* **2010,** *10,* 759–764. doi:10.1021/nl902000e
17. Parker, C. R.; Leary, E.; Frisenda, R.; Wei, Z.; Jennum, K. S.; Glibstrup, E.; Abrahamsen, P. B.; Santella, M.; Christensen, M. A.; Della Pia, E. A.; Li, T.; González, M. T.; Jiang, X.; Morsing, T. J.; Rubio-Bollinger, G.; Laursen, B. W.; Nørgaard, K.; van der Zant, H.; Agraït, N.; Nielsen, M. B. *J. Am. Chem. Soc.* **2014,** *136,* 16497–16507. doi:10.1021/ja509937k
18. Martín, N.; Sánchez, L.; Herranz, M. A.; Illescas, B.; Guldi, D. M. *Acc. Chem. Res.* **2007,** *40,* 1015–1024. doi:10.1021/ar700026t
19. Brunetti, F. G.; López, J. L.; Atienza, C.; Martín, N. *J. Mater. Chem.* **2012,** *22,* 4188–4205. doi:10.1039/c2jm15710a
20. Giacalone, F.; Segura, J. L.; Martín, N.; Guldi, D. M. *J. Am. Chem. Soc.* **2004,** *126,* 5340–5341. doi:10.1021/ja0318333
21. Molina-Ontoria, A.; Wielopolski, M.; Gebhardt, J.; Gouloumis, A.; Clark, T.; Guldi, D. M.; Martín, N. *J. Am. Chem. Soc.* **2011,** *133,* 2370–2373. doi:10.1021/ja109745a
22. Wielopolski, M.; Molina-Ontoria, A.; Schubert, C.; Margraf, J. T.; Krokos, E.; Kirschner, J.; Gouloumis, A.; Clark, T.; Guldi, D. M.; Martín, N. *J. Am. Chem. Soc.* **2013,** *135,* 10372–10381. doi:10.1021/ja401239r
23. Illescas, B. M.; Santos, J.; Martín, N.; Atienza, C. M.; Guldi, D. M. *Eur. J. Org. Chem.* **2007,** 5027–5037. doi:10.1002/ejoc.200700226
24. Pearson, D. L.; Tour, J. M. *J. Org. Chem.* **1997,** *62,* 1376–1387. doi:10.1021/jo962335y
25. Liu, S.-G.; Pérez, I.; Martín, N.; Echegoyen, L. *J. Org. Chem.* **2000,** *65,* 9092–9102. doi:10.1021/jo001149w
26. Herranz, M. A.; Yu, L.; Martín, N.; Echegoyen, L. *J. Org. Chem.* **2003,** *68,* 8379–8385. doi:10.1021/jo034894s
27. González, M. T.; Leary, E.; García, R.; Verma, P.; Herranz, M. A.; Rubio-Bollinger, G.; Martín, N.; Agraït, N. *J. Phys. Chem. C* **2011,** *115,* 17973–17978. doi:10.1021/jp204005v
28. Chen, F.; Tao, N. J. *Acc. Chem. Res.* **2009,** *42,* 429–438. doi:10.1021/ar800199a

29. Urban, C.; Écija, D.; Wang, Y.; Trelka, M.; Preda, I.; Vollmer, A.; Lorente, N.; Arnau, A.; Alcamí, M.; Soriano, L.; Martín, N.; Martín, F.; Otero, R.; Gallego, J. M.; Miranda, R. *J. Phys. Chem. C* **2010,** *114,* 6503–6510. doi:10.1021/jp911839b
30. Jain, A.; Rao, K. V.; Mogera, U.; Sagade, A. A.; George, S. J. *Chem. – Eur. J.* **2011,** *17,* 12355–12361. doi:10.1002/chem.201101813
31. Bryce, M. R.; Moore, A. J.; Hasan, M.; Ashwell, G. J.; Fraser, A. T.; Clegg, W.; Hursthouse, M. B.; Karaulov, A. I. *Angew. Chem., Int. Ed. Engl.* **1990,** *29,* 1450–1452. doi:10.1002/anie.199014501
32. Bryce, M. R.; Finn, T.; Batsanov, A. S.; Kataky, R.; Howard, J. A. K.; Lyubchik, S. B. *Eur. J. Org. Chem.* **2000,** 1199–1205. doi:10.1002/1099-0690(200004)2000:7<1199::AID-EJOC1199>3.0.CO;2-F
33. Peng, G.; Strange, M.; Thygesen, K. S.; Mavrikakis, M. *J. Phys. Chem. C* **2009,** *113,* 20967–20973. doi:10.1021/jp9084603
34. Bendikov, M.; Wudl, F.; Perepichka, D. F. *Chem. Rev.* **2004,** *104,* 4891–4946. doi:10.1021/cr030666m
35. González, M. T.; Zhao, X.; Manrique, D. Z.; Miguel, D.; Leary, E.; Gulcur, M.; Batsanov, A. S.; Rubio-Bollinger, G.; Lambert, C. J.; Bryce, M. R.; Agraït, N. *J. Phys. Chem.* **2014,** *118,* 21655–21662. doi:10.1021/jp506078a
36. Guédon, C. M.; Valkenier, H.; Markussen, T.; Thygesen, K. S.; Hummelen, J. C.; van der Molen, S. J. *Nat. Nanotechnol.* **2012,** *7,* 305–309. doi:10.1038/nnano.2012.37
37. Zotti, L. A.; Bürkle, M.; Pauly, F.; Lee, W.; Kim, K.; Jeong, W.; Asai, Y.; Reddy, P.; Cuevas, J. C. *New J. Phys.* **2014,** *16,* 015004. doi:10.1088/1367-2630/16/1/015004
38. Cuevas, J. C.; Scheer, E. *Molecular electronics: An Introduction to Theory and Experiment;* World Scientific Publishing Co Pte Ltd: Singapore, 2010; Vol. 1. doi:10.1142/7434
39. Lambert, C. J. *Chem. Soc. Rev.* **2015,** *44,* 875–888. doi:10.1039/C4CS00203B

License and Terms

BEILSTEIN JOURNAL OF ORGANIC CHEMISTRY

Regioselective synthesis of chiral dimethyl-bis(ethylenedithio)tetrathiafulvalene sulfones

Flavia Pop and Narcis Avarvari*

Full Research Paper

Open Access

Address:
Université d'Angers, CNRS, Laboratoire MOLTECH-Anjou, UMR 6200, UFR Sciences, Bât. K, 2 Bd. Lavoisier, 49045 Angers, France

Email:
Narcis Avarvari* - narcis.avarvari@univ-angers.fr

* Corresponding author

Keywords:
chirality; crystal structures; molecular materials; sulfones; tetrathiafulvalenes

Beilstein J. Org. Chem. **2015,** *11,* 1105–1111.
doi:10.3762/bjoc.11.124

Received: 04 April 2015
Accepted: 15 June 2015
Published: 02 July 2015

This article is part of the Thematic Series "Tetrathiafulvalene chemistry".

Guest Editor: P. J. Skabara

Abstract

Enantiopure (*R*,*R*) and (*S*,*S*)-dimethyl-bis(ethylenedithio)tetrathiafulvalene monosulfones have been synthesized by the aerial oxidation of the chiral dithiolates generated from the propionitrile-protected precursors. Both enantiomers crystallize in the orthorhombic chiral space group $P2_12_12_1$. They show a boat-type conformation of the TTF moiety, a rather rigid dithiin sulfone ring and the methyl groups in a bisequatorial conformation. Cyclic voltammetry measurements indicate fully reversible oxidation in radical cation and dication species.

Introduction

Chiral tetrathiafulvalene (TTF) derivatives have been addressed for the first time in the middle of 80s by Dunitz and Wallis through the synthesis of the (*S*,*S*,*S*,*S*)-enantiomer of tetramethyl-bis(ethylenedithio)tetrathiafulvalene (TM-BEDT-TTF) (Scheme 1) [1], thus opening opportunities towards the preparation of chiral molecular conductors [2]. Since then a large number of chiral TTF derivatives have been prepared [3], especially those derived from bis(ethylenedithio)tetrathiafulvalene (BEDT-TTF) [4]. Although numerous derivatives have been prepared only ten years ago different transport properties were observed for enantiopure and racemic conducting salts based on ethylenedithiotetrathiafulvalene-oxazoline (EDT-TTF-Ox) donors [5,6], due to a structural disorder effect [7]. Evidence was thus provided, and confirmed later on with a second complete series of conducting salts based on the same donors [8], that the presence of chiral centers can modulate the structural disorder of radical cation salts in the solid state, and subsequently, differences in their conducting properties can occur. A similar effect was observed more recently in the [TM-BEDT-TTF][I_3] family of enantiopure and racemic semiconducting salts [9]. In all these examples the crystal-cell parameters were similar for the enantiopure and racemic salts excepting the space groups which were non-centrosymmetric and centrosymmetric, respectively. On the other hand, complete different solid-state packings may be observed in enantiopure and racemic forms of the same donor, as recently described for a

series of mixed valence salts based on the dimethyl-ethylenedithiotetrathiafulvalene (DM-EDT-TTF) precursor (Scheme 1). Here the racemic salt was found to be metallic, while the enantiopure forms showed semiconducting behavior [10]. One of the most important results is the observation of a synergistic effect between chirality and conductivity in enantiopure mixed-valence metallic salts formulated as [DM-EDT-TTF]$_2$[ClO$_4$] [11]. This is referred to as the electrical magnetochiral anisotropy (eMChA) effect. This effect, which translates the influence of chirality on the transport properties measured in a parallel magnetic field [12], was previously observed only in bismuth wires and carbon nanotubes [13]. Another interesting research area is the redox modulation of the chiroptical properties described in derivatives such as TTF-allenes [14], TTF-helicenes [15], or TTF-paracyclophanes [16]. Thus, to address the different opportunities offered by the combination of chirality with the TTF motif, a certain number of families of precursors have been reported. They possess various types of chirality, i.e., stereogenic centers, axial, planar, helical chirality, and supramolecular chirality [17-21]. Since methylated BEDT-TTF derivatives such as dimethyl-bis(ethylenedithio)tetrathiafulvalene (DM-BEDT-TTF) [22-24], TM-BEDT-TTF [2,9,25,26] and DM-EDT-TTF [10] proved to be the most promising precursors for the preparation of chiral conductors, we were interested in the synthesis of functional derivatives thereof. One of the possibilities hardly addressed so far in TTF chemistry is the oxidation of the sulfur atoms into sulfoxides or sulfones. Indeed, only two reports deal with the oxidation of BEDT-TTF into BEDT-TTF monosulfoxides (Scheme 1), along with enantioselectivity issues [27,28]. We describe herein the synthesis, characterization and solid-state structures of the (*S*,*S*) and (*R*,*R*) enantiomers of DM-BEDT-TTF monosulfones **1** (Scheme 1).

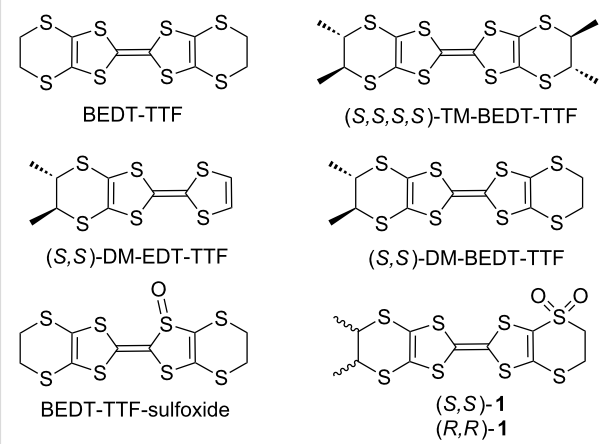

Scheme 1: BEDT-TTF and chiral derivatives.

Results and Discussion

In our previous studies dealing with the sulfoxidation of the BEDT-TTF donor we could selectively obtain the *inner* BEDT-TTF sulfoxide (Scheme 1) by using chiral sulfonyl-oxaziridines as oxidizing agent [27,28]. However, the *inner* BEDT-TTF sulfoxide was shown to be of only limited interest as precursor for molecular conductors, since it does not reversibly oxidize into a radical cation. This behavior is due to the moderate kinetic stability of the latter, which releases oxygen to transform into BEDT-TTF. Moreover, since the *inner* sulfur atoms present large orbital coefficients in the HOMO, the introduction of the electron-withdrawing oxygen atom induces a massive increase of the oxidation potential from the neutral to the radical cation states. We have then hypothesized that the oxidation of the *outer* sulfur atoms into sulfoxide or sulfone should only moderately influence the oxidation potential and thus provide more stable radical cation species. In order to access chiral precursors with controlled stereochemistry we decided to investigate the sulfoxidation of the DM-BEDT-TTF precursor.

Compounds (*S*,*S*)-**1** and (*R*,*R*)-**1** were synthesized in two steps from the corresponding enantiopure dithiole-thiones (*S*,*S*)-**5** and (*R*,*R*)-**5** and the dithiolone-dithiopropionitrile **4** (Scheme 2). In

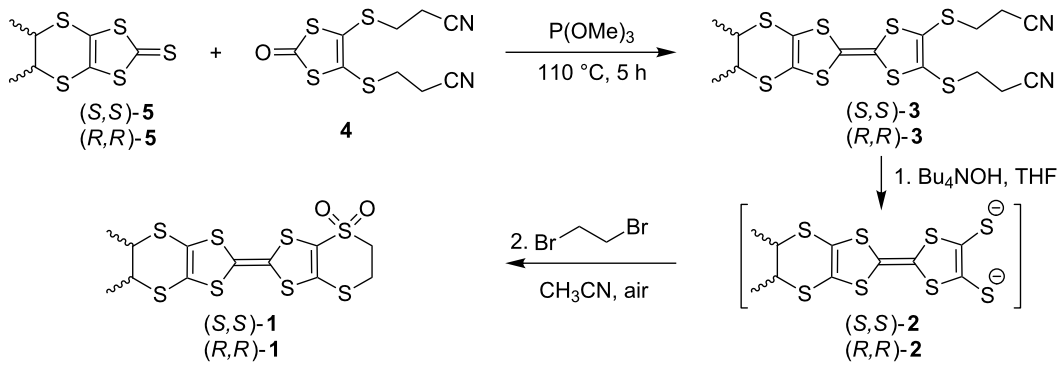

Scheme 2: Synthesis of the chiral sulfones (*S*,*S*)-**1** and (*R*,*R*)-**1**.

the first step the phosphite-mediated heterocoupling between the two units provides the enantiomeric DM-EDT-TTF-dithiopropionitriles (*S*,*S*)-**3** and (*R*,*R*)-**3** as the major products. Tetrabutylammonium hydroxide was then used to generate the corresponding dithiolates **2** in THF that, after solvent evaporation during which air was allowed in the Schlenk tube, were further refluxed in acetonitrile with 1,2-dibromoethane to afford the chiral monosulfones (*S*,*S*)-**1** and (*R*,*R*)-**1**. Thus, the oxidation of one of the outer sulfur atoms takes place in situ as the intermediate DM-EDT-TTF dithiolates are reactive towards oxygen. Interestingly, the reaction is regio- and chemoselective, as only compound **1** was isolated after column chromatography.

We have thus succeeded, through this simple strategy, to selectively oxidize one of the *outer* sulfur atoms of the DM-EDT-TTF donor, which represents a remarkable regio- and chemoselectivity.

Besides NMR (Figures S1 and S2 in Supporting Information File 1), mass spectrometry and elemental analysis, which are all concordant, the definite proof for the sulfone structure of **1** has been provided by single crystal X-ray diffraction analysis. Single crystals of the two enantiomers (*S*,*S*)-**1** and (*R*,*R*)-**1** were obtained by slow evaporation from dichloromethane/pentane or dichloromethane solutions, respectively. Although both enantiomers crystallize in the orthorhombic system (chiral space group $P2_12_12_1$), they are not isostructural, very likely because of the slightly different crystallization conditions. Indeed, the cell parameters are completely different and in the asymmetric unit of (*R*,*R*)-**1** there is one molecule and in that of (*S*,*S*)-**1** there are two independent molecules (Figure 1).

In both structures the methyl groups adopt equatorial positions, unlike the structure of DM-BEDT-TTF, in which they are axially oriented [22]. We have previously shown that for the TM-BEDT-TTF donor the axial orientation is slightly more favored in the gas phase than the equatorial one, but both can occur in the solid state [9,25]. In some cases even mixed (ax,ax,eq,eq) conformations have been observed in the solid state [25,26,29]. In the (*R*,*R*)-**1** molecule the dithiole and the methyl-substituted dihydrodithiin rings show rather strong distortions, with dihedral angles about the S···S hinges of 27.6° (S3–S8), 22.1° (S5–S6) and 46.1° (S1–S4). On the contrary, the dihydrodithiin sulfone ring is almost planar, with a S2···S7 folding angle of only 5.3°, certainly because of the rigidity imposed by the tetrahedral R_2SO_2 sulfur atom. The S=O bond lengths have values of 1.396(5) Å for S2=O1 and 1.380(5) Å for S2=O2, which are somewhat shorter than the usual values of 1.43–1.44 Å reported in the literature [30-32] (Table 1). Moreover, these S=O bonds are shorter when compared to those in *inner* TTF sulfoxides [27,28], yet the same feature was already observed in other sulfoxide/sulfone series [30,31]. The central C7=C8 bond measures 1.346(6) Å, which is a typical value for a neutral donor. In the packing the donors interact laterally along the *a* direction, with the shortest intermolecular S···S distance of 3.60 Å for S3···S7 (−1+x, y, z), forming chains which further dimerize through S6···S5 (−0.5+x, 0.5−y, 1−z) and S6···S8 (−0.5+x, 0.5−y, 1−z) contacts amounting to 3.54 and 3.59 Å, respectively. Then, the dimerized chains arrange perpendicular to each other in the *bc* plane (Figure 2).

Table 1: Selected bond distances for (*R*,*R*)-**1** and (*S*,*S*)-**1**.

Bond lengths (Å)		
(*R*,*R*)-**1**	(*S*,*S*)-**1 A**	(*S*,*S*)-**1 B**
C7=C8···1.346(6)	C5=C6···1.347(7)	C5=C6···1.347(7)
S5–C7···1.759(5)	S3–C5···1.770(5)	S3–C5···1.760(5)
S6–C7···1.748(5)	S4–C5···1.751(6)	S4–C5···1.755(5)
S8–C8···1.762(6)	S5–C6···1.741(6)	S5–C6···1.751(5)
S3–C8···1.771(6)	S6–C6···1.766(5)	S6–C6···1.750(5)
S2–O1···1.396(5)	S2–O1···1.395(5)	S1–O1···1.435(5)
S2–O2···1.380(5)	S2–O2···1.404(5)	S1–O2···1.430(4)

In the structure of (*S*,*S*)-**1** the overall configuration of the two independent molecules is similar, of boat type, with distortions

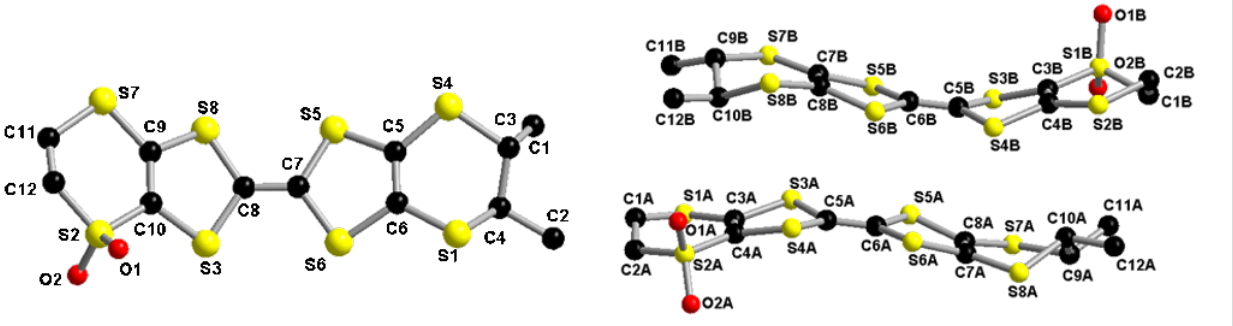

Figure 1: Molecular structure of (*R*,*R*)-**1** (left) and (*S*,*S*)-**1** (right) together with atom numbering scheme (H atoms have been omitted for clarity).

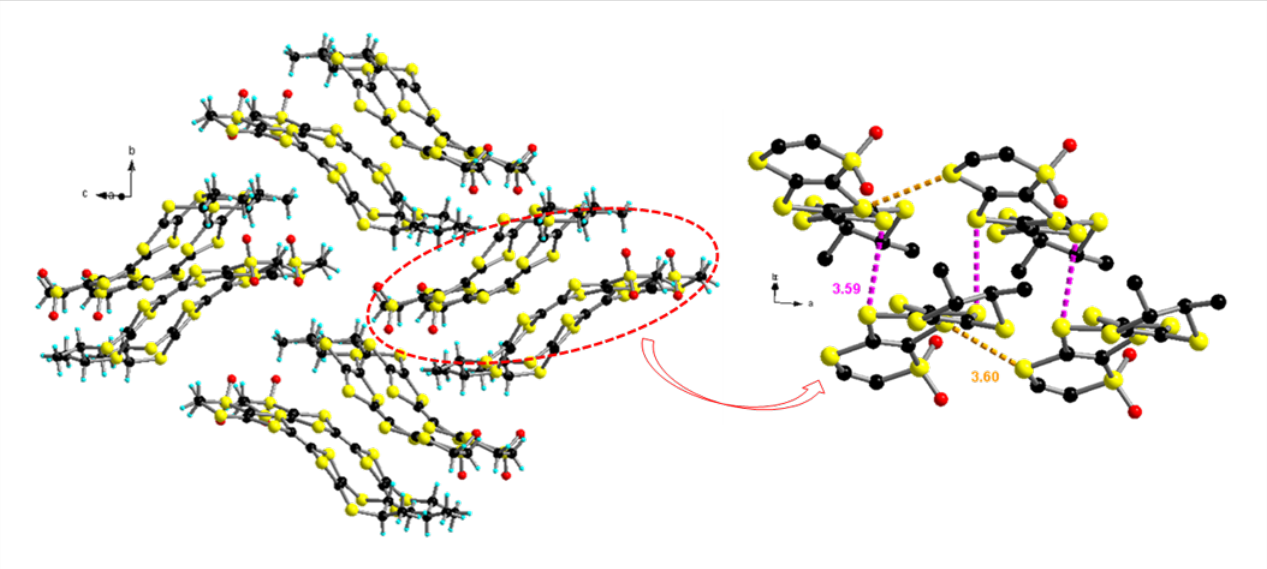

Figure 2: Packing of (*R*,*R*)-**1** in the *bc* plane (left) and detailed S···S interactions (only S3···S7 (−1+x, y, z) 3.60 Å and S6···S8 (−0.5+x, 0.5−y, 1−z) of 3.59 Å are highlighted) between molecules in each stack (right).

along the internal S···S axes in the same sense, having rather close values of 23.5° (S3A···S4A) and 16.7° (S5A···S6A) for molecule A, and 27.4° (S3B···S4B) and 14.4° (S5B···S6B) for molecule B. As far as the dihydrodithiin rings are concerned, the methyl-substituted ones are much less folded, according to the dihedral angles of 8.8° (S1A···S2A) and 16.5° (S1B···S2B), compared to those in the unsubstituted rings, amounting to 26.9° (S7A···S8A) and 22.1° (S7B···S8B). The S=O-bond lengths range between 1.395(5) and 1.435(5) Å, while the central C5=C6 bonds have the same value of 1.347(7) Å for both A and B molecules, typical for neutral donors (Table 1). (*S*,*S*)-**1** packs in *pseudo*-centrosymmetric head-to-tail dimers which are orthogonally disposed in an edge-to-face arrangement (Figure 3). The shortest intermolecular S···S distances within the dimers are 3.72 Å for S5A···S5B (2−x, −0.5+y, 0.5−z) and 3.76 Å for S6A···S5B (2−x, −0.5+y, 0.5−z), while

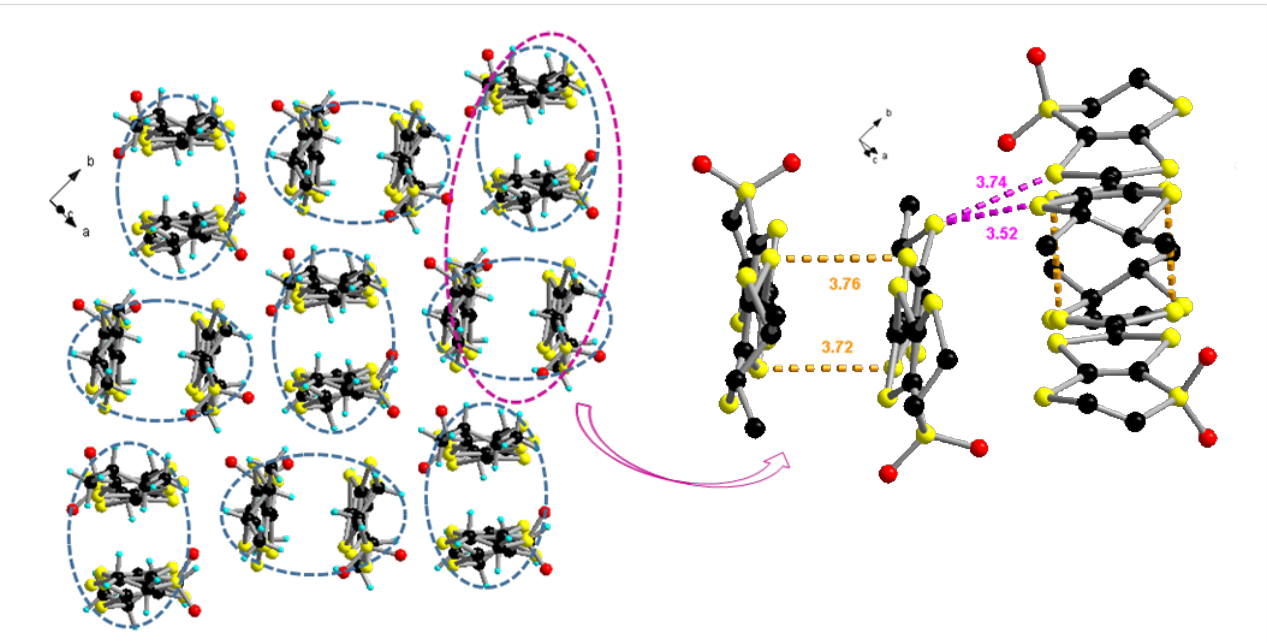

Figure 3: Packing of (*S*,*S*)-**1** in the *ab* plane (left) and detailed S···S intermolecular interactions within (highlighted S5A···S5B (2−x, −0.5+y, 0.5−z) 3.72 Å and S6A···S6B (2−x, −0.5+y, 0.5−z) 3.72 Å) and between (highlighted S5B···S8B (2−x, 0.5+y, 0.5−z) 3.72 Å and S3B···S8B (2−x, 0.5+y, 0.5−z) 3.74 Å) orthogonal dimers (right).

they are smaller between dimers, as for example S5B···S8B (2−x, 0.5+y, 0.5−z) (3.52 Å) or S6A···S7A (3−x, −0.5+y, 0.5−z) (3.49 Å).

A very important aspect related to the interest of these chiral TTF sulfones as precursors for molecular conductors is the stability of the radical cation species. As mentioned earlier, the major drawback of the *inner* BEDT-TTF sulfoxides is their irreversible oxidation, as the radical cations once generated lose oxygen to afford BEDT-TTF. However, in strike contrast with the behavior of the latter, cyclic voltammetry measurements for (*R*,*R*)-**1** and (*S*,*S*)-**1** show reversible two single-electron oxidation processes into radical cation and dication species at $\Delta E_{1/2}$ = +0.67 and 1.00 V vs SCE, respectively (Figure S3 in Supporting Information File 1). The first value is thus largely cathodically shifted with respect to the oxidation of the *inner* BEDT-TTF sulfoxide occurring at +0.95 V vs SCE, and only slightly anodically shifted when compared to the DM-BEDT-TTF donor [22].

Conclusion

Enantiopure (*R*,*R*) and (*S*,*S*)-dimethyl-bis(ethylenedithio)tetrathiafulvalene (DM-BEDT-TTF) monosulfones have been selectively prepared by the in situ aerial oxidation of a TTF dithiolate precursor followed by quenching with dibromoethane. Both enantiomers have been thoroughly characterized in solution and in the solid state by single crystal X-ray diffraction. The conformation of the enantiomers is very similar in the solid state, including the equatorial position of the methyl substituents, in spite of their different packing diagrams which are dominated by the intermolecular S···S interactions. The electrochemical behavior of these *outer* DM-BEDT-TTF sulfones is strikingly different from the one of the *inner* BEDT-TTF sulfoxide, as it shows fully reversible oxidation processes at much lower potentials. Accordingly, these new donors represent valuable precursors for crystalline chiral radical cation salts. Moreover, the partial reduction to the corresponding *outer* sulfoxides, which would generate an additional stereogenic center at the SO sulfur atom can be envisaged. These aspects are currently addressed in our laboratory.

Experimental

Materials and instrumentation: Reactions were carried out under argon; dry solvents were obtained from solvent drying machines. Nuclear magnetic resonance spectra were recorded on Bruker Avance DRX 300 and 500 spectrometers operating at 300 and 500 MHz for ^{1}H and 75 and 125 MHz for ^{13}C, respectively. Chemical shifts are expressed in parts per million (ppm) downfield from external TMS. The following abbreviations are used: d, doublet; t, triplet; m, multiplet. MALDI–TOF MS spectra were recorded on a Bruker Biflex-IIITM apparatus, equipped with a 337 nm N_2 laser. Elemental analyses were recorded using Flash 2000 Fisher Scientific Thermo Electron analyzer. The starting compounds **4** [33] and **5** [10] have been prepared as described in the literature.

Syntheses

(*S*,*S*)-3: A mixture of (*S*,*S*)-**5** (0.56 g, 2.21 mmol) and 3,3'-((2-oxo-1,3-dithiole-4,5-diyl)bis(sulfanediyl))dipropanenitrile (**4**, 1.23 g, 4.36 mmol, 2 equiv) in 10 mL of freshly distilled trimethylphosphite was heated under argon at 110 °C for 5 h. The solvent was evaporated in a rotary evaporator, and then 20 mL of toluene were added and evaporated. The last procedure was repeated twice. The product was dissolved in dichloromethane and passed through a silica column to remove the remaining phosphate, and then purified by chromatography using petroleum spirit/dichloromethane 1:1 followed by dichloromethane as eluent, to afford an orange solid (0.53 g, 48%). ^{1}H NMR (300 MHz, $CDCl_3$) δ 3.23–3.17 (m, 2H, -C*H*-CH_3), 3.06 (t, 2H, -CH_2-), 2.71 (t, 2H, -CH_2-), 1.42 (d, 6H, -CH_3) ppm; MALDI–TOF MS (*m*/*z*): $[M - CH_2CH_2CN)]^+$ 437.4; Anal. calcd for $C_{16}H_{16}N_2S_8$: C, 38.99; H, 3.27; N, 5.68; S, 52.05; found: C, 38.65; H, 3.05; N, 5.34; S, 52.43 (%).

(*R*,*R*)-3: The same synthetic procedure was followed as for the (*S*,*S*) enantiomer starting from (*R*,*R*)-**5**. Yield 55%. Anal. calcd for $C_{16}H_{16}N_2S_8$: C, 38.99; H, 3.27; N, 5.68; S, 52.05; found: C, 38.71; H, 3.08; N, 5.32; S, 52.51 (%).

DM-BEDT-TTF monosulfone (*S*,*S*)-1: After the solution of (*S*,*S*)-**3** (100 mg, 0.2 mmol) in 7 mL of dry THF was degassed for 10 min by bubbling argon through the solution, tetrabutylammonium hydroxide solution (1 M in methanol, 0.44 mL, 0.44 mmol) was added and the mixture was stirred at rt for 30 min. Then the THF was evaporated under vacuum, 10 mL of dry acetonitrile were added and the mixture was refluxed for 2 h. After the solution was concentrated the crude reaction mixture was chromatographed on silica gel using dichloromethane/pentane 1:1 to up to 4:1 as eluent to afford a yellow orange solid (27 mg, 30%). Single crystals were obtained by slow evaporation of a dichloromethane solution. ^{1}H NMR (500 MHz, CD_2Cl_2) δ 3.71–3.68 (m, 2H, -SCH_2-), 3.56–3.53 (m, 2H, -CH_2-S), 3.27–3.21 (m, 2H, S-C*H*-CH_3), 1.42 (d, 6H, -CH_3) ppm; ^{13}C NMR (100 MHz, CD_2Cl_2) δ 136.06, 120.59, 116.56, 112.02, 111.44, 50.10, 44.04, 30.38, 27.39, 21.36 ppm; MALDI–TOF MS (*m*/*z*): 444 $[M]^+$ (M_{calcd} = 443.86); Anal. calcd for $C_{12}H_{12}O_2S_8$: C, 32.41; H, 2.72; O, 7.19; S, 57.68; found: C, 32.72; H, 2.55; O, 6.95; S, 57.93 (%).

(*R*,*R*)-1: The same synthetic procedure was followed as for the (*S*,*S*)-enantiomer starting from (*R*,*R*)-**3**. Yellow orange solid (32 mg, 35%). Single crystals were obtained by slow evapor-

ation of a dichloromethane solution. Anal. calcd for $C_{12}H_{12}O_2S_8$: C, 32.41; H, 2.72; O, 7.19; S, 57.68; found: C, 32.68; H, 2.61; O, 7.01; S, 57.88 (%).

Crystallography: X-ray diffraction measurements were performed on a Nonius Kappa CCD diffractometer, using graphite-monochromated Mo Kα radiation (λ = 0.71073 Å). The structures were solved (SHELXS-97) by direct methods and refined (SHELXL-97) by full-matrix least-square procedures on F^2 [34]. The non-H atoms were refined with anisotropic displacement parameters. A summary of the crystallographic data and the structure refinement is given in Table 2. CCDC reference numbers: CCDC 1057825 (*R*,*R*)-**1** and CCDC 1057826 (*S*,*S*)-**1**. These data can be obtained free of charge from The Cambridge Crystallographic Data Centre via http://www.ccdc.cam.ac.uk/data_request/cif.

Table 2: Crystallographic data, details of data collection and structure refinement parameters for (*S*,*S*)-**1** and (*R*,*R*)-**1**.

	(*R*,*R*)-**1**	(*S*,*S*)-**1**
Moiety formula	$C_{12}H_{12}O_2S_8$	$C_{12}H_{12}O_2S_8$
M [gmol^{-1}]	444.70	444.70
T [K]	293(2)	293(2)
Crystal system	Orthorhombic	Orthorhombic
Space group	P*212121*	P*212121*
a [Å]	6.9459(9)	10.1062(9)
b [Å]	15.258(2)	11.5753(12)
c [Å]	16.523(3)	29.583(2)
α [°]	90.000	90.000
β [°]	90.000	90.000
γ [°]	90.000	90.000
V [Å^3]	1751.1(4)	3460.7(6)
Z	4	8
ρ_{calcd} [g cm^{-3}]	1.687	1.707
μ [mm^{-1}]	1.020	1.032
Goodness-of-fit on F^2	1.077	1.040
Final R1/*w*R2 [I > 2σ(I)]	0.0429/0.0809	0.0591/0.0978
R1/*w*R2 (all data)	0.0737/0.0910	0.1058/0.1089

Electrochemical studies: Cyclic voltammetry measurements were carried out with a Biologic SP-150 potentiostat in a glove box containing dry, oxygen-free (<1 ppm) argon at 293 K, by using a three-electrode cell equipped with a platinum millielectrode of 0.126 cm^2 area, an Ag/Ag$^+$ pseudo-reference electrode and a platinum-wire counter electrode. The potential values were then re-adjusted with respect to the saturated calomel electrode (SCE). The electrolytic media involved a 0.1 mol/L solution of (n-Bu_4N)PF_6 in CH_2Cl_2/acetonitrile 1:1. All experiments were performed at room temperature at 0.1 V/s.

Supporting Information

Supporting Information File 1

^{1}H NMR spectra of (*S*,*S*)-**3** and (*S*,*S*)-**1** and cyclic voltammogram of (*S*,*S*)-**1**.
[http://www.beilstein-journals.org/bjoc/content/supplementary/1860-5397-11-124-S1.pdf]

Acknowledgements

This work was supported by the National Agency for Research (ANR, Project 09-BLAN-0045-01), the CNRS and the University of Angers.

References

1. Wallis, J. D.; Karrer, A.; Dunitz, J. D. *Helv. Chim. Acta* **1986,** *69,* 69–70. doi:10.1002/hlca.19860690110
2. Karrer, A.; Wallis, J. D.; Dunitz, J. D.; Hilti, B.; Mayer, C. W.; Bürkle, M.; Pfeiffer, J. *Helv. Chim. Acta* **1987,** *70,* 942–953. doi:10.1002/hlca.19870700405
3. Avarvari, N.; Wallis, J. D. *J. Mater. Chem.* **2009,** *19,* 4061–4076. doi:10.1039/b820598a
4. Griffiths, J.-P.; Nie, H.; Brown, R. J.; Day, P.; Wallis, J. D. *Org. Biomol. Chem.* **2005,** *3,* 2155–2166. doi:10.1039/b502437d
5. Réthoré, C.; Fourmigué, M.; Avarvari, N. *Chem. Commun.* **2004,** 1384–1385. doi:10.1039/b402877e
6. Réthoré, C.; Fourmigué, M.; Avarvari, N. *Tetrahedron* **2005,** *61,* 10935–10942. doi:10.1016/j.tet.2005.08.104
7. Réthoré, C.; Avarvari, N.; Canadell, E.; Auban-Senzier, P.; Fourmigué, M. *J. Am. Chem. Soc.* **2005,** *127,* 5748–5749. doi:10.1021/ja0503884
8. Madalan, A. M.; Réthoré, C.; Fourmigué, M.; Canadell, E.; Lopes, E. B.; Almeida, M.; Auban-Senzier, P.; Avarvari, N. *Chem. – Eur. J.* **2010,** *16,* 528–537. doi:10.1002/chem.200901980
9. Pop, F.; Laroussi, S.; Cauchy, T.; Gómez-García, C. J.; Wallis, J. D.; Avarvari, N. *Chirality* **2013,** *25,* 466–474. doi:10.1002/chir.22210
10. Pop, F.; Auban-Senzier, P.; Frąckowiak, A.; Ptaszyński, K.; Olejniczak, I.; Wallis, J. D.; Canadell, E.; Avarvari, N. *J. Am. Chem. Soc.* **2013,** *135,* 17176–17186. doi:10.1021/ja408350r
11. Pop, F.; Auban-Senzier, P.; Canadell, E.; Rikken, G. L. J. A.; Avarvari, N. *Nat. Commun.* **2014,** *5,* No. 3757. doi:10.1038/ncomms4757
12. Rikken, G. L. J. A.; Fölling, J.; Wyder, P. *Phys. Rev. Lett.* **2001,** *87,* 236602. doi:10.1103/PhysRevLett.87.236602
13. Krstić, V.; Roth, S.; Burghard, M.; Kern, K.; Rikken, G. L. J. A. *J. Chem. Phys.* **2002,** *117,* 11315–11319. doi:10.1063/1.1523895
14. Hasegawa, M.; Sone, Y.; Iwata, S.; Matsuzawa, H.; Mazaki, Y. *Org. Lett.* **2011,** *13,* 4688–4691. doi:10.1021/ol201857f
15. Biet, T.; Fihey, A.; Cauchy, T.; Vanthuyne, N.; Roussel, C.; Crassous, J.; Avarvari, N. *Chem. – Eur. J.* **2013,** *19,* 13160–13167. doi:10.1002/chem.201301095
16. Kobayakawa, K.; Hasegawa, M.; Sasaki, H.; Endo, J.; Matsuzawa, H.; Sako, K.; Yoshida, J.; Mazaki, Y. *Chem. – Asian J.* **2014,** *9,* 2751–2754. doi:10.1002/asia.201402667
17. Saad, A.; Jeannin, O.; Fourmigué, M. *Tetrahedron* **2011,** *67,* 3820–3829. doi:10.1016/j.tet.2011.03.103

18. Danila, I.; Riobé, F.; Piron, F.; Puigmartí-Luis, J.; Wallis, J. D.; Linares, M.; Ågren, H.; Beljonne, D.; Amabilino, D. B.; Avarvari, N. *J. Am. Chem. Soc.* **2011,** *133,* 8344–8353. doi:10.1021/ja202211k
19. Danila, I.; Pop, F.; Escudero, C.; Feldborg, L. N.; Puigmartí-Luis, J.; Riobé, F.; Avarvari, N.; Amabilino, D. B. *Chem. Commun.* **2012,** *48,* 4552–4554. doi:10.1039/c2cc30789h
20. Awheda, I.; Krivickas, S. J.; Yang, S.; Martin, L.; Guziak, M. A.; Brooks, A. C.; Pelletier, F.; Le Kerneau, M.; Day, P.; Horton, P. N.; Akutsu, H.; Wallis, J. D. *Tetrahedron* **2013,** *69,* 8738–8750. doi:10.1016/j.tet.2013.07.089
21. Pop, F.; Melan, C.; Danila, I.; Linares, M.; Beljonne, D.; Amabilino, D. B.; Avarvari, N. *Chem. – Eur. J.* **2014,** *20,* 17443–17453. doi:10.1002/chem.201404753
22. Matsumiya, S.; Izuoka, A.; Sugawara, T.; Taruishi, T.; Kawada, Y. *Bull. Chem. Soc. Jpn.* **1993,** *66,* 513–522. doi:10.1246/bcsj.66.513
23. Matsumiya, S.; Izuoka, A.; Sugawara, T.; Taruishi, T.; Kawada, Y.; Tokumoto, M. *Bull. Chem. Soc. Jpn.* **1993,** *66,* 1949–1954. doi:10.1246/bcsj.66.1949
24. Pop, F.; Allain, M.; Auban-Senzier, P.; Martínez-Lillo, J.; Lloret, F.; Julve, M.; Canadell, E.; Avarvari, N. *Eur. J. Inorg. Chem.* **2014,** 3855–3862. doi:10.1002/ejic.201400125
25. Yang, S.; Pop, F.; Melan, C.; Brooks, A. C.; Martin, L.; Horton, P.; Auban-Senzier, P.; Rikken, G. L. J. A.; Avarvari, N.; Wallis, J. D. *CrystEngComm* **2014,** *16,* 3906–3916. doi:10.1039/c3ce42539h
26. Atzori, M.; Pop, F.; Auban-Senzier, P.; Clérac, R.; Canadell, E.; Mercuri, M. L.; Avarvari, N. *Inorg. Chem.* **2015,** *54,* 3643–3653. doi:10.1021/acs.inorgchem.5b00261
27. Chas, M.; Lemarié, M.; Gulea, M.; Avarvari, N. *Chem. Commun.* **2008,** 220–222. doi:10.1039/B714245E
28. Chas, M.; Riobé, F.; Sancho, R.; Minguíllon, C.; Avarvari, N. *Chirality* **2009,** *21,* 818–825. doi:10.1002/chir.20692
29. Pop, F.; Lacour, J.; Avarvari, N. *Rev. Roum. Chim.* **2012,** *57,* 457–462.
30. Wieland, T.; Götzendörfer, C.; Dabrowski, J.; Lipscomb, W. N.; Shoham, G. *Biochemistry* **1983,** *22,* 1264–1271. doi:10.1021/bi00274a043
31. Bouamaied, I.; Constable, E. C.; Housecroft, C. E.; Neuburger, M.; Zampese, J. A. *Dalton Trans.* **2012,** *41,* 10276–10285. doi:10.1039/c2dt30892d
32. de León, A.; Guerrero, M.; García-Antón, J.; Ros, J.; Font-Bardía, M.; Pons, J. *CrystEngComm* **2013,** *15,* 1762–1771. doi:10.1039/c2ce26687c
33. Svenstrup, N.; Rasmussen, K. M.; Hansen, T. K.; Becher, J. *Synthesis* **1994,** 809–812. doi:10.1055/s-1994-25580
34. *Programs for the Refinement of Crystal Structures;* University of Göttingen: Göttingen, Germany, 1996.

License and Terms

BEILSTEIN JOURNAL OF ORGANIC CHEMISTRY

Advances in the synthesis of functionalised pyrrolotetrathiafulvalenes

Luke J. O'Driscoll, Sissel S. Andersen, Marta V. Solano, Dan Bendixen, Morten Jensen, Troels Duedal, Jess Lycoops, Cornelia van der Pol, Rebecca E. Sørensen, Karina R. Larsen, Kenneth Myntman, Christian Henriksen, Stinne W. Hansen and Jan O. Jeppesen*

Full Research Paper

Open Access

Address:
Department of Physics, Chemistry and Pharmacy, University of Southern Denmark, Campusvej 55, DK-5230, Odense M, Denmark

Email:
Jan O. Jeppesen* - joj@sdu.dk

* Corresponding author

Keywords:
heterocycles; protecting groups; sulfur chemistry; tetrathiafulvalene; Ullman coupling

Beilstein J. Org. Chem. **2015,** *11,* 1112–1122.
doi:10.3762/bjoc.11.125

Received: 02 March 2015
Accepted: 13 May 2015
Published: 03 July 2015

This article is part of the Thematic Series "Tetrathiafulvalene chemistry".

Guest Editor: P. J. Skabara

Abstract

The electron-donor and unique redox properties of the tetrathiafulvalene (TTF, **1**) moiety have led to diverse applications in many areas of chemistry. Monopyrrolotetrathiafulvalenes (MPTTFs, **4**) and bispyrrolotetrathiafulvalenes (BPTTFs, **5**) are useful structural motifs and have found widespread use in fields such as supramolecular chemistry and molecular electronics. Protocols enabling the synthesis of functionalised MPTTFs and BPTTFs are therefore of broad interest. Herein, we present the synthesis of a range of functionalised MPTTF and BPTTF species. Firstly, the large-scale preparation of the precursor species *N*-tosyl-(1,3)-dithiolo[4,5-*c*]pyrrole-2-one (**6**) is described, as well as the synthesis of the analogue *N*-tosyl-4,6-dimethyl-(1,3)-dithiolo[4,5-*c*]pyrrole-2-one (**7**). Thereafter, we show how **6** and **7** can be used to prepare BPTTFs using homocoupling reactions and functionalised MPTTFs using cross-coupling reactions with a variety of 1,3-dithiole-2-thiones (**19**). Subsequently, the incorporation of more complex functionality is discussed. We show how the 2-cyanoethyl protecting group can be used to afford MPTTFs functionalised with thioethers, exemplified by a series of ethylene glycol derivatives. Additionally, the merits of 1,8-diazabicyclo[5.4.0]undec-7-ene (DBU) as an alternative to the most common deprotecting agent, $CsOH{\cdot}H_2O$ are discussed. Finally, we show how a copper-mediated Ullman-type reaction can be applied to the *N*-arylation of MPTTFs and BPTTFs using a variety of aryl halides.

Introduction

Tetrathiafulvalene (TTF) derivatives are of considerable interest in the fields of supramolecular chemistry and molecular machines [1-5], molecular and organic electronics [5-7], chemosensors [1,8-11], coordination chemistry [12-14], catalysis [15] and beyond [16-21]. This owes much to the strong electron-donor character of the TTF moiety and its derivatives,

which have been utilized in the formation of charge-transfer (CT) complexes for more than 40 years [21-23].

TTF (**1**) (Figure 1) is not aromatic according to the Hückel definition as its 14 π-electrons lack cyclic conjugation. Upon oxidation to the radical cation (**2**) and dication (**3**) states, a gain in aromaticity occurs: **2** contains a single aromatic, 6 π-electron 1,3-dithiolium system, and **3** possesses two such systems (Figure 1). These oxidations occur at low potential ($E^1_{1/2}$ = 0.34 V and $E^2_{1/2}$ = 0.73 V vs Ag/AgCl in MeCN [4]) and can be performed sequentially and reversibly. Additionally, both **2** and **3** are thermodynamically stable. These properties are responsible for the strong electron-donor character of TTF and its derivatives. Furthermore, the precise oxidation potential of a TTF derivative can be changed by the addition of electron-donating or electron-withdrawing substituents [4]. Usually, each of the three stable oxidation states possesses a distinct UV–vis absorption spectrum [4], facilitating studies of redox behaviour.

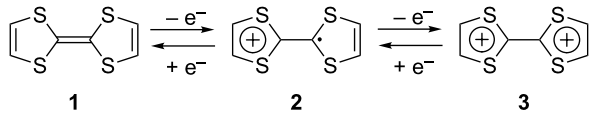

Figure 1: The sequential, reversible oxidation of TTF (**1**) to its stable radical cation (**2**) and dication (**3**) states.

To exploit the properties of TTF in more complex systems, various functionalised derivatives have been prepared, including both alkylated, arylated and annelated species [7]. A common complication encountered with such functionalised TTFs is the existence of *cis* and *trans* stereoisomers. The investigation of the properties of a single isomer is challenging, not only due to difficulties in the separation of the isomers, but also because it is possible for the isomers to interconvert in the presence of acid or light [24]. Studies of functionalised TTFs must therefore often use mixtures of isomers, although in some cases only one isomer exhibits the desired behaviour [9]. Isomeric mixtures can also complicate the interpretation of spectroscopic data.

These drawbacks led the group of Jeppesen and Becher to develop pyrrole-annelated TTF derivatives: monopyrrolotetrathiafulvalenes (MPTTFs, **4**) and bispyrrolotetrathiafulvalenes (BPTTFs, **5**) (Figure 2) [4,25]. The presence of either one or two fused pyrrole rings, respectively, eliminates *cis–trans* isomerism whilst still allowing for further functionalisation. Methodologies have been developed which facilitate the preparation of MPTTFs and BPTTFs independently substituted in almost all of the positions indicated in Figure 2. This ranges from the addition of simple alkyl, acyl or aryl substituents [13,19,26-28] to the preparation of fused ring systems [11,27], to the incorporation of MPTTFs and BPTTFs into more complex molecular architectures such as macrocycles [8,9,14], calix-pyrroles [1,10,11], calixarenes [29] and porphyrins [30]. Note that for MPTTFs, R^1 and R^2 can be either the same or different.

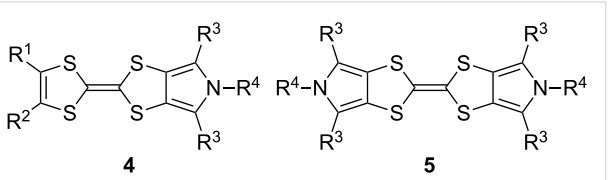

Figure 2: Structures and possible substitution positions of MPTTFs (**4**) and BPTTFs (**5**).

Here, we present recent developments in the synthesis of functionalised MPTTFs and BPTTFs. We report a more convenient and larger scale (>20 g) synthesis of the key building block *N*-tosyl-(1,3)-dithiolo[4,5-*c*]pyrrole-2-one (**6**), than that previously published [25], in addition to the synthesis of its dimethylated analogue, *N*-tosyl-4,6-dimethyl-(1,3)-dithiolo[4,5-*c*]pyrrole-2-one (**7**). We then provide a range of examples where **6** and **7** are used in the preparation of functionalised MPTTFs and BPTTFs. We expand on this by discussing subsequent additional functionalisation of MPTTFs and BPTTFs by two different methods: (i) the use of 2-cyanoethyl-protected thiols as a means to further functionalise MPTTFs with thioethers and (ii) copper-mediated *N*-arylation of both MPTTFs and BPTTFs.

Results and Discussion

An improved large-scale synthesis of *N*-tosyl-(1,3)-dithiolo[4,5-*c*]pyrrole-2-one (**6**)

The known compound **6** [4,25] is an important building block in the preparation of MPTTFs and BPTTFs. We have further developed the synthesis previously reported by our group [4,25] and can now isolate **6** in quantities in excess of 20 g. Our current large-scale synthetic strategy (Scheme 1) is comparable to that described in 2000 [25] but requires fewer intermediate purification steps. Diester **8** can be prepared from commercially available ethylene trithiocarbonate (**9**) and dimethyl acetylenedicarboxylate (**10**) at around 100 g scale in 74% yield (based on previously reported large-scale syntheses [31,32]). We have scaled up the reduction of **8** using sodium borohydride and lithium bromide to 40 g scale, obtaining diol **11** with only a small reduction in yield (77% vs 85% at 15 g scale [33]). Compound **11** is then treated with phosphorus tribromide to afford dibromide **12**. The scale up of this reaction to 36 g scale also results in a lower, but still acceptable yield (75% vs 91% at approximately 5 g scale [25]). The conversion of **12** to **6**

is achieved in three steps with minimal intermediate purification, beginning with up to 44 g of **12**. Reaction of **12** with sodium tosylamide (**13**) (prepared from tosylamide according to a literature procedure [34]) affords the cyclised product **14**. Crude material of sufficient purity for the following step can be isolated by precipitation (see the Experimental section in the Supporting Information File 1). Transchalcogenation of crude **14** affords **15** and aromatisation of crude **15** using 2,3-dichloro-5,6-dicyano-1,4-benzoquinone (DDQ) gives **6**, which is purified by column chromatography, in 52% overall yield (22.5 g) from **12**. We have also consistently obtained comparable yields of around 55% using the same method at approximately half this scale. The ability to isolate multigram quantities of **6**, which can be stored for years on the shelf, makes the subsequent synthesis of various MPTTF and BPTTF derivatives much more convenient and accessible.

Synthesis of *N*-tosyl-4,6-dimethyl-(1,3)-dithiolo[4,5-*c*]pyrrole-2-one (**7**)

To the best of our knowledge, the synthesis of **7**, the dimethylated analogue of **6**, has not been previously reported by other groups. *N*-Phenylated and *N*-Boc-protected analogues were, however, reported in 1996 [35]. Based on that work, we have developed a preparation of **7** (Scheme 2) [36]. Functionalised pyrrole **16** was prepared according to the literature [35,37] then tosylated in high yield to afford **17**. The reduction of the thiocyanate moieties with $LiAlH_4$ afforded the air-sensitive intermediate **18** (not characterised), which was treated with 1,1'-carbonyldiimidazole to afford **7**, in 83% yield over the two steps.

Preparation of functionalised MPTTFs and BPTTFs

Coupling reactions

Pyrrole-annelated TTF derivatives can be prepared from **6** and **7** by means of coupling reactions in triethyl phosphite (Scheme 3). The known homocoupling reaction of **6** affords the bis-tosylated BPTTF **5a** in high yield with minimal purification [25]. We have obtained a comparable yield (76% vs 84%) working at twice the previously published scale [25]. The equivalent reaction can be conducted using **7** to give BPTTF **5b** with a similar yield of 79% [36], a modest improvement on the reported yield of 73% for the Boc-protected analogue [35].

The synthesis of MPTTFs can be achieved using cross-coupling reactions between **6** and 1,3-dithiole-2-thiones **19** [38].

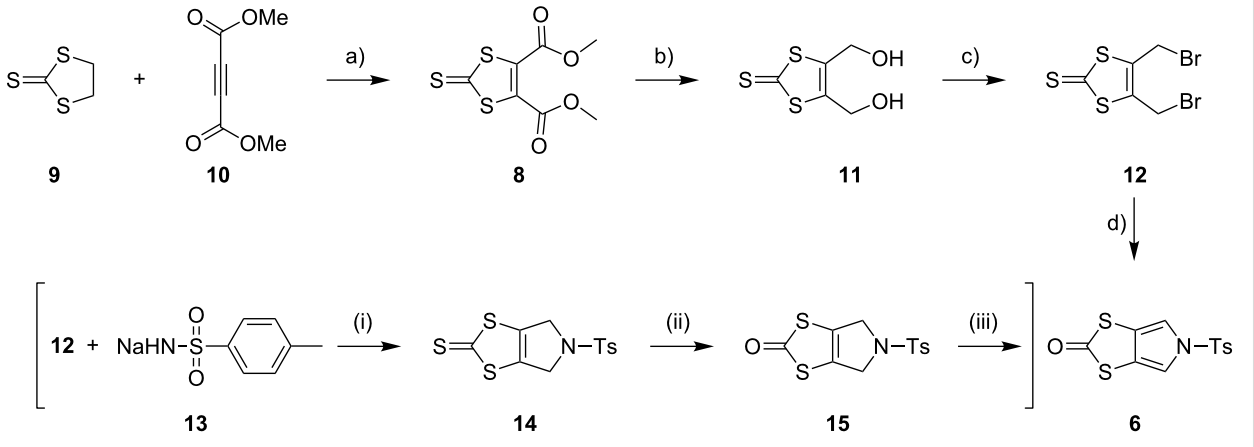

Scheme 1: Large-scale synthesis of **6**. Reagents and conditions: a) PhMe, reflux, 19 h, 74%; b) LiBr, $NaBH_4$, THF, MeOH, −10 °C → rt, 20 h, 77%; c) PBr_3, THF, 0 °C → rt, 20 h, 75%; d) (i) **13**, MeCN, DMF, 80 °C, 15 min, (ii) $Hg(OAc)_2$, $CHCl_3$, AcOH, rt, 24 h, (iii) DDQ, PhCl, reflux, 4 h, 52% (from **12**).

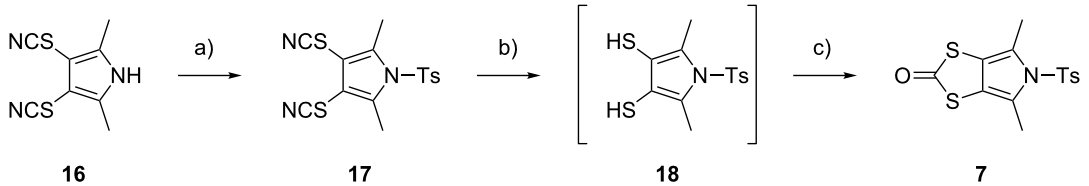

Scheme 2: Preparation of **7**. Reagents and conditions: a) TsCl, Et_3N, DMAP, MeCN, rt → reflux, 3.5 h, 82%; b) (i) $LiAlH_4$, THF, 0 °C, 2.5 h, (ii) AcOH, Et_2O, 0 °C; c) $(Im)_2CO$, THF, 0 °C, 1 h, 83% (from **17**).

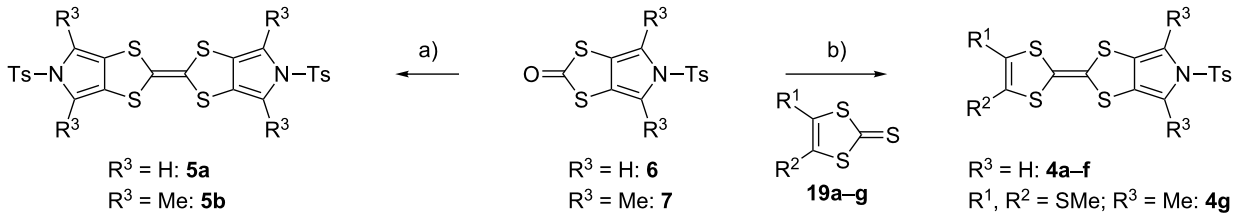

Scheme 3: Homo and cross-coupling reactions of **6** or **7** afford BPTTFs and MPTTFs, respectively. Reagents and conditions: a) $(EtO)_3P$, 120–130 °C, 5–5.5 h, 76–79%; b) $(EtO)_3P$, 120–135 °C, 1–4 h, 70–87%.

These reactions (Scheme 3 and Table 1) use an excess of **19** to minimise the formation of **5a** as a byproduct, making it possible to isolate tosylated MPTTFs (such as **4a**–**f**) in high yields. This is believed to be due to the higher reactivity of sulfur ylide intermediates (formed from 1,3-dithiole-2-thiones) with 1,3-dithiole-2-ones than with excess 1,3-dithiole-2-thiones [39].

Table 1 lists a selection of *N*-tosylated MPTTFs **4a**–**f** prepared from **6** and **19a**–**f**, respectively, with yields ranging from 70–87% despite the concomitant formation of homocoupled byproducts. Compound **7** (and related species [27]) can also be used in cross-coupling reactions, exemplified by its reaction with **19g** to give **4g** (Scheme 3 and Table 1) [36]. Our group has

Table 1: Cross-coupling reactions between 1,3-dithiole-2-ones and 1,3-dithiole-2-thiones affording MPTTFs.

1,3-Dithiole-2-one	1,3-Dithiole-2-thione	Product	% Yield
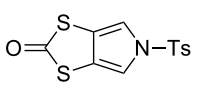 **6**	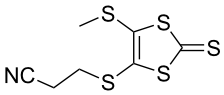 **19a**	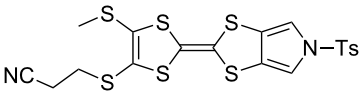 **4a**	85 (lit. 64 [41])
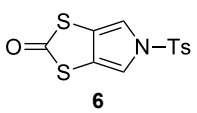 **6**	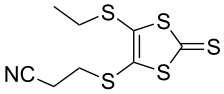 **19b**	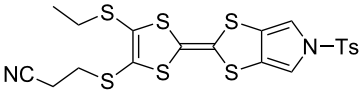 **4b**	83 (lit. 74 [42])
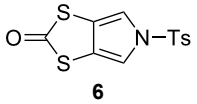 **6**	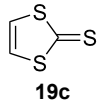 **19c**	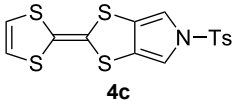 **4c**	71 (lit. 60 [28])
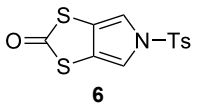 **6**	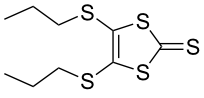 **19d**	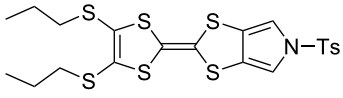 **4d**	87 (lit. 62 [43])
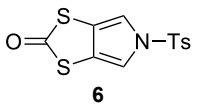 **6**	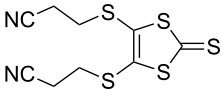 **19e**	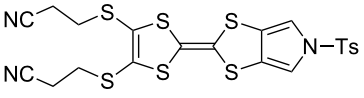 **4e**	70 (lit. 64 [25])
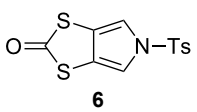 **6**	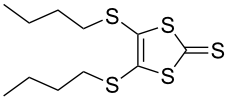 **19f**	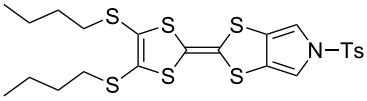 **4f**	85 [44]
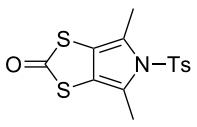 **7**	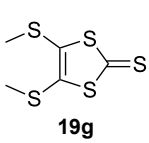 **19g**	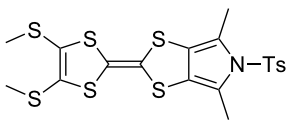 **4g**	80 [36]

previously shown that it is also possible to introduce substituents directly onto the pyrrole ring of MPTTF **4d** [40].

Further functionalisation of MPTTFs bearing a 2-cyanoethyl-protected thiol

The 2-cyanoethyl protecting group offers a convenient means of synthesising MPTTFs where one or both of R^1 and R^2 are thioethers. When only simple alkyl thioethers are targeted, it is often more effective to incorporate these moieties prior to the cross-coupling step that is used to form the TTF core, as described in the previous section. However, many functionalities or larger molecular architectures do not tolerate the harsh coupling conditions and must be added subsequently. The preparation of a series of analogous compounds can also be facilitated by preparing a common, protected MPTTF intermediate, such as **4a**, **4b** or **4e**, in large quantities, particularly in light of the good stability of the cyanoethyl and tosyl protecting groups.

As a simple example of this protocol, it has previously been shown that caesium hydroxide monohydrate ($CsOH·H_2O$) and methyl iodide can be used to accomplish the transformation of 2-cyanoethyl thioethers to methyl thioethers in high yield for both TTFs [38] and MPTTFs [25]. Thus deprotection and alkylation are achieved in a single synthetic step (e.g. the preparation of **4h** from **4a** in Scheme 4). Furthermore, when R^1 and R^2 are both 2-cyanoethyl thioethers (**4e**) these reagents can be used to selectively deprotect and alkylate only one of the two thiols, affording MPTTF **4a** (Scheme 4) [25]. Indeed, the direct preparation of **4h** from **4e** requires two iterative additions of base and alkylating agent. A wide range of other, more complex alkylating agents can be successfully used in place of methyl iodide. For example, functionalised ethylene glycol oligomers have been used in the preparation of rotaxanes and pseudorotaxanes [28,41,42,45].

Although $CsOH·H_2O$ is most commonly used, other bases are also known to remove the cyanoethyl protecting group from TTF derivatives [46]. However, some of these bases (e.g. sodium methoxide) are incompatible with the *N*-tosyl protecting group typically present during the synthesis of functionalised MPTTFs (see Scheme 3), and therefore cannot be used with these materials.

We have found that in many cases the use of 1,8-diazabicyclo[5.4.0]undec-7-ene (DBU, Scheme 5), rather than $CsOH·H_2O$, allows for a more convenient and consistent synthesis with a comparable or higher yield, which is also easier to conduct on a larger scale. DBU is an easily handled liquid which can be directly added to a deprotection reaction in a single portion. In contrast, $CsOH·H_2O$ is a highly hygroscopic solid which must typically be added dropwise as a solution in (a minimum of) methanol, in which it has low solubility. This dropwise addition is important to minimise deprotection of the tosyl group of MPTTFs, a side reaction which can be caused by the presence of small quantities of methoxide ions in the reaction mixture. As DBU is a non-nucleophilic base, such deprotection cannot occur. Note that unlike in the case of $CsOH·H_2O$ it is important to heat reactions using DBU to achieve good conversion. Thus, this base is unsuitable if temperature-sensitive moieties are present elsewhere in the molecule. Representative substitutions of MPTTFs [47] with alkyl halides **20**-X [48], **21**-X [49] and **22**-X [50] (where X is a halogen) using both bases are shown in Scheme 5 and Table 2. The products **4i–l** are used as building blocks in our work on rotaxanes and psuedorotaxanes [45,50].

When the preparation of the same product using each of the two bases is compared, it can be seen that the use of DBU rather than $CsOH·H_2O$ usually results in at least a modest increase in yield. We have prepared **4i** several times with each base and achieved more consistent yields with DBU (typically 88–90%) than with $CsOH·H_2O$ (typically 80–90%, occasionally lower), although the latter afforded the highest yield of **4i** we have obtained to date (92%). The largest difference in yields is seen for the preparations of **4k**, but it should be noted that the reac-

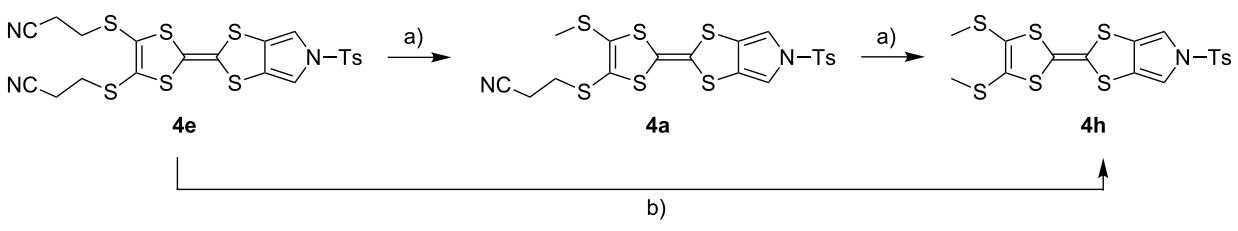

Scheme 4: Deprotection and methylation of cyanoethyl-protected thiol moieties on MPTTFs as reported by Jeppesen et al. [25]. Reagents and conditions: a) (i) 1 equiv $CsOH·H_2O$, MeOH, THF, rt, 1 h, (ii) MeI, THF, rt, 30 min; b) (i) 1 equiv $CsOH·H_2O$, MeOH, THF, rt, 1 h, (ii) MeI, THF, rt, 45 min, (iii) 1 equiv $CsOH·H_2O$, MeOH, THF, rt, 1 h, (iv) MeI, THF, rt, 30 min.

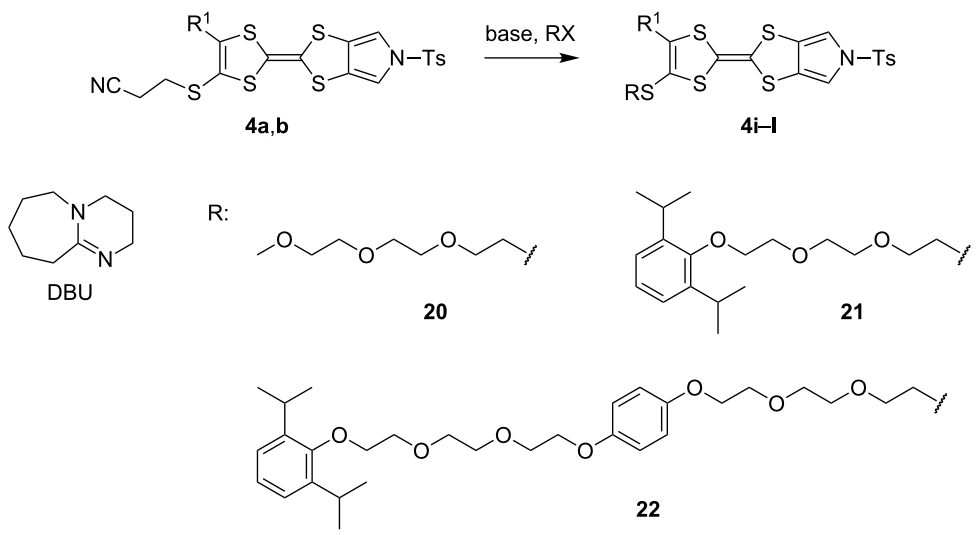

Scheme 5: Deprotection and alkylation of cyanoethyl-protected thiol moieties on MPTTFs using $CsOH·H_2O$ or DBU. Reagents and conditions are detailed in Table 2.

Table 2: Deprotection and alkylation of cyanoethyl-protected thiol moieties on MPTTFs using $CsOH·H_2O$ or DBU.

Substrate (R^1)	RX	Product	Base and conditions	% Yield
4b (SEt)	**20**-I	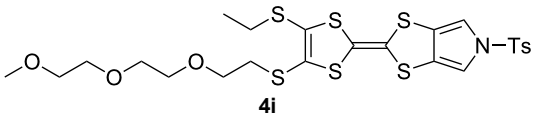 **4i**	$CsOH·H_2O$, THF, MeOH, rt, 16 h	92 (lit. 88 [45])
			DBU, THF, reflux, 20 h	90
4a (SMe)	**20**-I	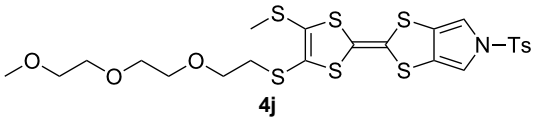 **4j**	$CsOH·H_2O$, THF, MeOH, rt, 2.5 h	87
			DBU, THF, reflux, 18 h	91
4a (SMe)	**21**-Br	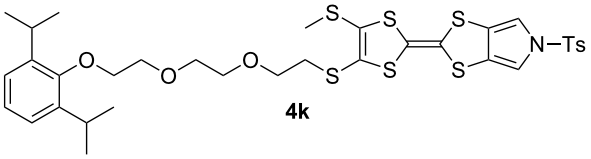 **4k**	$CsOH·H_2O$, THF, MeOH, rt, 20 h	53
4a (SMe)	**21**-I		DBU, THF, reflux, 17 h	93
4a (SMe)	**22**-I	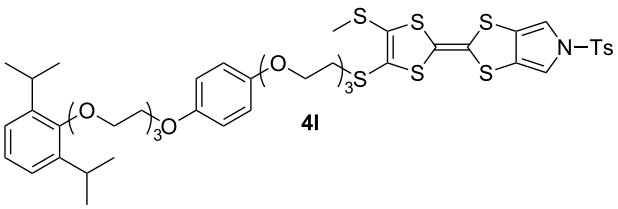 **4l**	$CsOH·H_2O$, THF, MeOH, rt, 18 h	88
			DBU, THF, reflux, 3 d	92

tion with $CsOH·H_2O$ used an alkyl bromide whereas that with DBU used the more reactive alkyl iodide analogue. Therefore, this effect may not relate to the change of base alone. In summary, the use of DBU as a deprotecting reagent was found to be high-yielding, consistent and more convenient than the use of $CsOH·H_2O$.

N-Arylation of MPTTFs and BPTTFs

N-Alkylation of MPTTFs and BPTTFs can be easily achieved using S_N2 reactions between a deprotonated pyrrole and a suitably activated aliphatic species [19,28]. *N*-Arylation of MPTTFs and BPTTFs, which allows an annelated TTF to be incorporated into a larger conjugated system, is less common,

although interest has increased in recent years. These reactions can be accomplished using a copper-mediated Ullman-type reaction, based on conditions reported by Buchwald and co-workers for the arylation of nitrogen-containing heterocycles and the amidation of aryl halides [51,52]. Examples of TTF derivatives synthesised using this protocol by other groups include: MPTTF and BPTTF-triarylamine conjugates (as possible charge-transport materials) [53], MPTTF-triarylborane conjugates (with possible applications as fluoride sensors) [54], and MPTTF-functionalised calix[4]arenes (which can bind to electron-deficient aromatics and form charge-transfer complexes) [29]. Alternative routes to *N*-arylated MPTTFs proceed through *N*-arylated (1,3)-dithiolo[4,5-*c*]pyrrole-2-ones or (1,3)-dithiolo[4,5-*c*]pyrrole-2-thiones (i.e. analogues of **6**). In some cases these can be prepared similarly to **6** [55], but an alternative route may be required if the desired aryl unit possesses reactive functional groups [12]. These routes are also limited to intermediates that can tolerate the harsh conditions of the subsequent coupling reaction used to form the TTF moiety. Our discussions here will be limited to copper-mediated C–N-bond formation, as we find this to be a flexible and convenient method.

Recent work in our laboratory has involved the *N*-arylation of MPTTFs, including both unsubstituted and thioether-substituted examples (Scheme 6 and Table 3). These materials have served as intermediates and model systems in the synthesis of, for example, donor–acceptor systems, chemosensors and materials with molecular electronics applications [44,56]. The *N*-tosyl protecting group of precursor MPTTFs (**4c**, **4d**, **4f** and **4g**) must first be removed. This can be achieved in excellent yield (89–95%) using sodium methoxide (Scheme 6). The deprotection of MPTTFs derived from **6** proceeded rapidly (15–40 min), whereas that of **4g**, derived from **7**, required 6 h, presumably because of the increased steric bulk of the substituted pyrrole ring. Copper-mediated coupling between the MPTTF products (**4c'**, **4d'**, **4f'** and **4g'**) and a range of aryl halides is then possible. In this study we have investigated several *p*-substituted species (**23**-X–**28**-X, Scheme 6).

As satisfactory results have been reported for similar arylations [29,53,54] when (±)-*trans*-1,2-diaminocyclohexane, **29** (Scheme 6), is used as the ligand, we also followed this approach, rather than using the costlier methylated analogue favoured by the Buchwald group [52]. To improve reaction yields, we made modifications to the published procedures [29,52-54], which typically utilise catalytic CuI in a sealed reaction vessel with 1,4-dioxane as solvent. Firstly, in our hands, comparable yields could be achieved using either THF or 1,4-dioxane as solvent; THF was therefore favoured to facilitate workup. We also saw improvement upon increasing the amount of CuI to 1–2.5 equiv (typically 2 equiv were used). We investigated the use of a microwave reactor (exemplified by the syntheses of **4m** and **4n** in Table 2, which were carried out under both sealed tube and microwave conditions), which typically allowed for shorter reaction times and resulted in higher

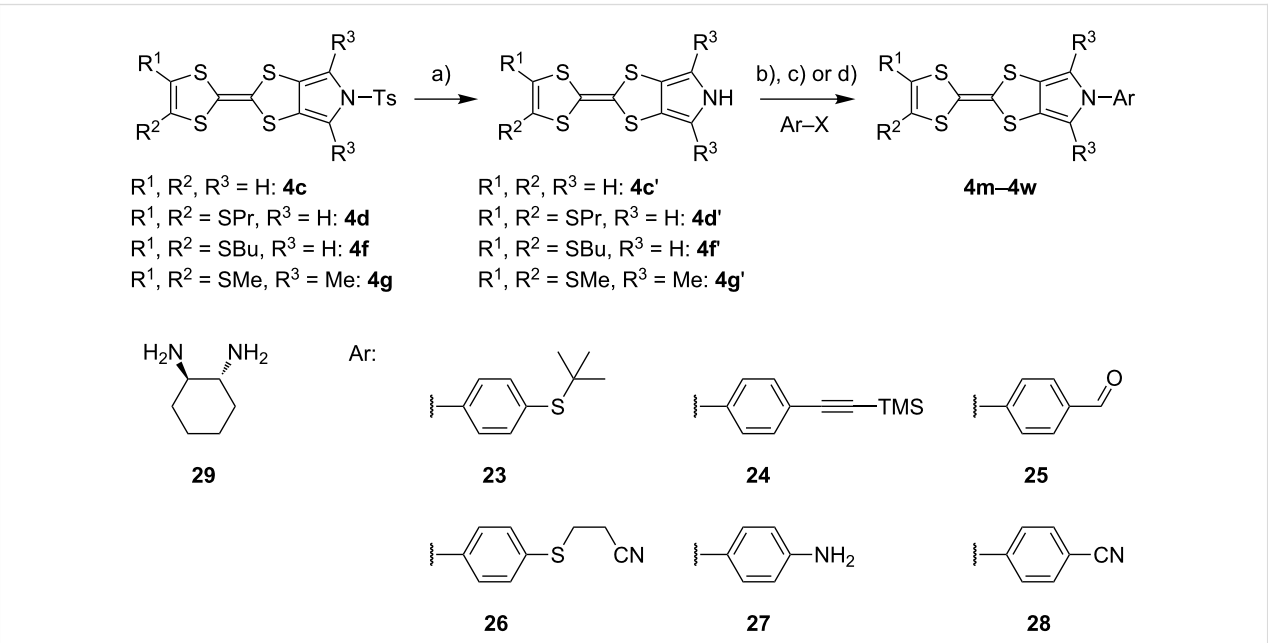

Scheme 6: Deprotection and *N*-arylation of tosylated MPTTFs. Reagents and conditions: a) NaOMe, THF, MeOH, reflux, 15 min–6 h, 89–95%; b) CuI, K_3PO_4, **29**, THF, 80–115 °C (sealed tube), 3–48 h, 25–68%; c) CuI, K_3PO_4, **29**, THF, 100–130 °C (microwave), 2–3 h, 51–93%; d) CuI, K_3PO_4, **29**, THF, reflux, 3 h, 67%.

Table 3: Copper-mediated *N*-arylation of MPTTFs.

MPTTF	Ar-X	Product	Conditions	% Yield
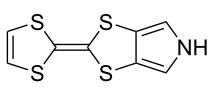 **4c′**	**23**-Br	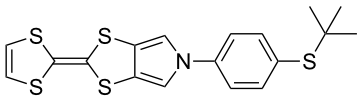 **4m**	ST[a]	35
			MW[b]	81
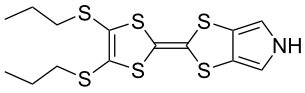 **4d′**	**23**-Br	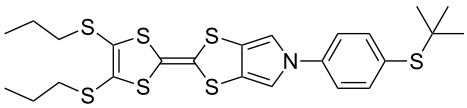 **4n**	ST	68
			MW	93
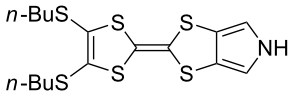 **4f′**	**24**-I	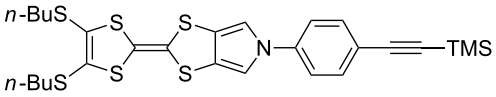 **4o**	Reflux[c]	67
			MW	54
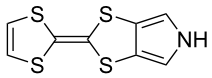 **4c′**	**25**-I	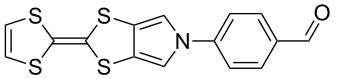 **4p**	ST	35
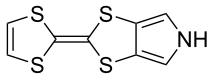 **4c′**	**26**-I	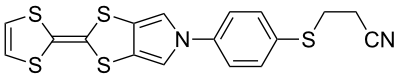 **4q**	ST	52
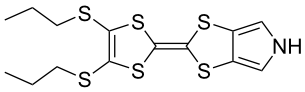 **4d′**	**26**-I	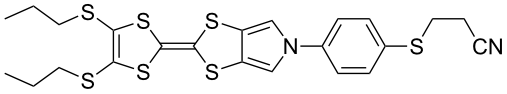 **4r**	ST	65
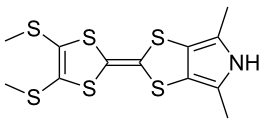 **4g′**	**23**-Br	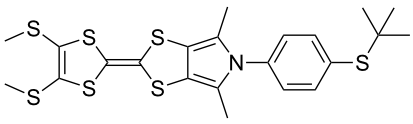 **4s**	ST	25
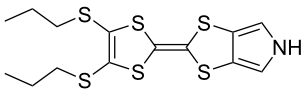 **4d′**	**25**-I	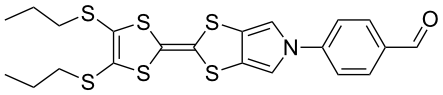 **4t**	MW	82 [56]
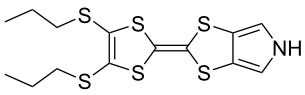 **4d′**	**26**-I	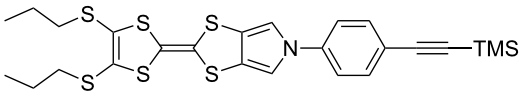 **4u**	MW	51
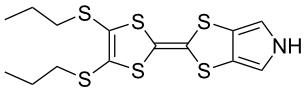 **4d′**	**27**-I	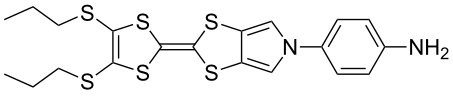 **4v**	MW	80
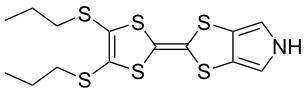 **4d′**	**28**-I	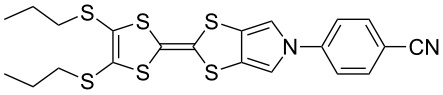 **4w**	MW	64

[a]ST = sealed tube conditions; [b]MW = microwave conditions; [c]Reflux = conventional reflux.

yields. Small alterations to base and ligand loading and reaction temperature were also made, but with no significant effects. A larger-scale synthesis of **4o** has also been conducted under conventional reflux conditions in good yield.

Scheme 6 and Table 3 show the results of reactions between MPTTFs **4c'**, **4d'**, **4f'** and **4g'** and aryl halides **23**-X–**28**-X to give *N*-arylated products **4m**–**w**. Acceptable yields can be obtained with both aryl bromides and aryl iodides, suggesting that the choice of halogen is not critical. *N*-Arylation of dimethylated MPTTF **4g'** gave the lowest yield amongst the reactions performed under sealed tube conditions, which may be attributable to its more sterically hindered pyrrole-*H*. The highest yielding reactions under sealed tube conditions gave comparable yields to the lowest yielding reactions under microwave conditions. In general, the microwave conditions give high yields and can tolerate a range of functional groups on the aryl halide. We believe that the higher yield of **4o** under conventional reflux as compared to microwave conditions relates to the significant increase in scale. This result indicates that the larger scale synthesis of related species should also be viable.

We have begun to extend the sealed tube protocol to the *N*,*N*-diarylation of BPTTFs with promising initial results (Scheme 7 and Table 4). Difficulties were encountered with the isolation, purification and characterisation of the targeted species, which appeared to relate to their extremely poor solubility. Nonetheless, it proved possible to synthesise **5c**–**f** (see Scheme 7 and Table 4), and accomplish some characterisation. The parent deprotected BPTTFs **5a'** and **5b'** were first prepared in near-quantitative yield, comparably to MPTTFs **4c'**, **4d'**, **4f'** and **4g'** (similarly, bulkier **5b'** required a much longer reaction time than **5a'**). In some cases **5a'** was observed to decompose when stored for periods of more than 24 h, although the nature of this decomposition is unclear. Therefore, these materials

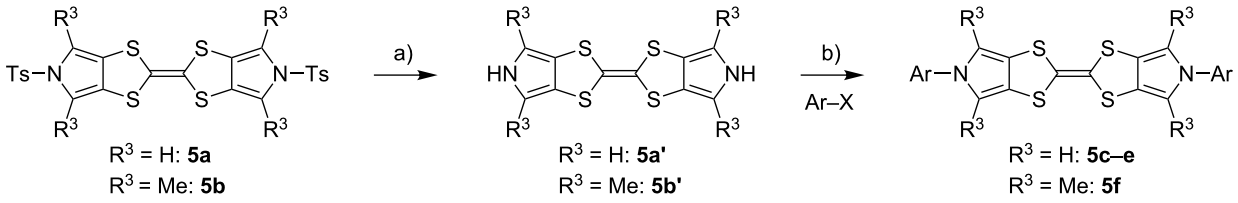

Scheme 7: Deprotection and *N*,*N*-diarylation of tosylated BPTTFs. Reagents and conditions: a) NaOMe, THF, MeOH, reflux, 30 min–8 h, 95–99%; b) CuI, K_3PO_4, **29**, THF or 1,4-dioxane, 98–110 °C (sealed tube), 22–65 h, 24–72%.

Table 4: *N*,*N*-Diarylation of BPTTFs.

Substrate	Ar–X	Product	% Yield
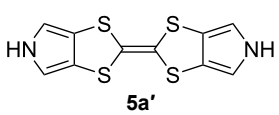 **5a'**	**23**-Br	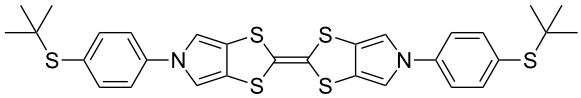 **5c**	42[a]/73[b]
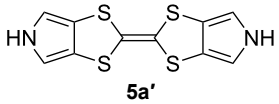 **5a'**	**25**-I	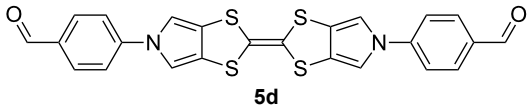 **5d**	45[a] [56]
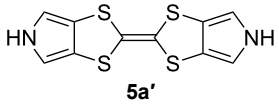 **5a'**	**26**-I	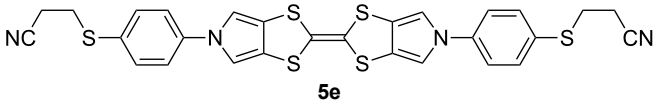 **5e**	24[a]
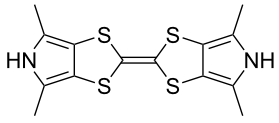 **5b'**	**23**-Br	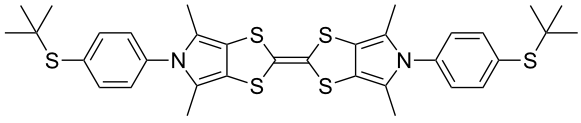 **5f**	40[a]/24[b]

[a]THF as solvent; [b]1,4-dioxane as solvent.

were prepared and isolated directly before the subsequent coupling reactions, and stored for no longer than 24 h before use. The isolated yields of the *N*,*N*-diarylated BPTTFs compare reasonably with the *N*-arylated MPTTF analogues discussed above, given that two C–N bonds are formed in these syntheses. For these systems we observed larger variation than for MPTTFs when the solvent was changed from 1,4-dioxane to THF; however, a different solvent gave the higher yield in each of the two cases where both solvents were used (**5c** and **5f**). We expect that further optimisation of these reactions can be achieved using microwave or larger scale conditions, and investigations are currently underway in our laboratory.

Conclusion

Pyrrole-annelated tetrathiafulvalenes (MPTTFs and BPTTFs) are versatile functional groups in many areas of chemistry. The large-scale synthesis of the key intermediate **6** improves the accessibility of these species and their derivatives. The related species **7** can be used to prepare further analogues. Compounds **6** and **7** can both be used to prepare BPTTFs and MPTTFs using homocoupling reactions or cross-coupling reactions with 1,3-dithiole-2-thiones (**19**), respectively. Additional functionalisation of MPTTFs and BPTTFs is important to allow their incorporation into systems with materials applications. The use of the 2-cyanoethyl protecting group allows thioether-functionalised MPTTFs to be prepared, including the addition of large ethylene glycol-based substituents utilised in the preparation of rotaxanes and pseudorotaxanes. *N*-Arylation of MPTTFs is an area of increasing interest and can be achieved using a copper-mediated reaction. We have applied this methodology to a range of aryl halides and achieved improved yields using microwave conditions. Optimisation of this arylation reaction is ongoing in our laboratory, including its extension to BPTTFs. We are continuing to improve and exploit these synthetic routes in our studies of MPTTF and BPTTF-based materials with applications in supramolecular chemistry, molecular electronics and as sensors.

Supporting Information

Supporting Information File 1

Experimental procedures and analytical data.
[http://www.beilstein-journals.org/bjoc/content/supplementary/1860-5397-11-125-S1.pdf]

Acknowledgements

We would like to acknowledge funding from EC FP7 ITN "MOLESCO" Project No. 606728, EC FP7 ITN "FUNMOLS" Project No. 212942, and the Danish Council for Independent Research – Natural Sciences (#11-106744).

References

1. Kim, D. S.; Sessler, J. L. *Chem. Soc. Rev.* **2015,** *44,* 532. doi:10.1039/C4CS00157E
2. Tian, J.; Ding, Y.-D.; Zhou, T.-Y.; Zhang, K.-D.; Zhao, X.; Wang, H.; Zhang, D.-W.; Liu, Y.; Li, Z.-T. *Chem. – Eur. J.* **2014,** *20,* 575. doi:10.1002/chem.201302951
3. Saha, S.; Flood, A. H.; Stoddart, J. F.; Impellizzeri, S.; Silvi, S.; Venturi, M.; Credi, A. *J. Am. Chem. Soc.* **2007,** *129,* 12159. doi:10.1021/ja0724590
4. Jeppesen, J. O.; Becher, J. *Eur. J. Org. Chem.* **2003,** *2003,* 3245. doi:10.1002/ejoc.200300078
5. Coskun, A.; Spruell, J. M.; Barin, G.; Dichtel, W. R.; Flood, A. H.; Botros, Y. Y.; Stoddart, J. F. *Chem. Soc. Rev.* **2012,** *41,* 4827. doi:10.1039/c2cs35053j
6. Liao, J.; Agustsson, J. S.; Wu, S.; Schonenberger, C.; Calame, M.; Leroux, Y.; Mayor, M.; Jeannin, O.; Ran, Y.-F.; Liu, S.-X.; Decurtins, S. *Nano Lett.* **2010,** *10,* 759. doi:10.1021/nl902000e
7. Jiang, H.; Yang, X.; Cui, Z.; Liu, Y.; Li, H.; Hu, W.; Kloc, C. *CrystEngComm* **2014,** *16,* 5968. doi:10.1039/c3ce41849a
8. Larsen, K. R.; Johnsen, C.; Hammerich, O.; Jeppesen, J. O. *Org. Lett.* **2013,** *15,* 1452. doi:10.1021/ol303308e
9. Trippé, G.; Levillain, E.; Le Derf, F.; Gorgues, A.; Sallé, M.; Jeppesen, J. O.; Nielsen, K.; Becher, J. *Org. Lett.* **2002,** *4,* 2461. doi:10.1021/ol0260829
10. Davis, C. M.; Lim, J. M.; Larsen, K. R.; Kim, D. S.; Sung, Y. M.; Lyons, D. M.; Lynch, V. M.; Nielsen, K. A.; Jeppesen, J. O.; Kim, D.; Park, J. S.; Sessler, J. L. *J. Am. Chem. Soc.* **2014,** *136,* 10410. doi:10.1021/ja504077f
11. Park, J. S.; LeDerf, F.; Bejger, C. M.; Lynch, V. M.; Sessler, J. L.; Nielsen, K. A.; Johnsen, C.; Jeppesen, J. O. *Chem. – Eur. J.* **2010,** *16,* 848. doi:10.1002/chem.200902924
12. Balandier, J.-Y.; Chas, M.; Dron, P. I.; Goeb, S.; Canevet, D.; Belyasmine, A.; Allain, M.; Sallé, M. *J. Org. Chem.* **2010,** *75,* 1589. doi:10.1021/jo902529e
13. Bivaud, S.; Balandier, J.-Y.; Chas, M.; Allain, M.; Goeb, S.; Sallé, M. *J. Am. Chem. Soc.* **2012,** *134,* 11968. doi:10.1021/ja305451v
14. Goeb, S.; Bivaud, S.; Dron, P. I.; Balandier, J.-Y.; Chas, M.; Sallé, M. *Chem. Commun.* **2012,** *48,* 3106. doi:10.1039/c2cc00065b
15. Lorcy, D.; Bellec, N.; Fourmigué, M.; Avarvari, N. *Coord. Chem. Rev.* **2009,** *253,* 1398. doi:10.1016/j.ccr.2008.09.012
16. Canevet, D.; Sallé, M.; Zhang, G.; Zhang, D.; Zhu, D. *Chem. Commun.* **2009,** 2245. doi:10.1039/b818607n
17. Bergkamp, J. J.; Decurtins, S.; Liu, S.-X. *Chem. Soc. Rev.* **2015,** *44,* 863. doi:10.1039/C4CS00255E
18. Romero-Nieto, C.; García, R.; Herranz, M. Á.; Ehli, C.; Ruppert, M.; Hirsch, A.; Guldi, D. M.; Martín, N. *J. Am. Chem. Soc.* **2012,** *134,* 9183. doi:10.1021/ja211362z
19. Liu, Y.; Zheng, N.; Chen, T.; Jin, L.; Yin, B. *Org. Biomol. Chem.* **2014,** *12,* 6927. doi:10.1039/C4OB01397B
20. Bryce, M. R. *J. Mater. Chem.* **2000,** *10,* 589. doi:10.1039/a908385e
21. Martin, N. *Chem. Commun.* **2013,** *49,* 7025. doi:10.1039/c3cc00240c
22. Ferraris, J.; Cowan, D. O.; Walatka, V.; Perlstein, J. H. *J. Am. Chem. Soc.* **1973,** *95,* 948. doi:10.1021/ja00784a066
23. Tayi, A. S.; Shveyd, A. K.; Sue, A. C. H.; Szarko, J. M.; Rolczynski, B. S.; Cao, D.; Kennedy, T. J.; Sarjeant, A. A.; Stern, C. L.; Paxton, W. F.; Wu, W.; Dey, S. K.; Fahrenbach, A. C.; Guest, J. R.; Mohseni, H.; Chen, L. X.; Wang, K. L.; Stoddart, J. F.; Stupp, S. I. *Nature* **2012,** *488,* 485. doi:10.1038/nature11395

24. Ballardini, R.; Balzani, V.; Becher, J.; Fabio, A. D.; Gandolfi, M. T.; Mattersteig, G.; Nielsen, M. B.; Raymo, F. M.; Rowan, S. J.; Stoddart, J. F.; White, A. J. P.; Williams, D. J. *J. Org. Chem.* **2000,** *65,* 4120. doi:10.1021/jo0001941
25. Jeppesen, J. O.; Takimiya, K.; Jensen, F.; Brimert, T.; Nielsen, K.; Thorup, N.; Becher, J. *J. Org. Chem.* **2000,** *65,* 5794. doi:10.1021/jo000742a
26. Gopee, H.; Nielsen, K. A.; Jeppesen, J. O. *Synthesis* **2005,** *2005,* 1251. doi:10.1055/s-2005-861879
27. Zong, K.; Cava, M. P. *J. Org. Chem.* **1997,** *62,* 1903. doi:10.1021/jo962303a
28. Nygaard, S.; Hansen, C. N.; Jeppesen, J. O. *J. Org. Chem.* **2007,** *72,* 1617. doi:10.1021/jo061962c
29. Düker, M. H.; Schäfer, H.; Zeller, M.; Azov, V. A. *J. Org. Chem.* **2013,** *78,* 4905. doi:10.1021/jo400502t
30. Nielsen, K. A.; Levillain, E.; Lynch, V. M.; Sessler, J. L.; Jeppesen, J. O. *Chem. – Eur. J.* **2009,** *15,* 506. doi:10.1002/chem.200801636
31. O'Connor, B. R.; Jones, F. N. *J. Org. Chem.* **1970,** *35,* 2002. doi:10.1021/jo00831a062
32. Melby, L. R.; Hartzler, H. D.; Sheppard, W. A. *J. Org. Chem.* **1974,** *39,* 2456. doi:10.1021/jo00930a043
33. Jeppesen, J. O.; Takimiya, K.; Thorup, N.; Becher, J. *Synthesis* **1999,** *1999,* 803. doi:10.1055/s-1999-3473
34. Mekelburger, H.-B.; Gro, J.; Schmitz, J.; Nieger, M.; Vögtle, F. *Chem. Ber.* **1993,** *126,* 1713. doi:10.1002/cber.19931260731
35. Zong, K.; Chen, W.; Cava, M. P.; Rogers, R. D. *J. Org. Chem.* **1996,** *61,* 8117. doi:10.1021/jo961282h
36. Solano, M. V.; Nielsen, M. B.; Jeppesen, J. O. *J. Heterocycl. Chem.* **2015,** in press.
37. Söderbäck, E.; Gronowitz, S.; Hörnfeldt, A.-B. *Acta Chem. Scand.* **1961,** *15,* 227. doi:10.3891/acta.chem.scand.15-0227
38. Simonsen, K. B.; Svenstrup, N.; Lau, J.; Simonsen, O.; Mørk, P.; Kristensen, G. J.; Becher, J. *Synthesis* **1996,** *1996,* 407. doi:10.1055/s-1996-4216
39. Konoike, T.; Namba, K.; Shinada, T.; Sakaguchi, K.; Papavassiliou, G. C.; Murata, K.; Ohfune, Y. *Synlett* **2001,** *2001,* 1476. doi:10.1055/s-2001-16806
40. Petersen, B. M.; Jeppesen, J. O.; Becher, J. *Synthesis* **2004,** *2004,* 2555. doi:10.1055/s-2004-831199
41. Jeppesen, J. O.; Perkins, J.; Becher, J.; Stoddart, J. F. *Org. Lett.* **2000,** *2,* 3547. doi:10.1021/ol006387s
42. Choi, J. W.; Flood, A. H.; Steuerman, D. W.; Nygaard, S.; Braunschweig, A. B.; Moonen, N. N. P.; Laursen, B. W.; Luo, Y.; DeIonno, E.; Peters, A. J.; Jeppesen, J. O.; Xu, K.; Stoddart, J. F.; Heath, J. R. *Chem. – Eur. J.* **2006,** *12,* 261. doi:10.1002/chem.200500934
43. Hansen, J. A.; Becher, J.; Jeppesen, J. O.; Levillain, E.; Nielsen, M. B.; Petersen, B. M.; Petersen, J. C.; Şahin, Y. *J. Mater. Chem.* **2004,** *14,* 179. doi:10.1039/b310733g
44. Salinas, Y.; Solano, M. V.; Sørensen, R. E.; Larsen, K. R.; Lycoops, J.; Jeppesen, J. O.; Martínez-Máñez, R.; Sancenón, F.; Marcos, M. D.; Amorós, P.; Guillem, C. *Chem. – Eur. J.* **2014,** *20,* 855. doi:10.1002/chem.201302461
45. Hansen, S. W.; Stein, P. C.; Sørensen, A.; Share, A. I.; Witlicki, E. H.; Kongsted, J.; Flood, A. H.; Jeppesen, J. O. *J. Am. Chem. Soc.* **2012,** *134,* 3857. doi:10.1021/ja210861v
46. Svenstrup, N.; Rasmussen, K. M.; Hansen, T. K.; Becher, J. *Synthesis* **1994,** *1994,* 809. doi:10.1055/s-1994-25580
47. We have obtained comparable results when using DBU to deprotect cyanoethyl protecting groups of non-annelated TTFs, but further details are beyond the scope of this paper.
48. Marquis, D.; Desvergne, J.-P.; Bouas-Laurent, H. *J. Org. Chem.* **1995,** *60,* 7984. doi:10.1021/jo00129a045
49. Ikeda, T.; Higuchi, M. *Tetrahedron* **2011,** *67,* 3046. doi:10.1016/j.tet.2011.03.009
50. Sørensen, A.; Andersen, S. S.; Flood, A. H.; Jeppesen, J. O. *Chem. Commun.* **2013,** *49,* 5936. doi:10.1039/c3cc42201a
51. Klapars, A.; Antilla, J. C.; Huang, X.; Buchwald, S. L. *J. Am. Chem. Soc.* **2001,** *123,* 7727. doi:10.1021/ja016226z
52. Antilla, J. C.; Baskin, J. M.; Barder, T. E.; Buchwald, S. L. *J. Org. Chem.* **2004,** *69,* 5578. doi:10.1021/jo049658b
53. Li, H.; Lambert, C. *Chem. – Eur. J.* **2006,** *12,* 1144. doi:10.1002/chem.200500928
54. Li, J.; Zhang, G.; Zhang, D.; Zheng, R.; Shi, Q.; Zhu, D. *J. Org. Chem.* **2010,** *75,* 5330. doi:10.1021/jo1007306
55. Nygaard, S.; Leung, K. C. F.; Aprahamian, I.; Ikeda, T.; Saha, S.; Laursen, B. W.; Kim, S.-Y.; Hansen, S. W.; Stein, P. C.; Flood, A. H.; Stoddart, J. F.; Jeppesen, J. O. *J. Am. Chem. Soc.* **2007,** *129,* 960. doi:10.1021/ja0663529
56. Solano, M. V.; Della Pia, E. A.; Jevric, M.; Schubert, C.; Wang, X.; van der Pol, C.; Kadziola, A.; Nørgaard, K.; Guldi, D. M.; Nielsen, M. B.; Jeppesen, J. O. *Chem. – Eur. J.* **2014,** *20,* 9918. doi:10.1002/chem.201402623

License and Terms

BEILSTEIN JOURNAL OF ORGANIC CHEMISTRY

New tris- and pentakis-fused donors containing extended tetrathiafulvalenes: New positive electrode materials for rechargeable batteries

Shintaro Iwamoto[1,2], Yuu Inatomi[1,3], Daisuke Ogi[1], Satoshi Shibayama[1], Yukiko Murakami[1], Minami Kato[1], Kazuyuki Takahashi[4], Kazuyoshi Tanaka[2], Nobuhiko Hojo[3] and Yohji Misaki[*1,5]

Full Research Paper

Open Access

Address:
[1]Department of Applied Chemistry, Graduate School of Science and Engineering, Ehime University, 3 Bunkyo-cho, Matsuyama, Ehime 790-8577, Japan, [2]Department, Molecular Engineering, Graduate School of Engineering, Kyoto University, Katsura, Kyoto 615-8520, Japan, [3]Panasonic Corporation, 1006 Kadoma, Kadoma, Osaka 571-8501, Japan, [4]Department of Chemistry, Graduate School of Science, Kobe University, 1-1 Rokkodai-cho, Nada-ku, Kobe 657-8501, Japan and [5]Elements Strategy Initiative for Catalysts and Batteries (ESICB), Kyoto University, Katsura, Kyoto 615-8520, Japan

Email:
Yohji Misaki* - misaki.yohji.mx@ehime-u.ac.jp

* Corresponding author

Keywords:
cyclic voltammetry; positive electrode materials; rechargeable battery; redox; tetrathiafulvalene

Beilstein J. Org. Chem. **2015,** *11,* 1136–1147.
doi:10.3762/bjoc.11.128

Received: 06 April 2015
Accepted: 19 June 2015
Published: 08 July 2015

This article is part of the Thematic Series "Tetrathiafulvalene chemistry".

Guest Editor: P. J. Skabara

Abstract

Derivatives of tris-fused TTF extended with two ethanediylidenes (**5**), tris- and pentakis-fused TTFs extended with two thiophene-2,5-diylidenes (**6**–**9**) were successfully synthesized. Cyclic voltammograms of the tetrakis(*n*-hexylthio) derivative of **5** and **7** (**5d**, **7d**) consisted of two pairs of two-electron redox waves and two pairs of one-electron redox waves. On the other hand, four pairs of two-electron redox waves and two pairs of one-electron redox waves were observed for the tetrakis(*n*-hexylthio) derivative of **9** (**9d**). Coin-type cells using the bis(ethylenedithio) derivatives of **5** (**5b**), **6** (**6b**) and the tetrakis(methylthio) derivatives of **5** (**5c**) and **8** (**8c**) as positive electrode materials showed initial discharge capacities of 157–190 mAh g^{-1} and initial energy densities of 535–680 mAh g^{-1}. The discharge capacities after 40 cycles were 64–86% of the initial discharge capacities.

Introduction

Tetrathiafulvalene (TTF, **1a**) and its analogues have attracted much attention as potential components for organic functional materials as well as multi-electron redox systems [1-5]. Fused TTF oligomers [5] are of considerable interest as multi-electron redox systems, because the TTF units strongly interact with each other. For example, a bis-fused TTF, 2,5-bis(1,3-dithiol-3-

ylidene)-1,3,4,6-tetrathiapentalene (BDT-TTP or simply TTP) exhibits four pairs of one-electron redox waves at +0.44, +0.62, +1.05 and +1.13 V (V vs SCE, in benzonitrile) [6]. The E_2–E_1 value is considerably larger than most dimeric TTF derivatives linked by σ-bond (typically 0.05–0.10 V) [7]. Fused TTF donors also play important roles in the development of highly functional materials. For example, TTP and its derivatives have yielded a large number of molecular conductors retaining metallic conductivity down to ≤4.2 K, because they have a tendency to construct two-dimensional molecular arrays through side-by-side sulfur···sulfur interaction [5,8]. On the other hand, a tris-fused TTF, 2,2'-bis[5-(1,3-dithiol-2-ylidene)-1,3,4,6-tetrathiapentanylidene] (TTPY, **2a**) and its derivatives have afforded highly conducting SbF_6^- and iodine salts of $\sigma_{rt} \approx 10^{-1}$–$10^{1}$ S cm^{-1} on compressed pellets [9,10].

Recently, we reported that TTP and TTPY can be utilized as positive electrode materials for rechargeable batteries [11]. All organic molecules exhibiting multi-electron redox behaviour seem to be promising as active materials for rechargeable batteries. However, most organic molecules have a crucial disadvantage, that is, they dissolve in organic solvents used for electrolyte solutions. TTF cannot be used as an active electrode material for rechargeable batteries for the above reason, while bis(ethylenedithio)-TTF (BEDT-TTF, **1b**) exhibits relatively good charge–discharge cycle performance because of its lower solubility in organic solvents [12]. However, the substitution of two ethylenedithio groups on TTF results in a significant decrease in the theoretical capacity (about half that of TTF). Utilization of polymerized materials is one of the solutions to decrease solubility. However, insertion of a linkage group, which is usually required to construct polymers, also results in considerable decrease in the theoretical capacity [13]. As for fused TTF oligomers, theoretical capacity rather increases as the number of TTF units increases because two carbons are shared in the two TTF units. TTP and TTPY are actually less soluble in organic solvents than TTF. In particular, TTPY is barely soluble in common solvents even in carbon disulfide. However, the maximum electrons cannot be utilized for TTP and TTPY batteries because TTP and TTPY dissolve in the electrolyte solutions in their maximum oxidation states (tetravalent for TTP and hexavalent for TTPY, respectively) [11].

Possible molecular modifications for TTPY to reduce solubility in electrolyte solvents are as follows; (i) introduction of rigid substituents such as the ethylenedithio group as mentioned above, (ii) use of a rigid extended-TTF unit, (iii) increase of the number of (extended) TTF units. As for the modification (ii), insertion of a π-spacer is sometimes useful. A vinylogous TTF (**3**, Figure 1) [14-16] shows lower solubility in ordinary organic solvents than TTF, although the thiophene-containing analog (**4**, Figure 1) [17-19] is more soluble than TTF. Increase of the TTF units might be the best way; however, the preparation of tetrakis- and/or pentakis-fused TTFs is not easy because of the low solubility of the precursor molecules. Insertion of thiophene spacers is a possible strategy for synthesizing fused TTF oligomers, because thiophene inserted precursors are more soluble than the TTF-type precursors as mentioned above. We succeeded in the synthesis of fused TTF pentamer and heptamer composed of the unit of **4** [20]. In this paper, we report the synthesis and electrochemical properties of vinyl extended TTPY analogue (**5b**–**d**) and tris- and pentakis-fused TTF analogues extended by the insertion of two thiophene rings (**6b**, **6d**, **7d**, **8c** and **9d**). We also report the charge–discharge properties of rechargeable batteries incorporating the methylthio and ethylenedithio derivatives of **5**, **6** and **8** (**5b**, **5c**, **6b** and **8c**) as a positive electrode material.

Results and Discussion

Synthesis

The synthesis of new donors was carried out according to Scheme 1. A trimethylphosphite-mediate cross coupling between a 1,3-dithiole-2-thione (**10**) [21] and 1,3-dithiol-2-one (**11**) [22-24] gave a TTF derivative with two ethoxyphosphoryl groups (**12**) in 63% yield. We adopted the cross-coupling reaction between the 1,3-dithiole-2-thione and the 1,3-dithiol-2-one derivatives for the following reasons. The homo-coupling reaction of **10** afforded **12** in low yields, and purification by column chromatography was difficult because of undesired byproducts. The homo-coupling reaction using **11** might give **12** in a good yield, however, toxic and expensive mercury(II) acetate has to be used for the synthesis of **11**. Thus, the cross-coupling reaction is useful for saving **11**. The Horner–Wadsworth–Emmons reaction of **12** with 2 equiv of aldehydes **13b**–**d** [16,25] in the presence of BuLi in THF at −78 °C gave the desired bis-adducts **5b**–**d** in 54−85% yields. Similarly, **6b**, **6c**, **7d**, **8c** and **9d** were obtained in 62–85% yields by the reaction of **12** with **14b,c**, **15d** [17-19] or **16c**, **17d** [26] in the presence of BuLi in THF. All the new donors were obtained as stable solids.

Theoretical calculations

We performed theoretical calculations of **5A**, **6Aa** and **7Aa** by using the Gaussian 09 program based on the density functional theory (DFT) at the B3LYP/6-31G(d) level [27]. Their HOMO and HOMO–*n* (*n* = 1–2 and 1–4) of the *trans* isomers of **5a**, **6a** and **8a** are shown in Figures 2–4, respectively. The shapes, energy levels and total energies of the *trans* and *cis* isomers were almost the same as each other. The HOMO of **5a** was distributed over the whole molecules. Molecular orbital coefficients were largely observed in the vinylogous TTF moieties rather than in the central TTF moiety (Figure 2). In the

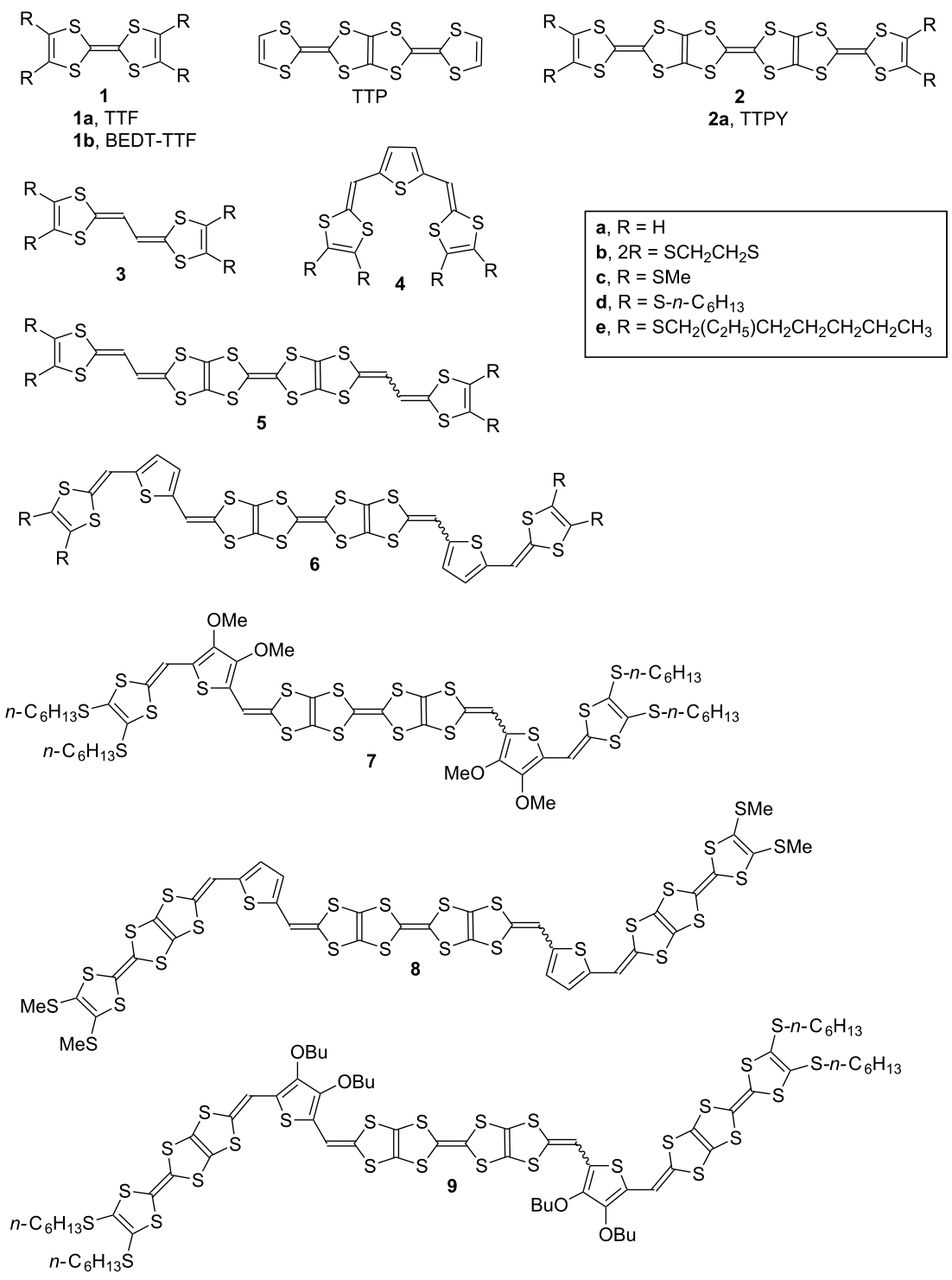

Figure 1: Chemical structures of **1**–**9** and TTP.

HOMO–1, most molecular orbital coefficients were found on the bilateral vinylogous TTF moieties. The HOMO–2 was mainly located on the central TTF unit. In the bilateral vinylogous TTF moieties, small molecular orbital coefficients were observed. The shapes of the HOMO, HOMO-1 and HOMO-2 of the thiophene extended donor **6a** resembled those of **5a** (Figure 3). The HOMO of **8a** spread mainly over the central TTF and the bilateral extended TTF moieties, and the TTF moieties at the both ends barely contributed to the HOMO (Figure 4). Similarly to **6a**, larger molecular orbital coefficients

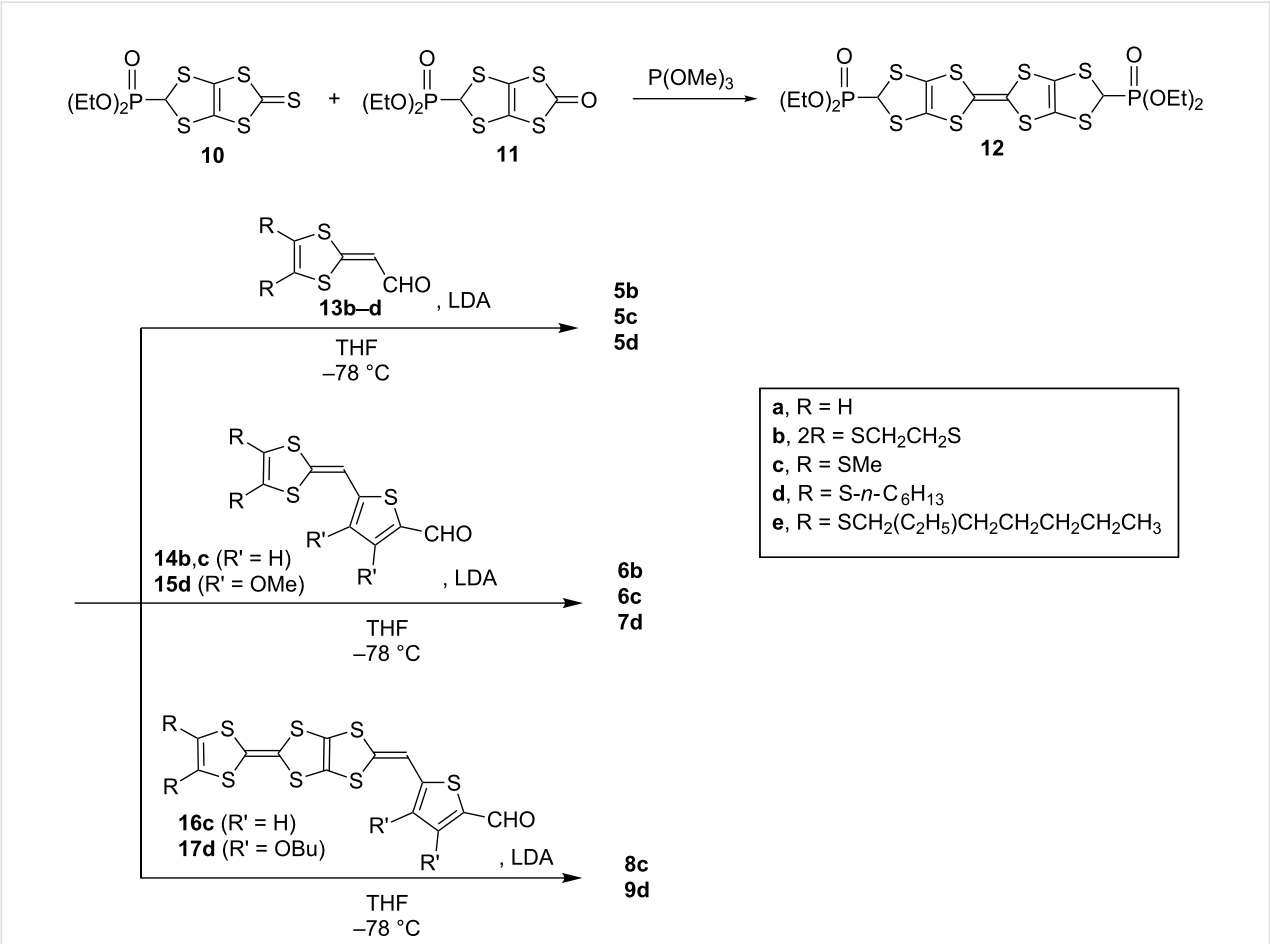

Scheme 1: Synthesis of **5**–**9**.

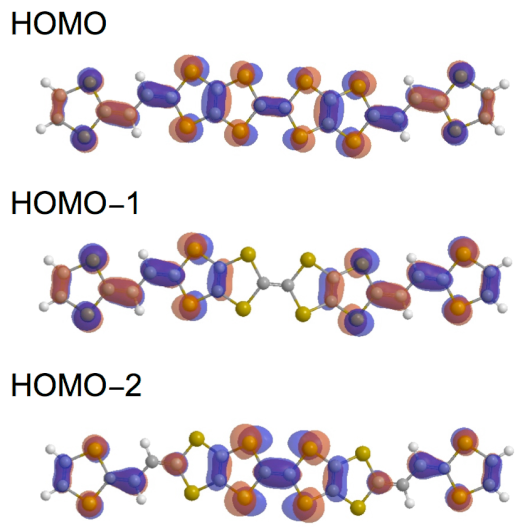

Figure 2: Molecular orbitals of **5a** (*trans* isomer).

of the sulfur atoms were found in the extended TTF moieties of **8a** rather than in the central TTF moiety. The HOMO–1 was mainly distributed on the two extended TTF moieties. Small molecular orbital coefficients were observed in the TTF moieties at the both ends. In contrast, the HOMO–2 was hardly distributed on the extended TTF units, but was substantially located on the three TTF units. The TTF moieties at the both ends considerably contributed to the HOMO–3. The HOMO–4 is distributed mainly on the central TTF moiety, although small molecular orbital coefficients were observed in the other donor units.

The orbital energies of the HOMO and HOMO–*n* (*n* = 1–2 and 1–4) for **5a**, **6a** and **8a** are summarized in Table 1. The orbital energies of HOMO of **5a**, **6a** and **8a** (−4.532 to −4.605 eV) are comparable to each other, and are higher by 0.18−0.25 eV than that of TTPY (−4.787 eV). If the oxidation relates to the orbital energy, the first oxidations of **5**–**9** might occur at lower potentials than TTPY. The energy differences between the HOMO and HOMO–1 of all the donors (0.041–0.113 eV) were smaller

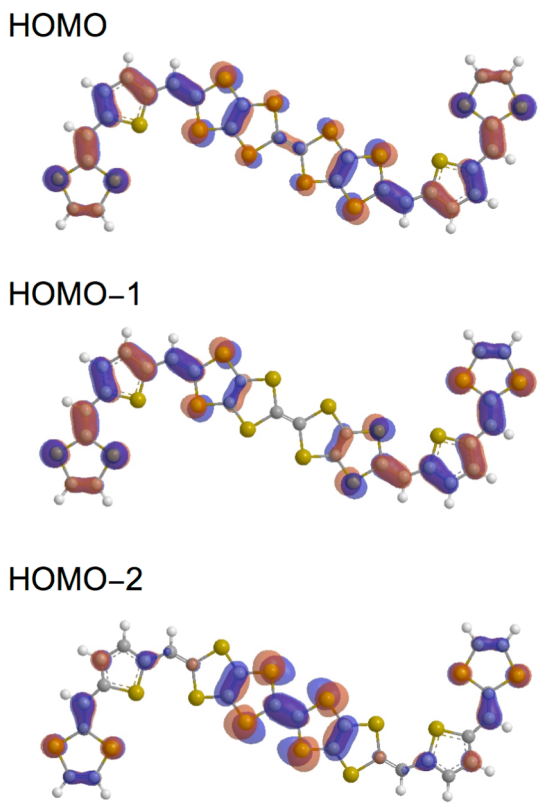

Figure 3: Molecular orbitals of **6a** (*trans* isomer).

than that of TTPY (0.186 eV). In particular, the orbital energies of the HOMO and HOMO–1 of **8a** (−4.602 and −4.643 eV, respectively) were close to each other, suggesting that the first four-electron oxidation of **8a** might occur in a narrow potential range. The HOMO–2 of **5a** and **6Aa** (−5.257 and −5.129 eV, respectively) and HOMO–4 of **8a** (−5.328 eV) were slightly higher than the orbital energy of the HOMO–2 of TTPY (−5.439 eV). These results suggest that the electrons at the HOMO–2 of **5a** and **6a** and HOMO–4 of **8a** might be removed more easily than those at the HOMO–2 of TTPY.

Table 1: Orbital energies (eV) of **5a**, **6a** and **8a**.

	5a	**6a**	**8a**	TTPY
HOMO	−4.605	−4.532	−4.602	−4.787
HOMO–1	−4.718	−4.589	−4.643	−4.973
HOMO–2	−5.257	−5.129	−4.967	−5.439
HOMO–3	–	–	−5.061	–
HOMO–4	–	–	−5.328	–

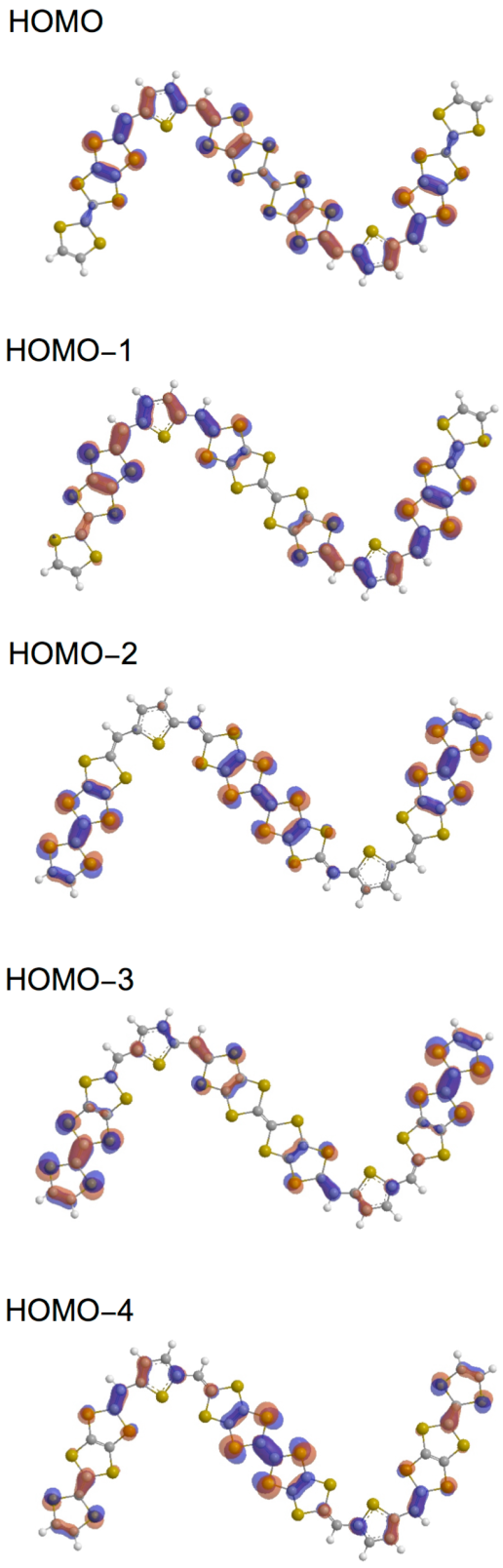

Figure 4: Molecular orbitals of **8a** (*trans* isomer).

Electrochemical properties

The redox behaviors of **5d**, **7d** and **9d** were investigated by using cyclic voltammetry. Deconvoluted cyclic voltammograms of **5d**, **7d** and **9d** measured in a carbon disulfide/benzonitrile (1:1, v/v) solution are shown in Figure 5. As for the tris-fused donors **5d** and **7d**, four pairs of redox waves were observed. The peak currents of the first and second redox waves were about double those of the others. The maximum number of electrons participating in the redox was six, considering that both donors have six redox-active 1,3-dithiol-2-ylidene (DT) sites. Thus, we think that the first and second redox waves correspond to two-electron redox processes and that the remaining waves correspond to one-electron transfer processes. The pentakis-fused donor **9d** shows six pairs of redox waves. The peak currents of the last two pairs of redox waves were about half as large as those of the others. Considering that **9d** has ten redox-active 1,3-dithiol-2-ylidene sites, it is suggested that the last two pairs of redox waves of **9d** correspond to one-electron transfer process, while the others correspond to two-electron transfer processes.

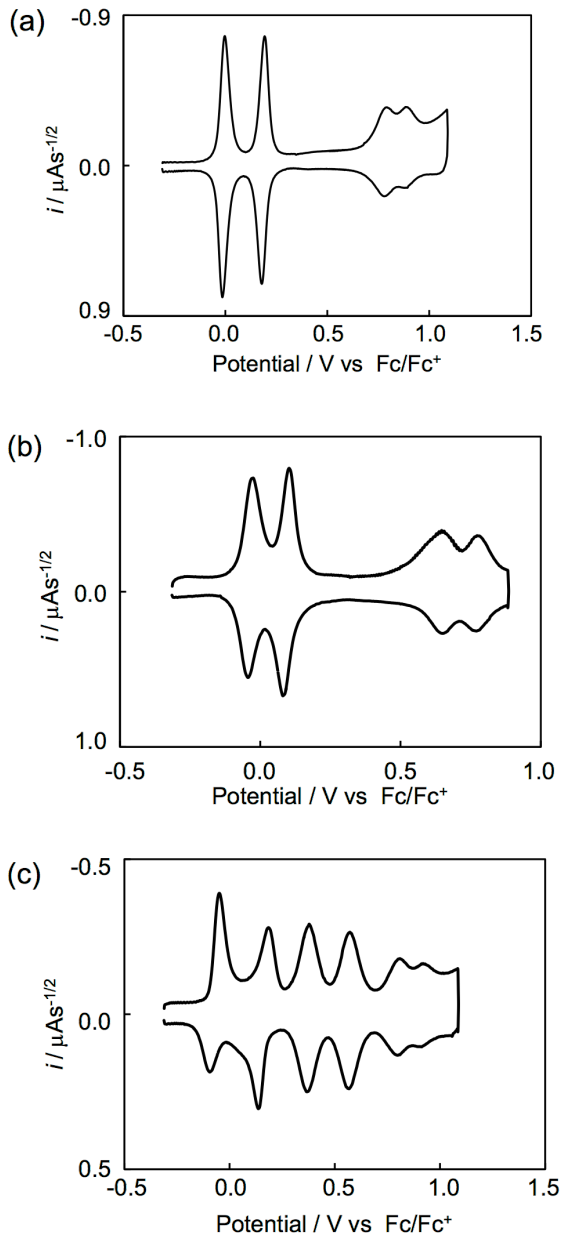

Figure 5: Deconvoluted cyclic voltammograms of (a) **5d**, (b) **7d** and (c) **9d**.

The redox potentials of **5d**, **7d** and **9d** are summarized in Table 2 together with their related compounds. The first two-electron redox potentials of **5d** (E_{m1} = −0.01 V) and **7d** (E_{m1} = −0.04 V) were more negative by 0.13 and 0.16 V than the first redox potential of a TTPY derivative **2e** (E_1 = +0.12 V) measured under the identical conditions. The first redox waves of **5d** and **7d** involved two-electron transfer processes, and that E_1 of the extended donors **3c** and **18** (−0.06 V) was lower than that of the TTF derivative **1c** (+0.03 V). These results suggest that two positive charges formed by the first two-electron oxidation process of **5d** and **7d** are presumably distributed mainly on each of the two extended TTF moieties so as to reduce on-site Coulomb repulsion (Scheme 2). Similarly, the two positive charges in $\mathbf{5d}^{4+}$ and $\mathbf{7d}^{4+}$ might be located mainly on each of the two extended TTF donors. Observation of two sequent one-electron redox waves in the higher potential region (+0.6 to +0.9 V) indicates that the central TTF moiety contributes to the remaining redox processes. The significant positive shifts of the E_5 and E_6 of **5d** and **7d** by 0.62–0.75 V and 0.41–0.63 V, respectively, compared to the E_1 and E_2 of **3c** is probably due to the strong electron-withdrawing effect by two dicationic extended TTF units in the tetracationic states. In other words, the presence of five and six positive charges in the molecules induces significantly large on-site coulomb repulsion. The E_5 and E_6 of **7d** are lower by 0.12–0.14 V than those of **5d**, suggesting that $\mathbf{7d}^{6+}$ is more stabilized than $\mathbf{5d}^{6+}$. The thiophene spacers inserted between two cationic 1,3-dithiole rings might reduce the intramolecular coulomb repulsion in $\mathbf{7d}^{6+}$.

As for **9d**, two positive charges in $\mathbf{9d}^{2+}$ are probably distributed mainly on each of the two thiophene-inserted TTF moieties, since the first redox wave of **9d** corresponds to a simultaneous two-electron transfer process, and the E_{m1} (−0.07 V) is comparable to the E_1 of **18** (−0.06 V) as shown in Scheme 3. The E_{m2} of **9d** (+0.16 V) is lower by 0.20 V than the E_3 of **19** (+0.36 V) [28], suggesting that the second redox process is contributed by two extended TTF moieties similarly to the first redox process. On the other hand, both the third and fourth redox waves involve two-electron transfer, and their

Table 2: Redox potentials of **5d**, **7d**, **9d** and their related compounds (V vs Fc/Fc^+, in benzonitrile/carbon disulfide 1:1, v/v).

Donor	E_1	E_2	E_3	E_4	E_5	E_6	E_7	E_8	E_9	E_{10}
	E_{m1}[a]		E_{m2}[a]		E_{m3}[a]		E_{m4}[a]			
5d	−0.01		+0.19		+0.79	+0.89				
7d	−0.04		+0.09		+0.65	+0.77				
9d	−0.07		+0.16		+0.38		+0.57		+0.81	+0.92
2e	+0.12	+0.19	+0.39		+0.87					
1c	+0.03	+0.36								
3c	−0.06	+0.05								
18	−0.06	+0.02								
19	+0.03		+0.36	+0.56						

[a] $E_{m1} = (E_1+E_2)/2$. $E_{m2} = (E_3+E_4)/2$. $E_{m3} = (E_5+E_6)/2$. $E_{m4} = (E_7+E_8)/2$.

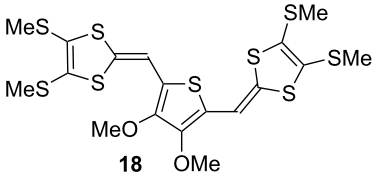

18

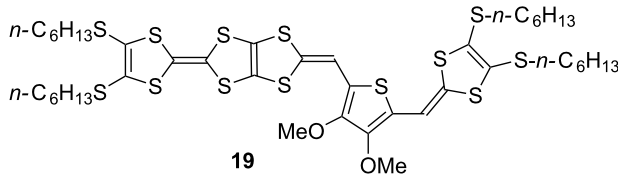

19

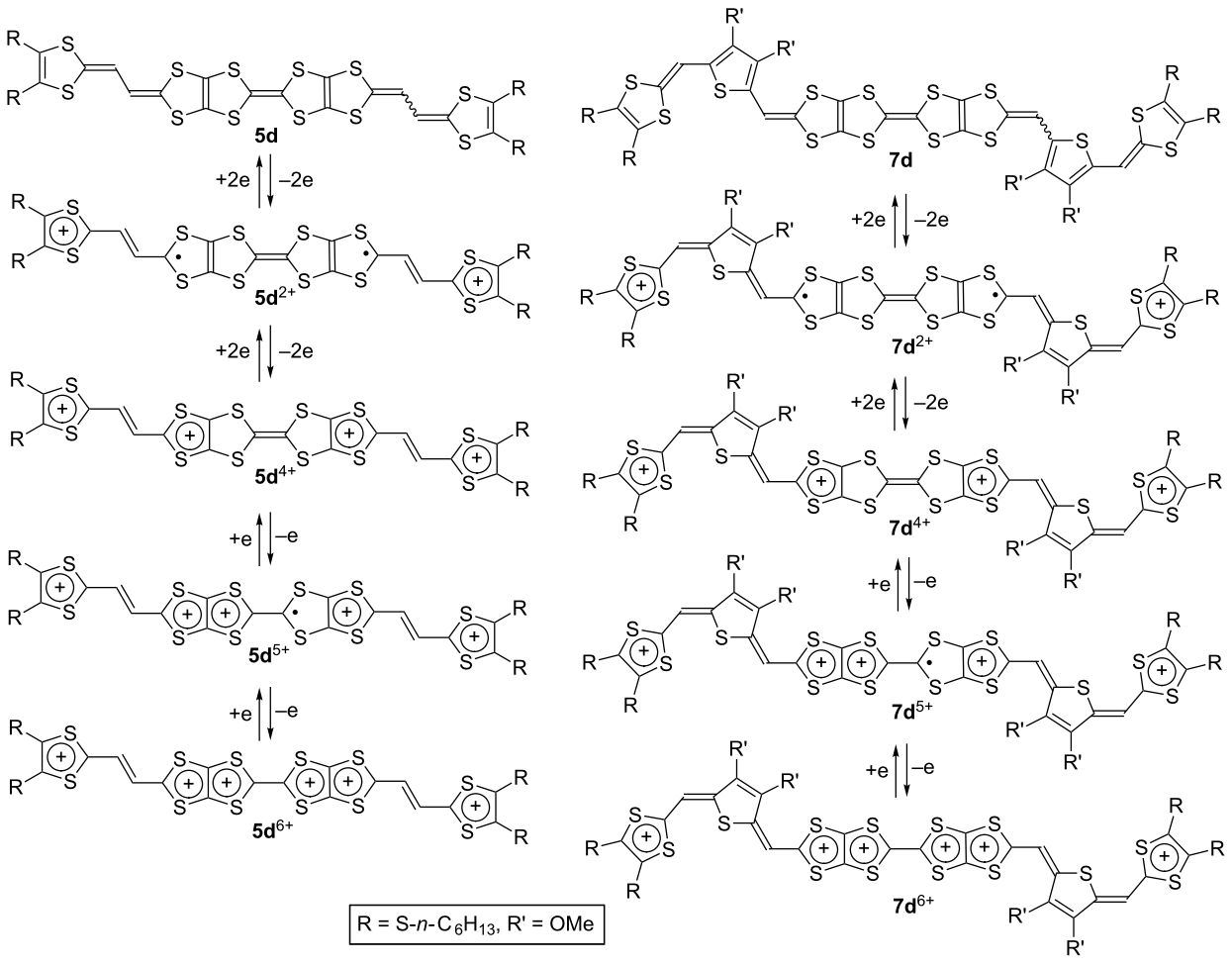

Scheme 2: Plausible redox processes of **5d** and **7d**.

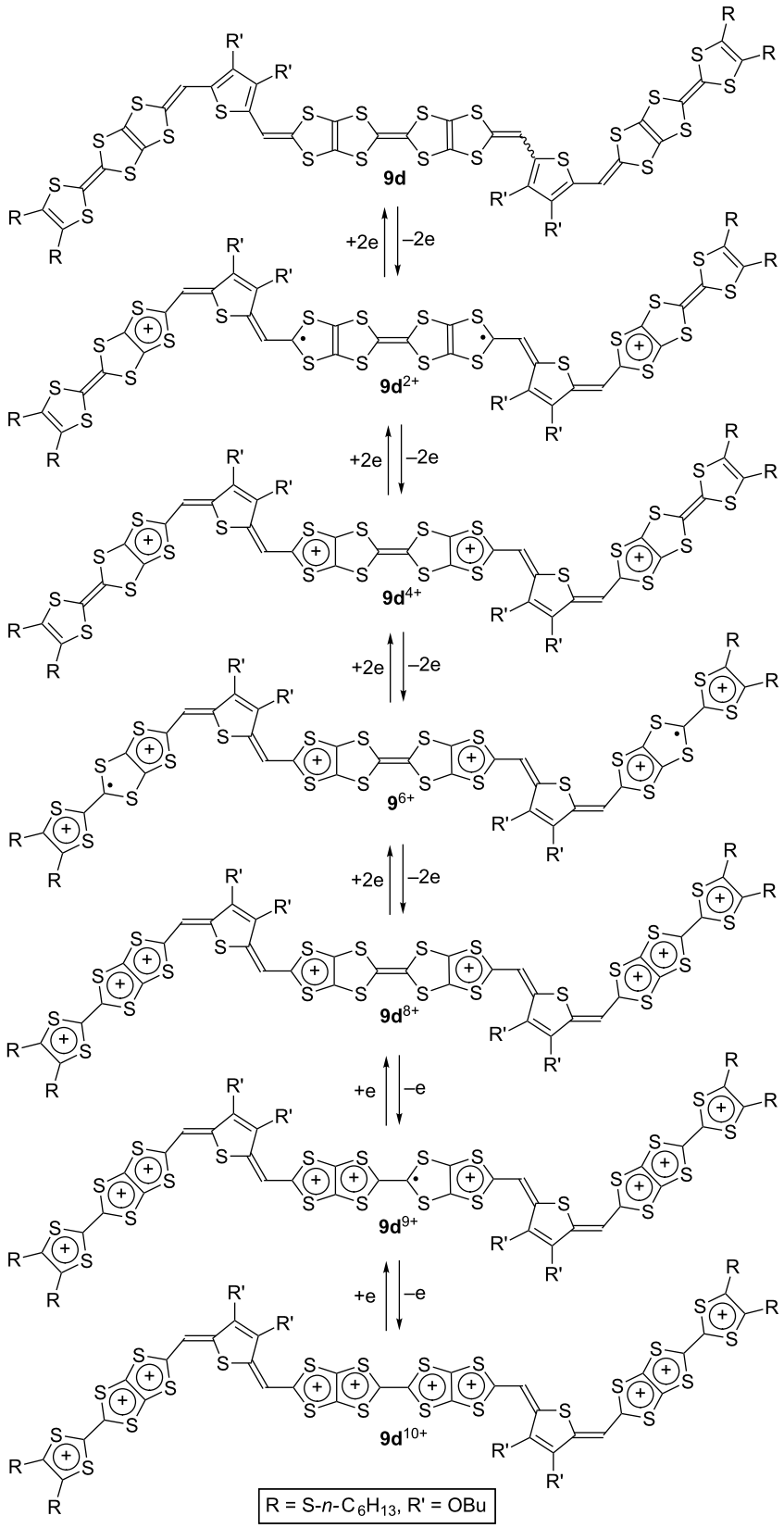

Scheme 3: Plausible redox process of **9d**.

potentials (E_{m3} = +0.38 V, E_{m4} = +0.57 V, respectively) are comparable to the E_3 and E_4 of **19** (E_3 = +0.36 V, E_4 = +0.56 V, respectively). Therefore, it is indicated that positive charges formed by the third and fourth redox processes are distributed over two TTF moieties at the both ends. The central TTF moiety contributes to the remaining two stages of the one-electron redox processes at +0.81 and +0.92 V, similarly to **5d** and **7d**.

Charge and discharge properties of rechargeable batteries

In order to examine the cell performance, IEC R2016 coin-type cells were fabricated using a positive electrode incorporating **5**, **6** and **8** (**5b, 5c, 6b** and **8c**) as positive electrode materials. The applied current densities were 40 mA g^{-1} (0.2 C rate) and 100 mA g^{-1} (0.5 C rate), respectively. The nominal charge capacity of a battery or an electrode is expressed as a C-rate. A 0.2 C rate means that the full discharge capacity reached in 5 h. Cyclic voltammetry in the solid state was carried out prior to the charge–discharge test so as to determine the turning back voltage (Supporting Information File 1, Figure S4). The electrodes incorporating **5b** and **5c** exhibited three indistinct oxidation peaks at 3.4, 3.6 V and 4.1 V. Multi-scan cycle voltammetry revealed a significant decay of redox waves at 4.1 V presumably due to dissolution of the oxidative species of **5b** and **5c** in the electrolyte solution. In contrast, there was no distinct decay of the redox waves at 3.6 V, suggesting that the oxidative species of **5b** and **5c** formed at 3.6 V barely dissolved in the electrolyte solution. In contrast, no distinct dissolution was observed for the **6b** and **8c** cells even at 4.2 V. Thus, we determined the turn-back voltages as 3.8 V for the **5b** and **5c** cells, and 4.2 V for the **6b** and **8c** cell.

The results are summarized in Table 3, and the first five charge–discharge curves of **5b**/Li and **6b**/Li cells cycled at room temperature are shown in Figure 6. A **5c** cell also exhibited charge–discharge curves similar to **5b**/Li and **6b**/Li cells. No distinct plateau was observed in both the charge and discharge processes for all the cells in spite of observation of well-separated redox waves in a solution. This is possibly due to the apparent overlap of the redox processes in the solid state (see also Figure S4 in Supporting Information File 1) [11]. The initial discharge capacities of **5b**/Li, **5c**/Li and **6b**/Li cells were 157, 168 and 158 mAh g^{-1}, respectively. They correspond to 93 and 99% of the theoretical capacity for the five-electron redox of **5b** and **5c**, and 94% of the theoretical capacity for the six-

Table 3: Charge–discharge parameters for the rechargeable batteries using **5**, **6** and **8**.

	5b/Li	**5c**/Li	**6b**/Li	**8c**/Li
Theoretical capacities for maximum electrons utilization indicated in parentheses (mAh g^{-1}).	203(6)	203(6)	169(6)	205(10)
1st Discharge capacity (mAh g^{-1})	157	168	158	190
Number of electron per molecule participating discharge	5	5	6	10
Average voltage for 1st discharge (V)	3.41	3.40	3.44	3.58
1st Energy density (mWh g^{-1})	535	571	544	680
40th Discharge capacity/1st discharge capacity (%)	86	73	74	64

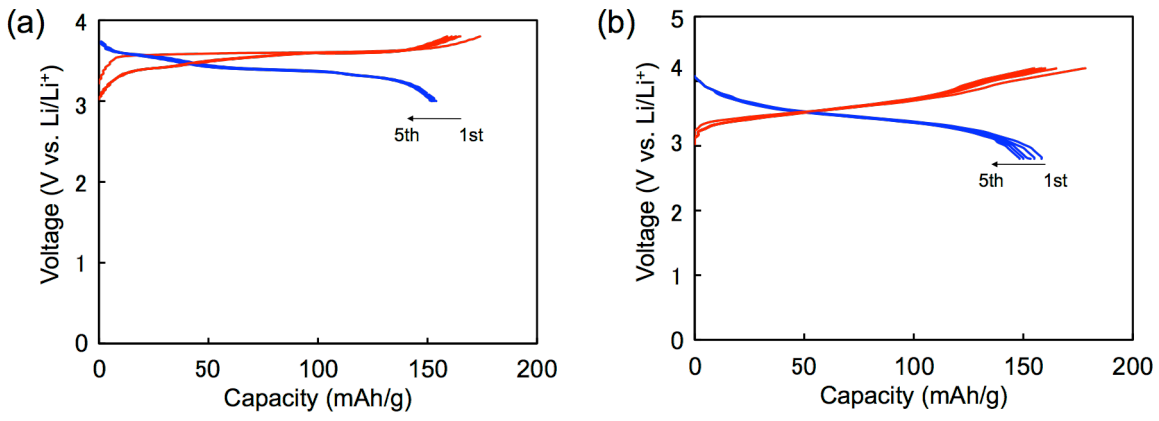

Figure 6: (a) Galvanostatic charge-discharge curves of (a) **5c**/Li and (b) **6b**/Li cells.

electron redox of **6b**, respectively. The first discharge capacities observed are comparable to those of the positive active materials for commercially available lithium ion batteries on the market (150–170 mAh g^{-1}). Cycle-life performances for **5b**/Li, **5c**/Li and **6b**/Li cells are shown in Figure 7. In all cases, the discharge capacities decreased gradually as the number of cycles increased. The discharge capacities after 40 cycles were 86, 73 and 74% of the first discharge capacities for **5b**/Li, **5c**/Li and **6b**/Li cells, respectively. The decrease in capacities for the cells using organic electrode materials might be attributed to elution of the positive electrode materials into the electrolyte solution. The result that the **5b** cell shows higher cycle performance than the other cells is consistent with the lower solubility of **5b** with rigid ethylenedithio substituents than **5c** with flexible methylthio substituents.

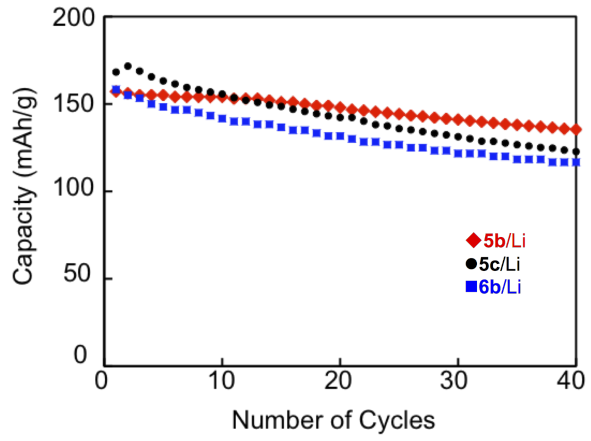

Figure 7: Cycle-life performances for **5b**/Li, **5c**/Li and **6b**/Li cells.

Figure 8 shows the first five charge–discharge curves of a **8c**/Li cell cycled at room temperature and their cycle performances up to 40 cycles. The initial charge and discharge capacities were 202 and 190 mAh g^{-1}, respectively. They correspond to 99% and 93% of the theoretical capacity for ten-electron utilization (205 mAh g^{-1}). This result strongly indicates that ten-electron redox per molecule participates in the charge and discharge processes. Similarly to the **5b**, **5c** and **6b** cells, the **8c**/Li cell shows no distinct plateau in both the charge and discharge processes in spite of observation of six pairs of redox waves in a solution. The initial discharge capacity of the **8c**/Li cell (190 mAh g^{-1}) is higher than those of the cathode active materials for commercially available lithium ion batteries. The discharge capacity after 40 cycles (121 mAh g^{-1}) was 64% of the first discharge capacity. The high cycle-life performance in spite of utilization of the highest oxidation state of +10 might be because of strong van der Waals force between the large π-electron frameworks of the thiophene-inserted pentakis-fused TTF.

The energy densities for the first discharge process (1st energy densities) calculated by multiples of the initial discharge capacity and the average voltage are also summarized in Table 3. The first energy densities of **5b**, **5c** and **6b** cells were 535–571 mWh g^{-1}, which are comparable to that of TTPY (543 mWh g^{-1} for four-electron utilization). On the other hand, the first energy density of **8c** cell (680 mWh g^{-1}) is larger which is larger by 110–150 mWh g^{-1} than those of the others. This value is also superior to the energy densities of most inorganic cathode materials for LIBs [29,30], **20**/Li (605 mWh g^{-1}) [31], and is slightly smaller than that of **21**/Li (700 mWh g^{-1}) [32] (Figure 9).

Conclusion

A TTF derivative with two phosphonate groups (**12**) is a useful building block for the synthesis of odd-numbered fused TTF donors containing extended TTF units. We have demonstrated that some derivatives of **5**, **6** and **8** can be utilized as positive electrode materials for rechargeable batteries. The **5b**/Li cell

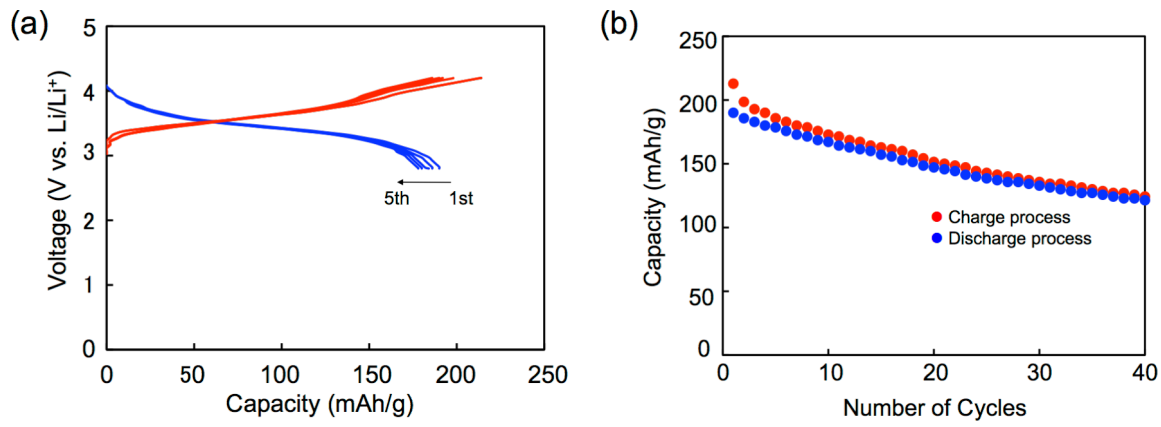

Figure 8: (a) Galvanostatic charge–discharge curves, and (b) cycle-life performances for a **8c**/Li cell.

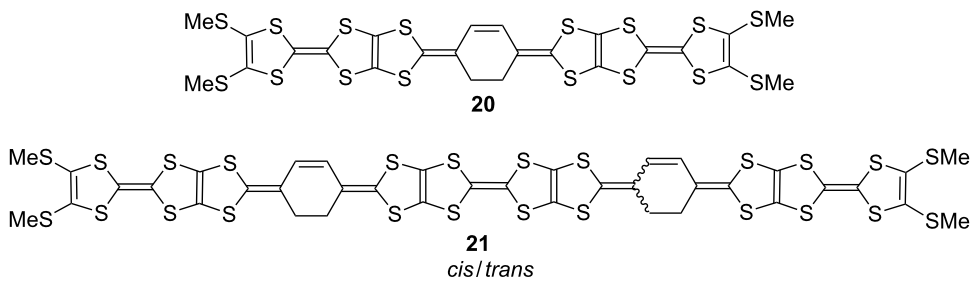

Figure 9: Molecular structures of **20** and **21**.

showed considerably higher cycle performance when the number of electrons is suppressed to five per molecule (5/6 of the maximum electrons). It is noted that the **6b** and **8c** cells showed good cycle performance in spite of utilizing the maximum amounts of electrons (six and ten electrons, respectively). The **8c** cell exhibited significantly high energy density (680 mWh g^{-1}) at the first discharge thanks to ten electrons utilization. The information obtained from the present work could be helpful in the molecular design and synthesis of new positive electrode materials for rechargeable batteries. We are engaged in the synthesis of the other derivatives of **5**, **6** and **8** containing unsubstituted derivatives and higher homologues of **5**, which are expected to exhibit higher charge–discharge performance than the materials described in this paper.

Supporting Information

Supporting Information File 1

Experimental details and spectroscopic data, optimized structures of **5a**, **6a** and **8a** (*trans* isomers) and cycle-life performances for rechargeable batteries using **5c**, **5b** and **6b**.
[http://www.beilstein-journals.org/bjoc/content/supplementary/1860-5397-11-128-S1.pdf]

Acknowledgements

This work is partially supported by a Grant-in-Aid for Scientific Research (No. 23550155), from the Ministry of Education, Culture, Sports, Science and Technology (MEXT), Japan, MEXT program "Elements Strategy Initiative to Form Core Research Center" (since 2012), and Grant-in-Aid for Research Promotion, Ehime University.

References

1. Yamada, J.; Sugimoto, T., Eds. *TTF Chemistry–Fundamental and Applications of Tetrathiafulvalene;* Kodansha-Springer: Tokyo, 2004.
2. Canevet, D.; Sallé, M.; Zhang, G.; Zhang, D.; Zhu, D. *Chem. Commun.* **2009,** 2245–2269. doi:10.1039/b818607n
3. Segura, J. L.; Martín, N. *Angew. Chem., Int. Ed.* **2001,** *40,* 1372–1409. doi:10.1002/1521-3773(20010417)40:8<1372::AID-ANIE1372>3.0.CO;2-I
4. Gorgues, A.; Hudhomme, P.; Sallé, M. *Chem. Rev.* **2004,** *104,* 5151–5184. doi:10.1021/cr0306485
5. Misaki, Y. *Sci. Technol. Adv. Mater.* **2009,** *10,* 024301. doi:10.1088/1468-6996/10/2/024301
6. Misaki, Y.; Matsui, T.; Kawakami, K.; Nishikawa, H.; Yamabe, T.; Shiro, M. *Chem. Lett.* **1993,** *22,* 1337–1340. doi:10.1246/cl.1993.1337
7. Iyoda, M.; Hasegawa, M.; Miyake, Y. *Chem. Rev.* **2004,** *104,* 5085–5114. doi:10.1021/cr030651o
8. Misaki, Y.; Fujiwara, H.; Yamabe, T.; Mori, T.; Mori, H.; Tanaka, S. *Chem. Lett.* **1994,** *23,* 1653–1656. doi:10.1246/cl.1994.1653
9. Nishikawa, H.; Kawauchi, S.; Misaki, Y.; Yamabe, T. *Chem. Lett.* **1996,** *25,* 43–44. doi:10.1246/cl.1996.43
10. Misaki, Y.; Kawakami, K.; Higuchi, N.; Nishikawa, H.; Yamabe, T. *Mol. Cryst. Liq. Cryst. Sci. Technol., Sect. A* **1996,** *284,* 337–344. doi:10.1080/10587259608037936
11. Inatomi, Y.; Hojo, N.; Yamamoto, T.; Watanabe, S.; Misaki, Y. *ChemPlusChem* **2012,** *77,* 973–976. doi:10.1002/cplu.201200197
12. Inatomi, Y.; Hojo, N.; Yamamoto, T.; Shimada, M.; Watanabe, S. presentation No. 167. In *ECS Meeting Abstracts 2008, MA2008-1,* 213th ECS meeting, Phoenix, May 22, 2008; The Electrochemical Society.
13. Oyaizu, K.; Suga, T.; Yoshimura, K.; Nishide, H. *Macromolecules* **2008,** *41,* 6646–6652. doi:10.1021/ma702576z
14. Yoshida, Z.; Kawase, T.; Awaji, H.; Sugimoto, I.; Sugimoto, T.; Yoneda, S. *Tetrahedron Lett.* **1983,** *24,* 3469–3472. doi:10.1016/S0040-4039(00)86015-3
15. Sugimoto, T.; Awaji, H.; Sugimoto, I.; Misaki, Y.; Kawase, T.; Yoneda, S.; Yoshida, Z.; Kobayashi, T.; Anzai, H. *Chem. Mater.* **1989,** *1,* 535–547. doi:10.1021/cm00005a015
16. Moore, A. J.; Bryce, M. R.; Ando, D. J.; Hursthouse, M. B. *J. Chem. Soc., Chem. Commun.* **1991,** 320–322. doi:10.1039/c39910000320
17. Hansen, T. K.; Lakshmikantham, M. V.; Cava, M. P.; Niziurski-Mann, R. E.; Jensen, F.; Becher, J. *J. Am. Chem. Soc.* **1992,** *114,* 5035–5039. doi:10.1021/ja00039a013
18. Takahashi, K.; Nihira, T.; Yoshifuji, M.; Tomitani, K. *Bull. Chem. Soc. Jpn.* **1993,** *66,* 2330–2334. doi:10.1246/bcsj.66.2330
19. Benahmed-Gasmi, A. S.; Frère, P.; Garrigues, B.; Gorgues, A.; Jubault, M.; Carlier, R.; Texier, F. *Tetrahedron Lett.* **1992,** *33,* 6457–6460. doi:10.1016/S0040-4039(00)79014-9
20. Misaki, Y.; Kubo, A.; Matsuda, W.; Fueno, H.; Tanaka, K. *Curr. Appl. Phys.* **2006,** *6,* 934–938. doi:10.1016/j.cap.2005.01.043

21. Misaki, Y.; Nishikawa, H.; Kawakami, K.; Uehara, T.; Yamabe, T. *Tetrahedron Lett.* **1992,** *33,* 4321–4324. doi:10.1016/S0040-4039(00)74250-X
22. Misaki, Y.; Higuchi, N.; Fujiwara, H.; Yamabe, T.; Mori, T.; Mori, H.; Tanaka, S. *Angew. Chem., Int. Ed. Engl.* **1995,** *34,* 1222–1225. doi:10.1002/anie.199512221
23. Misaki, Y.; Ohta, T.; Higuchi, N.; Fujiwara, H.; Yamabe, T.; Mori, T.; Mori, H.; Tanaka, S. *J. Mater. Chem.* **1995,** *5,* 1571–1579. doi:10.1039/jm9950501571
24. Takahashi, K.; Tanioka, H.; Fueno, H.; Misaki, Y.; Tanaka, K. *Chem. Lett.* **2002,** *31,* 1002–1003. doi:10.1246/cl.2002.1002
25. Moore, A. J.; Bryce, M. R. *Tetrahedron Lett.* **1992,** *33,* 1373–1376. doi:10.1016/S0040-4039(00)91626-5
26. Nakamura, K.; Shirahata, T.; Miyamoto, H.; Misaki, Y. *Heterocycles* **2011,** *83,* 2115–2126. doi:10.3987/COM-11-12277
27. *Gaussian 09,* Revision C.01; Gaussian, Inc.: Wallingford, CT, 2009.
28. Misaki, Y.; Sasaki, T.; Ohta, T.; Fujiwara, H.; Yamabe, T. *Adv. Mater.* **1996,** *8,* 804–807. doi:10.1002/adma.19960081006
29. Aravindan, V.; Gnanaraj, J.; Lee, Y.-S.; Madhavi, S. *J. Mater. Chem. A* **2013,** *1,* 3518–3539. doi:10.1039/c2ta01393b
30. Thackeray, M. M.; Wolverton, C.; Isaacs, E. D. *Energy Environ. Sci.* **2012,** *5,* 7854–7863. doi:10.1039/c2ee21892e
31. Kato, M.; Ogi, D.; Yao, M.; Misaki, Y. *Chem. Lett.* **2013,** *42,* 1556–1558. doi:10.1246/cl.130841
32. Kato, M.; Senoo, K.; Yao, M.; Misaki, Y. *J. Mater. Chem. A* **2014,** *2,* 6747–6754. doi:10.1039/c3ta14920j

License and Terms

BEILSTEIN JOURNAL OF ORGANIC CHEMISTRY

Thiazole-induced rigidification in substituted dithieno-tetrathiafulvalene: the effect of planarisation on charge transport properties

Rupert G. D. Taylor[1], Joseph Cameron[1], Iain A. Wright[1], Neil Thomson[1], Olena Avramchenko[1], Alexander L. Kanibolotsky[1,2], Anto R. Inigo[1], Tell Tuttle[1] and Peter J. Skabara[*1]

Full Research Paper

Open Access

Address:
[1]WestCHEM, Department of Pure and Applied Chemistry, University of Strathclyde, 295 Cathedral Street, Glasgow, G1 1XL, United Kingdom and [2]Institute of Physical-Organic Chemistry and Coal Chemistry, 02160 Kyiv, Ukraine

Email:
Peter J. Skabara[*] - peter.skabara@strath.ac.uk

* Corresponding author

Keywords:
non-covalent interactions; organic field effect transistor (OFET); organic semiconductors; tetrathiafulvalene; thiazole

Beilstein J. Org. Chem. **2015,** *11,* 1148–1154.
doi:10.3762/bjoc.11.129

Received: 24 April 2015
Accepted: 10 June 2015
Published: 10 July 2015

This article is part of the Thematic Series "Tetrathiafulvalene chemistry".

Associate Editor: J. P. Wolfe

Abstract

Two novel tetrathiafulvalene (TTF) containing compounds **1** and **2** have been synthesised via a four-fold Stille coupling between a tetrabromo-dithienoTTF **5** and stannylated thiophene **6** or thiazole **4**. The optical and electrochemical properties of compounds **1** and **2** have been measured by UV–vis spectroscopy and cyclic voltammetry and the results compared with density functional theory (DFT) calculations to confirm the observed properties. Organic field effect transistor (OFET) devices fabricated from **1** and **2** demonstrated that the substitution of thiophene units for thiazoles was found to increase the observed charge transport, which is attributed to induced planarity through S–N interactions of adjacent thiazole nitrogen atoms and TTF sulfur atoms and better packing in the bulk.

Introduction

The TTF moiety has received much attention in the field of organic electronics owing to its reliable redox behaviour [1], good charge transport properties [2] and scope for functionalisation [3]. This has led to widespread use of TTF-containing compounds in organic photovoltaic (OPV) devices [4-7] and in organic field effect transistors (OFETs), as both single crystals [8,9] and thin films [10,11] demonstrating charge carrier mobilities of up to 1.2 $cm^2\ V^{-1}\ s^{-1}$ [2] for single crystal devices. Similarly, oligothiophenes have demonstrated excellent properties for use in both light-emitting [12] and light-harvesting

devices [11,13]. Previously, our group reported a series of molecules containing various oligothiophenes fused to a TTF moiety through the central thiophene [11,14], which demonstrated thin film charge carrier mobilities of up to 8.61×10^{-3} cm^2 V^{-1} s^{-1} [11]. Crystallographic studies of the largest of these structures revealed significant twisting of the terminal thiophene units in septithiophene chains, leading to weak conjugation in this part of the molecule [14]. We reasoned that by replacing the terminal thiophene unit with a thiazole moiety, we could induce rigorous planarity throughout the structure and thus improve conjugation, packing and therefore charge transport properties.

A typical synthesis of a dithienoTTF is performed convergently: by constructing a half-unit functionalised with a 1,3-dithiol-2-one, that can undergo a triethyl phosphite-mediated homocoupling to synthesise the central dithienoTTF in the final step. Herein, we present an alternative divergent route to dithienoTTFs, by utilising 4,6,4',6'-tetrabromo-[2,2']bis(thieno[3,4-*d*][1,3]dithiolylidene) [15] as a core and appending heterocyclic arms through microwave assisted Stille couplings. It is worth noting that the tetrabromo-dithienoTTF core is still prepared via a triethyl phosphite-mediated homocoupling, but in this divergent route valuable heterocyclic groups can be introduced at the end of the synthesis, instead of being carried through from the outset.

Results and Discussion

Figure 1 shows the two novel dithienoTTFs **1** and **2** which were prepared according to the synthesis section below and studied in conjunction with a derivative **3** previously reported by our group [11].

Synthesis

Compounds **5** [15] and **6** [16] were prepared according to the relevant literature. Compound **4** was prepared in three steps starting with 1-bromooctan-2-one (Scheme 1). The substitution of the bromine atom for a thiocyanate group gave 1-thiocyanatooctan-2-one, which was subsequently cyclised under acidic conditions to give 2-bromo-4-hexylthiazole. Halogen–lithium exchange gave the lithiated thiazole which was quenched with trimethyltin chloride to afford **4** following purification via distillation.

Initial attempts at coupling **5** with **4** or **6** by using conventional heating methods proved ineffective due to the poor solubility of **5** in common organic solvents. However, under microwave conditions successful couplings could be readily achieved in dimethylformamide (DMF) at 160 °C (Scheme 2). It is noteworthy that in both cases no partially substituted TTFs were observed as reaction byproducts (due to the incomplete reaction of all the bromine atoms), and this is attributed to the increased solubility of the intermediates,

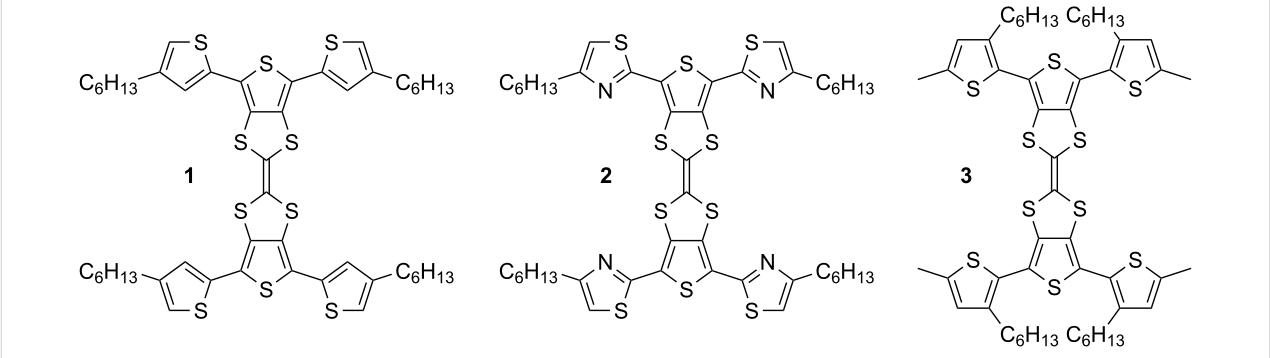

Figure 1: Compounds **1–3**.

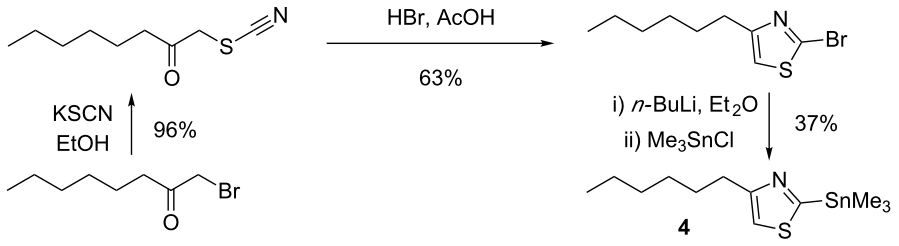

Scheme 1: Synthesis of compound **4**.

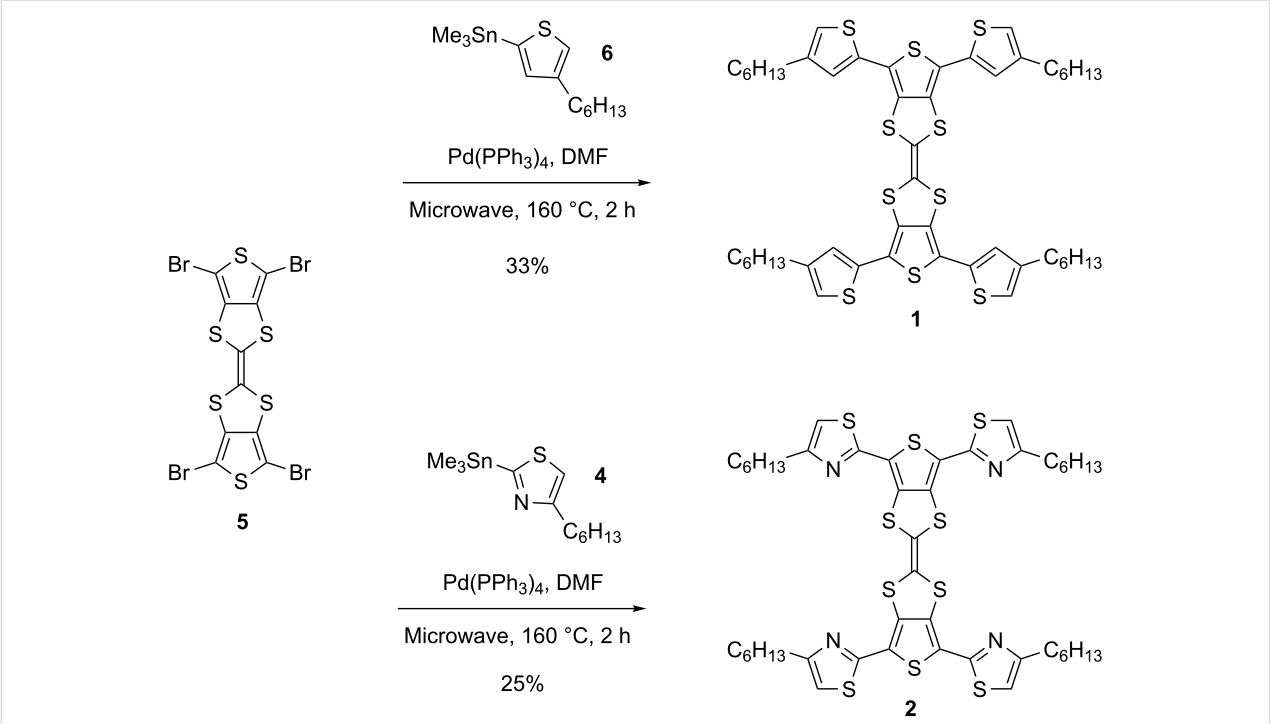

Scheme 2: Synthesis of compounds **1** and **2**.

which in turn increases their statistical likelihood of reacting further.

Optical and electrochemical properties

The optical properties of TTFs **1** and **2** were analysed by solution state UV–vis spectroscopy using dichloromethane (DCM) as the solvent (Figure 2). The obtained spectrum of compound **1** shows a maximum absorption at 380 nm and two less intense peaks at 308 nm and 274 nm. The most intensive absorption peak of **2** shows a 7 nm bathochromic shift compared to **1** and this main peak shows vibronic splitting, suggesting that compound **2** is planar, induced by S–N interactions. The main peak of compound **1** also has a slight shoulder suggesting a very small amount of vibronic splitting. There is also a broad shoulder present in the spectrum for compound **2** at 454 nm, showing evidence of charge transfer (CT) from the TTF to the electron-deficient thiazole units, facilitated due to their planarity. The structural properties of each compound will be expanded upon in the theoretical calculations section.

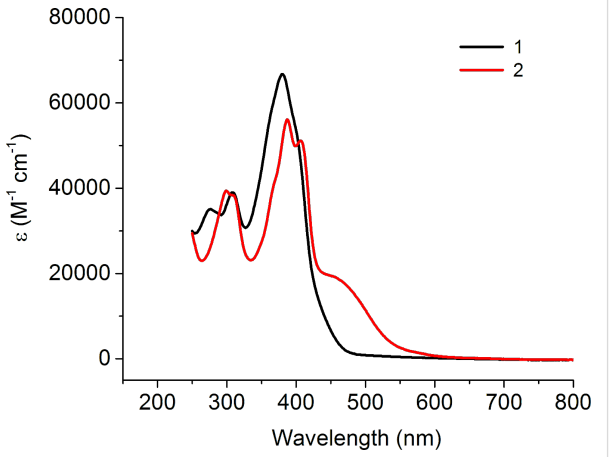

Figure 2: UV–vis absorption spectra of 10^{-5} M solutions of compounds **1** (black) and **2** (red) in dichloromethane.

Solution-state cyclic voltammetry was employed to determine the highest occupied molecular orbital (HOMO) and lowest unoccupied molecular orbital (LUMO) energy levels of TTF derivatives **1** and **2** (Figure 3). Full details of the measurements are given in Supporting Information File 1 and the results are summarised in Table 1.

The reduction waves of compounds **1** and **2** show two irreversible peaks. DFT calculations (Supporting Information File 1, Figure SI1) indicate that the reduction of these molecules primarily takes place across the triaryl units of the substituted TTF structures, with little involvement of the electron-rich TTF moiety. The LUMO energy level of compound **2** (−2.87 eV) is 0.25 eV lower than for compound **1** (−2.62 eV), which can be explained by the incorporation of electron-deficient thiazole units leading to the stabilisation of the LUMO orbital.

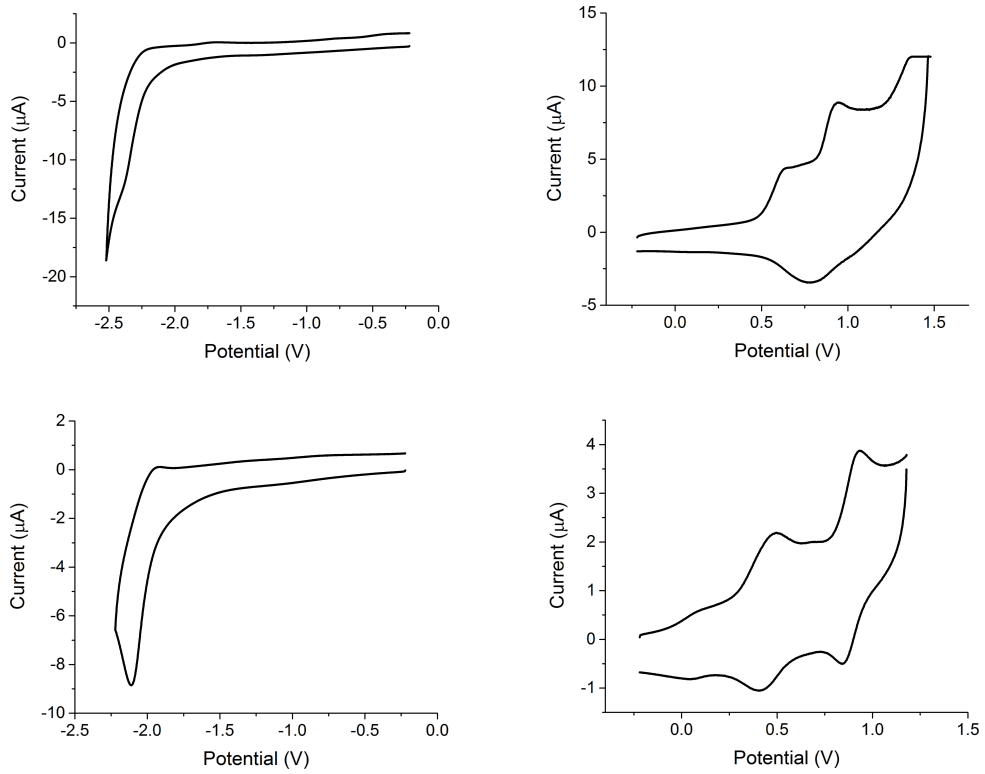

Figure 3: Cyclic voltammograms showing the reduction (left) and oxidation (right) of compounds 1 (top) and 2 (bottom) as 10^{-4} M solutions in dichloromethane.

Table 1: Summary of optical and electrochemical properties of compounds **1**–**3**.

Compound	λ_{max} (nm)	HOMO–LUMO gap (eV)[a]	HOMO (eV)[b]	LUMO (eV)[b]	E_{ox} (V)[c]	E_{red} (V)[c]
1	380	2.68 (2.86)	−5.30	−2.62	0.63, ir 0.94/0.78, qr 1.36/1.26, qr	−2.41, ir
2	387	2.22 (2.26)	−5.09	−2.87	0.49/0.41 0.93/0.84	−2.11/−1.94, ir
3 [11]	350	2.14 (2.92)	−5.06	−2.92	0.39/0.32 0.86/0.75 1.13/1.02, qr	−2.12, ir

[a]The electrochemical HOMO–LUMO gap calculated from the difference in HOMO and LUMO energy levels. The optical HOMO–LUMO gap is calculated from the onset of absorption and is shown in parentheses. [b]HOMO(LUMO) calculated from $E^{HOMO(LUMO)} = (-4.80 - E_{onset}^{ox(red)})$. [c]The cathodic and anodic peaks are reported for reversible and quasi-reversible (qr) waves. The peak values on both forward and reverse scans are reported for reversible and quasi-reversible (qr) waves. The peak value on forward scan is shown for irreversible (ir) waves. The peak values are referenced to Fc/Fc^+.

The oxidation of compound **1** shows an irreversible wave followed by two quasi-reversible waves. The three anodic peaks are well resolved but there is a non-resolved peak caused by overlap of the cathodic peaks on the reverse scan. Compound **2** appears to show a first oxidation wave at 0.09 V, however, this is an artefact due to a minor degree of aggregation induced by π–π stacking between some of the molecules. This is followed by two quasi-reversible waves with well-resolved peaks. DFT calculations (Supporting Information File 1, Figure SI1) show that the HOMO is localised on the central TTF unit suggesting that this is where the first oxidation of compounds **1** and **2** will occur. The HOMO of compound **2** (−5.09 eV) was found to be 0.21 eV higher than the HOMO calculated for compound **1** (−5.30 eV). Given that TTF **2** contains electron-deficient thiazole units, it might be expected that the HOMO is lower (further from the vacuum) than that of compound **1**, however this is not

the case. The increased HOMO of **2** is due to S–N interactions, resulting in donation from the nitrogen lone pair to the sulfur atoms of the TTF unit increasing the electron density on the TTF unit and destabilising the HOMO.

Theoretical calculations

DFT calculations were carried out using the CAM-B3LYP [17] functional and TZVP [18] basis set in dichloromethane with the SMD [19] solvent model implemented in Gaussian 09 [20]. In order to reduce computational cost, hexyl chains of **1**–**3** were reduced to methyl groups (Figure 4). The dihedral angle between the peripheral thiophene and TTF units in **3** is 62°, with the presence of the alkyl chain causing inter-ring twisting due to steric hindrance. This twist is lessened when the alkyl chain is placed in the 3-position, with **1** showing a 33° twist with respect to the central TTF unit. However, replacing the thiophene units of **1** and **3** with a thiazole in **2** leads to a structure with a dihedral angle of just 5°, suggesting the influence of favourable S–N interactions contributes to a more planar structure. The S and N atoms are separated by a distance of 3.01 Å, 0.34 Å shorter than the sum of the van der Waals radii of the two atoms (3.35 Å).

In the electrochemistry section of this paper we discussed how the S–N interactions cause destabilisation of the HOMO of **2**. The HOMO energies determined from the DFT calculations (Supporting Information File 1, Figure SI1) show that the HOMO of **1** (−6.61 eV) is lower in energy that that of **2** (−6.50 eV), which is consistent with the observed experimental trend.

Organic field-effect transistors (OFETs)

Compounds **1** and **2** were used in the fabrication of bottom-gate bottom-contact OFETs to give an indication on the applicability of these small molecules to organic semiconductor devices. The use of self-assembled monolayers (SAMs) was investigated with pentafluorobenzenethiol (PFBT) and octadecyltrichlorosilane (OTS), and chloroform and *o*-dichlorobenzene were compared for solution processing of the TTF derivatives. The output and transfer characteristics for devices fabricated using compound **2** with OTS and PFBT/OTS SAMs are shown in Figure 5 and Supporting Information File 1, Figure SI2, respectively and the results are summarised in Table 2.

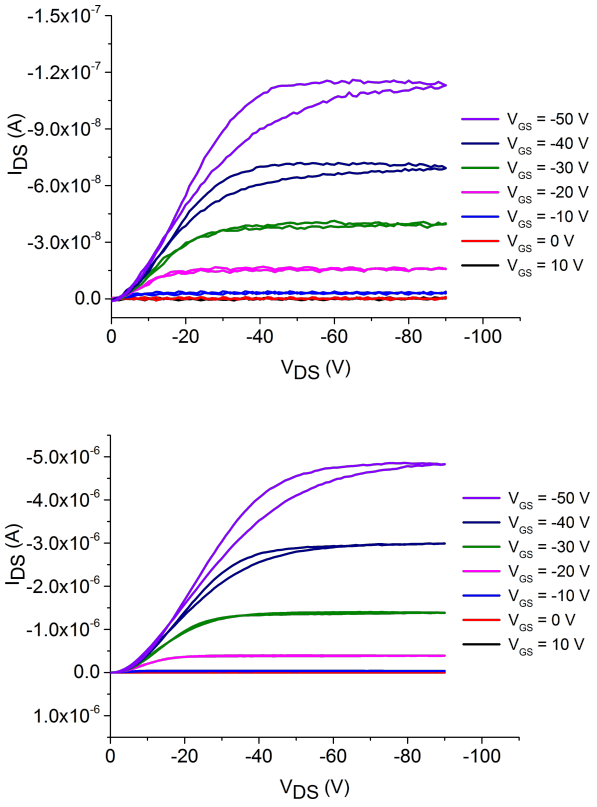

Figure 5: Output characteristics of OFETs fabricated using compound **2** in $CHCl_3$ with OTS (top) and PFBT/OTS (bottom) as self-assembled monolayers.

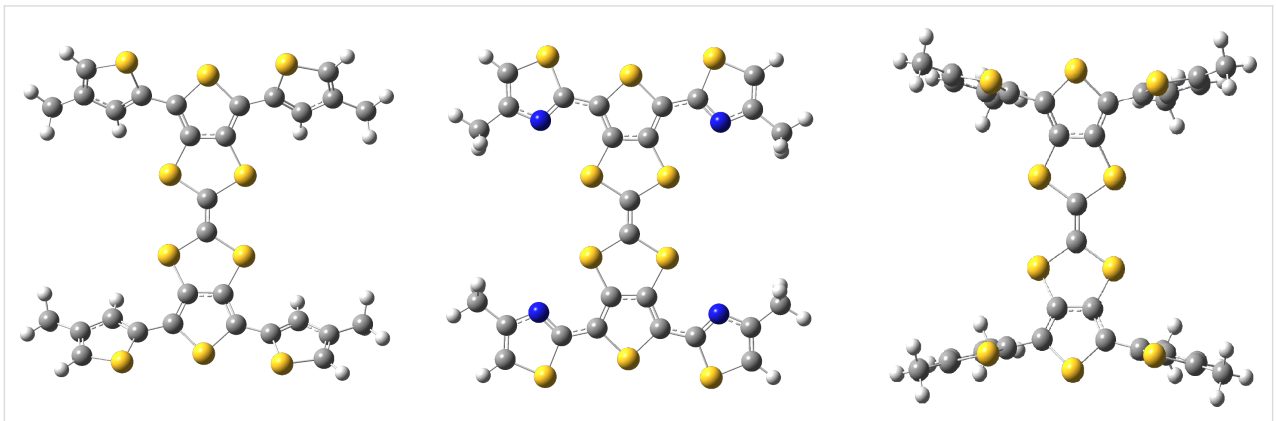

Figure 4: Optimised structures of **1** (left), **2** (centre) and **3** (right).

Table 2: OFET data produced from devices using $CHCl_3$ as the solvent for spin coating TTF **2**.

Compound	Self-assembled monolayers	μ_h ($cm^2\ V^{-1}\ s^{-1}$)	ON/OFF ratio	V_T (V)
2	OTS	1.35×10^{-5}	10^1	−30
	PFBT/OTS	3.47×10^{-4}	10^3	−34

The OFETs fabricated using only OTS as the SAM from a chloroform solution show an average saturation hole mobility of 1.35×10^{-5} $cm^2\ V^{-1}\ s^{-1}$ and an ON/OFF ratio of 10^1. However, the use of both PFBT and OTS SAMs and a chloroform solution of compound **2** results in a mobility of 3.47×10^{-4} $cm^2\ V^{-1}\ s^{-1}$, an increase of an order of magnitude. An increase is also observed in the ON/OFF ratio by two orders of magnitude to 10^3. There was no observed field-effect for devices fabricated using compound **2** in an *o*-dichlorobenzene solution or any OFETs fabricated using compound **1**.

Atomic force microscopy (AFM) was used in order to analyse the surfaces of the devices fabricated. Shown below in Figure 6 are images from devices containing compound **2** with OTS and PFBT/OTS SAMs. The images look similar with a combination of small and large clusters covering the surface. This suggests that the improvement in OFET performance with the addition of PFBT is due to improved charge injection, rather than an improvement in the morphology of the film. The OFETs were tested for n-type mobility but there was no field-effect observed.

Interestingly, despite OFETs fabricated from compound **1** showing no field-effect, films formed using this compound show a good degree of order. Figures SI3 and SI4 in Supporting Information File 1 show the surfaces of OFETs made using solutions of compound **1** in *o*-dichlorobenzene and chloroform, respectively. The film formed from spin-coating the *o*-dichlorobenzene solution shows the formation of long needle-like structures, whilst the film that results from spin-coating from the chloroform solution is less thick and shows needle-like structures which are shorter and wider. An explanation for the fact that there was no observed field-effect could be due to limited charge transport between the needles in these films.

Conclusion

By successfully coupling the tetrabrominated dithienoTTF (**5**) with stannylated intermediates **4** and **6** (via a four-fold Stille coupling), we have presented a novel route to substituted dithienoTTFs that does not necessitate the need for the synthesis of a half-unit and a final triethyl phosphite mediated homo-coupling. The resultant compounds, **1** and **2**, were fully characterised and their optical and electrochemical properties elucidated via UV–vis spectroscopy and cyclic voltammetry, and explained in conjunction with DFT level calculations. OFETs fabricated using **1** were found to have no observable field effect, but those fabricated from compound **2** were found to sustain charge carrier mobilities up to 3.47×10^{-4} $cm^2\ V^{-1}\ s^{-1}$.

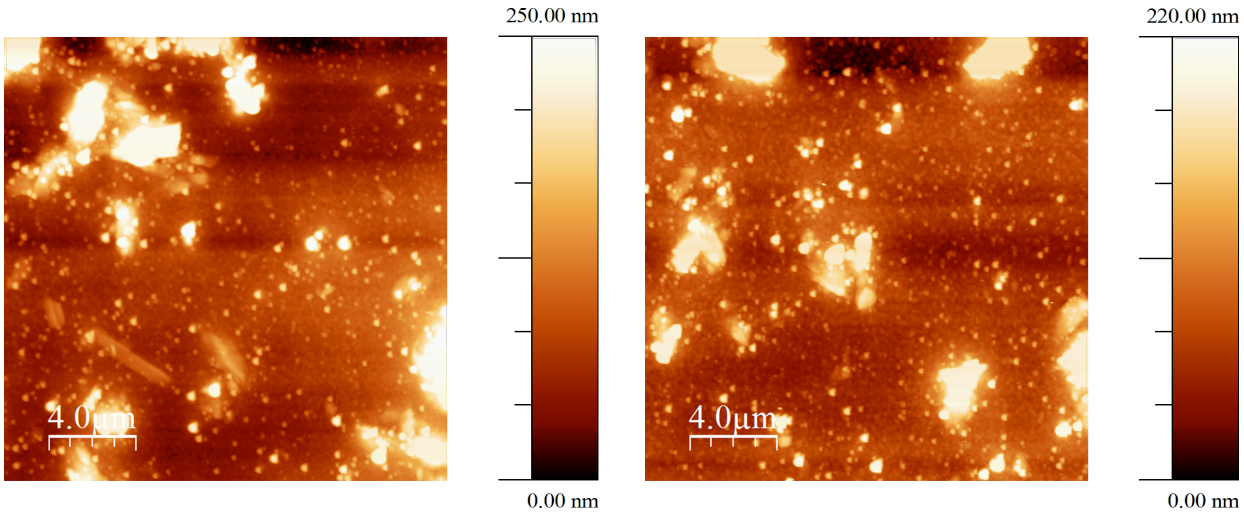

Figure 6: AFM images of OFET devices fabricated using compound **2** in $CHCl_3$ with OTS (left) and PFBT/OTS (right) as the SAMs.

The increased performance of thiazole TTF **2** is attributed to the planarising effect brought about by S–N interactions between the thiazole nitrogen atom and TTF sulfur atoms.

Supporting Information

Supporting Information File 1

Full experimental and characterisation for compounds **1**, **2** and **4**–**6**, as well as OFET fabrication methods and AFM images of OFETs containing **2**.
[http://www.beilstein-journals.org/bjoc/bjoc/content/supplementary/1860-5397-11-129-S1.pdf]

Acknowledgements

PJS thanks the Royal Society for a Wolfson Research Merit Award, ALK thanks the EPSRC for funding (EP/I029141), and RGDT thanks the EPSCR for funding (EP/L012200/1). We also thank the EPSRC UK National Mass Spectrometry Facility at Swansea University for their high resolution mass spectrometry service.

References

1. Martín, N. *Chem. Commun.* **2013,** *49,* 7025. doi:10.1039/c3cc00240c
2. Jiang, H.; Yang, X.; Cui, Z.; Liu, Y.; Li, H.; Hu, W.; Liu, Y.; Zhu, D. *Appl. Phys. Lett.* **2007,** *91,* 123505. doi:10.1063/1.2784970
3. Jiang, H.; Yang, X.; Cui, Z.; Liu, Y.; Li, H.; Hu, W.; Kloc, C. *CrystEngComm* **2014,** *16,* 5968. doi:10.1039/c3ce41849a
4. Arumugam, S.; Cortizo-Lacalle, D.; Rossbauer, S.; Hunter, S.; Kanibolotsky, A. L.; Inigo, A. R.; Lane, P. A.; Anthopoulos, T. D.; Skabara, P. J. *ACS Appl. Mater. Interfaces* **2015,** in press. doi:10.1021/am5080562
5. Bergkamp, J. J.; Decurtins, S.; Liu, S.-X. *Chem. Soc. Rev.* **2015,** *44,* 863. doi:10.1039/C4CS00255E
6. Brunetti, F. G.; López, J. L.; Atienza, C.; Martín, N. *J. Mater. Chem.* **2012,** *22,* 4188. doi:10.1039/c2jm15710a
7. Martín, N.; Sánchez, L.; Herranz, M. Á.; Illescas, B.; Guldi, D. M. *Acc. Chem. Res.* **2007,** *40,* 1015. doi:10.1021/ar700026t
8. Pfattner, R.; Mas-Torrent, M.; Bilotti, I.; Brillante, A.; Milita, S.; Liscio, F.; Biscarini, F.; Marszalek, T.; Ulanski, J.; Nosal, A.; Gazicki-Lipman, M.; Leufgen, M.; Schmidt, G.; Molenkamp, L. W.; Laukhin, V.; Veciana, J.; Rovira, C. *Adv. Mater.* **2010,** *22,* 4198. doi:10.1002/adma.201001446
9. Leufgen, M.; Rost, O.; Gould, C.; Schmidt, G.; Geurts, J.; Molenkamp, L. W.; Oxtoby, N. S.; Mas-Torrent, M.; Crivillers, N.; Veciana, J.; Rovira, C. *Org. Electron.* **2008,** *9,* 1101. doi:10.1016/j.orgel.2008.08.011
10. Geng, Y.; Pfattner, R.; Campos, A.; Hauser, J.; Laukhin, V.; Puigdollers, J.; Veciana, J.; Mas-Torrent, M.; Rovira, C.; Decurtins, S.; Liu, S.-X. *Chem. – Eur. J.* **2014,** *20,* 7136. doi:10.1002/chem.201304688
11. Wright, I. A.; Findlay, N. J.; Arumugam, S.; Inigo, A. R.; Kanibolotsky, A. L.; Zassowski, P.; Domagala, W.; Skabara, P. J. *J. Mater. Chem. C* **2014,** *2,* 2674. doi:10.1039/c3tc32571g
12. Ho, C.-L.; Yao, B.; Zhang, B.; Wong, K.-L.; Wong, W.-Y.; Xie, Z.; Wang, L.; Lin, Z. *J. Organomet. Chem.* **2013,** *730,* 144. doi:10.1016/j.jorganchem.2013.01.001
13. He, G.; Li, Z.; Wan, X.; Zhou, J.; Long, G.; Zhang, S.; Zhang, M.; Chen, Y. *J. Mater. Chem. A* **2013,** *1,* 1801. doi:10.1039/C2TA00496H
14. Wright, I. A.; Skabara, P. J.; Forgie, J. C.; Kanibolotsky, A. L.; González, B.; Coles, S. J.; Gambino, S.; Samuel, I. D. W. *J. Mater. Chem.* **2011,** *21,* 1462. doi:10.1039/C0JM02293D
15. Skabara, P. J.; Berridge, R.; McInnes, E. J. L.; West, D. P.; Coles, S. J.; Hursthouse, M. B.; Müllen, K. *J. Mater. Chem.* **2004,** *14,* 1964. doi:10.1039/b400809j
16. Barbarella, G.; Bongini, A.; Zambianchi, M. *Macromolecules* **1994,** *27,* 3039. doi:10.1021/ma00089a022
17. Yanai, T.; Tew, D. P.; Handy, N. C. *Chem. Phys. Lett.* **2004,** *393,* 51. doi:10.1016/j.cplett.2004.06.011
18. Schäfer, A.; Huber, C.; Ahlrichs, R. *J. Chem. Phys.* **1994,** *100,* 5829. doi:10.1063/1.467146
19. Marenich, A. V.; Cramer, C. J.; Truhlar, D. G. *J. Phys. Chem. B* **2009,** *113,* 6378. doi:10.1021/jp810292n
20. *Gaussian 09;* Gaussian, Inc.: Wallingford, CT, U.S.A., 2009.

License and Terms

BEILSTEIN JOURNAL OF ORGANIC CHEMISTRY

Tetrathiafulvalene-based azine ligands for anion and metal cation coordination

Awatef Ayadi[1,2], Aziz El Alamy[3], Olivier Alévêque[1], Magali Allain[1], Nabil Zouari[2], Mohammed Bouachrine[3] and Abdelkrim El-Ghayoury*[1]

Full Research Paper

Open Access

Address:
[1]Laboratoire MOLTECH Anjou, Université d'Angers, UFR Sciences, UMR 6200, CNRS, Bât. K, 2 Bd. Lavoisier, 49045 Angers Cedex, France, [2]Laboratoire de Physico-chimie de l'état solide, Université de Sfax, Route de Soukra; Km 4; BP: 802, 3038, Sfax, Tunisia and [3]MEM, High School of Technology (ESTM), University, Moulay Ismail, Meknès, Morocco

Email:
Abdelkrim El-Ghayoury* - abdelkrim.elghayoury@univ-angers.fr

* Corresponding author

Keywords:
azine ligand; fluoride sensing; rhenium; tetrathiafulvalene; X-ray

Beilstein J. Org. Chem. **2015,** *11,* 1379–1391.
doi:10.3762/bjoc.11.149

Received: 24 March 2015
Accepted: 12 July 2015
Published: 07 August 2015

This article is part of the Thematic Series "Tetrathiafulvalene chemistry".

Guest Editor: P. J. Skabara

Abstract

The synthesis and full characterization of two tetrathiafulvalene-appended azine ligands, namely 2-([2,2'-bi(1,3-dithiolylidene)]-4-yl)-6-((2,4-dinitrophenyl)hydrazono)methyl)pyridine (**L1**) and 5-([2,2'-bi(1,3-dithiolylidene)]-4-yl)-2-((2,4-dinitrophenyl)hydrazono)methyl)pyridine (**L2**) are described. The crystal structure of ligand **L1** indicates that the ligand is completely planar with the presence of a strong intramolecular N3–H3···O1 hydrogen bonding. Titration experiments with inorganic anions showed that both ligands are suitable candidates for the sensing of fluoride anions. Ligand **L2** was reacted with a Re(I) cation to yield the corresponding rhenium tricarbonyl complex **3**. In the crystal structure of the newly prepared electroactive rhenium complex the TTF is neutral and the rhenium cation is hexacoordinated. The electrochemical behavior of the three compounds indicates that they are promising for the construction of crystalline radical cation salts.

Introduction

Tetrathiafulvalene (TTF) is known to have excellent electron-donating properties resulting in stable radical cation ($TTF^{\bullet+}$) and dication (TTF^{2+}) species from two sequential and reversible oxidation processes. The huge interest in the synthesis of TTF and its very numerous derivatives [1] has been initiated by the high electrical conductivity discovered in a chloride salt of TTF [2] and metallic behavior in the charge-transfer complex with 7,7,8,8-tetracyano-*p*-quinodimethane (TCNQ) [3]. These systems have played a major role for the preparation of molecular materials designed for various applications. They have been, for example, used as electron donor molecules to prepare electrically (super)conducting crystalline materials [4-7], as solar energy systems [8,9] or even as donor moieties in nonlinear optical (NLO) materials [10,11]. In the last decades one of the biggest challenges in materials science is devoted to the preparation of multifunctional molecular materials that can

potentially exhibit, in solution and/or in solid state, synergy or coexistence between two or more different physical properties. In order to address this issue, many efforts have been devoted to the association of a binding or coordinating unit to the redox-active TTF moiety. This strategy has led for example, in solid state, to the preparation of electroactive metal complexes that combine magnetic and electrical properties [12-17]. In solution, TTF-based redox-responsive receptors for neutral and/or charged guest sensing applications have been prepared [18-22]. On this ground, chemosensors capable of recognizing anionic and/or cationic species constitute an important area of increasing research in supramolecular chemistry, considering the ubiquitous properties of both anions and metal cations [23-27]. In fact, anions are involved in a large number of biological and chemical processes [28-31]. Note that fluoride is of particular interest among the other inorganic anions because of its both beneficial (e.g., preventing dental caries and treatment of osteoporosis) and detrimental (e.g., fluorisis) effects on human health [32-34]. Many TTF derivatives have been used to coordinate or to bind separately metal cations [35] or inorganic anions [36], however only few examples were used for both inorganic anions and metal cations coordination [37].

Herein we report the synthesis and electronic properties of two new multifunctional TTF-based azine ligands that integrate distinctive functional groups as depicted in Scheme 1 and thus capable of coordinating both metal cations as well as inorganic anions. The sensing studies for inorganic anions are discussed. Metal cation complexation studies of the new ligands afforded the formation and the structural characterization of a neutral rhenium complex.

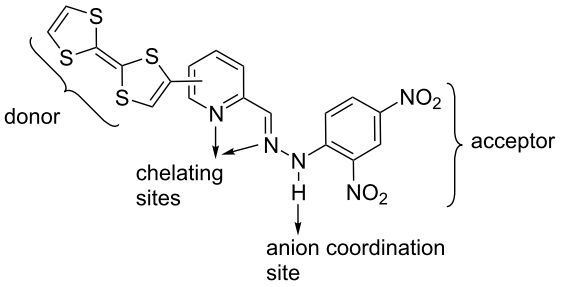

Scheme 1: Multifunctional TTF-appended azine ligands.

Results and Discussion

Synthesis of the ligands L1 and L2

The protocol followed for the synthesis of the new azine ligands **L1** and **L2** is summarized in Scheme 2. The reaction of 6-bromo-2-pyridinecarboxaldehyde or 5-bromo-2-pyridinecarbox-

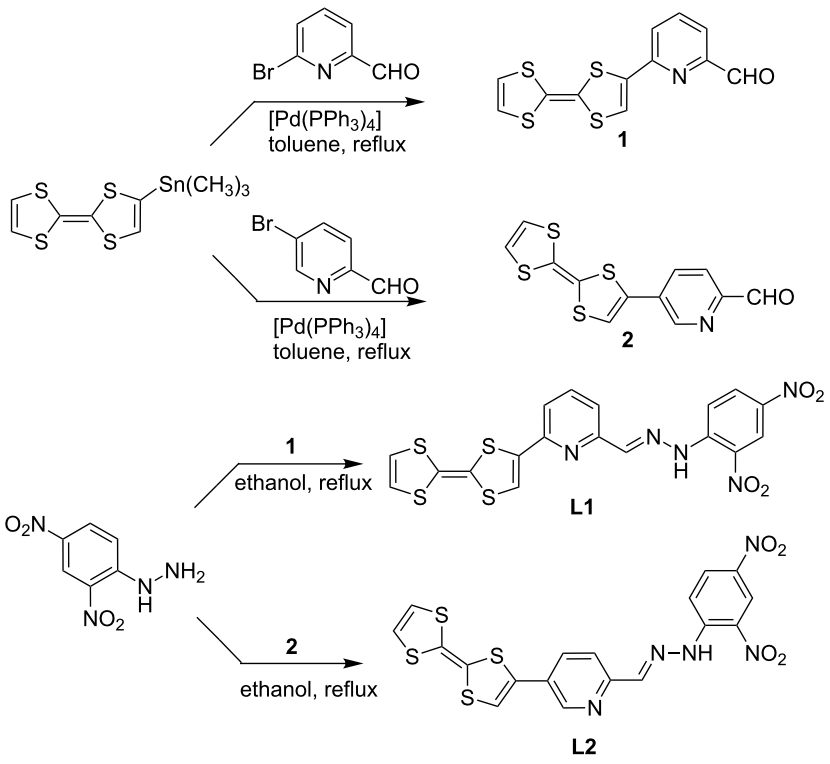

Scheme 2: Synthetic scheme for TTF-based azine ligands **L1** and **L2**.

aldehyde with one equivalent of TTF-$SnMe_3$ under the Stille coupling conditions, using [$Pd(PPh_3)_4$] as catalyst in toluene, afforded the intermediates 6-([2,2'-bi(1,3-dithiolylidene)]-4-yl)picolinaldehyde (**1**, previously described in reference [38]) and 5-([2,2'-bi(1,3-dithiolylidene)]-4-yl)picolinaldehyde (**2**) in good yields (60% and 65%, respectively), after chromatographic work-up. Condensation of pyridinealdehyde-functionalized TTF **1** or **2** with 2,4-dinitrophenylhydrazine, in refluxing ethanol, afforded the desired ligands **L1** and **L2** in 75% and 63% isolated yields, respectively. The structures of the new ligands were characterized by ^1H and ^{13}C NMR, UV–visible and IR spectroscopy, high resolution mass spectrometry and elemental analysis.

Crystal structure description

Details about data collection and structure refinement are given in Table 1. Crystallographic data for the structural analysis have been deposited within the Cambridge Crystallographic Data Centre, CCDC 1055120 (ligand **L1**) and CCDC 1055119 (complex **3**).

Suitable single crystals for X-ray analysis have been grown for ligand **L1** upon recrystallization from DMSO solution. Ligand **L1** crystallizes as dark plates in the orthorhombic system, space group Pbca and selected bond lengths and angles are depicted in Table 2. As it can be seen in Figure 1, ligand **L1** is completely planar. The dihedral angle between the dinitrophenylhydrazone and pyridine planes is 2.67 (2)° which is slightly lower than the dihedral angle observed in the case of the pyridine-2-carbaldehyde 2,4-dinitrophenylhydrazone that is 3.88 (8)° [39]. The molecular conformation of the ligand is stabilized by a strong intramolecular N3–H3···O1 (2.015 (6) Å) hydrogen bond making the dinitrophenyl ring coplanar with the hydrazone unit and also by an intramolecular short contact S4···N1

Table 1: Crystal data and structure refinement for ligand **L1** and complex **3**.

compound	Ligand **L1**	Complex **3**
Empirical formula	$C_{78}H_{62}N_{20}O_{19}S_{19}$	$C_{42}H_{24}Cl_2N_{10}O_{15}Re_2S_8$
fw	2192.62	1608.49
T (K)	293(2)	180.0(1)
wavelength (Å)	0.71073	1.54184
cryst syst	Orthorhombic	Triclinic
space group	Pbca	*P*1
a (Å)	7.353(3)	8.591(1)
b (Å)	30.35(1)	11.501(1)
c (Å)	20.894(6)	15.567(2)
α (deg)	90	99.494(8)
β (deg)	90	100.97(1)
γ (deg)	90	94.926(8)
V (Å^3)	4663(3)	1478.3(3)
Z	*2*	1
D_c (g cm^{-3})	1.562	1.807
abs coeff (mm^{-1})	0.517	11.955
F(000)	2252	778
cryst size (mm^3)	0.26 x 0.04 x 0.02	0.2061 x 0.0406 x 0.0194
θ range for data collection (deg)	3.01–24.98	2.94–72.85
Tmin/Tmax	0.867 / 0.990	0.656 / 1.000
reflns collected	32107	8638
indep reflns	4078	5473
completeness (%)	99.5	96.8
R(int)	0.1083	0.1495
refinement method	full-matrix least squares on F^2	full-matrix least squares on F^2
Data with [$I > 2\sigma(I)$] /restraints/param	1974/ 0 / 280	3616 / 7 / 361
GOF on F^2	1.093	1.041
final *R* indices [$I > 2\sigma(I)$]	R1 = 0.0947, wR2 = 0.1705	R1 = 0.0987, wR2 = 0.2569
R indices (all data)	R1 = 0.2089, wR2 = 0.2046	R1 = 0.1458, wR2 = 0.2810
largest diff. peak and hole (e Å^{-3})	0.255 and −0.310	2.290 and −2.053
X-ray wavelength radiation	Mo K_α	Cu K_α

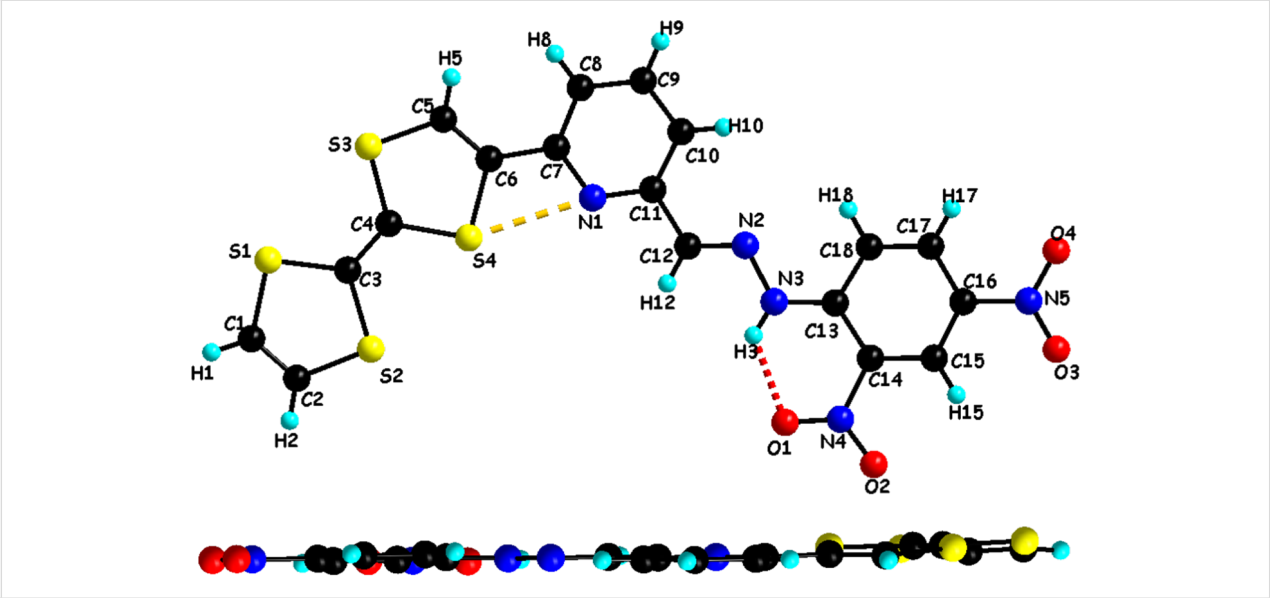

Figure 1: Crystal structure of ligand **L1** with atom numbering scheme (top) and a side view of the molecule (bottom).

Table 2: Selected bond lengths (Å) and angles (°) in **L1**.

Bond length (Å)			
C1–S1	1.749(8)	C6–C7	1.487(9)
C1–C2	1.310(9)	C7–N1	1.361(8)
C2–S2	1.745(7)	N1–C11	1.324(8)
C3–S2	1.789(7)	C11–C12	1.463(9)
C3–S1	1.748(8)	C12–N2	1.256(8)
C3–C4	1.349(9)	N2–N3	1.383(7)
C4–S3	1.741(7)	N3–C13	1.340(8)
C4–S4	1.779(7)	C13–C14	1.431(9)
S4–C6	1.777(6)	C14–N4	1.474(9)
C6–C5	1.337(8)	N4–O1	1.217(8)
Angle values (°)			
N1–C11–C10	123.7(7)	N2–N3–C13	119.0(6)
C12–N2–N3	117.2(6)	C18–C13–N3	120.3(6)
C11–C12–N2	121.9(7)	C13–C14–N4	120.9(7)

(2.824(6) Å) that makes the TTF unit and the pyridine ring coplanar.

In the solid state, the packing arrangement in **L1** is characterized by the self-assembly between the TTF donor unit and the dinitrophenyl acceptor unit forming head-to-tail dimers. Moreover, the plane-to-plane distance between the donor and acceptor moieties is $d = 3.39$ Å, showing an evident overlap that is comparable to the reported intermolecular charge-transfer complexes [35]. This overlap develops along *a*-axis forming infinite columns (Figure 2). These columns are linked together along *c*-axis through hydrogen bonding occurring between TTF-C-H and NO_2 (TTF-C–H1···O3-NO 2.493(6) Å).

In the *b*-direction, the columns of stacked head to tail molecules are connected laterally through S···O heteroatom contacts ($d = 3.16$ Å, Figure S1, Supporting Information File 1) resulting in alternating stacks with a "zig zag" like manner with an angle of rotation of 135.6° (Figure 3).

UV–visible absorption spectroscopy

The UV–visible absorption spectra of the ligands **L1** and **L2** were recorded in a mixture of dichloromethane/acetonitrile solution (9/1, v/v, $C = 2 \times 10^{-5}$ M) at room temperature (Figure 4). The two ligands exhibit strong electronic absorption bands between $\lambda = 300$ nm and 450 nm which are assigned to the $\pi \rightarrow \pi^*$ and $n \rightarrow \pi^*$ absorption bands resulting from the different units of the two ligands (TTF moiety, pyridyl ring and the dinitrophenylhydrazone group). As compared to ligand **L1**, **L2** exhibits an additional absorption band around $\lambda = 516$ nm which is attributed to an intramolecular charge transfer (ICT) excitation from the TTF donor moiety to the dinitrophenylhydrazone accepting group. These results from a strong π-electronic delocalization that occurs in ligand **L2** leading to a resonance structure that involves the C=N hydrazone bond as it can be seen in (Figure S2, Supporting Information File 1).

Theoretical calculations

Theoretical calculations based on density functional theory (DFT) methods have been performed with the Gaussian 09 program [40]. Becke's three-parameter gradient-corrected functional (B3LYP) with 6-31G (d) basis in vacuum was used for

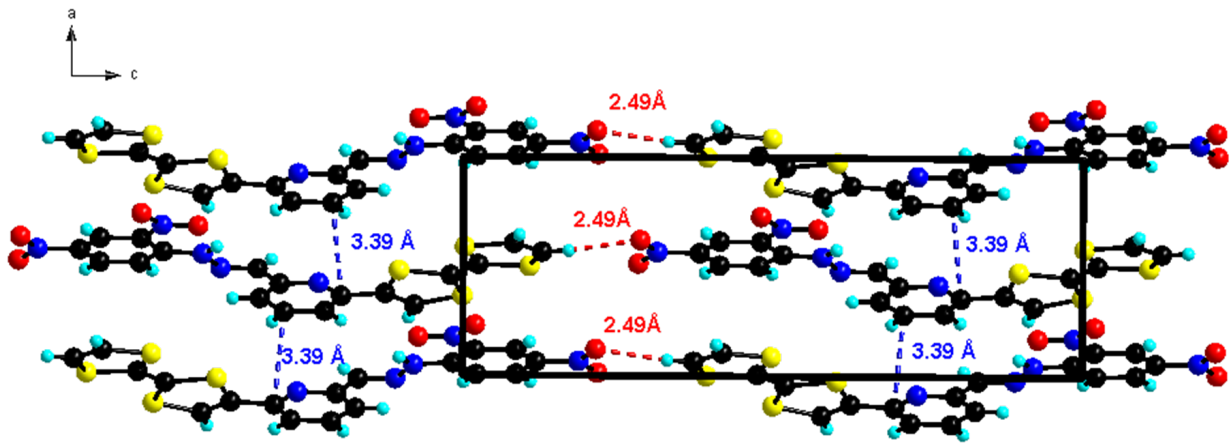

Figure 2: Partial crystal packing of ligand **L1** with formation of head to tail dimers that stack along *a*-axis forming columns that are connected through hydrogen bonding along *c*-axis.

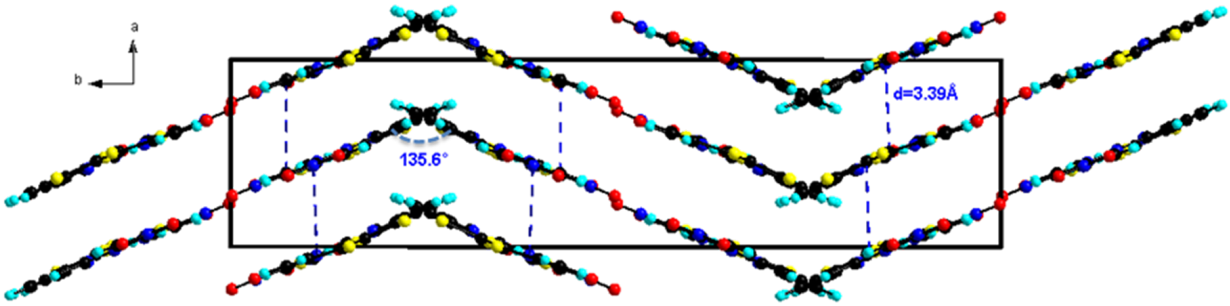

Figure 3: Packing diagram of **L1** showing the orientation of the columns of head to tail dimers.

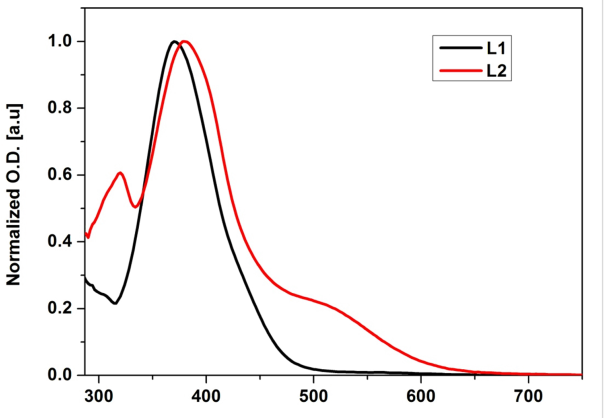

Figure 4: UV–visible absorption spectra of ligands **L1** and **L2** (*c* 2.5 × 10^{-5} M in (dichloromethane/acetonitrile, 9:1, v/v)), room temperature.

full geometry optimization of the two ligands. The resulting frontier molecular orbitals (Figure 5) for ligands **L1** and **L2** indicate that the electron density of the highest occupied molecular (HOMO) orbitals develop exclusively on the TTF fragment. The LUMO orbital for ligand **L1** is essentially distributed on the nitrophenylhydrazino group with a small participation of the pyridyl ring, while for ligand **L2** it is distributed on the π-extended system with a small participation of the external ethylenic atom of the TTF moiety which is confirming the good electronic conjugation in this ligand. The same behavior is observed for the TTF pyridine carboxaldehyde precursors **1** and **2** (Figure S3, Supporting Information File 1).

Cyclic voltammetry

The electrochemical behavior of the electroactive precursors **1** and **2** as well as of ligands **L1** and **L2** was investigated by cyclic voltammetry (Figure 6 and Table 3). The measurements in the case of precursors **1** and **2** show two reversible oxidations at E_{1ox} = +0.26 V, E_{2ox} = +0.75 V and E_{1ox} = +0.32 V, E_{2ox} = +0.77 V vs Ag/Ag^{+}, respectively, that are anodically shifted when compared to the ones of the free TTF because of the presence of the electron deficient pyridinecarboxaldehyde moiety. In addition, E_{1ox} of **2** is anodically shifted when

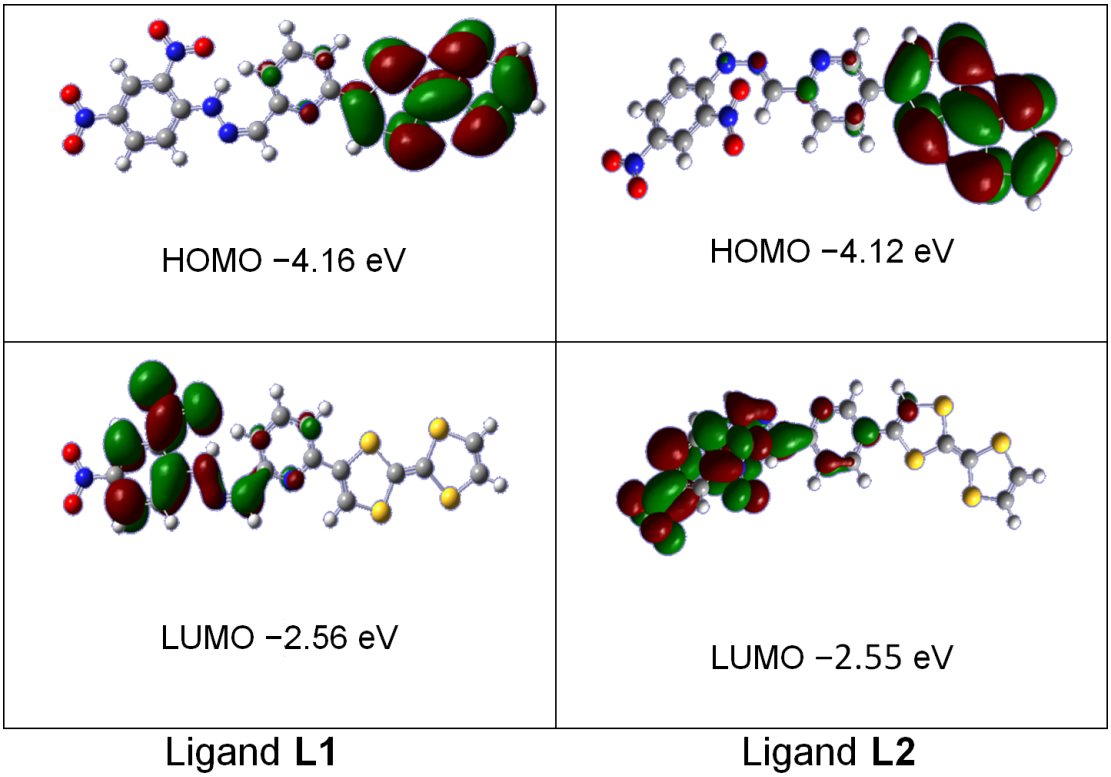

Figure 5: HOMO–LUMO Frontier orbitals representation for ligands **L1** and **L2**.

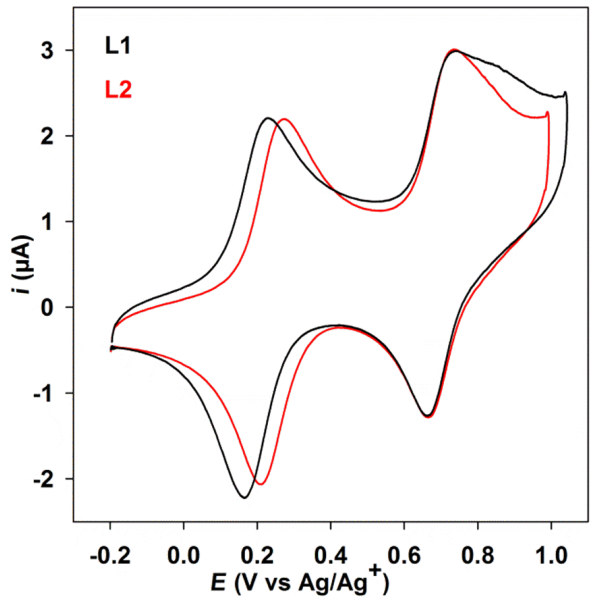

Figure 6: Cyclic voltammograms of ligands **L1** and **L2** (2×10^{-5} M) in CH_2Cl_2/CH_3CN (9:1, v/v) at 100 mV·s^{-1} on a glassy carbon electrode with *n*-Bu_4NPF_6 (0.1 M).

Table 3: Apparent redox potentials (V) of molecular compounds **1**, **2**, **L1** and **L2** reported vs Ag/Ag^+ (0.01 M) in 0.1 M $TBAPF_6$ in CH_2Cl_2/CH_3CN 3:1 on glassy carbon electrode at 100 mV·s^{-1}.

compound	E_{ox1}	E_{ox2}
1	0.26	0.75
2	0.32	0.77
L1	0.20	0.70
L2	0.25	0.70

compared with E_{1ox} of **1**, indicating a strong π-electron conjugation in precursor **2**. As for **1** and **2**, ligands **L1** and **L2** show two reversible oxidations at E_{1ox} = +0.20 V, E_{2ox} = +0.70 V and E_{1ox} = +0.25 V, E_{2ox} = +0.70 V vs Ag/Ag^+, respectively) that are cathodically shifted when compared to the ones of **1** and **2** indicating that the pyridine-hydrazone group is less electron deficient than the corresponding pyridinecarboxaldehyde. In addition, E_{1ox} of **L2** is also anodically shifted when compared with E_{1ox} of **L1** because of the strong π-electron conjugation in ligand **L2** and this is in agreement with the bathochromic shift observed for **L2** in the UV–visible absorption spectra.

Sensing properties of the azine ligands for anions

It is known that phenylhydrazone groups are able to act as optical sensors particularly for fluoride anions [41-45]. Thus, the colorimetric sensing abilities of the two ligands **L1** and **L2**

were investigated by adding various anions such as hydrogensulfate, acetate, iodine and fluoride (used as tetrabutylammonium salts) in a mixture of dichloromethane/acetonitrile (9:1, v/v). Addition of increasing amounts of F^- causes a dramatic change in color from yellow to violet that can be observed by the naked eye (Figure S4 in Supporting Information File 1), which is accompanied by the formation of a new broad absorption band centered at about 510 nm in the case of ligand **L1**. In the case of ligand **L2**, addition of F^- (Figure 7) causes also a dramatic change in color from light orange to violet that can be observed by the naked eye (Figure S5 in Supporting Information File 1), that is accompanied by a decrease of the intense absorption band centered at about 380 nm and the increase of the ICT absorption band centered around 540 nm. This change is likely due to the deprotonation of the hydrazone nitrogen which causes an enhancement of charge transfer from the TTF unit and the deprotonated nitrogen to the electron poor 2,4-dinitrophenyl moiety [36]. A remarkable feature is the occurrence of a quite well defined isosbestic point at 420 nm and 447 nm for **L1** and **L2**, respectively, indicating that **L1** or **L2** coexist with only one species upon addition of TBAF. Note that upon addition of other inorganic anions such as bromide, chloride or hydrogensulfate we have observed a negligible absorption changes while in the case of acetate anion a moderate absorption changes are obtained (Figures S6 and S7 in Supporting Information File 1) [46].

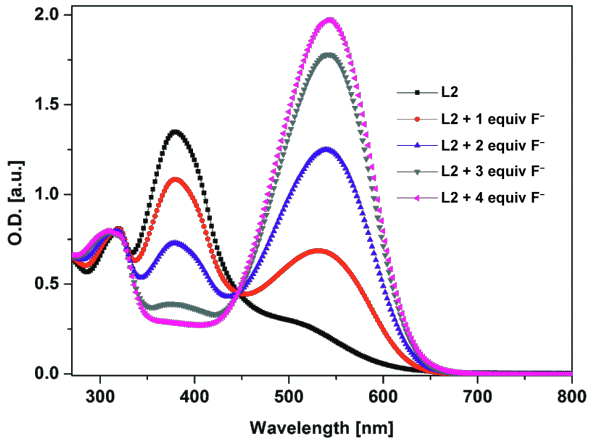

Figure 7: UV–visible spectral changes of ligand **L2** (2×10^{-5} M in CH_2Cl_2/CH_3CN, 9/1) upon addition of TBAF.

Treatment of an electrolytic solution of ligand **L1** or **L2** with an increasing amount of fluoride anion (tetrabutylammonium fluoride trihydrate in a CH_2Cl_2/CH_3CN mixture) involve the presence, as previously seen for fluoride anion sensing [47], and mainly on the first cycle, of the pre-wave superimposed on the wave of oxidation of the ligands. We clearly see on the second cycle a negligible change of the oxidation potential of the ligand which is very likely because of the large distance between the TTF and the fluoride coordinating unit (Figure S8 in Supporting Information File 1).

In order to get further supports to the observed optical sensing and to get deeper insights into the interactions between **L1** or **L2** and fluoride, ^{1}H NMR titration experiments were performed in DMSO-d_6 (Figure 8 and Figure S9 in Supporting Information File 1). The measurements indicate that the N–H peak disappears after addition of one equivalent of TBAF while the other aromatic proton resonances of **L1** or **L2** exhibit an upfield shift. These results tend to be consistent with the deprotonation of the N–H group and the delocalization of the negative charge over the π-conjugated system as previously observed TTF dinitrophenylhydrazone [36]. Note that there is no change in the ^{1}H NMR spectrum observed for other anions.

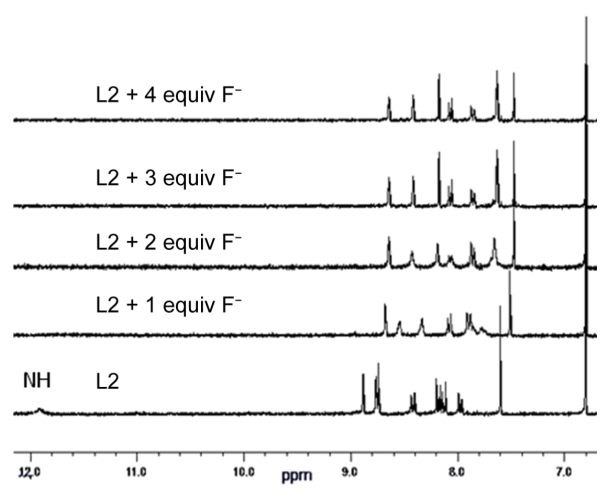

Figure 8: ^{1}H NMR spectra of ligand **L2** ($4 \cdot 10^{-3}$ M in DMSO-d_6) upon addition of successive aliquots of TBAF (DMSO-d_6).

Synthesis and crystal structure of a neutral rhenium complex

Few metal complexes based on ruthenium cations have been previously prepared with dinitrophenylazine type ligands [48,49]. These reports indicate that the pyridinedinitrophenylazine type ligands are good candidates for the formation of metal complexes. We have therefore investigated the complexation of **L1** and **L2** with various metal cations and we succeeded in the crystallization of a neutral rhenium metal complex with ligand **L2**. Thus, the equimolar reaction between **L2** and the $[Re(CO)_5Cl]$ precursor performed in refluxing toluene, under no light and inert atmosphere, afforded a mononuclear neutral complex **3** described as $[Re\mathbf{L2}(CO)_3Cl]\cdot 0.5H_2O$ as a dark precipitate [50]. Single crystals of **3** were obtained by recrystallization from acetone/hexane solution. Details about data collection and structure refinement are given in Table 1. As expected,

the resulting metal complex **3** is composed of one ligand **L2** coordinated to $Re(CO)_3Cl$ fragment through two nitrogen atoms of the pyridine and the C=N hydrazone group (Figure 9). Upon complexation, the ligand acquires a *cis*-conformation of the hydrazinopyridine moiety in contrast to the *trans*-conformation observed for free ligand **L1** (see Figure 1 and Figure 9). Within the complex, the rhenium center is surrounded by the bidentate chelating **L2** ligand, three carbonyl ligands arranged in a facial fashion, and a chlorine atom and its coordination sphere presents the expected, although slightly distorted, octahedral geometry. The angle formed by the rhenium center and N atoms equals to 73.6(5)° which is smaller than the angle of 90° adopted in an ideal octahedron. In addition, in the complex the C–Re–C angles identified as C19–Re1–C20, C19–Re–C21, C20–Re–C21 are 87.7°, 91.7° and 90.9°, respectively, which are close to 90° indicating that CO ligands are almost linearly coordinated to the rhenium(I) cation. The length of the two Re–N bonds are (N1–Re1 2.20(1) Å) and N2–Re1 2.18(1) Å, and the formal double bond character C=N is maintained (C12–N2 1.32(2) Å). All three Re–CO bond lengths are very close, and the Re–C–O angles present minor deviations from linear structure, values ranging from 165(2)° to 177(2)° (Table 4).

In the crystal structure, the chlorine atom coordinated to rhenium is involved in an intramolecular C–H···Cl hydrogen bonding with the hydrogen from the pyridyl ring with a distance of 2.581(6) Å. In addition, it is involved in an intermolecular hydrogen bonding with a neighboring molecule by a strong TTF-C–H···Cl bond (2.659(6) Å) resulting in the formation of dimers that are formed with a $R_2^2(16)$ cyclic motif (grey filling in Figure 10) as it was previously observed within a catechol-appended TTF derivative [51].

Table 4: Selected bond lengths (Å) and angles (°) in complex **3**.

Bond length (Å)			
N1–Re1	2.20(1)	C20–Re1	1.96(2)
N2–Re1	2.18(1)	C19–Re1	1.89(2)
Cl1–Re1	2.39(8)	C11–N1	1.35(2)
C21–Re1	2.19(1)	C11–C12	1.43(2)
Angle values (°)			
C19–Re1–C20	87.7(9)	N2–Re1–N1	73.6(5)
C19–Re1–C21	91.7(7)	C21–Re1–Cl1	172.7(4)
C20–Re1–C21	90.9(7)	C19–Re1–Cl1	89.7(6)
C19–Re1–N2	174.2(6)	C20–Re1–Cl1	96.3(7)
C20–Re1–N2	97.4(8)	N1–Re1–Cl1	86.1(4)
C19–Re1–N1	101.1(7)	N2–Re1–Cl1	92.4(4)
C20–Re1–N1	170.8(8)	O5–C19–Re1	177(2)
C21–Re1–N2	85.6(5)	O6–C20–Re1	177(2)
		O7–C21–Re1	165(2)

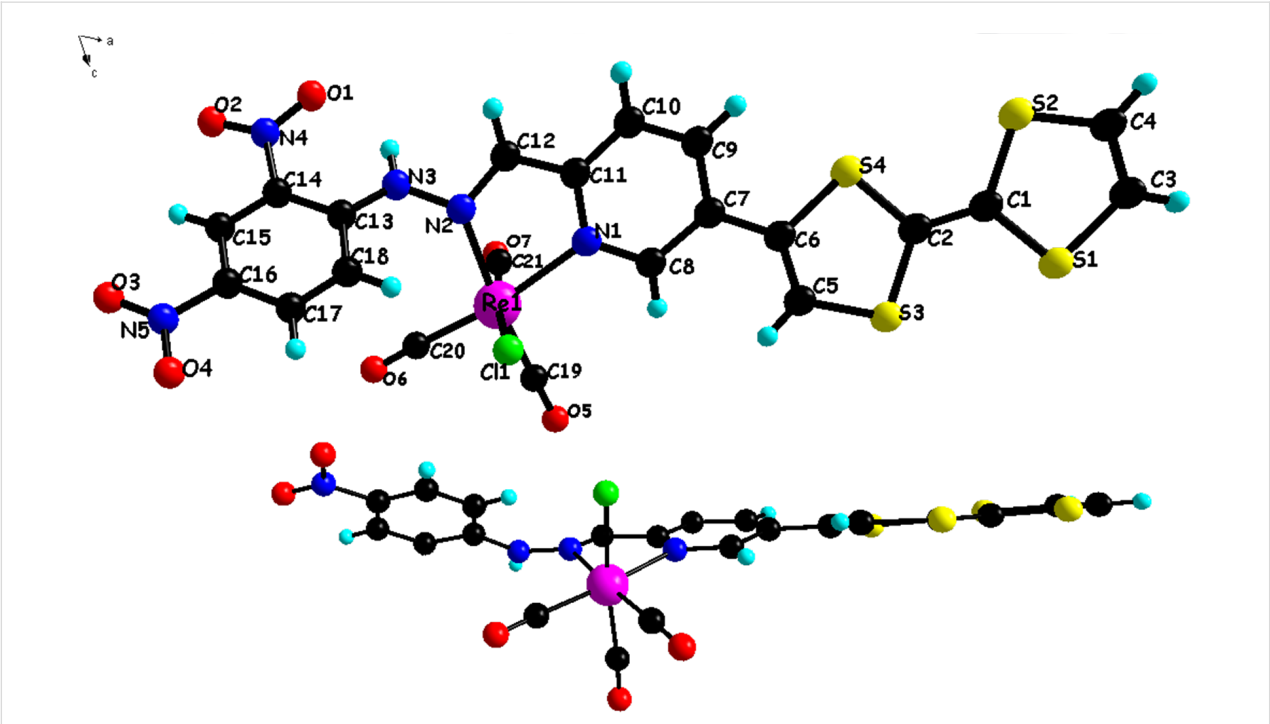

Figure 9: Crystal structure of complex **3** with atom numbering scheme (top) and a side view of the molecule (bottom). Water molecules are omitted for clarity.

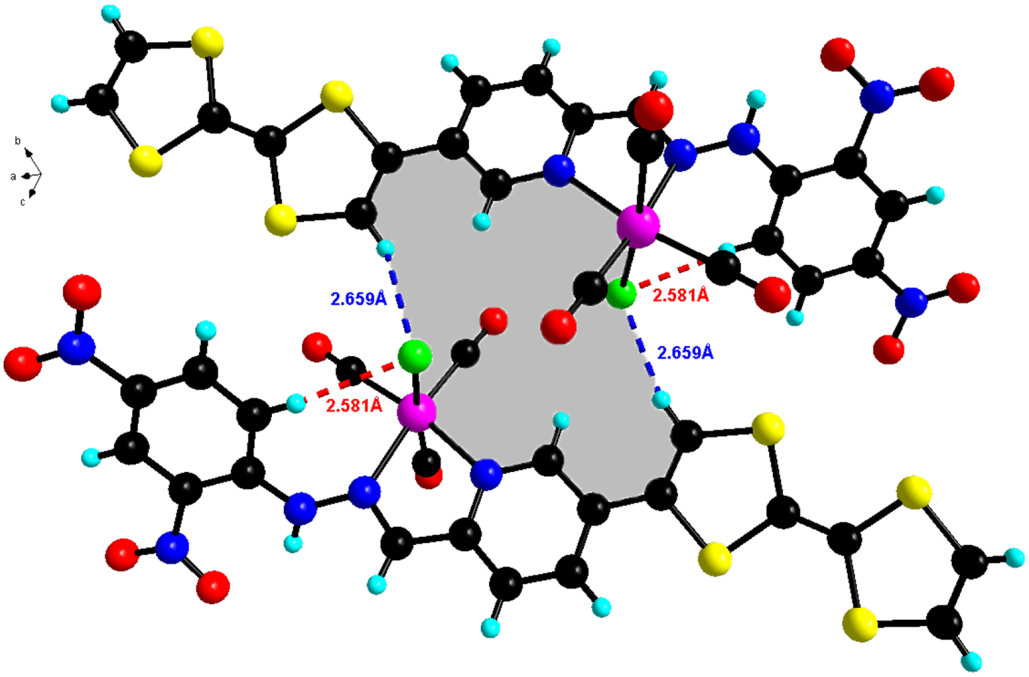

Figure 10: Pattern of intramolecular and intermolecular contacts in **3**. Two molecules are linked by pairs of strong TTF-C–H···Cl hydrogen bonds forming $R_2^2(16)$ cyclic motifs (in grey filling).

Adjacent dimers interact through hydrogen bonding interaction C–H···O (H···O 2.70(2) Å) formed between the NO_2 group and an aromatic C–H that results in the establishment of $R_2^2(10)$ cyclic motifs (blue filling in Figure 11) and N–H···O (H···O 2.32(2) Å) hydrogen bonds formed between the second NO_2 group and N–H that form $R_2^2(12)$ cyclic motifs (grey filling in

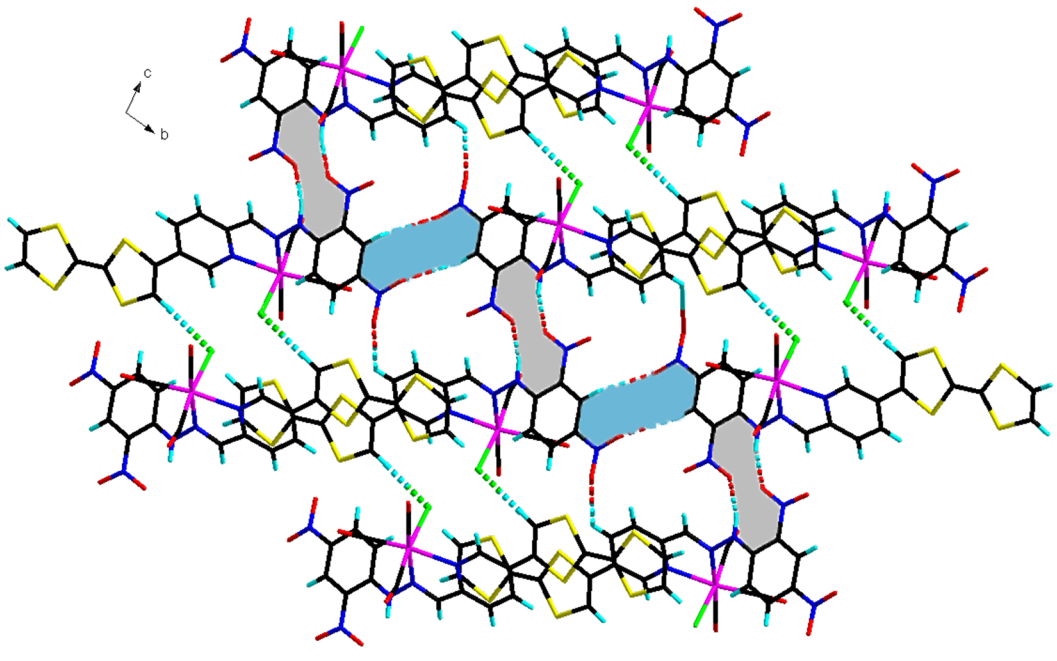

Figure 11: Layered structure of complex **3** viewed along the *a*-axis. The dimers are linked together through hydrogen bonding that form $R_2^2(10)$ in blue filling and $R_2^2(12)$ in grey filling cyclic motifs.

Figure 11). This hydrogen bonding link therefore the molecules together into layers parallel with the *bc* crystallographic plane. The dimers of the resulting layers form a stack along *a*-axis through S···S contacts (d(S···S) being between 3.70(6) and 3.90(7) Å) resulting into a 3D supramolecular network.

The UV–visible absorption spectrum of the rhenium complex **3** recorded in a mixture of dichloromethane/acetonitrile (9:1, v/v) at room temperature (c 1.1×10^{-4} M) presents the same features as the free ligand **L2** with a red shift of the different absorption bands (Figure S10 in Supporting Information File 1). The ICT trasnsition suffers a bathochromic shift by about 100 nm as compared with the free ligand which indicates an increase of the electron acceptor effet of the ligand upon complexation with rhenium which acts as strong Lewis acid.

After complexation, the redox behavior of the TTF moiety is maintained. We note a positive shift of the two oxidation potentials in the case of complex **3** by about 90 mV and 100 mV (Figure S11 in Supporting Information File 1). This increase of the oxidation potential suggests that the rhenium fragment is acting as an electron acceptor by decreasing the electron density on the TTF unit. This behavior is in agreement with the electronic absorption experiments and confirms the strong electronic conjugation in ligand **L2**. The electrochemical behavior observed for **L2** and its corresponding rhenium complex **3** indicate that this compounds are valuable candidates for the electrochemical formation of air-stable radical cation crystalline salts [16].

Conclusion

Two multifunctional ligands which associate an electron-donating TTF unit with an electron-accepting dinitrophenyl group as well as a coordinating pyridine azine moiety were successfully synthesized. Ligand **L2** exhibit a strong electronic conjugation between the donor and the acceptor resulting in the occurrence of an intramolecular charge transfer (ICT) band between the two fragments. Single crystals of ligand **L1** have been obtained and its crystal structure indicates the ligand is completely planar with the occurrence of a strong intramolecular as well as intermolecular hydrogen bonding. Inorganic anions titration experiments showed that the two ligands are suitable candidates for the sensing of fluoride anions. Metal cation-coordination experiments afforded the obtaining of a neutral electroactive rhenium(I) complex. The crystal structure of this complex indicates the formation of dimers that are connected through strong hydrogen bonding. The electrochemical behavior of both the ligands and the neutral rhenium(I) complex suggests that crystalline radical cation salts can be readily obtained upon chemical and/or electrochemical oxidation. The complexation abililty of the two novel electroactive ligands toward transition metal cations such as Cu(II), Fe(II), Co(II), etc is in progress.

Experimental

General information

NMR spectra were recorded on a Bruker Avance DRX 300 spectrometer operating at 300 MHz for ^{1}H NMR and 75 MHz for ^{13}C NMR. Chemical shifts are expressed in parts per million (ppm) downfield from external TMS. UV–visible spectra were recorded at room temperature in quartz cuvettes using Perkin Elmer spectrophotometer. Mass spectra were collected with Bruker Biflex-III TM. IR spectra were recorded on a Bruker vertex 70. Elemental (C, H and N) analyses were performed on a Thermo-Scientific Flash 2000 Organic Elemental Analyzer. Cyclic voltammetry (CV) experiments were performed in a three-electrode cell equipped with a platinum millielectrode as the working electrode , a platinum wire as a counter electrode and a silver wire Ag/Ag^+ used as a reference electrode. The electrolytic media involved a 0.1 mol/L solution of (n-Bu_4N)PF_6 in dichloromethane/acetonitrile (9:1, v/v). Melting points were measured with a Melting Point Apparatus SMP3.

X-ray single-crystal diffraction data for complex **3** were collected at 180 K on an Agilent SuperNova diffractometer equipped with Atlas CCD detector and mirror monochromated micro-focus Cu K_α radiation (λ = 1.54184 Å). For ligand **L1**, crystal data were collected at 293 K on a Bruker KappaCCD diffractometer, equipped with a graphite monochromator utilizing MoKα radiation (λ = 0.71073Å). The two structures were solved by direct methods, expanded and refined on F^2 by full matrix least-squares techniques using SHELX97 programs (G.M. Sheldrick, 1998). All non-H atoms were refined anisotropically and the H atoms were included in the calculation without refinement. Multiscan empirical absorption was corrected using the SADABS program (Bruker AXS area detector scaling and absorption correction, v2008/1, Sheldrick, G.M., (2008)) for ligand **L1** and using the CrysAlisPro program (CrysAlisPro, Agilent Technologies, V1.171.37.35g, 2014) for complex **3**. For ligand **L1**, the structure refinement showed disordered electron density which could not be reliably modeled and the program PLATON/SQUEEZE were used to remove the scattering contribution corresponding to dimethyl sulfoxide solvent from the intensity data. The assumed solvent composition (3 DMSO per asymmetric unit) was used in the calculation of the empirical formula, formula weight, density, linear absorption coefficient and F(000). For complex **3**, the largest difference peak and hole of 2.29 $eÅ^{-3}$ observed is relatively high and it can be attributed to bad absorption correction. As the Gaussian absorption method does not improve the refinement, we have chosen the empirical absorption correction. This residual electronic density is located around the Re metal ion.

6-([2,2'-Bi(1,3-dithiolylidene)]-4-yl)picolinaldehyde (1): This compound was prepared as previously described [38]. Stannylated tetrathiafulvalene (0.50 g, 1.36 mmol) and 6-bromo-2-pyridinecarboxaldehyde (0.34 g, 1.36 mmol) were dissolved in toluene (20 mL) and $[Pd(PPh_3)_4]$ (0.156 g, 0.135 mmol) was added. The reaction mixture was heated for 48 hours at 110 °C. After evaporation of the solvent under reduced pressure, the obtained residue was then passed over a silica gel column chromatography using a gradient of eluent (pentane/dichloromethane, 3:1, v/v). After solvent evaporation, a solid was obtained in 60% yield, (0.250 g, 0.809 mmol); mp 152 °C; ^{1}H NMR (300 MHz, DMSO-d_6) δ 9.95 (s, 1H), 8.19 (d, J = 7.21 Hz, 1H), 8.10 (t, J = 7.89 Hz, 1H), 7.88 (s, 1H), 7.85 (d, J = 7.50 Hz, 1H), 6.78 (s, 2H) ppm; ^{13}C NMR (75 MHz, DMSO-d_6) δ 193.3, 152.0, 150.9, 138.8, 136.7, 124.2, 122.3, 121.2, 120.7, 120.5, 112.3, 107.5 ppm; anal. calcd for $C_{12}H_7NOS_4$: C, 46.58; H, 2.28; N, 4.53; found: C, 46.16; H, 2.22; N, 4.43; MALDI–TOF MS calcd: m/z = 309.5. found: m/z = 308.9 $[M]^+$; HRMS (M): calcd for $C_{12}H_7NOS_4$: 308.9410; found: 308.9413.

5-([2,2'-Bi(1,3-dithiolylidene)]-4-yl)picolinaldehyde (2): This compound was prepared by following the same procedure as for compound **1**. Yield (65%); mp 191 °C; ^{1}H NMR (300 MHz, DMSO-d_6) δ 9.98 (s, 1H), 8.97 (d, J = 1.65 Hz, 1H), 8.07 (dd, J = 6.42 Hz, J = 2.08 Hz, 1H), 7.96 (d, J = 8.30 Hz, 1H), 7.78 (s, 1H), 6.81 (s, 2H) ppm; ^{13}C NMR (75 MHz, DMSO-d_6) δ 193.2, 151.5, 147.4, 134.7, 131.8, 130.8, 122.6, 122.5, 120.7, 120.6, 114.2, 105.7 ppm; anal. calcd for $C_{12}H_7NOS_4$: C, 46.58; H, 2.28; N, 4.53; found: C, 46.54; H, 2.20; N, 4.51; MALDI–TOF MS calcd: m/z = 309.5. found: m/z = 308.9 $[M]^+$. HRMS (M): calcd for $C_{12}H_7NOS_4$: 308.9410; found: 308.9404.

2-([2,2'-Bi(1,3-dithiolylidene)]-4-yl)-6-((2,4-dinitrophenyl)-hydrazono)methyl)pyridine (L1): 2,4-Dinitrophenylhydrazine (0.150 g, 0.757 mmol) and 6-([2,2'-bi(1,3-dithiolylidene)]-4-yl)picolinaldehyde (**1**, 0.234 g, 0.757 mmol) were dissolved in ethanol (20 mL) and three drops of acetic acid were added. The resulting solution was refluxed overnight. After cooling to room temperature, a dark precipitate was formed which was filtered and washed with ethanol then dried under vacuum to afford a dark powder of ligand **L1**, 75% (0.277 g, 0.567 mmol); mp 264 °C; ^{1}H NMR (300 MHZ, DMSO-d_6) δ 11.87 (s, 1H, -NH), 8.90 (d, J = 2.60 Hz, 1H), 8.78 (s, 1H), 8.43 (dd, J = 6.48 Hz, J = 2.70 Hz, 1H), 8.19 (d, J = 9.40 Hz, 1H), 7.98 (m, 3H), 7.78 (s, 1H), 6.78 (s, 2H) ppm; ^{13}C NMR (75 MHz, DMSO-d_6) δ 160.8, 154.6, 147.3, 144.7, 141.6, 140.6, 138.4, 134.2, 134.1, 131.0, 130.2, 129.2, 123.3, 120.5, 117.5 ppm; selected IR bands (cm^{-1}): 1614, 1499, 1333; anal. calcd for $C_{18}H_{11}N_5O_4S_4$: C, 44.15; H, 2.26; N, 14.30, found: C, 43.54; H, 2.22; N, 13.66; MALDI–TOF MS calcd: m/z = 489.6. found: m/z = 489.1 $[M]^+$; HRMS (M): calcd for $C_{18}H_{11}N_5O_4S_4$: 488.9694; found: 488.9687.

5-([2,2'-bi(1,3-dithiolylidene)]-4-yl)-2-((2,4-dinitrophenyl)-hydrazono)methyl)pyridine (L2): This ligand was prepared by following the same procedure used for **L1**. Yield: 63%; mp 257 °C; ^{1}H NMR (300 MHz, DMSO-d_6) δ 11.88 (s, 1H, -NH), 8.88 (d, J = 2.64 Hz, 1H), 8.75 (d, J = 2.34 Hz , 1H), 8.72 (s, 1H), 8.41 (dd, J = 6.96 Hz, J = 2.63 Hz, 1H), 8.17 (d, J = 9.63 Hz, 1H), 8.11 (d, J = 8.13 Hz , 1H), 7.96 (dd, J = 5.99 Hz, J = 2.40 Hz, 1H), 7.58 (s, 1H), 6.79 (s, 2H) ppm; ^{13}C NMR (75 MHz, DMSO-d_6) δ 152.6, 148.6, 147, 144.7, 138.3, 134.2, 131.3, 130.8, 130.3, 128.6, 123.3, 121.1, 120.7, 117.7, 113.6, 106.3 ppm; selected IR bands (cm^{-1}): 1612, 1508, 1325; anal. calcd for $C_{18}H_{11}N_5O_4S_4$: C, 44.15; H, 2.26; N, 14.30; S, 26.19, found: C, 43.69; H, 2.16; N, 13.98; S, 26.01; MALDI–TOF MS calcd: m/z = 489.6. found: m/z = 489.0 $[M]^+$; HRMS (M): calcd for $C_{18}H_{11}N_5O_4S_4$: 488.9694; found: 488.9703.

Rhenium(I) complex [ReL2(CO)$_3$Cl] 3: To a solution of ligand **L2** (0.025 g, 0.051 mmol) in a mixture of toluene and dichloromethane (3:1, v/v) solution was added $[Re(CO)_5Cl]$ (0.027 g, 0.076 mmol). The mixture was refluxed for 6 hours under nitrogen atmosphere. After cooling the resulting mixture to room temperature, the solvent was removed by a rotary evaporator. The brown residue was extracted with dichloromethane and recrystallized from acetone/hexane solvent mixture to yield complex **3** as black crystals with 81% yield (0.033 g, 0.041 mmol); mp > 360 °C; ^{1}H NMR (300 MHz, DMSO-d_6) δ 12.35 (s, 1H), 9.36 (m, 1H), 9.02 (s, 1H), 8.91 (s, 1H), 8.32 (m, 3H), 8.0 (s, 1H), 7.84 (m, 1H), 6.83 (s, 2H) ppm; ^{13}C NMR (75 MHz, DMSO-d_6) δ 197.6, 196.8, 193.0, 152.5, 148.5, 147.6, 144.7, 138.2, 136.4, 134.1, 131.2, 130.8, 130.2, 129.2, 128.5, 123.3, 121.0, 120.7, 117.7, 113.6, 106.3 ppm; selected IR bands (cm^{-1}): 2018, 1868, 1614, 1497, 1333; MALDI–TOF MS calcd: m/z = 795.3. found: m/z = 795.2 $[M]^+$; HRMS (M): calcd for $C_{21}H_{11}O_7N_5S_4ReCl$: 794.8787; found: 794.8781.

Supporting Information

Supporting Information File 1

Additional analytical data.
[http://www.beilstein-journals.org/bjoc/content/supplementary/1860-5397-11-149-S1.pdf]

Acknowledgements

The Johnson-Matthey company is acknowledged for the generous providing of palladium salt.

References

1. Bendikov, M.; Wudl, F.; Perepichka, D. F. *Chem. Rev.* **2004,** *104,* 4891–4946. doi:10.1021/cr030666m
2. Wudl, F.; Wobschall, D.; Hufnagem, E. J. *J. Am. Chem. Soc.* **1972,** *94,* 670–672. doi:10.1021/ja00757a079
3. Ferraris, J.; Cowan, D. O.; Walatka, V.; Perlstein, J. H. *J. Am. Chem. Soc.* **1973,** *95,* 948–949. doi:10.1021/ja00784a066
4. Molecular conductors. *Chem. Rev.* **2004,** *104,* 4887–5782.
5. Martín, N. *Chem. Commun.* **2013,** *49,* 7025–7027. doi:10.1039/c3cc00240c
6. Williams, J. M.; Ferraro, J. R.; Thorn, R. J.; Carlson, K. D.; Geiser, U.; Wang, H. H.; Kini, A. M.; Whangbo, M.-H. *Organic Superconductors (Including fullerenes), Synthesis, Structure, properties and Theory;* Prentice Hall: Upper Saddle River, NJ, U.S.A., 1992.
7. Bryce, M. R.; Murphy, L. C. *Nature* **1984,** *309,* 119–126. doi:10.1038/309119a0
8. McCall, K. L.; Morandeira, A.; Durrant, J.; Yellowlees, L. J.; Robertson, N. *Dalton Trans.* **2010,** *39,* 4138–4145. doi:10.1039/b924660f
9. Wenger, S.; Bouit, P.-A.; Chen, Q. L.; Teuscher, J.; Di Censo, D.; Humphry-Baker, R.; Moser, J.-E.; Delgado, J. L.; Martín, N.; Zakeeruddin, S. M.; Grätzel, M. *J. Am. Chem. Soc.* **2010,** *132,* 5164–5169. doi:10.1021/ja909291h
10. de Lucas, A. I.; Martín, N.; Sánchez, L.; Seoane, C.; Andreu, R.; Garín, J.; Orduna, J.; Alcalá, R.; Villacampa, B. *Tetrahedron* **1998,** *54,* 4655–4662. doi:10.1016/S0040-4020(98)00182-3
11. González, M.; Segura, J. L.; Seoane, C.; Martín, N.; Garín, J.; Orduna, Jesús; Alcalá, R.; Villacampa, B.; Hernández, V.; López Navarrete, J. T. *J. Org. Chem.* **2001,** *66,* 8872–8882. doi:10.1021/jo010717k
12. Ouahab, L. *Chem. Mater.* **1997,** *9,* 1909–1926. doi:10.1021/cm9701217
13. Coronado, E.; Galán-Marcós, J. R.; Gómez-García, C. J.; Laukhin, V. *Nature* **2000,** *408,* 447–449. doi:10.1038/35044035
14. Ouahab, L.; Enoki, T. *Eur. J. Inorg. Chem.* **2004,** 933–941. doi:10.1002/ejic.200300869
15. Coronado, E.; Day, P. *Chem. Rev.* **2004,** *104,* 5419–5448. doi:10.1021/cr030641n
16. Setifi, F.; Ouahab, L.; Golhen, S.; Yoshida, Y.; Saito, G. *Inorg. Chem.* **2003,** *42,* 1791–1793. doi:10.1021/ic026211h
17. Nihei, M.; Takahashi, N.; Nishikawa, H.; Oshio, H. *Dalton Trans.* **2011,** *40,* 2154–2156. doi:10.1039/C0DT01092H
18. Canevet, D.; Sallé, M.; Zhang, G.; Zhang, D.; Zhu, D. *Chem. Commun.* **2009,** 2245–2269. doi:10.1039/b818607n
19. Nielsen, M. B.; Lomholt, C.; Becher, J. *Chem. Soc. Rev.* **2000,** *29,* 153–164. doi:10.1039/a803992e
20. Segura, J. L.; Martín, N. *Angew. Chem., Int. Ed.* **2001,** *40,* 1372–1409. doi:10.1002/1521-3773(20010417)40:8<1372::AID-ANIE1372>3.0.CO;2-I
21. Yamada, J.; Sugimoto, T. *TTF Chemistry: Fundamentals & Applications of Tetrathiafulvalene;* Kodansha and Springer: Tokyo, Japan and Berlin, Germany, 2004.
22. Hardouin-Lerouge, M.; Hudhomme, P.; Sallé, M. *Chem. Soc. Rev.* **2011,** *40,* 30–43. doi:10.1039/B915145C
23. Lehn, J. M. Chapter 3. *Supramolecular Chemistry: Concepts and Perspectives;* Wiley-VCH: New York, NY, U.S.A., 1995.
24. Bianchi, E.; Bowman-James, K.; García-España, E. *Supramolecular Chemistry of Anions;* Wiley-VCH: New York, NY, U.S.A., 1997.
25. Schmidtchen, F. P.; Berger, M. *Chem. Rev.* **1997,** *97,* 1609–1646. doi:10.1021/cr9603845
26. Beer, P. D. *Acc. Chem. Res.* **1998,** *31,* 71–80. doi:10.1021/ar9601555
27. Bowman-James, K. *Acc. Chem. Res.* **2005,** *38,* 671–678. doi:10.1021/ar040071t
28. Sessler, J. L.; Gale, P. A.; Cho, W. S. *Anion Receptor Chemistry;* Royal Society of Chemistry: Cambridge, United Kingdom, 2006.
29. Caltagirone, C.; Gale, P. A. *Chem. Soc. Rev.* **2009,** *38,* 520–563. doi:10.1039/B806422A
30. Gale, P. A.; García-Garrido, S. E.; Garric, J. *Chem. Soc. Rev.* **2008,** *37,* 151–190. doi:10.1039/B715825D
31. Suksai, C.; Tuntulani, T. *Chem. Soc. Rev.* **2003,** *32,* 192–202. doi:10.1039/b209598j
32. Kirk, K. L. *Biochemistry of the Halogens and Inorganic Halides;* Biochemistry of the Elements, Vol. 9A+B; Springer: New York, NY, U.S.A., 1991; pp 58 ff. doi:10.1007/978-1-4684-5817-6
33. Hudnall, T. W.; Chiu, C.-W.; Gabbaï, F. P. *Acc. Chem. Res.* **2009,** *42,* 388–397. doi:10.1021/ar8001816
34. Lee, C.-H.; Miyaji, H.; Yoon, D.-W.; Sessler, J. L. *Chem. Commun.* **2008,** 24–34. doi:10.1039/B713183F
35. Belhadj, E.; El-Ghayoury, A.; Cauchy, T.; Allain, M.; Mazari, M.; Sallé, M. *Eur. J. Inorg. Chem.* **2014,** 3912–3919. doi:10.1002/ejic.201402073 And references therein.
36. Xiong, J.; Cui, L.; Liu, W.; Beves, J. E.; Li, Y.-Y.; Zuo, J.-L. *Tetrahedron Lett.* **2013,** *54,* 1998–2000. doi:10.1016/j.tetlet.2013.02.005 And references therein.
37. Shi, Z.; Han, Q.-H.; Li, X.-Y.; Shao, M.-Y.; Zhu, Q.-Y.; Dai, J. *Dalton Trans.* **2011,** *40,* 7340–7347. doi:10.1039/c1dt10353a
38. Chahma, M.; Wang, X. S.; van der Est, A.; Pilkington, M. *J. Org. Chem.* **2006,** *71,* 2750–2755. doi:10.1021/jo0525938
39. Yu, M.; Fan, Z.; Jing, Z.-L.; Chen, X.; Diao, C.-H.; Deng, Q.-L. *Acta Crystallogr.* **2005,** *E61,* o3342–o3343. doi:10.1107/S160053680502934X
40. *Gaussian03,* Revision B.04; Gaussian, Inc.: Pittsburgh, PA, U.S.A., 2003.
41. Zhou, L.; Zhang, X.; Wu, S. *Chem. Lett.* **2004,** *33,* 850–851. doi:10.1246/cl.2004.850
42. Chawla, H. M.; Sahu, S. N.; Shrivastava, R.; Kumar, S. *Tetrahedron Lett.* **2012,** *53,* 2244–2247. doi:10.1016/j.tetlet.2012.02.083
43. Sun, Y.; Liu, Y.; Guo, W. *Sens. Actuators, B* **2009,** *143,* 171–176. doi:10.1016/j.snb.2009.09.038
44. Li, J.; Lin, H.; Cai, Z.; Lin, H. *Spectrochim. Acta, Part A* **2009,** *72,* 1062–1065. doi:10.1016/j.saa.2008.12.045
45. Upadhyay, K. K.; Mishra, R. K.; Kumar, V.; Chowdhury, P. K. R. *Talanta* **2010,** *82,* 312–319. doi:10.1016/j.talanta.2010.04.041
46. Amendola, V.; Esteban-Gómez, D.; Fabbrizzi, L.; Licchelli, M. *Acc. Chem. Res.* **2006,** *39,* 343–353. doi:10.1021/ar050195l
47. Jia, H.-P.; Forgie, J. C.; Liu, S.-X.; Sanguinet, L.; Levillain, E.; Le Derf, F.; Sallé, M.; Neels, A.; Skabara, P. J.; Decurtins, S. *Tetrahedron* **2012,** *68,* 1590–1594. doi:10.1016/j.tet.2011.11.087
48. Singh, A.; Chandra, M.; Sahay, A. N.; Pandey, D. S.; Pandey, K. K.; Mobin, S. M.; Carmen Puerta, M.; Valerga, P. *J. Organomet. Chem.* **2004,** *689,* 1821–1834. doi:10.1016/j.jorganchem.2004.02.037
49. Sarjit Singh, K.; Mozharivskyj, Y. A.; Thöne, C.; Rao Kollipara, M. *J. Organomet. Chem.* **2005,** *690,* 3720–3729. doi:10.1016/j.jorganchem.2005.05.001
50. Liu, W.; Heinze, K. *Dalton Trans.* **2010,** *39,* 9554–9564. doi:10.1039/c0dt00393j

51. El-Ghayoury, A.; Leliège, A.; Allain, M.; Batail, P. *Tetrahedron Lett.* **2013,** *54,* 4015–4018. doi:10.1016/j.tetlet.2013.05.060

License and Terms

BEILSTEIN JOURNAL OF ORGANIC CHEMISTRY

Synthesis of racemic and chiral BEDT-TTF derivatives possessing hydroxy groups and their achiral and chiral charge transfer complexes

Sara J. Krivickas[1,2], Chiho Hashimoto[1], Junya Yoshida[1], Akira Ueda[1], Kazuyuki Takahashi[1,3], John D. Wallis[4] and Hatsumi Mori[*1]

Full Research Paper

Open Access

Address:
[1]The Institute for Solid State Physics, the University of Tokyo, 5-1-5 Kashiwanoha, Kashiwa, Chiba, 277-8581, Japan, [2]The University of Adelaide, Adelaide, South Australia, 5005 Australia, [3]Department of Chemistry, Graduate School of Science, Kobe University, Kobe, Hyogo 657–8501, Japan and [4]School of Science and Technology, Nottingham Trent University, Clifton Lane, Nottingham, NG11 8NS, UK

Email:
Hatsumi Mori* - hmori@issp.u-tokyo.ac.jp

* Corresponding author

Keywords:
BEDT-TTF; chiral molecular crystal; hydrogen bonding; hydroxy group; molecular conductors

Beilstein J. Org. Chem. **2015,** *11,* 1561–1569.
doi:10.3762/bjoc.11.172

Received: 08 June 2015
Accepted: 21 August 2015
Published: 08 September 2015

This article is part of the Thematic Series "Tetrathiafulvalene chemistry".

Guest Editor: P. J. Skabara

Abstract

Chiral molecular crystals built up by chiral molecules without inversion centers have attracted much interest owing to their versatile functionalities related to optical, magnetic, and electrical properties. However, there is a difficulty in chiral crystal growth due to the lack of symmetry. Therefore, we made the molecular design to introduce intermolecular hydrogen bonds in chiral crystals. Racemic and enantiopure bis(ethylenedithio)tetrathiafulvalene (BEDT-TTF) derivatives possessing hydroxymethyl groups as the source of hydrogen bonds were designed. The novel racemic *trans-vic*-(hydroxymethyl)(methyl)-BEDT-TTF **1**, and racemic and enantiopure *trans-vic*-bis(hydroxymethyl)-BEDT-TTF **2** were synthesized. Moreover, the preparations, crystal structure analyses, and electrical resistivity measurements of the novel achiral charge transfer salt θ^{21}-[(*S,S*)-**2**]$_3$[(*R,R*)-**2**]$_3$(ClO_4)$_2$ and the chiral salt α'-[(*R,R*)-**2**]ClO_4(H_2O) were carried out. In the former θ^{21}-[(*S,S*)-**2**]$_3$[(*R,R*)-**2**]$_3$(ClO_4)$_2$, there are two sets of three crystallographically independent donor molecules [(*S,S*)-**2**]$_2$[(*R,R*)-**2**] in a unit cell, where the two sets are related by an inversion center. The latter α'-[(*R,R*)-**2**]ClO_4(H_2O) is the chiral salt with included solvent H_2O, which is not isostructural with the reported chiral salt α'-[(*S,S*)-**2**]ClO_4 without H_2O, but has a similar donor arrangement. According to the molecular design by introduction of hydroxy groups and a ClO_4^- anion, many intermediate-strength intermolecular hydrogen bonds (2.6–3.0 Å) were observed in these crystals between electron donor molecules, anions, and included H_2O solvent, which improve the crystallinity and facilitate the extraction of physical properties. Both salts are semiconductors with relatively low resistivities at room temperature and activation energies of 1.2 ohm cm with E_a = 86 meV for θ^{21}-[(*S,S*)-**2**]$_3$[(*R,R*)-**2**]$_3$(ClO_4)$_2$ and 0.6 ohm cm with E_a = 140 meV for α'-[(*R,R*)-**2**]$_2$$ClO_4$($H_2O$),

respectively. The variety of donor arrangements, θ^{21} and two kinds of α'-types, and their electrical conductivities of charge transfer complexes based upon the racemic and enantiopure (*S,S*)-**2**, and (*R,R*)-**2** donors originates not only from the chirality, but also the introduced intermolecular hydrogen bonds involving the hydroxymethyl groups, perchlorate anion, and the included solvent H_2O.

Introduction

The chiral crystals without an inversion center have attracted much interest recently. Non-centrosymmetric crystals can exhibit a variety of physical properties related to their crystal class [1]; optical and magneto-optical phenomena such as second-harmonic generation, Faraday and Kerr effects, magneto-chiral dichroism, and electrical and magneto-electrical phenomena such as piezoelectricity, pyroelectricity, ferroelectricity and electrical magnetochiral anisotropy. Rikken et al. observed magneto-chiral dichroism in a europium complex [2,3] and also electrical magneto-chiral anisotropy in carbon nanotubes where small changes in the resistance of the chiral carbon nanotubes in a magnetic field were observed between enantiomers [4-6].

One method of constructing chiral crystals is through the use of chiral molecules as building blocks. Tetrathiafulvalene derivatives such as TTF (**3**) and BEDT-TTF (**4**) have been investigated considerably due to their ability to form radical cation salts with interesting conductive and magnetic properties (Figure 1). The influence of chirality in the TTF molecules on the crystal structure and physical properties has been shown by Avarvari's (*R*)-, (*S*)- and racemic (±)-(ethylenedithio(tetrathiafulvalene)methyloxazoline)$_2$X, (**5**$_2$X, X = AsF_6 [7], PF_6 [8]) where disorder within the racemic salt leads to lower conductivity. Recently, Pop et al., have also reported electrical magnetochiral anisotropy in chiral molecular conductors, (*R,R*)- and (*S,S*)-[dimethyl-(ethylenedithio)tetrathiafulvalene]$_2ClO_4$ (**6**$_2ClO_4$) [9,10].

Although there is a relatively large number of chiral TTF derivatives, only a few conducting properties for chiral cation salts have been so far reported, for those based upon tetramethyl-**4** [11-15], **5** [7,8], **6** [9,10], and X-dimethyl-(ethylenedithio)tetrathiafulvalene (X = ethylenedithio [16,17], ethylenedioxy [18], and pyrazino [19]), due to the difficulty of chiral-crystal growth. In order to improve the crystallinity, the inclusion of hydroxy groups in the BEDT-TTF molecule has been postulated to produce hydrogen bonding interactions between electron-donor molecules, electron-acceptor molecules, and anions in the subsequent radical cation salts [20-22]. This may lead to improved order in the crystalline state, which in turn may help the observation of physical properties of the salts. Previously, the synthesis of racemic-**2** [21,22], the preliminary synthesis of enantiopure (*R,R*)- and (*S,S*)-**2,** and the preparation, and crystal structure of the radical cation salt α'-[(*S,S*)-**2**]$_2ClO_4$ [22] have been reported. In this article, we report the syntheses of novel racemic-**1** and enantiopure (*R,R*)- and (*S,S*)-**2** possessing one or two hydroxymethyl groups, and the preparations, crystal structures, and electrical resistivities of the achiral charge transfer complex θ^{21}-[(*S,S*)-**2**]$_3$[(*R,R*)-**2**]$_3(ClO_4)_2$ and the chiral complex α'-[(*R,R*)-**2**]$_2ClO_4(H_2O)$, in comparison with

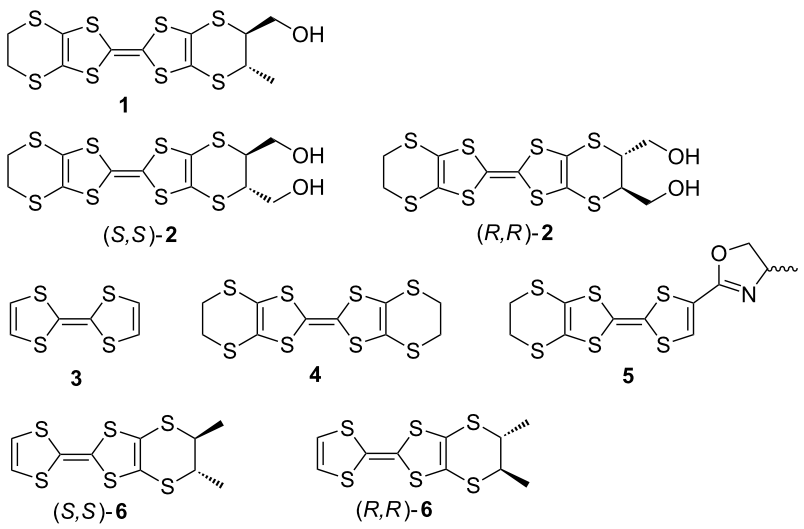

Figure 1: Molecular structures of *trans-vic*-(hydroxymethyl)(methyl)-BEDT-TTF (**1**), *trans-vic*-bis(hydroxymethyl)-BEDT-TTF (**2**), TTF (**3**), BEDT-TTF (**4**), EDT-TTF-methyl-oxazoline **5**, and *trans*-dimethyl-EDT-TTF (**6**).

those of α'-[(*S*,*S*)-**2**]$_2$ClO$_4$. The effects of introducing hydrogen bonds between hydroxymethyl groups of donors and ClO_4^- anions in charge transfer complexes are also discussed.

Results and Discussion

Syntheses of racemic-**1**, enantiopure (*S*,*S*)- and (*R*,*R*)-**2** and evaluation of their electrochemical properties

The synthesis of the racemic *trans-vic*-(hydroxymethyl)(methyl)-BEDT-TTF (**1**) was performed in a similar manner to racemic **2** [22]. The *trans*-alkene **8** was reacted with trithione **7** under standard Diels–Alder cycloaddition conditions in refluxing toluene to afford a mixture of the *trans*-(*S*,*S*)- and (*R*,*R*)-**9** in 56% yield (Scheme 1). The purchased alkene contained a small amount of the *cis*-isomer (*trans*-form:*cis*-form 96:4), but the *cis*-product can be removed by simple recrystallization of the thione **9** from hexane/dichloromethane. The racemic donor **1** could then be synthesized following procedures whereby the alcohol functionality is protected as acetate, **10**, the thione **10** is then converted to the oxo-analogue **11** using mercuric acetate and acetic acid in chloroform. Oxo compound **11** was then cross-coupled with 1.2 equivalents of thione **12** in triethyl phosphite to afford the racemic protected donor **13** in reasonable yield (37%). Basic hydrolysis of the acetyl protecting group afforded the racemic donor **1** in an 81% yield. The syntheses of enatiopure donors **1** and the preparations of their charge transfer complexes are under way.

Moreover, enantiopure (*S*,*S*)-**2** and (*R*,*R*)-**2** were also synthesized as shown in Scheme 2. Chiral HPLC was performed using a JAIGEL-OA7500 column on a JAI LC-908 recycling preparative system using the solvent system methanol/water 7:3 to separate (*S*,*S*)- and (*R*,*R*)-**14**. The obtained dihydroxy-thione (*S*,*S*)-**14** was protected as a diacetate to give (*S*,*S*)-**15**, which was converted to the oxo-form (*S*,*S*)-**16**, and coupled with

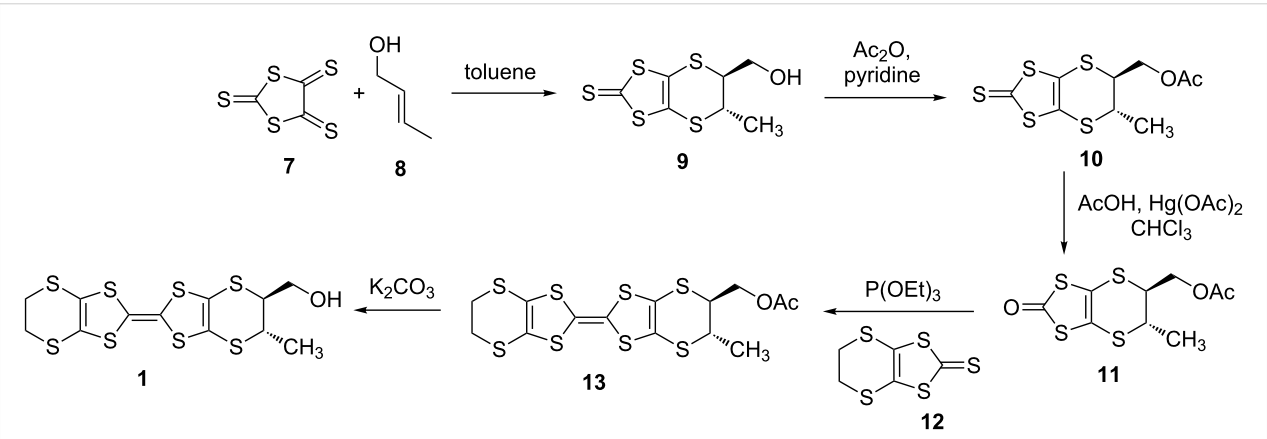

Scheme 1: Synthesis of donor *trans*-**1**.

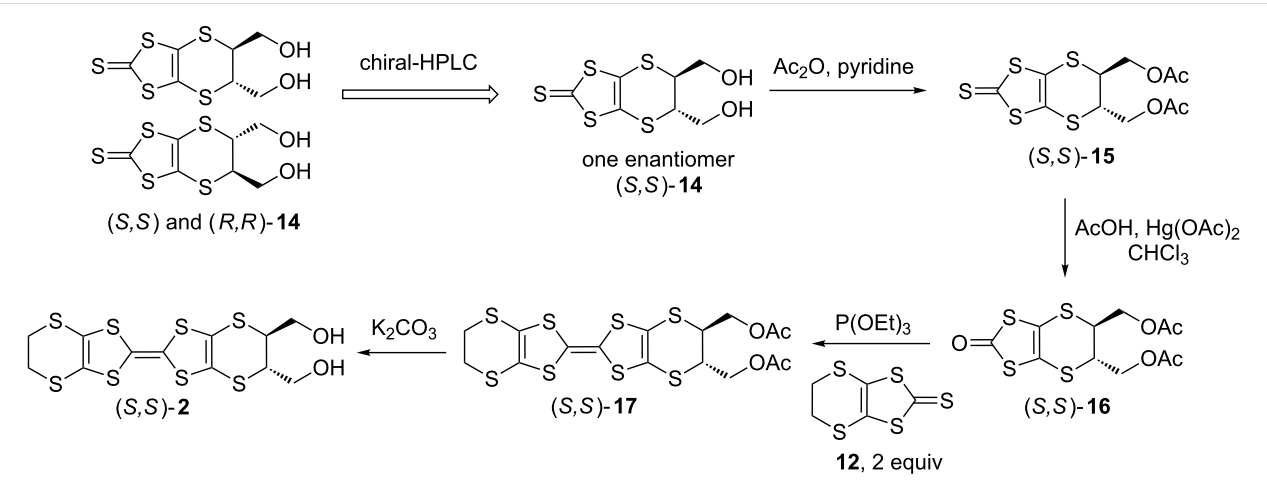

Scheme 2: Synthesis of enantiopure donor (*S*,*S*)-**2**.

2 equivalents of **12** to give (*S,S*)-**17**. Deprotection under basic conditions afforded enantiopure (*S,S*)-**2**. The other enantiomer (*R,R*)-**2** was synthesized in the same manner.

The cyclic voltammetry measurement on racemic-**1** indicated the first and second oxidation potentials ($E^1_{1/2}$, $E^2_{1/2}$) and their difference ΔE (= $E^2_{1/2} - E^1_{1/2}$) to be 0.52, 0.83, and 0.31 V by utilizing glassy carbon as working electode with 0.1 M tetrabutylammonium perchlorate in benzonitrile. These potentials are similar to those of (*S,S*)- and (*R,R*)-**2** with $E^1_{1/2}$, $E^2_{1/2}$, and ΔE of 0.52, 0.80, and 0.28 V, respectively.

Preparations of single crystals for achiral charge transfer salt θ^{21}-[(*S,S*)-2**]$_3$[(*R,R*)-**2**]$_3$(ClO_4)$_2$ and chiral charge transfer salt α'-[(*R,R*)-**2**]$_2ClO_4(H_2O)$.** The single brown plate crystals of θ^{21}-[(*S,S*)-**2**]$_3$[(*R,R*)-**2**]$_3$(ClO_4)$_2$ were grown by the oxidation of the racemic donor **2** (7 mg) in the presence of tetrabutylammonium perchlorate (44 mg) in dichloromethane (24 mL) at room temperature under a constant current of 0.5 μA under a N_2 atmosphere during the course of 6 days. The other chiral brown plate crystal of α'-[(*R,R*)-**2**]$_2ClO_4(H_2O)$ was prepared electrochemically by utilizing (*R,R*)-**2** (5 mg) and tetrabutylammonium perchlorate (40 mg) in dichloromethane (9 mL) at 0.5 μA for 5 days.

Crystal structures of achiral charge transfer salt θ^{21}-[(*S,S*)-2**]$_3$[(*R,R*)-**2**]$_3$(ClO_4)$_2$ and chiral charge transfer salt α'-[(*R,R*)-**2**]$_2ClO_4(H_2O)$.** The crystal structure of θ^{21}-[(*S,S*)-**2**]$_3$[(*R,R*)-**2**]$_3$(ClO_4)$_2$ is depicted in Figure 2. The lattice parameters are listed in Table S1 in Supporting Information File 1. The crystallographically independent molecules are two (*S,S*)-**2** (molecules A and C indicated by red in Figure 2b), one (*R,R*)-**2** (molecules B indicated by blue), and one ClO_4^- anion. The unit cell contains six donor molecules, consisting of three (*S,S*)-**2** (molecules A, B', and C) and three (*R,R*)-**2** (molecules A', B and C'), and two ClO_4^- anions. Molecules in a pair, X and X' (X = A, B, and C) are related by an inversion center, so that the space group is centrosymmetric *P*-1 (No. 2). The donor arrangement is the θ^{21}-type, where transvers inclination pattern is ++−++−... (+ and − represent upward and downward slopes,

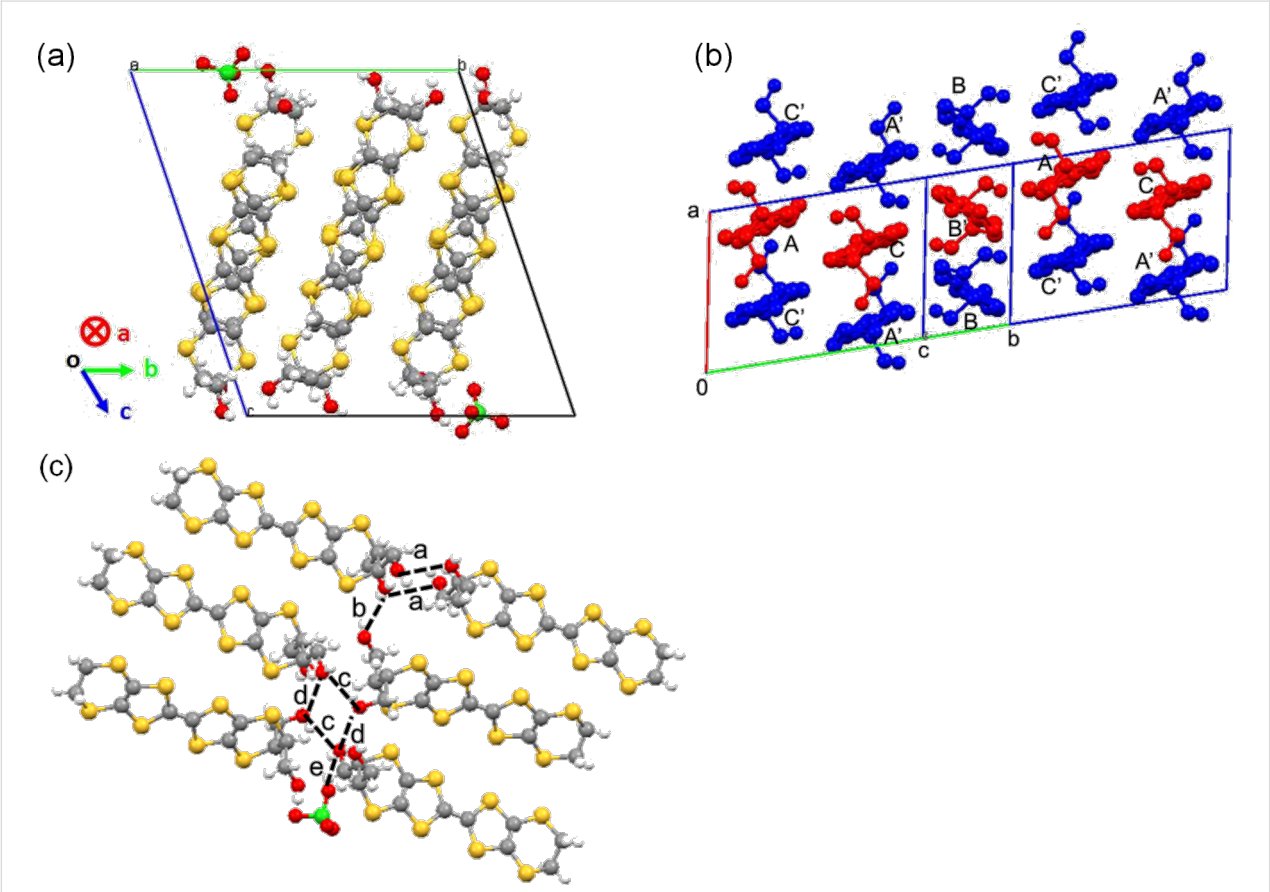

Figure 2: (a) Crystal structure, (b) θ^{21}-type donor arrangement of molecules A and A' [(*S,S*) and (*R,R*)-**2** indicated by red and blue with charge of +0.59(8)], B and B' [(*R,R*) and (*S,S*)-**2**, blue and red with +0.23(7)], and C and C' [(*S,S*) and (*R,R*)-**2**, red and blue with +0.18(8)], and (c) O···O hydrogen bond contacts of achital charge transfer salt θ^{21}-[(*S,S*)-**2**]$_3$[(*R,R*)-**2**]$_3$(ClO_4)$_2$; *a* = 2.89(1), *b* = 2.90(1), *c* = 2.879(8), *d* = 2.837(8), *e* = 2.94(1) Å.

respectively), whereas the usual θ^{11}-type has the +−+−+−... pattern [23]. In every (+) and (−)-stacking column, the alternate (*R,R*)–(*S,S*)–(*R,R*)–(*S,S*)- chiral donors indicated by blue–red–blue–red are stacked such as C'AC'A..., A'CA'C..., or BB'BB'... in head-to-tail fashion (Figure 2b). Moreover, the molecules with the same chirality, (*R,R*) or (*S,S*), are arranged side-by-side along the *b*-axis. The charge of each molecule is estimated by bond analyses; as shown in Table S2 (Supporting Information File 1) [24], the charges of molecules A, B, and C are +0.59(8), +0.23(7), and +0.18(8), respectively. In the (+) stacking column, the charge rich A (+0.59(8)) and charge poor C (+0.18(8)) stack, whereas B with the medium charge (+0.23(7)) is arranged in the (−)-column, constructing the appropriate charge balance. The introduced hydroxymethyl groups are set to axial positions for donors A, B, and C (Figure 2b). Following the molecular design, many intermediate-strength intermolecular O···O hydrogen bonds (<2.6–3.0 Å) between hydroxymethyl groups in the donors (*a* = 2.89(1), *b* = 2.90(1), *c* = 2.879(8), and *d* = 2.837(8) Å in Figure 2c), and between a hydroxymethyl group in the donor and a ClO_4^- anion (e = 2.94(1) Å) were observed, presumably helping the crystallinity of the complex based upon chiral molecules.

The crystal structure of the chiral salt α'-[(*R, R*)-**2**]$_2$$ClO_4$($H_2O$) is shown in Figure 3. The crystallographically independent molecules are two (*R,R*)-**2** donors, one ClO_4^- anion, and one

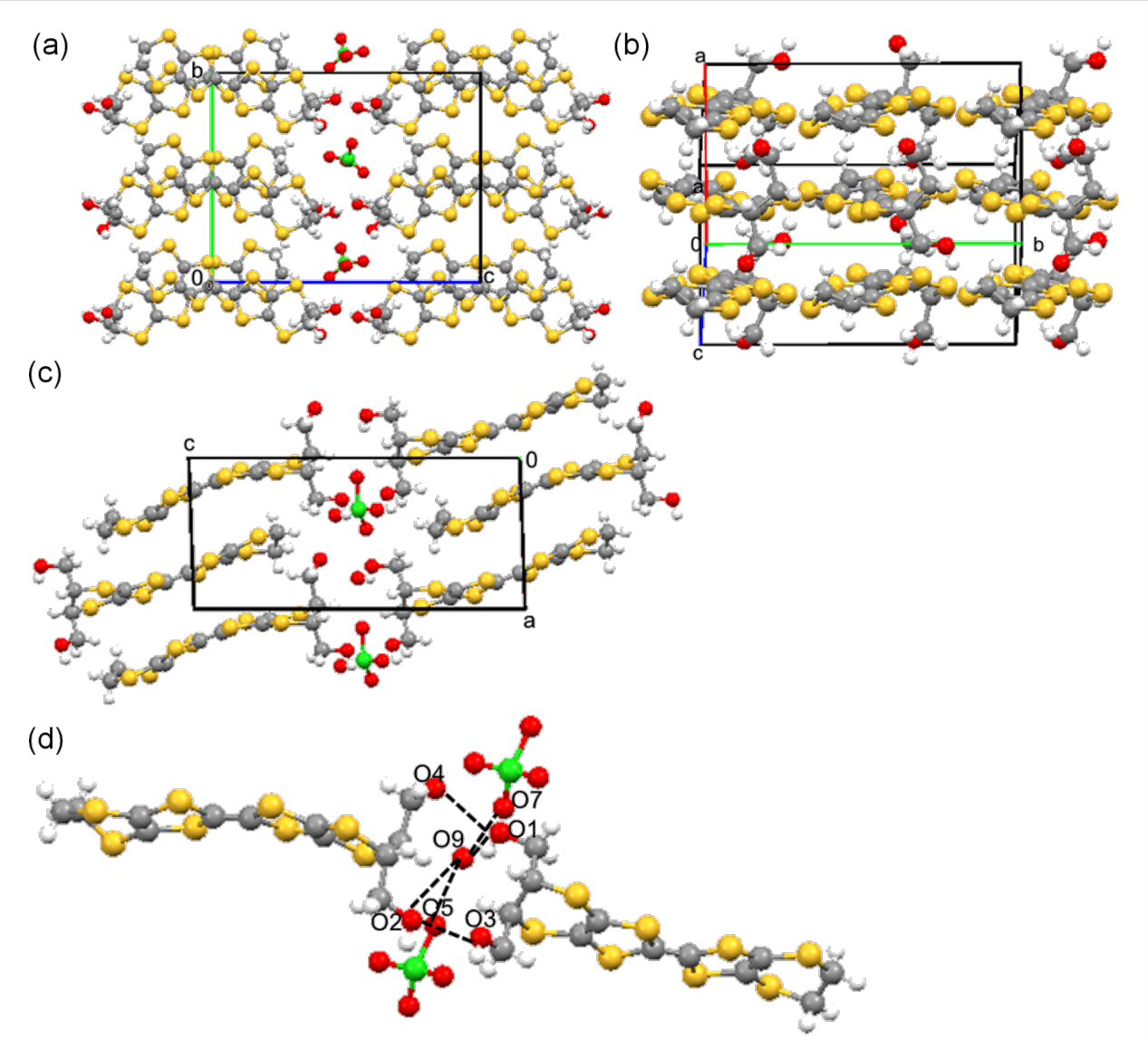

Figure 3: Crystal structure (a) viewed along the *a*-axis, (b) donor arrangement, (c) viewed along the *b*-axis, and (d) intermolecular hydrogen bond contacts for chiral charge transfer salt α'-[(*R,R*)-**2**]$_2$$ClO_4$($H_2O$). The calculated hydrogen bonds are as follows; *r*(O1···O4) = 2.67(3), *r*(O1···O9) = 3.00(3), *r*(O2···O3) = 2.67(2), *r*(O2···O9) = 2.85(3), *r*(O5···O9) = 2.62(6), and *r*(O7···O9) = 2.90(6) Å.

H_2O molecule as an included solvent. There are four donors, two anions, and two H_2O solvents in the unit cell. The enantiopure (*R,R*)-**2** donors stack in a head-to-tail manner and twisted with respect to each other along the *a*-axis, namely the α'-type donor arrangement [25].

The hydroxymethyl groups project from the molecular BEDT-TTF plane in axial positions (Figure 3c). According to the molecular design, the intermolecular moderate hydrogen bonds between the oxygen atoms in hydroxymethyl groups of (*R,R*)-**2** donors are observed such as *r*(O1···O4) = 2.67(3) and *r*(O2···O3) = 2.67(2) Å (Figure 3d). The other hydrogen bonds are found between the oxygen atoms of either included H_2O solvent and hydroxymethyl groups such as *r*(O1···O9) = 3.00(3) and *r*(O2···O9) = 2.85(3) Å, or of a solvent H_2O and an anion ClO_4^- such as *r*(O5···O9) = 2.62(6) and *r*(O7···O9) = 2.90(6) Å. These hydrogen bonds contribute to forming this chiral crystal.

This chiral crystal α'-[(*R,R*)-**2**]$_2$$ClO_4$($H_2O$) is not isostructural to the other enantiopure crystal α'-[(*S,S*)-**2**]$_2$$ClO_4$, previously reported (Table S1, Supporting Information File 1) [22]. The crystallographically independent donors are two for α'-[(*R,R*)-**5**]$_2$$ClO_4$($H_2O$) in the space group $P2_1$ (No. 4), but one for α'-[(*S,S*)-**5**]$_2$$ClO_4$ in *P*2 (No. 3). Although this α'-[(*R,R*)-**2**]$_2$$ClO_4$($H_2O$) crystal includes a H_2O solvent molecule and α'-[(*S,S*)-**2**]$_2$$ClO_4$ does not in the same preparation conditions, both salts have the similar α'-type donor arrangements.

Electrical resistivities for the achiral charge transfer salt θ^{21}-[(*S,S*)-2]$_3$[(*R,R*)-2]$_3$(ClO_4)$_2$ and the chiral salt α'-[(*R,R*)-2]$_2$$ClO_4$($H_2O$). Temperature dependences of electrical resistivites for the achiral charge transfer salt θ^{21}-[(*S,S*)-**2**]$_3$[(*R,R*)-**2**]$_3$(ClO_4)$_2$ and the chiral salt α'-[(*R,R*)-**2**]$_2$$ClO_4$($H_2O$) are shown in Figure 4. The resistivities at room temperature are very similar, 1.2 and 0.6 ohm cm for θ^{21}-[(*S,S*)-**2**]$_3$[(*R,R*)-**2**]$_3$(ClO_4)$_2$ and α'-[(*R,R*)-**2**]$_2$$ClO_4$($H_2O$), respectively. Both salts show semiconducting behaviour and the activation energy of θ^{21}-[(*S,S*)-**2**]$_3$[(*R,R*)-**2**]$_3$(ClO_4)$_2$ is E_a = 86 meV which is lower than that of α'-[(*R,R*)-**2**]$_2$$ClO_4$($H_2O$) which has E_a = 140 meV.

Conclusion

In summary, we have synthesized redox-active racemic and enantiopure donors of BEDT-TTF derivatives containing one or two hydroxymethyl groups, the novel racemic *trans-vic*-(hydroxymethyl)(methyl)-BEDT-TTF **1** and enantiopure *vic*-bis(hydroxymethyl)-BEDT-TTF **2**. By successful molecular design to introduce intermolecular hydrogen bonds, the achiral charge transfer salt θ^{21}-[(*S,S*)-**2**]$_3$[(*R,R*)-**2**]$_3$(ClO_4)$_2$ and the chiral salt α'-[(*R, R*)-**2**]ClO_4(H_2O) could be obtained, and their crystal structure analyses and measurements of electrical resistivities were performed. In the racemic complex θ^{21}-[(*S,S*)-**2**]$_3$[(*R,R*)-**2**]$_3$(ClO_4)$_2$, (*S,S*)-**2** and (*R,R*)-**2** donors stack alternately along the *a*-axis and the same chiral (*S,S*)-**2** (or (*R,R*)-**2**) donors are arranged in the side-by-side interaction to construct the stripe chirality order. The latter chiral salt α'-[(*R,R*)-**2**]ClO_4(H_2O) is not isostructural with α'-[(*S,S*)-**2**]ClO_4 without H_2O, but has a similar α'-type donor arrangement. According to the molecular design, both crystals have many moderate-strength hydrogen bonds of 2.6–3.0 Å between donor molecules, ClO_4^- anions, and H_2O, which contribute to crystallinity based upon chiral molecules and allow the investigation of physical properties. The promising strategy of chiral crystal growth will lead to the development of the versatile functionalities of molecular chiral crystals.

Experimental

General information

The parent racemic-**2** (Figure 1) was synthesized according to the literature [22]. ^{1}H NMR (300 MHz) and ^{13}C NMR (75 MHz) spectra were measured with a JEOL JNM-AL300

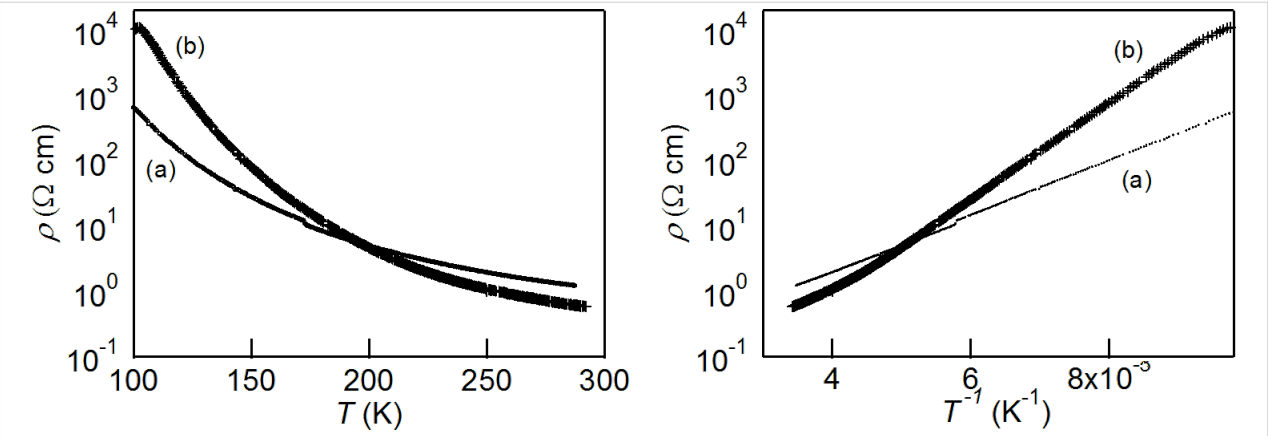

Figure 4: Temperature dependences of electrical resistivities for (a) achiral charge transfer salt θ^{21}-[(*S,S*)-**2**]$_3$[(*R,R*)-**2**]$_3$(ClO_4)$_2$ and (b) chiral salt α'-[(*R,R*)-**2**]$_2$$ClO_4$($H_2O$).

spectrometer with $CDCl_3$ as solvent using Me_4Si or residual solvent as an internal standard. Cyclic voltammetry (CV) measurements were performed on an ALS 610DB electrochemical analyzer in benzonitrile containing 0.1 M tetrabutylammonium perchlorate (working electrode: Pt, counter electrode: Pt wire, reference electrode: saturated calomel electrode (SCE)) [22]. EI-mass spectra were obtained with a JEOL JMS-AX500 spectrometer. X-ray crystallographic measurements were made on a Rigaku AFC-7R diffractometer (Mo Kα, λ = 0.71073 Å). The crystal structures were solved by direct methods and refined with full-matrix least-squares technique using Crystal Structure (ver. 4.0.1, Rigaku Co. and Rigaku Americas Co.). Anisotropic thermal parameters were applied to all non-hydrogen atoms. The hydrogen atoms were generated geometrically (C–H = 0.960 Å). The direct current electrical conductivity measurement was made by the conventional four-probe method using carbon paste and gold wires.

Synthesis of racemic-1

***trans*-5-(Hydroxymethyl)-6-methyl-5,6-dihydro[1,3]dithiolo[4,5-*b*][1,4]dithiine-2-thione (9).** A solution of trithione **7** (1 g, 5.1 mmol, 1 equiv) and alkene **8** (0.52 mL, 6.12 mmol, 1.2 equiv, *trans*-form 96%) in toluene (50 mL) was refluxed overnight. The toluene was removed under reduced pressure and the crude material purified by column chromatography (silica gel, 2:1 hexane:ethyl acetate) to afford the *trans*-thione **9** as a brown powder (with small amounts of the *cis* derivative). This material was recrystallized from dichloromethane/hexane to give the *trans*-thione **9** as a brown powder (0.77g, 56%). ^{1}H NMR (300 MHz, $CDCl_3$) δ 1.55(d, *J* = 6.6 Hz, 3H), 1.98 (dd, *J* = 5.1, 6.6 Hz, 1H), 3.36 (ddd, *J* = 3.9, 6.3, 7.5 Hz, 1H), 3.64 (dq, *J* = 3.9, 6.9 Hz, 1H), 3.86 (m, 2H); ^{13}C NMR (75 MHz, $CDCl_3$) δ 21.90, 37.07, 49.95, 64.89, 120.20, 120.46, 207.57.

***trans*-5-(Acetoxymethyl)-6-methyl-5,6-dihydro[1,3]dithiolo[4,5-*b*][1,4]dithiine-2-thione (10).** To a solution of thione **9** (482 mg, 1.80 mmol, 1 equiv) in pyridine (5 mL) was added acetic anhydride (202 mg, 1.98 mmol, 1.1 equiv). The reaction mixture was stirred overnight under argon at room temperature. Dichloromethane (50 mL) was added, the organic phase was washed with 1 M HCl (2 × 50 mL) and water (50 mL), dried over $MgSO_4$, filtered and reduced in vacuo to give the required product **10** as a brown oil (560 mg, 100%). The material was used in the next step without further purification. ^{1}H NMR (300 MHz, $CDCl_3$) δ 1.50 (d, *J* = 6.9 Hz, 3H), 2.03 (s, 3H), 3.42 (ddd, *J* = 3.9, 6.6, 7.8 Hz, 1H), 3.50 (dq, *J* = 3.9, 6.9 Hz, 1H), 4.22 (dd, *J* = 7.5, 11.7 Hz, 1H), 4.27 (dd, *J* = 6.0, 11.7 Hz, 1H); ^{13}C NMR (75 MHz, $CDCl_3$) δ 20.69, 21.82, 37.13, 45.86, 65.66, 119.44, 119.82, 170.33, 207.20.

***trans*-5-(Acetoxymethyl)-6-methyl-5,6-dihydro[1,3]dithiolo[4,5-*b*][1,4]dithiine-2-one (11).** To a solution of thione **10** (560 mg, 1.81 mmol, 1 equiv) in chloroform (30 mL) was added mercuric acetate (843 mg, 2.71 mmol, 1.5 equiv) and acetic acid (5 mL). The reaction mixture was stirred for 3 hours at room temperature. The solution was filtered, washed with sat. $NaHCO_3$ (2 × 50 mL) and water (50 mL), dried over $MgSO_4$, filtered and reduced in vacuo to give the oxo compound **11** (480 mg, 90%) as a yellow solid. ^{1}H NMR (300 MHz, $CDCl_3$) δ 1.53 (d, *J* = 6.6 Hz, 3H), 2.03 (s, 3H), 3.40 (ddd, *J* = 3.9, 6.3, 7.2 Hz, 1H), 3.46 (dq, *J* = 3.9, 6.6 Hz, 1H), 4.28 (m, 2H); ^{13}C NMR (75 MHz, $CDCl_3$) δ 20.73, 21.80, 38.50, 47.59, 65.82, 110.40, 110.61, 116.36, 170.43.

***trans-vic*-Acetoxymethyl-methyl-BEDT-TTF (13).** A solution of thione **12** (439 mg, 1.96 mmol, 1.2 equiv) and the oxo-compound **11** (480 mg, 1.63 mmol, 1 equiv) in triethyl phosphite (10 mL) was stirred overnight at 90 °C. After cooling, hexane was added and the precipitate collected by vacuum filtration and purified by column chromatography (silica gel, 4:1 hexane/ethyl acetate) to afford the cross-coupled product **13** as a red-orange solid (280 mg, 37%). ^{1}H NMR (300 MHz, $CDCl_3$) δ 1.44 (d, *J* = 6.6 Hz, 3H), 2.05 (s, 3H), 3.26 (s, 4H), 3.38 (ddd, *J* = 3.9, 6.3, 7.5 Hz, 1H), 3.43 (dq, *J* = 3.9, 6.6 Hz, 1H), 4.18 (dd, *J* = 7.5, 11.4 Hz, 1H), 4.24 (dd, *J* = 6.3, 11.4 Hz, 1H); ^{13}C NMR (75 MHz, $CDCl_3$) δ 20.75, 21.58, 30.06, 37.80, 46.56, 65.80, 110.54, 110.77, 110.97, 111.86, 113.69, 170.35.

***trans-vic*-Hydroxymethyl-methyl-BEDT-TTF (1).** A solution of the acetyl protected BEDT-TTF **13** (280 mg, 0.596 mmol, 1 equiv) and K_2CO_3 (95 mg, 0.894 mmol, 1.5 equiv) in MeOH/H_2O/THF (5 mL/5 mL/5 mL) was stirred overnight at room temperature under an argon atmosphere. Water (50 mL) and dichloromethane (100 mL) were added, the organic layer separated and washed with water (2 × 50 mL). The organic layer was dried over $MgSO_4$, filtered and evaporated to give the crude product that was purified by column chromatography (silica gel, ethyl acetate) to afford the *trans*-racemic BEDT-TTF derivative **1** as an orange powder (210 mg, 81%). ^{1}H NMR (300 MHz, $CDCl_3$) δ 1.43 (d, *J* = 6.6 Hz, 3H), 1.85 (br s, 1H), 3.22 (s, 4H), 3.24 (m, 1H), 3.46 (dq, *J* = 3.6, 6.6 Hz, 1H), 3.71 (m, 2H); ^{13}C NMR (75 MHz, DMSO-d_6) δ 21.29, 29.58, 37.39, 50.37, 63.98, 110.03, 110.11, 110.44, 111.62, 112.93, MS *m*/*z*: $[M - OH]^+$ calcd for $C_{12}H_{11}S_8$, 411; found, 410.8627.

Synthesis of (*S,S*)-**2**

(*S,S*)-*trans*-5,6-Bis(acetyloxymethyl)-5,6-dihydro-1,3-dithiolo[4,5-*b*]-1,4-dithiin-2-thione ((*S,S*)-15). A solution of the dihydroxythione (*S,S*)-**14** (25 mg, 0.088 mmol, 1 equiv) in pyridine (1 mL) and acetic anhydride (0.02 mL, 1.96 mmol, 20 equiv) was stirred at room temperature overnight under an

argon atmosphere. The reaction mixture was taken up in dichloromethane and washed briefly with 1 M HCl (2 × 50 mL) and water (50 mL). The organic layer was dried over $MgSO_4$, filtered and the volatiles removed in vacuo to give the crude enantiopure diacetoxythione (*S,S*)-**15** (32 mg, quantitative). The isolated product was used in the next step without further purification. ^{1}H NMR (300 MHz, $CDCl_3$) δ 2.12 (s, 6H), 3.79 (m, 2H), 4.32 (dd, *J* = 8.1, 11.4 Hz, 2H), 4.42 (dd, *J* = 6.0, 11.4 Hz, 2H); ^{13}C NMR (75 MHz, $CDCl_3$) δ 20.69, 40.06, 64.71, 118.79, 170.28, 206.49.

(*S,S*)-*trans*-5,6-Bis(acetoxymethyl)-5,6-dihydro-1,3-dithiolo[4,5-*b*]-1,4-dithiin-2-one ((*S,S*)-16). To a solution of thione (*S,S*)-**15** (32 mg, 0.087 mmol, 1 equiv) in chloroform (10 mL) was added mercuric acetate (35 mg, 0.11 mmol, 1.3 equiv) and acetic acid (0.5 mL). The reaction mixture was stirred for 3 hours, after which it was filtered, washed with (sat.) $NaHCO_3$ (3 × 50 mL) and water (50 mL). The organic layer was dried over $MgSO_4$, filtered and the solvent removed under reduced pressure to afford the oxo compound (*S,S*)-**16** (28 mg (93%). ^{1}H NMR (300 MHz, $CDCl_3$) δ 2.12 (s, 6H), 3.76 (m, 2H), 4.38 (dd, *J* = 7.5, 11.4 Hz, 2H), 4.45 (dd, *J* = 5.7, 11.4 Hz, 2H); ^{13}C NMR (75 MHz, $CDCl_3$) δ 20.69, 41.40, 64.84, 109.72, 170.35, 187.57.

(*S,S*)-*trans-vic*-Bis(acetyloxymethyl)-BEDT-TTF ((*S,S*)-17). A solution of thione **12** (64 mg, 0.16 mmol, 2 equiv) and oxo compound (*S,S*)-**16** (50 mg, 0.14 mmol, 1 equiv) in triethyl phosphite (2 mL) was stirred at 90 °C for 5 hours. After cooling hexane was added, the precipitate collected and purified by column chromatography (silica gel, hexane/ethyl actetate) to afford the enantiopure cross coupled product (*S,S*)-**17** (34 mg, 47%). ^{1}H NMR (300 MHz, $CDCl_3$) δ 2.09 (s, 6H), 3.29 (s, 4H), 3.69 (m, 2H), 4.25 (dd, *J* = 7.8, 11.4 Hz, 2H), 4.34 (dd, *J* = 6.0, 11.4 Hz, 2H); ^{13}C NMR (75 MHz, $CDCl_3$) δ 20.73, 30.17, 40.88, 64.93, 110.43, 113.92, 170.35.

(*S,S*)-*trans-vic*-Bis(hydroxymethyl)-BEDT-TTF ((*S,S*)-2). K_2CO_3 (27 mg, 0.193 mmol, 3 equiv) was added to a solution of the acetyl protected BEDT-TTF ((*S,S*)-**17**, 34 mg, 0.064 mmol) in MeOH/THF/H_2O (1 mL/1 mL/1 mL). The reaction mixture was stirred for 3 hours under an argon atmosphere, after which no starting material remained (TLC control). Dichloromethane (100 mL) was added and the organic layer washed with water (2 × 20 mL). The organic layer was dried over $MgSO_4$, filtered and the solvent was removed under reduced pressure. The crude material was purified by column chromatography (silica gel, 1:1 hexane/ethyl acetate) to afford the desired product (*S,S*)-**2** (23 mg, 80%) as a red–pink solid. ^{1}H NMR (300 MHz, DMSO-d_6) δ 3.34 (s, 4H), 3.58 (m, 4H), 3.71 (m, 2H), 4.44 (m, 2H); ^{13}C NMR (75 MHz, DMSO-d_6) δ 30.83, 45.82, 67.40, 111.24, 111.38, 111.97, 114.44.

Supporting Information

Supporting Information File 1

CD spectra of (*S,S*)-**2** and (*R,R*)-**2**, crystal data for θ^{21}-[(*S,S*)-**2**]$_3$[(*R,R*)-**2**]$_3$(ClO_4)$_2$, α'-[(*R,R*)-**2**]$_2ClO_4(H_2O)$, and α'-[(*S,S*)-**2**]$_2ClO_4$ (Table S1), charge estimation of θ^{21}-[(*S,S*)-**2**]$_3$[(*R,R*)-**2**]$_3$(ClO_4)$_2$ (Table S2, Figure S2), and NMR data (Figures S3-1–S3-18).
[http://www.beilstein-journals.org/bjoc/content/supplementary/1860-5397-11-172-S1.pdf]

Acknowledgements

This work was partially supported by Grants in-Aid for Scientific Research (Nos. 26810044, 24340074, and 26610096) from Japan Society for the Promotion Science (JSPS), Japan, the Yazaki Memorial Foundation for Science and Technology and the Mitsubishi Foundation.

References

1. Inoue, K.; Ohkoshi, S.; Imai, H. Chiral Molecule-Based Magnets. In *Magnetism: Molecules to Materials V;* Miller, J.; Drillon, M., Eds.; Wiley-VCH: Weinheim, 2005; pp 41–70.
2. Rikken, G. L. J. A.; Raupach, E. *Nature* **1997,** *390,* 493–494. doi:10.1038/37323
3. Rikken, G. L. J. A.; Raupach, E. *Phys. Rev. E* **1998,** *58,* 5081–5084. doi:10.1103/PhysRevE.58.5081
4. Rikken, G. L. J. A.; Fölling, J.; Wyder, P. *Phys. Rev. Lett.* **2001,** *87,* 236602. doi:10.1103/PhysRevLett.87.236602
5. Krstić, V.; Roth, S.; Burghard, M.; Kern, K.; Rikken, G. L. J. A. *J. Chem. Phys.* **2002,** *117,* 11315–11319. doi:10.1063/1.1523895
6. Krstić, V.; Rikken, G. L. J. A. *Chem. Phys. Lett.* **2002,** *364,* 51–56. doi:10.1016/S0009-2614(02)01243-5
7. Réthoré, C.; Avarvari, N.; Canadell, E.; Auban-Senzier, P.; Fourmigué, M. *J. Am. Chem. Soc.* **2005,** *127,* 5748–5749. doi:10.1021/ja0503884
8. Madalan, A. M.; Réthoré, C.; Fourmigué, M.; Canadell, E.; Lopes, E. B.; Almeida, M.; Auban-Senzier, P.; Avarvari, N. *Chem. – Eur. J.* **2010,** *16,* 528–537. doi:10.1002/chem.200901980
9. Pop, F.; Auban-Senzier, P.; Frackowiak, A.; Ptaszyński, K.; Olejniczak, I.; Wallis, J. D.; Canadell, E.; Avarvari, N. *J. Am. Chem. Soc.* **2013,** *135,* 17176–17186. doi:10.1021/ja408350r
10. Pop, F.; Auban-Senzier, P.; Canadell, E.; Rikken, G. L. J. A.; Avarvari, N. *Nat. Commun.* **2014,** *5,* 3757. doi:10.1038/ncomms4757
11. Wallis, J. D.; Karrer, A.; Dunitz, J. D. *Helv. Chim. Acta* **1986,** *69,* 69–70. doi:10.1002/hlca.19860690110
12. Karrer, A.; Wallis, J. D.; Dunitz, J. D.; Hilti, B.; Mayer, C. W.; Bürkle, M.; Pfeiffer, J. *Helv. Chim. Acta* **1987,** *70,* 942–953. doi:10.1002/hlca.19870700405
13. Wallis, J. D.; Dunitz, J. D. *Acta Crystallogr., Sect. C: Cryst. Struct. Commun.* **1988,** *44,* 1037–1039. doi:10.1107/S0108270188001593

14. Matsumiya, S.; Izuoka, A.; Sugawara, T.; Taruishi, T.; Kawada, Y. *Bull. Chem. Soc. Jpn.* **1993,** *66,* 513–522. doi:10.1246/bcsj.66.513
15. Avarvari, N.; Wallis, J. D. *J. Mater. Chem.* **2009,** *19,* 4061–4076. doi:10.1039/B820598A
16. Zambounis, J. S.; Mayer, C. W.; Hauenstein, K.; Hilti, B.; Hofherr, W.; Pfeiffer, J.; Bürkle, M.; Rihs, G. *Adv. Mater.* **1992,** *4,* 33–35. doi:10.1002/adma.19920040106
17. Krivickas, S. J.; Ichikawa, A.; Takahashi, K.; Tajima, H.; Wallis, J. D.; Mori, H. *Synth. Met.* **2011,** *161,* 1563–1565. doi:10.1016/j.synthmet.2011.05.019
18. Konoike, T.; Iwashita, K.; Yoshino, H.; Murata, K.; Sasaki, T.; Papavassiliou, G. C. *Phys. Rev. B* **2002,** *66,* 245308. doi:10.1103/PhysRevB.66.245308
19. Zambounis, J. S.; Pfeiffer, J.; Papavassiliou, G. C.; Lagouvardos, D. J.; Terzis, A.; Raptopoulou, C. P.; Delhaès, P.; Ducasse, L.; Fortune, N. A.; Murata, K. *Solid State Commun.* **1995,** *95,* 211–215. doi:10.1016/0038-1098(95)00231-6
20. Leurquin, F.; Ozturk, T.; Pilkington, M.; Wallis, J. D. *J. Chem. Soc., Perkin Trans. 1* **1997,** 3173–3177. doi:10.1039/A704364C
21. Brown, R. J.; Brooks, A. C.; Griffiths, J.; Vital, B.; Day, P.; Wallis, J. D. *Org. Biomol. Chem.* **2007,** *5,* 3172–3182. doi:10.1039/b709823e
22. Krivickas, S. J.; Hashimoto, C.; Takahashi, K.; Wallis, J. D.; Mori, H. *Phys. Status Solidi C* **2012,** *9,* 1146–1148. doi:10.1002/pssc.201100728
23. Mori, T.; Mori, H.; Tanaka, S. *Bull. Chem. Soc. Jpn.* **1999,** *72,* 179–197. doi:10.1246/bcsj.72.179
24. Guionneau, P.; Kepert, C. J.; Bravic, G.; Chasseau, D.; Truter, M. R.; Kurmoo, M.; Day, P. *Synth. Met.* **1997,** *86,* 1973–1974. doi:10.1016/S0379-6779(97)80983-6
25. Mori, T. *Bull. Chem. Soc. Jpn.* **1999,** *72,* 2011–2027. doi:10.1246/bcsj.72.2011

License and Terms

BEILSTEIN JOURNAL OF ORGANIC CHEMISTRY

Star-shaped tetrathiafulvalene oligomers towards the construction of conducting supramolecular assembly

Masahiko Iyoda*[1] and Masashi Hasegawa[2]

Review

Open Access

Address:
[1]Department of Chemistry, Graduate School of Science and Engineering, Tokyo Metropolitan University, Hachioji, Tokyo 192-0397, Japan and [2]Department of Chemistry, School of Science, Kitasato University, 1-15-1 Kitasato, Minami-ku, Sagamihara, Kanagawa 252-0373, Japan

Email:
Masahiko Iyoda* - iyoda@tmu.ac.jp

* Corresponding author

Keywords:
conducting fibers; star-shaped molecules; supramolecular assembly; tetrathiafulvalene oligomers

Beilstein J. Org. Chem. **2015,** *11,* 1596–1613.
doi:10.3762/bjoc.11.175

Received: 15 June 2015
Accepted: 20 August 2015
Published: 10 September 2015

This article is part of the Thematic Series "Tetrathiafulvalene chemistry".

Guest Editor: P. J. Skabara

Abstract

The construction of redox-active supramolecular assemblies based on star-shaped and radially expanded tetrathiafulvalene (TTF) oligomers with divergent and extended conjugation is summarized. Star-shaped TTF oligomers easily self-aggregate with a nanophase separation to produce supramolecular structures, and their TTF units stack face-to-face to form columnar structures using the fastener effect. Based on redox-active self-organizing supramolecular structures, conducting nanoobjects are constructed by doping of TTF oligomers with oxidants after the formation of such nanostructures. Although radical cations derived from TTF oligomers strongly interact in solution to produce a mixed-valence dimer and π-dimer, it seems to be difficult to produce nanoobjects of radical cations different from those of neutral TTF oligomers. In some cases, however, radical cations form nanostructured fibers and rods by controlling the supramolecular assembly, oxidation states, and counter anions employed.

Introduction

Tetrathiafulvalene (TTF) chemistry first attracted enthusiastic attention of chemists and physicists on high electrical conductivity and superconductivity with high T_c temperature. Recently, however, TTF and its derivatives are frequently employed as a redox-active moiety for organic electronic devices such as field-effect-transistors (FET), dye-sensitized solar cells (DSC), positive electrode materials for rechargeable batteries, and electrochromic (EC) materials [1].

TTF derivatives are versatile building blocks to form aggregates in the solid state with interesting conducting and magnetic behavior [2]. Although these properties are mainly originated from specific interactions between molecules having one or more unpaired electrons [3,4], neutral TTF and its derivatives also easily form stacked columnar structures with face-to-face π···π stacking and side-by-side S···S interactions in the crystalline state. Furthermore, weak intermolecular interactions

(hydrogen bonding, metal coordination, CT interaction, π···π stacking, van der Waals interaction, etc.) play an important role in the formation of the three-dimensional (3D) crystal structures [5]. For the construction of nanostructured objects, π···π, S···S, and other weak intermolecular interactions first accelerate self-aggregation of molecules in solution [6-8] and then produce the functional one-dimensional (1D) or two-dimensional (2D) supramolecular structures, which are very important in advanced nanosciences [9-11]. For the formation of the nanostructured objects such as fibers, rods, tubes, and particles, amphiphilic TTFs having a rigid core and long alkyl chains are one of the best molecular systems. The self-assembly of TTF derivatives in solid and on surface gives rise to a long-distance dynamic ordering as compared with single crystals.

Among the recent researches on TTF and its derivatives, radially expanded or star-shaped multi-TTFs with C_3 and C_6 symmetries have attracted considerable attention in the field of materials science because of their divergent and extended π-conjugation. Various C_3-symmetric compounds incorporating three conjugated TTF units were designed and synthesized to realize TTF-based conducting organic magnets using ferromagnetic interaction between the two TTF radical cations [12-21]. On the other hand, compounds with a hexagonal molecular symmetry were used as core structures for constructing conductive fibers and functional dyes [22,23]. Furthermore, various multifunctional TTF-based supramolecular architectures have been designed and synthesized to realize molecular sensors, redox switches, multi-input systems for logic gates, electrochemically-driven conformational controls, molecular clips and tweezers, and redox-controlled gelation processes. TTF-based supramolecular chemistry in solution was thoroughly outlined in recent reviews of Jeppesen, Nielsen, and Becher (2004) [24], Iyoda, Hasegawa, and Miyake (2004) [25,26], Sallé and Zhang (2009) [27], and Martin (2009, 2012) [28,29]. However, limited examples of redox-active nanostructures in the solid state were summarized so far. Therefore, this review focuses on the conducting nanostructures of TTF derivatives in the solid state, together with association behavior in solution.

Review

Redox-active radially expanded TTF oligomers in solution and the solid state

TTF oligomers with radially expanded structures can be expected to demonstrate multifunctional properties because a central core and TTF branches exhibit individual and/or cooperative functionalities [25]. For example, dendrimers composed of central benzenoid cores and TTF branches are cited as representative examples [30-33]. Other functional units such as fullerenes [34,35], cyclodextrins [36], porphyrin [37], and phthalocyanine [38-40] can also be introduced into the core of radial oligo-TTFs. As shown in Figure 1, TTF-annelated porphyrin **1** was synthesized by Becher and co-workers in 2001 [37]. Reflecting its strong π-donor ability, **1** was oxidized spontaneously in solution to afford $\mathbf{1}^{\bullet+}$ under ambient conditions. Multifunctional TTF-crown ether-substituted phthalocyanine (Pc) **2a** and its copper(II) complex **2b** were reported by Amabilino, Rowan, Nolte, and co-workers in 2005 [40]. The giant molecule **2a** self-aggregated in chloroform–dioxane to form a gel. TEM images of the xerogel exhibited helical molecular tapes nanometer wide and micrometer long. A cyclic voltammetry (CV) study on **2b** showed the redox properties expected for Pc and TTF, and doping of **2b** in CH_2Cl_2 with I_2 produced a radical cation species.

Among radially expanded TTFs, Jeppesen, Becher, Nielsen, Sessler, and co-workers reported TTF-calix[4]pyrrole **3** as a valuable supramolecular receptor, and **3** easily incorporated 1,3,5-trinitrobenzene (TNB) in the cavity to form **4** (**3**:TNB = 1:2) (Figure 2) [41,42]. Furthermore, in the presence of halide ions, **3** formed the C_{60} complex **5**, in which C_{60} was bound within the bowl-like cup of the TTF-calix[4]pyrrole core in a ball-and-socket binding mode [43].

Recently, the C_3-symmetric compounds **6a**,**b** incorporating three TTF residues were reported by Amabilino, Avarvari, and co-workers (Figure 3) [21]. The three TTF units with chiral citronellyl and dihydrocitronellyl chains led to helical one-dimensional stacks in solution to produce fibers that have morphologies depending on the nature of the chiral alkyl group, although an achiral counterpart showed no helicity. C_3-symmetric truxene-TTFs **7a–c** were synthesized by Ortí, Martín, and co-workers (Figure 3) [44].

The pioneering studies on the synthesis of tetrakis(1,3-dithiol-2-ylidene)cyclobutane (**8**) and related [5] and [6]radialenes **9** and **10a**,**b** were reported by Yoshida and co-workers in the 1980's (Figure 4). These π-expanded TTFs **8–10a**,**b** exhibited unique X-ray structures and multi-redox behavior [45-47].

Conducting supramolecular assembly of oligo-TTFs

The electric conductivities of doped nanofibers and nanorods derived from TTF and its derivatives are measured by mounting them on Au electrodes with a μm-sized spacing. On the other hand, the conductivities of the corresponding neutral nanoobjects are determined by pulse-radiolysis or flash-photolysis time-resolved microwave conductivity techniques [48,49]. Current-sensing atomic force microscopy (CS-AFM) and combination of scanning tunneling microscopy and spectroscopy (STM/STS) are also employed for determining the

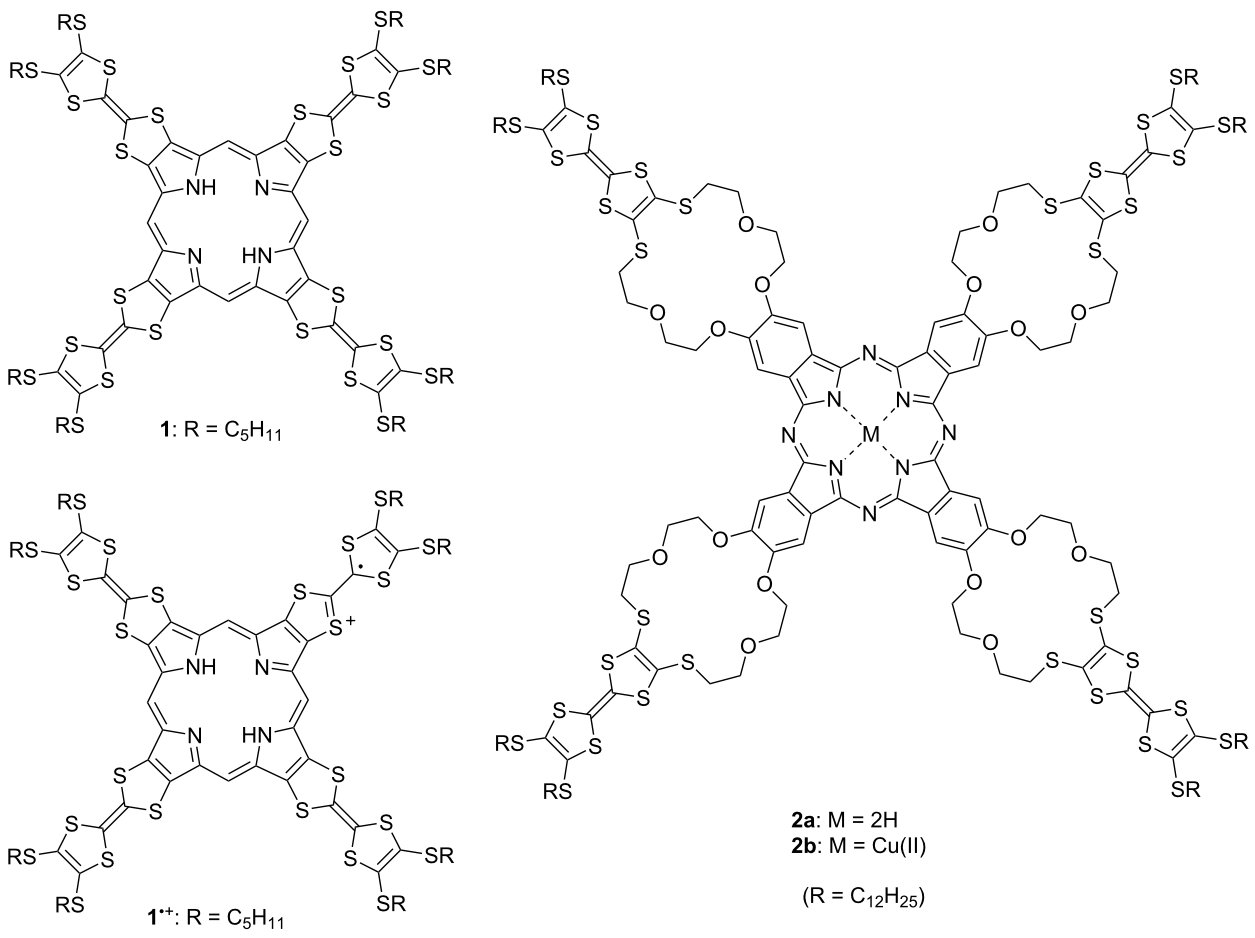

Figure 1: Radially expanded TTF oligomers **1** and **2a**,**b**.

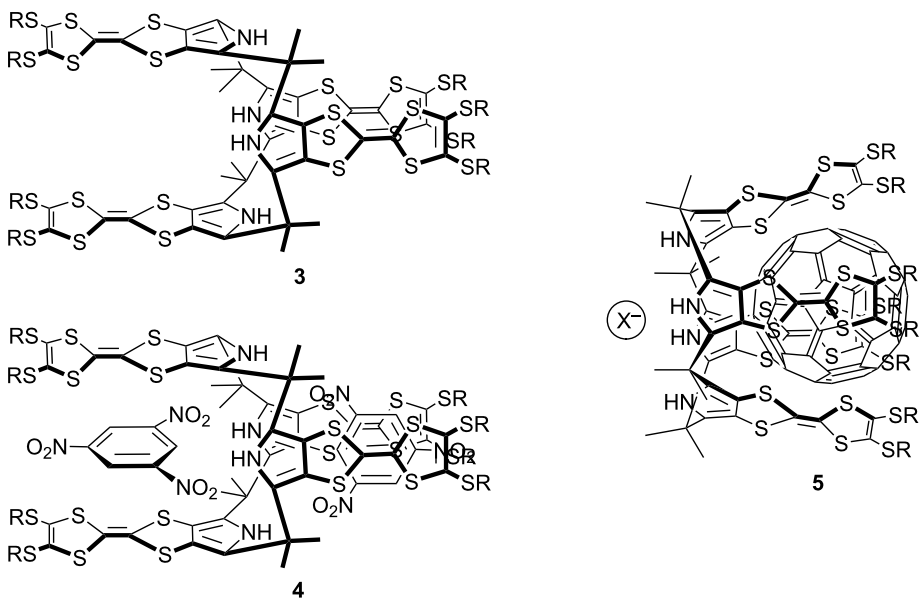

Figure 2: TTF-calix[4]pyrrole **3** and its TNT and C_{60} complexes **4** and **5**.

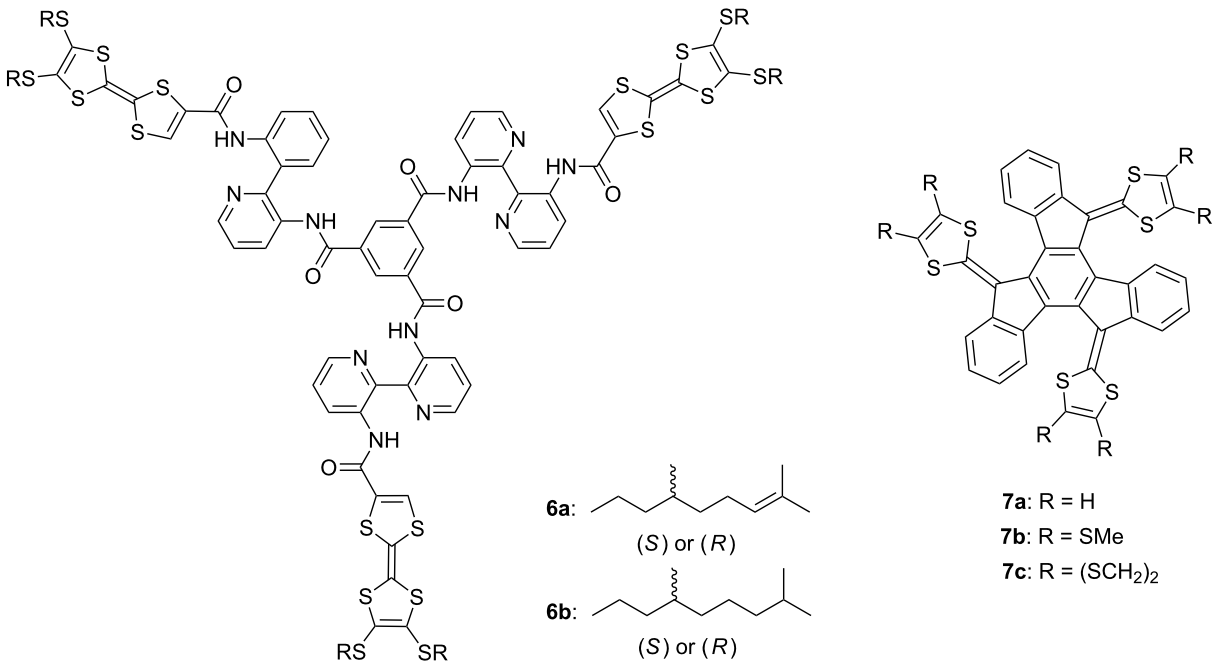

Figure 3: C_3-symmetric TTF derivatives **6a**,**b** and **7a–c**.

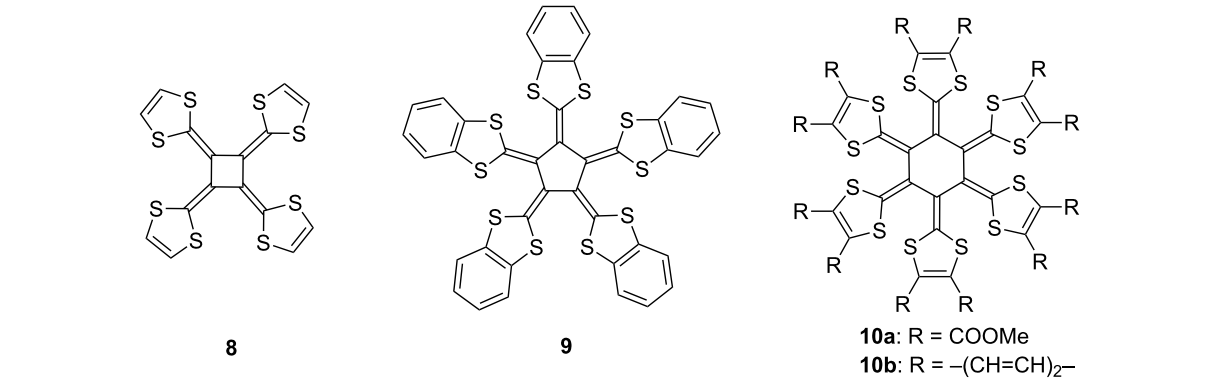

Figure 4: Radially expanded TTF derivatives **8**, **9**, and **10a**,**b**.

conductivities of nanoobjects [50,51]. The electrical conductivity of nanostructures mainly depends on the alignment of stacked TTFs or their radical salts. The first fibrous material was fabricated by using arborol-TTF **11** in 1994 by Joergensen, Bechgaard, and co-workers (Figure 5) [52]. Although **11** showed no conductivity, Bryce and co-workers synthesized arborol-functionalized TTF derivative **12** in 2003, whose doped film exhibited a moderate level of conductivity ($\sigma_{rt} \approx 10^{-4}$ S cm^{-1}) [53]. In 2005, several groups reported the formation of nanofibers using amphiphilic TTFs (**13** and **14**) (Figure 5) [54-56] After that, many research efforts have been focused on the construction of conducting nanoobjects possibly employed as nanosized electric wires, wirings, molecular switches, and devices. Some neutral nanoobjects derived from TTFs show electroconductivity owing to the fastener effect [57]; however, the oxidation of face-to-face stacked TTFs easily generates highly conducting states with unfilled band structure. Thus, the doping of neutral nanoobjects with iodine is generally used for preparing conducting nanostructures. Chemically oxidized TTFs in solution are also available for preparing conducting nanofibers.

The fastener effect [57], which enhances the face-to-face interaction between the two TTFs, can be used to construct conducting nanostructured fibers in the neutral state, and doping of the fibers with iodine affords black conducting fibers. For example,

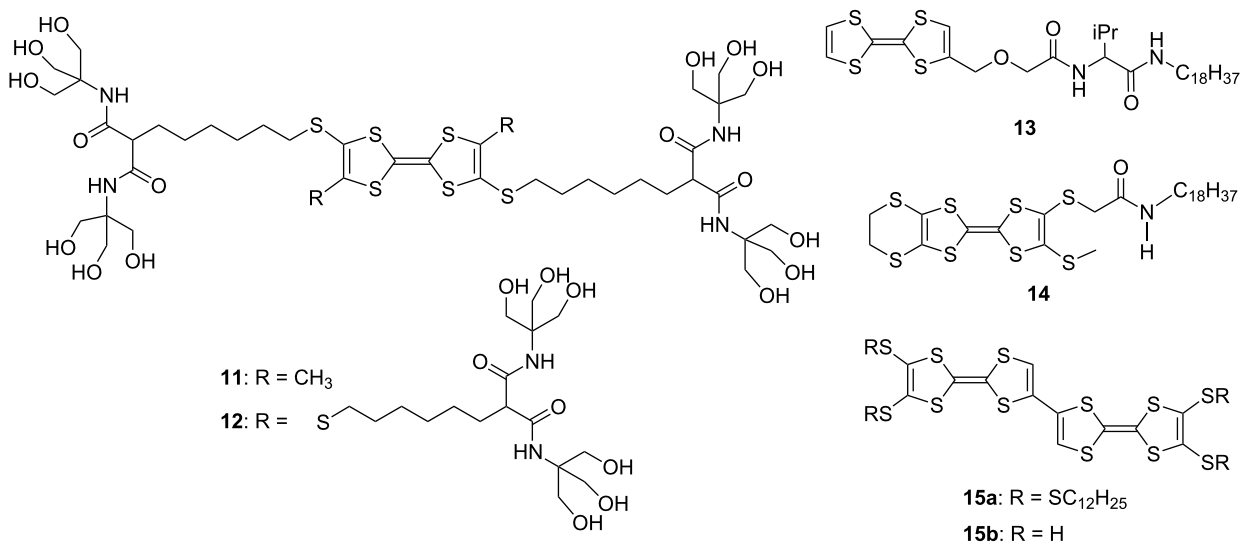

Figure 5: Amphiphilic TTFs **11–14** and **15a**,**b**.

the bi-TTF derivative **15a** with long alkylthio chains as substituents was synthesized (Figure 5) [58]. Bi-TTF **15a** formed reddish orange rods which exhibited a bulk conductivity of $\sigma_{rt} = 1.0 \times 10^{-6}$ S cm^{-1} without doping. The p-type semiconductivity was detected by CS-AFM. Furthermore, the doping of **15a** with iodine and bromine vapors afforded black conducting complexes ($\sigma_{rt} = 1.1 \times 10^{-4}$ and 1.5×10^{-4} S cm^{-1}, respectively).

For conjugated TTF dimers linked by π-systems or chalcogen atoms, intramolecular through-bond and/or through-space interactions can be expected between two TTF parts. The intramolecular through-bond interaction between the two TTF parts linked in a head-to-tail manner is calculated to be weak in the ground state [25]. Thus, the conjugation of the two neutral TTF parts in **16–19** is weak (Figure 6) [59]. In the cyclic voltammetry (CV) measurements, tetraethylthio-bi-TTF **16** showed two one-electron and one two-electron redox waves (Table 1), while other TTF dimers of **17–19** exhibited only two two-electron reversible redox waves corresponding to TTF/TTF$^{\bullet+}$ and TTF$^{\bullet+}$/TTF^{2+} at a normal scan rate (100 mV s^{-1}). As shown in Table 1, however, steady-state electronic spectra of **16**$^{\bullet+}$, **17**$^{\bullet+}$, and **18**$^{\bullet+}$ show intramolecular interaction between TTF and TTF$^{\bullet+}$, and the absorption maxima were observed at ca. 450 and 750 nm, together with broad absorption of intramolecular CT interactions between two TTF units at 1400, 1300, 1200 nm, respectively. The magnitude of these broad absorption bands is clearly affected by the distance between two TTFs, and TTF

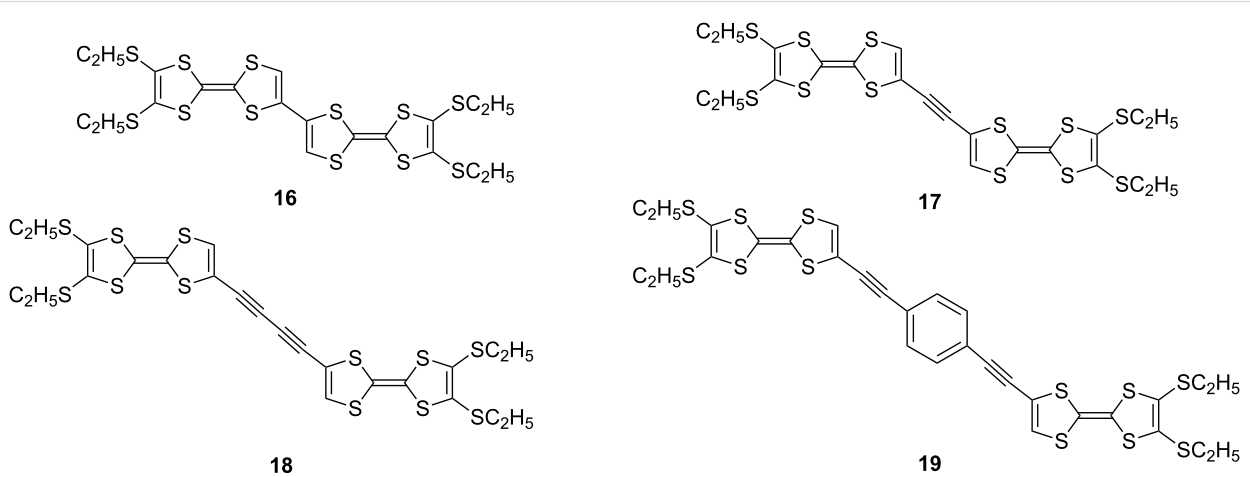

Figure 6: TTF dimers linked by σ-bond (**16**) and conjugated π-systems (**17–19**).

Table 1: Redox potentials of **16–19** and absorption maxima of monocations $\mathbf{16}^{\bullet+}$, $\mathbf{17}^{\bullet+}$, $\mathbf{18}^{\bullet+}$ and $\mathbf{19}^{\bullet+}$, and dications $\mathbf{16}^{2+}$, $\mathbf{17}^{2+}$, $\mathbf{18}^{2+}$ and $\mathbf{19}^{2+}$ [25,59].

Compound	Redox potentials[a] vs Fc/Fc^+			Absorption maxima[b]	
	$E_{1/2}^1$ (V)	$E_{1/2}^2$ (V)	$E_{1/2}^3$ (V)	Monocation (nm)	Dication (nm)
16	0.06	0.17	0.44	772, 1400 br	816, 1098 sh
17	0.11	0.42		778, 1300 br	808
18	0.12	0.42		790, 1200 br	804
19	0.08	0.38		790	796

[a]Potentials were measured by cyclic voltammetry (CV) in benzonitrile against a Ag/Ag^+ electrode and adjusted to the Fc/Fc^+ potential. [b]Measured in CH_2Cl_2/CH_3CN (4:1) using $Fe(ClO_4)_3$ as the oxidation reagent.

dimer $\mathbf{19}^{\bullet+}$ linked with a longer spacer exhibited no intramolecular CT absorption band. Moreover, the longest absorption maxima of the dications $\mathbf{16}^{2+}$, $\mathbf{17}^{2+}$, and $\mathbf{18}^{2+}$ exhibit a bathochromic shift of 44, 30, and 14 nm, respectively, from the corresponding absorption maximum of $\mathbf{16}^{\bullet+}$, $\mathbf{17}^{\bullet+}$, and $\mathbf{18}^{\bullet+}$ due to the head-to-tail orientation of two $TTF^{\bullet+}$ (Davydov red shift) [25]. It is worth noting that the redox behavior of TTF dimers in CV measurements are sensitive to the concentration and the solvent used, and pristine bi-TTF **15b** showed two reversible two-electron redox waves at −0.03 and 0.38 V vs Fc/Fc^+ in benzonitrile under normal conditions [25,60].

Conducting nanostructure formation from star-shaped oligo-TTFs

Although pristine TTF does not self-associate in solution due to the low association constant for dimerization, the mixed-valence (MV) dyad $(TTF/TTF)^{\bullet+}$ and the dicationic dyad $(TTF^{\bullet+})_2$, so-called π-dimer, are formed in concentrated solution or at low temperature [61]. On the other hand, the synergy of either the fastener effect or π-expansion allows star-shaped C_3-symmetric oligo-TTFs **22** and **23** to self-associate both in solution and in the solid state even in neutral state [18]. Compounds **22** and **23** were synthesized in good yields by Sonogashira coupling reaction of 1,3,5-triethynylbenzene with **20** and 1,3,5-triiodobenzene with **21**, respectively (Scheme 1). X-ray analysis of **22** revealed the columnar structure, in which the three TTF units stack in face-to-face manner to form single crystals (Figure 7).

In the case of **23** with butyl chains, this molecule dimerized in $CDCl_3$ solution ($K_2 = 1.58 \pm 0.30\ M^{-1}$ at 293 K). The chemical shift of the central benzene ring clearly shifted higher field with an increase of concentration or lowering temperature. The observed shift is attributed to the shielding effect from the neighboring molecule that settles in face-to-face mode. The thermodynamic parameters were estimated to be $\Delta H = -9.43$ kJ mol^{-1} and $\Delta S = -28.3$ J mol^{-1} by the van't Hoff plot (Table 2 and Supporting Information File 1). The self-association behavior is significantly affected by the solvent. While no association was observed in benzene-d_6 solution in the concentration ranges of 0.7–21 mM even at low temperatures, a larger K_2 value was estimated in $CDCl_3$–CD_3CN solution (3:7 v/v,

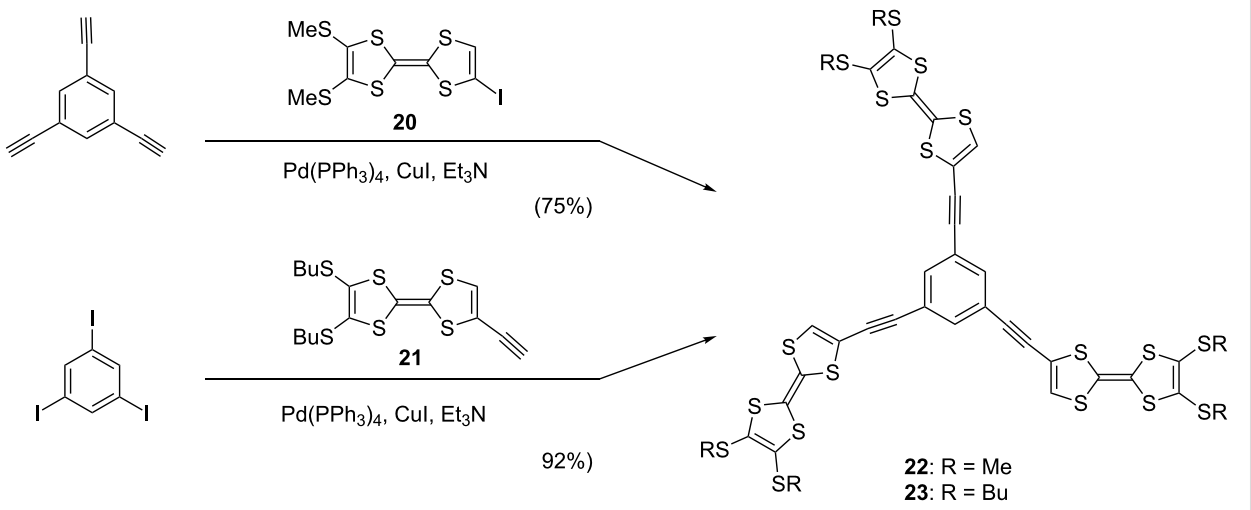

Scheme 1: Synthesis of star-shaped TTF trimers **22** and **23**.

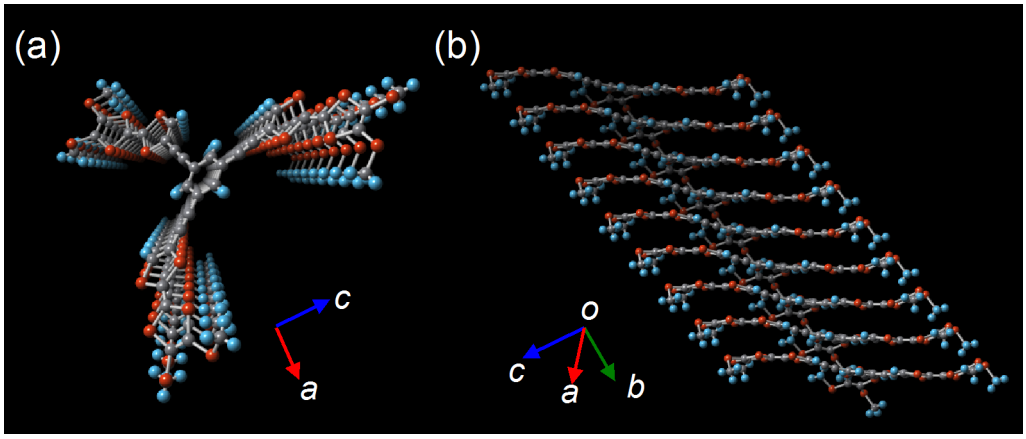

Figure 7: Projections of the molecular array of **22** in crystal structure (a) along with the *c* axis and (b) from side view.

Table 2: Association (dimerization) constants and thermodynamic parameters of **23** in various solvents[a].

Solvent	K_2 (M^{-1})[b]	ΔG (kJ mol^{-1})[b]	ΔH (kJ mol^{-1})	ΔS (J mol^{-1})
$CDCl_3$	1.58	−1.13	−9.41	−28.2
$CDCl_3$–CD_3CN (3:7)	5.01	−3.64	−16.6	−43.1
benzene-d_6	–[c]	–[c]	–[c]	–[c]

[a]Parameters were estimated from titration experiments using ^{1}H NMR with the assumption of the dimerization process of **23**. [b]At 298 K. [c]No association was observed.

K_2 = 5.01 ± 0.98 M^{-1} at 293 K). Moreover, only a small concentration dependence of the chemical shift, which could not be used for determination of the K_2 value, was observed in acetone–CS_2 solution owing to very weak self-association. These results clearly suggest that the association behavior is driven by intermolecular π–π, S···S, and/or S···H interactions in solution. Note that these K_2 values of **23** in the neutral state are similar to that of the mixed valence dimer ($TTF^{\bullet+}$ + TTF) (K_2 = 6.0 M^{-1}) and much larger than that of the π-dimer ($TTF^{\bullet+}$ + $TTF^{\bullet+}$) (K_2 = 0.6 M^{-1}) described in the literature [61].

Strong self-association of **23** was observed in the oxidation state. CV analysis of **23** in a dilute CH_2Cl_2 solution (1.9×10^{-5} M) showed two three-electron redox waves at 0.05 and 0.40 V vs Fc/Fc^+ corresponding to the formation of $\mathbf{23}^{3+}$ and $\mathbf{23}^{6+}$, whereas a similar CV analysis of **23** in a concentrated CH_2Cl_2 solution (1.2×10^{-3} M) displayed three reversible waves at −0.04, 0.14, and 0.47 V vs Fc/Fc^+ corresponding to the formation of $(\mathbf{23})_2^{3+}$, $(\mathbf{23})_2^{6+}$, and $(\mathbf{23})_2^{12+}$ (Figure S2, Supporting Information File 1). Interestingly, the three cationic species $\mathbf{23}^{\bullet+}$, $\mathbf{23}^{2+}$ and $\mathbf{23}^{3+}$ prepared by chemical oxidation with $Fe(ClO_4)_3$ in CH_2Cl_2/CH_3CN (4:1) showed a strong self-association, and electronic spectra of $\mathbf{23}^{\bullet+}$ and $\mathbf{23}^{2+}$ exhibited marked intermolecular charge resonance (CR) bands at λ_{max} 2000 (br, ε 1500) and 2000 (br, ε 1700) owing to the face-to-face mixed valence interaction (Figure 8), and $\mathbf{23}^{3+}$ exhibited a typical Davydov blue shift (λ_{max} 738 nm, ε 27000) as compared with **19** (λ_{max} 796 nm, Table 1) [25]. To determine the

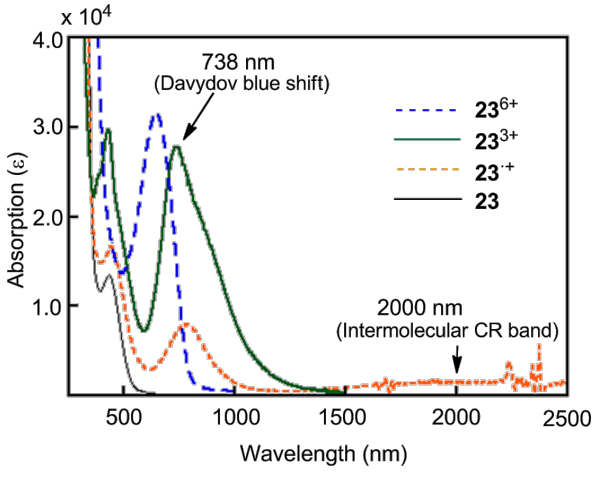

Figure 8: UV–vis/NIR spectra of **23**, $\mathbf{23}^{\bullet+}$, $\mathbf{23}^{3+}$, and $\mathbf{23}^{6+}$.

conducting behavior of **22** and **23**, a pellet of **22** was treated with iodine to produce a semiconducting black solid ($\sigma_{rt} = 3.6 \times 10^{-4}$ S cm^{-1}), whereas a similar doping of **23** with iodine resulted in the formation of the conducting liquid.

Radially expanded TTF oligomers with a large central π-surface can be expected to show effective intra- and intermolecular delocalization of electrons in the neutral and mixed-valence states. Furthermore, the supramolecular self-assembly of these large molecules having nanophase separation is a promising way of realizing molecular switches and devices [62-65]. With this in mind, hexadehydrotris(TTF)[12]annulenes **28** and **29** and dodecadehydrotris(TTF)[18]annulenes **30** and **31** were synthesized using palladium-mediated coupling reactions (Scheme 2) [20,25,26,66-68]. Tris(TTF)[12]annulenes **28** and **29** were pepared by Sonogashira coupling of **26** with **24** and **27** with **25** in 25 and 36% yields, respectively. For the synthesis of **30** and **31**, cyclotrimerization of **24** and **25** with a stoichiometric amount of $PdCl_2(PPh_3)_2$ and CuI in triethylamine–THF was employed to afford **30** and **31** in 32 and 29% yields, respectively. Although tris(TTF)[18]annulenes are stable at room temperature in air, tris(TTF)[12]annulenes **28** and **29** gradually decomposed under ambient conditions due to the instability of central 4n π-electron system.

In order to investigate the effect of fused two TTF units on the cyclic conjugation and the interaction of the two TTF units in the neutral and cationic states, TTF-fused annulenes **33** [69] and radiannulenes **34** and **35** [70] were synthesized using a Sonogashira coupling in moderate yields (Figure 9).

The thermodynamic study on the self-aggregation of tris(TTF)annulenes indicates that the aggregation of **28**, **30**, and **31** is an enthalpically driven process that is entropically disfavored (Table 3) [68], although the aggregation of planar macrocyclic belts is both enthalpically and entropically driven [71]. The TTF[18]annulene **30** has smaller ΔH and ΔS values than the TTF[12]annulene **28**, suggesting a higher stacking ability and a larger ring size for **30**. Alkyl-substituted TTF[18]annulene **32** was reported to show almost no aggregation behavior in solution [72]. However, the slightly more amphiphilic **31** exhibits self-aggregation in benzene, toluene, and cyclohexane owing to a slightly larger nanophase separation in **31**. It is worth noting that the self-aggregation of TTF-annulenes results in the

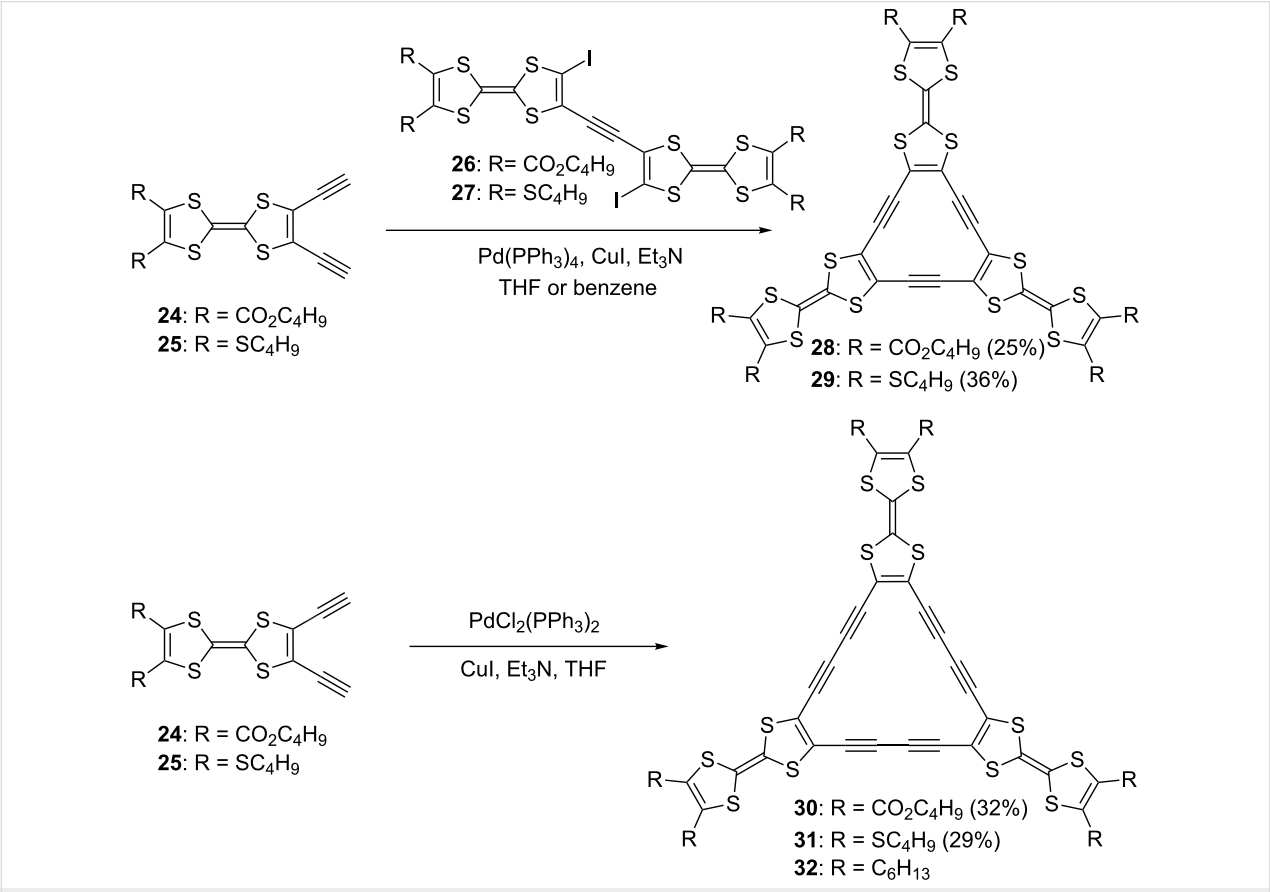

Scheme 2: Synthesis of tris(TTF)[12]annulenes **28** and **29** and tris(TTF)[18]annulenes **30** and **31**, together with hexyl-substituted tris(TTF)[18]annulene **32**.

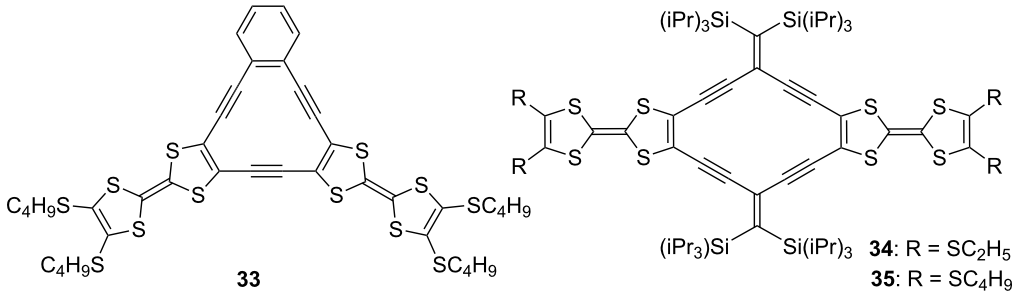

Figure 9: TTF-fused annulene **33** and radiannulenes **34** and **35**.

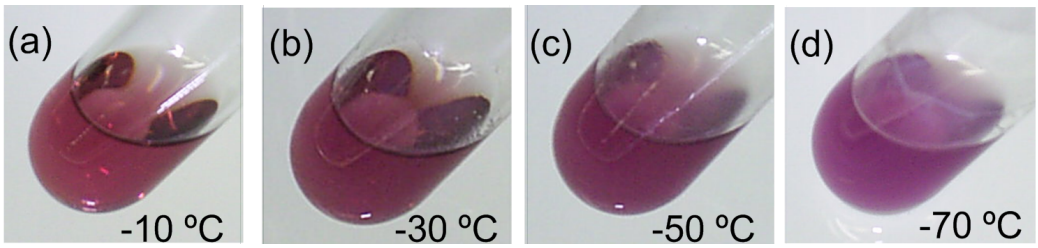

Figure 10: Colors of **30** solutions a–d in toluene (0.025 mM) at various temperatures. (a) λ_{max}: 511 nm, (b) λ_{max}: 512 nm, (c) λ_{max}: 517 nm, (d) λ_{max}: 520 nm. Reprinted with permission from [68]. Copyright 2012 Chemical Society of Japan.

Table 3: Self-aggregation data in toluene-d_8.[a]

Comp.	Δ*G* (kJ mol^{-1}) at 303 K	Δ*H* (kJ mol^{-1})	Δ*S* (J mol^{-1}·K^{-1})
28	−11.8	−32.0	−66.3
30	−14.5	–37.8	−77.0
31	−10.1	−21.5	−37.1

[a]Determined with concentration/temperature-dependent ^{1}H NMR assuming an infinite association model [68].

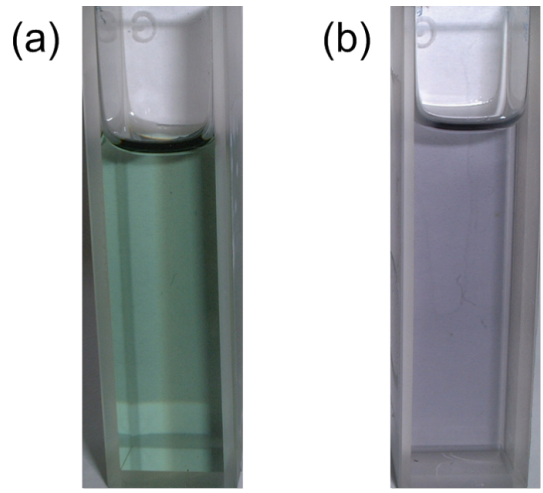

Figure 11: Solutions of **33**. (a) In CS_2, λ_{max}: 608 nm. (b) In CH_2Cl_2, λ_{max}: 577 nm. Reprinted with permission from [69]. Copyright 2004 Royal Society of Chemistry.

appearance of solvatochromism and thermochromism [68]. As shown in Figure 10, **30** exhibits a supramolecular thermochromism in toluene, and the color at −10 °C is reddish purple, whereas the color at −70 °C is purple. On the other hand, as shown in Figure 11, a solution of **33** exhibits deep green in CS_2 but purple in CH_2Cl_2 [69].

CV analysis of **28**–**34** in solution showed different behaviors (Table 4). The [12]annulenes **28**, **29**, and **33** exhibited two reversible one-electron reductions due to the smooth reduction of the 12π electron system to a 14π electron system, whereas the [18]annulenes **30** and **31** showed an irreversible reduction wave, due to the unfavorable reduction of the aromatic 18π electron system. On the other hand, all the molecules exhibited reversible oxidation waves in CH_2Cl_2 based on the high HOMO levels of TTF units. Another important feature in the CV data of **28**–**32** is broadening or splitting of the first oxidation wave, indicating intra- and/or intermolecular interactions between TTF units [68]. Interestingly, the first oxidation potential of **28** and **29** splited at the slow scanning rate of 3 mV s^{-1} owing to the intermolecular mixed-valence interaction between the TTF$^{\bullet+}$

Table 4: Redox potentials of **28**–**34** measured by CV[a].

Compound	$E_{1/2}^{red2}$ (V)	$E_{1/2}^{red1}$ (V)	$E_{1/2}^{ox1}$ (V)	$E_{1/2}^{ox2}$ (V)
28[b]	−1.52 (1e)	−1.16 (1e)	0.38 (3e) [0.29, 0.44][c]	0.66 (3e)
29[b]	−1.78 (1e)	−1.41 (1e)	0.21 (3e) [0.12, 0.26][c]	0.49 (3e)
30[b]	–[d]	–1.35[e]	0.43 (3e)[f]	0.70 (3e)
31[b]	–[d]	–1.48[e]	0.14 (1e), 0.29 (2e)	0.53 (3e)
32[g]	–[d]	–1.40[e]	0.20 (3e)	0.64 (3e)
33[b,i]	−1.87 (1e)	–1.50 (1e)	0.19 (2e)[f,h]	0.46 (2e)[h]
34[i]	−1.52 (1e)	−1.16 (1e)	0.20 (1e), 0.29 (1e)	0.61 (2e)

[a]Conditions: 0.1 M Bu_4NClO_4, 100 mV s^{-1}, Pt as a working electrode, Ag/Ag^+ as a reference electrode, Pt wire as a counter electrode. Potentials were referenced to Fc/Fc^+. Solvent: THF for reduction, and CH_2Cl_2 for oxidation. [b]Concentration: 0.1 mM. [c]Measured at 3 mV s^{-1}. [d]Not observed. [e]Irreversible process. [f]Broad redox wave. [g]According to [72]. [h]Solvent: benzonitrile. [i]According to [70].

and TTF moieties under diffusion-controlled conditions. In the case of **31**, the first oxidation potential ($E_{1/2}$ = 0.14 V vs Fc/Fc^+) is lower than that of **32** with alkyl groups ($E_{1/2}$ = 0.20 V). Since the first oxidation potential of **31** in a dilute solution broadened but did not split ($E_{1/2}^{ox1}$ in CH_2Cl_2: 0.23 (3e) V), the potential of **31** at 0.14 V (Table 4) reflected the strong intermolecular interaction between the $TTF^{\bullet+}$ and TTF moieties in $\mathbf{31}^{\bullet+}$. By comparison with the known UV–vis/NIR spectra of mixed valence dimers [18,73], the association constant K_a of $\mathbf{31}^{\bullet+}$ measured in CH_2Cl_2–MeCN 4:1 assuming an infinite association model [74] is large ($K_a = 3.12 \pm 0.48 \times 10^5$ M^{-1} at 298 K) owing to 18 sulfur atoms in **31**. Therefore, the oxidation of **31** solution (0.1 mM) in CH_2Cl_2 first forms $(\mathbf{31})_2^{2+}$ owing to the intermolecular mixvalence interaction between the $TTF^{\bullet+}$ and TTF moieties, and the further oxidation forms $\mathbf{31}^{3+}$ [68]. In summary, the oxidation of **28**–**31** showed multistep processes owing to intra- and/or intermolecular interactions between TTF units. In the case of [18]annulene **31**, the first oxidation potential splited in two with the strong intermolecular interaction in $\mathbf{31}^{\bullet+}$. TTF-functionalized radiaannulenes (RAs) **34** and **35** also exhibit multiple redox states [70]. CV analysis of **34** shows the two reversible one-electron reductions as the reduction of the RA core, whereas the three reversible oxidations at 0.20, 0.29, and 0.61 V correspond to the formation of $\mathbf{34}^{\bullet+}$, $\mathbf{34}^{2+}$, and $\mathbf{34}^{4+}$. Therefore, the redox behavior of **34** is similar to those of **28**, **29**, and **31**.

The [18]annulenes **30** and **31** formed a fibrous structure in H_2O–THF 1:1, and **31** required longer time for fiber formation than **30** owing to weaker association constant in solution (K_a in toluene-d_8 at 303 K = 634 M^{-1} (**30**), 101 M^{-1} (**31**)) [67,68]. Both **30** and **31** fibers showed roughly the same behavior for doping with iodine, and the color of fibers quickly changed from bluish purple to dark brown due to the partial oxidation of **30** and **31** as shown Figure 12 (the maximum conductivities: **30** σ_{rt} 2.0×10^{-2} S cm^{-1}, **31** σ_{rt} 2.6×10^{-3} S cm^{-1}). The color of the doped fibers gradually returned to the original bluish purple under vacuum, but the speed of the iodine desorption for fiber **31** was very slow. The conductivity of the doped pellet prepared from fiber **30** is estimated to be ca. 1000 times higher than that of the neutral fiber (before doping: σ_{rt} $3 \times 10{-}^6$ S cm^{-1}, after doping: σ_{rt} 3×10^{-3} S cm^{-1}) [68].

Star-shaped pyrrole-fused TTF oligomers **38**–**43** were synthesized by nucleophilic aromatic substitution (S_NAr) reactions of fluorinated benzenes with the pyrrolyl sodium salts derived from **36** and **37** in moderate yields (Scheme 3) [23]. X-ray analysis of **38** revealed that the three TTF units are bent simply to fill an empty space and stacked to form a columnar structure. The torsion angle between the mean planes of the pyrrole and central benzene is 7–32°, indicating the conformational flexibility of the pyrrole–benzene linkage. The calculated torsion angles between the pyrroles and central benzenes of **38**, **40**, and **42** are 34, 45, and 59°, respectively, and the non-planar structures of **38**, **40**, and **42** are in good agreement with the high-field shift of α-protons of pyrroles in the ^1H NMR spectra: δ 6.89 (**38**), 6.41 (**40**), 5.93 ppm (**42**). Star-shaped TTF 10-mer **44** was also synthesized by S_NAr reaction of the sodium salt of **36** with decafluorobiphenyl (44%) [75] (Figure 13).

In the CV measurements (Figure 14), tetrasubstituted **40** shows typical two reversible oxidation waves at $E_{1/2}^{ox1}$ = 0.044 and $E_{1/2}^{ox2}$ = 0.35 V (vs Fc/Fc^+). However, trisubstituted **38** and hexasubstituted **42** exhibit split and broad first peaks, respectively, at −0.086 and 0.020 V (**38**) and 0.097 V (**42**), followed by second peaks at 0.45 V (**38**) and 0.37 V (**42**). The CV data of tetrasubstituted **40** suggests no intramolecular charge delocalization between the adjacent TTF units. The splitting and broadening of the first oxidation waves in **38** and **42** are considered to be caused by intermolecular interactions between the neutral and cationic TTF units.

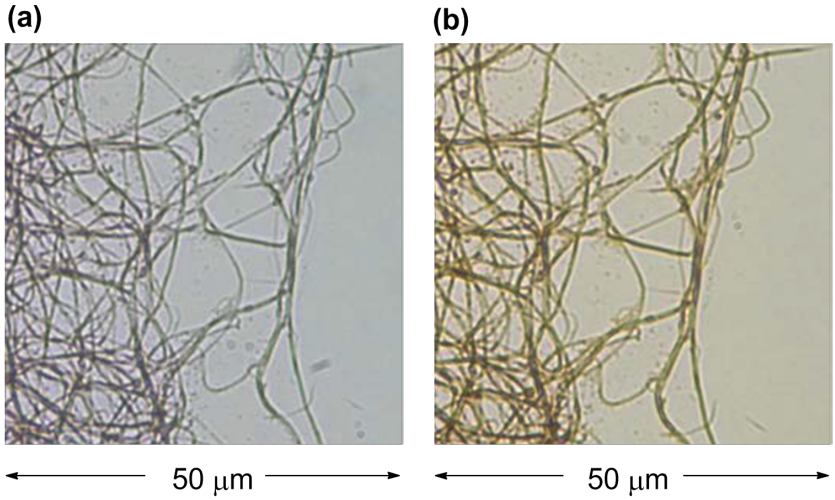

Figure 12: Optical micrographs (1000× magnified) of fibers, prepared from **30** in THF–H_2O 1:1, on a glass plate at 23 °C. (a) Before iodine doping. (b) After iodine doping (3 min). Reprinted with permission from [26]. Copyright 2010 Royal Society of Chemistry.

As shown in Figure 15, the stepwise chemical oxidation of **38**, **40**, and **42** with $Fe(ClO_4)_3$ in CH_2Cl_2–CH_3CN 2:1 exhibits the typical changes in the absorption spectra. The addition of $Fe(ClO_4)_3$ up to 1 equiv with respect to each of the TTF units causes new absorption maxima at longer wavelength region (blue to green spectra). For the oxidation of **40**, the changes show several isosbestic points, indicating that each TTF unit is oxidized from the neutral to the radical cation ($TTF^{\bullet+}$) in a stepwise manner (Figure 15b). On the other hand, for **38** and **42**, there are no isosbestic points (Figure 15a,c). For **38**, a new broad peak around 1850 nm (intermolecular CR absorption) appears in the presence of 1.5 equiv of $Fe(ClO_4)_3$, which is attributed to the formation of an intermolecular face-to-face mixed valence complex. These results are consistent with the peak splitting of the CV. Furthermore, CV analysis of **44** exhibited two reversible ten-electron redox waves corresponding to the formation of $\mathbf{44}^{10+}$ and $\mathbf{44}^{20+}$.

Trisubstituted **38** showed polymorphism and formed single crystals from CH_2Cl_2, whereas it produced a yellow fibrous material from CH_2Cl_2–hexane 1:4. X-ray diffractometry (XRD) exhibited that fiber **38** possesses a hexagonal columnar structure different from single crystals. Furthermore, the spin-coated film of **38** has an amorphous structure. Interestingly, doping of single crystals, hexagonal fiber, and amorphous film of **38** with iodine vapor produced black CT-complexes having different assembled structure. After doping, electric conductivity of single crystals was $\sigma_{rt} = 1.8 \times 10^{-2}$ S cm^{-1} and the fiber was 1.9×10^{-2} S cm^{-1}, whereas the amorphous film was 2.5×10^{-3} S cm^{-1}. The difference in the conductivity reflects the molecular level alignments. Other star-shaped oligomers **39–44** also formed nanostructures fibers, particles and film, and doping with iodine produced black complexes which exhibited electric conductivities of $\sigma_{rt} = 2.7 \times 10^{-3}$–$2.4 \times 10^{-2}$ S cm^{-1} in spite of the non-planarity of the molecular frame of **39–44**.

The pyridazine-3,6-diol-annulated TTF derivative **45** produced trimer **46** via hydrogen bonds in a THF–H_2O solution (Scheme 4), in which micrometer-sized fibrous material was gradually formed [76]. The compressed pellet of the **46** fibers showed an electrical conductivity of $\sigma_{rt} = 2.3 \times 10^{-4}$ S cm^{-1} after doping with iodine vapor. The addition of ethylene diamine triggered the reorganization of the supramolecular structure **46**, and fine nanoscopic fibers composed of **45** and ethylene diamine (1:1) were produced from the $CHCl_3$ solution. A compressed pellet of the fibers of $\mathbf{45}{\cdot}H_2NCH_2CH_2NH_2$ exhibited an electrical conductivity in the range of $\sigma_{rt} = 1.5$–10.0×10^{-5} S cm^{-1} after iodine doping.

Recently, conducting nanofibers derived from the self-assembly of TTF-appended dipeptides were reported [77]. Conductivity measurements performed on the nanofibers of TTF-appended dipeptides indicate a remarkable enhancement in the conductivity after doping with TCNQ ($\sigma_{rt} = 1 \times 10^{-5}$ S cm^{-1}).

Conducting nanostructures prepared from cation radicals

Molecular conductors derived from CT complexes and radical salts of TTFs are widely known [1], and mixed-valence $(TTF_2)^{n+}$ ($0 < n < 1$) was reported to form self-accembled conducting nanofibers ($\sigma_{rt} = \sim 10^{-2}$ S cm^{-1}) [78-82]. However, there is only a limited number of examples of nanofibers and nanorods prepared from CT complexes and radical salts of star-shaped and radially expanded TTF oligomers. One typical

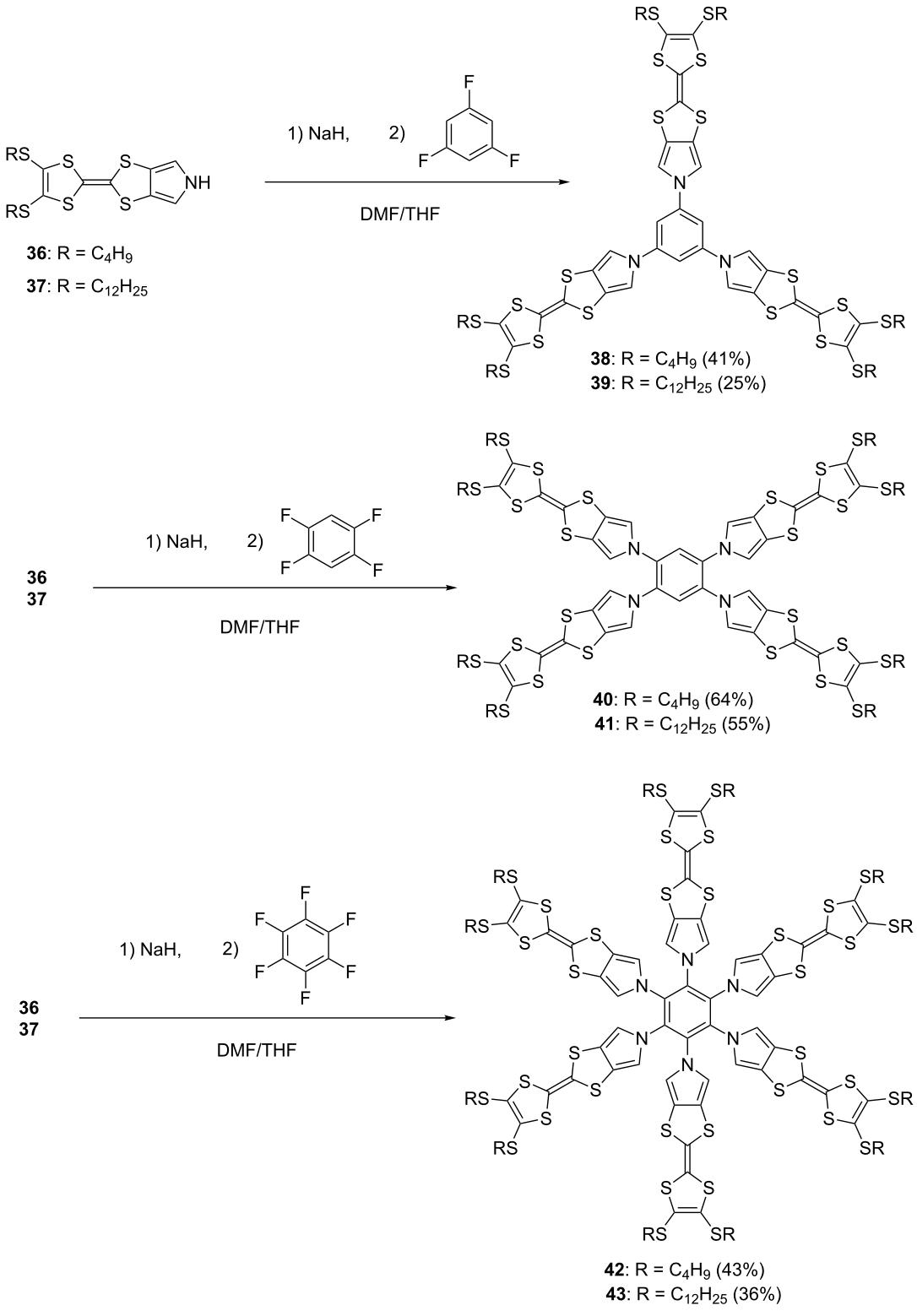

Scheme 3: Star-shaped TTF oligomers **38–43**.

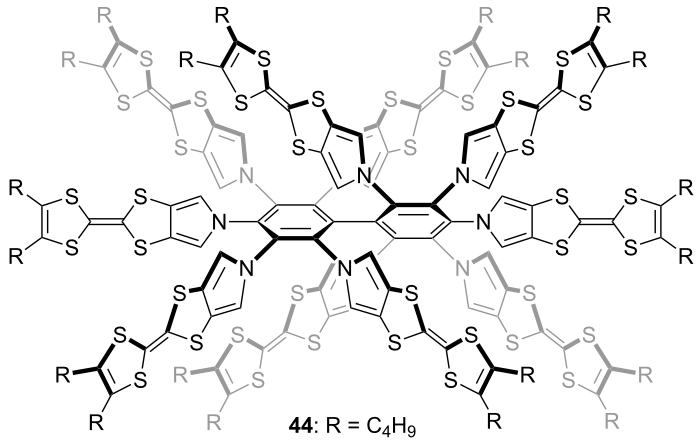

Figure 13: Star-shaped TTF 10-mer **44**.

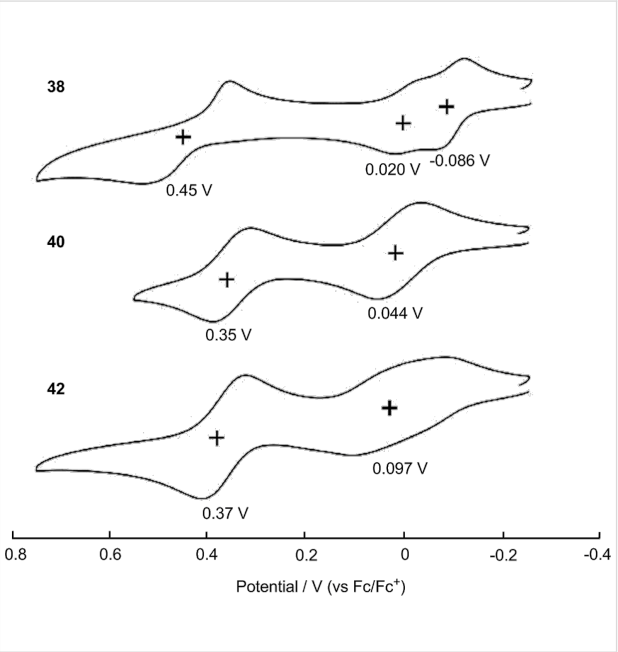

Figure 14: Cyclic voltammograms of **38**, **40**, and **42** (0.1 mM) in benzonitrile with 0.1 M *n*-Bu_4PF_6 as a supporting electrolyte, $Ag/AgNO_3$ as a reference electrode, glassy carbon as a working electrode, Pt wire as a counter electrode, and a scan rate of 100 mV s^{-1}. Values are half-wave potentials. Adapted with permission from [23]. Copyright 2011 American Chemical Society.

example is the conducting CT complex $\mathbf{47}^{2+}\cdot(TCNQF_4^{\bullet-})_2$ of amphiphilic TTF **47** and $TCNQF_4$ (Figure 16) [83,84]. The fiber structure with typical dimensions of 2.5 nm (height) × 50 nm (width) × 1 μm (length) was constructed on a mica substrate by using the Langmuir–Blodgett (LB) technique, and the conductivity of the film composed the $\mathbf{47}^{2+}\cdot(TCNQF4^{\bullet-})_2$ fiber was found to be on the order of $\sigma_{rt} = 10^{-3}$ S cm^{-1}.

The stacking behavior of TTF in solution and in the solid state was employed as a driving force to construct higher aggregates by using the star-shaped hexakis(tetrathiafulvalenylethynyl)benzene **48** (Figure 17a). The TTF-hexamer **48** was synthesized by Sonogashira coupling of **21** with hexaiodobenzene (52%) [22]. As expected, **48** strongly self-aggregates in $CHCl_3$ ($K_a = 2.1 \times 10^4$ M^{-1}, 23 °C) and in other common organic solvents. To construct nanoobjects, a $CHCl_3$ solution of **48** was diluted with hexane to afford dark blue fibers with a slim and curled fiber structure (40–90 nm wide, 30–100 nm thick and more than 10 μm long) (Figure 17b). On the other hand, a dark blue film was formed by casting a solution of **48** on a glass surface (Figure 17c). XRD studies on the fiber and the film of **48** revealed that the fiber has a hexagonal alignment, whereas the film has a lamellar structure with lateral order and π···π stacking. It is worth noting that the film of **48** prepared by casting a 0.1 wt % solution of **48** in $CHCl_3$ exhibited a low carrier mobility of $\mu = 3 \times 10^{-6}$ cm^2 V^{-1} s^{-1}, indicating a lamellar structure vertical to the substrate surface.

Oxidation of **48** with 1 and 3 equiv of $Fe(ClO_4)_3$ produced the analytically pure monocation $\mathbf{48}^{\bullet+}ClO_4^-$ and trication $\mathbf{48}^{3+}(ClO_4^-)_3$, respectively. The cationic species $\mathbf{48}^{\bullet+}ClO_4^-$ and $\mathbf{48}^{3+}(ClO_4^-)_3$ strongly self-aggregate in $CHCl_3$ ($K_a = 2.3$–2.5×10^6 M^{-1}) and rather weakly aggregate in THF. Interestingly, in THF, $\mathbf{48}^{\bullet+}ClO_4^-$ and $\mathbf{48}^{3+}(ClO_4^-)_3$ exhibited the formation of stacked cylindrical structures with a radius of 11 Å and a height of 14–16 Å by small-angle X-ray scattering (SAXS). ESR spectra of $\mathbf{48}^{\bullet+}$ and $\mathbf{48}^{3+}$ in $CHCl_3$ at 23 °C showed 100% of spin for $\mathbf{48}^{\bullet+}$ and 33% of spin for $\mathbf{48}^{3+}$. Therefore, the spin–spin interaction in $\mathbf{48}^{\bullet+}$ is weak, whereas the spin–spin interaction in $\mathbf{48}^{3+}$ is strong.

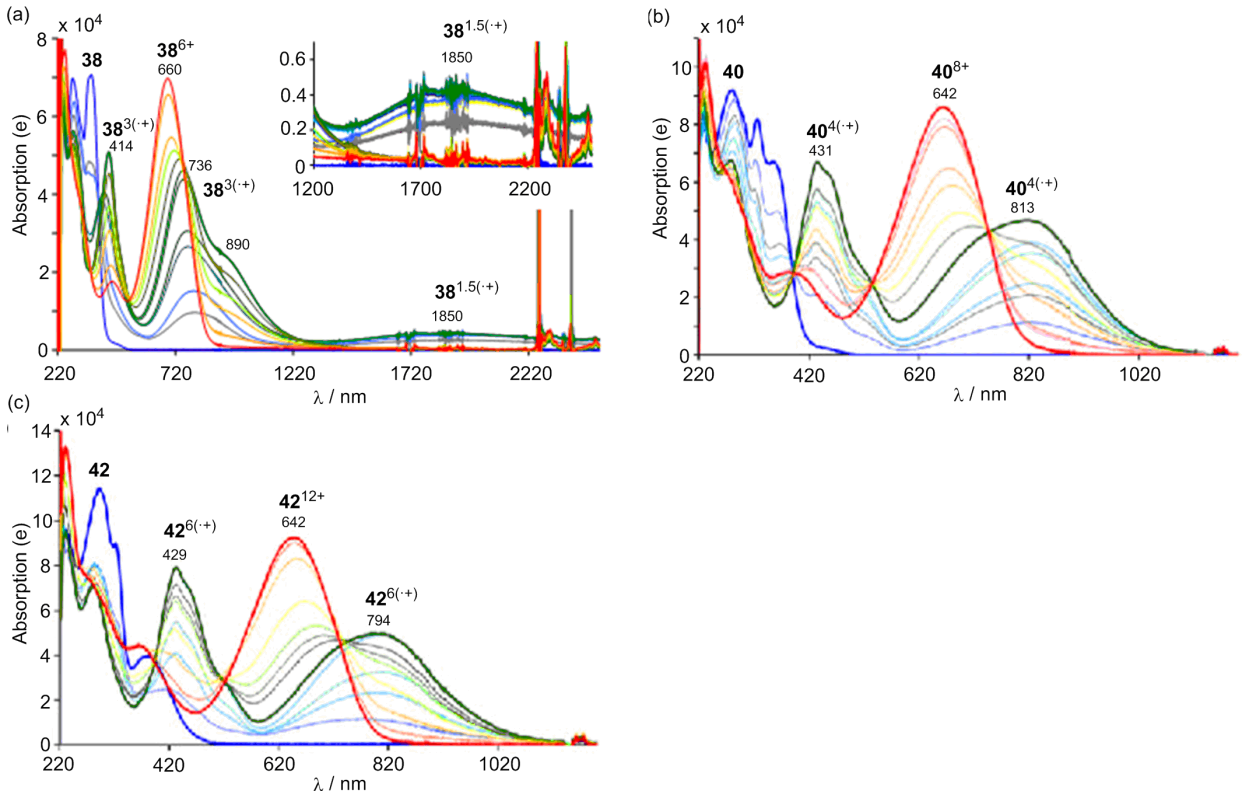

Figure 15: Stepwise oxidation of (a) **38** (0.02 mM), (b) **40** (0.05 mM), and (c) **42** (0.03 mM) with incremental addition of $Fe(ClO_4)_3$ in a mixture of CH_2Cl_2–CH_3CN (2:1, v/v) at 25 °C. The blue line indicates the neutral absorption spectra, the green line the multiple TTF radical cations $\mathbf{38}^{3(\bullet+)}$, $\mathbf{40}^{4(\bullet+)}$, and $\mathbf{42}^{6(\bullet+)}$, and the red line the TTF dications $\mathbf{38}^{6+}$, $\mathbf{40}^{8+}$, and $\mathbf{42}^{12+}$. Adapted with permission from [23]. Copyright 2011 American Chemical Society.

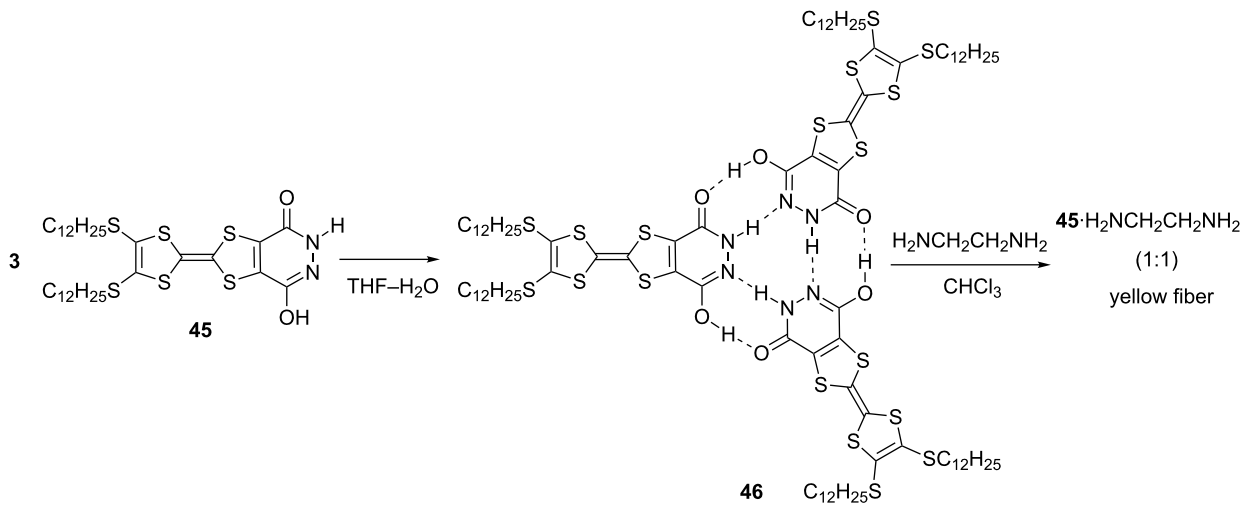

Scheme 4: Pyridazine-3,6-diol-TTF **45** and its trimer **46**.

The monocation $\mathbf{48}^{\bullet+}ClO_4^-$ easily formed a hexagonal fiber from $CHCl_3$–hexane solution, probably owing to the strong aggregation properties and molecular shape of the stacked $\mathbf{48}^{\bullet+}ClO_4^-$, whereas trication $\mathbf{48}^{3+}(ClO_4^-)_3$ produced a nanoparticle having a low internal regularity, presumably owing to the strong intermolecular $TTF^{\bullet+}$–$TTF^{\bullet+}$ interaction of $\mathbf{48}^{3+}$. A cast film of $\mathbf{48}^{\bullet+}ClO_4^-$ shows a lamellar structure vertical to the substrate in a similar manner to the neutral **48** (Figure 17c). Inter-

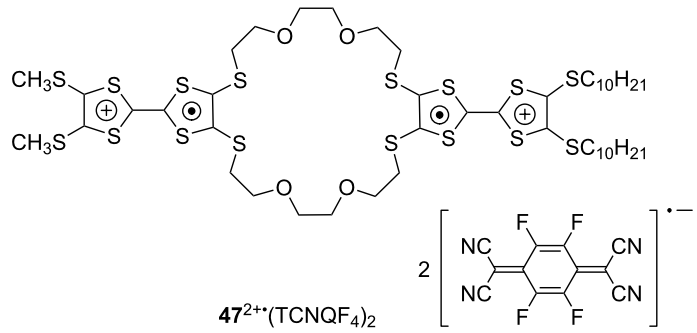

Figure 16: CT-complex of **47** with $TCNQF_4$.

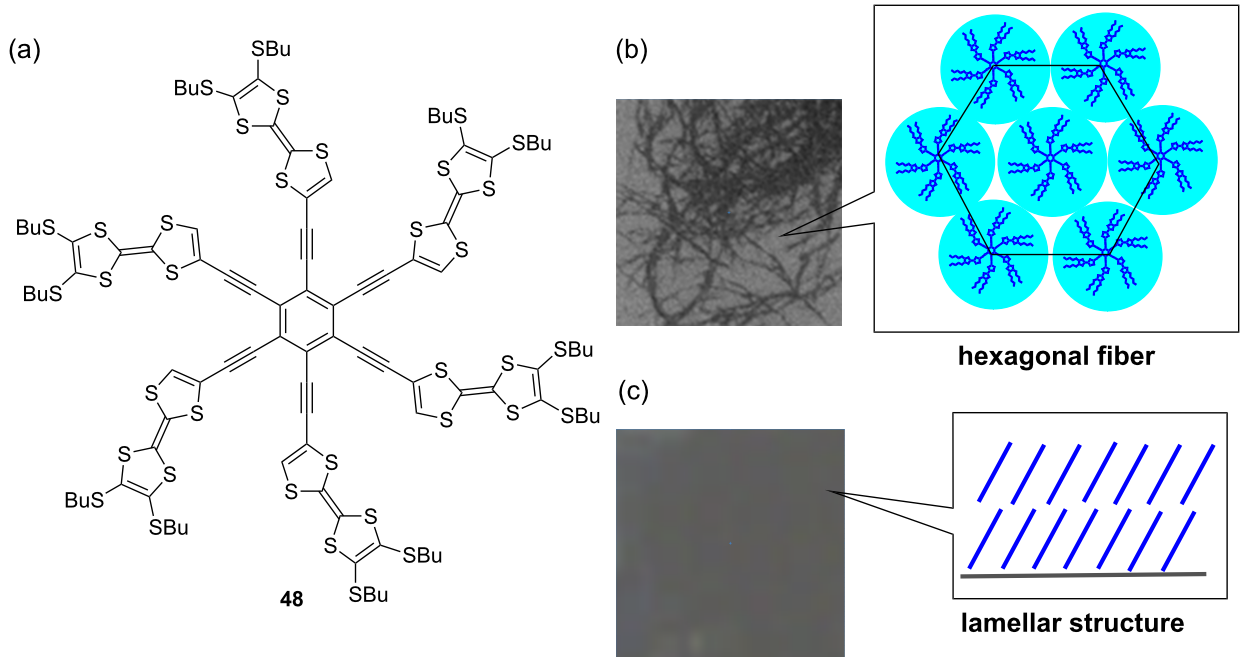

Figure 17: (a) Star-shaped TTF hexamer **48**. (b) Optical image of **48** fiber with a hexagonal structure. (c) Optical image of **48** film with a lamellar structure. Adapted with permission from [22]. Copyright 2007 American Chemical Society.

estingly, the structural difference between nanofiber and film of $\mathbf{48}^{\bullet+}ClO_4^-$ leads to the different electric conductivities of wires (σ_{rt} = 1.1 × 10^{-3} S cm^{-1}) and film (σ_{rt} = 3.1 × 10^{-5} S cm^{-1}) depending on their stacking structures.

Cation radicals of pyrrole-fused TTF trimer **38** also formed conducting nanostructures when a CH_2Cl_2 solution of $\mathbf{38}^{1.5(\bullet+)}$ was mixed with an excess amount of hexane. The XRD pattern of the fiber $\mathbf{38}^{1.5(\bullet+)}$ is composed of a lamellar structure different from the neutral **38** fiber and an exhibited electric conductivity of σ_{rt} = 2.9 × 10^{-4} S cm^{-1}. The lower conductivity of the fiber $\mathbf{38}^{1.5(\bullet+)}$ as compared to the doped **38** fiber (σ_{rt} = 1.9 × 10^{-2} S cm^{-1}) may be due to the difference in their internal structures.

Conclusion

The construction of nanoobjects based on the self-assembly of TTFs were rapidly advanced, and a large number of functional properties such as electronic, magnetic, and optical properties were recently reported. Based on these developments of nanoscience, the construction of conducting nanoobjects has also been investigated to realize electrochemically-driven conformational control, redox-controlled gelation processes, redox switches, and molecular sensors. Furthermore, semiconductive

fibers and rods of TTFs can be utilized for nanosized electric wires and wirings in nanoelectronics. The next key innovation in TTF-based nanoobjects is the fulfillment of nanofiber and nanorod with metallic conductivity and superconductivity. To achieve a high electric conductivity, further knowledge is necessary to fabricate a closely stacked ionic state with unfilled bands. If these innovative systems can be implemented, conducting nanoobjects find functions in a variety of mass use devices.

Supporting Information

Supporting Information File 1

Determination of association constants (K_2) of **23** by NMR and cyclic voltammetry analysis of **23**.
[http://www.beilstein-journals.org/bjoc/content/supplementary/1860-5397-11-175-S1.pdf]

Acknowledgements

This work was partly supported by a Grant-in-Aid for Scientific Research from JSPS and by Strategic Japanese-German Cooperative Program of JST (Japan Science and Technology Corporation). We thank Prof. Tohru Nishinaga (Tokyo Metropolitan University) and Prof. Masayoshi Takase (Ehime University) for their helpful assistance.

References

1. Batail, P. *Chem. Rev.* **2004,** *104,* 4887–4890. doi:10.1021/cr040697x
2. Yamada, Y.; Sugimoto, T. *TTF Chemistry. Fundamentals and Applications of Tetrathiafulvalene;* KODANSHA–Springer: New York, NY, U.S.A., 2004.
3. Ishiguro, T.; Yamaji, K.; Saito, G. *Organic Superconductors,* 2nd ed.; Springer Series in Solid-State Sciences, Vol. 88; Springer: Berlin, Germany, 1998. doi:10.1007/978-3-642-58262-2
4. Saito, G.; Yoshida, Y. *Bull. Chem. Soc. Jpn.* **2007,** *80,* 1–137. doi:10.1246/bcsj.80.1
5. Desiraju, G. R. *Angew. Chem., Int. Ed. Engl.* **1995,** *34,* 2311–2327. doi:10.1002/anie.199523111
6. Lehn, J.-M. *Science* **2002,** *295,* 2400–2403. doi:10.1126/science.1071063
7. Hoeben, F. J. M.; Jonkeijm, P.; Meijer, E. W.; Schenning, A. P. H. J. *Chem. Rev.* **2005,** *105,* 1491–1546. doi:10.1021/cr030070z
8. Whitesides, G. M.; Grzybowski, B. *Science* **2002,** *295,* 2418–2421. doi:10.1126/science.1070821
9. Nayak, S.; Lyon, L. A. *Angew. Chem., Int. Ed.* **2005,** *44,* 7686–7708. doi:10.1002/anie.200501321
10. Gomar-Nadal, E.; Puigmartí-Luis, J.; Amabilino, D. B. *Chem. Soc. Rev.* **2008,** *37,* 490–504. doi:10.1039/B703825A
11. Li, C.; Bai, H.; Shi, G. *Chem. Soc. Rev.* **2009,** *38,* 2397–2409. doi:10.1039/b816681c
12. Bryce, M. R.; Marshallsay, G. J.; Moore, A. J. *J. Org. Chem.* **1992,** *57,* 4859–4862. doi:10.1021/jo00044a020
13. Formigué, M.; Johannsen, I.; Boubekeur, K.; Nelson, C.; Batail, P. *J. Am. Chem. Soc.* **1993,** *115,* 3752–3759. doi:10.1021/ja00062a047
14. Iyoda, M.; Fukuda, M.; Yoshida, M.; Sasaki, S. *Synth. Met.* **1995,** *70,* 1171–1172. doi:10.1016/0379-6779(94)02806-A
15. Iyoda, M.; Fukuda, M.; Yoshida, M.; Sasaki, S. *Chem. Lett.* **1994,** *23,* 2369–2372. doi:10.1246/cl.1994.2369
16. González, A.; Segura, J. K.; Martín, N. *Tetrahedron Lett.* **2000,** *41,* 3083–3086. doi:10.1016/S0040-4039(00)00344-0
17. Kanibolotsky, A.; Roquet, S.; Cariou, M.; Leriche, P.; Turrin, C.-O.; de Bettingnies, R.; Caminade, A.-M.; Majoral, J.-P.; Khodorkovsky, V.; Gorgues, A. *Org. Lett.* **2004,** *6,* 2109–2112. doi:10.1021/ol049648x
18. Hasegawa, M.; Takano, J.-i.; Enozawa, H.; Kuwatani, Y.; Iyoda, M. *Tetrahedron Lett.* **2004,** *45,* 4109–4112. doi:10.1016/j.tetlet.2004.03.150
19. Jia, H.-P.; Liu, S.-X.; Sanguine, L.; Levillain, E.; Decurtins, S. *J. Org. Chem.* **2009,** *74,* 5727–5729. doi:10.1021/jo901054b
20. Hara, K.; Hasegawa, M.; Kuwatani, Y.; Enozawa, H.; Iyoda, M. *Heterocycles* **2010,** *80,* 909–915. doi:10.3987/COM-09-S(S)122
21. Pop, F.; Melan, C.; Danila, I.; Linares, M.; Beljonne, D.; Amabilino, D. B.; Avarvari, N. *Chem. – Eur. J.* **2014,** *20,* 17443–17453. doi:10.1002/chem.201404753
22. Hasegawa, M.; Enozawa, H.; Kawabata, Y.; Iyoda, M. *J. Am. Chem. Soc.* **2007,** *129,* 3072–3073. doi:10.1021/ja069025+
23. Takase, M.; Yoshida, N.; Nishinaga, T.; Iyoda, M. *Org. Lett.* **2011,** *13,* 3896–3899. doi:10.1021/ol2014279
24. Jeppesen, J. O.; Nielsen, M. B.; Becher, J. *Chem. Rev.* **2004,** *104,* 5115–5131. doi:10.1021/cr030630u
25. Iyoda, M.; Hasegawa, M.; Miyake, Y. *Chem. Rev.* **2004,** *104,* 5085–5113. doi:10.1021/cr030651o
26. Hasegawa, M.; Iyoda, M. *Chem. Soc. Rev.* **2010,** *39,* 2420–2427. doi:10.1039/b909347h
27. Canevet, D.; Sallé, M.; Zhang, G.; Zhang, D.; Zhu, D. *Chem. Commun.* **2009,** 2245–2269. doi:10.1039/b818607n
28. Pérez, E. M.; Illescas, B. M.; Herranz, M. Á.; Martín, N. *New J. Chem.* **2009,** *33,* 228–234. doi:10.1039/B816272G
29. Brunetti, F. G.; López, J. L.; Atienza, C.; Martín, N. *J. Mater. Chem.* **2012,** *22,* 4188–4205. doi:10.1039/c2jm15710a
30. Christensen, C. A.; Bryce, M. R.; Batsanov, A. S.; Becher, J. *Chem. Commun.* **2000,** 331–332. doi:10.1039/A909882H
31. Christensen, C. A.; Bryce, M. R.; Becher, J. *Synthesis* **2000,** 1695–1704. doi:10.1055/s-2000-8203
32. Zou, L.; Xu, W.; Shao, X.; Zhang, D.; Wang, Q.; Zhu, D. *Org. Biomol. Chem.* **2003,** *1,* 2157–2159. doi:10.1039/b301587d
33. Le Derf, F.; Levillain, E.; Trippé, G.; Gorgues, A.; Sallé, M.; Sebastían, R.-M.; Caminade, A.-M.; Majoral, J.-P. *Angew. Chem., Int. Ed.* **2001,** *40,* 224–227. doi:10.1002/1521-3773(20010105)40:1<224::AID-ANIE224>3.0.CO;2-O
34. Kreher, D.; Cariou, M.; Liu, S.-G.; Levillain, E.; Veciana, J.; Rovira, C.; Gorgues, A.; Hudhomme, P. *J. Mater. Chem.* **2002,** *12,* 2137–2159. doi:10.1039/b201695h
35. Mas-Torrent, M.; Rodrígues-Mias, R. A.; Solà, M.; Molins, M. A.; Pons, M.; Vidal-Gancedo, J.; Veciana, J.; Rovira, C. *J. Org. Chem.* **2002,** *67,* 566–575. doi:10.1021/jo010748f
36. Bras, Y. L.; Sallé, M.; Leriche, P.; Mingotaud, C.; Richomme, P.; Møller, J. *J. Mater. Chem.* **1997,** *7,* 2393–2396. doi:10.1039/a704005i
37. Becher, J.; Brimert, T.; Jeppesen, J. O.; Pedersen, J. Z.; Zubarev, R.; Bjørnholm, T.; Reitzel, N.; Jensen, T. R.; Kjaer, K.; Levillain, E. *Angew. Chem., Int. Ed.* **2001,** *40,* 2497–2500. doi:10.1002/1521-3773(20010702)40:13<2497::AID-ANIE2497>3.0.CO;2-F

38. Cook, M. J.; Cooke, G.; Jafari-Fini, A. *Chem. Commun.* **1996,** 1925. doi:10.1039/CC9960001925
39. Farren, C.; Christensen, C. A.; FitzGerald, S.; Bryce, M. R.; Beeby, A. *J. Org. Chem.* **2002,** *67,* 9130. doi:10.1021/jo020340y
40. Sly, J.; Kasák, P.; Gomar-Nadal, E.; Rovira, C.; Górriz, L.; Thordardarson, P.; Amabilino, D. B.; Rowan, A. E.; Nolte, R. J. M. *Chem. Commun.* **2005,** 1255–1257. doi:10.1039/b416034g
41. Nielsen, K. A.; Cho, W.-S.; Jeppesen, J. O.; Lynch, V. M.; Becher, J.; Sessler, J. L. *J. Am. Chem. Soc.* **2004,** *126,* 16296–16297. doi:10.1021/ja044664a
42. Nielsen, K. A.; Bähring, S.; Jeppesen, J. O. *Chem. – Eur. J.* **2011,** *17,* 11001–11007. doi:10.1002/chem.201101266
43. Davis, C. M.; Lim, J. M.; Larsen, K. R.; Kim, D. S.; Sung, Y. M.; Lyons, D. M.; Lynch, V. M.; Nielsen, K. A.; Jeppesen, J. O.; Kim, D.; Park, J. S.; Sessler, J. L. *J. Am. Chem. Soc.* **2014,** *136,* 10410–10417. doi:10.1021/ja504077f
44. Pérez, E. M.; Sierra, M.; Sánchez, L.; Torres, M. R.; Viruela, R.; Viruela, P. M.; Ortí, E.; Martín, N. *Angew. Chem., Int. Ed.* **2007,** *46,* 1847–1851. doi:10.1002/anie.200604327
45. Sugimoto, T.; Awaji, H.; Misaki, Y.; Yoshida, Z.; Kai, Y.; Nakagawa, H.; Kasai, N. *J. Am. Chem. Soc.* **1985,** *107,* 5792–5793. doi:10.1021/ja00306a030
46. Sugimoto, T.; Misaki, Y.; Arai, Y.; Yamamoto, Y.; Yoshida, Z.; Kai, Y.; Kasai, N. *J. Am. Chem. Soc.* **1988,** *110,* 628–629. doi:10.1021/ja00210a069
47. Sugimoto, T.; Misaki, Y.; Kajita, T.; Yoshida, Z.; Kai, Y.; Kasai, N. *J. Am. Chem. Soc.* **1987,** *109,* 4106–4107. doi:10.1021/ja00247a042
48. Warman, J. M.; de Haas, M. P.; Dicker, G.; Grozema, F. C.; Piris, J.; Debije, M. G. *Chem. Mater.* **2004,** *16,* 4600–4609. doi:10.1021/cm049577w
49. Kroeze, J. E.; Savenije, T. J.; Vermeulen, M. J. W.; Warman, J. M. *J. Phys. Chem. B* **2003,** *107,* 7696–7705. doi:10.1021/jp0217738
50. Kostecki, R.; Schnyder, B.; Alliata, D.; Song, X.; Kinoshita, K.; Kötz, R. *Thin Solid Films* **2001,** *396,* 36–43. doi:10.1016/S0040-6090(01)01185-3
51. Müllen, K.; Rabe, J. P. *Acc. Chem. Res.* **2008,** *41,* 511–520. doi:10.1021/ar7001446
52. Joergensen, M.; Bechgaard, K.; Bjoernholm, T.; Sommer-Larsen, P.; Hansen, L. G.; Schaumburg, K. *J. Org. Chem.* **1994,** *59,* 5877–5882. doi:10.1021/jo00099a012
53. Le Gall, T.; Pearson, C.; Bryce, M. R.; Petty, M. C.; Dahlgaard, H.; Becher, J. *Eur. J. Org. Chem.* **2003,** 3562–3568. doi:10.1002/ejoc.200300286
54. Kitamura, T.; Nakaso, S.; Mizoshita, N.; Tochigi, Y.; Shimomura, T.; Moriyama, M.; Ito, K.; Kato, T. *J. Am. Chem. Soc.* **2005,** *127,* 14769–14775. doi:10.1021/ja053496z
55. Kitahara, T.; Shirakawa, M.; Kawano, S.-i.; Beginn, U.; Fujita, N.; Shinkai, S. *J. Am. Chem. Soc.* **2005,** *127,* 14980–14981. doi:10.1021/ja0552038
56. Wang, C.; Zhang, D.; Zhu, D. *J. Am. Chem. Soc.* **2005,** *127,* 16372–16373. doi:10.1021/ja055800u
57. Inokuchi, H.; Saito, G.; Seki, K.; Wu, P.; Tanf, T. B.; Mori, T.; Imaeda, K.; Enoki, T.; Higuchi, Y.; Inaka, K.; Yasuoka, N. *Chem. Lett.* **1986,** *15,* 1263–1266. doi:10.1246/cl.1986.1263
58. Honna, Y.; Isomura, E.; Enozawa, H.; Hasegawa, M.; Takase, M.; Nishinaga, T.; Iyoda, M. *Tetrahedron Lett.* **2010,** *51,* 679–682. doi:10.1016/j.tetlet.2009.11.106
59. Iyoda, M.; Hasegawa, M.; Takano, J.-i.; Hara, K.; Kuwatani, Y. *Chem. Lett.* **2002,** *32,* 590–591. doi:10.1246/cl.2002.590
60. Iyoda, M.; Kuwatani, Y.; Ueno, U.; Oda, M. *Chem. Commun.* **1992,** 158–159. doi:10.1039/c39920000158
61. Rosokha, S. V.; Kochi, J. K. *J. Am. Chem. Soc.* **2007,** *129,* 828–838. doi:10.1021/ja064166x
62. Benniston, A. C. *Chem. Soc. Rev.* **2004,** *33,* 573–578. doi:10.1039/B309963F
63. Wouters, D.; Schubert, U. S. *Angew. Chem., Int. Ed.* **2004,** *43,* 2480–2495. doi:10.1002/anie.200300609
64. Wassel, R. A.; Gorman, C. B. *Angew. Chem., Int. Ed.* **2004,** *43,* 5120–5123. doi:10.1002/anie.200301735
65. Palermo, V.; Samorì, P. *Angew. Chem., Int. Ed.* **2007,** *46,* 4428–4432. doi:10.1002/anie.200700416
66. Enozawa, H.; Hasegawa, M.; Takamatsu, D.; Fukui, K.-i.; Iyoda, M. *Org. Lett.* **2006,** *8,* 1917–1920. doi:10.1021/ol0605530
67. Enozawa, H.; Hasegawa, M.; Isomura, E.; Nishinaga, T.; Kato, T.; Yamato, M.; Kimura, T.; Iyoda, M. *ChemPhysChem* **2009,** *10,* 2607–2611. doi:10.1002/cphc.200900545
68. Enozawa, H.; Takahashi, T.; Nishinaga, T.; Kato, T.; Hasegawa, M.; Iyoda, M. *Bull. Chem. Soc. Jpn.* **2012,** *85,* 1120–1137. doi:10.1246/bcsj.20120135
69. Hara, K.; Hasegawa, M.; Kuwatani, Y.; Enozawa, H.; Iyoda, M. *Chem. Commun.* **2004,** 2042–2043. doi:10.1039/b407200f
70. Lincke, K.; Frellsen, A. F.; Parker, C. R.; Bond, A. D.; Hammerich, O.; Nielsen, M. B. *Angew. Chem., Int. Ed.* **2012,** *51,* 6099–6102. doi:10.1002/anie.201202324
71. Hanai, Y.; Rahman, M. J.; Yamakawa, J.; Takase, M.; Nishinaga, T.; Hasegawa, M.; Kamada, K.; Iyoda, M. *Chem. – Asian J.* **2011,** *6,* 2940–2945.
72. Andersson, A. S.; Kilså, K.; Hassenkam, T.; Gisselbrecht, J.-P.; Boudon, C.; Gross, M.; Nielsen, M. B.; Diederich, F. *Chem. – Eur. J.* **2006,** *12,* 8451–8459. doi:10.1002/chem.200600986
73. Hasegawa, M.; Daigoku, K.; Hashimoto, K.; Nishikawa, H.; Iyoda, M. *Bull. Chem. Soc. Jpn.* **2012,** *85,* 51–60. doi:10.1246/bcsj.20110224
74. Martin, R. B. *Chem. Rev.* **1996,** *96,* 3043–3064. doi:10.1021/cr960037v
75. Takase, M.; Yoshida, N.; Narita, T.; Fujio, F.; Nishinaga, T.; Iyoda, M. *RSC Adv.* **2012,** *2,* 3221–3224. doi:10.1039/c2ra00035k
76. Inoue, R.; Hasegawa, M.; Mazaki, Y. *Chem. Lett.* **2015,** *44,* 448–450. doi:10.1246/cl.141165
77. Nalluri, S. K. M.; Shivarova, N.; Kanibolotsky, A. L.; Zelzer, M.; Gupta, S.; Frederix, P. W. J. M.; Skabara, P. J.; Gleskova, H.; Ulijn, R. V. *Langmuir* **2014,** *30,* 12429–12437. doi:10.1021/la503459y
78. Tatewaki, Y.; Hatanaka, T.; Tsunashima, R.; Nakamura, T.; Kimura, M.; Shirai, H. *Chem. – Asian J.* **2009,** *4,* 1474–1479. doi:10.1002/asia.200900044
79. Tanaka, K.; Kunita, T.; Ishiguro, F.; Naka, K.; Chujo, Y. *Langmuir* **2009,** *25,* 6929–6933. doi:10.1021/la900219b
80. Ahn, S.; Kim, Y.; Beak, S.; Ishimoto, S.; Enozawa, H.; Isomura, E.; Hasegawa, M.; Iyoda, M.; Park, Y. *J. Mater. Chem.* **2010,** *20,* 10817–10823. doi:10.1039/c0jm02628j
81. Tanaka, K.; Matsumoto, T.; Ishiguro, F.; Chujo, Y. *J. Mater. Chem.* **2011,** *21,* 9603–9607. doi:10.1039/c1jm11161b
82. Jain, A.; Rao, K. V.; Mogera, U.; Sagade, A. A.; George, S. J. *Chem. – Eur. J.* **2011,** *17,* 12355–12361. doi:10.1002/chem.201101813
83. Akutagawa, T.; Ohta, T.; Hasegawa, T.; Nakamura, T.; Christensen, C. A.; Becher, J. *Proc. Natl. Acad. Sci. U. S. A.* **2002,** *99,* 5028–5033. doi:10.1073/pnas.082644299
84. Akutagawa, T.; Kakiuchi, K.; Hasegawa, T.; Noro, S.-i.; Nakamura, T.; Hasegawa, H.; Mashiko, S.; Becher, J. *Angew. Chem., Int. Ed.* **2005,** *44,* 7283–7287. doi:10.1002/anie.200502336

BEILSTEIN JOURNAL OF ORGANIC CHEMISTRY

Polythiophene and oligothiophene systems modified by TTF electroactive units for organic electronics

Alexander L. Kanibolotsky*[1,2], Neil J. Findlay[1] and Peter J. Skabara*[1]

Review

Open Access

Address:
[1]WestCHEM, Department of Pure and Applied Chemistry, University of Strathclyde, 295 Cathedral Street, Glasgow, G1 1XL, United Kingdom and [2]Institute of Physical-Organic Chemistry and Coal Chemistry, 02160 Kyiv, Ukraine

Email:
Alexander L. Kanibolotsky* - alexander.kanibolotsky@strath.ac.uk;
Peter J. Skabara* - peter.skabara@strath.ac.uk

* Corresponding author

Keywords:
donor; oligothiophene; organic electronics; polythiophene; semiconductor; tetrathiafulvalene

Beilstein J. Org. Chem. **2015,** *11,* 1749–1766.
doi:10.3762/bjoc.11.191

Received: 23 May 2015
Accepted: 30 August 2015
Published: 28 September 2015

This article is part of the Thematic Series "Tetrathiafulvalene chemistry".

Associate Editor: S. C. Zimmerman

Abstract

The aim of this review is to give an update on current progress in the synthesis, properties and applications of thiophene-based conjugated systems bearing tetrathiafulvalene (TTF) units. We focus mostly on the synthesis of poly- and oligothiophenes with TTF moieties fused to the thiophene units of the conjugated backbone either directly or via a dithiin ring. The electrochemical behaviour of these materials and structure–property relationships are discussed. The study is directed towards the development of a new type of organic semiconductors based on these hybrid materials for application in organic field effect transistors and solar cells.

Introduction

Sulfur-rich π-functional systems are important building blocks in materials chemistry. Among them, tetrathiafulvalene (TTF) electron donor and polythiophene (PT) conjugated systems are highly popular classes of organic compounds which have shown fascinating conducting and electronic properties. The advantages of PT-based materials are their synthetic versatility, excellent film-forming properties and potential to increase the dimensionality of charge carrier transport [1] by involving π–π stacking interactions. Varying the substituents of the conjugated backbone allows control over the polymer's effective conjugation length and electronic properties, whilst also influencing the extent of inter-chain interactions. Two of the most studied polythiophene materials for organic electronics are regioregular poly(3-hexylthiophene) (P3HT) [2,3] and poly(3,4-ethylenedioxythiophene) (PEDOT) [4], which is highly conductive in its doped state. P3HT has become a benchmark polymer semiconductor for both bulk hetero-junction solar cells (BHJSCs) [5] and organic field effect transistors (OFETs) [6,7], whereas the PEDOT:poly(styrene sulfonate) salt (PEDOT:PSS) was originally investigated for antistatic applications but is now commercially available for its use as a hole-injecting/collecting material for organic light emitting diodes (OLEDs) and BHJSCs. So far, various electroactive units have been anchored aside the polythiophene backbone, including ferrocene [8], por-

phyrin [9], 2-carboxyanthraquinone [10], 1,3-dithiole-2-ylidenefluorene [11,12], dithiinoquinoxaline [13,14] and fullerene C_{60} [15,16]. The incorporation of acceptor units into a conjugated network is a standard way to narrow the HOMO/LUMO band gap and examples of such units include dioxopyrrolopyrrole (DPP) [17-19], benzodifuranone [20] and boron-dipyrromethene (BODIPY) [21,22].

As a different class of electroactive materials, TTF derivatives are well-known as reversible redox systems with low potentials of oxidation to cation radical and dication species. The high level of stability observed for the oxidised TTF π-electron system arises from the aromatic nature of the oxidised 1,3-dithiolium rings and this has triggered tremendous efforts directed toward the synthesis of compounds with TTF donor units and subsequent investigation of their properties. Since the first discovery of the semiconducting properties of TTF and its cation radical [23], and the metallic behaviour of the TTF-TCNQ charge transfer complex [24], great attention was focused on the preparation of TTF mixed valance state materials, which showed superconducting properties [25]. Fusing the TTF unit with dithiin rings in bis(ethylenedithio)tetrathiafulvalene (BEDT-TTF) led to the extension of 1D π–π stacking intermolecular interactions in a donor sheet of a mixed valance state system to 2D with a significant contribution from S···S non-covalent interactions [26]. This gave a record transition temperature among TTF mixed valence ambient pressure superconductors in the salt κ-(BEDT-TTF)$_2$Cu[N(CN)$_2$]Br [27]. In an attempt to create macromolecular compounds with multi-electron redox activity and to further increase the dimensionality of their intermolecular interactions in the solid phase, the TTF units were incorporated into dendritic structures [28-32]. The extraordinary propensity of TTF and its doped species to aggregate was the reason for using this unit in the design of gelators [33,34].

Combining the exceptional donor strength of TTF and excellent film-forming properties of a conjugated polymer (CP) opens up the possibility to create promising materials with interesting redox behaviour. So far the TTF unit has been used for redox modification of various CP systems [35] including incorporation within the conjugated backbone [36,37], as a pendant unit [38-40] and direct fusion to the π-conjugated system of the polymer [41,42]. Incorporation of a TTF unit into a PT architecture allows the creation of interesting hybrid redox systems with a wide range of electro-activities. The goal of this review is to provide an update on the synthesis of TTF-PT hybrid conjugated systems, their properties and their application to organic electronics. Both electrodeposition and chemical polymerisation will be considered as methods of producing the PT conjugated backbone. In some cases poly(ethynylene/vinylene) homologues will be considered for comparison. Additionally, monodispersed tetrathiafulvalene-oligothiophene (TTF-OT) conjugated systems will be discussed as their well-defined structures provide a stronger insight into structure–property relationships.

Review

PT conjugated systems with TTF units within the polymer backbone or as pendant units

The most straightforward way to modify PT conjugated systems is to incorporate the TTF unit into the polymer backbone or attach it as a pendant unit, as only minor modifications to the synthesis of the TTF/thiophene monomer are required. Both chemical [43] and electrochemical polymerisation [44] have been used to incorporate a TTF moiety within the polythiophene backbone. Yamamoto coupling of diiodo monomers **1a** and **1b** provided polymer **1c**, albeit with a modest molecular weight (M_w = 5800 Da) compared to that of the polymer **1d**, which was obtained by Sonogashira coupling of **1b** with **1e** and exhibited a partial solubility in THF with M_w = 610000 Da (THF soluble fraction) [43] (Scheme 1).

Polymer properties in the solid state are hugely important for organic electronics applications, with the electronic properties of materials being greatly affected by film morphology. The

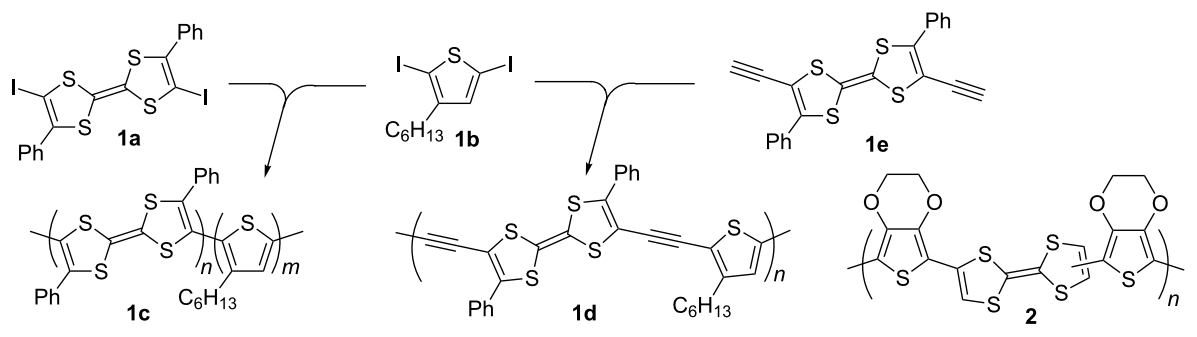

Scheme 1: The synthesis of PT based conjugated systems with the TTF unit incorporated within the polymer backbone.

electropolymerisation technique creates a simple test for the viability of a certain structural motif in the PT chain and is considered both as a potential route for the synthesis of a new functional CP and also as a method for the modification of an electrode surface [45]. The electrodeposition of a polymer has a number of advantages over any chemical protocol: 1) it is cheap and can be performed on a very small scale; 2) it requires no reagent or catalyst and is very clean; 3) due to the interfacial nature of a polymer growth the spectro-electrochemical investigation of the polymer film is straightforward; 4) it provides control over the morphology through the choice of solvent, electrolyte and/or the method of electrodeposition. TTF has been incorporated into a CP backbone by electropolymerisation of its bis(EDOT) derivative to afford polymer **2** [44] (Scheme 1). All the polymers (**1c,d** and **2**) exhibited electroactivity of the TTF units. Due to a break in conjugation of the polymers in their neutral state there is no electrochemical signature of the PT backbone. As such, the aforementioned systems cannot be considered as true TTF-PT systems.

The first example of the electrochemical preparation of PT with a pendant TTF-carboxylic unit (**3**) was reported by the Bryce group [46] (Scheme 2). The mixture of CH_2Cl_2 with $PhNO_2$, to supress the electrochemical activity of TTF during electropolymerisation, was used as a solvent. Another example of a TTF-PT hybrid polymer (**4**), now with an ester linkage between the tetrathio-TTF derivative and the PEDOT polymer backbone, has also been reported [47]. The TTF-functionalised EDOT monomer unit allowed the authors to manage the electropolymerisation in an acetonitrile:CH_2Cl_2 mixture using both potentiodynamic and potentiostatic electrodeposition. Nevertheless, the labile ester bond and its potential cleavage remain an issue due to formation of acid upon electropolymerisation.

Roncali and co-workers used more reliable ether bonds to anchor a TTF moiety to a thiophene monomer via a long aliphatic spacer group, avoiding the effect of steric interactions between pendant TTF units and increasing the conjugation length of the PT backbone (Scheme 2). They successfully electropolymerised TTF-modified thiophene monomer **5a** to polymer **6a** from a nitrobenzene monomer solution [48]. Cyclic voltammetry of the polymer thin film revealed the splitting of the first oxidation wave during the cathodic run, which the authors attributed to a stepwise reduction from the aggregated radical cation to an intermediate mixed valence state, then further reduction to the neutral species. To decrease the difference in the oxidation potential of TTF and that of the thiophene backbone of the monomer, the TTF-modified bithiophene compounds **5b–d** were used as monomers for electropolymerisation to **6b–d** [49]. The appearance of an additional, well-defined oxidation wave in the CV, as the first oxidation wave was split in both anodic and cathodic runs, was evident for all polymers, but clearest for **6c**. This was assigned to the formation of a mixed valence state and aggregated cation radical [50]. The relative increase in the peak current during oxidation to the dication, compared to that of cation radical formation, was explained by an additional contribution to charge transport from the doped PT backbone [49]. The oxidation of the latter did not contribute significantly to the CV of the polymer films due to the much stronger electrochemical response of the TTF. However, from a separate experiment in which the authors electropolymerised monomer **5c** (2×10^{-2} M) in the presence of a double excess of a non-modified bithiophene monomer **7** [49], the contribution from the PT backbone oxidation in the CV of the final copolymer was clear. However, it was unresolved from the wave of TTF^{2+} formation during the anodic run (Figure 1).

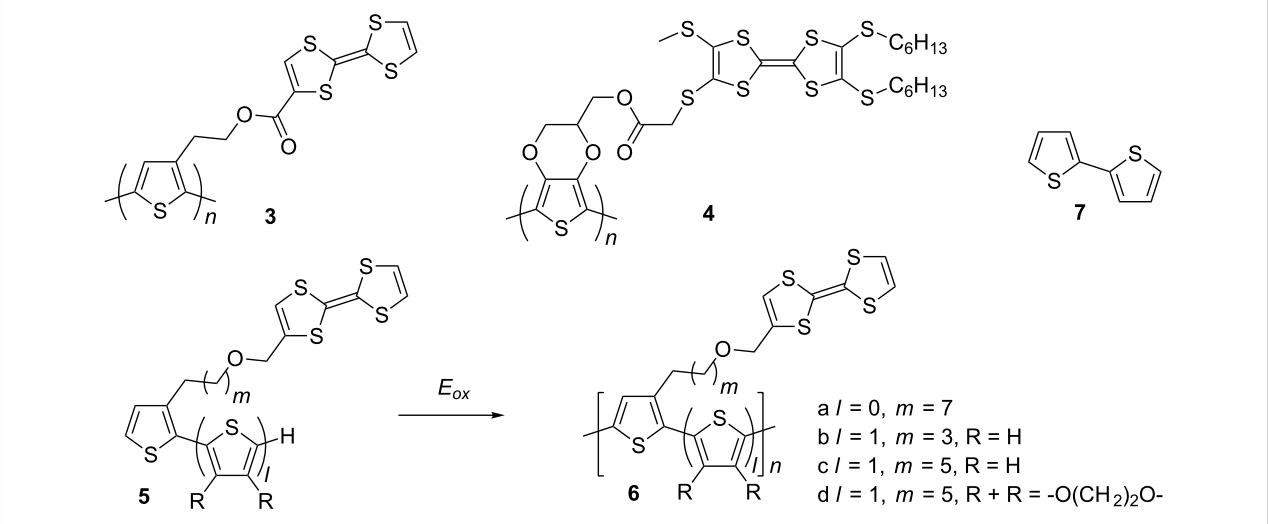

Scheme 2: PT with pendant TTF units, prepared by electropolymerisation.

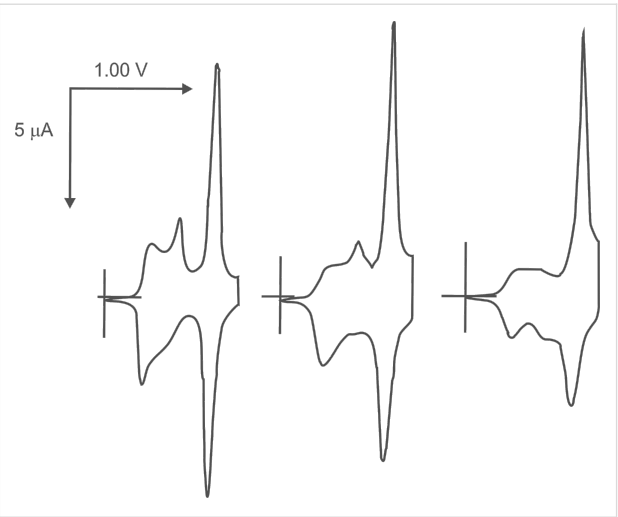

Figure 1: Cyclic voltammograms of copolymers electrodeposited from nitrobenzene solutions of TTF modified monomer **6c** and nonsubstituted bithiophenes **7**. Left: 2×10^{-2} M of **6c**; middle: 2×10^{-2} M of **6c** + 1×10^{-2} M of **7**; right: 2×10^{-2} M of **6c** + 4×10^{-2} M of **7**; ref. SCE, 0.1 M (TBA)PF_6 in acetonitrile as an electrolyte. Reproduced with permission from [49]. Copyright 1998 Wiley-VCH.

An alternative way of preparing PT hybrid materials with TTF pendant groups was to modify the pre-polymerised PT containing an appropriate functionality with a TTF derivative. The Roncali group reported electropolymerisation of EDOT monomers **8a,b** bearing a ω-iodo-functionalised aliphatic chain to polymers **9a,b**, which was followed by the heterogeneous reaction of the polymeric film with TTF thiolates **10a** [51] and **10c** [52] to produce the polymers **11a–d** (Scheme 3). The polymers **11a,c** were also prepared by electropolymerisation of the corresponding TTF functionalised monomers **12a,c** [52]. The electrochemical response from the polymeric film of **11c**, prepared by functionalising prepolymerised PEDOT **9a** with thiolatoTTF **10c**, and that prepared by direct electropolymerisation of **12c** turned out to be very similar, confirming that the heterogeneous derivatisation of **9a** with **10c** was rapid and quantitative with no significant effect on the integrity of the polymer. The crown ether TTF modified polymers **11c,d** were tested for electrochemical recognition of Ba^{2+} ions. At [Ba^{2+}] saturation concentration of 4 mM the shifts of the first CV peak for **11c** and **11d** films were +60 and +30 mV with a TTF electrode coverage of 1.4×10^{-9} and 9×10^{-9} mol/cm^2, respectively.

A recent example of the chemical preparation of PT with pendant TTF-units has been reported [53] (Scheme 4) where direct arylation polymerisation of quaterthiophene **13a** and 3-(acetoxymethyl)thiophene (**13b**), followed by acidic hydrolysis of the ester groups in polymer **13c**, provided the polymer **13d** with hydroxy groups for further modification by ω-bromooctyloxymethylTTF **13f** . The CV of the final PT-TTF compound **13e** showed mainly the characteristics of the PT backbone; due to the low content of the TTF unit in the polymer **13e**, the two oxidation waves related to formation of TTF cation radical and dication were not apparent in the CV of the film, but were discernible in solution state. Pure **13e**, and **13e** with a small amount of the parent poly(3,3'''-didodecyl-2,2':5',2'':5'',2'''-quaterthiophene) (PQT12) (5 or 10 wt %), did not exhibit any OFET activity due to hole trapping by the TTF unit. This hole trapping was explained to be the reason for a negative Seebeck coefficient of the non-doped polymer **13e** and was used for sensing trinitrotoluene (TNT) using the drain-source current-increase response to TTF-TNT complexation in an OFET fabricated from **13e** with 5% of PQT12.

Conjugated OT systems with fused TTF units

Synthesis of the monomer units

Incorporation of a TTF unit into a PT architecture via fusion to the polymer backbone allows the realisation of highly diverse electroactive conjugated systems with different contributions to the properties from each of the components. In contrast to polymers where TTF is attached as a pendant unit or incorporated

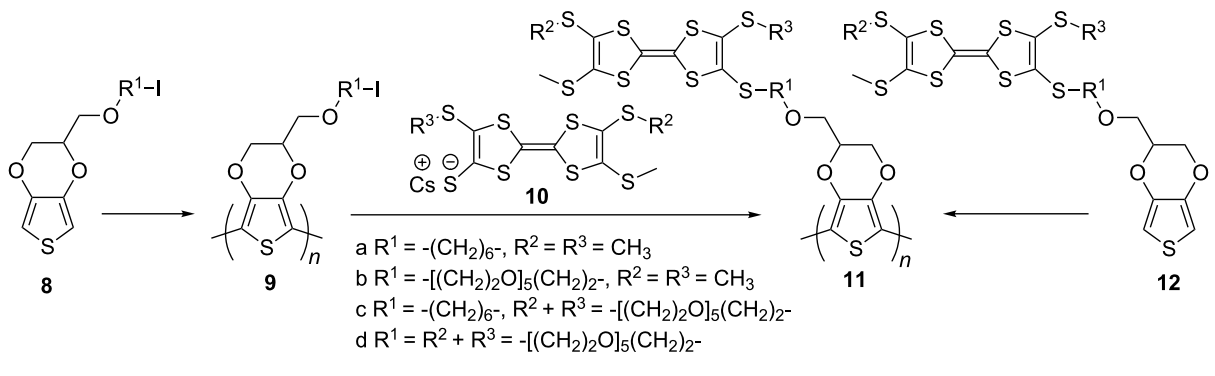

Scheme 3: PT with pendant TTF units prepared by electropolymerisation and post-modification of polymerised PT through iodoalkyl functionality.

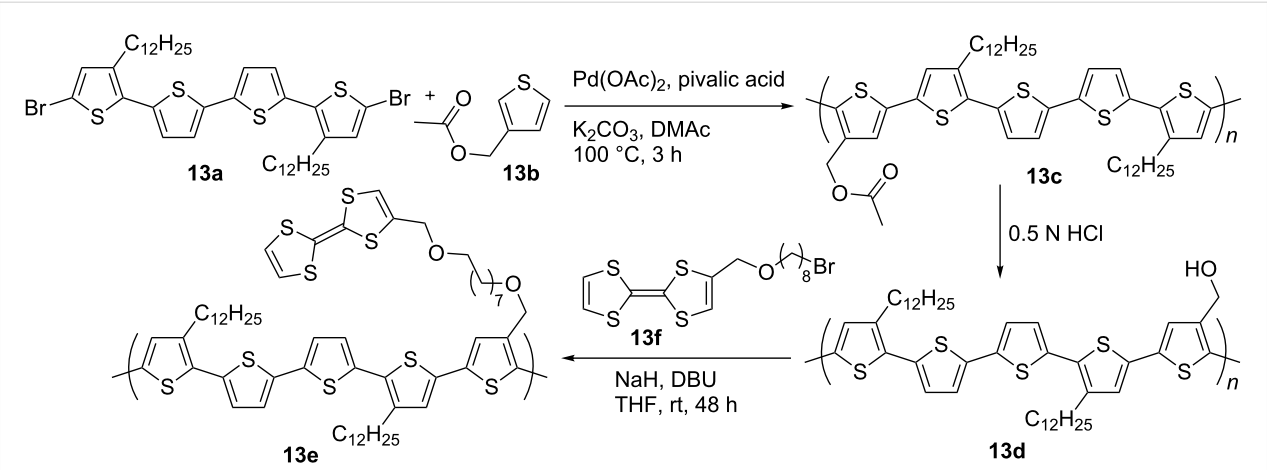

Scheme 4: Synthesis of PT with pendant TTF by post-modification of the polymer prepared by direct arylation.

within a PT backbone, the construction of the TTF unit in this case is normally performed through coupling of the corresponding dithiol units, with one or both of them already fused to the monomer thiophene backbone precursor. The retrosynthetic scheme for these monomers with direct fusion of the TTF unit to a thiophene **14a–c** is shown in Scheme 5, with the key building block thieno[3,4-*d*][1,3]dithiole-2-one **15a–c**.

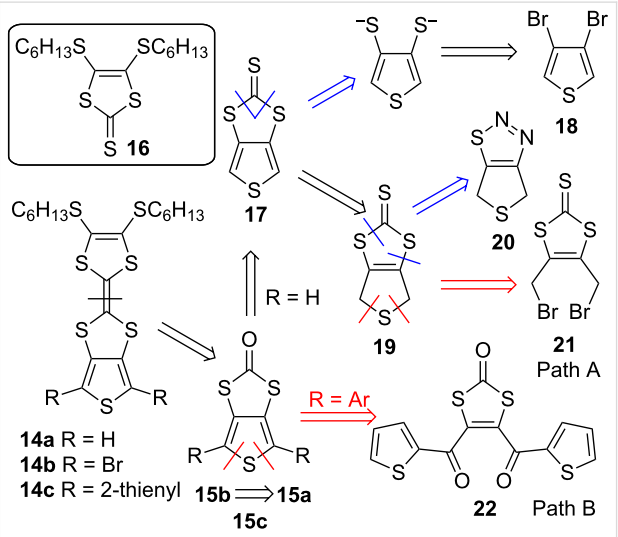

Scheme 5: Retrosynthetic scheme for the synthesis of the monomer building block which is required for the preparation of PT with TTF directly fused to the polymer backbone. Bis(bromomethyl) derivative **21** and diketone **22** are starting compounds for synthetic pathways A and B, respectively.

Where there is no substitution at the α-position of the thiophene monomer, e.g., **14a**, triethylphosphite mediated heterocoupling of **15a** with 4,5-bis(hexylthio)-1,3-dithiole-2-thione (**16**) proceeds in low yield (20–30%) [54]. However, the same procedure for the synthesis of dibromo derivative **14b** turned out to be more effective, with the monomer **14b** being isolated in 70% yield [55]. The starting compound required for this, 4,6-dibromothieno[3,4-*d*][1,3]dithiole-2-one (**15b**), can be efficiently obtained by brominating compound **15a**, which in turn is synthesised by mercury(II) acetate assisted transchalcogenation reaction from the corresponding thione **17**. Unsubstituted thieno[3,4-*d*][1,3]dithiole-2-thione (**17**) can be constructed by building up either of its two rings, involving cyclisation of a suitable precursor already containing one existing heterocycle. The construction of the 1,3-dithiole-2-thione unit of **17** can be completed using 3,4-dibromothiophene (**18**) as a starting material [56], or by oxidation of dihydroderivative **19** obtained from 4,6-dihydrothieno[3,4-*d*][1,2,3]thiadiazole (**20**) [57,58]. However, the most reliable method for the synthesis of 4,6-dihydrothieno[3,4-*d*][1,3]dithiole-2-thione (**19**) is cyclisation of 4,5-bis(bromomethyl)-1,3-dithiole-2-thione (**21**) [59] (synthetic pathway A).

For 4,6-diaryl substituted thienodithiole-2-ones, e.g., 4,6-di(thiophen-2-yl)thieno[3,4-*d*][1,3]dithiol-2-one (**15c**), construction of the thiophene directly onto the dithiole ring seems to be the only strategy, which can be readily achieved by reductive cyclisation of diketone **22** [60] (synthetic pathway B). Compound **22** is normally synthesised by transchalcogenation from the corresponding 1,3-dithiole-2-thione derivative. One method for the synthesis of 1,3-dithiole-2-thione with electron-acceptor substituents [61] is the reaction of readily accessible ethylene trithiocarbonate (**23**) [62] with electron-deficient acetylene compounds (Scheme 6). By reacting **23** with **24a** this method provides diester **25a** in good yield [63]. Compound **25a** can be reduced to diol **25d** [64] and further converted by either the Appel method [59] or by reaction with PBr_3 [65] into dibromomethyl compound **21**, which is required for synthetic pathway A.

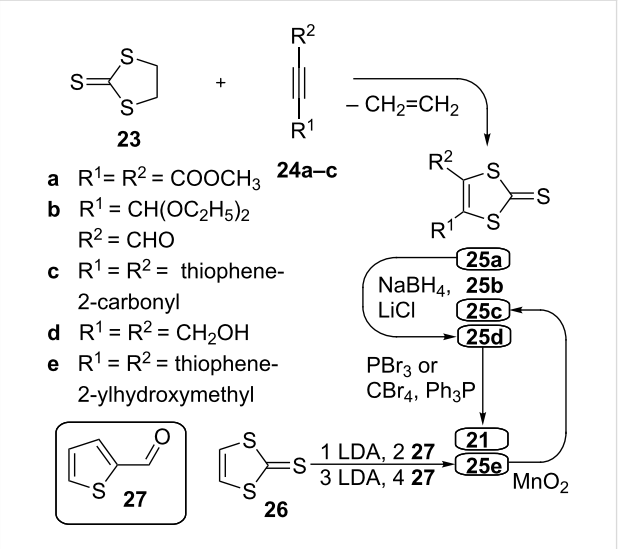

Scheme 6: Synthesis of bisfunctionalised derivatives of vinylene trithiocarbonate **21** and **25c** required for synthetic pathways A and B, respectively.

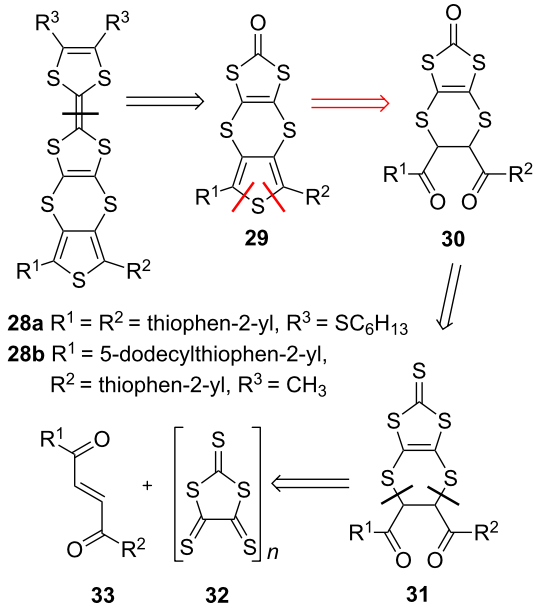

Scheme 7: Retrosynthetic scheme for the synthesis of the building block which is required for the preparation of PT with TTF fused to a polymer backbone via a dithiin ring (synthetic pathway C).

Even though the reaction of **23** with acetylene compound **24b** (containing only one electron-withdrawing group) is efficient, affording **25b** with a 60% yield [66], attempts to invoke cycloaddition of **23** and **24c** in a similar manner led to a poor yield of **25c** (8%) [60]. An efficient method for the synthesis of **25c** – a compound required for synthetic pathway B – was found to be repeated sequential lithiation of vinylene trithiocarbonate (**26**) [67] followed by subsequent trapping of the lithium organic species with thiophenecarboxaldehyde **27** [60]. The diol **25e**, formed as a product of this reaction, is unstable and undergoes various rearrangments [68,69] in acidic conditions. Hence, it is preferably oxidised directly to the more stable diketone **25c** without delay.

The retrosynthetic scheme for the monomer units **28a,b** with thieno-dithiino-dithiole type fusion is shown in Scheme 7. Similar to the aforementioned synthetic pathway B, the strategy for the synthesis of **29** involves construction of the thiophene ring by cyclisation of diketone **30** (synthetic pathway C).

The diketone **31** is constructed through the cycloaddition reaction of diacylethene **33** with oligomer **32**, readily available by oxidation of bis(tetraethylammonium) bis(2-thioxo-1,3-dithiole-4,5-dithiolato)zincate with iodine [70]. This versatile strategy can be applied where R^1 and R^2 are either aromatic or aliphatic [71]. The application of the strategy has been utilised for both symmetric **28a** [60] and asymmetric **28b** systems [72].

Polymers with fused TTF units

The electronic characterisation for monomer units **14a–c** and **28a** is shown in Table 1.

Table 1: Electrochemical and UV–vis absorption data for the monomer compounds **14a–c**, and **28a** in CH_2Cl_2 solution. The oxidation potentials are shown vs Ag/AgCl reference.

Compound	$E^{1/2}{}_{1ox}$, V	$E^{1/2}{}_{2ox}$, V	$E^{p}{}_{3ox}$, V	λ_{max}, nm
14a	0.74	1.10	2.18	324
14b	0.95	1.31	–	337
14c	0.64	1.02	1.55	373
28a	0.64	0.99	1.52	344

Electropolymerisation of monomer compounds **14a**, **14c** and **28a** [73] was attempted. Due to the high oxidation potential (see Table 1) of the thiophene unit in the fused system **14a** (2.18 V vs Ag/AgCl), electropolymerisation for this compound was unsuccessful (Scheme 8). Surprisingly, the other two monomers, both with a similar, low $E^{p}{}_{3ox}$ – attributed to oxidation of the terthiophene unit (**14c** (1.55 V vs Ag/AgCl) and **28a** (1.52 V vs Ag/AgCl)) – showed different behaviour upon repetitive voltammetric cycling over the range of 0.0–1.6 V vs Ag/AgCl. Although upon electrodeposition of **14c** onto the surface of a working electrode a red film appeared, it was non-polymeric in nature. On the contrary, the electropolymerisation of **28a** under the same conditions exhibited a reproducible polymer growth of **34**.

The CV of polymer **34** exhibited the characteristic electrochemical signature of the TTF-unit – two reversible oxidation waves

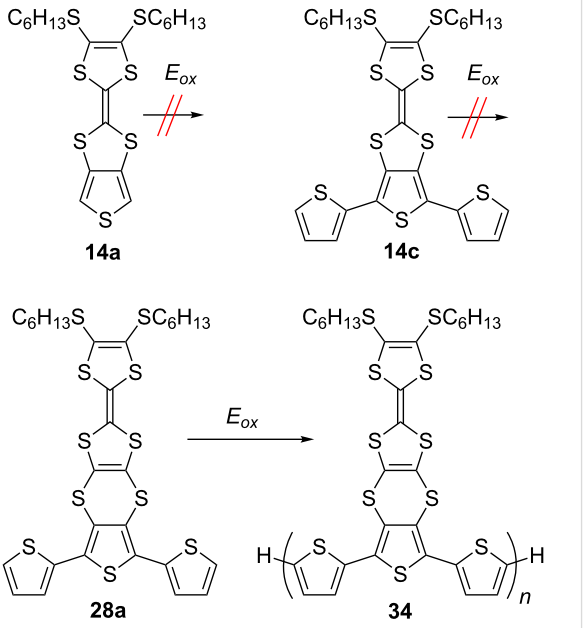

Scheme 8: The monomers **14a**, **14c** and electropolymerisation of **28a**.

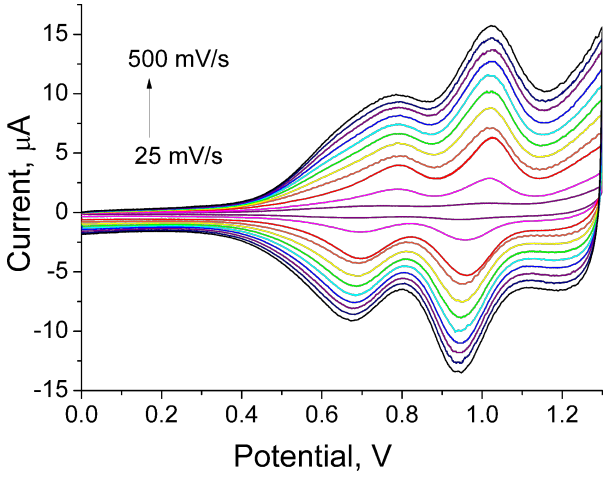

Figure 2: Cyclic voltammograms of a thin film of **34** at various scan rates (25 mV, 50 × *n* mV/s, *n* = 1–10). Adapted with permission from [73].Copyright 2000 The Royal Society of Chemistry.

to a cation radical and a dication, with a linear dependence of peak currents upon scan rates. Similar to PT systems with a pendant TTF unit [49], the peak current of the second wave was noticeably higher than that of the first (Figure 2). There are three possible reasons for such behaviour that can be considered: 1) the interaction between the TTF units would cause the partial splitting of the first oxidation wave with poorly resolved components – attributed to oxidation of the neutral TTF into a mixed valence state and further to an aggregated cation radical; 2) contrary to formation of the cation radical, the oxidation to the dication is not limited by charge transport through the film as the conductivity of the latter is ensured by both charged TTF species and the polaron charge carrier route; 3) the oxidation potential of the polymer backbone is likely to be in the same region as the potential for TTF^{2+} formation, although the contribution to the current from the normally irreversible oxidation of the PT backbone would be small due to the high TTF content in the polymer.

The as grown polymer exhibited two broad absorption peaks at 459 and 833 nm, indicating that the polymer film exists in a doped state. The aforementioned peaks can be assigned to the cation radical of the TTF unit and are very similar to the absorption features of tetraalkylthiotetrathiafulvalene cation radical [31,32]. The doped film exhibited excellent stability and its absorption characteristics did not change despite treatment with hydrazine. However, de-doping was achieved with repetitive scanning of the polymer film over the range of −0.3–0 V vs Ag/AgCl for 2 hours [73]. After de-doping, the polymer **34** exhibited an absorption band with a maximum at ca. 490 nm and extending to ca. 736 nm, with an optical band gap of 1.69 eV (Table 2). For a simple π-conjugated polymer the difference between the oxidation and reduction onsets constitute the electrochemical band gap [74,75]. For polymer **34**, if the first oxidation wave was taken into consideration, the electrochemical band gap was found to be 1.39 eV. However, if the second oxidation wave was considered the band gap was calculated to be 1.81 eV, a value slightly higher than the aforemen-

Table 2: Characterisation of the polymers **34**, **35**, **37**, and **39**.

Polymer	M_n, Da	PDI	Condition	$E^{1/2}_{1ox}$, V	$E^{1/2}_{2ox}$, V	E^{pc}_{1red}, V	λ_{max}, nm (E_g^{opt}, eV)	
							CH_2Cl_2	Film
34	–	–	Film	0.77	1.09	−1.21	–	494 (1.69)
35	3437	1.32	CH_2Cl_2	0.81	1.10	−1.15	466(1.86)	487 (1.75)
37	4886	2.40	CH_2Cl_2	0.69	1.07	−1.65	456	496 (1.82)
39	3158	1.19	CH_2Cl_2	0.89	1.31	–	578	–
			Film	0.91[a]	1.35[a]	−0.96	–	598 (1.45)

[a]Due to the irreversible nature of the oxidation waves, the anodic peak values E^{pa}_{ox} are shown.

tioned optical band gap of the polymer (1.69 eV). This is to be expected considering that upon oxidation of the PT backbone the electron must be removed from a polymer already containing oxidised TTF moieties. The agreement between the optical and electrochemical band gaps in this case infers that the oxidation of the PT backbone in the polymer **34** occurs at the potential close to the second oxidation wave of the TTF unit. A more detailed spectroelectrochemical study [76] of the polymer **34** film deposited on ITO glass revealed an electrochemical signature of both oxidised TTF species ($TTF^{+\bullet}$, TTF^{2+}) [31,32] and polarons (vide infra).

To investigate the properties of PT-TTF systems with the TTF moiety directly fused to a thiophene backbone, chemical polymerisation of suitably functionalised monomers was carried out (Scheme 9). For all chemically synthesised polymers a Soxhlet extraction (with methanol, acetone and CH_2Cl_2) has been used as a method of purification and to narrow their polydispersity. Using Yamamoto coupling compound **14b** was polymerised. Use of DMF alone as solvent led to a polymer that was sparingly soluble in CH_2Cl_2 [77]. However, a mixture of DMF:toluene (1:1) as a medium for Yamamoto polymerisation afforded polymer **35** as a dark purple solid in 95% yield [55]. Polymer **35** is the analogue of the polymer which could have been obtained had the monomer **14a** been suitable for electropolymerisation, while Stille coupling of dibromo monomer **14b** with 5,5'-bis(trimethylstannyl)-2,2'-bithiophene (**36**) [78] was used to circumvent problems with the electropolymerisation of terthiophene **14c**, and to chemically synthesise the analogous polymer **37** [76]. By reacting monomer **14b** and 1,2-bis(tributylstannyl)ethylene (**38**) [79], polymer **39** was synthesised using the Stille coupling protocol [76].

The number average molecular weight (M_n) revealed by GPC analysis (Table 2) corresponds to about 7 thienoTTF monomer units per polymer chain for **35** and **37**, and about 6 units for **39**. MALDI–TOF MS characterisation was only successful for polymer **39** and showed a series of peaks with a mass difference of 516 Da, corresponding to the mass of the 2-(4,5-bis(hexylthio)-1,3-dithiol-2-ylidene)thieno[3,4-*d*][1,3]dithiol-4,6-diyl-alt-vinylene repeating unit. The mass spectra confirmed that the polymer was end-capped with a thienoTTF unit, with the terminal bromo substituents still intact. The highest mass peak of 5290 Da registered by MALDI–MS corresponds to 10 thienoTTF units, which is significantly higher than the aforementioned M_n measured by GPC.

Table 2 displays the electrochemical and UV–vis absorption characteristics of the polymers. The peaks corresponding to the absorption maximum occurred in the range 450–500 nm for polymers **34**, **35** and **37**, with the optical band gap being in the range of 1.7–1.9 eV. When comparing the spectra in CH_2Cl_2 solutions to those of the solid film, the red shift in absorption is due to the emergence of π–π interactions in the solid state. Compared to the aforementioned polymers, poly(thienylene-vinylene) (PTV) **39** exhibited a red-shifted absorption with maxima occurring at 578 and 598 nm in CH_2Cl_2 and as a thin film, respectively.

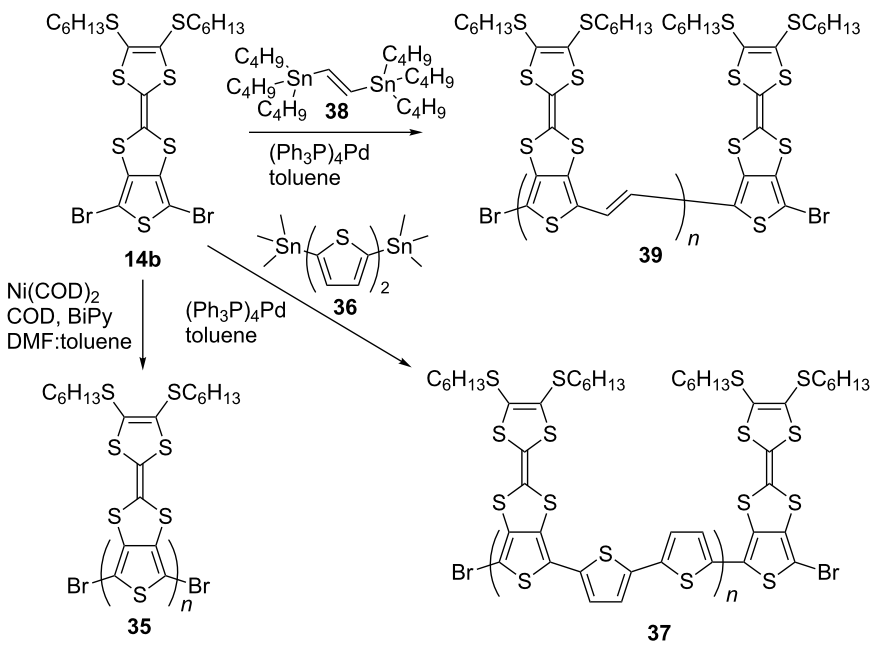

Scheme 9: Chemical polymerisation of **14b** into polymers **35**, **37** and **39**.

The CVs in CH_2Cl_2 solution of **35** and **37** (Table 2) revealed two quasi-reversible oxidation waves that are shifted to lower potentials compared to the corresponding reversible oxidation waves of monomer **14b** (+0.91 and +1.31 V, see Table 1). Monomer **14b** has a weaker donating ability due to the strong electron-withdrawing inductive effect of the terminal bromo substituents, while the PTV polymer **39** exhibited almost identical oxidation potentials to monomer **14b**. On the other hand, both oxidation waves of the TTF unit in polymers **35**, **37**, and **39** shifted to significantly higher potentials in comparison to those of the non-brominated monomer compound **14a** (+0.46 and +0.83 V, see Table 1) [54]. This can be explained by: 1) the electron-withdrawing effect of the polymer backbone and 2) the electrostatic interaction between the oxidised TTF units within the polymer backbone. The degree to which these polymer oxidation potentials shift is in the order **37** < **35** < **39**, which roughly follows the expected charge density of the doped polymer backbone. The chronocoulometry experiment during bulk electrolysis of **35** and **39** revealed that approximately two electrons were released per monomer unit; this is much more than one would expect from a simple PT that normally donates one electron per 3–10 thiophene units [80]. To the best of our knowledge, **35** is the most dopable polythiophene in the literature, with respect to the level of oxidation that is achieved per repeating unit, the excellent electrochemical reversibility observed, and the modest potential window in which the highly doped state is attained. Even for a stable doped system, for example a PEDOT sample heavily doped with polystyrenesulfonic (PSSH) or *p*-toluenesulfonic (TosH) acid, the doping level is 3–5 units per one positive charge [81,82]. So, the presence of TTF units fused to each thiophene of the PT backbone creates a polymer with a greatly enhanced p-doping ability. The direct fusion in this case of two electroactive units (TTF and PT) inhibits any electrochemical activity from the polymer backbone and the electrochemistry of the material is dominated by the TTF unit.

The inhibition of the polymer backbone's electrochemical activity was confirmed by spectroelectrochemistry of **39**, which indicated no change of the π–π* transition upon applying potentials up to +2.0 V. The CV of **39** shows an irreversible first oxidation wave, and the band gap calculated from the first oxidation onset agreed well with the optical band gap. The former indicates the possibility of significant interchain interactions between the TTF unit and the polymer backbone.

Upon oxidation, the film of polymer **37** exhibited a broad ill-defined band extending from 700 nm into the near infrared range. The intensity of the π–π* transition in this case diminished upon oxidation, but this band still remained the most intense feature of the spectrum across the entire potential range (Figure 3a). The spectoelectrochemistry of polymer **34** revealed more drastic changes in the spectra upon oxidation of the film, where the resolved absorption signature of a cation radical, dication and polaron can be observed (Figure 3b). As the applied potential is increased, two peaks appear: one at 460 nm that overlaps with the backbone π–π* transition, and a second centred at 800 nm. Those peaks were observed in the spectrum of the doped polymer film (Figure 3b) and could be assigned to the absorption of the cation radical of the TTF unit. With further increase in the applied potential the TTF cation radical UV–vis signature diminishes and a strong absorption band at 700 nm,

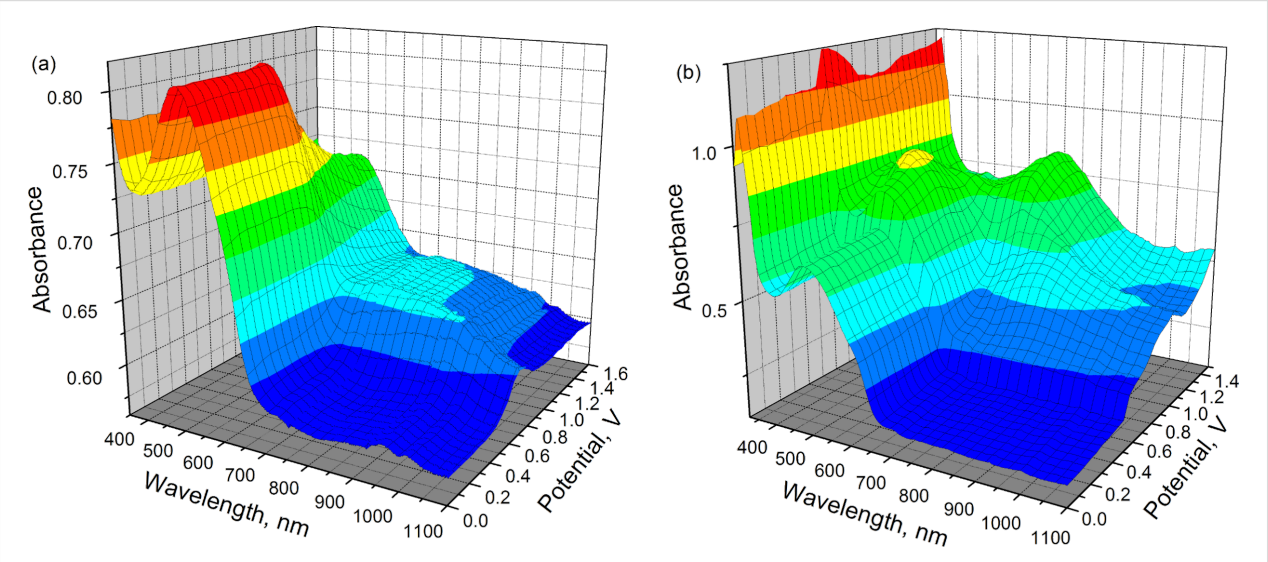

Figure 3: Spectroelectrochemistry of polymers **37** (a) and **34** (b) as thin films deposited on the working electrode. Adapted with permission from [76]. Copyright 2006 The American Chemical Society.

along with a broad absorption in the NIR region, appear. The former can be assigned to the absorption of the dication of the TTF unit and both bands to a polaron formation. Therefore, for **34** the spectroelectrochemistry unequivocally confirms the electrochemical activity of the polymer backbone, which is involved in the formation of polarons at potentials close to the second oxidation potential of the TTF unit.

The polymer **39**, which has the lowest band gap, was tested as a donor material for BHJSCs with $PC_{61}BM$ as the acceptor. The OPV performance is shown in Table 3. The estimation of HOMO and LUMO levels by electrochemical analysis gave values of −5.24 and −3.78 eV, respectively, indicating a small offset between the LUMO of **39** and $PC_{61}BM$ (ca. −3.8 eV) [83,84]. This is the main reason for the small short circuit current density (J_{sc}) and low efficiency of the cell. Due to the possible presence of efficient interchain interactions between the TTF units and the PTV backbone (vide supra) in the film of polymer **39**, another important factor that should be considered is photoinduced charge transfer. Photoexcitation of **39** can lead to an increase in the donor ability of the TTF unit due to a greater contribution of the quinoidal structure to the excited polymer backbone, and foster electron transfer from the TTF moiety to $PC_{61}BM$ (Scheme 10). However, further hole transfer from the TTF unit to the PTV backbone may still limit dissociation of the $(TTF^{+\bullet})(PC_{61}BM^{-\bullet})$ bound pair.

The surprising inertness of **14c** towards electropolymerisation can be circumvented by replacing the thiophene units in the monomer terthiophene backbone with more electron-rich moieties, such as pyrrole and EDOT. Bisthienylpyrrolo-TTF monomer compounds **40** and **41**, which were synthesised by Stille coupling of diiodopyrrolo-TTF **42** with trimethylstannyl derivatives of EDOT **43** and hexylthiophene **44**, were efficiently electropolymerised (Scheme 11) into polymers **45** and **46**, respectively [85]. Note that these latter two polymers are analogues of polymer **37**. Polymer **47**, synthesised by Stille polymerisation of **42** and **38**, is an analogue of the polymer **39**. A direct comparison between the obtained polymers with pyrroloTTF and thienoTTF units showed that the incorporation of an electron-rich pyrrole unit into the conjugated backbone leads to materials with a wider band gap as they are less stable

Table 3: Performance of BHJSCs fabricated from the thiophene-TTF hybrid systems.

Compound	Acceptor	Solvent	P_{inc}, mW cm^{-2}	J_{sc}, mA cm^{-2}	V_{oc}, V	FF	PCE, %
39	$PC_{61}BM$	CB	80	0.68	0.52	0.30	0.13
48	none	o-DCB	100	1.8	0.61	0.28	0.31
48	$PC_{71}BM$	$CHCl_3$	100	4.9	0.66	0.31	1.0
48	$PC_{71}BM$	o-DCB	100	8.0	0.71	0.32	1.8
54 (n = 1)	$PC_{71}BM$	$CHCl_3$	100	7.44	0.70	0.33	1.7
54 (n = 1)	$PC_{71}BM$	o-DCB	100	9.81	0.78	0.33	2.5

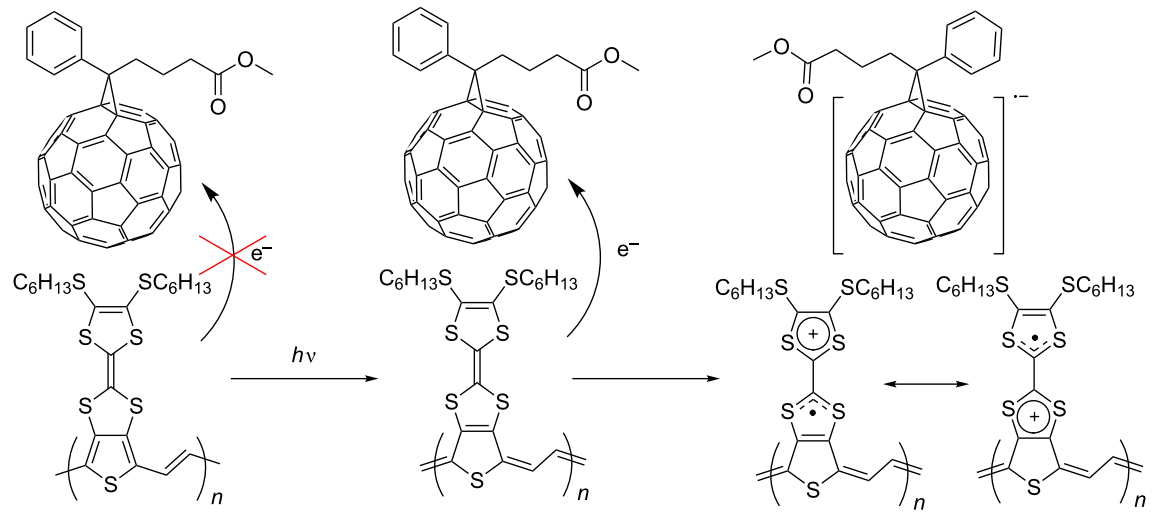

Scheme 10: Photoinduced charge transfer from the TTF of polymer **39** to $PC_{61}BM$.

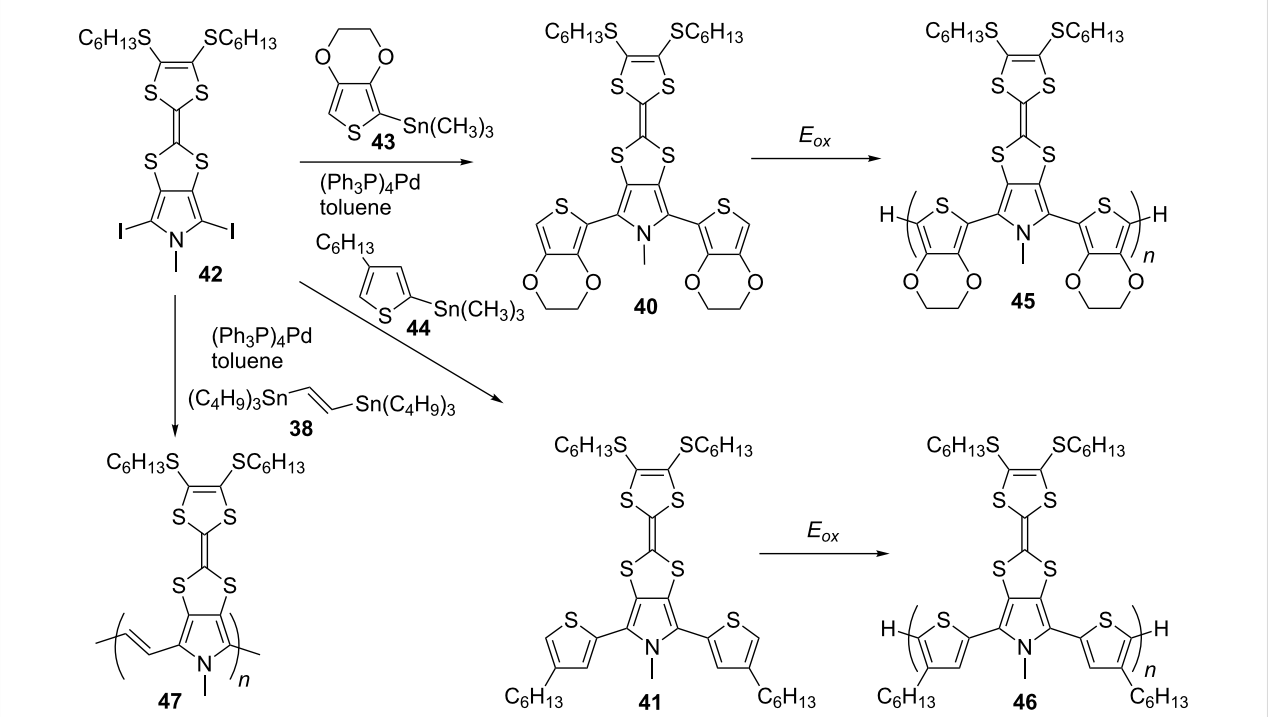

Scheme 11: Electropolymerisation of **40** and **41** into polymers **45** and **46**, respectively, and Stille polymerisation of **42** into polymer **47**.

to n-doping. The pyrrole unit lowers the oxidation potentials of the TTF moieties but the electrochemical dominance of the TTF is lost in the pyrrolo-TTF polymers.

Another analogue of polymer **37** includes the 2,5-bis(2-octyldodecyl)-1,4-dioxopyrrolo[3,4-*c*]pyrrole (DPP) unit incorporated within the PT backbone [86]. The polymer **48** was prepared by Suzuki coupling polymerisation of diboronic ester **49** and dibromothieno-TTF **50** (Scheme 12). The latter was synthesised following the aforementioned synthetic pathway A. The incorporation of the DPP π-acceptor into the conjugated backbone led to a polymer with a narrow optical band gap (E_g^{opt} = 1.32 eV in CH_2Cl_2 solution), with the expected lower value of E_g^{opt} = 1.26 eV in the film due to π–π stacking interactions. The value of the HOMO/LUMO levels (−5.13/−3.49 eV) in the film were noticeably different from those in solution (−4.95/−3.55 eV), which suggested significant donor–acceptor interactions in the solid phase between the DPP and TTF units.

OFET device fabrication employing polymer **48** exhibited p-type semiconductor behaviour, with the best performance from devices using the bottom contact top gate configuration [87]. The hole mobility values calculated in the saturated region were found to be 3.8×10^{-2} and 5.3×10^{-2} cm^2 V^{-1} s^{-1} for OFETs fabricated via spincoating the semiconductor from solution in chlorobenzene and chloroform, respectively. The strong

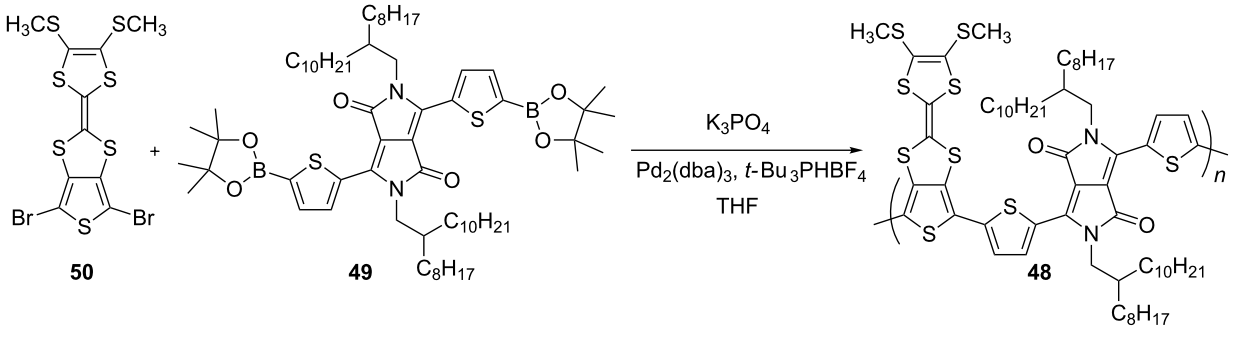

Scheme 12: The synthesis of polymer **48**.

propensity of **48** to aggregation led to the tightly packed grain morphology of the film cast from chlorobenzene with small sized crystalline domains (Figure 4). On the contrary, using chloroform the high solvation energy of the TTF unit and the carbonyl groups of the DPP moieties made the rate of nucleation lower compared to the rate of grain growth, so the size of the crystalline domain in the film was higher in this case. These larger crystalline domains in films spin-coated from chloroform were beneficial for field effect mobility.

None of the OFETs showed any n-type mobility. The extended character of the HOMO residing on the dithienyl-thieno-TTF unit and the localised nature of the LUMO led to donor–acceptor interactions in the solid phase, making it impossible for efficient overlap between LUMOs, which would normally be required for an efficient n-type semiconductor.

BHJSCs were fabricated from **48** as the electron donor and $PC_{71}BM$ as the electron acceptor using *ortho*-diclorobenzene (*o*-DCB) and chloroform as solvents (Table 3). The devices prepared with *o*-DCB showed up to a two-fold increase in power conversion efficiency (PCE) compared to those obtained by spincoating the blend from chloroform, which is due to a more homogeneous blend morphology leading to improved charge carrier transport and increased J_{sc}. Since the use of *o*-DCB as the solvent for spincoating provided better performance for BHJSCs than chloroform, it was used for the fabrication of a single material organic solar cell (SMOSC) (Table 3). The SMOSC performance is modest compared to that of similar devices fabricated using donor–acceptor block copolymers [88-90]. Nevertheless, the value of the PCE (0.31%) is higher than one would expect from a SMOSC fabricated from polymer **48** as a semiconductor, since it has no obvious donor–acceptor phase separation and is lacking efficient electron mobility.

TTF-oligothiophene systems with well-defined structures

The monodisperse analogue of polymer **34**, bearing two TTF units and capped with dodecyl chains at the terminal positions, was synthesised using chemical coupling protocols, or alternatively via electrochemical oxidation of terthiophene **28b** (Scheme 13) [72]. The latter was synthesised by the aforementioned synthetic pathway C.

The electrochemical method for the preparation of sexithiophene **51** was achieved by potentiostatic oxidative electrodimerization of **28b** in a mixture of 2:1 CH_2Cl_2/hexane, with 0.1 M tetrabutylammonium hexafluorophosphate as the supporting electrolyte. On a larger scale, chemical oxidation by $FeCl_3$ in nitrobenzene was used which after purification, afforded **51** in a 24% yield. Lithiation of compound **28b** with LDA and successive trapping of the aryllithium compound with perfluorohexyl iodide afforded iodoterthiophene **52** in a 74% yield. Compound **52** was used to explore other possibilities for synthesising sexithiophene **51**, including Ullmann and Yamamoto coupling, which provided **51** in 43 and 10% yield, respectively. Sexithiophene **51** exhibited a strong propensity to aggregate even in chloroform solution, hence an interpretable ^1H NMR spectrum was only obtained in a mixture of $CDCl_3$ with CS_2.

In CH_2Cl_2 solution, the chemically synthesised product showed a π–π* transition peak at 443 nm, with a HOMO–LUMO gap of 2.32 eV, a value very similar to that of the parent sexithiophene **53** [91]. For the electrochemically prepared film of **51**, there

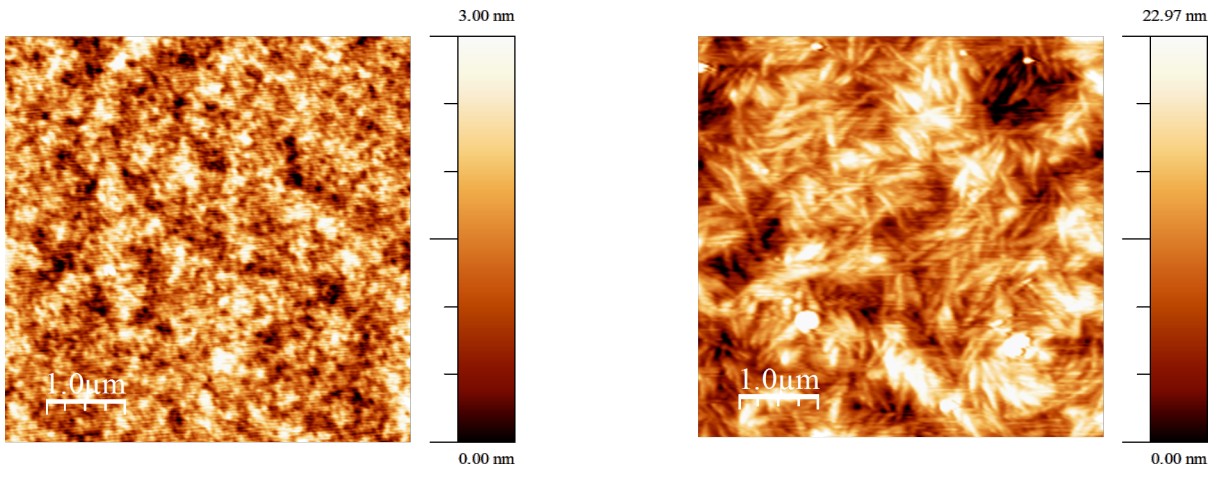

Figure 4: Tapping mode AFM height images of polymer **48** film spin-coated from chlorobenzene (left) and chloroform (right) solutions on ODTS treated SiO_2 substrate. Reproduced with permission from [87]. Copyright 2015 The American Chemical Society.

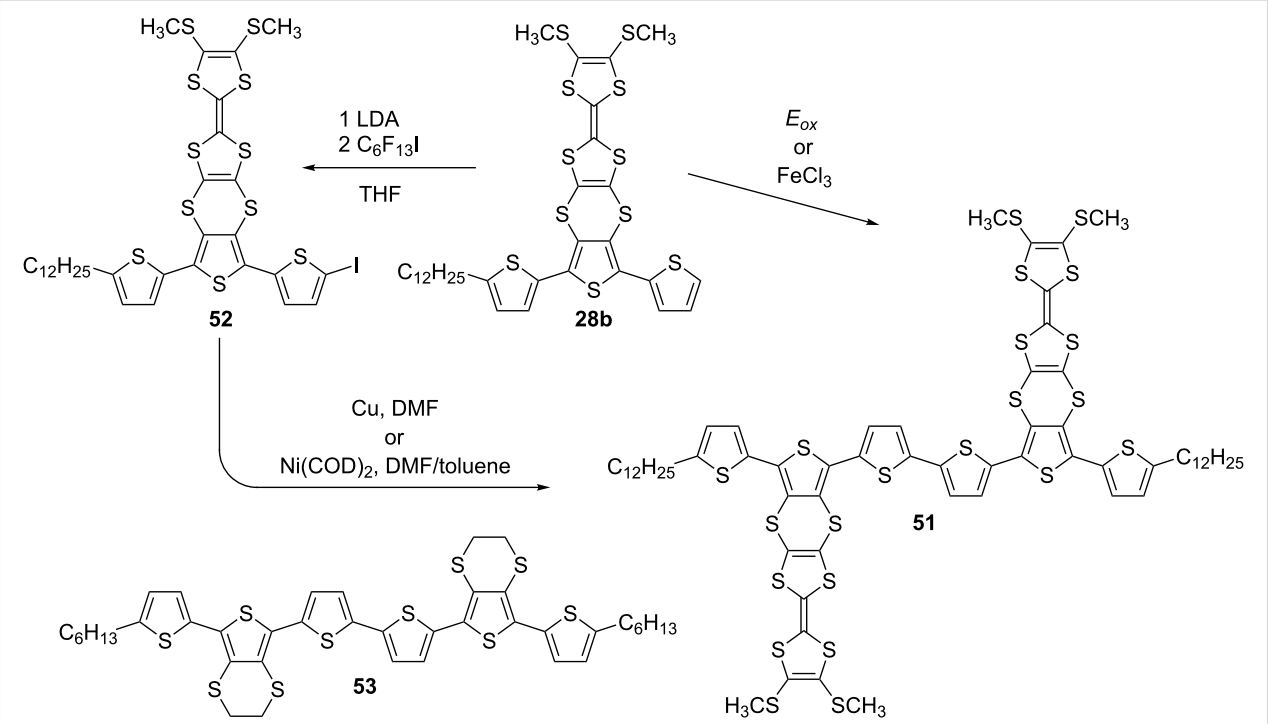

Scheme 13: The synthesis of TTF-sexithiophene system **51** and the structure of the parent sexithiophene **53**.

were two broad bands with maxima centred at 449 and 735 nm, confirming the doped state of the film and the presence of a cation radical centred on the TTF unit. After de-doping, a single broad band remained with its maximum red-shifted compared to that of the solution state spectrum of the chemically synthesised sexithiophene **51**; this is evidence of a strong π–π stacking interaction upon aggregation in the solid state. The electrochemistry of compound **51** is similar for both solution and solid state samples, with the main feature being the overlap between the second oxidation peak of the TTF and the oxidation of the sexithiophene backbone.

A series of hybrid electroactive compounds **54** (n = 0–2) with two oligothiophenes directly fused to one TTF unit was recently reported [92,93]. Here, triethylphosphite mediated homocoupling of the corresponding oligothiophenes **55** (n = 0–2) containing a central thieno[3,4-*d*][1,3]dithiole-2-one unit proceeded smoothly, with yields of 77% for n = 0, 82% for n = 1 and 39% for n = 2 (Scheme 14).

The oligothiophene half-unit precursors, **55** (n = 0–2), were synthesised following synthetic pathway B. The electrochemical and optical properties of **54** (n = 0–2) are shown in Table 4.

The optical properties of **54** (n = 0–2) in solution (Table 4) follow a general trend of decreasing the absorption onset, while increasing the conjugation length. The electrochemistry of each

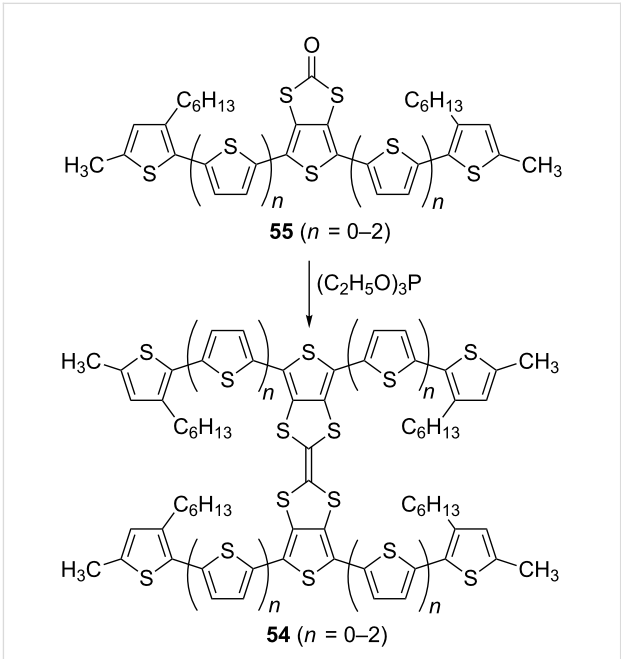

Scheme 14: The synthesis of TTF-oligothiophene H-shaped systems **54** (n = 0–2).

H-shaped system **54** (n = 0–2) on the other hand is not so straightforward. While the first and the second oxidation waves are easily identified and assigned for **51** (vide supra), for **54** (n = 0–2) it is only the first oxidation wave which can be

Table 4: The properties of monodisperse oligothiophene-TTF systems in dichloromethane solution.

	51	**54** (*n* = 0)	**54** (*n* = 1)	**54** (*n* = 2)
E_{1ox}, V[a]	+0.29/0.21	+0.39/+0.32	+0.27/+0.21	+0.26/+0.23
E_{2ox}, V[a]	+0.53/0.45	+0.86/+0.75	+0.54/+0.48	+0.66/+0.49
E_{3ox}, V[a]	–	+1.13	+0.76/+0.71	+0.97/+0.94
E_{4ox}, V[a]	–	–	+0.97/+0.89	–
E_{red}, V[a]	–	–2.12	–2.19	−1.98
HOMO[b], eV	−4.93	–5.06	–4.96	−4.95
LUMO[b], eV	–	–2.92	–2.81	−3.00
HOMO–LUMO gap, eV	–	2.14	2.15	1.95
λ_{max}, nm	443	351	431	461
Absorption onset, eV	2.32	2.92	2.45	2.20

[a]The electrochemical data are referenced against the Fc/Fc^+ couple. Both E^{pa} and E^{pc} or anodic peak value (E^{pa}, if the wave is irreversible) for the oxidation waves and cathodic peak values (E^{pc}) for the reduction waves are quoted. [b]HOMO/LUMO values were calculated using the formula HOMO/LUMO = $-E^{onset}_{ox}/E^{onset}_{red} - 4.80$.

unequivocally assigned to the first oxidation potential of the TTF unit. It is interesting to note that the terthiophene-TTF H-shaped system **54** (*n* = 0) exhibits a significantly higher potential for the formation of $TTF^{+\bullet}$ than that of the quinqui- and septithiophene systems **54** (*n* = 1–2). This can be explained by the increased π-donating ability of the oligothiophene with a higher conjugation length due to a more pronounced contribution of the quinoidal resonance structure. This effect is only possible for hybrid systems with a TTF unit directly fused to the PT backbone (Scheme 15).

Quinqui- and septithiophene TTF bridge systems **54** (*n* = 1–2) are prone to strong aggregation in solution and, as with **51**, a mixture of chloroform with CS_2 was used for NMR spectroscopy in these cases. For compound **54** (*n* = 2) the absorption spectrum as a thin film exhibits a maximum at 496 nm and is red-shifted by 35 nm compared to the solution state spectrum, suggesting strong intermolecular interactions in the solid phase.

Single crystal X-ray diffraction of **54** (*n* = 2) (Figure 5) revealed that the molecules in the solid state are essentially planar, apart from a significant torsion angle of 33° between the terminal thiophene A and the thiophene B.

The angle between planes D and F is 5.79°, with the inter-ring distance being 3.74 Å. The angle between thiophenes C and G is higher (18.36°) but the two S-atoms are involved in a weak non-covalent interaction with a distance of 3.81 Å between them. The strong π–π stacking interaction and the presence of multiple S–S non-covalent interactions in the H-shaped TTF-oligothiophene system **54** (*n* = 2) made this compound a promising p-type organic semiconductor material. The time of flight mobility for this compound was found to increase from 1.4×10^{-6} to 1.1×10^{-5} cm^2 V^{-1} s^{-1}, as the electric field increases from 1×10^5 to 4×10^5 V cm^{-1} [92].

Compound **54** (*n* = 1) was tested as a solution processable p-type semiconductor in OFETs using two solvents for spin-coating – chloroform and chlorobenzene [93]. A bottom contact, bottom gate device configuration was used with an n-doped silicon gate and a SiO_2 dielectric layer. After annealing at 120 °C, AFM imaging indicated a closely packed grain-like

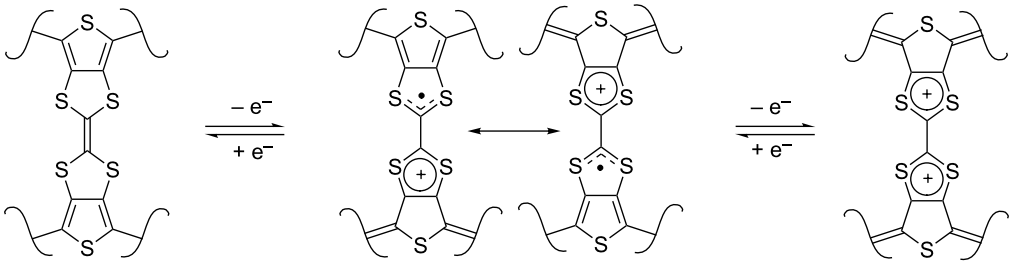

Scheme 15: The oxidation of a fused TTF-oligothiophene system.

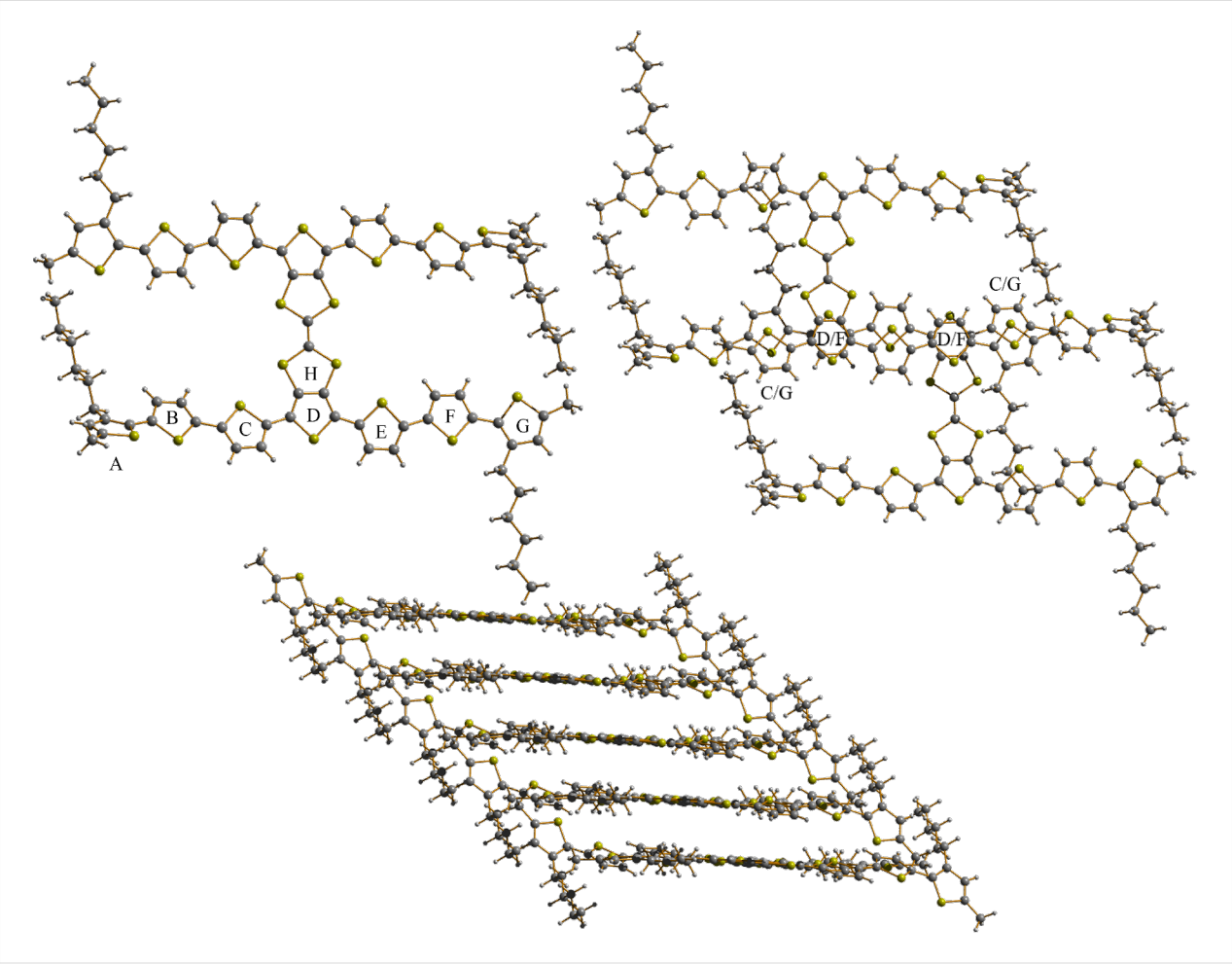

Figure 5: Molecular structure and packing arrangement of compound **54** (n = 2). Adapted by permission from [92]. Copyright 2011 The Royal Society of Chemistry.

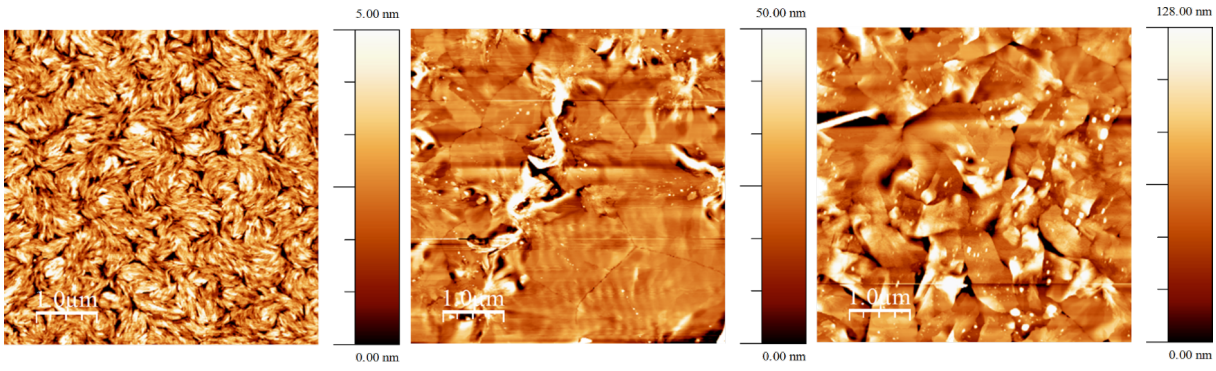

Figure 6: AFM tapping mode images of the compound **54** (n = 1) film cast on an untreated SiO_2 substrate surface from solutions in chlorobenzene (left), $CHCl_3$ (centre) and on an ODTS treated SiO_2 substrate from $CHCl_3$ (right). Reproduced with permission from [93]. Copyright 2014 The Royal Society of Chemistry.

surface morphology of the film cast from chlorobenzene as a result of the strong propensity of H-shaped TTF-quinquithiophene **54** (n = 1) to aggregate in this solvent (Figure 6, left). Upon spin-coating and further annealing, the rate of nucleation exceeded the rate of grain growth, leading to the small size of the crystalline domain. An OFET mobility of

1.41×10^{-4} cm^2 V^{-1} s^{-1} calculated in the saturation region was observed. An increase in the field effect mobility (to $\mu = 1.17 \times 10^{-3}$ cm^2 V^{-1} s^{-1}) by almost an order of magnitude was observed in devices cast from chloroform. As with polymer **48**, tapping mode AFM of the organic semiconductor film spin-coated from this solvent revealed that, after annealing, the surface morphology consisted of large crystalline domains with a smooth grain boundary (Figure 6, centre). Such a striking difference in morphology of the films cast from chlorobenzene and $CHCl_3$ is explained by the high energy of solvation of **54** (n = 1) in chloroform, which leads to a higher crystallisation rate compared to the rate of nucleation during spin-coating and subsequent annealing. When substrates with a pre-treated *n*-octadecyltrichlorosilane (ODTS) SiO_2 surface were used for spin-coating from a $CHCl_3$ solution, the surface morphology remained essentially the same (Figure 6, right), with a further increase in mobility ($\mu = 8.61 \times 10^{-3}$ cm^2 V^{-1} s^{-1}) observed due to the beneficial effects of large crystalline domains on the field effect mobility.

Compound **54** (n = 1) was tested as a donor material in BHJSCs. The results are presented in Table 3. Similar to polymer **48**, the device prepared by spin-coating the blend of **54** (n = 1) and $PC_{71}BM$ from solution in *o*-DCB showed a higher performance than that fabricated with $CHCl_3$, with a short circuit current density (increased up to 9.81 mA cm^{-2}) being more affected by the solvent than the open circuit voltage (0.78 V). AFM revealed a smoother surface morphology of the donor–acceptor blend film cast from *o*-DCB than that when chloroform was used as solvent.

Conclusion

The series of poly- and oligothiophene based compounds bearing TTF units reported so far in the literature have been discussed. The most interesting properties were exhibited by polymers where TTF units were incorporated alongside the conjugated backbone, allowing for the different charge transport mechanisms on the basis of TTF mixed valence states and polarons to be observed. Upon positioning the TTF unit in the vicinity of the polymer backbone, a variation of electrochemical behaviour is observed, including complete dominance by the TTF units and, at times, independent activity of both electroactive entities.

The initial idea of creating materials with hybrid charge transport on the basis of the polaron mechanism and the mixed valence state of doped TTF units has developed now into efforts to use the TTF unit as a handle for controlling the morphology of organic semiconductors in the solid state. The great challenge in this field is to design hybrid materials where the position of the TTFs relative to the polymer backbone and the choice of optimised processing conditions allow tuning of the energy levels and the intrinsic charge carrier mobility in order to achieve maximum device performance.

Acknowledgements

PJS thanks the Royal Society for a Wolfson Research Merit Award and ALK thanks the EPSRC for funding (EP/I029141 and EP/K00042X).

References

1. Skabara, P. J.; Arlin, J.-B.; Geerts, Y. H. *Adv. Mater.* **2013,** *25,* 1948–1954. doi:10.1002/adma.201200862
2. Chen, T. A.; Rieke, R. D. *J. Am. Chem. Soc.* **1992,** *114,* 10087–10088. doi:10.1021/ja00051a066
3. McCullough, R. D.; Tristram-Nagle, S.; Williams, S. P.; Lowe, R. D.; Jayaraman, M. *J. Am. Chem. Soc.* **1993,** *115,* 4910–4911. doi:10.1021/ja00064a070
4. Groenendaal, L.; Jonas, F.; Freitag, D.; Pielartzik, H.; Reynolds, J. R. *Adv. Mater.* **2000,** *12,* 481–494. doi:10.1002/(SICI)1521-4095(200004)12:7<481::AID-ADMA481>3.0.CO;2-C
5. Dang, M. T.; Hirsch, L.; Wantz, G.; Wuest, J. D. *Chem. Rev.* **2013,** *113,* 3734–3765. doi:10.1021/cr300005u
6. Sirringhaus, H.; Tessler, N.; Friend, R. H. *Science* **1998,** *280,* 1741–1744. doi:10.1126/science.280.5370.1741
7. Cho, S.; Lee, K.; Yuen, J.; Wang, G.; Moses, D.; Heeger, A. J.; Surin, M.; Lazzaroni, R. *J. Appl. Phys.* **2006,** *100,* 114503. doi:10.1063/1.2400796
8. Zotti, G.; Zecchin, S.; Schiavon, G.; Berlin, A.; Pagani, G.; Canavesi, A. *Chem. Mater.* **1995,** *7,* 2309–2315. doi:10.1021/cm00060a019
9. Schäferling, M.; Bäuerle, P. *J. Mater. Chem.* **2004,** *14,* 1132–1141. doi:10.1039/b313296j
10. Iraqi, A.; Crayston, J. A.; Walton, J. C. *J. Mater. Chem.* **1998,** *8,* 31–36. doi:10.1039/a703397d
11. Skabara, P. J.; Serebryakov, I. M.; Perepichka, I. F.; Sariciftci, N. S.; Neugebauer, H.; Cravino, A. *Macromolecules* **2001,** *34,* 2232–2241. doi:10.1021/ma0015931
12. Skabara, P. J.; Berridge, R.; Serebryakov, I. M.; Kanibolotsky, A. L.; Kanibolotskaya, L.; Gordeyev, S.; Perepichka, I. F.; Sariciftci, N. S.; Winder, C. *J. Mater. Chem.* **2007,** *17,* 1055–1062. doi:10.1039/B609858D
13. Goldenberg, L. M.; Skabara, P. J.; Roberts, D. M.; Berridge, R.; Ortí, E.; Viruela, P. M.; Pou-Amérigo, R. *J. Mater. Chem.* **2000,** *10,* 2458–2465. doi:10.1039/b003914o
14. Berridge, R.; Wright, S. P.; Skabara, P. J.; Dyer, A.; Steckler, T.; Argun, A. A.; Reynolds, J. R.; Harrington, R. W.; Clegg, W. *J. Mater. Chem.* **2007,** *17,* 225–231. doi:10.1039/B613879A
15. Palermo, E. F.; Darling, S. B.; McNeil, A. J. *J. Mater. Chem. C* **2014,** *2,* 3401–3406. doi:10.1039/c3tc32512a
16. Chan, S.-H.; Lai, C.-S.; Chen, H.-L.; Ting, C.; Chen, C.-P. *Macromolecules* **2011,** *44,* 8886–8891. doi:10.1021/ma201425d
17. Bijleveld, J. C.; Zoombelt, A. P.; Mathijssen, S. G. J.; Wienk, M. M.; Turbiez, M.; de Leeuw, D. M.; Janssen, R. A. J. *J. Am. Chem. Soc.* **2009,** *131,* 16616–16617. doi:10.1021/ja907506r
18. Zhang, K.; Tieke, B.; Forgie, J. C.; Skabara, P. J. *Macromol. Rapid Commun.* **2009,** *30,* 1834–1840. doi:10.1002/marc.200900442

19. Zhang, K.; Tieke, B.; Forgie, J. C.; Vilela, F.; Parkinson, J. A.; Skabara, P. J. *Polymer* **2010,** *51,* 6107–6114. doi:10.1016/j.polymer.2010.10.054
20. Zhang, K.; Tieke, B.; Forgie, J. C.; Vilela, F.; Skabara, P. J. *Macromolecules* **2012,** *45,* 743–750. doi:10.1021/ma202387t
21. Cortizo-Lacalle, D.; Howells, C. T.; Gambino, S.; Vilela, F.; Vobecka, Z.; Findlay, N. J.; Inigo, A. R.; Thomson, S. A. J.; Skabara, P. J.; Samuel, I. D. W. *J. Mater. Chem.* **2012,** *22,* 14119–14126. doi:10.1039/c2jm32374e
22. Forgie, J. C.; Skabara, P. J.; Stibor, I.; Vilela, F.; Vobecka, Z. *Chem. Mater.* **2009,** *21,* 1784–1786. doi:10.1021/cm9004823
23. Wudl, F.; Wobschall, D.; Hufnagel, E. J. *J. Am. Chem. Soc.* **1972,** *94,* 670–672. doi:10.1021/ja00757a079
24. Ferraris, J.; Cowan, D. O.; Walatka, V.; Perlstein, J. H. *J. Am. Chem. Soc.* **1973,** *95,* 948–949. doi:10.1021/ja00784a066
25. Jérome, D. *Chem. Rev.* **2004,** *104,* 5565–5592. doi:10.1021/cr030652g
26. Seo, H.; Hotta, C.; Fukuyama, H. *Chem. Rev.* **2004,** *104,* 5005–5036. doi:10.1021/cr030646k
27. Kini, A. M.; Geiser, U.; Wang, H. H.; Carlson, K. D.; Williams, J. M.; Kwok, W. K.; Vandervoort, K. G.; Thompson, J. E.; Stupka, D. L. *Inorg. Chem.* **1990,** *29,* 2555–2557. doi:10.1021/ic00339a004
28. Bryce, M. R.; Devonport, W.; Goldenberg, L. M.; Wang, C. *Chem. Commun.* **1998,** 945–951. doi:10.1039/a800536b
29. Christensen, C. A.; Becher, J.; Goldenberg, L. M.; Bryce, M. R. *Chem. Commun.* **1998,** 509–510. doi:10.1039/A707504I
30. Beeby, A.; Bryce, M. R.; Christensen, C. A.; Cooke, G.; Duclairoir, F. M. A.; Rotello, V. M. *Chem. Commun.* **2002,** 2950–2951. doi:10.1039/b209765f
31. Kanibolotsky, A.; Roquet, S.; Cariou, M.; Leriche, P.; Turrin, C.-O.; de Bettignies, R.; Caminade, A.-M.; Majoral, J.-P.; Khodorkovsky, V.; Gorgues, A. *Org. Lett.* **2004,** *6,* 2109–2112. doi:10.1021/ol049648x
32. Kimura, H.; Konishi, K.; Muraoka, S.-y.; Shirahata, T.; Misaki, Y. *Chem. Lett.* **2014,** *43,* 843–845. doi:10.1246/cl.140092
33. Yang, X.; Zhang, D.; Zhang, G.; Zhu, D. *Sci. China: Chem.* **2011,** *54,* 596–602. doi:10.1007/s11426-011-4225-y
34. Nalluri, S. K. M.; Shivarova, N.; Kanibolotsky, A. L.; Zelzer, M.; Gupta, S.; Frederix, P. W. J. M.; Skabara, P. J.; Gleskova, H.; Ulijn, R. V. *Langmuir* **2014,** *30,* 12429–12437. doi:10.1021/la503459y
35. Inagi, S.; Naka, K.; Chujo, Y. *J. Mater. Chem.* **2007,** *17,* 4122–4135. doi:10.1039/b708640g
36. Kashimura, Y.; Goto, T.; Nakashima, H.; Furukawa, K.; Wang, E.; Li, H.; Hu, W.; Torimitsu, K. *Jpn. J. Appl. Phys.* **2010,** *49,* 01AB08. doi:10.1143/JJAP.49.01AB08
37. Jia, H.-P.; Forgie, J. C.; Liu, S.-X.; Sanguinet, L.; Levillain, E.; Le Derf, F.; Sallé, M.; Neels, A.; Skabara, P. J.; Decurtins, S. *Tetrahedron* **2012,** *68,* 1590–1594. doi:10.1016/j.tet.2011.11.087
38. Zhang, X.; Wang, C.; Lai, G.; Zhang, L.; Shen, Y. *New J. Chem.* **2010,** *34,* 318–324. doi:10.1039/B9NJ00520J
39. Zhang, X.-C.; Wang, C.-Y.; Lai, G.-Q.; Zhang, L.; Shen, Y.-J. *Polym. Bull.* **2011,** *66,* 893–903. doi:10.1007/s00289-010-0322-x
40. Zhang, L.; Li, M.; Wang, C.; Lai, G.; Shen, Y. *Polym. Bull.* **2013,** *70,* 353–369. doi:10.1007/s00289-012-0841-8
41. Hou, Y.; Wan, X.; Yang, M.; Ma, Y.; Huang, Y.; Chen, Y. *Macromol. Rapid Commun.* **2008,** *29,* 719–723. doi:10.1002/marc.200800023
42. Hou, Y.; Chen, Y.; Liu, Q.; Yang, M.; Wan, X.; Yin, S.; Yu, A. *Macromolecules* **2008,** *41,* 3114–3119. doi:10.1021/ma702864c
43. Yamamoto, T.; Shimizu, T. *J. Mater. Chem.* **1997,** *7,* 1967–1968. doi:10.1039/a704753c
44. Zotti, G.; Zecchin, S.; Schiavon, G.; Berlin, A.; Huchet, L.; Roncali, J. *J. Electroanal. Chem.* **2001,** *504,* 64–70. doi:10.1016/S0022-0728(01)00429-6
45. Roncali, J. *J. Mater. Chem.* **1999,** *9,* 1875–1893. doi:10.1039/a902747e
46. Bryce, M. R.; Chissel, A. D.; Gopal, J.; Kathirgamanathan, P.; Parker, D. *Synth. Met.* **1991,** *39,* 397–400. doi:10.1016/0379-6779(91)91766-4
47. Zhang, L.; Li, M.; Wang, C.; Wang, Y.; Shen, Y. *J. Appl. Polym. Sci.* **2013,** *127,* 3356–3364. doi:10.1002/app.37803
48. Thobie-Gautier, C.; Gorgues, A.; Jubault, M.; Roncali, J. *Macromolecules* **1993,** *26,* 4094–4099. doi:10.1021/ma00068a004
49. Huchet, L.; Akoudad, S.; Roncali, J. *Adv. Mater.* **1998,** *10,* 541–545. doi:10.1002/(SICI)1521-4095(199805)10:7<541::AID-ADMA541>3.0.CO;2-1
50. Huchet, L.; Akoudad, S.; Levillain, E.; Roncali, J.; Emge, A.; Bäuerle, P. *J. Phys. Chem. B* **1998,** *102,* 7776–7781. doi:10.1021/jp982593u
51. Besbes, M.; Trippé, G.; Levillain, E.; Mazari, M.; Le Derf, F.; Perepichka, I. F.; Derdour, A.; Gorgues, A.; Sallé, M.; Roncali, J. *Adv. Mater.* **2001,** *13,* 1249–1252. doi:10.1002/1521-4095(200108)13:16<1249::AID-ADMA1249>3.0.CO;2-W
52. Trippé, G.; Le Derf, F.; Lyskawa, J.; Mazari, M.; Roncali, J.; Gorgues, A.; Levillain, E.; Sallé, M. *Chem. – Eur. J.* **2004,** *10,* 6497–6509. doi:10.1002/chem.200400303
53. Sinha, J.; Lee, S. J.; Kong, H.; Swift, T. W.; Katz, H. E. *Macromolecules* **2013,** *46,* 708–717. doi:10.1021/ma3019365
54. Skabara, P. J.; Müllen, K. *Synth. Met.* **1997,** *84,* 345–346. doi:10.1016/S0379-6779(97)80774-6
55. Skabara, P. J.; Berridge, R.; McInnes, E. J. L.; West, D. P.; Coles, S. J.; Hursthouse, M. B.; Müllen, K. *J. Mater. Chem.* **2004,** *14,* 1964–1969. doi:10.1039/b400809j
56. Shu, P.; Chiang, L.; Emge, T.; Holt, D.; Kistenmacher, T.; Lee, M.; Stokes, J.; Poehler, T.; Bloch, A.; Cowan, D. *J. Chem. Soc., Chem. Commun.* **1981,** 920–921. doi:10.1039/c39810000920
57. Rovira, C.; Santalō, N.; Veciana, J. *Tetrahedron Lett.* **1989,** *30,* 7249–7252. doi:10.1016/S0040-4039(01)93950-4
58. Rovira, C.; Veciana, J.; Santalo, N.; Tarres, J.; Cirujeda, J.; Molins, E.; Llorca, J.; Espinosa, E. *J. Org. Chem.* **1994,** *59,* 3307–3313. doi:10.1021/jo00091a017
59. Skabara, P. J.; Müllen, K.; Bryce, M. R.; Howard, J. A. K.; Batsanov, A. S. *J. Mater. Chem.* **1998,** *8,* 1719–1724. doi:10.1039/a803027h
60. Skabara, P. J.; Serebryakov, I. M.; Roberts, D. M.; Perepichka, I. F.; Coles, S. J.; Hursthouse, M. B. *J. Org. Chem.* **1999,** *64,* 6418–6424. doi:10.1021/jo990198+
61. O'Connor, B. R.; Jones, F. N. *J. Org. Chem.* **1970,** *35,* 2002–2005. doi:10.1021/jo00831a062
62. Lee, A. W. M.; Chan, W. H.; Wong, H. C. *Synth. Commun.* **1988,** *18,* 1531–1536. doi:10.1080/00397918808081310
63. Liu, B.; Wu, B.; Xu, J.; Wu, Z.; Zhao, Y.; Zheng, X.; Wang, H. *J. Raman Spectrosc.* **2010,** *41,* 1185–1193. doi:10.1002/jrs.2580
64. Fox, M. A.; Pan, H.-I. *J. Org. Chem.* **1994,** *59,* 6519–6527. doi:10.1021/jo00101a009
65. Jeppesen, J. O.; Takimiya, K.; Jensen, F.; Brimert, T.; Nielsen, K.; Thorup, N.; Becher, J. *J. Org. Chem.* **2000,** *65,* 5794–5805. doi:10.1021/jo000742a

66. Salle, M.; Gorgues, A.; Jubault, M.; Boubekeur, K.; Batail, P. *Tetrahedron* **1992,** *48,* 3081–3090. doi:10.1016/S0040-4020(01)92250-1
67. Guziec, F. S., Jr.; Russo, J. M.; Torres, F. F.; Long, G. C.; Tellez, M. R. *J. Chem. Soc., Perkin Trans. 1* **1989,** 1068–1070. doi:10.1039/p19890001068
68. Serebryakov, I. M.; Skabara, P. J.; Perepichka, I. F. *J. Chem. Soc., Perkin Trans. 2* **1999,** 1405–1410. doi:10.1039/a901178a
69. Vilela, F.; Skabara, P. J.; Mason, C. R.; Westgate, T. D. J.; Luquin, A.; Coles, S. J.; Hursthouse, M. B. *Beilstein J. Org. Chem.* **2010,** *6,* 1002–1014. doi:10.3762/bjoc.6.113
70. Svenstrup, N.; Becher, J. *Synthesis* **1995,** 215–235. doi:10.1055/s-1995-3910
71. Berridge, R.; Serebryakov, I. M.; Skabara, P. J.; Ortí, E.; Viruela, R.; Pou-Amérigo, R.; Coles, S. J.; Hursthouse, M. B. *J. Mater. Chem.* **2004,** *14,* 2822–2830. doi:10.1039/b404545a
72. Kanibolotsky, A. L.; Kanibolotskaya, L.; Gordeyev, S.; Skabara, P. J.; McCulloch, I.; Berridge, R.; Lohr, J. E.; Marchioni, F.; Wudl, F. *Org. Lett.* **2007,** *9,* 1601–1604. doi:10.1021/ol070366h
73. Skabara, P. J.; Roberts, D. M.; Serebryakov, I. M.; Pozo-Gonzalo, C. *Chem. Commun.* **2000,** 1005–1006. doi:10.1039/b001943g
74. Roncali, J. *Chem. Rev.* **1997,** *97,* 173–206. doi:10.1021/cr950257t
75. Bredas, J.-L. *Mater. Horiz.* **2014,** *1,* 17–19. doi:10.1039/C3MH00098B
76. Berridge, R.; Skabara, P. J.; Pozo-Gonzalo, C.; Kanibolotsky, A.; Lohr, J.; McDouall, J. J. W.; McInnes, E. J. L.; Wolowska, J.; Winder, C.; Sariciftci, N. S.; Harrington, R. W.; Clegg, W. *J. Phys. Chem. B* **2006,** *110,* 3140–3152. doi:10.1021/jp057256h
77. Skabara, P. J.; Roberts, D. M.; Ray, A. K.; Umare, S. S.; Hassan, A. K.; Nabok, A. V.; Müllen, K. Tetrathiafulvalene Units. In *Electronic, Optical and Optoelectronic Polymers and Oligomers;* Jabbour, G. E.; Sariciftci, N. S., Eds.; Materials Research Society: Michigan, 2002; Vol. 665, pp 45–52.
78. Kotani, S.; Shiina, K.; Sonogashira, K. *J. Organomet. Chem.* **1992,** *429,* 403–413. doi:10.1016/0022-328X(92)83188-N
79. Renaldo, A. F.; Labadie, J. W.; Stille, J. K. *Org. Synth.* **1989,** *67,* 86–97. doi:10.15227/orgsyn.067.0086
80. Roncali, J. *Chem. Rev.* **1992,** *92,* 711–738. doi:10.1021/cr00012a009
81. Zotti, G.; Zecchin, S.; Schiavon, G.; Louwet, F.; Groenendaal, L.; Crispin, X.; Osikowicz, W.; Salaneck, W.; Fahlman, M. *Macromolecules* **2003,** *36,* 3337–3344. doi:10.1021/ma021715k
82. Kim, E.-G.; Brédas, J.-L. *J. Am. Chem. Soc.* **2008,** *130,* 16880–16889. doi:10.1021/ja806389b
83. Han, G. D.; Collins, W. R.; Andrew, T. L.; Bulović, V.; Swager, T. M. *Adv. Funct. Mater.* **2013,** *23,* 3061–3069. doi:10.1002/adfm.201203251
84. Holliday, S.; Ashraf, R. S.; Nielsen, C. B.; Kirkus, M.; Röhr, J. A.; Tan, C.-H.; Collado-Fregoso, E.; Knall, A.-C.; Durrant, J. R.; Nelson, J.; McCulloch, I. *J. Am. Chem. Soc.* **2015,** *137,* 898–904. doi:10.1021/ja5110602
85. Kanibolotsky, A. L.; Forgie, J. C.; Gordeyev, S.; Vilela, F.; Skabara, P. J.; Lohr, J. E.; Petersen, B. M.; Jeppesen, J. O. *Macromol. Rapid Commun.* **2008,** *29,* 1226–1230. doi:10.1002/marc.200800154
86. Cortizo-Lacalle, D.; Arumugam, S.; Elmasly, S. E. T.; Kanibolotsky, A. L.; Findlay, N. J.; Inigo, A. R.; Skabara, P. J. *J. Mater. Chem.* **2012,** *22,* 11310–11315. doi:10.1039/c2jm31502e
87. Arumugam, S.; Cortizo-Lacalle, D.; Rossbauer, S.; Hunter, S.; Kanibolotsky, A. L.; Inigo, A. R.; Lane, P. A.; Anthopoulos, T. D.; Skabara, P. J. *ACS Appl. Mater. Interfaces* **2015**. doi:10.1021/am5080562
88. Zhang, Q.; Cirpan, A.; Russell, T. P.; Emrick, T. *Macromolecules* **2009,** *42,* 1079–1082. doi:10.1021/ma801504e
89. Wang, J.; Higashihara, T. *Polym. Chem.* **2013,** *4,* 5518–5526. doi:10.1039/c3py00979c
90. Sommer, M.; Huettner, S.; Thelakkat, M. *J. Mater. Chem.* **2010,** *20,* 10788–10797. doi:10.1039/c0jm00665c
91. Mason, C. R.; Skabara, P. J.; Cupertino, D.; Schofield, J.; Meghdadi, F.; Ebner, B.; Sariciftci, N. S. *J. Mater. Chem.* **2005,** *15,* 1446–1453. doi:10.1039/b415610b
92. Wright, I. A.; Skabara, P. J.; Forgie, J. C.; Kanibolotsky, A. L.; González, B.; Coles, S. J.; Gambino, S.; Samuel, I. D. W. *J. Mater. Chem.* **2011,** *21,* 1462–1469. doi:10.1039/C0JM02293D
93. Wright, I. A.; Findlay, N. J.; Arumugam, S.; Inigo, A. R.; Kanibolotsky, A. L.; Zassowski, P.; Domagala, W.; Skabara, P. J. *J. Mater. Chem. C* **2014,** *2,* 2674–2683. doi:10.1039/c3tc32571g

License and Terms

BEILSTEIN JOURNAL OF ORGANIC CHEMISTRY

[2.2]Paracyclophane derivatives containing tetrathiafulvalene moieties

Laura G. Sarbu[1,2], Lucian G. Bahrin[1,2], Peter G. Jones[3], Lucian M. Birsa[*1,2] and Henning Hopf[*2]

Letter

Open Access

Address:
[1]Department of Chemistry, "Al. I. Cuza" University of Iasi, 11 Carol I Bv., RO-700506 Iasi, Romania, [2]Institute of Organic Chemistry, Technical University of Braunschweig, Hagenring 30, D-38106 Braunschweig, Germany and [3]Institute of Inorganic and Analytical Chemistry, Technical University of Braunschweig, Hagenring 30, D-38106 Braunschweig

Email:
Lucian M. Birsa[*] - lbirsa@uaic.ro; Henning Hopf[*] - h.hopf@tu-bs.de

* Corresponding author

Keywords:
dithiocarbamates; 1,3-dithiolium salts; [2.2]paracyclophane; regioselective bromination; stereoisomers; tetrathiafulvalenes

Beilstein J. Org. Chem. **2015,** *11,* 1917–1921.
doi:10.3762/bjoc.11.207

Received: 27 July 2015
Accepted: 24 September 2015
Published: 15 October 2015

This article is part of the Thematic Series "Tetrathiafulvalene chemistry".

Guest Editor: P. J. Skabara

Abstract

The synthesis of [2.2]paracyclophane derivatives containing tetrathiafulvalene units has been accomplished by the coupling reaction of 4-([2.2]paracyclophan-4-yl)-1,3-dithiol-2-thione in the presence of trimethylphosphite. The 1,3-dithiol-2-thione derivative was in turn synthesized by the regioselective bromination of 4-acetyl[2.2]paracyclophane, then through the corresponding dithiocarbamates and 1,3-dithiolium salts.

Introduction

Tetrathiafulvalene (TTF) and its derivatives have been extensively studied with respect to their applications as organic metals and superconductors [1,2]. These properties are a consequence of the π-donor properties of TTF and of its important intermolecular interactions in the solid state through extended π-orbitals. The design of new tetrathiafulvalene derivatives has targeted those systems where the intermolecular interactions between planar molecules are more effective and the solid-state architecture tends to be as stacks or layers with their long axes mutually parallel.

[2.2]Paracyclophane and its derivatives has been the subject of particular interest since their discovery, more than six decades ago [3-5]. Most of the unique properties of these cyclophanes are the result of the rigid framework and the short distance between the two aromatic rings within the [2.2]paracyclophane

unit. Besides investigations of the geometry and of transannular interactions, special attention has been paid to the ability of these compounds to form charge-transfer complexes [6-9].

A recent report has appeared concerning the synthesis of a [2.2]paracyclophane doubly substituted by a dimeric tetrathiafulvalene in a *pseudo-ortho* substitution pattern [10]. This compound exhibited novel chiroptical properties. Prompted by these observations, we decided to investigate the synthesis of a tetrathiafulvalene that incorporates two [2.2]paracyclophane units.

Results and Discussion

The synthesis of [2.2]paracyclophanes containing a tetrathiafulvalene moiety, follows a general route that involves the synthesis of the corresponding [2.2]paracyclophane-substituted 1,3-dithiol-2-ylium salts. These compounds are known to provide tetrathiafulvalenes under specific conditions [11-13]. The synthetic strategy for the incorporation of the 1,3-dithiol-2-ylium ring in the [2.2]paracyclophane framework involves a three-step reaction sequence, starting from 4-acetyl[2.2]paracyclophane (**1**) (Scheme 1).

The first step consists of the regioselective monobromination of 4-acetyl[2.2]paracyclophane (**1**) at the α-position to the carbonyl group to form 2-bromo-1-([2.2]paracyclophan-4-yl)ethan-1-one (**2**). The starting 4-acetyl[2.2]paracyclophane has been prepared according to the reported procedure [14]. In order to avoid the formation of side products during the bromination process [15], the synthesis of compound **2** has been accomplished using the molecular complex of bromine with dioxane [16]. However, although this reagent has often been employed in mild and selective bromination reactions [17], there are some difficulties concerning its isolation and handling [18]. In order to avoid these problems, we generated the reagent by mixing one equivalent of bromine with one equivalent of dioxane and adding dry dioxane to the resulting solid until the dissolution was complete. This solution was then added dropwise at room temperature to a solution of one equivalent of ketone **1** in dioxane, providing 2-bromo-1-([2.2]paracyclophan-4-yl)ethan-1-one (**2**) in 81% yield.

The reactions of α-bromophenones with salts of dithiocarbamic acid, readily available from the reaction of secondary amines with carbon disulfide, represent an accessible route to variously substituted phenacyl carbodithioates [19]. Following this synthetic protocol, we obtained dithiocarbamates **4a**–**c** by reacting 2-bromo-1-([2.2]paracyclophan-4-yl)ethan-1-one (**2**) with sodium *N*,*N*-dimethyldithiocarbamate (**3a**), pyrrolidinium pyrrolidine-1-carbodithioate (**3b**) and morpholinium morpholine-4-carbodithioate (**3c**), respectively. These compounds were obtained as colorless crystals in 80% isolated yields. The structures of dithiocarbamates **4a**–**c** were inferred from their analytical and spectral data; thus the ^{1}H NMR spectra include the expected signals for the aliphatic hydrogen atoms from the dialkylamino groups, and the ^{13}C NMR spectra show the signals at ca. 196 ppm attributable to the thiocarbonyl group. Finally, the structure of 2-([2.2]paracyclophan-4-yl)-2-oxoethyl-*N*,*N*-dimethyldithiocarbamate (**4a**) was unambiguously confirmed by X-ray crystallography (Figure 1). The molecular dimensions confirm the extensive p–π conjugation within the dithiocarbamate group; the N(1)–C(19) bond length is 1.341(3) Å, some 0.12 Å shorter than N(1)–C(20) and N(1)–C(21), which are essentially σ-bonds. The cyclophane group displays the usual

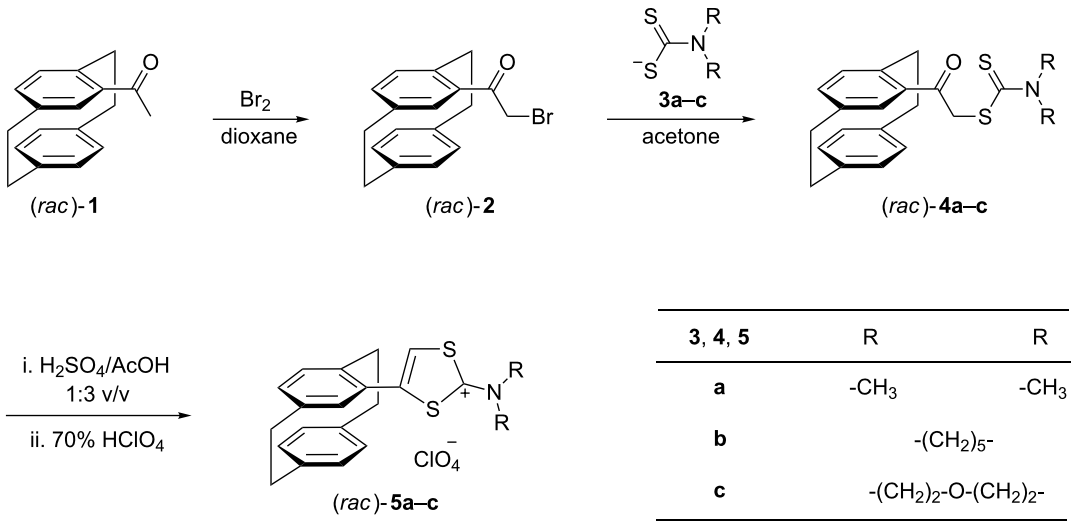

Scheme 1: Synthesis of 2-*N*,*N*-dialkylamino-4-([2.2]paracyclophan-4-yl)-1,3-dithiol-2-ylium perchlorates **5**.

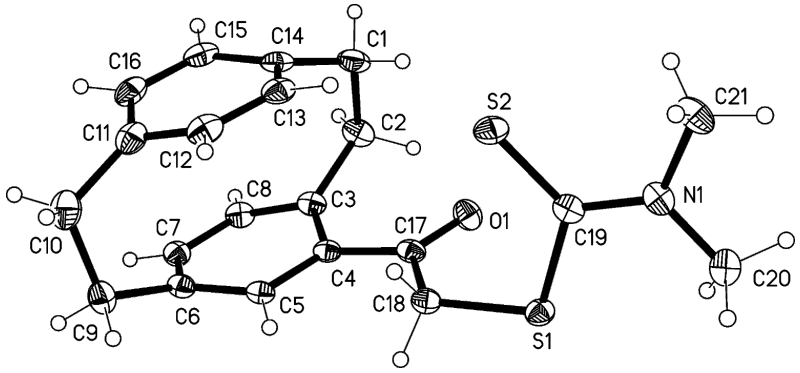

Figure 1: Molecular structure of compound **4a**. Ellipsoids represent 30% probability levels. Selected molecular dimensions (Å, °): N(1)–C(19) 1.341(3), N(1)–C(20) 1.458(3), N(1)–C(21) 1.471(3), N(1)–C(19)–S(2) 123.19(17), N(1)–C(19)–S(1) 113.85(17), S(2)–C(19)–S(1) 122.89(13).

indicators of strain (e.g., lengthened bridge bonds and widened bridge angles, flattened boat conformations for the rings). The moieties C3/4/5/17/18/O1 and C19/20/21/S1/S2/N1 are to a good approximation planar and subtend an interplanar angle of 80°. Short intramolecular contacts H13···S2 2.83 Å and H2B···O1 2.29 Å are observed. CCDC-1412356 contains the supplementary crystallographic data for compound **4a** (see also Supporting Information File 1). These data can be obtained free of charge from the Cambridge Crystallographic Data Center via http://www.ccdc.cam.ac.uk/data_request/cif.

The third step, the synthesis of 1,3-dithiol-2-ylium salts, consists of an acid-catalyzed cyclocondensation of phenacyl carbodithioates **4**. Using a concentrated sulfuric acid–glacial acetic acid mixture (1:3, v/v) [20], the cyclization of carbodithioates **4a**–**c** takes place under mild reaction conditions. After 10 min at 80 °C the homogeneous reaction mixture was cooled to room temperature and 70% $HClO_4$ and water were added. Filtration and recrystallization of the precipitate gave perchlorates **5a**–**c** as colorless crystals, in 58–81% yield (Scheme 1). The heterocyclization of carbodithioates **4** is supported by their spectral data. The IR spectra revealed the disappearance of the absorption band corresponding to the carbonyl group (ca. 1680 cm^{-1}) and the presence of new, strong and broad absorption bands at 1000–1100 cm^{-1}, corresponding to the perchlorate anion. The ^1H NMR spectra of 1,3-dithiol-2-ylium perchlorates indicate the absence of the AB quartet pattern of the methylene hydrogen atoms from compounds **4**. The ^{13}C NMR spectra also confirm the successful synthesis of 1,3-dithiol-2-ylium salts **5** by the disappearance of the carbonyl and thiocarbonyl carbon atoms present in the carbodithioate spectra, as well as the appearance of a new signal at a very low field (ca. 180 ppm) which corresponds to the electron-deficient C-2 atom.

1,3-Dithiolium salts are valuable precursors for tetrathiafulvalenes. There are two main synthetic approaches that are mainly based on the exploitation of the electron-deficient character of the C-2 carbon atom. One of these involves the conversion of 2-*N*,*N*-dialkylamino-1,3-dithiolium salts into the corresponding 2-unsubstituted 1,3-dithiolium salts, followed by the homocoupling of the carbene intermediate that is generated under basic conditions. Unfortunately, our attempts to synthesize the 2-unsubstituted derivative from 1,3-dithiolium perchlorates **5a**–**c** in the presence of tetrafluoroboric acid led to the degradation of the substrate. The second approach for the synthesis of tetrathiafulvalenes involves the desulfurative coupling of 1,3-dithiol-2-thiones in the presence of alkyl phosphites. 1,3-Dithiol-2-thiones are easily available by the treatment of 1,3-dithiol-2-ylium salts with sodium sulfide [21]. Thus, by treating perchlorates **5a**–**c** with sodium sulfide nonahydrate, at room temperature in ethanol, we obtained 4-([2.2]paracyclophan-4-yl)-1,3-dithiol-2-thione (**6**) as a yellow solid in 41% isolated yield (Scheme 2).

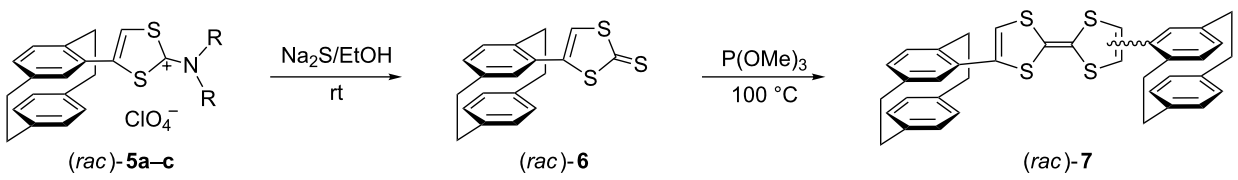

Scheme 2: Synthesis of tetrathiafulvalenes **7**.

Unexpectedly, the yield of 1,3-dithiol-2-thione **6** was found to be dependent on the nature of the dialkylamino substituent and to the volume of the solvent used. The best results were obtained by employing 2-(*N*,*N*-dimethylamino)-4-([2.2]paracyclophan-4-yl)-1,3-dithiol-2-ylium perchlorate (**5a**) as a substrate for this reaction. The formation of 1,3-dithiol-2-thione **6** is supported by the NMR and mass spectrometry data. Moreover, the structure of 1,3-dithiol-2-thione **6** was confirmed by X-ray crystallography (Figure 2). The asymmetric unit contains two molecules, which differ in the orientation of the 1,3-dithiol-2-thione group relative to the cyclophane; the torsion angle C3–C4–C17–S3 is −45.9° in the first molecule but −142.4° in the second. CCDC-1412357 contains the supplementary crystallographic data for compound **6** (see also Supporting Information File 1). These data can be obtained free of charge from The Cambridge Crystallographic Data Center via http://www.ccdc.cam.ac.uk/data_request/cif.

The desulfurative dimerization of 1,3-dithiol-2-thione **6** was effected by heating it with trimethyl phosphite at 100 °C (Scheme 2). Purification of the crude reaction mixture by column chromatography resulted in a mixture of inseparable isomeric tetrathiafulvalenes **7** in 17% yield. Since compound **6** already exhibits planar chirality (racemate R_p/S_p), the theoretical number of stereoisomers of the tetrathiafulvalene **7** should be six as follows: *cis*-(S_p,S_p) with *cis*-(R_p,R_p) and *trans*-(S_p,S_p) with *trans*-(R_p,R_p) for the parallel orientation of the ethano bridges, and the mesoforms *cis*-(S_p,R_p) and *trans*-(S_p,R_p) for the angular orientation of the ethano bridges. The NMR spectrum of the purified tetrathiafulvalene indicates the presence of 4 isomers, most probably the two pairs of racemates and the two mesoforms.

Although the separation of the isomers has not yet been successful, this synthetic pathway indicates that it is feasible to incorporate of [2.2]paracyclophane as an extended π-system onto a tetrathiafulvalene core. Further research will target a decrease in the theoretical number of isomers and their isolation in order to investigate their structural and chiroptical properties.

Conclusion

The synthesis of as yet inseparable isomeric tetrathiafulvalenes has been performed by desulfurative dimerization of a [2.2]paracyclophane-substituted trithione. The latter compound was obtained from the corresponding 1,3-dithiol-2-ylium cation. This was in turn synthesized through a three-step procedure, starting with the regioselective bromination of 4-acetyl[2.2]paracyclophane.

Supporting Information

Supporting Information File 1

Detailed experimental procedures, supplementary spectroscopic and X-ray data.
[http://www.beilstein-journals.org/bjoc/content/supplementary/1860-5397-11-207-S1.pdf]

Acknowledgements

L.M.B. is indebted to the Alexander von Humboldt Foundation for a stay in Braunschweig. This work was supported by a grant of the Romanian National Authority for Scientific Research, CNDI–UEFISCDI, project number 51/2012.

References

1. Yamada, J. In *TTF Chemistry Fundamentals and Applications of Tetrathiafulvalene;* Yamada, J.; Sugimoto, T., Eds.; Kodansha and Springer: Tokyo, 2004.
2. Bendikov, M.; Wudl, F.; Perepichka, D. F. *Chem. Rev.* **2004,** *104,* 4891–4946. doi:10.1021/cr030666m
3. Brown, C. J.; Farthing, A. C. *Nature* **1949,** *164,* 915–916. doi:10.1038/164915b0
4. Cram, D. J.; Steinberg, H. *J. Am. Chem. Soc.* **1951,** *73,* 5691–5704. doi:10.1021/ja01156a059

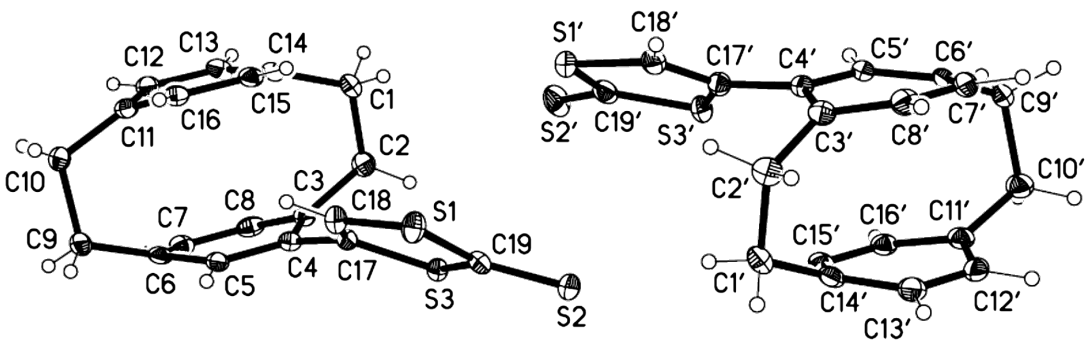

Figure 2: Molecular structure of compound **6** (two independent molecules). Ellipsoids represent 30% probability levels.

5. Vögtle, F.; Neumann, P. *Synthesis* **1973,** 85–103. doi:10.1055/s-1973-22137
6. Staab, H. A.; Knaus, G. H.; Henke, H.-E.; Krieger, C. *Chem. Ber.* **1983,** *116,* 2785–2807. doi:10.1002/cber.19831160807
7. Boekelheide, V. *Top. Curr. Chem.* **1983,** *113,* 87–143. doi:10.1007/3-540-12397-0_2
8. Hopf, H.; Marquard, C. Strain Release in Aromatic Molecules: The [2_n] Cyclophanes. In *Strain and its Implications in Organic Chemistry;* de Meijere, A.; Blechert, S., Eds.; Kluwer: Dordrecht, 1989; pp 297–332. doi:10.1007/978-94-009-0929-8_21
9. Vögtle, F. *Cyclophane Chemistry, Synthesis, Structure and Reactions;* Wiley: Chichester, 1993; pp 71–111.
10. Kobayakawa, K.; Hasegawa, M.; Sasaki, H.; Endo, J.; Matsuzawa, H.; Sako, K.; Yoshida, J.; Mazaki, Y. *Chem. – Asian J.* **2014,** *9,* 2751–2754. doi:10.1002/asia.201402667
11. Narita, M.; Pittman, C. U., Jr. *Synthesis* **1976,** 489–514. doi:10.1055/s-1976-24099
12. Schukat, G.; Richter, A. M.; Fanghänel, E. *Sulfur Rep.* **1987,** *7,* 155–231. doi:10.1080/01961778708082503
13. Schukat, G.; Fanghänel, E. *Sulfur Rep.* **1993,** *14,* 245–383. doi:10.1080/01961779308055019
14. Truesdale, E. A.; Cram, D. J. *J. Org. Chem.* **1980,** *45,* 3974–3981. doi:10.1021/jo01308a005
15. Mamyrbekova, Z. A.; Soldatova, S. A.; Abelentsev, V. I.; Solov'eva, T. I.; Guryshev, V. N.; Soldatenkov, A. T. *Pharm. Chem. J.* **1994,** *28,* 198–202. doi:10.1007/BF02218999
16. Pasaribu, S. J.; Williams, L. R. *Aust. J. Chem.* **1973,** *26,* 1327–1331. doi:10.1071/CH9731327
17. Dombrovski, A. V. *Russ. Chem. Rev.* **1961,** *30,* 635–639. doi:10.1070/RC1961v030n12ABEH003011
18. Billimoria, J. D.; Maclagen, N. F. *J. Chem. Soc.* **1954,** 3257–3262. doi:10.1039/jr9540003257
19. Lungu, N. C.; Sandu, I.; Chirita, P.; Birsa, M. L. *Rev. Chim. (Bucharest, Rom.)* **2013,** *64,* 697–700.
20. Sarbu, L. G.; Lungu, N. C.; Forna, N.; Birsa, M. L. *Rev. Chim. (Bucharest, Rom.)* **2013,** *64,* 1404–1407.
21. Birsa, M. L. *Synth. Commun.* **2003,** *33,* 3071–3076. doi:10.1081/SCC-120022483

License and Terms

BEILSTEIN JOURNAL OF ORGANIC CHEMISTRY

Urethane tetrathiafulvalene derivatives: synthesis, self-assembly and electrochemical properties

Xiang Sun[1], Guoqiao Lai[2], Zhifang Li[2], Yuwen Ma[1], Xiao Yuan[1], Yongjia Shen[1] and Chengyun Wang*[1]

Full Research Paper

Open Access

Address:
[1]Key Laboratory for Advanced Materials and Institute of Fine Chemicals, East China University of Science and Technology, 130 Meilong Road, Shanghai 200237, China and [2]Key Laboratory of Organosilicon Chemistry and Material Technology of Ministry of Education, Hangzhou Normal University, Hangzhou 310012, China

Email:
Chengyun Wang* - cywang@ecust.edu.cn

* Corresponding author

Keywords:
hydrogen bond; nanoribbon; self-assembly; tetrathiafulvalene; urethane

Beilstein J. Org. Chem. **2015,** *11,* 2343–2349.
doi:10.3762/bjoc.11.255

Received: 17 July 2015
Accepted: 13 November 2015
Published: 27 November 2015

This article is part of the Thematic Series "Tetrathiafulvalene chemistry".

Guest Editor: P. J. Skabara

Abstract

This paper reports the self-assembly of two new tetrathiafulvalene (TTF) derivatives that contain one or two urethane groups. The formation of nanoribbons was evidenced by scanning electron microscopy (SEM) and X-ray diffraction (XRD), which showed that the self-assembly ability of $\mathbf{T_1}$ was better than that of $\mathbf{T_2}$. The results revealed that more urethane groups in a molecule did not necessarily instigate self-assembly. UV–vis and FTIR spectra were measured to explore noncovalent interactions. The driving forces for self-assembly of TTF derivatives were mainly hydrogen bond interactions and π–π stacking interactions. The electronic conductivity of the $\mathbf{T_1}$ and $\mathbf{T_2}$ films was tested by a four-probe method.

Introduction

In recent years, there has been an enormous increase of interest in functional organic nanomaterials, given that they are promising materials with a variety of applications including optoelectronic and bioelectronic devices [1,2]. The mechanism behind the formation of functional organic nanomaterials is generally accepted to be the self-assembly of supermolecules, which is constructed through weak noncovalent interactions such as π–π stacking, van der Waals interactions, charge transfer and H-bonding interactions [3-6]. Generally speaking, H-bonding interactions are the key intermolecular interactions in molecular self-assembly systems. Therefore, molecules containing urea, amide and other similar groups have been investigated because these molecules can easily generate intermolecular hydrogen bonds [7-9].

Tetrathiafulvalene (TTF) derivatives have been widely investigated in the fields of supramolecular and materials chemistry due to their great potential application in molecular electronics,

for example, as switches and conductors [10-14]. As we all know, TTF derivatives can form charge transfer (CT) complexes with electron acceptors such as tetracyanoquinodimethane (TCNQ), and the CT complexes of TTF derivatives and TCNQ exhibit high electrical conductivity [14-16]. Therefore, TTF derivatives are extensively used in the field of functional organic conductive nanomaterials.

Herein, we designed and synthesized two compounds, **T_1** and **T_2**, which contain TTF units and urethane groups (Figure 1). The combination of the urethane group (forming hydrogen bonds) and the TTF unit (forming π–π stacking) may promote the formation of nanostructures. To the best of our knowledge, urethane groups have been rarely introduced into the molecular structure of TTF derivatives to generate an H-bonding chain.

Results and Discussion

Synthesis and characterization

The synthetic routes for two newly designed TTF derivatives containing one or two urethane groups are shown in Scheme 1. Compounds **2** [17], **3** [18], **4** [19], **5** [19], **6** [18,20] and **7** [18,21] were synthesized from commercially available starting materials according to the reported methods. Compound **8** [18,21] was obtained by the reaction of **7** with 2-chloroethyl isocyanate in dry and degassed toluene. Finally, the TTF derivative **T_1** was obtained in acceptable yield (72%). For the synthesis of **T_2**, urethane groups were introduced first, and then the coupling reaction was carried out. The new compounds **T_1** and **T_2** were characterized by ^{1}H, ^{13}C NMR, HRMS–ESI (for the spectra see Supporting Information File 1) and elemental analysis. In addition, other intermediates previously reported in the literature were also characterized by ^{1}H NMR, ^{13}C NMR, and EIMS.

Self-assembly and SEM investigation of T_1 and T_2

The studies showed that **T_1** and **T_2** gels were not formed in several common solvents such as hexane, chloroform, dichloromethane, tetrahydrofuran, toluene, diethyl ether, acetone, dimethylformamide, ethanol, methanol and acetonitrile when they were heated and cooled by the methods reported in the literature [2-4]. A loose gel of **T_1** was observed in ethyl acetate when the concentration was increased to 20 mg/mL. However, the precipitate of **T_2** was obtained under the same conditions. Moreover, their micromorphology was recorded with SEM images (Figure 2). The samples were prepared by different methods (drop-coating, spin-coating). The experiments were performed as follows: the solid compounds were completely dissolved in ethyl acetate while heating, then cooled to room temperature. The studies showed that drop-coating was better than direct spin-coating, likely because slow solvent evaporation is more conducive to the formation of regular structure. The SEM images of the **T_1** films (Figure 2a, drop-coated from a diluted **T_1** solution) showed that regular helical nanoribbons were observed. The diameter of the nanoribbons was approximately 500 nm with a length of >20 μm. Although nanoribbons were observed in the SEM images of **T_2** (Figure 2b), they showed no similar ordered structure.

In addition, the X-ray diffraction (XRD) patterns of **T_1** and **T_2** nanoribbons were taken (Supporting Information File 1, Figure S7). The XRD pattern of **T_1** showed three sharp peaks at 7.4°, 14.9° and 22.1°, which suggested that a lamellar stacking organization was formed [4]. This was not the case for the XRD pattern of **T_2**. In general, intermolecular hydrogen bonding is the main driving force behind self-assembly. Although **T_2** contains two urethane groups and **T_1** contains one urethane group, the self-assembly ability of **T_2** is not better than that of

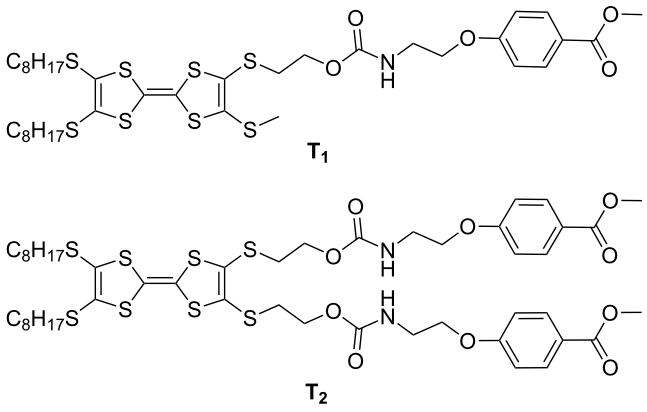

Figure 1: Molecular structure of TTF derivatives **T_1** and **T_2**.

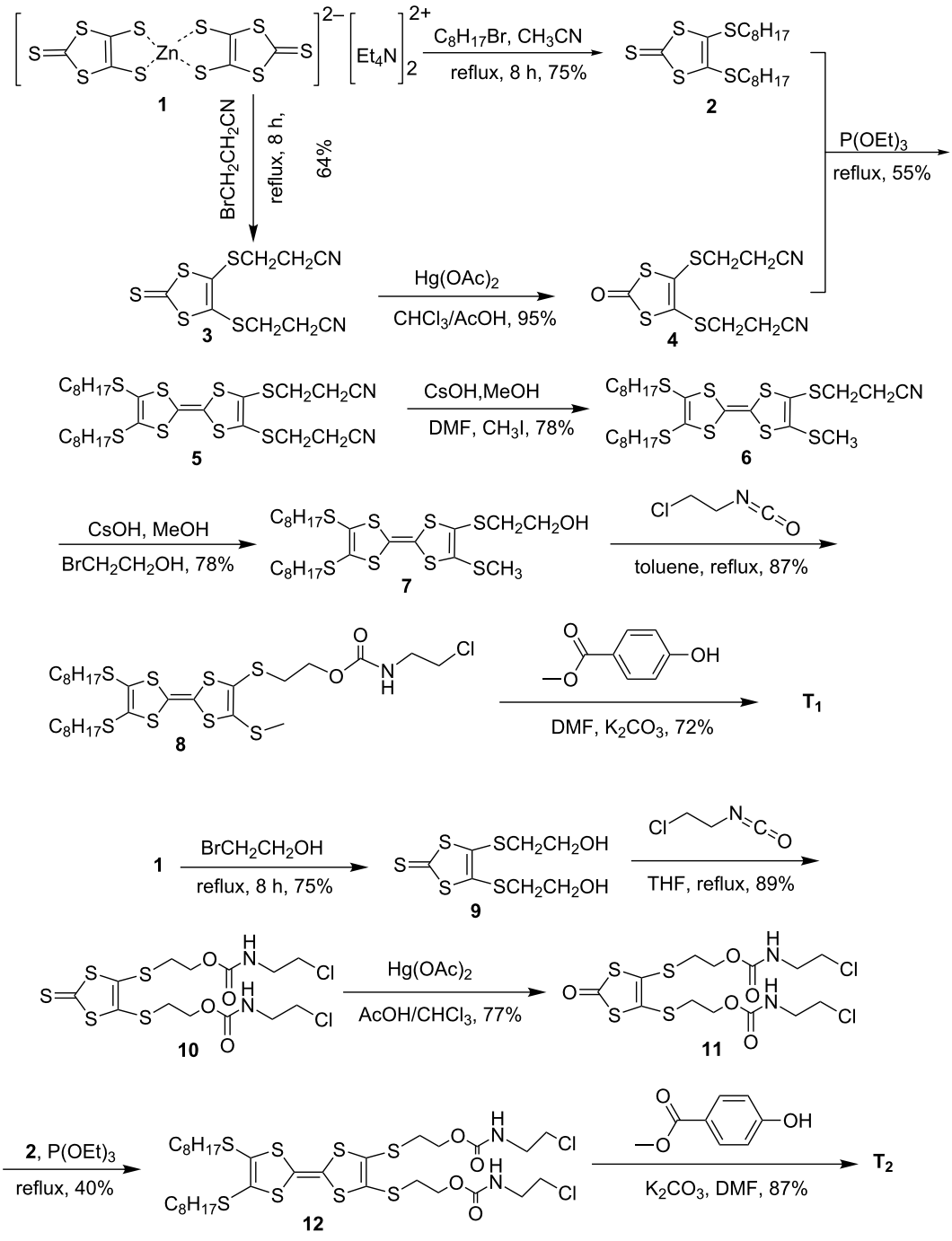

Scheme 1: The synthetic routes of compounds $\mathbf{T_1}$ and $\mathbf{T_2}$.

$\mathbf{T_1}$. We concluded that more intramolecular hydrogen bonds were formed in molecules of $\mathbf{T_2}$ instead of intermolecular hydrogen bonds in ethyl acetate, which was not conducive to form regular nanoribbons.

UV–vis and FTIR spectroscopy

To study the intermolecular interactions, the UV–vis absorption spectra of $\mathbf{T_1}$ and $\mathbf{T_2}$ in ethyl acetate at different concentrations were measured (Figure 3a,b). Figure 3a shows that the two absorption peaks of $\mathbf{T_1}$ are blue-shifted from 314 nm and 338 nm (1×10^{-6} M) to 294 nm and 315 nm (aggregated solid state). This was also observed for $\mathbf{T_2}$, which illustrated that π–π interactions and H-aggregation occurred with the increase in concentration [22-24]. To further study the driving forces for the self-assembly of $\mathbf{T_1}$ and $\mathbf{T_2}$, FTIR spectra were also measured (Figure 4a,b). The FTIR spectra of $\mathbf{T_1}$ showed an

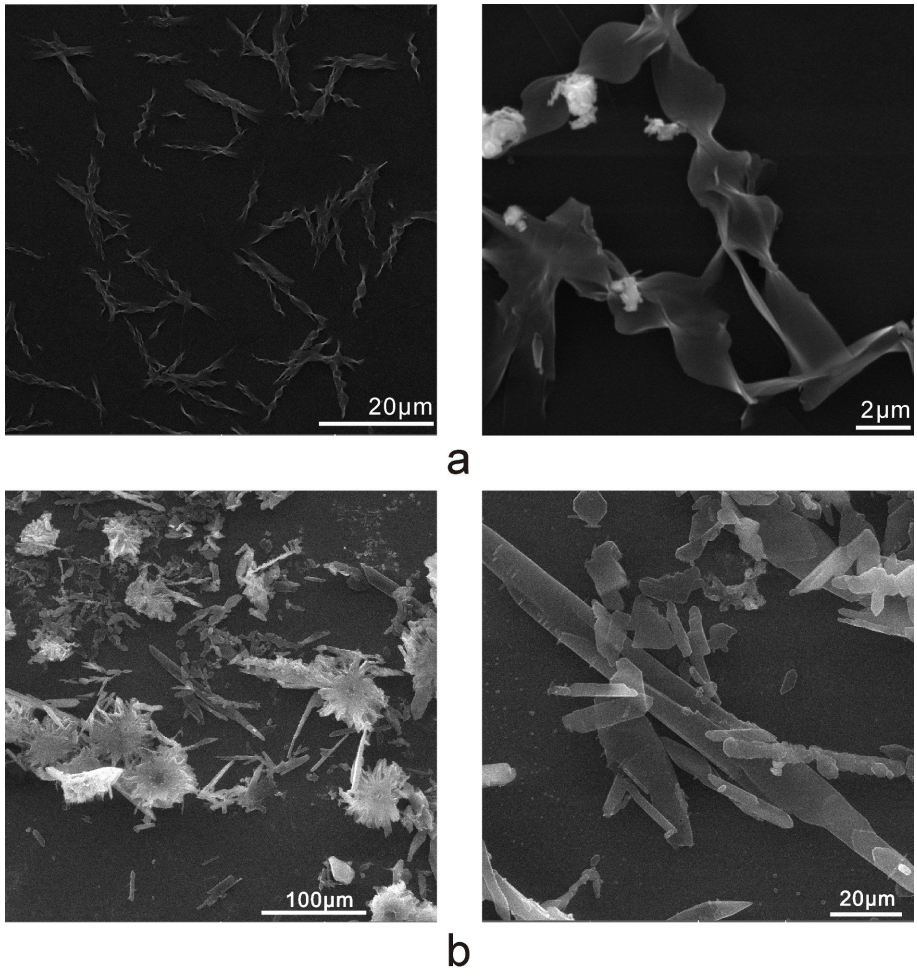

Figure 2: SEM images of $\mathbf{T_1}$ (a) and $\mathbf{T_2}$ (b) films on glass substrates (drop-coated from diluted $\mathbf{T_1}$ or $\mathbf{T_2}$ solution).

absorption peak at 3352 cm^{-1} for the N–H stretching vibration, 1706 cm^{-1} for amide I and 1519 cm^{-1} for amide II related to the urethane groups. The same situation was observed for $\mathbf{T_2}$. The absence of a free N–H stretching vibration (around 3400 cm^{-1}) and a free C=O stretching vibration (around 1720 cm^{-1}) suggested that strong hydrogen bonds between urethane groups were formed [25,26]. These results indicated that π–π interactions and hydrogen bonding were the main driving forces behind the self-assembly.

In addition, UV−vis and FTIR spectra were measured to explore the formation of the charge-transfer complexes. TTF derivates are representative electron donors, while TCNQ is a typical electron acceptor. When one equivalent of TCNQ was added to the solution of $\mathbf{T_1}$ in ethyl acetate, TCNQ radical anion species ($TCNQ^{\bullet-}$) and TTF radical cation species ($TTF^{\bullet+}$) were formed, which was possibly supported by the increase of the absorption bands around 600–900 nm (Figure 5a) [2,4]. Moreover, the UV–vis spectra of self-assembled nanoribbons doped with iodine were collected. It was concluded that the assembled solid structures were maintained. Figure 5b shows the UV–vis spectrum of $\mathbf{T_1}$ (thin film on glass) before and after iodine doping. Upon exposure to iodine vapor for 30 min in a sealed container, a new absorption band was observed at approximately 850 nm, which suggested the formation of the CT complex [27].

IR spectra of TCNQ, $\mathbf{T_1}$/TCNQ, and $\mathbf{T_2}$/TCNQ are shown in Figure 4c–e. In contrast to those of $\mathbf{T_1}$ and $\mathbf{T_2}$, the N–H and C=O stretching bands of the amide groups were not obviously shifted after doping with TCNQ. This indicated that the doping did not change the hydrogen-bonded structures.

Cyclic voltammetry (CV)

The cyclic voltammetry experiments were carried out to explore the electrochemical properties of the TTF compounds. The cyclic voltammograms of $\mathbf{T_1}$ and $\mathbf{T_2}$ were measured in dry and

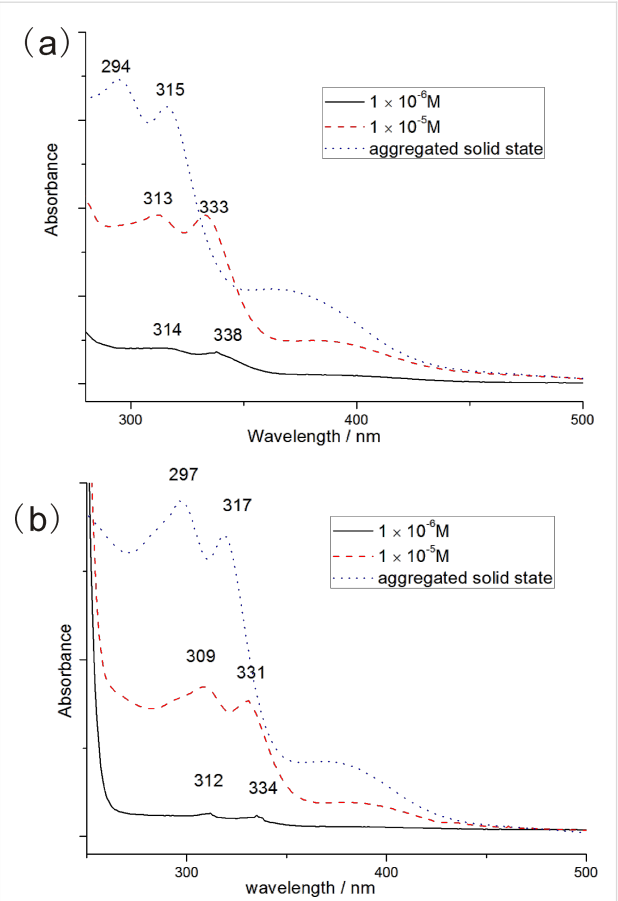

Figure 3: The UV–vis spectra of $\mathbf{T_1}$ (a) and $\mathbf{T_2}$ (b) at different concentrations in ethyl acetate.

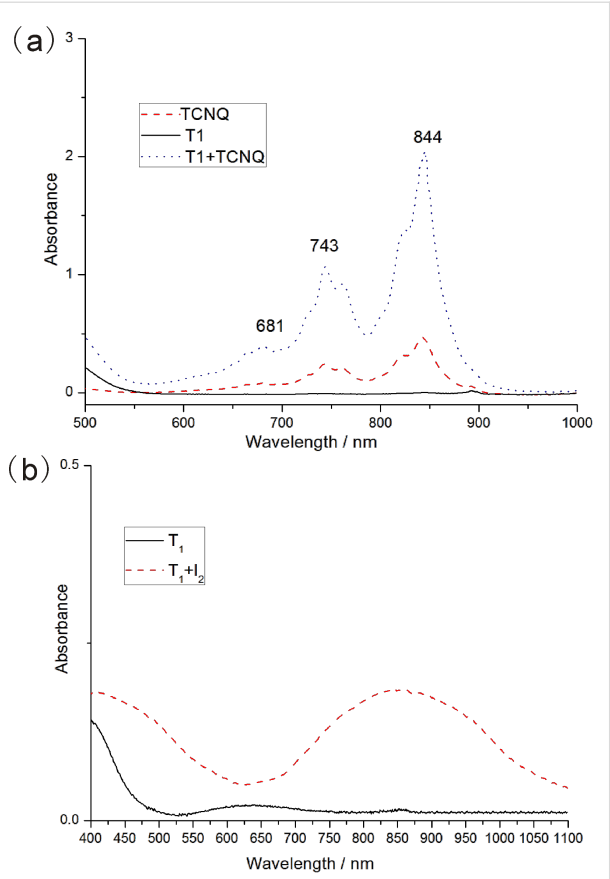

Figure 5: (a) UV–vis spectra of $\mathbf{T_1}$ solutions TCNQ and $\mathbf{T_1}$/TCNQ in ethyl acetate (1×10^{-3} M). (b) UV–vis spectra of $\mathbf{T_1}$ before and after iodine doping for 30 min.

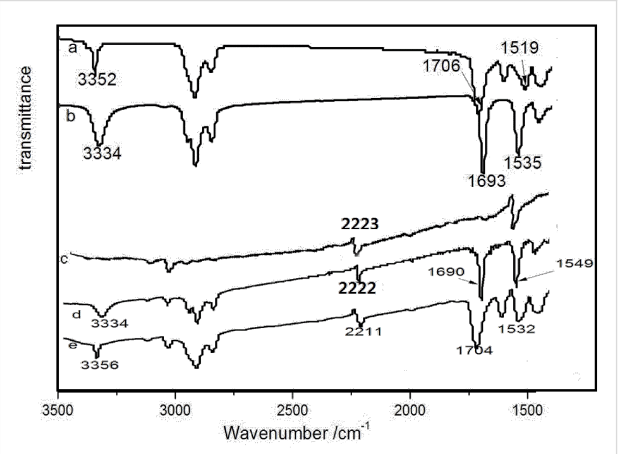

Figure 4: IR spectra of (a) $\mathbf{T_1}$, (b) $\mathbf{T_2}$, (c) TCNQ, (d) $\mathbf{T_2}$/TCNQ, and (e) $\mathbf{T_1}$/TCNQ.

degassed dichloromethane solution [28]. Both $\mathbf{T_1}$ and $\mathbf{T_2}$ displayed two, reversible, one-electron redox couples, in which the first oxidation at $E_{1/2}^{ox1}$ = +0.628 V ($\mathbf{T_1}$) and +0.643 V ($\mathbf{T_2}$) (vs Ag/AgCl) was in the anodic window. This indicated the successive reversible oxidation of neutral TTF (TTF^0) to the radical cation ($TTF^{\bullet+}$). The second oxidation at $E_{1/2}^{ox2}$ = +0.958 V ($\mathbf{T_1}$) and +0.973 V ($\mathbf{T_2}$) (vs Ag/AgCl) corresponded to the reversible oxidation of the radical cation ($TTF^{\bullet+}$) to the dication (TTF^{2+}) (Figure 6). Both the first-wave and the second-wave oxidation potentials of $\mathbf{T_2}$ were higher (15 mV) than those of $\mathbf{T_1}$, which indicated that introduction of another urethane group resulted in a decrease of the electron-donating ability.

Cyclic voltammograms were also measured to explore the formation of the charge-transfer complex. For the mixture of $\mathbf{T_1}$ and TCNQ, five oxidation potentials at $E_{1/2}^{ox1}$ = −0.956 V (I), $E_{1/2}^{ox2}$ = −0.368 V (II), $E_{1/2}^{ox3}$ = +0.221 V (III), $E_{1/2}^{ox4}$ = +0.527 V (IV), and $E_{1/2}^{ox5}$ = +0.852 V (V) (vs saturated calomel electrode, SCE) were clearly discernible (Figure 7). The first three oxidation potentials belonged to $TCNQ^{2-}/TCNQ^{-}$ (I), $TCNQ^{-}/TCNQ^0$ (II) and $TCNQ^0/TCNQ^+$ (III), which were all lower than those of TCNQ ($E_{1/2}^{ox1}$ = −0.954 V(I), $E_{1/2}^{ox2}$ = −0.341 V(II), $E_{1/2}^{ox3}$ = +0.224 V(III)). The (IV) and (V) processes could be assigned to $TTF^{\bullet+}/TTF^0$ (IV) and $TTF^{\bullet 2+}/TTF^{\bullet+}$ (V), which

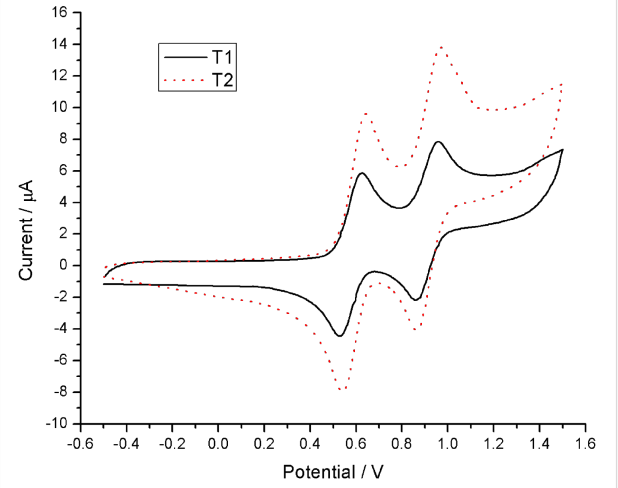

Figure 6: Cyclic voltammograms of $\mathbf{T_1}$ and $\mathbf{T_2}$ in DCM. Conditions: 0.1 M tetrabutylammonium hexafluorophosphate, 100 mV s^{-1}, Ag/AgCl as the reference electrode, Pt wire as the counter electrode, and glassy carbon as the working electrode; measured under argon at 20 °C. Concentration: 1 mM for $\mathbf{T_1}$ and 1 mM for $\mathbf{T_2}$.

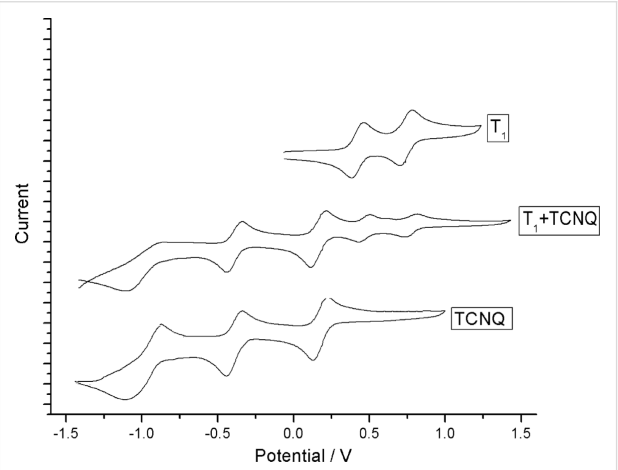

Figure 7: Cyclic voltammograms of $\mathbf{T_1}$ and TCNQ in DCM. Conditions: 0.1 M tetrabutylammonium hexafluorophosphate, 100 mV s^{-1}, saturated calomel electrode (SCE) as the reference electrode, Pt wire as the counter electrode, and glassy carbon as the working electrode; measured under argon at 20 °C. Concentration: 1 mM for $\mathbf{T_1}$ and 1 mM for TCNQ.

were all higher than those of $\mathbf{T_1}$ ($E_{1/2}^{ox1}$ = +0.514 V (I), $E_{1/2}^{ox2}$ = +0.841 V (II)). These changes indicated the formation of the CT complex.

Electrical conductivity measurements

The electrical conductivity of thin films obtained from the $\mathbf{T_1}$ and $\mathbf{T_2}$ samples with TCNQ (1:1 molar)/I_2 (30 min) were further evaluated. To eliminate the influence of contact resistance, the four-probe method was carried out instead of the two-probe method [29,30]. To prepare the thin films, a diluted ethyl acetate solution was dropcasted onto a glass substrates (20 mm × 20 mm) and dried overnight at 40 °C under vacuum. The $\mathbf{T_1}$ and $\mathbf{T_2}$ films in the neutral state before doping behaved as typical, undoped semiconductors ($\sigma < 10^{-9}$ S cm^{-1}) at room temperature. Nevertheless, for $\mathbf{T_1}$, the conductivity increased to 5.8×10^{-6} S cm^{-1} when doped with TCNQ and to 3.0×10^{-6} S cm^{-1} when exposed to iodine vapor. As for $\mathbf{T_2}$, the results were 6.3×10^{-7} S cm^{-1} when doped with TCNQ and 1.8×10^{-7} S cm^{-1} when exposed to iodine vapor. These results indicated their CT complexes can function as semiconducting materials.

Conclusion

In summary, we demonstrated that $\mathbf{T_2}$ (containing two urethane groups) formed amorphous structures while $\mathbf{T_1}$ (possessing one urethane group) formed nanoribbons. The self-assembly ability of $\mathbf{T_1}$ was better than that of $\mathbf{T_2}$, and the results revealed that more urethane groups in a molecule did not necessarily lead to more efficient self-assembly. This may be associated with the formation of intramolecular hydrogen bonds in the $\mathbf{T_2}$ molecule. The formation of hydrogen bonds between urethane groups and the π–π stacking interaction from TTF units were regarded as the main driving forces behind the self-assembly process. Cyclic voltammetry showed that the TTF derivatives underwent two reversible oxidation processes. In addition, the doping of nanoribbons by TCNQ/iodine resulted in the formation of charge transfer states exhibiting semiconducting properties. There is significant potential for the application of the conducting nanoribbons in molecular electronics devices.

Supporting Information

Supporting Information File 1

Experimental section and copies of ^{1}H, ^{13}C NMR spectra, MS and XRD pattern of $\mathbf{T_1}$ and $\mathbf{T_2}$.
[http://www.beilstein-journals.org/bjoc/content/supplementary/1860-5397-11-255-S1.pdf]

Acknowledgments

The reseach leading to these results was funded by the National Natural Science Foundation of China (Nos.20872035, and 21576087), Hangzhou Normal University, and the East China University of Science and Technology.

References

1. Hirst, A. R.; Escuder, B.; Miravet, J. F.; Smith, D. K. *Angew. Chem., Int. Ed.* **2008,** *47,* 8002–8018. doi:10.1002/anie.200800022
2. Nalluri, S. K. M.; Shivarova, N.; Kanibolotsky, A. L.; Zelzer, M.; Gupta, S.; Frederix, P. W. J. M.; Skabara, P. J.; Gleskova, H.; Ulijn, R. V. *Langmuir* **2014,** *30,* 12429–12437. doi:10.1021/la503459y

3. Giansante, C.; Raffy, G.; Schäfer, C.; Rahma, H.; Kao, M.-T.; Olive, A. G. L.; Del Guerzo, A. *J. Am. Chem. Soc.* **2011,** *133,* 316–325. doi:10.1021/ja106807u
4. Liu, Y.; Zheng, N.; Li, H.; Yin, B. *Soft Matter* **2013,** *9,* 5261–5269. doi:10.1039/c3sm50614b
5. Pratihar, P.; Gosh, S.; Stepanenko, V.; Patwardhan, S.; Grozema, F. C.; Siebbeles, L. D. A.; Würthner, F. *Beilstein J. Org. Chem.* **2010,** *6,* 1070–1078. doi:10.3762/bjoc.6.122
6. Banerjee, S.; Das, R. K.; Terech, P.; de Geyer, A.; Aymonier, C.; Loppinet-Serani, A.; Raffy, G.; Maitra, U.; Del Guerzo, A.; Desvergne, J. P. *J. Mater. Chem. C* **2013,** *1,* 3305–3316. doi:10.1039/c3tc30104d
7. George, M.; Tan, G.; John, V. T.; Weiss, R. G. *Chem. – Eur. J.* **2005,** *11,* 3243–3254. doi:10.1002/chem.200401066
8. Goyal, N.; Mangunuru, H. P. R.; Parikh, B.; Shrestha, S.; Wang, G. *Beilstein J. Org. Chem.* **2014,** *10,* 3111–3121. doi:10.3762/bjoc.10.328
9. Skilling, K. J.; Citossi, F.; Bradshaw, T. D.; Ashford, M.; Kellam, B.; Marlow, M. *Soft Matter* **2014,** *10,* 237–256. doi:10.1039/C3SM52244J
10. Wang, C.; Zhang, D.; Zhu, D. *J. Am. Chem. Soc.* **2005,** *127,* 16372–16373. doi:10.1021/ja055800u
11. Jeppesen, J. O.; Becher, J. *Eur. J. Org. Chem.* **2003,** 3245–3266. doi:10.1002/ejoc.200300078
12. Yang, X.; Zhang, G.; Zhang, D.; Zhu, D. *Langmuir* **2010,** *26,* 11720–11725. doi:10.1021/la101193z
13. Gomar-Nadal, E.; Veciana, J.; Rovira, C.; Amabilino, D. B. *Adv. Mater.* **2005,** *17,* 2095–2098. doi:10.1002/adma.200500348
14. Bryce, M. R. *Chem. Soc. Rev.* **1991,** *20,* 355–390. doi:10.1039/cs9912000355
15. PuigmartÍ-Luis, J.; Laukhin, V.; Pérez del Pino, Á.; Vidal-Gancedo, J.; Rovira, C.; Laukhina, E.; Amabilino, D. B. *Angew. Chem., Int. Ed.* **2007,** *46,* 238–241. doi:10.1002/anie.200602483
16. Puigmartı-Luis, J.; Pérez del Pino, Á.; Laukhina, E.; Esquena, J.; Laukhin, V.; Rovira, C.; Vidal-Gancedo, J.; Kanaras, A. G.; Nichols, R. J.; Brust, M.; Amabilino, D. B. *Angew. Chem., Int. Ed.* **2008,** *47,* 1861–1865. doi:10.1002/anie.200704864
17. Massue, J.; Bellec, N.; Chopin, S.; Levillain, E.; Roisnel, T.; Clérac, R.; Lorcy, D. *Inorg. Chem.* **2005,** *44,* 8740–8748. doi:10.1021/ic051017r
18. Lyskawa, J.; Oçafrain, M.; Trippé, G.; Le Derf, F.; Sallé, M.; Viel, P.; Palacin, S. *Tetrahedron* **2006,** *62,* 4419–4425. doi:10.1016/j.tet.2006.02.054
19. Zhang, X.; Wang, C.; Lai, G.; Zhang, L.; Shen, Y. *New J. Chem.* **2010,** *34,* 318–324. doi:10.1039/B9NJ00520J
20. Benbellat, N.; Le Gal, Y.; Golhen, S.; Gouasmia, A.; Ouahab, L. *Synth. Met.* **2012,** *162,* 1789–1797. doi:10.1016/j.synthmet.2012.08.018
21. Tatewaki, Y.; Watanabe, T.; Watanabe, K.; Kikuchi, K.; Okada, S. *Dalton Trans.* **2013,** *42,* 16121–16127. doi:10.1039/c3dt51464a
22. Su, L.; Bao, C.; Lu, R.; Chen, Y.; Xu, T.; Song, D.; Tan, C.; Shi, T.; Zhao, Y. *Org. Biomol. Chem.* **2006,** *4,* 2591–2594. doi:10.1039/b602520j
23. Kitamura, T.; Nakaso, S.; Mizoshita, N.; Tochigi, Y.; Shimomura, T.; Moriyama, M.; Ito, K.; Kato, T. *J. Am. Chem. Soc.* **2005,** *127,* 14769–14775. doi:10.1021/ja053496z
24. Ding, Z.; Zhao, Q.; Xing, R.; Wang, X.; Ding, J.; Wang, L.; Han, Y. *J. Mater. Chem. C* **2013,** *1,* 786–792. doi:10.1039/C2TC00125J
25. Demir-Ordu, Ő.; Şimşir, H.; Alper, K. *Tetrahedron* **2015,** *71,* 1529–1539. doi:10.1016/j.tet.2015.01.042
26. Zhang, Y.; Liang, C.; Shang, H.; Ma, Y.; Jiang, S. *J. Mater. Chem. C* **2013,** *1,* 4472–4480. doi:10.1039/c3tc30545g
27. Le Gall, T.; Pearson, C.; Bryce, M. R.; Petty, M. C.; Dahlgaard, H.; Becher, J. *Eur. J. Org. Chem.* **2003,** 3562–3568. doi:10.1002/ejoc.200300286
28. Vilela, F.; Skabara, P. J.; Mason, C. R.; Westgate, T. D. J.; Luquin, A.; Coles, S. J.; Hursthouse, M. B. *Beilstein J. Org. Chem.* **2010,** *6,* 1002–1014. doi:10.3762/bjoc.6.113
29. Akutagawa, T.; Kakiuchi, K.; Hasegawa, T.; Nakamura, T.; Christensen, C. A.; Becher, J. *Langmuir* **2004,** *20,* 4187–4195. doi:10.1021/la049950e
30. Skabara, P. J.; Berridge, R.; McInnes, E. J. L.; West, D. P.; Coles, S. J.; Hursthouse, M. B.; Müllen, K. *J. Mater. Chem.* **2004,** *14,* 1964–1969. doi:10.1039/b400809j

License and Terms